STRENGTHENING OF REINFORCED CONCRETE BEAMS USING CARBON FIBRE REINFORCED PLASTIC

Amin Ali Ahmed Abdulmajid

B.Sc, M.Sc

Thesis submitted for the Degree of

Doctor of Philosophy

Heriot-Watt University

School of the Built Environment

Edinburgh, United Kingdom

March 2007

Abstract

Strengthening of reinforced concrete beams using external bonded FRP composites is a relatively new approach. The consensus among researchers is that adding FRP composites to the tension face of a beam improves the mechanical properties of the strengthened section. However, applying FRP to the tension face only becomes ineffective if a high ratio of tension steel reinforcement has been used. This thesis therefore focuses on study of the performance of simply supported reinforced concrete beams strengthened with bonded carbon fibre reinforced plastic, CFRP, laminates on both the tension and compression faces.

A series of beams subjected to symmetrical two point loadings were tested. Different parameters including the position of the CFRP (only on the tension face, the compression face or both), the thickness of the CFRP on the compression beam face, the ratio of the tension steel reinforcement and the end anchorage at the tension face of the beam were investigated. Test results showed that adding CFRP to the compression face of an over-reinforced strengthened beam could increase the flexure strength up to 1.4 times of that beam strengthened on tension only. Adding CFRP to the compression face of a strengthened beam decreases, at any load level, the mid-span deflection and increases the stiffness compared to the strengthened on tension face. No significant changes in the first cracking loads were found between the two types of reinforcement concrete beams. Buckling of the CFRP laminates from the compression face of a strengthened beam was a major failure mode.

A simplified analytical model to determine load-deflection behaviour was developed. A nonlinear finite element program, LUSAS, was used to analyse some of the tested beams. A design procedure, based on the material models given in BS 8110, has been developed to determine the ultimate flexural strength of the section.

The tests results are compared with the analytical results and good correlation was found.

To almighty Allah who helped me to complete this work

To the soul of my parents

To my wife, my children and my family for their love, support and encouragement

Acknowledgments

I would like to express my sincere thank to my supervisor Professor Ian May for his unlimited help, in the form of guidance, advice and encouragement. Professor Ian May has been a source of help by providing great ideas and guidance throughout this research.

I would like to thank Heriot-Watt University, particularly the School of the Built Environment, for supporting this research by providing test materials and using the different equipment in the laboratories.

The technicians of the structural and materials laboratories are gratefully acknowledged for their help and advice during the experimental investigation. I would like to particularly thank, Steve Ritch, Graeme Sorley and Tom A Scott.

I am obliged to all members and friends of the School of the Built Environment, particularly Spyros Themelis, for their encouragement and assistance through the research.

ACADEMIC REGISTRY
Research Thesis Submission

Name: Amin Ali Ahmed Abdulmajid	
School/PGI: The Built Environment	
Version: *(i.e. First, Resubmission, Final) : Final*	Degree Sought: PhD

Declaration

In accordance with the appropriate regulations I hereby submit my thesis and I declare that:

1) the thesis embodies the results of my own work and has been composed by myself
2) where appropriate, I have made acknowledgement of the work of others and have made reference to work carried out in collaboration with other persons
3) the thesis is the correct version of the thesis for submission*.
4) my thesis for the award referred to, deposited in the Heriot-Watt University Library, should be made available for loan or photocopying, subject to such conditions as the Librarian may require
5) I understand that as a student of the University I am required to abide by the Regulations of the University and to conform to its discipline.

** Please note that it is the responsibility of the candidate to ensure that the correct version of the thesis is submitted.*

Signature of Candidate: 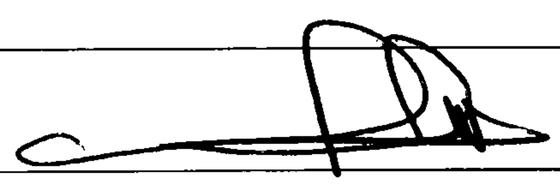	Date: 23-03-07

Submission

Submitted By *(name in capitals)*: Amin Abdelmajid.	
Signature of Individual Submitting: 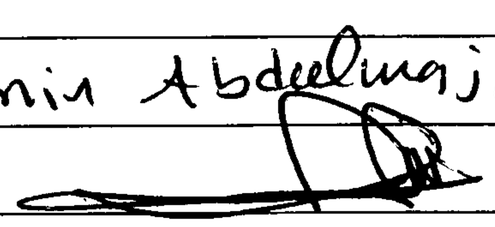	
Date Submitted: 23-03-07	

For Completion in Academic Registry

Received in the Academic Registry by *(name in capitals)*: C RUSSELL	
Method of Submission HANDED IN. *(Handed in to Academic Registry; posted through internal/external mail)*:	
Signature: C Russell	Date:

October 2004

Table of Contents

Notations and Abbreviations

FRP	fibre reinforced plastic
CFRP	carbon fibre reinforced plastic
GFRP	glass fibre reinforced plastic
AFRP	aramad fibre reinforced plastic
UCF	unidirectional carbon fibre
ρ_b	balanced ratio of tensile reinforcement
ρ_s	ratio of tensile steel reinforcement
ρ_{sc}	ratio of compressive steel reinforcement
ρ_f	ratio of external tensile fibre composite reinforcement
ρ_{fc}	ratio of external compressive fibre composite reinforcement
ρ_{fl}	the lower limit of CFRP ratio that avoids yielding of the tensile steel bars
ρ_{fu}	the upper limit of CFRP ratio that avoids the CFRP rupture
ρ_{sv}	the volume ratio between the steel stirrups and the concrete core measured to the outside of stirrups
ε_y	steel strain at yield
ε_s	steel strain
ε	the concrete compressive strain
ε_{cu}	ultimate concrete strain
ε_f	CFRP strain
ε_{fu}	ultimate strain in tension CFRP
ε_{fcu}	ultimate strain in compression CFRP
ε_t	the concrete tensile strain
ε_{su}	the failure strain of steel reinforcement
ε_{sh}	strain-hardening of the internal steel reinforcement
ε_{aci}	strain at the centre of the compression concrete strip
ε_{ati}	strain at the centre of the tension concrete strip
ε_{to}	tensile strain of concrete at the end of softening curve
ε_{cp}	uniaxial strain of concrete at the peak uniaxial compressive stress

ε_{co}	uniaxial strain of concrete at the end of the compressive softening curve
ε_f	tensile strain in CFRP
ε_{fc}	compressive strain in CFRP
ε_s	tensile strain in steel reinforcement
ε_{sc}	compressive strain in steel reinforcement
ε_0	concrete strain at maximum stress defined in equations 5.1 and 5.2
E_s	steel elastic modulus
E_{s1}	hardening slope of steel reinforcement
E_{fib}	elastic modulus of the fibre
E_{mat}	elastic modulus of the matrix
E_c	initial tangent modulus of concrete
E_f	the modulus of elasticity of the CFRP in tension
E_{fc}	the modulus of elasticity of the CFRP in compression
f_y	yield stress of steel reinforcement
f_f	tensile stress of the composite
f_{fib}	tensile stress of the fibre
f_{mat}	tensile stress of the matrix
f_{cu}	compressive strength of concrete cube
f_{cy}	compressive strength of concrete cylinder
f_{sp}	splitting tensile strength of concrete
f_f	tensile stress of CFRP
f_{fc}	compression stress of CFRP
f_{yv}	yield strength of the steel stirrups
f_{su}	the ultimate stress of steel reinforcement
f_t	the concrete tensile stress
f_{yv}	the yield strength of the steel stirrups
A_f	cross-sectional area of externally bonded laminate in tension
A_{fc}	cross-sectional area of externally bonded laminate in compression

A_{fib}	cross-sectional area of the fibre
A_{mat}	cross-sectional area of the matrix
A_s	cross-sectional area of tensile steel bars
A_{sc}	cross-sectional area of compressive steel bars
A_e	the area of concrete in tension
b	beam breadth
h	beam depth
d_f	beam depth includes CFRP thickness
d_s	effective beam depth
d_{sc}	concrete cover in compression
b_f	width of external bonded plate in tension
b_{fc}	width of external bonded plate in compression
ℓ	concrete cylinder length
d	concrete cylinder diameter
b_n	width of the concrete core measured to the outside of stirrups
s_h	spacing between the vertical steel stirrups
t_a	the thickness of the adhesive layer
t_f	thickness of externally bonded plate in tension
t_{fc}	thickness of externally bonded plate in compression
x	distance from the outermost fibre in the compression zone to the neutral axis
$x_l = x_u$	minimum and maximum value of the neutral axis that avoids CFRP rupture and yielding of tensile steel defined in equations 5.47 and 5.51 respectively
a_c	depth of the concrete strip layer in compression
a_t	depth of the concrete strip layer in tension
l_t	number of concrete strips in the tension zone
l_c	number of concrete strips in the compression zone
j	number of the targeted concrete strip in compression
p	number of the targeted concrete strip in tension
y_{ci}	distance from the centroid of the compression strip to the neutral axis

y_{ti}	distance from the centroid of the tension strip to the neutral axis
L_s	shear span
L_s/d_s	shear span to effective depth ratio
Ø	steel bar diameter
$\bar{y}$	distance between the composite plate and neutral axis of the strengthened beam
L	the buckling length
V_{fib}	volume fraction of the fibre
W_{fib}	weight fraction of the fibre
W_{mat}	weight fraction of the matrix
V_{mat}	volume fraction of the matrix
P_u	ultimate load
P_b	buckling load
η_1	ultimate load enhancement ratio for a beam strengthened in tension and compression faces/unstrengthened beam
η_2	ultimate load enhancement ratio for a beam strengthened in both tension and compression faces/ strengthened on tension
Z_{tr}	uncracked first moment of area of the plated section transformed to concrete
I_{fc}	the moment of inertia of the CFRP in compression
I_c and I_f	moments of inertia of the concrete and the plate beams, respectively
μ_φ	curvature ductility index
μ_D	deflection ductility index
μ_E	energy ductility index
M	bending moment
M_f	predicted moment at flexural debonding at plate end
M_{end}	predicted debonding moment at plate end
V_s	predicted debonding shear force at plate end
V_{end}	predicted debonding shear force
V_c	concrete shear force in the concrete beam
v	average concrete shear stress in the concrete beam
v_c	resisting concrete shear stress in the concrete beam
v_s	shear stress caused by steel stirrups

$l_{\min} = l_{\max}$	Minimum and maximum crack spacing, respectively
u	The average bond strength between the steel tension reinforcement and concrete
$\sum O_{bars}$	the total perimeter of the tension reinforcing steel bars
u_f	the average bond shear strength between the FRP and the concrete
G_a	the shear modulus of the adhesive layer
q	the distributed load on the concrete beam
τ	shear stress at the plate end
σ	the peeling stress at the plate end
σ_c	equivalent concrete strength
F_c	total internal compressive force resisted by the concrete above the neutral axis
F_{sc}	total internal compressive force resisted by the compression reinforcement
F_{fc}	compressive force resisted by the external compressive CFRP reinforcement
T_c	total internal tensile force resisted by the uncracked concrete under the neutral axis
F_s	total internal tensile force resisted by the tensile reinforcement
F_f	tensile force resisted by the external tensile CFRP reinforcement
φ	beam curvature
θ	rotation at any point along beam span
v	deflection at a considered point
Δx	length of the segment considered along the beam span
k_1	mean concrete stress factor for rectangular block
k_2	depth of the stress block centroid factor
n	depth ratio d_s / d_f
n_1	depth ratio d_s / d_{sc}
m	depth ratio d_{sc} / d_f
r_{op}	ratio between yield and the peak uniaxial compressive stresses

CHAPTER 1
INTRODUCTION

1.1 General

Strengthening of reinforced concrete members may be required because of the reduction of strength due to deterioration of reinforcement or due to increased loading. Deterioration of the reinforcement in concrete structures can be considered as one of the main problems of structural degradation. This leads to reductions in the resistance capability of the structure at both the ultimate and serviceability conditions. The factors that can cause degradation of concrete structures include carbonation and chloride attack, mechanical damage and reinforcement corrosion. Increases in loads can occur due to a change in use, or due to design or construction effects [1]. Further reasons for strengthening could be the upgrading of resistance to withstand underestimated loads; increasing the load carrying capacity for higher permitted loads; eliminating premature failure due to inadequate detailing. [2]

Strengthening of concrete structural members can be achieved by replacing poor quality or defective material with that of a better quality. An alternative method is by attaching additional load-bearing material to the structure. Important techniques for these include concrete overlaying with additional reinforcement bars, external pre-stressing and externally bonded materials using epoxy resin. The external bonded materials can be FRP or steel plates. The major difficulty in strengthening is achieving compatibility of the behaviour between the existing and the new material used in the repair work. These materials may have properties such as elastic modulus and thermal coefficients of expansion quite different to those of the original. Structural behaviour must also be compatible for all load situations including both dead and dynamic load conditions [2].

Bonding of steel plates to the surface of existing members has been widely used for strengthening concrete structures. This is because it is inexpensive, relatively quick and easy to install, full interaction between the steel plate and concrete surface can be obtained, and it has little effect on the overall dimensions on the structure.

Bonding of steel plates to the tension zones of flexural concrete members in existing beams in buildings and bridges was first reported in 1960 [3] and 1964 [4], respectively. The use of the technique has grown and has been recognised as suitable for the strengthening and stiffening of structures and has become common practice for the retrofitting and repair of building structures. [5, 6] In spite of the extensive use of steel plates in practice, these have some disadvantages. For example, they are heavy which affects their transportation, handling and installation; the lengths of plates available are limited, which necessitates the difficult task of forming joints. In addition, it is necessary for expensive falsework to hold the plates in position during the adhesive curing period, to prepare the steel surface for bonding and thereafter to protect plates against corrosion [7]. Because of the disadvantages mentioned above, other materials have been considered. These are fibre-reinforced polymer-matrix composites, also called fibre-reinforced plastic (FRP). Currently, three types of FRP composites are available: glass fibre (GFRP), aramid fibre (AFRP) and carbon fibre (CFRP). These materials are constructed in the form of plates or laminates. The main differences between the two composite systems are that plates have specific thickness and they can be applied/stuck directly to the concrete surface. There can be some difficulty in applying them on curved surfaces. However, fabric systems are more flexible in that any number of layers can be added and they can be applied on any surface geometry.

FRP materials possess the qualities of high strength to weight ratio, resulting in lower installation costs and the possibility of their application to the structure with little disruption. In addition, FRP materials have mechanical and physical properties superior to those of steel, particularly with respect to tensile stress, fatigue strength, corrosion resistance, toughness and thermal properties. Therefore, because of the need to repair and retrofit rapidly deteriorating infrastructure in recent years, the potential market for using fibre-reinforced composites for repair of a wider range of applications is now being realized to a much greater extent.

As a result of the wide acceptance of the advantages of these materials, numerous studies have been carried out in recent years into the strengthening of reinforced concrete beams using FRP composites. The literature review in Chapter two illustrates that FRP composite has been widely used on the tension face to strengthen both simply

supported and continuous reinforced concrete beams. Research has shown that the application of FRP composite to the tension face of an over-reinforced beam does not lead to a significant increase in the flexural strength. To overcome this problem it has been suggested that CFRP laminates should be bonded both the tension and compression faces of the simply supported beam in this investigation.

1.2 Aims of research

The aims of the research are summarised as follows:

1. To investigate the increase in the flexural strength by bonding CFRP laminates on the compression face of unstrengthened simply supported reinforced concrete beams.
2. To investigate failure mechanisms of the strengthened reinforced concrete beams, namely peeling and debonding of external bonded CFRP, and particularly buckling of the compression CFRP.
3. To carry out and provide guidance on the use of the nonlinear finite element method for modelling simply supported beams strengthened with external CFRP on both the tension and the compression faces.
4. To develop design guidelines for reinforced concrete beams strengthened with external CFRP on both the tension and the compression faces.

1.3 Research programme

The research comprised an experimental programme, theoretical analyses and FE analyses.

A test programme of twenty-three reinforced approximately half full size concrete beams, which were tested under four point loadings with various shear spans, was carried out. In the experimental programme the following test series were carried out:

- Series-I, which comprised under-reinforced beams with a low ratio of tension steel and low shear span to effective depth.
- Series-II, which comprised under-reinforced beams, and also had a low shear span to effective depth.

The parameters investigated in series I and II were: CFRP laminate lengths, anchorages at the ends of the CFRP laminates into the tension face and the contribution to the flexural strength caused by tension strengthening and tension and compression strengthening.

- Series-III, which comprised over-reinforced beams and high shear span to effective depth ratio.
- Series-IV, which comprised over-reinforced beams with a high ratio of tension steel and a high span to effective depth ratio. In this series, small cross-section beams were tested.

In series III and IV, the thickness of the compression CFRP was investigated. In addition, the contribution to the flexural strength and the strain in the CFRP laminates when buckling of the CFRP laminate occurred were investigated.

A moment-curvature model was developed using Microsoft Excel. The model is capable of predicting the flexural strength behaviour of a section at any incremental moments.

A program using MATLAB [8] for predicting deflections based on the finite difference method has also been developed.

The simplified material models given in BS8110 (1997) [9] have been adopted for a design procedure. The model is able to predict, directly, the value of the neutral axis depth, x, at failure, for the different flexural modes of the composite section and the flexural strength.

Comparisons between the experimental results and those obtained from the analytical models, the design procedure and the non-linear finite element analysis, LUSAS 13.5,[10] have been conducted.

The components parts of the research programme are shown in Figure 1.1.

1.4 Outline of the thesis

The contents of the eight chapters and three appendices are as follows:

Chapter 1 is a general introduction to the reasons for the deterioration of reinforced concrete structures and the different repair and strengthening techniques that have been successfully developed, including the technique that has been investigated in this research, externally bonded FRP laminates. The reasons for choosing FRP composites as an appropriate strengthening approach compared with steel plates are described. The reasons for adding FRP composites on the compression face of the beams are also discussed. The aims of the research are presented.

Chapter 2 contains a critical review of previous research into the repair and strengthening of reinforced concrete beams using external reinforcement. Different strengthening techniques for reinforced concrete elements are presented. The effect of bonding FRP materials on the external concrete surfaces on the engineering and physical properties, i.e. flexural strength, deflection, ductility and stiffness, are presented. The common failure modes and the existing models for reinforced concrete beams strengthened externally with FRP composites are also discussed. The review identifies the areas that need further investigation.

Chapter 3 contains a description of the experimental investigation of strengthened reinforced concrete simply supported beams. The materials used in the test specimens, including the CFRP coupons, and the test procedure of the main reinforced beams are described. The results of the tension tests of CFRP coupons are discussed.

Chapter 4 contains a description of the test results. Several parameters have been investigated: in particular, the influence of the amount of both the internal steel and the external CFRP reinforcement and the position of the external CFRP on the beam

faces (i.e. on the tension face, the compression face or both the tension and compression faces). Crack patterns, failure modes, deflection and curvature responses and the strains in different elements of the section are discussed.

Chapter 5 provides a description of the different theoretical models used to predict the behaviour of sections strengthened with CFRP. The models are:

- the simplified analysis models, which are based on the moment-curvature relationship and load-deflection.
- the simplified design procedure, which is based on the rectangular stress block for concrete approach of BS 8110, and
- the numerical non-linear finite element analysis, using the LUSAS software computer package[11].

Chapter 6 presents a comparison between the experimental results and those from the models described in Chapter 5. Two main sections are included in this chapter. The first section compares the experimental results conducted in the current study with those obtained from the analytical formulation, the simplified design procedure and the FE analysis models. In this section, load-deflection relationships, moment-curvature relationships, strains in the internal steel reinforcement, strains in the external CFRP reinforcement and crack patterns obtained from the FE analysis are investigated. The second section validates the results of the ultimate bending capacity and the failure modes obtained from the simplified analytical model and the design procedure model, described in Chapter 5-Section 5.3.3 and Section 5.4, with respect to the experimental results obtained from the literature and those carried out in the current study.

Chapter 7 contains a description of a case study to investigate the influence of some parameters on the flexural strength and failure modes of a reinforced concrete beam strengthened on the tension face and on both the tension and compression faces of the beam. A parametric survey was conducted which included the effect of the FRP composite ratio on the tension, the tension and compression, the internal steel reinforcement ratio and the concrete compressive strength. The parametric study

was carried out using the simplified analysis model and the design procedure for flexural design discussed in Sections 5.3.3 and 5.4, respectively.

Chapter 8 outlines the principal findings obtained from the research and gives recommendations for future work.

Appendix A illustrates the crack patterns and failure modes for some of the tested beams.

In Appendix B two worked examples using the design procedure described in Chapter 4 are given.

Appendix C describes the derivation procedure of the depth of the neutral axis design formulae, Section 5.4.4, that are used for calculating the ultimate bending capacity of a strengthened beam.

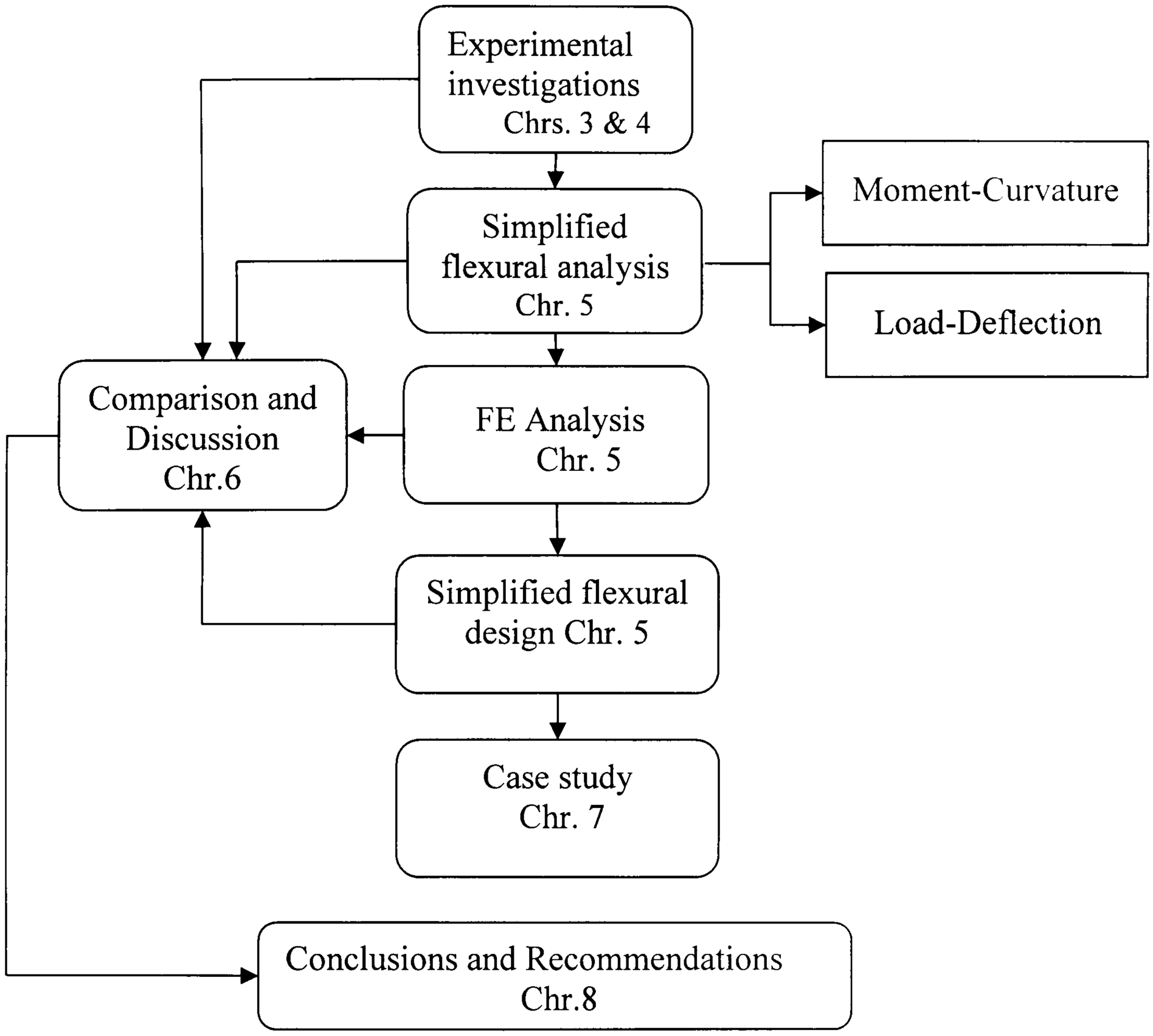

Figure 1.1: Research programme adopted

CHAPTER 2
LITERATURE REVIEW

2.1 General introduction

The requirement to strengthen an existing concrete structure may arise from a variety of reasons, as mentioned in Chapter One. These reasons justify the ever-increasing demand for the repair and strengthening of concrete structures. It was mentioned earlier in Chapter One that the crucial aim of strengthening a structure is to increase its load-carrying capacity with reference to its previous condition. External bonded FRP composite used in this research is one of the techniques that are used for the flexural strengthening of reinforced concrete members; a brief review of other strengthening techniques is also given in the literature survey carried out in this Chapter. The literature survey given in this chapter is divided into two main parts. The first part contains a brief description of some of the other techniques for structural strengthening, which is not the subject of this thesis. The second part contains a description of the flexural strengthening of reinforced concrete beams using external bonded FRP composite reinforcement, as this is the subject of this research.

2.2 Techniques for the Strengthening of Reinforced Concrete Members

2.2.1 Introduction

This section contains a description of some strengthening techniques for reinforced concrete structures that have been developed. Established techniques are:

- Concrete overlaying with additional reinforcement
- Miscellaneous

2.2.2 Concrete overlaying with additional reinforcement

Concrete overlaying involves adding additional concrete and is accompanied by additional reinforcing steel bars. Concrete overlaying can be implemented either to the tension or compression zone of a reinforced concrete beam. When this technique is implemented onto the tension zone of a reinforced concrete beam, e.g. a simply supported beam, the concrete mix is projected into place using a nozzle. In such case the overlaying is referred to as Gunite [11] in the UK and Shotcrete by the American Concrete Institute (ACI). In the UK, the size of the aggregate used is less than 10 mm; however, in the ACI the size can exceed 10mm. In this technique the capability of the strengthened length to transfer shear stresses between the old and the new concrete needs careful evaluation [12]. It has been reported that most concrete overlaying durability failures occur because of peeling off of the strengthened length owing to bond failure rather than failure of the material itself [13].

An experimental study carried out by Pham-Thanh *et al.* (1995) [14] tested nine reinforced concrete bridge slabs strengthened by fixing an additional layer of mesh reinforcement below the slab soffit and then covering this with a layer of sprayed concrete. The thickness of the sprayed reinforced concrete layers varied between 0.5 and 1 of that of the original slabs. The ultimate flexural strength of some of the slabs strengthened using this technique increased by 3 times.

Diab (1997) [15] carried out an experimental study of the strengthening of reinforced concrete beams sprayed with concrete. The study comprised adding longitudinal tensile steel bars and an additional thickness of sprayed concrete. Four beams were cast with the same dimensions. One was kept as an unstrengthened beam, one beam was loaded to cracking load and the final two beams were loaded to service loads. Then, each loaded beam was strengthened with an additional thickness of 70 mm of ordinary concrete sprayed to the tension zone, Figure 2.1. This corresponded to 0.2 of the total beam depth. The load tests were repeated and the average ultimate strength of the three strengthened beams increased in relation to the unstrengthened beam by 2.5 times. The strengthened beams showed high ductility before failure. No slippage between the two

concrete layers was observed until failure. The results were validated by mathematical modelling. Good agreement was observed between the calculated and the measured results.

Recently, beams with rectangular and channel shaped cross sections were experimentally investigated by Haldane and Ziara (1999)[16]. The study was carried out by casting a concrete overlay onto the upper surface of the beams, compression zone. To prevent diagonal and inter-laminar shear failures, the stirrups in the regions of the supports in the overlay were welded to the stirrups in the original beam. The thickness of the concrete added to the rectangular beam was similar to that of the unstrengthened beam depth. The thickness ratio of the concrete added onto the top face of the channel beam was 0.25 of the unstrengthened beam depth; however, it was similar to the slab thickness of the unstrengthened beams. The channel shaped beam was loaded on the top face of the channel. The results showed that each of the strengthened beams acted as a monolithic unit and failed in a flexural manner. The flexural strength of the strengthened beams was increased by 1.63 times compared with the unstrengthened beams. Ziara (2000) [17] has proposed a design approach for strengthening structural concrete beams using physically connected concrete overlays based on the experiments carried out by Haldane and Ziara (1999)[16]. The results of the experiments and the design method correlated well.

Öztürk and Ayvaz (2002)[18] investigated the effect of V connecting bars and U connecting stirrups on the flexure strength of strengthened reinforced concrete beams, Figure 2.2. V shaped connecting bars were welded to both the old and the new longitudinal reinforcement. U shaped connecting stirrups were welded to the stirrups of the old longitudinal reinforcement. The thickness ratio of the additional concrete layer was 0.25 of the depth of the unstrengthened beam. Using the two techniques provided a good anchorage between the existing and the additional reinforcement. The final failure occurred by flexure. It was found that the ultimate strengths of the strengthened beams produced by using both techniques were approximately 2.5 times of the unstrengthened beam.

2.2.3 Miscellaneous

Three additional techniques are explained in this section, external prestressing, external unbonded reinforcement and finally the CARDIFRC technique.

External prestressing

In this technique, the prestress is produced by tendons which are placed outside the structure. One of the advantages of external prestressing is its applicability to several structural materials; for example, reinforced and prestressed concrete, and masonry walls. The use of the external prestress tendons in some new bridges in the UK began in 1960 [19]. Strengthening with external unbonded prestressed tendons is widely used; however, the technique is limited to developed countries because of the expense of the technique [12].

External un-bonded reinforcement

This technique employs unstressed reinforcing bars which are retro-fitted to the existing beam from outside the cross-section, and anchored at the ends of the beams, Figure 2.3. This technique may offer significant advantages, because of the ease of installation over alternative strengthening techniques, for simply supported beams. Cairns and Rafeeqi (1997)[20] investigated experimentally the influence of three parameters, namely the loading arrangement, the effective depth of external unbonded bars, and the ratio of internal reinforcement, on the structural behaviour of simply supported beams strengthened using unbonded external reinforcement. The results showed that using this strengthening technique for reinforced concrete beams improved their serviceability behaviour. The flexural capacity of the strengthened beam increased by up to average of

1.85 over the unstrengthened beam with some reduction in ductility. The increase in the flexural strength was found to be higher for lightly reinforced beams.

Theoretical and experimental studies on the use of external unbonded ordinary tensile reinforcement bars for strengthening reinforced concrete simply supported beams have been conducted by Cairns and Rafeeqi [21,22]. It was reported that normal plane section behaviour assumptions cannot be used directly when this technique is used because the external reinforcement is not bonded to the beam throughout its span, but is anchored only at the ends. To keep the longitudinal unbonded bars following the curvature of the original beam, deflectors were used. A numerical model based on section analysis, and incorporating non-linear behaviour of both materials and geometric effects, was proposed by Cairns and Rafeeqi [21,22]. The numerical model predicted the enhancements in ultimate strength accurately, but was less successful in the prediction of deflection when compared with the measured results.

The CARDIFRC technique

The CARDIFRC [23] technique is a new approach which can be used as an alternative approach to externally bonded plates of either steel or FRP. This technique, based on a material compatible with concrete, is currently under development at Cardiff University. The method uses high-performance fibre-reinforced concrete. The constituent materials could be mixed and fabricated to form plates or strips with a thickness of between 16 mm to 20 mm and length as required. The fabricated strips must be cured at room temperature for one day before demolding, and then followed by a hot-curing at 90°C for nine days. Subsequently, the strips are bonded to the concrete surface in a similar way to steel plates and FRP plates using epoxy. Test results have shown that bonding CARDIFRC strips to the tension face and to the sides of the beam is a promising method for improving the flexural and shear strength, as well as the serviceability of damaged beams. It is stated that the current method may be used when there is a need to improve the durability of existing structures.

2.3 External Plate Bonding of either Steel or FRP Composite

2.3.1 Introduction

External reinforcement has been used for the flexural repair and strengthening of reinforced concrete beams for several years. The literature survey in this section describes the flexural strengthening of reinforced concrete beams using external bonded steel plates and FRP composites. The main objective of this section is to establish the previous research and that currently being carried out and to understand the behaviour of externally strengthened beams so that further research areas can be identified.

As mentioned in Section 1.1, epoxy resins were used as early as the 1960's to bond steel plates to the tension zones of flexural concrete members of buildings and bridges [3]. The second recorded case was in Durban, South Africa, in 1964, where epoxy-bonded steel plates were used to strengthen the flexural zones of concrete beams in an apartment building, in which part of the reinforcing steel had been accidentally omitted during construction [4]. A subsequent application of steel plates bonded to the tension faces of structural members was the strengthening of bridges on the M5 Motorway at Quinton, England in (1975) [24].

Bonding external steel plates on the tension face of reinforced concrete has been investigated for flexural strengthening of simply supported reinforced concrete beams, for example Jones *et al.* (1980) [25], Swamy *et al.* (1987) [26], Oehlers and Moran (1990) [27] and Oehlers *et al.* (1992) [6].

FRP composite materials have been used in the strengthening of reinforced concrete beams as a result of the wide acceptance of their advantages in recent years, as discussed in Section 1.1. Extensive research on the use of FRP materials for strengthening flexural of reinforced concrete beams has been carried out. Experimental

and analytical research in this area has been conducted; for example An *et al.* (1991) [28], Ritche *et al.*(1991) [29], Sharif *et al.* (1994) [30], Meier and Winstorfer (1995) [31], Arduini *et al.* (1997) [32], Arduini and Nanni (1997) [1], Garden *et al.* (1998) [7], Malek *et al.* (1998) [33], Saadatmanesh and Malek (1998) [34], Swamy and Mukhopadhyaya (1999) [35] , Speadi *et al.* (2000) [36], Mukhopadhyaya and Swamy (2001) [37], Rahimi and Hutchinson (2001) [38], Pham and AL-Mahaidi (2004) [39] and Thomsen *et al.* (2004) [40].

Some experimental studies of the strengthening reinforced concrete continuous beams using FRP materials have been carried out: these include studies by Arduini *et al.* (1997) [41], Grace *et al.* (1999) [42], Tann and Deplak (2000) [43] , and Grace (2001) [44]. More recently, Ashour *et al.* (2004) [45] carried out an experimental study validated by theoretical calculation for strengthened reinforced concrete continuous beams.

With reference to the above mentioned studies, it is obvious that most of the experimental research on tension face-strengthened beams with both steel plates and FRP materials to increase flexural strength and stiffness, reported in the literature, has been on simply supported beams. No study has been reported using external FRP or steel plates on the compression face of a beam. Therefore, the review of literature described in this chapter is focused on the strengthening of a reinforced concrete beam on the tension face.

Extensive research has been carried out on using external reinforcement either steel plates or FRP materials on the tension face of a reinforced concrete beam [25-40], a comprehensive review showing experimental observations and analytical results in the current research is given. This will focus on:

- Properties of FRP composites
- Mechanical properties gained by flexural strengthening
- Failure modes
- Plate-end peeling models
- Analytical models for strengthened beams
- Flexural design models

- Finite element models
- Parameters effecting strengthened beams

2.3.2 Properties of FRP composites

FRP composites comprise fibre and resin, the primary role of the resins in the FRP is to provide lateral support to the fibres and to protect the fibres from physical and chemical effects caused by the surroundings [46].

There are many types of fibres in general use. The most important types commonly used in structural applications, as reported in Chapter 1, are Carbon fibres, Aramid fibres, and Glass fibres.

The main characteristics of various common reinforcing fibres are given in Table 2.1 [46], whilst the mechanical properties of the FRP composites, fibre and the adhesive, are given in Table 2.2 [47]. The values given in Table 2.2 may be considered as indicative values and do not give exactly a particular composite product in which the actual properties of the composite are directly related to the fibre volume fraction in the composite, FVF.

Regardless of the type of fibre or forming method employed, all three FRP materials given in Table 2.2 have similar stress-strain behaviour: linear elastic up to rupture in both tension and compression. Figure 2.4 shows the tension stress-strain curves for CFRP, GFRP, AFRP and mild steel. These curves show clearly the brittle behaviour of FRP materials compared with the ductile behaviour of steel.

FRP has excellent strength in both tension and compression. The mechanical properties of the FRP composite in the longitudinal direction are influenced by the properties of fibre and resin, the fibre/resin surface interaction, the fibre volume fraction (FVF), and the fibre orientation [48]. The stiffness of the composite depends on the fibre stiffness and

the FVF. The axial tensile strength of the composite is directly dependent on the fibre's ultimate strength, the fibre's FVF and the resin stiffness [46,48].

2.3.3 Mechanical properties gained by flexural strengthening

Adding external material, either plates or laminates, to the surfaces of reinforced concrete beams using resins or bolts or both together can substantially improve the mechanical and physical properties of stiffened sections, particularly with FRP materials. The term resin herein refers to epoxy. The bolts can be anchor bolts or expansion anchors for use with steel plates, or fibre anchors for use with FRP composites.

Several experimental studies have been selected to present the benefits to be gained from bonding steel plates or FRP materials to the tension face of reinforced concrete beams. For example, strengthening of RC beams using steel plates has been carried out by, e.g. Jones *et al.* (1980) [25], Swamy *et al.* (1987) [26], and Jones *et al.* (1988) [5]. Using this technique increased the range of elastic behaviour, reduced the tensile strain in the concrete caused by the composite action, and delayed the appearance of the first visible cracks [25]. Furthermore, a significant strength enhancement was achieved with increasing flexural stiffness [25, 26], reduced cracking [26, 5], deflections [5] and surface deformation at all levels of loads, and increased the ultimate flexural capacity, with a range of 1.1-1.15 compared with that of the unstrengthened beams [25].

Several experimental studies have reported similar results gained from using FRP materials as external reinforcement on reinforced concrete beams e.g. Saadatmanesh and Ehsani (1990) [49], An *et al.* (1991) [28], Ritche *et al.* (1991) [29], Sharif *et al.* (1994) [30], Chajes *et al.* (1994) [50], Bonacci and Maalej (2000) [51], Ramana *et al.* (2000) [52], Rahimi and Hutchinson (2001) [38], Bonacci *et al.* (2001) [53], Shin and Lee (2003) [54], Grace *et al.* (2003) [55] and Alagusundaramoorthy *et al.* (2003) [56]. The consensus among researchers is that adding FRP materials to the tension faces of reinforced concrete beams increases the flexural strength and stiffness, and conversely decreases the mid-span deflection and

reduces the crack size. All strengthened beams showed similar increases in stiffness and flexural strength ranging from 1.2 to 2 times over the serviceability loads of the unstrengthened beams, while the ultimate flexural strength increased from 1.28 to 1.97 [29]. Similarly, Chajes *et al.* (1994) [50] showed that strengthening reinforced concrete beams with FRP laminates increases the flexure strength by 1.45 to 1.53 and the stiffness by 1.4 over the unstrengthened beams. However, deflection capacities (defined as a ratio between the central deflection at peak load of a strengthened beam and that of unstrengthened beams) reduced by 0.9 to 0.7 [51].

An excellent study presented by Bonacci and Maalej (2001) [53] assessed the behaviour trends of beams strengthened with the externally bonded FRP materials. The analysis involved a total of 127 specimens from 23 separate experimental studies as a database. It was found that one-third of the specimens with external reinforcement showed strength increases of 1.5 or more in combination with a considerable reduction in deflection capacity when compared with the unstrengthened beams.

Most recently, Pham and AL-Mahaidi (2004) [39] carried out an experimental and analytical study using sixteen simply supported rectangular reinforced concrete beams strengthened with CFRP laminates on the tension face. All the beams were tested using four point loads with a clear span of 2300 mm between the supports and a shear span of 700 mm. The beam width was 140 mm and the CFRP laminate width was 100 mm. Variables in the test included the length of the CFRP, the area of the tension reinforcement, the concrete cover, the number of CFRP laminates and the amount of the shear reinforcement. All the strengthened beams exhibited both high stiffness and ultimate load compared with the unstrengthened beams. The ultimate strengths of strengthened beams were increased by 1.3 to 1.5 of that of the unstrengthened beams.

With regard to ductility of simply supported beams strengthened with FRP composites, Spadea *et al.* (1998)[57], Mukhopadhyaya *et al.* (1998)[58] and Swamy and Mukhopadhyaya (1999) [35] described three measures. These measures are curvature ductility index (μ_φ), deflection ductility index (μ_D) and energy dissipation ductility index (μ_E). Ductility indices were calculated from the following:

$$\mu_{\varphi} = \frac{\varphi_u}{\varphi_y} \tag{2-1}$$

$$\mu_D = \frac{D_u}{D_y} \tag{2-2}$$

$$\mu_{\mathrm{E}} = \frac{\mathrm{E}_u}{\mathrm{E}_y} \tag{2-3}$$

where φ_u, D_u and E_u are the beam curvature, mid-span deflection and the area under load-deflection curve, respectively, at ultimate load and φ_y, D_y and E_y are the beam curvature, mid-span deflection and the area under load-deflection curve, respectively, at yield load of the tensile reinforcement.

Spadea *et al.* (2001)[59] carried out an experimental study using 11 rectangular reinforced concrete simply supported beams strengthened with CFRP plates on the tension face. The study focused on investigating the strength and the assessment of the ductility indices as mentioned above. The variables in the experimental programme were the longitudinal steel ratio, the volume of internal stirrups, and the location and configuration of external anchorages along the beam span. The beam length was 5m and the cross-section was 140 mm x 300 mm. The tensile steel reinforcement varied between 0.65% and 1.14%. Three beams were unstrengthened and two beams were strengthened with a single CFRP plate bonded to the tension face but without any external anchorages for the bonded plate. The remaining six beams also contained one single bonded CFRP plate at the tension face. These beams were provided with external anchorages at the plate ends and intermediate anchorages distributed along the beam span. The study concluded that adding CFRP plates to the tension face of a beam without external anchorages exhibited less ultimate strengths than that with external anchorages when both were compared with the unstrengthened beams. The higher contribution to the ultimate strengths occurred with beams that have the lower tensile ratios of tension steel. The ductility indices defined in equations 2-1 to 2-3 were found realistically reflect the physical and structural response of reinforced concrete beams strengthened with a bonded CFRP laminate with or without external anchorages. By choosing one of the beam series which were tested for example, series-A included

unstrengthened beam A2, strengthened beam but without any external anchorages for the bonded plate A2.2 and beam strengthened but with external anchorages and other intermediate anchorages distributed along the beam span A2.3 were provided.

	Curvature Ductility index (μ_φ)	Deflection ductility index (μ_D)	Energy ductility index (μ_E)
A2, unstrengthend	11.5	7.5	17.4
A2.2, strengthened without anchorages	3.0	4.8	13.2
A2.3, strengthened with anchorages	4.0	5.8	16.1

The ductility values given above imply that curvature, deflection and energy indices are found to increase for reinforced concrete beams strengthened with a bonded CFRP laminates at the tension face with external anchorages compared with those without. It is also recommended that using the intermediate anchorages, which are distributed along the beam span for reinforced concrete beams strengthening on tension faces for future applications, is needed.

2.3.4 Failure modes

Reinforced concrete members strengthened externally with steel plates or FRP can fail either by the classical mode of failures of reinforced concrete beams or because of loss of composite action.

The classical modes of failure in reinforced concrete beam are:

- Flexural failure
- Shear failure

Failures related to loss of composite action can be summarised as follows:

- Steel yielding followed by FRP rupture
- Plate-end failure
- Debonding failure

A brief discussion will be given in the following sections. Most of the discussion will be focused on the failures that are related to loss of a composite action, particularly plate-end failure and debonding failure. Plate-end failure may occur in the form of peeling or separation of the plate at the plate ends. The most common plate-end failure reported is peeling and this mode is normally initiated due to the concentration of the flexural and shearing forces in the adhesive layer [60]. Debonding failure normally occurs away from the plate end [60]. Usually, as the load is further increased, the formation of the flexural or a mixed flexure shear crack away from the plate ends in this mode causes high stresses in the FRP along the crack, and finally debonding of the FRP occurs. This can arise if the bonding adhesive is weak or has not been properly applied. Further details on Plate-end failure and debonding failure will be given in 2.3.4.4 and 2.3.4.5.

2.3.4.1 Flexural failure

If the failure at the ends of the plate is prevented, the ultimate flexural capacity of the beam is reached when either yielding of the tensile steel reinforcement followed by concrete crushing, or by crushing of the concrete, Figure 2.5. When the beam section is under-reinforced internally with tensile steel and a relatively low amount of the external FRP on the tension face of the beam added, the tensile steel reinforcement yields before concrete crushing. If a large amount of FRP is added on the tension face of an under-reinforced beam, the ultimate flexural capacity of the beam is reached by crushing of the concrete and the tensile steel reinforcement does not reach yield. Beams which fail by concrete crushing before yielding of the tensile steel reinforcement, when a large amount of FRP was used, have shown considerable reduction in the ductility compared with the unstrengthened beam [61].

2.3.4.2 Shear Failure

A reinforced concrete beam may reach its shear limit prior to flexural failure if sufficient shear reinforcement is not provided [61], Figure 2.6. Adding external reinforcement to the tension face of the beam provides little contribution to shear

resistance [62]. Teng *et al.* (2002) [47] reported that shear strengthening of reinforced concrete beams should be carried out simultaneously with flexural strengthening, to ensure that the required flexural strength is not compromised by shear failure and that flexural failure still precedes shear failure.

2.3.4.3 Steel yielding followed by FRP rupture

FRP rupture generally occurs following the yielding of the longitudinal tensile steel bars. FRP rupture occurs if the beam section is under-reinforced internally with tension steel and the external FRP ratio is relatively low. This failure mode is shown in Figure 2.7. The FRP reinforcement must be well anchored for this failure mode to take place [53].

2.3.4.4 End-plate failure

As mentioned earlier, premature end plate failure often occurs. Two end-plate failure modes are reported normally separation of concrete cover, Figure 2.8a, and separation of the plate from the concrete, Figure 2.8b. In the first failure mode the concrete cover is attached to the plate, and the failure is related to peeling forces; however, in the second failure mode only very small particle of cementitious materials are attached to the plate. Separation of the plate is normally related to the adhesive properties or surface condition.

The first mode of end-plate failure is described as premature peeling failure by Oehlers and Moran (1990)[27], Oehlers (1992)[6], and Moahmed Ali *et al.* (2001) [63]. This mode of failure has been referred to elsewhere as end-of-plate failure through concrete e.g. Ritchie *et al.* (1991) [29]; local shear failure, Saadatmanesh and Malek (1998) [34] ; and concrete rip-off failure, Sharif *et al.* (1994) [30] and Nguyen *et al.* (2001) [64].

In this study the first mode of failure will be referred to as peeling failure. Peeling failure can start at the plate ends owing to stress concentration caused by the discontinuity of the plate; this form of failure is induced by both the applied vertical shear forces [6,65] and the applied moments at the plate ends [27]. Garden and Hollaway (1998) [66] have reported that the formation of a crack in the concrete at or near the plate end propagates to the level of the horizontal tension reinforcement which leads the separation of the concrete cover, and then the tension reinforcement can be clearly seen.

Oehlers and Moran (1990)[27] and Oehlers (1992) [6] investigated peeling failures of reinforced concrete beams externally strengthened with steel plates. Two types of peeling failure were identified: flexural peeling and flexural-shear peeling. Flexural peeling can be observed in strengthened beams with the plate ending in a constant bending moment region, for which a peeling crack associated with a flexural crack causes plate separation, Figure 2.9. Flexure-shear peeling is observed in strengthened beams with the plate ending in the shear span. This mode occurs due to the sudden propagation of the peeling crack associated with a diagonal flexural-shear crack, Figure 2.10.

With regard to the mechanism of flexural peeling, Oehlers [67] reported that this kind of peeling occurs when the attached plate tends to stay straight while the beam deforms owing to the applied moment; this deformation induces a crack propagating inwards from the plate ends, forming a crack plane parallel with the plane of the plate, Figure 2.11. It was also reported that the effect of flexure on debonding can be prevented by terminating the external plate at a section near to zero moment.

A comparison of the flexural peeling mechanism for steel and FRP plates strengthened simply supported beam, loaded with two equal point loads, was reported by Mohamed Ali *et al.*[63]. Tests comprised five beams with the plates on tension face and three beams with similar plate lengths but bonded to the sides of the beam without any tension face strengthening. The dimensions of the beams were 150mm wide, 250mm deep, and the total length was 3000mm. The two point loads were equally spaced at 600mm for each. The length of the bonded plates was 600mm and ended in the region of the constant

bending moment. It was observed that the peeling mechanism was the same for both steel and FRP, but the magnitudes of the flexural peeling resistance were different. When the scatter between the magnitudes of the test results and the magnitudes of the theoretical results for FRP strengthened beam and steel strengthened beams was removed, beams strengthened with FRP showed a lesser increment in the flexure peeling capacities than steel strengthened beams. The scatter between the magnitudes of the test and the theoretical results for FRP strengthened beam and steel strengthened beams in such cases was adjusted by considering the experimental flexural peeling capacities for the steel strengthened beams were made equal to the corresponding theoretical magnitudes and for the FRP strengthened beams, all the test results were multiplied by this factor.

Olivier (1999) [68] discussed the mechanism of flexure peeling and referred to the fact that peeling cracks are very similar to the cracking mechanism of concrete splitting in tension specimens, or in the flexure-shear failure of beams without stirrups.

Ritchie *et al.* (1991) [29] carried out tests on sixteen simply supported reinforced concrete beams subjected to two equal point loads, strengthened with FRP plates on the tension face. End plate anchorages were used in some of the strengthened beams. The plates were bonded along the beam tension face and ended close to the beam support. It was noted that many of strengthened beams failed by peeling. The failure modes were initiated by cracking starting from the end of the plate and propagating at about a 45-degree angle up to the internal longitudinal steel, then continuing horizontally through the concrete at the level of the reinforcing steel.

Based on the analysis of some tests of simply supported reinforced concrete beams strengthened with FRP loaded with four equal point loads, Sebastian (2001) [69] reported that, peeling failure occurred due to the curvature imbalance at the plate ends between the curvature in the plate and that which exists in the beam. Three cases for end-plate peeling to occur in simply supported single span strengthened beams were also reported:

- in beams with low shear span where high shear bond stresses near the supports can be produced
- in beams where the plates are curtailed far from the supports, where the shear bond stress can be amplified due to the plate-end effect
- in beams where a stiff plate is used, where high bond stresses near the plate curtailment can be involved

Recently, Pham and AL-Mahaidi (2004) [39] carried out an experimental and analytical study using sixteen simply supported rectangular reinforced concrete beams strengthened with CFRP laminates on the tension face. Details of the beam tested are described in 2.3.3. The study concluded that peeling failure started from the CFRP ends and failed due to the formation of shear cracks at the steel reinforcement level at the root of the concrete teeth between shear cracks.

The consensus among researchers is that peeling failure is initiated by the high interfacial shear and normal stresses near the plate ends when it exceeds the strength of the weakest element, which is the concrete.

The second form of end-plate failure, Figure 2.8b, the separation of the plate, occurs by debonding of the laminate or the plate from the concrete interface, which is caused by a propagating crack starting from the ends of the plate, close to the adhesive layer. This mode has been investigated in experiments by Saadatmanesh and Ehsani (1991) [70] who tested one control beam, four rectangular beams and one T-beam. The cross section of the rectangular beams was 455 mm width and 205mm depth. The flange width and the thickness of the T-beam were 610mm and 75mm, respectively. The total depth of the T-beam was 455 mm; the thickness of the web was 205mm. The beam span, between the supports, was 4570mm. GFRP plates were bonded to the tension face of each beam and cut off at 16mm of the beam supports. The T-beam failed by sudden premature separation of the plate. This was due to poor workmanship used in the surface preparation and bonding.

Teng *et al.* (2002) [47] referred to this mode by plate-end interfacial debonding, because it occurs in the concrete adjacent to the concrete-to-adhesive interface. It was also added that the risk of this failure is increased by using poorer adhesives, and not only the poor workmanship reported by Saadatmanesh and Ehsani (1991) [70].

It can be mentioned that the mechanism of crack formation at or near the plate end is well understood. The cracks formation that occurs at the plate ends is the most important factors in the splitting of concrete cover; however, the adhesive properties and/or poor workmanship are responsible for the separation of the plate. Although many publications have been issued concerning strengthening of reinforced concrete beams further research is needed to investigate the efficiency of the anchorage techniques that should be used at the plate end in terms of inhibiting or preventing end-peeling failure.

2.3.4.5 Debonding failure

In most cases, this mode of failure occurs in the constant moment region. Debonding may be initiated at a flexural or a mixed flexure-shear crack and propagate towards the plate ends, Figure 2.12. Debonding failure has been observed in a number of experimental studies. For example, debonding initiated by flexural cracks has been reported by Oehlers (2001) [67], Saadatmanesh and Ehsani (1991) [70], Bonacci and Maalej, (2000) [51] and initiated by flexure-shear cracks by Garden *et al.* (1998) [66], Swamy and Mukhopadhyaya (1999)[35], Meier (1995)[71], and Pham and AL-Mahaidi (2004) [39].

Oehlers [67] believed that the mechanism of debonding is caused by axial peeling, Figure 2.13. This was interpreted as "…the 'infinite' strains that have to be accommodated where the plate crosses the crack induce debonding cracks that propagate away from the flexural crack, as shown. The axial load *A,* Figure 2.14, in the plate is resisted by the uncracked concrete at the end of the peeling crack as well as by aggregate interlock or friction across the crack interface".

Teng *et al.* (2002) [47], with respect to the mechanism of the flexural crack that induced FRP debonding, reported that when a major crack is formed in the concrete, the tensile stresses released by the cracked concrete are transferred to the FRP plate. Accordingly, high interfacial stresses, peeling and shear, along the adhesive-to-concrete interface, between the FRP and the concrete, are induced near the crack. With further increases in the applied loading, the tensile stresses in the concrete near the crack, and hence the interfacial stresses, are increased. When these stresses reach critical values, debonding starts at the crack and then propagate towards one of the plate ends.

For flexure-shear crack induced debonding failure, the relative vertical displacement between the two faces of the crack, Figure 2.15, produces peeling stresses on the FRP plate-to-concrete interface [35, 71, 72]. These stresses finally lead the FRP plate to debond.

Many experimental studies have reported the debonding mechanism in reinforced concrete beams strengthened using steel plates or FRP plates, however, only a few studies have reported similar mechanisms in reinforced concrete cantilever slabs strengthened using GFRP strips: these include studies by Teng *et al.* (2000) [73] , Teng *et al.* (2001) [74] and Lam and Teng (2001) [75].

Tests of twenty-one specimens of reinforced concrete cantilever slabs with different variables were carried out. Two GFRP strips were bonded to the tension face of the concrete slab, Figure 2.16. The overall dimensions of the cantilever slabs were nominally 700mm long, 500mm wide and 100mm thick; various tension steel ratios from 0.28% to1.13% were used. The total dimensions of the GFRP strips were varied; 600 and 800 mm length, 40 and 80 mm wide, and 1.27-1.92 mm thickness per strip were used. The GFRP strips were anchored into the fixed end of the cantilever slab; at the free end three different schemes were used:

1. the GFRP strips without anchoring
2. the GFRP strips were wrapped around slab edge through slab thickness using a similar material of GFRP strips

3. two fibre anchors for each GFRP strip were prepared and installed close to the fixed end and at the mid-span of the slab

In all the tests, a line load across the tension face of the slab at the free end was applied.

The test results showed that as the line load was increased, the deflection increased and cracks started to appear near the fixed end, in the interface layer between the concrete and GFRP. With further load increase, these cracks joined each other to form a major crack and debonding started soon after. Debonding propagated from the fixed end to the free end of the slab as the deformation continued to occur. Debonding of the GFRP was observed in the slabs strengthened using the first and the second schemes.

In slabs strengthened using the third scheme, when the fibre anchors were used, debonding of the GFRP strips was prevented and the slabs finally failed by tensile rupture of the GFRP. It was concluded that debonding of the GFRP strips occurred at the location where the bending moment is maximum and using the fibre anchors was found to prevent debonding failure.

2.3.5 Plate-end peeling models

Plate-end peeling failure of strengthened beams has become a matter of concern for many researchers, mainly with respect to identifying the characteristic forms of existing debonding strength models, as discussed in Section 2.3.4.4. An extensive search of the literature has found many debonding strength models which have been developed either for FRP or steel strengthened reinforced concrete beams. A brief review for these models has been given here.

2.3.5.1 Upper limit of the longitudinal shear stresses

a) Shear capacity based models

- **The Model of Oehlers *et al.***

Oehlers *et al.* (1990) [27],(1992) [6] developed a strength model for calculating debonding forces at the steel plate ends of the plated reinforced simply supported beams subjected to either four or three point bending. Two expressions for calculating debonding forces, based on the position of the tension plate termination, were proposed. For a plate terminating in the constant moment region, the flexural moment M_f that causes the plate to debond was proposed by the following expression:

$$M_f = \frac{E_c I_c f_{sp}}{0.901 E_f t_f} \qquad (2\text{-}4)$$

where E_c and E_f are the moduli of elasticity of the concrete and the plate respectively, I_c the cracked second moment of area of the plated section transformed to concrete, f_{sp} the cylinder splitting tensile strength of concrete, and t_f the plate thickness.

For a plate terminating near the support, it was proposed that debonding occurs when the shear force at the plate end ,$V_{s,}$ reaches the shear capacity of the concrete, V_c, in the reinforced concrete beam without the contribution from the shear reinforcement. Hence, based on the experimental observations, [6] the following empirical formula was proposed:

$$V_s = V_c = [1.4 - (d_s/2000)]\, b d_s\, [\rho_s f_{cy}]^{1/3} \qquad (2\text{-}5)$$

where $\rho_s = A_s / b d_s$ is the ratio of tensile steel reinforcement, A_s the area of steel tension reinforcement, b the section width, d_s the effective depth of the section and f_{cy} is the concrete cylinder compressive strength in N/mm^2.

For cases where both the shear force and the moment at the plate end are significant, the following interaction equation was used to describe the failure envelope, Figure 2.17.

$$\frac{M_{end}}{M_f} + \frac{V_{end}}{V_s} \leq 1.17 \tag{2-6}$$

and

$$M_{end} \leq M_f \tag{2-7}$$

$$V_{end} \leq V_s \tag{2-8}$$

M_f and V_s are the moment and shear force at the plate end, respectively, causing plate debonding when the plate end is terminated in a region of constant moment and shear, respectively.

- **Smith and Teng model**

Smith and Teng (2002) [76] compared equation 2-6 against the test data for FRP strengthened beams. The plot showed that no interaction appeared to exist between the moment and the shear force, and the shear force at failure is always greater than V_s, as predicted by equation 2-5. Accordingly, the shear force that causes failure is proposed to be given by

$$V_{end} = \alpha V_c \tag{2-9}$$

The factor α =1.4 is recommended for use to design against all forms of plate end debonding failures. V_c is given by equation 2-5.

b) Concrete tooth models

- **Raoof and Zhang Models**

The concept of a concrete tooth was first described in Zhang *et al.* (1995) [77]. Based on this concept, Zhang *et al.* (1995) [77], Zhang *et al.* (1997) [78] developed a strength model to predict concrete cover separation failures in steel plated beams. The concrete cover between two successive cracks forms a concrete tooth which can deform as a cantilever under the longitudinal shear stresses at the adhesive level, as shown in Figure 2.18. The bending moment due to these shear stresses about the tooth root will result in transverse tensile stresses at the level of the internal steel reinforcement adjacent to the external plate. When these tensile stresses exceed the tensile strength of the concrete, peeling failure will occur.

As there are minimum and maximum crack spacings, l_{min} and l_{max} obtained from equations 2-10 and 2-11 respectively, the shear stresses at the adhesive level causing peeling failure also have upper and lower limits. The lower limit of the shear stresses is calculated from equation 2-12, whereas the upper limit of the shear stresses is twice the lower limit.

$$l_{\min} = \frac{A_e f_{sp}}{u(\Sigma O_{bars} + b_f)} \tag{2-10}$$

$$l_{\max} = 2l_{\min} \tag{2-11}$$

$$\tau_{\min} = \frac{f_{sp} l_{\min}}{6h'} \frac{b}{b_f} \tag{2-12}$$

where A_e is the area of concrete in tension, Figure 2.19, u the steel-to-concrete average bond strength, ΣO_{bars} the total perimeter of the tension reinforcing bars, b_f is the external plate width, h' is the clear cover depth as shown in Figure 2.18b. It is assumed that $u = 0.28\sqrt{f_{cu}}$, in N/mm^2, and $f_{sp} = 0.36\sqrt{f_{cu}}$, in N/mm^2, where f_{cu} is the concrete cube compressive strength. For the case of an reinforced concrete beam with a single layer of steel tension reinforcement, A_e is twice the distance from the centroid of the tension reinforcement to the external fibre of the tension face of the reinforced concrete beam multiplied by the width of the reinforced concrete beam.

- **Wang and Ling's model**

Wang and Ling (1998) [79] proposed a modification to the tooth model of Zhang *et al.* (1995) [78] to make it suitable for FRP-strengthened beams. This involved modifying the average bond strength between the concrete and the plate, leading to the following formula for the minimum crack spacing:

$$l_{\min} = \frac{A_e f_{sp}}{u \Sigma O_{bars} + u_f b_f} \tag{2-13}$$

$$u = 0.313\sqrt{f_{cy}} \ , \tag{2-14}$$

where

u = the average bond strength between the steel tension reinforcement and concrete.

f_{cy} = the cylinder compressive strength and

f_{cy} = 0.8 f_{cu}, while u_f is the average bond shear strength between the FRP and the concrete and was taken as 1.96 N/mm^2.

2.3.5.2 Ultimate shear and peeling stresses at plate end

- **The models of Roberts and Ziraba *et al.***

Roberts (1989)[80] studied the equilibrium of a small part of a steel plate bonded to a simply supported beam to determine the shear and transverse normal (peeling) stresses at the plate end. Elastic behaviour for the materials was assumed. The longitudinal shear stress, τ, and the peeling stress, σ, along the adhesive layer at the plate end, respectively, were calculated from the following formulae:

$$\tau = C_1 V_o \tag{2-15}$$

$$\sigma = C_2\ \tau \tag{2-16}$$

where

$$C_1 = \frac{t_f (d_f - x)}{I_c}\left[1 + \frac{M_o}{V_o}\sqrt{\frac{G_a}{E_f t_f t_a}}\right] \tag{2-17}$$

$$C_2 = \left(\frac{3E_a t_f}{E_f t_a}\right)^{0.25} \tag{2-18}$$

The parameters E_a, G_a and t_a are the modulus of elasticity, shear modulus and thickness of the adhesive layer, respectively. E_f and t_f are the elasticity modulus and thickness of the plate, respectively. d_f is the total beam depth including the plate thickness, x is the neutral axis depth of the transformed strengthened cracked section, I_c is the second moment of area of this transformed cracked section, and M_o and V_o are the bending moment and the shear farce at the plate end respectively.

The influence of the concrete compressive strength ,f_c' , and the concrete tensile strength, f_t, on the shear and peeling stresses at the plate end for the equations developed by Roberts (1989)[80] was investigated by Ziraba *et al.* (1994) [81]. The following formulae were proposed:

$$\tau = 35 f_t \left(\frac{C_1 V_o}{f_c'} \right)^{\frac{5}{4}} \qquad (2\text{-}19)$$

$$\sigma = 1.1\, C_2\, \tau \qquad (2\text{-}20)$$

where C_1 and C_2 are parameters calculated from equations 2-17 and 2-18.

- **Saadatmanesh and Malek's model**

Saadatmanesh and Malek (1998)[34] developed a debonding strength model to predict concrete cover separation in FRP-plated beams based on the assumption that concrete cover failure is related to high stresses at the plate end. Linear elastic behaviour for the materials was assumed. The shear stress τ and the normal (peeling) stress σ are found from a closed-form solution derived by Malek *et al.* (1998) [33] while the longitudinal stress was found from a section bending analysis. The closed-form solution for determining the bending moment was derived assuming the following quadratic formula

$$M_{(xo)} = a_1 x_o^2 + a_2 x_o + a_3 \qquad (2\text{-}21)$$

where x_o is the distance along the soffit plate from its left end. And a_1, a_2, a_3 are the constants of the bending moment $M_{(xo)}$ polynomial for a beam subjected to a uniformly distributed load, q. The shear, τ, stress at the plate end is expressed by the following equation:

$$\tau = t_f (b_4 \sqrt{A} + b_3) \tag{2-22}$$

where

$$A = \frac{G_a}{t_a t_f E_f} \tag{2-23}$$

$$b_2 = \frac{E_f}{Z_{tr} E_c} (2a_1 x_o + a_2) \tag{2-24}$$

$$b_3 = E_f \left[\frac{1}{Z_{tr} E_c} (a_1 x_o^{\,2} + a_2 x_o + a_3) + 2b_1 \frac{t_a t_f}{G_a} \right] \tag{2-25}$$

The parameters a_1, a_2, a_3 are derived from equation 2-21; furthermore, Z_{tr} is the uncracked first moment of area of the plated section transformed to concrete; t_a is the thickness of the adhesive layer; t_f is the plate thickness; E_f and E_c are Young's modulus of the plate and the concrete, respectively, and G_a is the shear modulus of the adhesive layer.

The maximum normal (peeling), σ, stress at the plate end is expressed by the following equation:

$$\sigma = \frac{K_n}{2\beta^3} \left(\frac{V_p}{E_f I_f} - \frac{V_c + \beta M_o}{E_c I_c} \right) + \frac{q E_f I_f}{b_f E_c I_c} \tag{2-26}$$

where

$$\beta = \left(\frac{K_n b_f}{4 E_f I_f}\right)^{1/4} \text{; and } \quad K_n = E_a / t_a \tag{2-27}$$

$$V_c = V_o - b_f \bar{y} t_f (b_3 \sqrt{A} + b_2) \tag{2-28}$$

$$V_p = -b_f t_f{}^2 (b_3 \sqrt{A} + b_2)/2 \tag{2-29}$$

where, I_c and I_f are moments of inertia of the concrete and the plate beams, respectively; $\bar{y}$ is distance between the composite plate and neutral axis of the strengthened beam; b_f is the width of composite plate; M_o is the bending moment in the concrete beam at the location of he plate end; q is the distributed load on the concrete beam; and V_o is the shear force in the concrete beam at the location of the plate end.

- **Smith and Teng's model**

Smith and Teng (2001)[82] developed analytical solutions for the interfacial shear and normal stresses at the plate end of reinforced concrete strengthened beams. The derivations of these solutions are described in terms of adherends 1 and 2, where adherent 1 is the beam and adherend 2 is the soffit plate. Linear elastic behaviour for derivations of axial, bending and shear between the two adherends is assumed.

The general expressions for the interfacial, shear $\tau(x)$, and normal $\sigma(x)$, stresses for all load cases and applicable over the whole lengths of the soffit plate are given as follows:

$$\tau(x) = z_1 V(x) + \frac{z_2}{\lambda} M(0) e^{-\lambda x} + \tau^*(x) \tag{2-30}$$

$$\sigma(x) = e^{-Bx}[C_1 \cos(Bx) + C_2 \sin(Bx)] - s_1 \frac{d\tau(x)}{dx} - s_2 q \tag{2-31}$$

where

$V(x)$ and $M(0)$ are the applied shear force at any point along the soffit plate and the applied bending moment at the end of the soffit plate, respectively. The shear

stress, $\tau^*(x)$, varies for each load case provided by specific formulae detailed in reference [82]. Expressions λ, z_1, s_1, s_2, B, C_1 and C_2, based on the section geometry and materials properties of the composite section, are given in Smith and Teng (2001)[82].

2.3.6 Analytical models for strengthened beams

Moment-Curvature relationship

Ritchie *et al.* (1991) [29] and An *et al.* (1991) [28] developed an iterative technique to determine the moment-curvature relationship of a reinforced concrete beam strengthened with an external plate on its tension face. The technique is based on assuming values for the compressive concrete strain on the extreme fibre and the neutral axis depth. Once these values are assigned, the concrete between the extreme compression fibre and the depth of the neutral axis is divided into strips. For all the strips across the beam depth, the average strains were determined based on a linear distribution. The stresses and hence the forces are then calculated on the strips and in the tension reinforcement, and summed to give the total force. The depth of the neutral axis was then adjusted until the sum of the compressive forces equalled the sum of the tensile forces. The bending moment and the corresponding curvature are then determined. The compressive strain on the extreme fibre is increased and a similar process is carried out. Consequently, the moment-curvature relationship of a strengthened section could be evaluated. An *et al.* (1991) [28] limited the extreme compression strain to a value of 0.003, as proposed by the ACI Building Code [83]. Ritchie *et al.* (1991), [29] however, confirmed that the ultimate strength of the section is not limited by a specified value of the extreme compression strain. The strain at the extreme compression fibre of a beam should be incrementally increased to a level where either the moment capacity of the section is reduced or the up to ultimate strain of the tensile reinforcement. The technique of Ritchie *et al.* (1991) [29] has been adopted in the current study, further details are given in Chapter 5.

Load-Deflection relationship

Despite the large amount of experimental work reported in the literature on using external reinforcement of steel plates, FRP plates or laminates on the tension face of the reinforced concrete beam for strengthening, only a few analytical studies for calculating the load-deflection relationship have been developed.

Ross *et al.* (1999) [84] developed an approximate analytical solution, based on elastic-plastic section analysis for predicting load-deflection behaviour of simply supported beam strengthened with FRP on the tension face, loaded statically in three-point bending. The analytical solution was developed to determine the deflection of the beam at the mid-span only and not for any section along the beam. The load-deflection curve was divided into 4 regions, Figure 2.20. In each region, a linear load-deflection relationship was assumed. The strain and stress distributions in the cross sections for regions 1 to 4 are given in Figure 2.21. Trilinear curves for modelling concrete in compression and the tensile steel were utilised. For the FRP, linear stress-strain behaviour up to rupture was assumed. In region 1, the behaviour of the concrete and tensile steel bars was assumed to be elastic. In region 2, a cracked section was assumed and consequently the concrete in tension was not active and at the end of this region the tensile steel yielded. In region 3, the tensile steel behaviour is inelastic, having passed the yield stress. At the end of region 3, the concrete in compression reached its peak compression stress, trilinear stress-strain relationship for concrete in compression. In region 4, the concrete in compression is assumed to have reached its ultimate strain, strain softening, and the equivalent rectangular distribution of the stresses was considered. For each region of the load-deflection relationship, the flexure stiffness of the strengthened beam, the bending moment of the internal forces at the beam mid-span were calculated. Hence, the applied load and consequently the mid-span deflection, based on a constant factor obtained in the derivation of beam midspan deflection for three point bending, of the beam can be determined.

In estimating deflections of reinforced concrete flexural members, ACI 318-95[-] recommends the use of an effective moment of inertia which includes the effect of stiffness variation caused by nonuniform cracking of the concrete along the length of the beam. Because the ACI's calculation of the effective moment of inertia of FRP-strengthened reinforced concrete beams does not accurately represent the flexural stiffness characteristics, El-Mihilmy and Tedesco (2000) [85] represented an alternative approximate solution for estimating the effective moment of inertia for these beams. This solution was incorporated into a rational procedure for calculating deflections of these types of beams. The load-deflection relationship of FRP-strengthened on tension face of reinforced concrete beams described in three stages:

1. precracked beam, before concrete cracking
2. cracked beam, after concrete cracking and before yielding of steel reinforcement
3. postcracked beam, after yielding of the tensile steel reinforcement and the ultimate flexural strength of the section

For the precracked beam, the cracking moment and the mid-span deflection were calculated using the linear elastic analysis. For each of the cracked beam and postcracked beam, an analytical equation for calculating the effective moment of inertia was reported. In the cracked beam, the concrete stress-strain curve was assumed to be linear until yielding of the tensile steel reinforcement. The effective moment of inertia at yielding of the steel was assumed to be equal to the cracked moment of inertia. The curvature of the postcracked beam was calculated by integrating the idealized bilinear moment-curvature relationships of the FRP-strengthened beams. The bending moments at ultimate and at yielding of the tensile steel reinforcement were calculated, based on satisfying the force's equilibrium. The mid-span deflection, assuming elastic analysis, was then calculated, based on the effective second moment of inertia of the strengthened reinforced concrete beam.

2.3.7 Flexural design models

Many design models for calculating the ultimate flexural strength of reinforced concrete beams strengthened with steel plates or FRP have been developed. These design models

consider only flexural failure of the strengthened beam by FRP rupture, Figure 2.7, or concrete crushing, Figure 2.5 [28, 34, 50,75, 86, 87, 88]. However, with regard to preventing plate failure, some recommendations have been drawn up [87]. The Concrete Society Technical Report 55 (2000) [87], classified the failure modes of reinforced concrete beams strengthened by end-plate failure and debonding, Section 2.3.4. End-plate failure occurs due to peeling. To avoid peeling, the ratio of the plate width to plate thickness was limited by no more than 5 for steel plates; however, a greater ratio for FRP is acceptable. To prevent peeling failure, the longitudinal shear stress between the FRP and the substrate at ultimate limit state is limited to be no more than 0.8 N/mm^2. To avoid debonding failure, it was recommended that the strain in the FRP plate should not exceed 0.8% when the applied load is uniformly distributed. When a point load on the beam is applied, this value is reduced to 0.6% particularly at the hogging regions close to supports of continuous beams, where high shear force and bending moment are present. Ashour (2002) [88] recommended that the area of the FRP should be limited between upper and lower limits to ensure ductile behaviour of the strengthened sections, Section 5.4.4.

2.3.8 Finite element analysis

Finite element analysis has been widely used in the analysis of reinforced concrete structure, particularly in the analysis of reinforced concrete beams. Experimental studies have been used to validate the results obtained from this approach. A few reported studies [32, 38, 89] on finite element analysis of reinforced concrete beams strengthened with external FRP reinforcement have presented some explanations.

Hong *et al.* (1997) [89] used ABAQUS software for modelling four point loading reinforced concrete simply supported beams strengthened with external CFRP plates. Two beams using FE analysis were analysed and the results compared with the experiments. 1D and 2D finite element analyses for one half of the beam were conducted. A constant strain one dimensional beam element and 8-noded plane element CPS8 were used for modelling concrete in 1D and 2D, respectively. The internal tensile reinforcing steel and the external plate reinforcement were modelled as bar elements

embedded in the concrete. It was found that the analytical results obtained by FE correlated well with the experiment. Several variables, using a parametric study based on the 1D modelling analyses, were also investigated by Hong *et al.* (1997) [89]. The variables are concrete strength, tensile steel ratio and the thickness of the steel plate. It was found that the adding CFRP plate on the tension face of a beam achieved a significant increase in the flexural strength in the section that had a relatively low tension steel ratio when compared with the unstrengthened beam. The concrete strength significantly contributed to the ductility and affected the stiffness and the flexure strength of the strengthened beam. Increasing the thickness of the external plate increased the stiffness and the flexure capacity of the strengthened beam. However, the opposite effect on the ductility of the strengthened beam was observed.

Arduni *et al.* (1997) [32] used 2D and 3D finite element analysis for reinforced concrete simply supported beams strengthened with external FRP plates and laminates. A perfect bond between the FRP and the concrete was assumed, and FRP reinforcement was applied directly over the concrete elements. Different types of failures were observed, ranging from FRP rupture to concrete shear failure, and it was found that these failure modes were affected by FRP type, thickness and bonded length of the FRP material. After concrete cracking, the load-deflection curve produced by the numerical models exhibited higher stiffness than the measured results. It was also found that the load capacity of the strengthened beams determined from the numerical solutions is less than the measured. This was justified as a result of convergence problems caused by the opening of abundant cracks as the applied load increased.

Rahimi and Hutchinson (2001) [38] used LUSAS software to model reinforced concrete simply supported beams strengthened with external FRP plates. A 2D nonlinear FE model was used. Due to the symmetry of the beams about the mid-span, half of the beams were modelled. Concrete beams were modelled with 4 and 8-noded quadrilateral isoperimetric elements. The steel reinforcing bars were modelled with two and three noded elements. A single row of 4 and 8-noded elements was used to model the FRP and the adhesive. A perfect bond between the adhesive and the concrete was assumed. It was found that the numerical solutions were sensitive to the value of concrete tensile strength, but a value of 1.5 N/mm^2 provided good correlation with the experimental

results. The sizes of mesh used in this study were relatively coarse and did not make a difference in the results, particularly when compared with beams having much finer mesh [90]. The study concluded that the detachment of the bonded external plate from the concrete, at ultimate loads, is governed by limiting the principal stress value at the concrete /FRP plate interface. The exact location of this value depends on a number of factors, including plate material type and thickness.

2.3.9 Parameters effecting strengthened beams

All previous studies discussed in this research emphasized that a good degree of strengthening could be achieved by bonding external FRP or steel plates to the tension face of the concrete beam. However, the essential degree of strengthening obtainable is related to many factors, such as the geometrical dimensions and properties of the bonded materials, surface condition, adequate anchorages at the plate ends, the amount of the tensile steel and the compressive concrete strength. A detailed investigation on the effect of such parameters is given below.

2.3.9.1 Geometry and properties of external bonded materials

The geometrical dimensions of the external bonded reinforced materials, such as plates or laminates, adhesive thickness, or both together, and their properties play an important role in the composite action, and consequently controlling the failure mode and the flexural strength, of the strengthened section as discussed in the following:

Plate, adhesive thickness

With steel plates for example increasing plate thickness or adhesive thickness reduces cracking and deformation but not at the same rate. The stiffening effect produced by increasing adhesive thickness decreases as the plate thickness increases [26].

Tripi *et al.* (2000)[91] reported that local deformations in a reinforced concrete beam strengthened with the external CFRP laminates are effected by the thickness of the epoxy. Large relative displacements between the CFRP laminates and the concrete tension surface at the location of through-cracks occurred when a thicker epoxy was used. Thicker epoxy also resulted in large spacings between adjacent through-cracks.

The relationship between the ductile behaviour of the repaired reinforced concrete beams and the thicknesses of the GFRP plate was investigated by Sharife *et al.* (1994) [30]. An inversely proportional relationship was noted: increasing plate thickness decreased the ductility of the strengthened reinforced concrete beams. The failure mechanism at the plate end was found to depend on the plate thickness. Low thickness produced low shear and peeling stresses at the plate end, and the final failure was observed by either concrete crushing or FRP rupture at mid-span of the beam. A high thickness however increased shear and peeling stresses at the plate end and consequently caused peeling failure. Also, increasing plate thickness increased shear stress [38,92] and peeling stress [38] at the plate ends. In addition, the thicker plates led to peeling failure however it can be delayed by gluing plates to the lateral faces [32]. Furthermore, increasing the plate thickness increased the stiffness and reduced the internal tensile steel reinforcement strains compared with those of the unstrengthened beam at the same value of the applied load [26,38]. This implies that the strength enhancement could be obtained by using this technique; however, increasing the thickness of either adhesive or plate can cause brittle failure.

Plate width, length

Most recently, the CFRP plate width in a strengthened reinforced concrete beam, was studied using nonlinear analysis based on a bond-slip model by Thomsen *et al.* (2004) [40]. Complete anchorages at the plate ends were assumed. It was noticed that using small plate widths led to peeling failure with a little enhancement in the flexure strength of the strengthened beam. In contrast, using large plate widths caused rupture of the CFFP

plates, associated with high flexure strength enhancement of the strengthened beam, compared with that failed by peeling failure. However, large plate widths introduced higher energy ductility than the small plate widths. In all cases studied by Thomsen *et al.* (2004), the widths of the CFRP plates were varied while the areas were kept constant. Furthermore, larger widths led to more cost-effective strengthening [93]. Extending the length of the CFRP plate close to the entire beam supports avoided peeling failure and the flexural strength was increased compared with that of the beam strengthened with smaller length [40,64]. Moreover, Thomsen *et al.* (2004) [40] reported that increasing the length of the CFRP plate at the beam tension face, which has a constant area, increased the flexural strength of the strengthened beam, and the failure modes were changed from peeling at the plate end to debonding at mid-span.

All the studies that have been carried out, using FRP composite or steel plates in strengthening of reinforced concrete beams, indicated that there is a good enhancement of strength, but the gained strength is accompanied with brittle failure. This failure depends on the several factors for example, the geometrical dimensions of the external plate and the adhesive, the mechanical properties of the external bonded materials and the linear behaviour between the bond stress and the slip of the bonded materials.

2.3.9.2 Surface preparation and installation methods

The effect of surface preparation on the bonded interface between FRP laminates and concrete members is considered an important factor for achieving a high level of strengthening. Arduni and Nanni (1997) [1] used two methods for preparing the concrete surface of reinforced concrete beams strengthened with CFRP laminates: sanding and sand blasting. The first one was used to remove the small particles and smooth the sharp corners of the concrete specimens, since the concrete surface was of good quality. However, in the second one the coarse aggregate was exposed. It was found that sand blasting was slightly more effective than the normal sanding. In the specimens where sand blasting was used, high loads and deflections with no change in the failure mechanism were observed.

Two methods for concrete surface treatment with using FRP laminates were discussed by Toutanji and Ortiz (2001)[94]. The first consists of sanding the concrete surface using an ordinary sander to the thin layer of mortar accumulated on the surfaces. The second treatment was by water jet using an intensifier pump machine. It was observed that surface treatment by water jet produced a better bonding strength than surface treatment by sander. Grit blasting or water jetting techniques were recommended [95] for use in surface preparation of concrete prior to the adhesive layer being used.

Varying the application methods of FRP composites on the concrete surface may have a part in the effect on the strengthened elements. Three methods: hand lay-up system, pre-preg system, and vacuum injection system of FRP composite applications were experimentally studied by Täljsten and Elfgren (2000)[96] to evaluate the efficiency of using these materials in shear strengthening.

In the first method, hand lay-up system, the adhesive was applied to the primed concrete surface and the CFRP strips were placed on the surface. Subsequently, the reinforcement was soaked with the resin using a roller.

The second method is the unidirectional pre-preg system. In this method the carbon fibres are impregnated with epoxy adhesive to form a pre-preg tape. The basic difference between pre-preg system and the conventional hand lay-up is that using the prepreg the impregnation of the fibres is made prior to moulding. Figure 2.22 shows the different components used in the application of pre-preg tape on strengthening concrete beams. The application procedure of pre-preg tape to the concrete surface is summarised as follows.

1. An adhesive film is placed on the concrete surface to provide extra adhesive to the pre-preg tape.
2. The pre-preg tape is placed over the adhesive film.
3. A peel ply is placed on the pre-preg tape, to make the removal of the vacuum bag from the hardened composite easier.

4. A breather is placed on the peel ply to evacuate an excess of epoxy.
5. The vacuum bag is applied and sealed against the concrete using tapes. A hole is made in the bag which is connected to a vacuum pump.
6. A heating element is placed over the vacuum bag and is heated up to 100°C, with an increase of 2°C /min. The maximum temperature is maintained for 4 hours and then the temperature is reduced at a rate of 2°C /min.

There are several advantages of using the pre-preg system: e.g. it can be laid up in any direction to give the required orientation, and requires less handling of the epoxy adhesive at the work site. However, it also has some disadvantages, such as materials cost is higher for impregnated fabrics, and also because there is a need for several operations to be considered before the strengthening is achieved. In addition, the pre-preg tape needs to be stored under cold conditions until application. Another source[46] referred to this approach as being impractical for construction because of the complexity of heating treatment.

The third method is the vacuum-injection system. The implementation of this method is carried out by covering the concrete surface with FRP fabrics. A vacuum bag and plastic film is then laid on the FRP fabrics and the sides of the bags are sealed to the concrete surface. The vacuum is applied at the outlet in the bag, and an epoxy adhesive is supplied at the inlet.

From a comparison of the three methods, it is observed that hand lay-up is easy to apply to the concrete beams and good results can be achieved. However, in special applications, for example in warm surroundings, pre-pregs can be used because the glass transition temperature of this resin could be increased. Exceeding the glass transition temperature is accompanied by a reduction in mechanical properties.

2.3.9.3 End-anchorage techniques

Stress concentrations at the plate ends can cause premature failure. Therefore, end anchorage techniques have been used to prevent end-plate failure of strengthened beam.

Several experimental studies have been carried out, using either mechanical bolts [5,30] or prefabricated U-shapes [30, 35,58,97].

Jones *et al.* (1988) [5] used different schemes of steel bolts for anchoring longitudinal steel plates for reinforced concrete beams, loaded with four equal point loads, Figure 2.23. It was found that the plate end peeling was delayed and the failure load of the bolted plated beams was increased compared to the un-bolted plated beams. After peeling occurred, the bolts prevented complete plate separation and the beams were able to carry more load. The final failure of the bolted beams was due to concrete crushing. The contribution of the bolts in increasing the failure load was 9% compared with that where the peeling failure occurred. All the bolted and unbolted beams studied by Jones *et al.* (1988) [5] were designed to have the same theoretical failure load assuming no plate-peeling. The bolted beams exhibited small increase in the failure load when the concrete failed by crushing compared with the un-bolted beams which failed by plate-peeling. End-plate peeling, when occurs, can be influenced by many factors i.e. the magnitude of the stresses at the plate, the geometrical dimension of the plate, etc. The important point here is that the use of the steel bolts for anchoring longitudinal steel plates for reinforced concrete beams delays peeling, avoids the complete separation of the plate and failure due to concrete crushing can be achieved.

Alagusundaramoorthy *et al.* (2003) [56] reported that the flexural strength of reinforced concrete beams was increased when strengthened with CFRP laminates on the tension face and anchored with steel bolts at the laminate ends compared with the un-anchored beam.

Providing fibreglass angles with relatively height at the plate ends increased the load-capacity of the strengthened beam; however, it was found to be an ineffective anchorage technique to prevent peeling failure, Figure 2.24a [29]. U-shaped steel confinements at the plate ends, Figure 2.24b, were effective in preventing end plate failure and increasing flexural strength of the strengthened beams [5,30,35,58,98]. Mukhopadhyaya *et al.* (1998) [58], and Swamy and Mukhopadhyaya (1999) [35] found that debonding of the external steel plates can occur along the beam span. However, using additional U-shaped steel

confinements which were distributed along the shear span, Figure 2.25, was found to be effective in enhancing the flexural strength of the beam strengthened with CFRP plate. Bencardino *et al.* (2002) [98] reported that anchoring the ends of the FRP laminates in strengthened beams has an important role to play in preventing peeling failure. It was noted that adding additional U-shaped fibre confinements, distributed along the beam span, can prevent local intermediate cracks at critical sections.

Anchoring FRP plates or laminates with mechanical anchors can be used in both beams and slabs. Fibre anchors were used to anchor GFRP strips to the tension faces of the cantilever reinforced concrete slabs, Figure 2.16 [74]. It was found that using mechanical fibre anchors inhibited the crack propagation which caused debonding at the location of the anchors and the final failure was due to concrete crushing.

From the discussion presented above, it can be mentioned that using different techniques of anchorage, either bolts or U-shapes, may not completely prevent plate end failure; however, by delaying the onset of plate end failure the flexural strength of the strengthened beam can be increased. Therefore, further experimental research using different anchorage techniques is required in this area.

2.3.9.4 Internal tensile steel ratio

The effect of the internal tensile steel reinforcement ratio of beams strengthened with external FRP composite on the flexural strength has been studied in several experimental investigations [38, 64, 70, 84]. Changes in the mechanism of failure caused by strengthening over-reinforced concrete sections have been investigated in studies by Ross *et al.* (1999) [84,] Nguyen *et al.* (2001) [64] and Rahimi and Hutchinson (2001) [38].

Higher enhancement in the flexural strength was achieved for smaller ratios of the internal tension steel reinforcement [64, 70, 84]. Ross *et al.* (1999) [84] reported that increasing the strength enhancement of over-reinforced strengthened reinforced concrete sections

required an increase in the amount of FRP. However, increasing the thickness of FRP caused plate end peeling. It was also stated that the degree of strengthening enhancement was affected by the ratio of the FRP composite to tensile steel reinforcement. Nguyen *et al.* (2001) [64] found that the under-reinforced beam strengthened with CFRP plate on the tension face failed by shear while the over reinforced beam failed by peeling. The two beams, assuming prefect bond between CFRP plate and the concrete, were designed to fail in flexural failure.

Rahimi and Hutchinson (2001) [38] found that increasing the amount of the external CFRP or GFRP laminates on the tension faces of over-reinforced simply supported beams achieved little increase in the flexural strength compared with un-strengthened beams. At failure the separation of the plates was combined with concrete crushing. It was also found that the beams strengthened with CFRP laminates exhibited a higher increase in the flexural strength than those strengthened with GFRP laminates. This was interpreted as a result of the higher elastic modulus of the CFRP laminates.

2.3.9.5 Compressive strength of concrete

Swamy and Mukhopadhya (1999) [35] investigated the effect of concrete strength on the mode of failure in reinforced concrete beams strengthened with CFRP plates. Two beams were reinforced internally and externally with similar ratios. The concrete strengths in the two beams were 45 and 66 N/mm^2. It was found that the beam which had the higher concrete strength exhibited an increase in strength of around 9% at failure compared with that having the lower concrete strength. The beam which had the higher concrete strength failed as a result of plate end separation; however, the beam which had the lower concrete strength failed in flexure. Sawmy and Mukhopadhya (1999) [35] also found that the maximum plate strain at failure was nearly the same in the two beams. This was justified by the fact that the CFRP tension debonding was a function of the concrete strength, where at cracking the beam which had the higher concrete strength released a greater amount of energy due to the higher degree of concrete brittleness compared with that which had the lower concrete strength. Bencardino *et al.* (2002) [98] has reported that the final failure of a strengthened beam is

influenced by the strength of concrete and the reinforcement conditions of the original beam.

2.4 Reflections on literature review

Various strengthening techniques to enhance the flexural strength of reinforced concrete beams have been reviewed. All the techniques revised have been found to be effective in increasing the flexural strength of the strengthened elements. The main points which emerge from the review of the literature on using external steel plates or FRP composite, which is the principal method used in the current investigation, are given in the following:

- Externally bonded plates or laminates on the tension face of a reinforced concrete beam are an effective technique for strengthening beam. The technique can increase flexural strength and stiffness.

- Strengthening of over-reinforced beams on the tension face does not achieve a significant increase in the flexural strength compared with under-reinforced beams. In addition, increasing the thickness of the external reinforcement at the tension face of the beam, keeping the same area of the plate, causes peeling failure.

- Increases in the amount of external reinforcement, particularly FRP composite, on the tension face of an under-reinforced beam tends to change the failure mode from an under-reinforced mode to an over-reinforced mode. However, increasing the thickness of the FRP with keeping the same area of the plate also causes peeling failure.

- Brittle failure at the end of the plate or debonding of the external reinforcement from the concrete surface along the beam length is the dominant failure mode.

- Several debonding models have been developed to assess the shear and peeling stresses at the plate end at which peeling failure takes place. Emerging end-anchorage techniques at the plate are an excellent method for inhibiting peeling failure, so that the ultimate capacity of the strengthened section could be reached. The effect of using these anchorage techniques in the debonding models developed however was not considered.

From the above review, the benefits of adding FRP plates or laminates on the tension face of a reinforced concrete beam have been identified. However, minimal increases in the flexural strengths can be achieved by using this technique on over-reinforced beam sections. Additionally, with increased thickness of FRP plates or laminates on such sections leads to a change in the failure mechanism, particularly at the plate ends. Therefore, this thesis discusses research focused on adding CFRP laminates to the tension and compression faces of the simply supported over-reinforced beams.

Table 2.1: Typical properties of common reinforcing fibres [46]

Fibre	Tensile strength (N/mm^2)	Young's modulus (kN/mm^2)	Density (kg/m^3)
Carbon	2100- 7100	220- 900	1740- 2200
Glass	3445- 4890	72 –87	2460- 2580
Aramid	3150- 3600	58- 160	1390-1470

Table 2.2: Typical properties of common FRP composites [47]

Unidirectional FRP composite laminate	Tensile strength (N/mm^2)	Young's modulus (kN/mm^2)	Density (kg/m^3)	Fibre content % by weight
Carbon/epoxy CFRP	1200-2250	120-250	1600-1900	65-75
Glass/polyester GFRP	400-1800	20-55	1600-2000	50-80
Aramid/epoxy AFRP	1000-1800	40-125	1050-1250	60-70

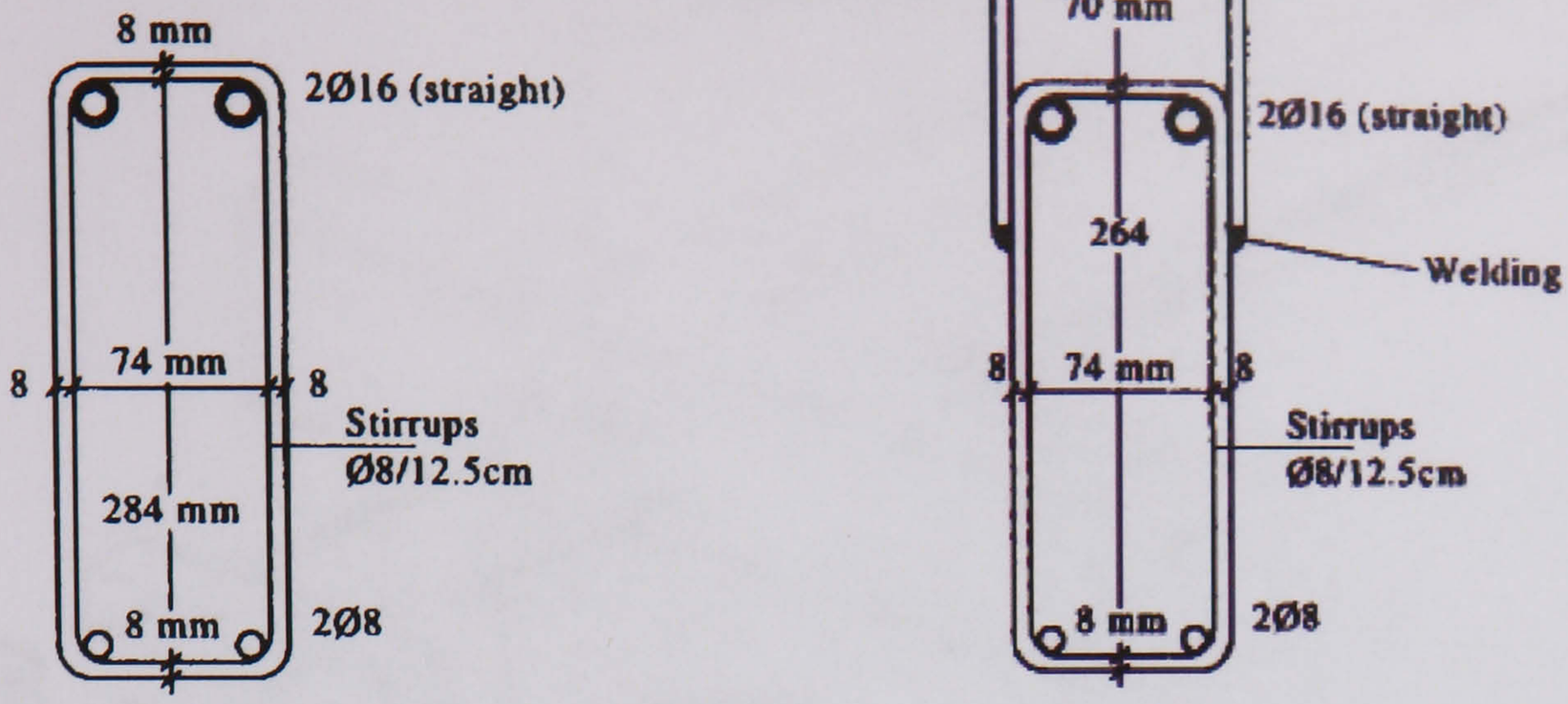

Figure 2.1: Concrete overlaying strengthening: detail for steel reinforcing bars for tested beams in (a) unstrengthened and (b) strengthened (after Diab [15])

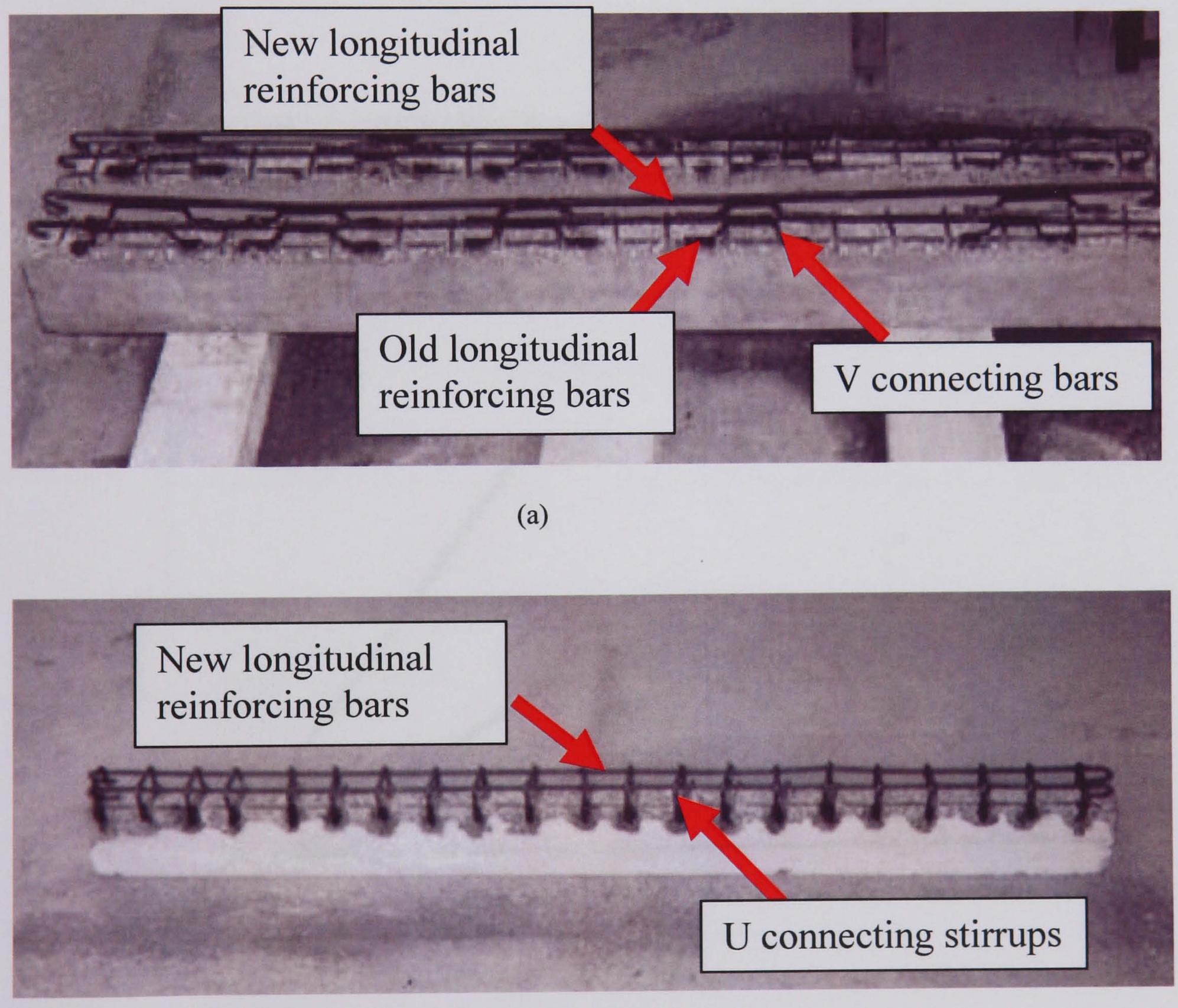

Figure 2.2: A test beam to be strengthened with : a) V connecting bars ; b) U connecting stirrups , Öztürk and Ayvaz (2002)[18]

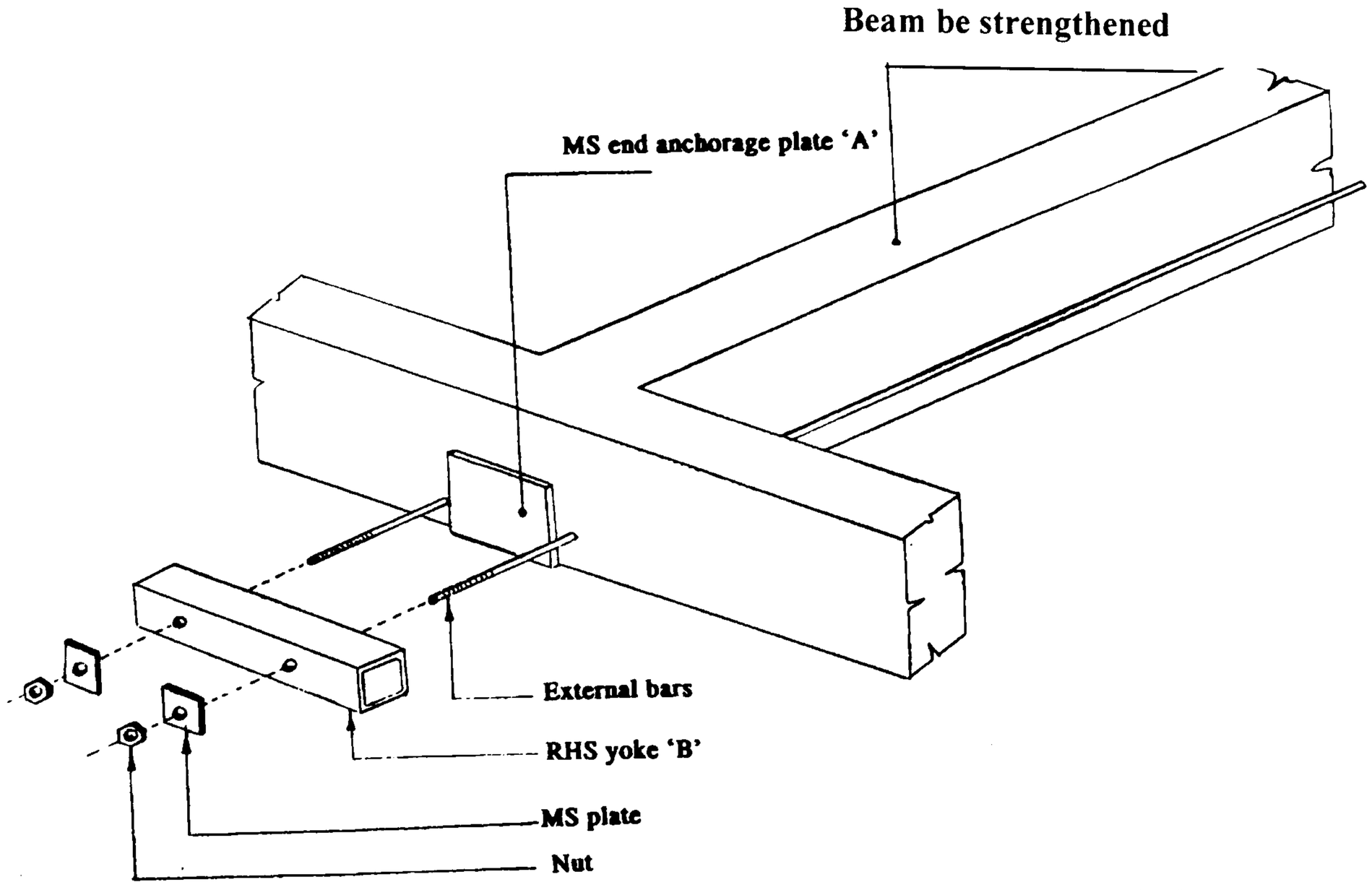

Figure 2.3: External un-bonded bars for strengthening RC beam. (After Rafeeqi [12])

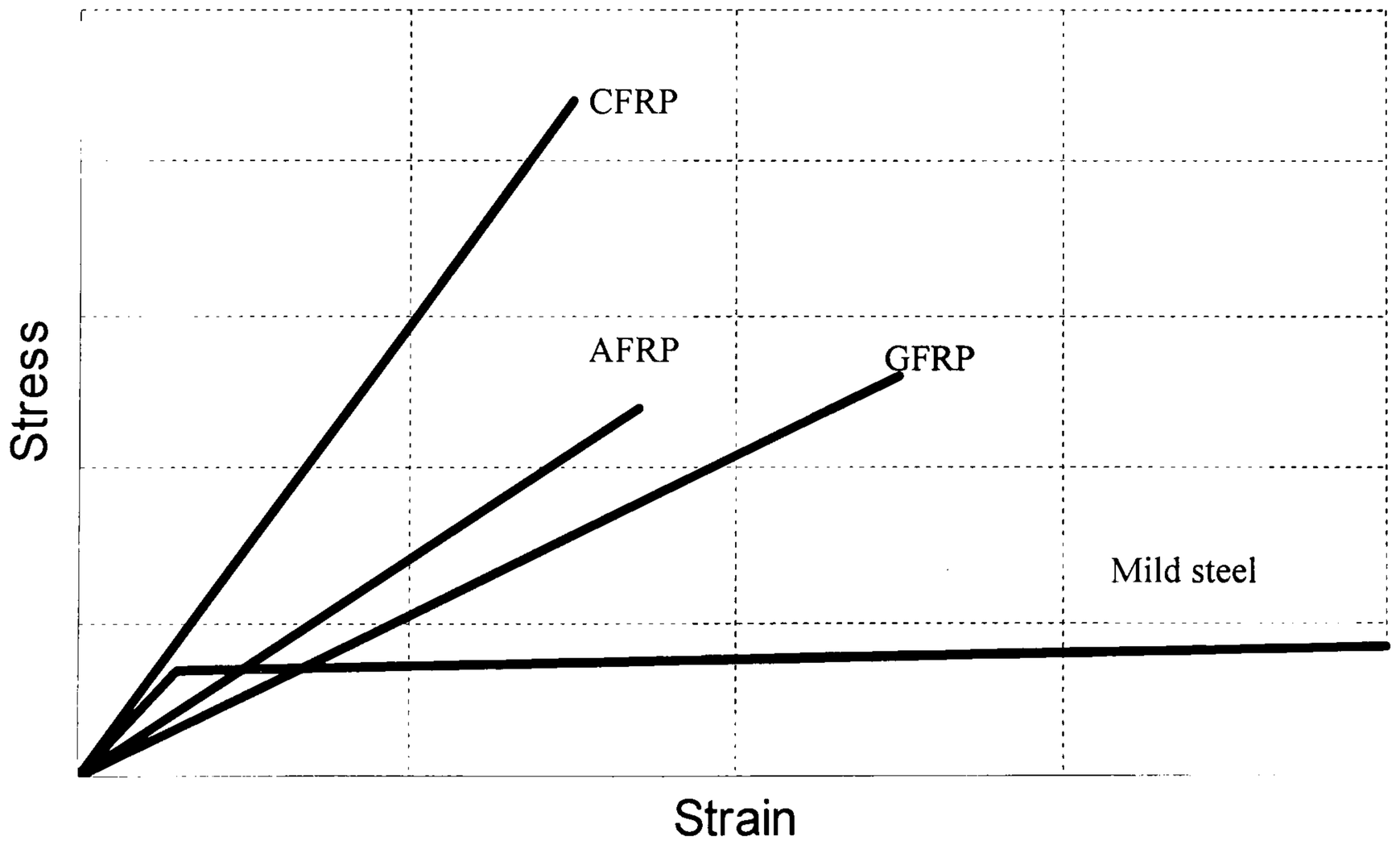

Figure 2.4: Stress-strain relationship for FRP materials and steel reinforced in strengthened concrete

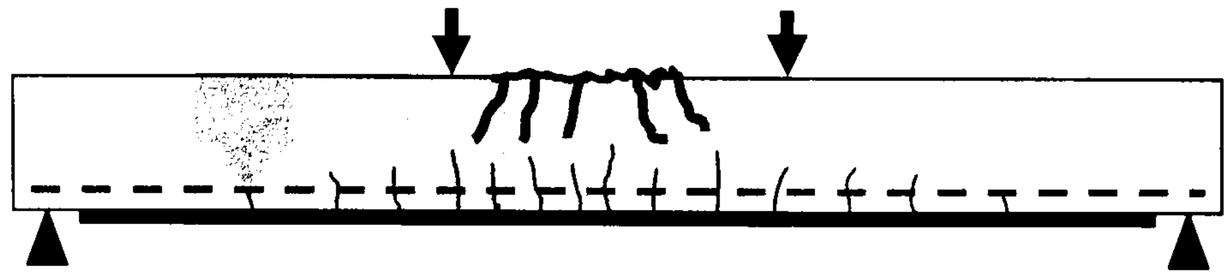

Figure 2.5: Flexural failure

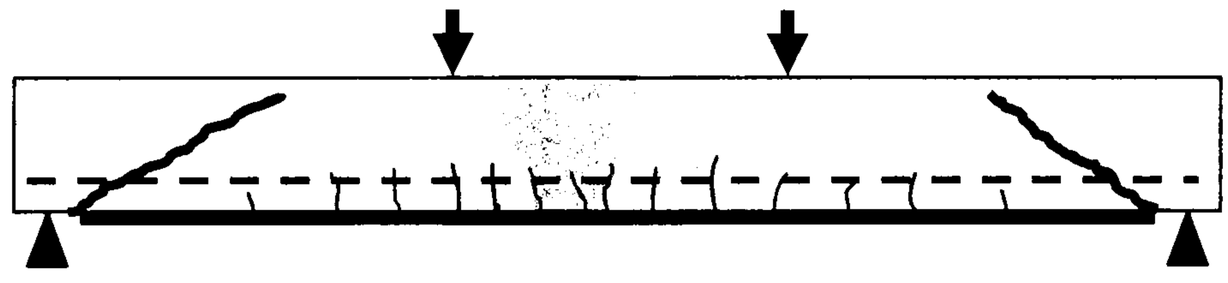

Figure 2.6: Shear failure

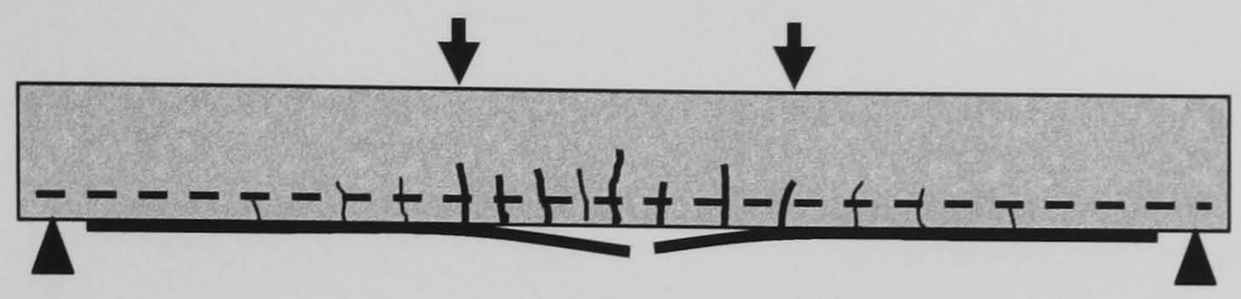

Figure 2.7: Steel yielding followed by FRP rupture

(a)

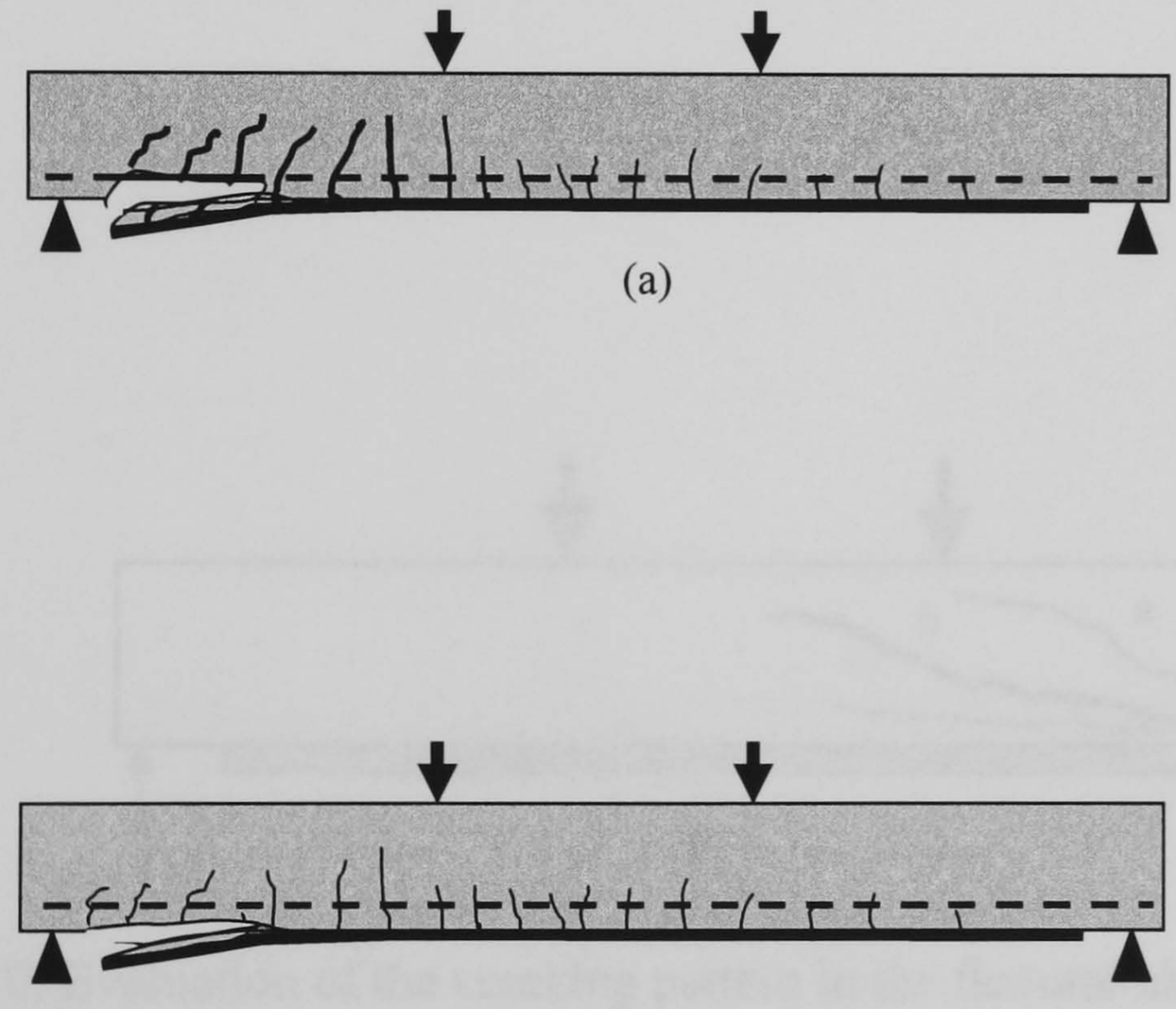

(b)

Figure 2.8: End-plate failure, a) peeling failure, b) plate separation from the concrete surface

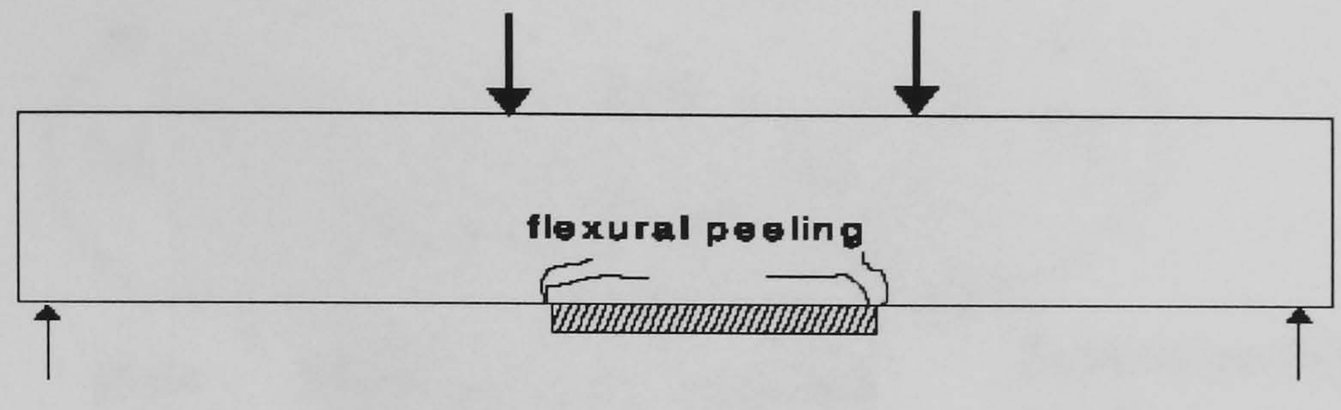

Figure 2.9: Flexure peeling, (After Oehlers 1990 [27])

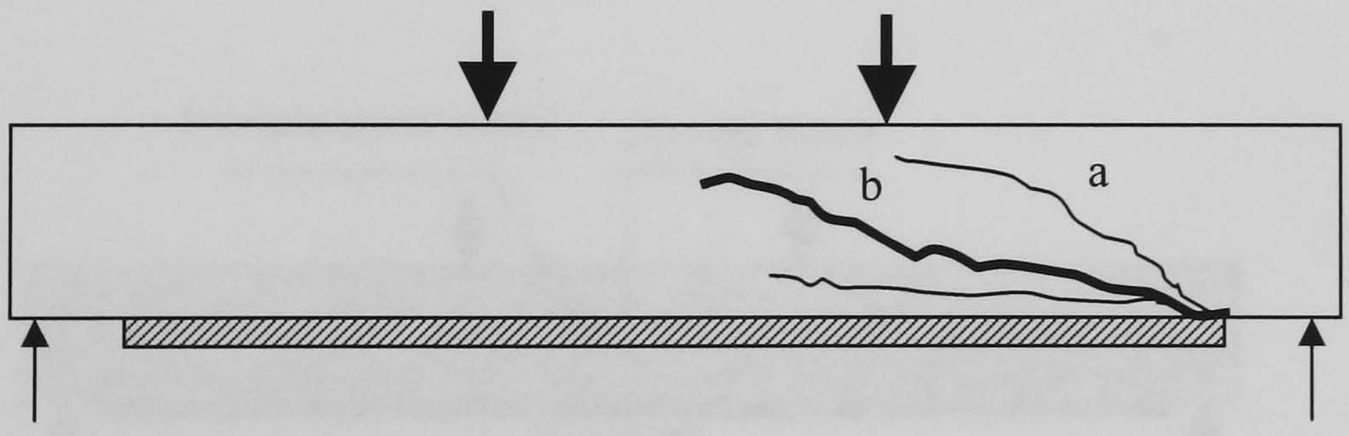

Figure 2.10: Evaluation of the cracking pattern in the flexural-shear peeling failure of strengthened beams: a) onset of peeling, b) at failure

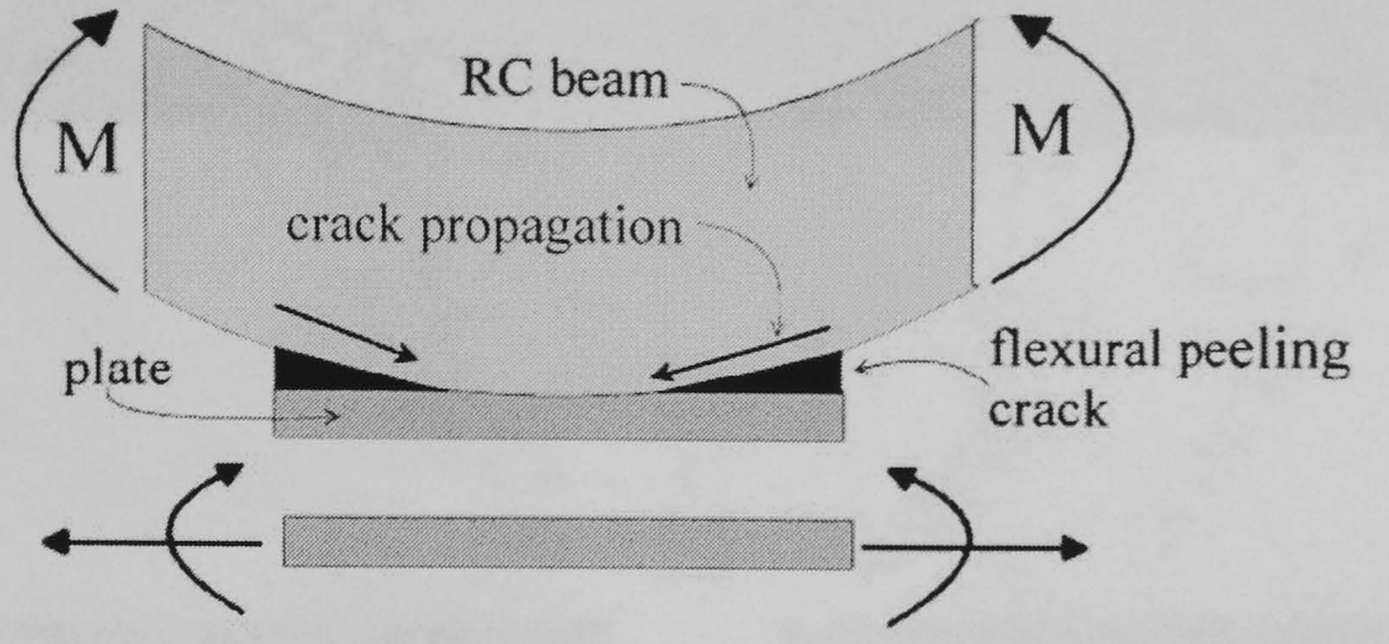

Figure 2.11: Flexure peeling mechanism (After Oehlers, 2001)[67]

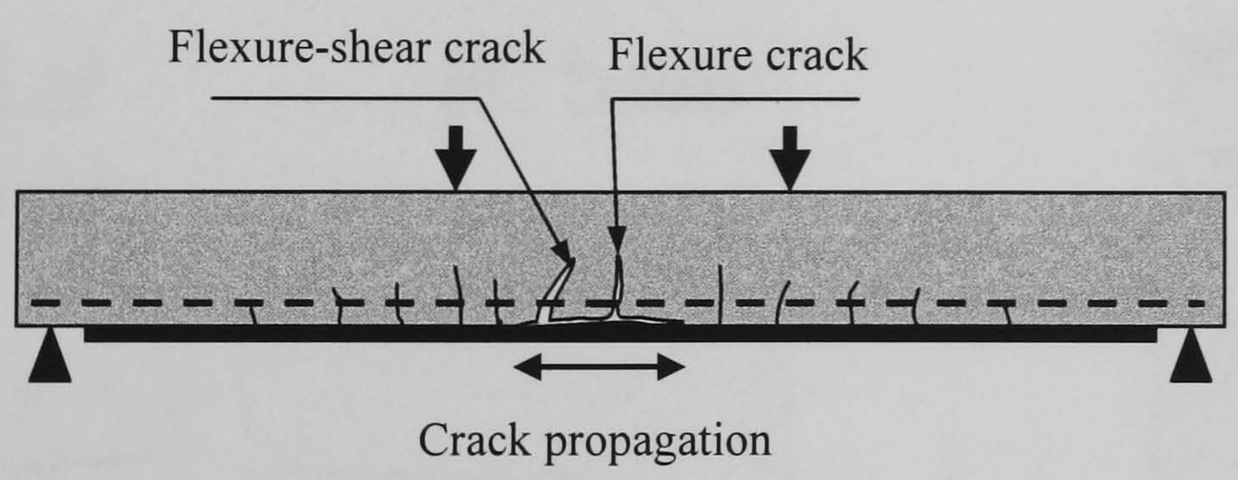

Figure 2.12: Debonding failure

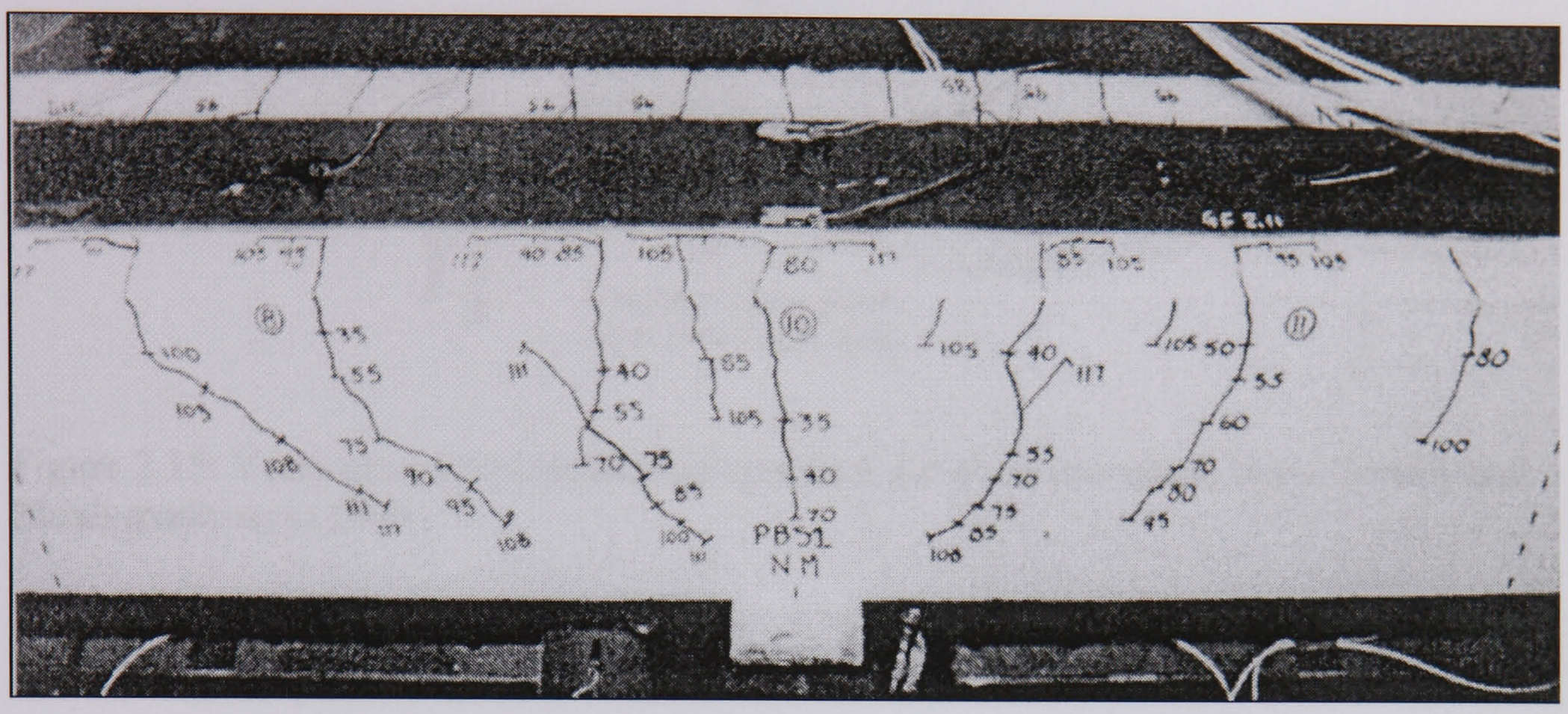

Figure 2.13: Flexure peeling of a steel plated beam, Oehlers (2001) [67]

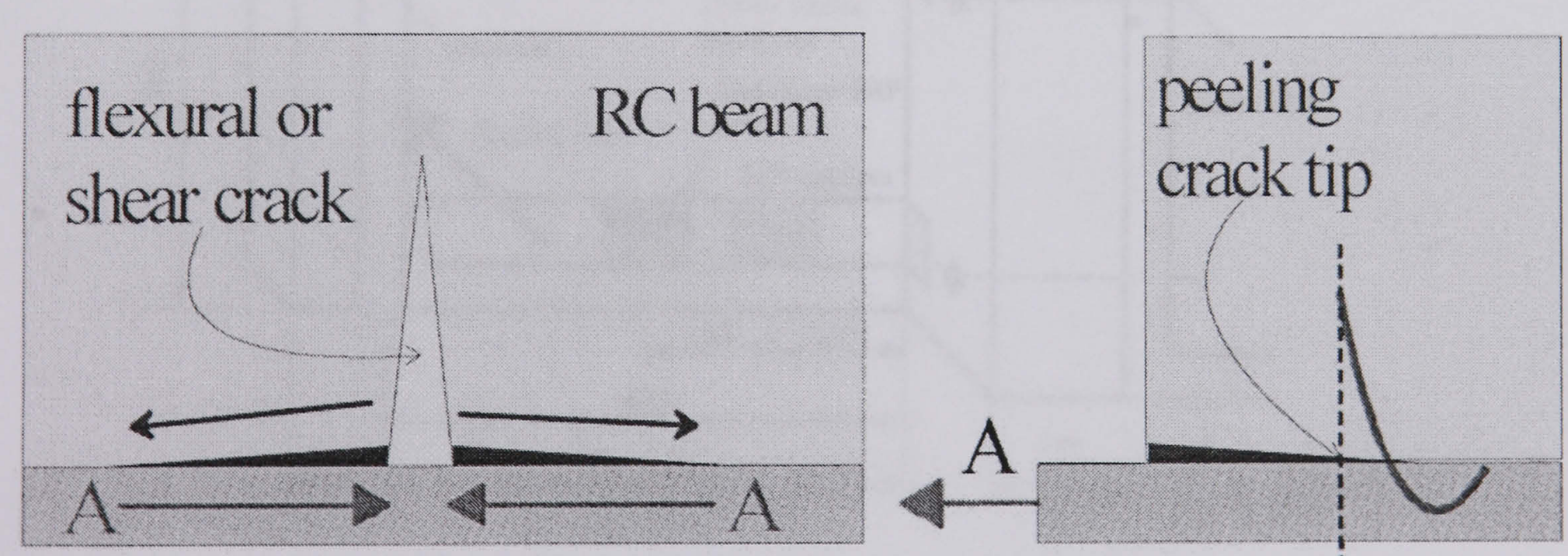

Figure 2.14: Flexure peeling mechanism, Oehlers (2001) [67]

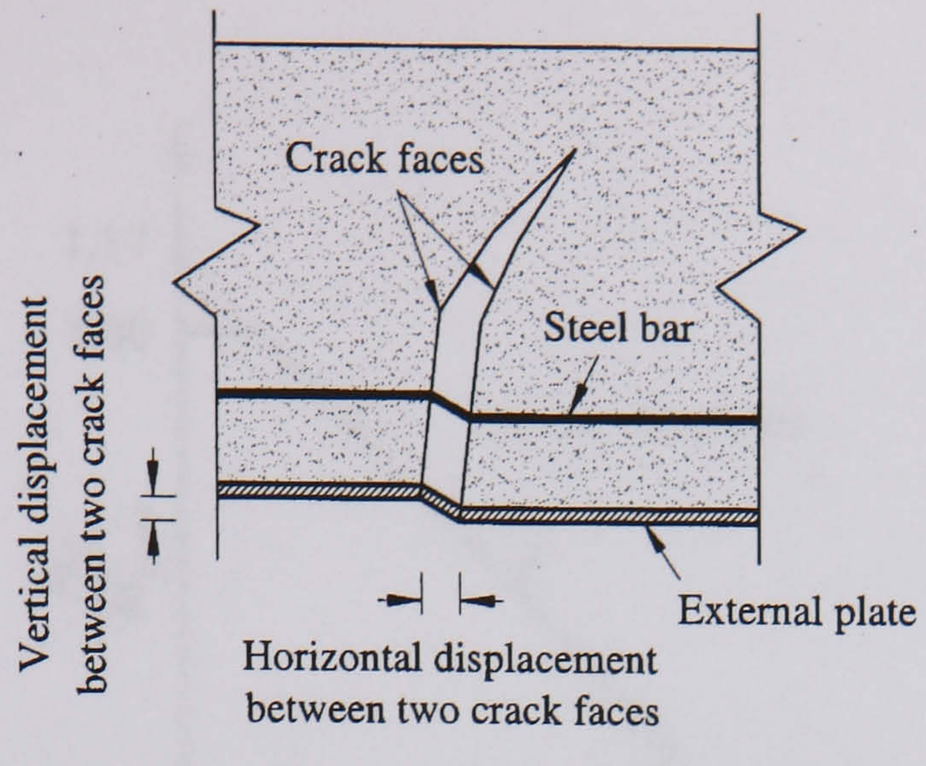

Figure 2.15: Vertical and horizontal displacements between two crack faces, Swamy and Mukhopadhyaya (1999) [35]

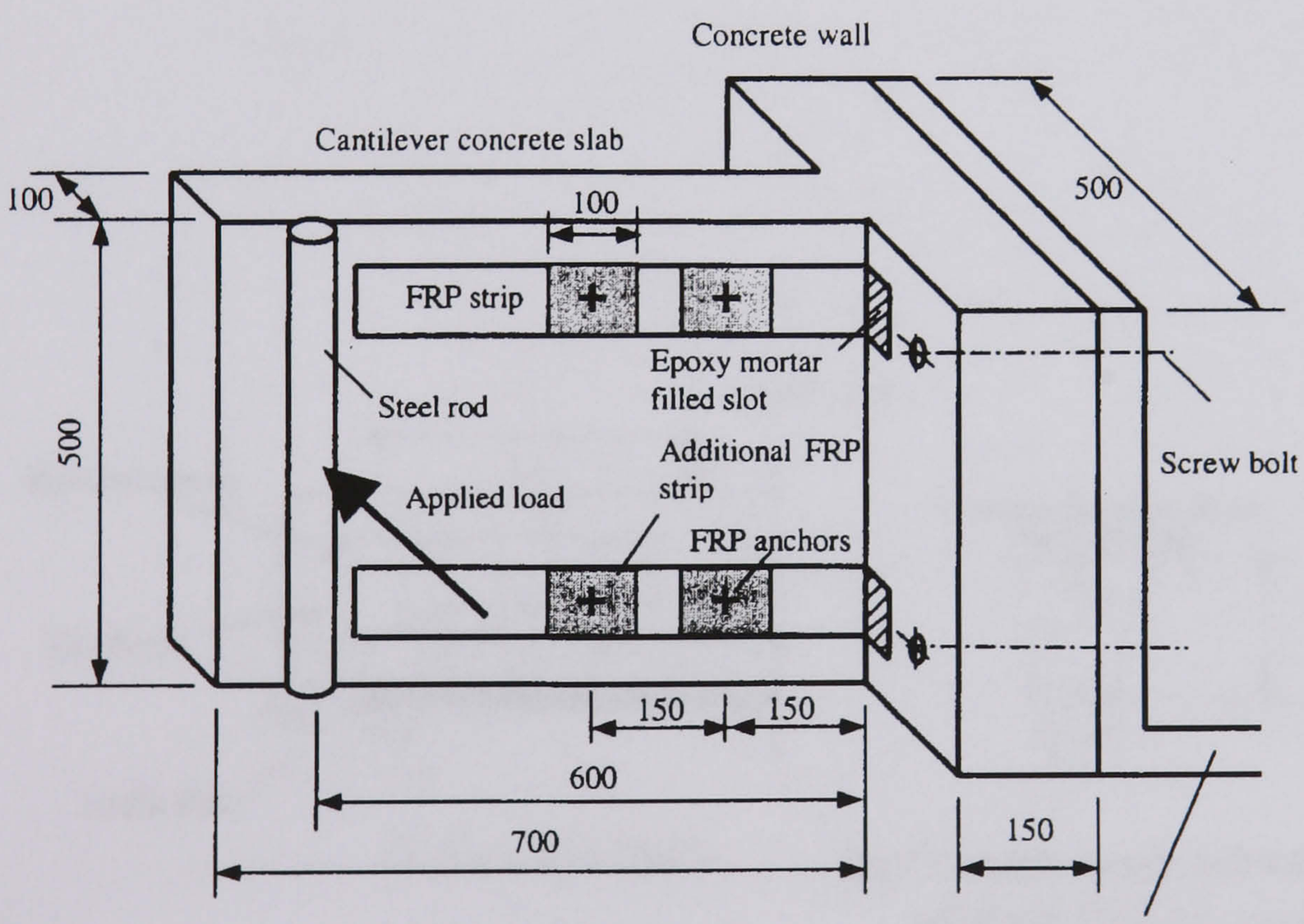

Figure 2.16: Overall dimensions of specimens and test set-up, Lam and Teng (2001)[75]

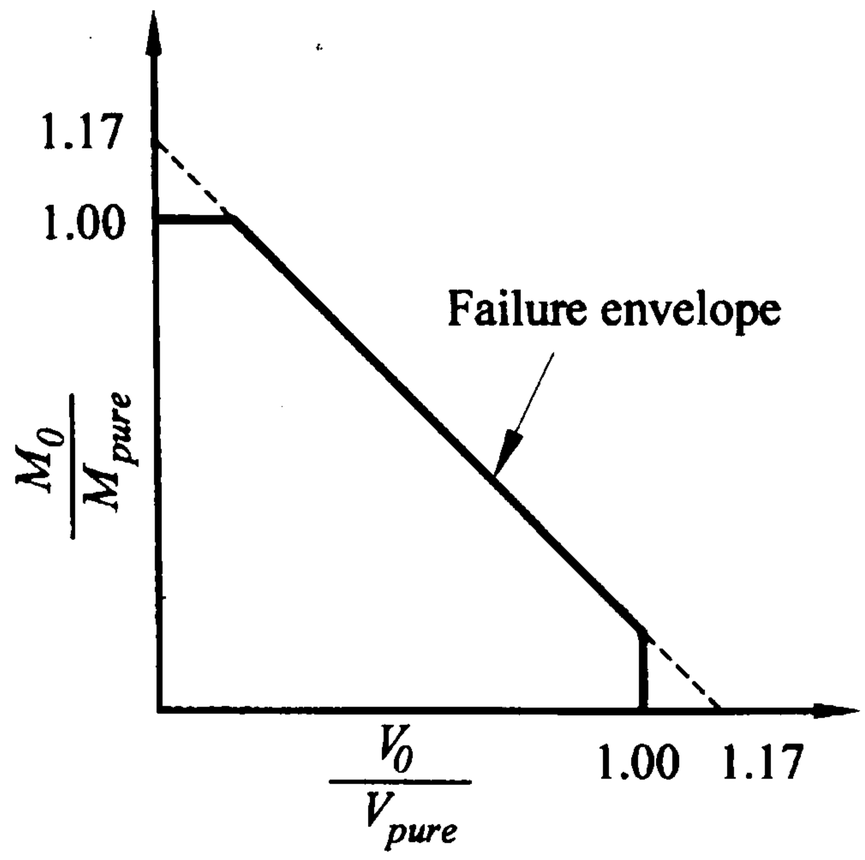

Figure 2.17: Peeling failure envelope proposed by Oehlers (1992) [6]

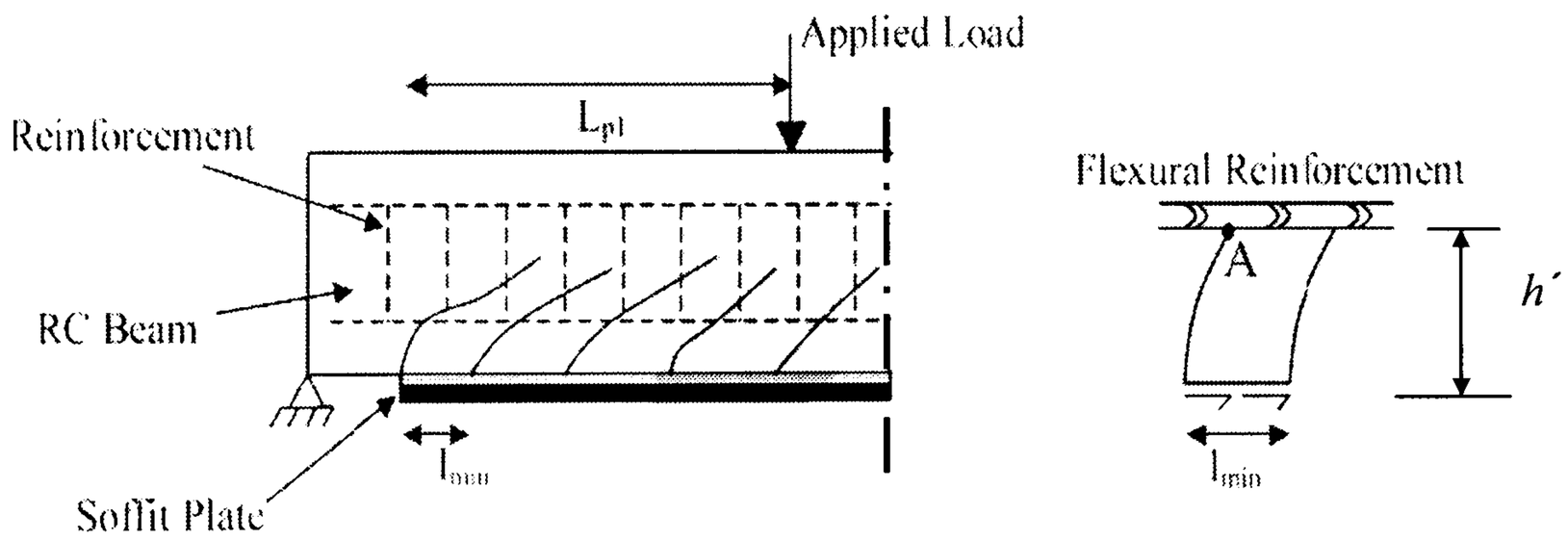

(a) Cracked beam

(b) Concrete tooth between two adjacent flexure cracks

Figure 2.18: Concrete tooth model, Zhang *et al.* (1995) [77]

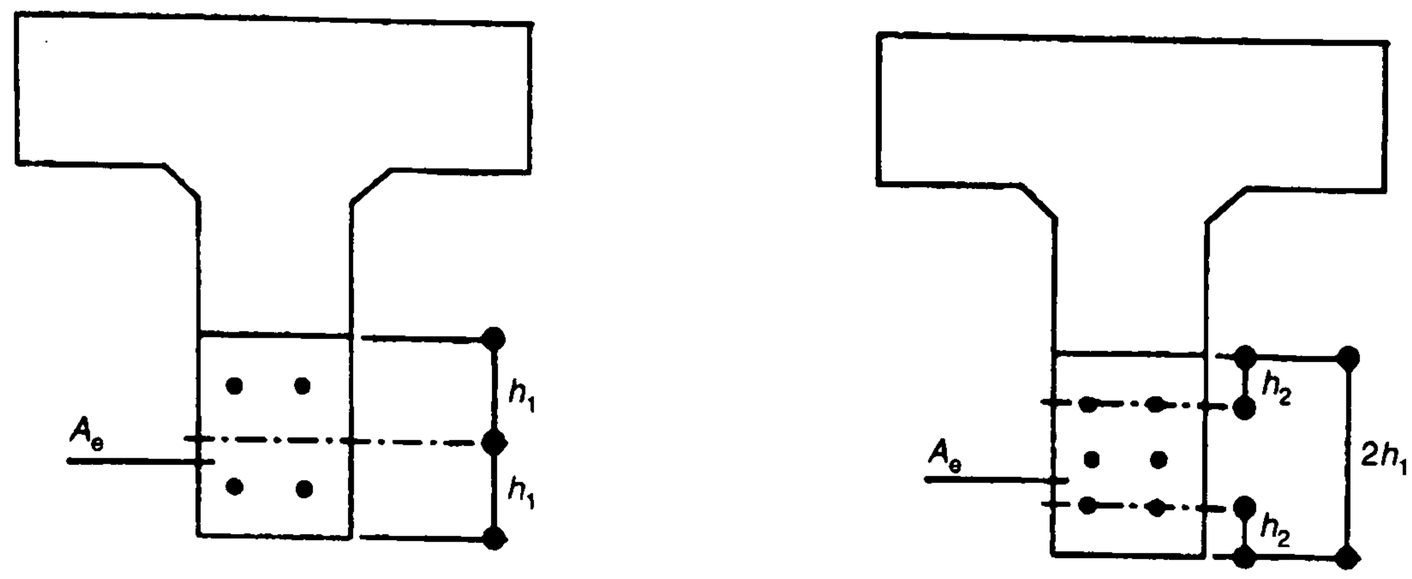

Figure 2.19: Assumed concrete area in tension, Zhang *et al.* (1995) [77]; a) two layers of steel reinforcement and; b) Three layers of steel reinforcement

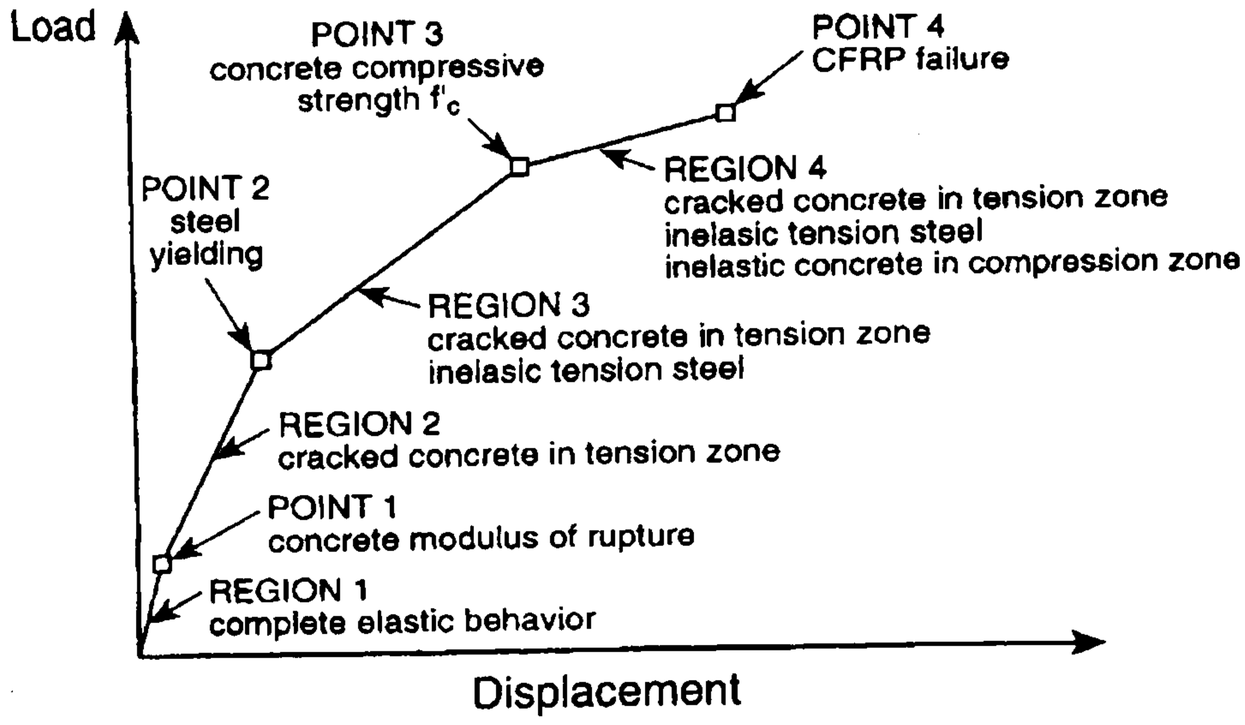

Figure 2.20: Load-displacement response assumptions used in beam section analysis, Ross *et al.* (1999)[84]

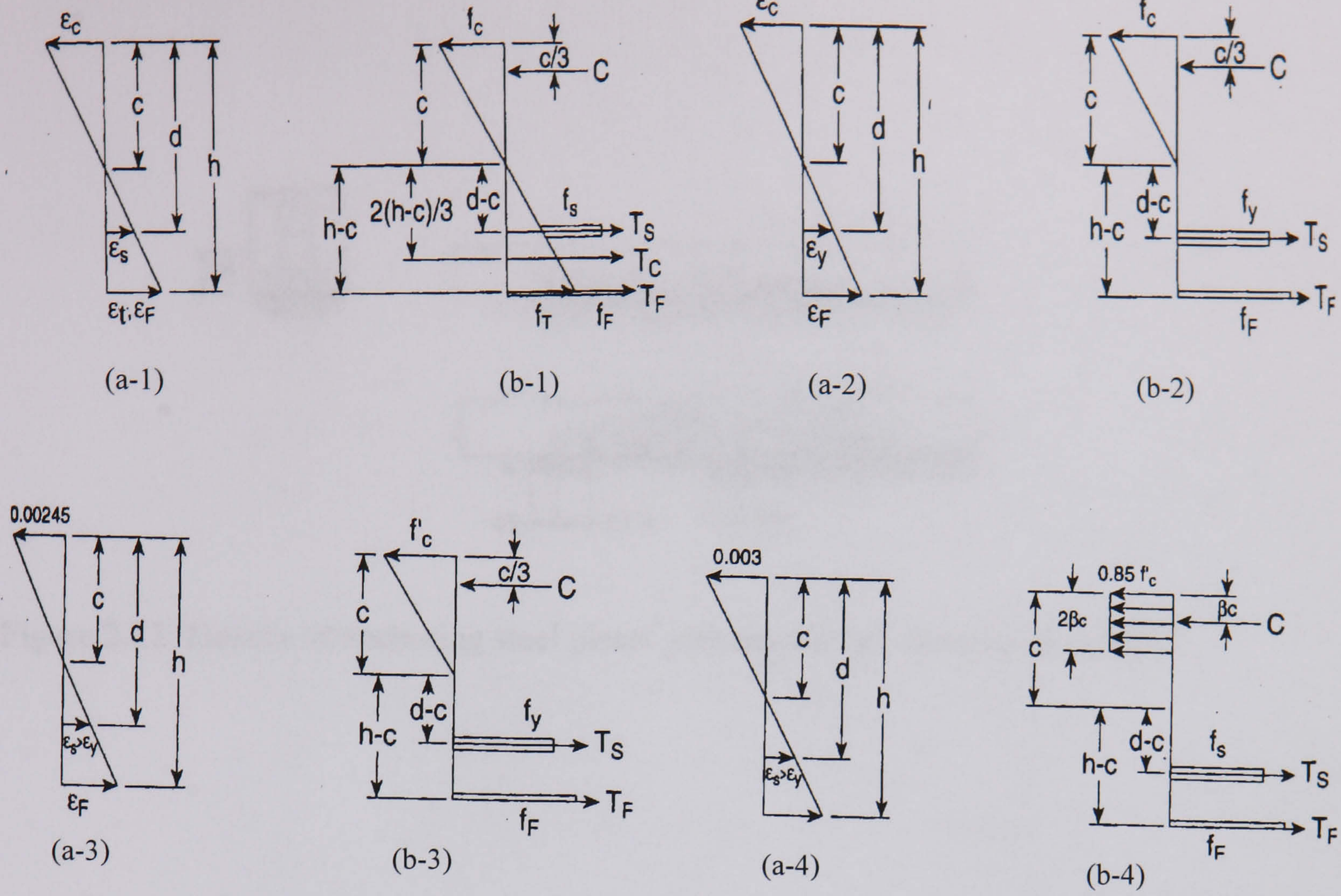

Figure 2.21: Strain and stress distributions in cross section for regions 1-4: (a) strain and (b) stress, Ross et al. (1999) [84]

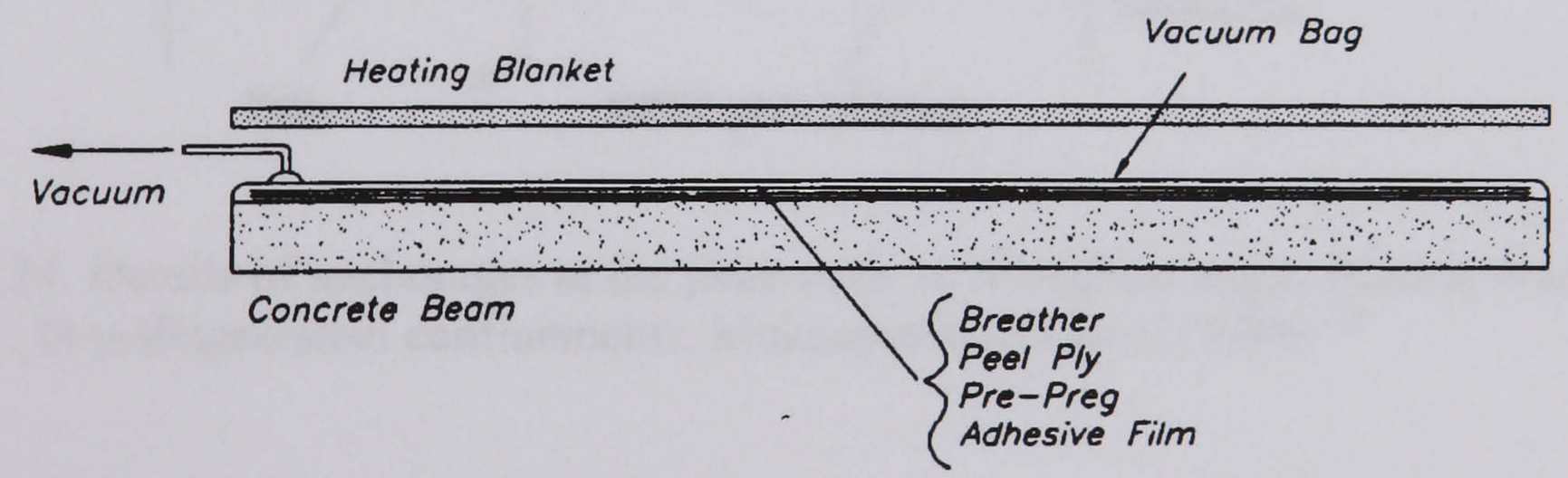

Figure 2.22: Pre-preg system for strengthening purpose, Täljsten and Elfgren (1999) [96]

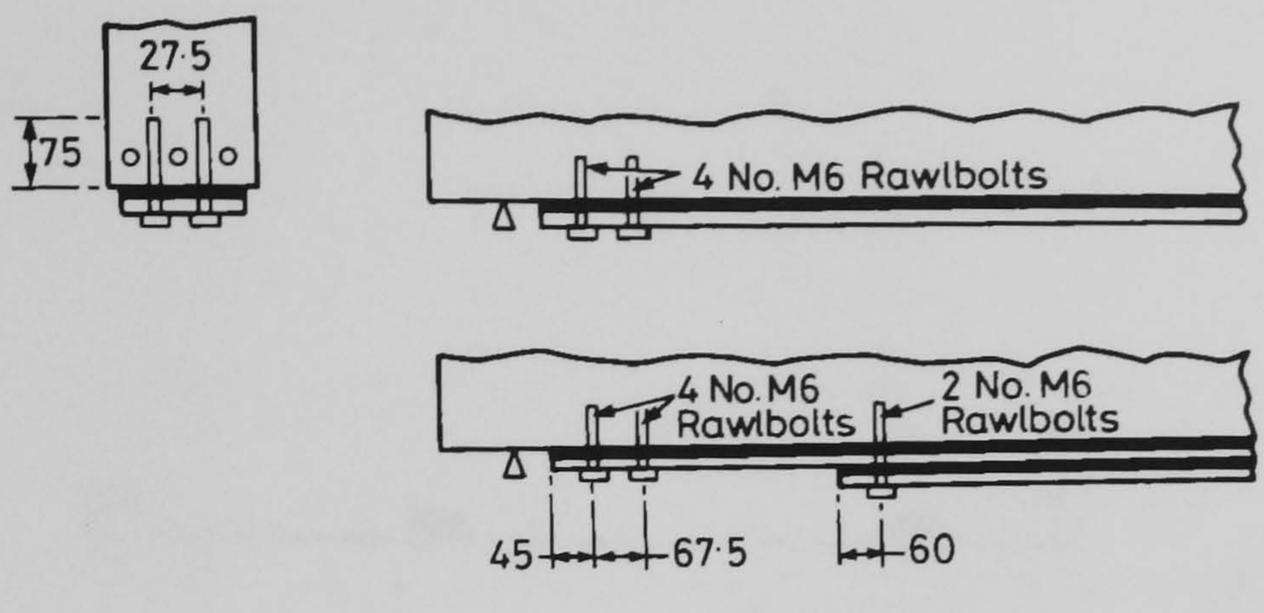

Figure 2.23: Details of anchoring steel plates with steel bolts, Jones *et al.* (1988) [5]

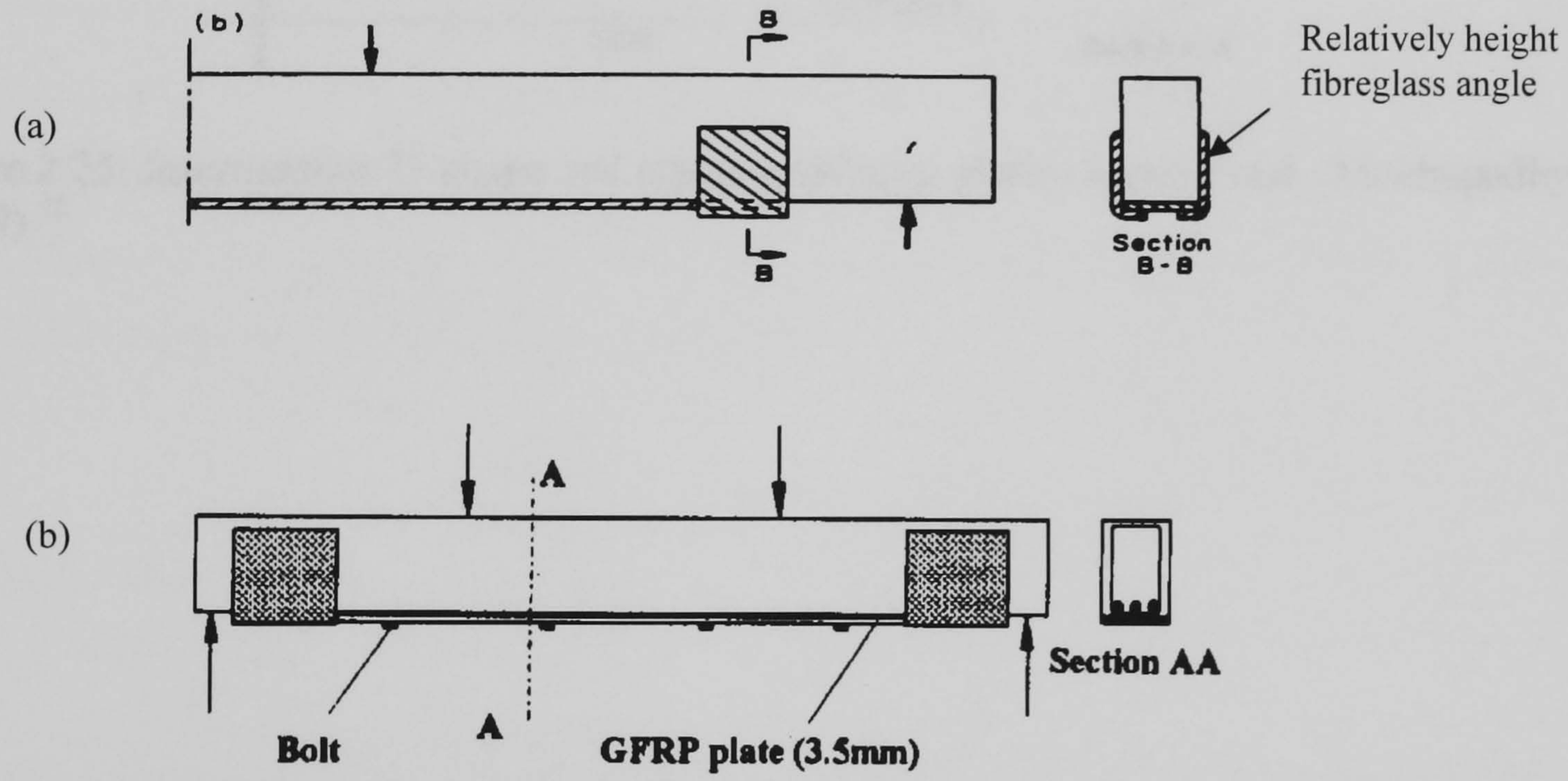

Figure 2.24: Details of anchorages at the plate ends: a) fibreglass angle, Ritchie *et al.* (1991)[29] ; b) u-shaped steel confinements, Mukhopadhyaya *et al.(*1998) [58]

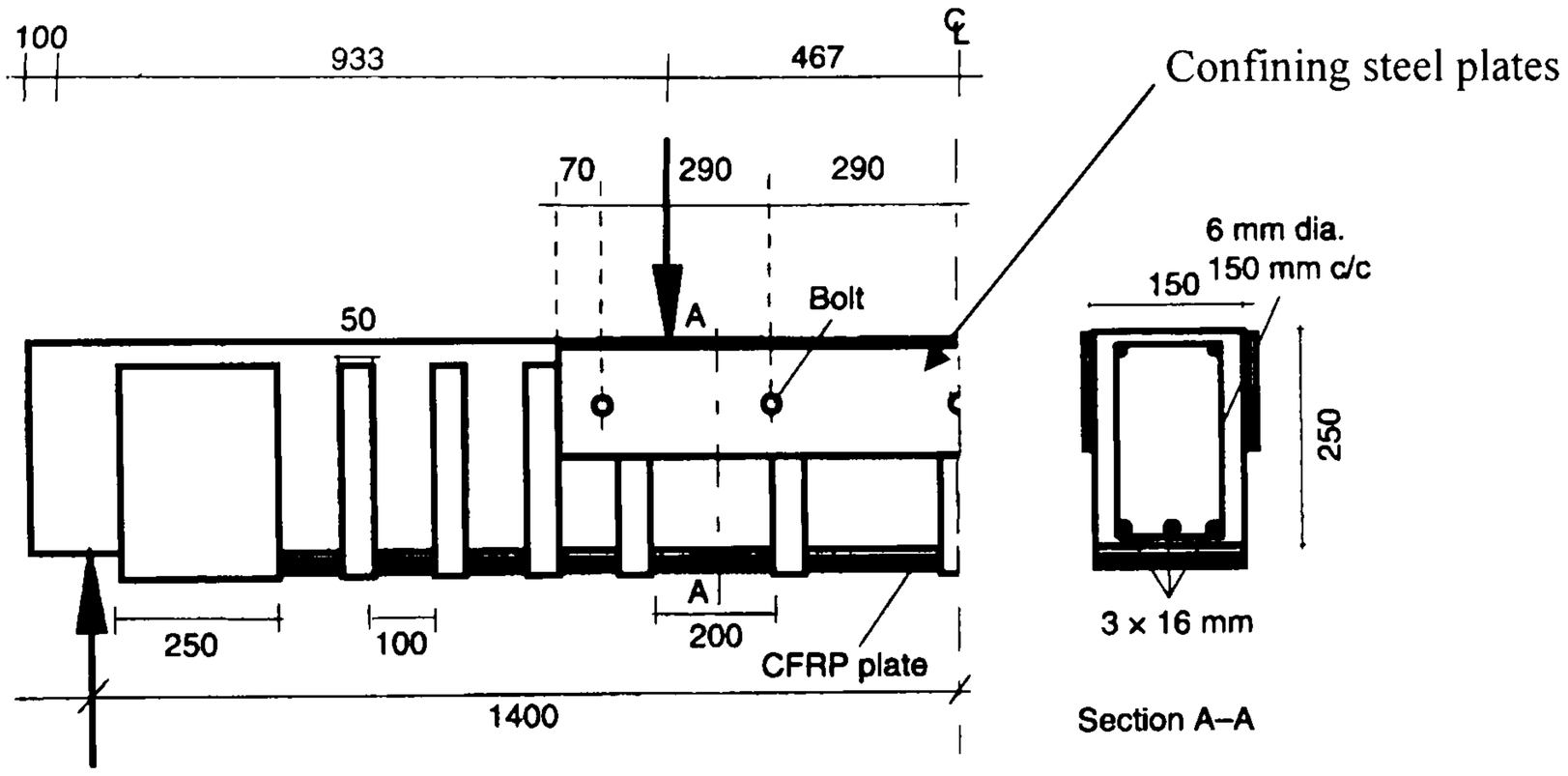

Figure 2.25: Intermediate U-shape and lateral confining plates, Swamy and Mukhopadhyaya (1999) [35]

CHAPTER 3

EXPERIMENTAL INVESTIGATION

3.1 Introduction

This Chapter describes the materials used in the test specimens and the data collection techniques used in the experimental investigation which was performed to investigate the flexural behaviour of reinforced concrete simply supported beams strengthened with external CFRP laminates. The strengthening technique using CFRP laminates was applied to both the tension and the compression faces of the reinforced concrete beams.

The three main sections in the Chapter are Section 3.2, Materials, Section 3.3 Tension tests of CFRP coupons and Section 3.4, Experimental investigation of reinforced concrete beams. A brief discussion is given within the three sections to give information about the materials and their properties, specimen preparation and testing procedure and the instrumentation used. All materials preparation and testing was carried out in the Structures Laboratory at Heriot-Watt University.

3.2 Materials

This section presents a brief description of all materials used in this investigation. The materials include Carbon fibre reinforced plastic, Section 3.2.1, Structural adhesive, Section 3.2.2, Steel reinforcement Section 3.2.3 and Concrete Section 3.2.4.

3.2.1 Carbon fibre reinforced plastic fabrics

In this investigation a composite laminate was developed to be placed on the compression and tension faces of the reinforced concrete beams in order to strengthen beams. Unidirectional Carbon Fibre, UCF, (UT-C200) was used. UT-C200 is a carbon

in Unitex with a nominal weight of 200 g/m^2. The selection of this type was for two reasons, it is easier to apply by the hand lay up technique, and secondly unidirectional carbon fibre reinforcement fabrics offer a high tensile strain and strength capacity in the longitudinal direction. The average tensile modulus, tensile strength and density are 235 kN/mm^2 and 3500 N/mm^2, and 1.8 g/cm^3, respectively.

3.2.2 Structural adhesive

Ampreg 20 was selected to be used with the UCF in the current investigation. This comprises an epoxy resin and hardener, and is convenient for use in hand lay-up applications. It has established itself as the benchmark laminating resin in many industries [48]. The epoxy resin and hardener were mixed together in a specified ratio, Section 3.3.2.1, to give the adhesive action. The component physical and mechanical properties of resin / hardener are illustrated in Table 3.1.

The composite materials, unidirectional carbon fibre (UCF), epoxy resin and hardeners were provided by SP-Systems Composite Engineering Materials UK. Details of the mechanical properties of the composite materials taken from the manufacture's data sheets are presented in Table 3.1 and Section 3.2.1. The mechanical properties of laminates were not given in the manufacture's data sheet; therefore two different methods were carried out to determine the elastic modulus E_f and the ultimate strength f_f of the CFRP laminates. The methods are the experimental method and the predictive method based on the micromechanics analysis theory, the methods and the result comparisons will be described in Sections 3.3.3, 3.3.4 and 3.3.5.

3.2.3 Steel reinforcement

8 mm, 10 mm, and 16 mm diameter high yield steel and 6 mm mild steel were utilized in the test programme. Tensile tests were conducted to determine the mechanical characteristics. The properties measured were the yield strength f_y, elastic modulus E_s

ultimate strength f_{su} and the elongation at fracture. Three tensile specimens for each bar were prepared and axially tested according to EN 10002-1:2001(E) [99] for each rebar. A Denison extensometer Model 7609C1 with 50 mm original gauge length was used to measure the elongation throughout the elastic stage. Once the loaded bar reached yield, the extensometer was removed. Subsequently, the elongation was increased in 2 mm increments to the failure measured using a divider. In the plastic stage, the procedure consisted of taking a series of load readings from the testing machine with corresponding elongation readings from the mechanical divider. The load-elongation results were then converted to a stress-strain diagram.

The average values for yield strength, elasticity modulus, ultimate strength and the elongation percentage are given in Table 3.2. Figures 3.1a, 3.1b and 3.1c show typical measured stress-strain relationship for bar diameters of 6, 8 and 16 mm, respectively. The yield strength f_y and Young's modulus E_s are also noted. For bars which did not indicate significant yield strength, i.e. the high yield steel bars, the 0.2% proof stress was used in calculation. Details of the different steel bars used in this investigation are given in Table 3.2.

3.2.4 Concrete

3.2.4.1 Constituent materials

Ordinary Portland cement, Type I was used throughout the investigation. The cement was ordered as required for each stage and was not stored more than three months prior to use.

Graded sand, Quartz type, according to zone 2 classification of BS 812 [100] was used. The fineness modulus of the sand was 3.16 (from sieves analysis test).

The coarse aggregate used was crushed, aggregate of maximum size 10 mm. This size was chosen at it was convenient for the specimens size.

3.2.4.2 Mix proportions

Concrete mix proportions used through this study were designed to have an expected compressive cube strength between 25-40 N/mm^2 at 28 days. The main factors that have an effect on the concrete strength are the water to cement ratio W/C, aggregate amount, cement content and the percentage of sand in the aggregate composition. Trial mixes based on the design procedure BS 5328 [101] of the constituent materials were carried out. It was found that when the size of the coarse aggregate is small, increasing the ratio of the sand in the aggregate component instead of increasing the amount of the cement can improve the concrete compressive strength. So, a ratio of 1:1 of both sand and coarse aggregate was used. Concrete mix proportions for the various target strengths are given in Table 3.3.

3.2.4.3 Mixing, casting and curing procedures

The constituents were weighed and the aggregate and cement were placed in a 1.5 m diameter mixing pan. The aggregate and cement were mixed dry for two minutes to ensure complete mixing, the water was then added gradually, by hand, taking a few minutes. The mixer was allowed to rotate until the concrete was of uniform consistency and colour. Mixing time was about 3 minutes after the addition of the water.

Wooden forms were cleaned, prior to concrete mixing, of any traces in the concrete or dirt, and oiled. The beam reinforcement cage was placed in the wooden forms. All the beams were cast with the tension face of the beams on the base of the wooden forms. The concrete was placed by hand, normally in two layers. An electrical vibrator was used for compacting each layer of all beams, except the specimens, series-IV. Hand compacting of the specimens in series-IV was carried out. Cubes and cylinders for each mix were cast, and were compacted on a vibrating table. The time of vibration was 20-30 seconds, to ensure no segregation of the cement paste from the mix occurred. The top surface of the placed concrete was levelled with a hand trowel. The measured slump values for all mixes are reported in Table 3.3

The membrane curing method for the specimens was used; this method could be called a water-barrier method. It relies on the prevention of the losses of water from the surface of the concrete, without the possibility of external water ingressing into it. The top face of the beams was covered with polythene sheets for 24 hours after completion of casting and levelling. The sides of the wooden moulds were removed after 24 hours of casting. All specimens were numbered and dated, and left under the same conditions of curing for 7 days.

3.2.4.4 Compression strength

The compressive strength test might be considered the most rigorous destructive test for hardened concrete. All cubes and cylinders were prepared in accordance with BS1881-108 [102], BS1881-110 [103]. All test specimens were removed from the casting moulds after 24 hrs and membrane curing method, Section 3.2.4.3, was processed. A Tonipac 3000 compression machine was used for testing all specimens.

The average compressive, f_{cu}, strength of three cubes and two cylinders, f_{cy}, for each beam, except the specimens of series-IV, was recorded and is presented in Table 3.4. For the single batch of concrete for the specimens of series-IV, the average of three cubes and three cylinders were tested and are also recorded in Table 3.4. All test specimens; cubes and cylinders were tested immediately after testing the relevant beam.

3.2.4.5 Tensile strength

Two cylinders,150 mm diameter and 300 mm long, obtained from the concrete mix, for each beam, were tested to measure splitting tensile strength in accordance with ASTM C496-90 [104]. A Denison machine with a maximum load capacity of 2000 kN was used. In this test the concrete cylinder is loaded along the length until splitting failure occurs across the diameter. Concrete specimens were placed in the centring machine cross

heads with 3 mm thick plywood strips positioned along the top and bottom of the loading plane. The splitting strength f_{sp} is expressed by

$$f_{sp} = \frac{2P}{\pi \ell d} \tag{3-1}$$

where P is the maximum applied load, ℓ and d are the cylinder length and diameter, respectively. All splitting strengths obtained from the cylinder tests are presented in Table 3.4. In cases in which the splitting test is unavailable, the splitting strength of the concrete, f_{sp}, can be estimated [105] from the original cylinder strength, f_{cy}, using

$$f_{sp} = 0.53\sqrt{f_{cy}} \tag{3-2}$$

The experimental results conducted in the current study, Table 3.4, were calibrated using equation 3-2. It was found that these results gave an average difference of 3% higher than the experiments. This may be attributed to the limited number of the conducted tests.

3.2.4.6 Modulus of elasticity

One of the most important elastic properties of concrete is its modulus of elasticity, E_c. The modulus of elasticity E_c can be determined from the change of stress with respect to the strain in the elastic range. In concrete, the stress is generally not proportional to the strain, and the stress-strain relationship is non-linear. Therefore, there are different methods that have been considered for determining the elastic deformations of hardened concrete. All the methods are obtained from stress-strain curve of concrete cylinders. From these methods are the initial tangent modulus, tangent modulus at a given plastic strain, and secant modulus at a stress $0.5\, f_{cy}$. In some cases the last method is called the E-Chord modulus, and is represented by the slope of a straight line passing at $0.5\, f_{cy}$ [106].

The initial tangent modulus of the hardened concrete E_c was determined using equation 3-3, with accordance of BS8110 [107]

$$E_c = 5500\sqrt{\frac{f_{cu}}{\gamma_m}} \qquad (\mathrm{N/mm^2}) \tag{3-3}$$

where f_{cu} is the cube strength ($\mathrm{N/mm^2}$) and γ_m is a partial safety factor (for the tests taken as $\gamma_m = 1.0$). The initial modulus of concrete, E_c, was calculated based on equation 3-3 and presented in Table 3.4.

3.3 Tension Tests of CFRP Coupons

3.3.1 Introduction

In order to meet the objectives of this investigation it was necessary to determine the mechanical properties of the CFRP laminates. The laminates properties are characterised by the modulus of elasticity and the tensile strength at failure. The ultimate strength, elastic modulus, and failure strain can be calculated from the theoretical analyses as in section 3.3.4. These properties were experimentally determined by using coupons from the CFRP laminates, section 3.3.3. Two different amounts of epoxy were used to produce the CFRP coupons that were tested, in order to investigate the effect of the amount of epoxy on the volume fibre fractions in the CFRP laminate and consequently the ultimate strength. The first amount of epoxy added was based on the manufacture's instructions and the second was 2.5 times the first. The CFRP laminates tested were distinguished by A and B, respectively.

The mixing of the CFRP materials was carried out according to the manufacture's instructions. The preparation of laminate specimens, moulding, machining, and testing were carried out according to ASTM D3641 [108], ISO 294 [109], 2818 [110] and 3167 [111], respectively. The preparation of the CFRP specimens is described in Section 3.3.2. The

method used to experimentally determine the ultimate strength of the CFRP is described in Section 3.3.3, Section 3.3.4 describes the use of micromechanics analysis to predict the elastic modulus and the maximum strength. The results and discussion of the testing and prediction methods are presented in Section 3.3.5.

3.3.2 CFRP specimen preparations

3.3.2.1 CFRP laminates

A steel mould 350 mm long, 300 mm-wide and 4 mm deep was prepared for casting the CFRP laminate. A silicon paste was used to fill any gaps between the members of the mould. The steel mould was placed on a horizontal surface, and sandpaper was used to remove debris materials and dust from the mould base surface. The interior area of the steel mould was then covered with a very thin layer of Vaseline to prevent sticking of the bonded material to the steel surface. Then, a layer of aluminium sheet was placed on the surface and carefully rolled using rubber roller. The epoxy resin to hardener was mixed in the proportions 1:1/4. The resin was applied by brush over a 300 mm square area which was marked on the aluminium surface. The unidirectional fibre was then placed on it. A relatively stiff rubber roller was used for rolling the unidirectional fibre in the longitudinal direction to ensure the adhesive was distributed throughout the fibre textile.

Finally a further layer of aluminium sheet was placed on the top face of the composite laminate, and then carefully rolled using the rubber roller to remove any voids in the composite interlayer. The CFRP laminate was left for 3 days at room temperature of 23 ^{o}C to cure. After curing the aluminium sheets were removed carefully from the CFRP laminate.

The CFRP laminate was squared using an electric saw to avoid any disruption of the laminate edges. A proposed width of composite laminate in the longitudinal fibre direction was then marked and cut to produce test specimens for composite density. It is

important to assess the density of the fabricated sheet from which the volume fibre fraction, VF, in the composite laminate is then easily calculated.

The remaining part of the CFRP laminate was kept for coupons for tensile tests. Details of the coupons are shown in Figure 3.2. In order to carry out the tensile tests for the CFRP coupons, the gripped ends of the specimen in the test machine should be thicker than that of the specimen. Hence, end tabs were provided. In order to bond the end tabs, the ends on each side of the CFRP laminate were sanded with the sandpaper to roughen the surface. The sanded area was then cleaned with acetone to remove debris and dust from the laminate surface. The end tabs were prepared from the same unidirectional carbon fibre UCF as in the body of the coupon. The UCF was cut into four rectangle pieces each 60 mm wide and 300 mm long. The required amount of epoxy corresponding to the bonded area ends was evaluated, and the mixing process presented earlier was repeated. The steel mould was placed on a horizontal surface, and the same process previously presented was repeated. The bonded areas of the CFRP ends and aluminium sheet were marked to approximately the same dimensions of UCF pieces. Epoxy was brushed on the marked aluminium area, and then the UCF pieces were bonded. A relatively stiff rubber roller was used for rolling the UCF strips in the fibre direction, and another layer of epoxy was then brushed on the top face of UCF strips. Subsequently, epoxy was brushed carefully on the marked areas on the CFRP laminate, and then the laminate was placed normal to the length of the bonded UCF pieces. Another two UCF pieces were placed on the top face of the laminate and the same process of rolling and covering with aluminium was carried out as described previously. The bonded parts (CFRP laminate, adhesive, and aluminium fabrics) were left to cure at room temperature for 7 days before final preparation of the coupons.

3.3.2.2 CFRP coupons

The CFRP laminate including the end strips, as discussed in Section 3.3.2.1, was marked to produce test coupons 15 mm wide and 250 mm long, in the longitudinal direction parallel to the fibre axis of the CFRP laminate. The laminate together with the shoulders was cut into test coupon specimens, as shown in Figure 3.2. During cutting the coupon specimens, the saw rate was relatively slow to avoid possible damage to the

specimen. At high rates of saw motion the saw bits would tend to dissipate the carbon fibres and rip them from the stiff adhesive, damaging the specimen. Six and five CFRP coupons were prepared from the laminates for types A and B, respectively. The width of each specimen was recorded at three different locations with a digital micrometer along the length between the machine grips, and it was found to be an average of 14.98 mm. The length of all specimens was approximately 250 mm. The thickness of the coupon specimens was evaluated from the density of the fabricated laminates according to ASTM Standard, D 792 [112] as will be mentioned in section 3.3.5.

A longitudinal line was marked at the centre of each specimen to orient the demec buttons, perpendicular reference lines were marked at a distance of 25 mm apart from the centre. The surface of the specimen was then cleaned and conditioned to remove any dirt, oil, scratches, or other impurities that may affect the bond strength. The demec buttons were fixed using super glue on the perpendicular reference lines at the centre of each test specimen. A calibration demec bar was used to orient steel demec buttons on the specimen, by keeping a constant 50 mm original gauge length.

In order to determine the mechanical properties, the elastic modulus and tensile strength, of the CFRP coupons it was necessary to measure the axial strain corresponding to the increments of load up to failure. A mechanical extensometer with a gauge length of 50 mm was attached to the specimens, Figure 3.2, and the extension was recorded for each load increment up to failure.

3.3.3 Experimental method

The CFRP coupon specimens were tested according to ASTM D3039 [113] and EN ISO 527-5 [114], using a 100 kN, Instron testing machine. Each specimen was aligned and clamped in the machine grips. The free span between the grips of each specimen was approximately 132 mm and the average measured thickness of the composite coupons tested was 0.40 mm and 0.90 mm for types A and B, respectively. Displacements were measured using a mechanical extensometer as in Section 3.3.2.2. Each specimen was loaded at a rate of 0.5 mm/min, until failure. Failure was defined as the maximum load

that could be applied during the test. Displacement readings were recorded for increments of load of 0.2 kN up to the coupon rupture. Load and displacement for each increment was converted to stress and strain as in Figure 3.3.

The ultimate tensile strength of the coupons for the two types of CFRP specimens, type A and type B, was determined from the maximum load, while the tensile modulus was determined from the gradient of the stress-strain curve, by using the 20 % and 80% points of the maximum stress, Figure 3.4. The stress-strain relationship was observed for six and five CFRP coupons tested in type A and B, respectively, and all specimens showed elastic behaviour up to the maximum load. Figure 3.3 shows a typical stress-strain relationship for specimens (III) in A and (II) in B.

Tables 3.5 and 3.6 show the measured elastic modulus, the ultimate stress and the failure strain of each coupon specimen for type A and B. Tables 3.5 and 3.6 also present the mean values (average) of the elasticity modulus, the ultimate stress and the ultimate strain. The mean values of the elasticity modulus and the ultimate stress were different in specimens A and B, due to the increased ratio of the matrix in specimen B compared with specimen A.

It was found that, Tables 3.5 and 3.6, increasing the amount of epoxy in the composite coupons decreased the elastic modulus and the ultimate stress. Therefore, the amount of the epoxy used in the A coupons, which produced a high volume fraction 26% and consequently lower thickness, was used for the external CFRP laminates for the strengthened reinforced concrete beams. The elastic modulus and the composite stress at failure were 61938 N/mm^2 and 802.4 N/mm^2, respectively. As the CFRP laminate presented a linear behaviour, it is assumed that the same behaviour occurred in compression.

3.3.4 CFRP Micromechanical prediction method

The mechanical characteristics of the composite laminate can be estimated based on composite theory. The elastic modulus and the failure strength for unidirectional CFRP were predicted using the micromechanical behaviour of laminates method described by Barbero [115]. Knowing the mechanical and physical properties, of the fibre and epoxy materials, i.e. density, tensile modulus and tensile strength, and the weight fractions of the constituent, the mechanical properties for the composite laminate then can be determined using the theory. The predicted model was developed for the uniaxial fibre direction and based on the following assumptions:

- Fibres to be continuous in the composite
- Fibres to be uniform in properties and diameter
- Prefect bonding exists between fibres and the matrix
- Fibres parallel throughout the composite and also lie in the direction of the load
- The composite materials are linear elastic up to failure

The volume fractions and weight fractions are related to the densities of the composite, the fibre and the matrix. The weight fractions of the composite are known, but the volume fractions are typically used in the predicted strength analysis of the composite materials. The weight fractions to volume fraction conversion relationships are:

$$V_{fib} = \frac{D_f}{D_{fib}} W_{fib} \tag{3-5}$$

$$V_{mat} = \frac{D_f}{D_{mat}} W_{mat} \tag{3-6}$$

where the volume fractions, weight fractions, and densities are denoted by V, W and D, respectively. The subscripts fib, mat and f refer to fibre, matrix and composite respectively.

From the assumptions made, the contributions of the fibre and matrix materials to the average composite properties are proportional to their volume fractions, the rule of

mixtures. These properties to be determined are the tensile stress and the elastic modulus of the composite. The tensile stress of the composite is given by:

$$f_f = f_{fib} V_{fib} + f_{mat} V_{mat} \tag{3-7}$$

The predicted elastic modulus for the composite E_f in the longitudinal direction is given by:

$$E_f = E_{fib} V_{fib} + E_{mat} V_{mat} \tag{3-8}$$

where E_{fib} and E_{mat} are the elastic modulus for the fibre and matrix, respectively.

The fibre volume fractions, V_{fib}, for the CFRP laminate specimens A and B were calculated from the density tests, and were found to be 26% and 11% for A and B, respectively. The materials properties given in section 3.2.1 and Table 3.1 were used in equations 3.5 to 3.8 to obtain the predicted value for tensile strength and the elastic modulus of the composite in the fibre direction. The predicted values for the CFRP laminates A and B are given in Table 3.7.

3.3.5 Comparison of results

To predict the values of the elastic modulus and the ultimate strength of the composite coupons, it is necessary to determine an accurate value of the fibre volume fraction in the composite coupons. Once the weight fraction of fibre W_{fib} has been determined then the fibre fraction V_{fib} can be calculated. The obtained fibre volume fractions used in this investigation were 26 % and 11% for CFRP coupon types A and B, respectively. The coupon densities for types A and B from the experiment were found to be 1.34 g/cm^2 and 1.26 g/cm^2, respectively. The average measured thickness was 0.40 mm and 0.90 mm for types A and B, respectively. The differences in the densities and the

thicknesses are due to the increase in the amount of epoxy added to the composite coupons, the fibre fraction being kept unchanged.

Table 3.7 contains the predicted results and summarises the experimental results. It can be seen from Table 3.7 that the experimental results were lower than the predicted values for all the properties investigated. As Table 3.7 indicates, there is little difference between the measured and the predicted value for the composite elasticity modulus of coupons type A, which had fibre volume fractions, V_{fib}, of 26%. The predicted values for the ultimate stress of the two composite coupons, A and B, were greater than the measured. This might be due to a relative orientation of the fibres to the direction of loading in the composite. This can occur during preparation of the laminate. In such cases Weeton *et al.* (1987) [116] and Marcus (1973)[117] reported that a significant decrease in the composite stress occurs when the fibres are not orientated in the direction of loading. Moreover, the reduction in the composite stress is affected by the angle between the fibres and the tensile axis of the specimen.

The average failure strains for the composites are also shown in Table 3.7. The predicted values were found by dividing the predicted ultimate tensile strength by the modulus of elasticity. The large difference in the failure strain was expected due to the fact that the stress-strain relationships for the composites were not linear at the initial stages of the tests, Figure 3.4. This behaviour has been found elsewhere [118].

3.4. Experimental Investigation of Reinforced Concrete Beams

3.4.1 General

This section describes all aspects related to the testing of the reinforced concrete beams. Design and analysis of the beams are discussed in Section 3.4.2. Three types of reinforced concrete beams having different dimensions and various ratios of external CFRP laminates and internal steel reinforcements have been tested, Section 3.4.3. The following subsections are included: test programme, Section 3.4.3, which describes the

various series and strengthening scheme for the specimens; all aspects related to surface preparation and installing of CFRP laminates, Section 3.4.4 and Section 3.4.5 respectively, and; testing procedure and instrumentation is discussed in Section 3.4.6.

3.4.2 Design and analysis of the beams

In this research, the primary concern was to analyse and design various beam elements. The results obtained from experiments are used to validate the results predicted by the simplified analysis model, Section 5.3.3, and the simplified model for flexural design, Section 5.4.

Because both the simplified model analysis and the design did not include shear failure, the beams were designed to fail in flexure before shear failure would occur. Therefore, the shear stresses in the beams tested were calculated according to BS 8110 [9]. The bending capacity, the shear stresses, the shear links design and their arrangements are given in an example in appendix B.

3.4.3 Test programme and strengthening scheme

Twenty three reinforced concrete beams, divided into four series, were tested. The series were: series-I which comprised under-reinforced sections with a low ratio of tensile steel reinforcement, less than 1%, and a low shear span to effective depth. Series-II comprised under-reinforced sections with a high ratio of tensile steel reinforcement, between 1% and 2%, and also low shear span to effective depth ratio. In this series, end anchorages at the beam tension face were included. Series-III comprised over-reinforced sections with a relatively low ratio of tensile steel reinforcement, between 2% and 3%, and high span to effective depth. Series-IV comprised over-reinforced sections with a high ratio of tensile steel reinforcement, greater than 3%, high span to effective depth ratio and small cross-sections. Details of the internal steel reinforcement and the external CFRP for the beams are given in Table 3.9. All beams were rectangular in cross-section. The layout of the steel reinforcement and CFRP laminates for beam III6-OL-TC beam are illustrated in Figure 3.5.

All specimens were detailed to ensure a flexural mode of failure and loaded to failure under four point bending. The design for each Series is discussed in sections 3.4.3.1, 3.4.3.2 and 3.4.3.3.

In series-I and II, the breadth and the depth of the beams were 120 mm and 160 mm, respectively, while the distance between the supports and the overall length of the beam were 1100 mm and 1300 mm, respectively. The intermediate distance between the two load points was 400 mm, see Figures 3.6 and 3.7. The shear span to effective depth ratio was approximately 2.65 for the beams in the two series.

In series-III, the breadth and the depth of the beams were also 120 mm and 160 mm, respectively, while the distance between the supports and the overall length of the beam was 2500 mm and 2800 mm, respectively. The intermediate distance between two load points was 500 mm, see Figure 3.8. The shear span to effective depth ratio was approximately 7.2 for the beams in this series.

In series-IV, the breadth and the depth were 65 mm and 80 mm, respectively, while the distance between the supports and the overall length of the beam was 1100 mm and 1300 mm, respectively. The intermediate distance between two load points was 200 mm, see Figure 3.9. The shear span to effective depth ratio was approximately 9 for the beams in this series.

As mentioned earlier the beam specimens were divided into four series however, because the CFRP ratio applied to the compression beam face was slightly lower in Series-II, therefore Series-II might be better to be discussed with Series-I.

To distinguish the beams, three part identifiers were used. The first part represents the series number, group number in the series and beam number in the group. The second

part represents the ratio of the tensile steel reinforcements (U and O are under-and over-reinforced section and L and H are lower and higher steel ratio, respectively). The last part represents the external CFRP on the beam section i.e. UN unstrengthened, T strengthened on the tension face and TC strengthened on both the tension and compression faces. For example: beam I25-UL-TC means that this beam belongs to series-I, group number 2 and beam number 5, the section was under-reinforced with low ratio of tension steel, the section was strengthened on both tension and compression. Beam III2-OL-T means that this beam belongs to series-III, beam number 2 in the series, the section was over-reinforced with low ratio of tension steel and the section was strengthened on the tension face. The different combinations of the internal steel reinforcement and the external CFRP reinforcement used in the test programme are given in Tables 3.8 and 3.9.

3.4.3.1 Specimens of Series-I & II

The specimens in Series-I can be divided into two groups. The first group comprised three unstrengthened reinforced concrete beams, with different steel ratios (to give under reinforced and over reinforced beams), and were designed to investigate the failure mechanism, validate the prediction results and to assist in setting up the test procedure, and instrumentation, details of the beams are given in Table 3.8. The beams are I11-UH-UN, I12-UH-UN and I13-OL-UN.

The second group comprised five reinforced concrete beams which had 0.54% internal tension reinforcement. The beams of the second group are I21-UL-UN, I22-UL-T, I23-UL-TC, I24-UL-TC and I25-UL-TC. Vertical links of 6 mm bar diameter at 50 mm centres were provided through each beam length in order to prevent shear failure, see Tables 3.8 and 3.9. I21-UL-UN was considered as a control beam while the remaining specimens of this group were strengthened with the CFRP laminates. Further details including the layout of the steel reinforcement are illustrated in Figure 3.6.

The parameters investigated in the second group were the laminate lengths and anchorages at the ends of the composite laminates, on the beam tension face, and the

contribution to the beam flexural strength by either placing of the CFRP laminate on the tension face, or placing them on both the tension and compression faces.

In the second group, four of the beams, I22-UL-T, I23-UL-TC, I24-UL-TC and I25-UL-TC were externally strengthened with CFRP laminates. End laminate anchors, U-shaped, were provided to the tension face of I22-UL-T, I23-UL-TC beams. The ratio of the tension and the compression CFRP composite used was 0.92% and 0.61 %, corresponding to 3 and 2 laminates, respectively see Table 3.9. I22-UL-T was strengthened on the tension face only. 2-CFRP laminates were placed on the compression face of I23-UL-TC, I24-UL-TC and I25-UL-TC. The laminate length was terminated 50 mm from the external beam supports on the tension face in I22-UL-T and I23-UL-TC, while the laminate was extended to the beam ends in I24-UL-TC and I25-UL-TC, Figure 3.6. A full width, 120 mm CFRP laminate was utilized on both the tension and the compression beam faces. One CFRP U-shaped 100 mm wide was placed at each end of the external CFRP laminate. Adding CFRP U-shapes to the laminate ends was to prevent any premature failure due to laminate debonding. I25-UL-TC was strengthened with the same reinforcement configuration of I24-UL-TC to validate the results of the later beam. Further details including the layout of the CFRP composites and the position of the U-shaped wrapping are given in Table 3.10 and Figure 3.6.

Series II comprised three beams. All beams were internally reinforced with steel ratio of 1.3% and 0.65 % in tension and in compression, respectively, Table 3.9. Vertical links of 8 mm bar diameter at 100 mm centres were provided throughout each beam. In fact, this series was designed and tested prior to the second group of series-I. Shear failure was the dominant failure mode of this series because the spacing between the shear links was too large, therefore, CFRP U-shaped wrappings were provided at the laminate ends as anchorages with the arrangements as shown in Figure 3.7.

The ratio of the tension steel reinforcement used in series-II beams was higher than that used in the second group of series-I, Table 3.9. In addition a low ratio of compression steel was included. Series-II comprised three strengthened beams, II1-UH-T, II2-UH-TC and II3-UH-TC. Low ratios of CFRP composites were placed to both beam tension

and compression faces. The ratios of the tension and the compression CFRP laminate were 0.31% and 0.13 % to correspond of one CFRP laminate, Tables 3.9 and 3.10. II1-UH-T was strengthened in the tension face only. In the three beams, the laminate on the tension face was terminated at 50 mm from the external beam supports. Due to the large spacing between the shear links, end U-shaped anchors were provided to the tension faces of the beams. The width and the number of the external U-shaped anchors were varied. The utilised U-shaped width was 100 mm and 250 mm in II2-UH-TC, II3-UH-TC beams and II1-UH-T, respectively, Table 3.10 and Figure 3.7. Further details, including the layout of the steel reinforcement and CFRP laminates are illustrated in Figure 3.7.

3.4.3.2 Specimens of Series-III

The parameters investigated in series-III were the effectiveness of CFRP laminate on the compression beam face for varying ratios of CFRP, and the value of the strain reached when buckling of the compression CFRP laminate takes place.

Series-III comprised six beams; all beams had the same ratio of steel tension reinforcement but different quantities of external CFRP laminates, Table 3.8. The ratios of the internal steel reinforcement were 2.4% and 0.34% for tension and the compression, respectively, Table 3.9. A high ratio of the tension steel reinforcement was used in this series. This was to ensure that the beams were over-reinforced and the final failure was due to concrete crushing. However, this ratio is low when compared to that in series-IV as will be discussed later. Vertical links of 6 mm bar diameter at 50 mm centres were provided throughout beam spans in order to prevent shear failure, see Table 3.8. The shear span to effective depth ratio was approximately 2.7 larger than that used for beams of series-I&II. Increasing the shear span to effective depth ratio in this series was to produce low applied moment, large deflection and to investigate the mechanism of CFRP buckling at mid-span of the beam.

III1-OL-UN and III4-OL-UN, unstrengthened beams, were designed to fail by concrete crushing. Six CFRP laminates were placed on the tension face of the two beams, III2-OL-T and III5-OL-T, which represents a composite ratio of 1.72%. III2-OL-T and III5-OL-T were not strengthened on the compression face and considered to be the reference beams for III3-OL-TC and III6-OL-TC. III3-OL-TC and III6-OL-TC had six and ten CFRP laminates, respectively, placed on the beam compression face which represents composite ratios of 1.71% and 2.84%, respectively. The laminates on the tension faces were extended to the beam ends while the compression laminates terminated at 100 mm from the external beam supports. A full width, 120 mm CFRP width was used in all strengthened beams. Further details including the layout of the steel reinforcement and CFRP laminates are given in Tables 3.8, 3.9, 3.10 and Figures 3.5 and 3.8.

3.4.3.3 Specimens of series-IV

The main objective of series-IV was to investigate the increases in the flexure strength and buckling mechanism of CFRP laminates when added to the compression face of over-reinforced beams, especially in the presence of a high tensile steel ratio and to investigate the concrete strain when the CFRP debonds.

Series-IV can be divided into two groups. The first group comprised two beams and the second comprised four beams. The beams of the first group were IV11-OL-TC and IV12-OL-TC while the beams of the second group are IV21-OH-UN, IV22-OH-C, IV23-OH-C and IV24-OH-C. In both groups the ratio of CFRP and the internal steel were chosen in such way that over reinforced failures occurred, Tables 3.8 and 3.9. All beams of these series have a length of 1300 mm and breadth of 65 mm. The total depth of specimens was 80 mm. In the second group there was a notch of 5 mm deep at mid-beam span to ensure that the failure would occur in these locations. Further details of the two groups are as follows.

In the first group, the two beams were internally reinforced with two 8 mm bars, which give a steel ratio of 2.81%. CFRP laminates were placed on both the tension and compression face of the two beams of this group. The ratio of CFRP, in the first group,

on both the tension and compression beam faces was 1.34% which corresponds of two laminates, 60 mm width and 0.4 mm thickness for each. The thickness of the CFRP was measured in the coupon tests, Section 3.3.3. The CFRP laminates extended to the ends of beam IV11-OL-TC while the CFRP laminates were terminated at 50 mm from the external supports in beam IV12-OL-TC. In beam IV12-OL-TC, U-shaped CFRP with steel anchor bolts were provided as shown in Figure 3.9. In the two beams, the anchoring technique used either extending the laminates to the beam-ends, or using both U-shaped and steel anchors in order to prevent end laminate debonding at the beam tension face.

In the second group, the beams were reinforced with two bars 10 mm in diameter, which represents a steel ratio of 4.4 %. The internal tensile steel ratio used in this series was high, see Table 3.9, to meet the corresponding strength increases due to increasing of CFRP laminates without reaching the yield of the tensile steel reinforcement. A rectangular notch 3 mm wide and 5 mm deep was included at mid span of the compression face as shown in Figure 3.9; beam IV21-OH-UN. This was to ensure that the failure would occur at mid span of the specimen.

IV21-OH-UN was a control test the other three beams, IV22-OH-C, IV23-OH-C and IV24-OH-C, were strengthened on the compression face only by applying different laminates of CFRP. The ratios of the CFRP used in IV22-OH-C, IV23-OH-C and IV24-OH-C beams were 1.34%, 2.7% and 4% corresponding to 2, 4 and 6 laminates, respectively. The compression laminates were terminated at 50 mm from the external support, U-shaped CFRP were provided along the shear span of the strengthened beam as shown in Figure 3.9. Use of U-shaped CFRP on the shear length was to prevent shear failure because no vertical steel links were included in the sections. Further details including the layout of the steel reinforcement, CFRP composites and the position of U-shaped CFRP along the shear spans are illustrated in Figure 3.9.

3.4.4 Surface preparation

Before application of the CFRP the concrete substrate was initially roughened using a round wire brush in a drill four days after casting the beams. Once the coarse aggregate was exposed, a sandstone was used to remove the remaining cementatious materials from it. A compressor vacuum, 20 bars, was used to clean the surfaces and remove any dust or loose particles from the concrete surface. The top faces of the second group beams of series-IV are shown in Figure 3.10.

3.4.5 Preparing and installing CFRP composites

Dependent on the amount of the unidirectional fibre layers required, the role of UCF was placed on a clean horizontal table and longitudinal strips of the correct length and the width were cut, Figures 3.11a and 3.11b. The surface of concrete beam, required to be strengthened, was prepared as described in section 3.4.4, then the surface was cleaned using acetone to remove dirt and small particles, see Figure 3.11c, prior to placing the CFRP laminates.

Two-component adhesives, epoxy resin and standard hardener, were prepared in accordance with the manufacture's recommendations and applied to the concrete substrate by brush. The mixing ratio of the component and laminating time are given in Table 3.1. After mixing, the adhesive was applied by brush to the concrete surface. The layer of UCF then placed by hand and pressed onto the adhesive using rubber roller, to ensure a full distribution through the fibres. Another layer of adhesive and layer of UCF were applied over the previous CFRP laminate. This process was repeated for each of the required number of laminates. Subsequently, the laminated beam was left to cure for at least 7 days before testing.

3.4.6 Testing procedure and instrumentation

3.4.6.1 Loading arrangement and loading equipment

The loading arrangement used is shown in Figures 3.5 and 3.12. All beams were loaded under four point loading. Each beam was simply supported on two end rollers; the beam load was applied by hydraulic jacks at two points. The test frame was such that the beam was tested upside down, Figure 3.12. ENERPAC RC-106 hydraulic jacks, which had a 32 mm ram diameter and 150 mm stroke with a capacity of 100 kN, reacted against an independent steel frame. High tensile bars carried the reactions from the beam to the steel frame, which were bolted to steel plates attached to a steel beam. The load was transmitted to the beam through a rectangular solid steel plate of 150 length, 60 mm width, and 20 mm thickness. One of the two intermediate supports, between the top of the ram and the contacting steel plate, was designed to act as a roller so that tilting of the plate during the loading process was allowed to occur. When testing strengthened beams, a rubber pad with a thickness of 6 mm was placed between the beam surface and the steel plate in order to minimize the abrasion between the steel plate and the composite laminates, in the unstrengthened reinforced concrete control beams a plaster paste was used. Similar rectangular solid steel plates at the external supports were used.

3.4.6.2 Loading procedure

Before loading the specimen, the beams were painted white to assist in identifying cracking during the tests. Demec buttons and the electronic strain gauges were installed to the beam sides and on the CFRP laminates as will be discussed in section 3.4.6.4. The beam was then placed in the test frame and all readings of the instrumentation were initialised.

All specimens were tested under load control. All specimens were subjected to 2 load cycles. The first cycle was formed to cause cracking stage and continued up to approximate 60% of ultimate failure, the second cycle was formed to failure of the

specimens. In the first cycle the load increments were 2 kN and 3 kN while in the second cycle were 1kN and 1.5 kN in series (I and-III) and series-II, respectively. In series-IV only one load cycle, with load increments of 0.5 kN, was carried out up to failure. The load increments as proposed were applied. After application of the load it immediately dropped, the final values of the load were recorded. The larger specimens with external CFRP laminate strengthened took between 4 and 5 hours to test to failure, whereas the time taken for the control beams was between 3 and 4 hours.

After each load increment, cracks were marked on the beam surface with marker pen to trace the crack propagation. Crack patterns and any distinguishable behaviour noticed during the test such as a release of sound was recorded. All tests were carried beyond the maximum load and were stopped only when either catastrophic failure occurred, e.g. due to rupture of composite or extensive crushing of concrete.

3.4.6.3 Load cells and displacement measures

The hydraulic jack, section 3.4.6.1, applied vertical load via two intermediate load cells. Because of the symmetry of the beam, each load was approximately half of the total load on the beam. RDP-43/8219-05 load cells manufactured by RDP-Electronic Ltd and having a maximum capacity of 100 kN were installed between 8 mm steel plates, bolted and held together, Figure 3.11d. This process was carried out to protect the load cells from any damage during the test. The whole unit, load cell and the steel plates were positioned concentrically on each ram in both intermediate beam two points. The beam specimen then was set up for test. The loads recorded in both load cells were continuously displayed on RDP transducer indicator E 308 and were recorded for each load increment.

Four mechanical dial gauges, total displacement 25 mm and 0.01 mm accuracy, were installed on the test beam, three for measuring the vertical deflection of the beam at mid span and under the point loads, and one was placed at the end of the beam, to measure the horizontal movement or lateral movement.

3.4.6.4 Surface strains

Strains in the concrete through the beam depth were recorded using Demec gauges. Strains at the tension CFRP laminates at the mid span of the beam were recorded for some beams using Demec gauges. The locations of the strain readings are shown in Figure 3.13. Electrical resistance strain gauges were installed on the CFRP laminates.

Two Demec gauges were used. The original gauge length for the two Demec gauges were 150 mm and 50 mm with 2500 division and strain of 1.08×10^{-5} and 2.54×10^{-5} mm/mm per each division, respectively. A Demec gauge of 150mm was used in series-I, II and III.A Demec gauge 50 mm was used in the second group beams of series-IV. Strains in the concrete were recorded for each load increment.

Electrical resistance strain gauges were installed on the CFRP laminate on the compression beam face and, in some cases to the laminate on the tension face, to assess the strain distribution along the laminate length. The use of the electrical resistance strain gauges on the compression face was necessary because the beam was tested in an upside-down position. The electrical resistance strain gauges were placed on the compression CFRP laminate at mid-span, as in Figure 3.13. As the output, the readings of the strain gauges at each load increment were amplified and then fed into a data acquisition computer module.

Table 3.1: Properties of the structural adhesive (epoxy/ standard hardener)

Property	
Mix ratio (by weight)	100: 25 (resin / standard hardener)
Mix density	1.18 g/cm^3
Laminate working	1.5 -3 hr
Gel Time 150g @25°C	45 min
Tensile strength, 28day @25°C	75.2 (N/mm^2)
Tensile modulus, 28day @25°C	3.81 (kN/mm^2)
Laminating compressive strength, 28day @25°C	448 (N/mm^2)

Table 3.2: Mechanical properties of steel reinforcement used in beams

bar diameter (mm)	Yield strength, f_y (N/mm^2)	Ultimate strength, f_{su} (N/mm^2)	Elasticity modulus, E_s (kN/mm^2)	Elongation percentage, (%)	Remarks
6	368	465	200	29.0	plain mild steel
8	490	530	202	18.4	high yield deformed
10	527	590	207	15.2	high yield deformed
16	530	643	212	18.1	high yield deformed

Table 3.3: Mix proportions and the slump test values for all concrete mixes

For Target cube crushing strength between 25-40 N/mm^2	
Materials	Weight (kg/m^3)
Water to Cement ratio	0.62-0.68
Water	205-225
Cement	330-360
Fine aggregate	1080-908
Coarse aggregate	726-908
Slump	40-140 mm

Table 3.4: Concrete properties for beams tested

Series no.	Beam ref.	f_{cu} [1] (N/mm^2)	f_{cy} [1] (N/mm^2)	f_{sp} [1] (N/mm^2)	E_c [2] (N/mm^2)
I	I11-UH-UN	31.71	24.6	2.51	30971
	I12-UH-UN	32.01	24.62	2.43	31118
	I13-OL-UN	32.85	25.65	2.45	31523
	I21-UL-UN	23.8	21.21	2.92	26832
	I22-UL-T	25.27	22.72	2.45	27648
	I23-UL-TC	26.8	21.83	2.65	28473
	I24-UL-TC	30.51	24.0	2.71	30380
	I25-UL-TC	35.7	28.7	2.9	32862
II	II1-UH-T	36.47	29.08	2.65	33215
	II2-UH-TC	34.07	26	2.47	32103
	II3-UH-TC	35.63	27.27	2.58	32830
III	III1-OL-UN	36.97	30	2.38	33442
	III2-OL-T	37.48	30.1	2.68	33672
	III3-OL-TC	39.96	31.5	2.81	34768
	III4-OL-UN	39.8	31.3	3.2	34698
	III5-OL-T	40.2	33.1	3.35	34872
	III6-OL-TC	40.53	36.37	3.55	35015
IV	IV11-OL-TC	34.43	24	2.36	32272
	IV12-OL-TC	35.7	28.7	2.73	32862
	IV21-OH-UN	36.26	29.4	2.64	33119
	IV22-OH-C	36.26	29.4	2.64	33119
	IV23-OH-C	36.26	29.4	2.64	33119
	IV24-OH-C	36.26	29.4	2.64	33119
1: measured ; 2 : calculated based on equation 3.3					

Table 3.5: Mechanical properties for CFRP coupons type (A)

Specimen	E_f (N/mm^2)	f_f (N/mm^2)	ε_f %
I	66138.8	875.9	1.37
II	66137.6	787.0	1.2
III	68051.5	885.2	1.37
IV	61637.0	720.2	1.18
V	55187.6	795.8	1.44
VI	54476.0	750.0	1.41
Mean (Average)	61938.0	802.4	1.33

Table 3.6: Mechanical properties for CFRP coupons type (B)

Specimen	E_f (N/mm^2)	f_f (N/mm^2)	ε_f %
I	29000.4	366.1	1.25
II	26471.8	383.1	1.48
III	27870.4	356.2	1.28
IV	28319.6	406.3	1.46
V	29239.8	401.0	1.34
Mean (Average)	28180.4	382.5	1.36

Table 3.7: Experimental and predicted results for composite coupons for A and B

Composite Property	Specimen (A)		Specimen (B)		Difference (%)	
	e	*p*	*e*	*p*	(A)	(B)
Elasticity modulus, E_f (kN/mm^2)	61.9	63.2	28.2	29.1	2.0	3.0
Ultimate stress, f_f (N/mm^2)	802.4	960.3	382.5	456.6	16.4	16.2
Failure strain ε_f (%)	1.33	1.52	1.36	1.57	12.5	13.4
The subscripts *e* and *p* represent the experimental and predicted values, respectively						

Table 3.8: Beam geometry and reinforcement details

Series no.	Beam ref.	Beam Dimensions				Internal reinforcement				Shear links, diameter and spacing (mm)	Remarks
						Ten. bars		Comp. bars			
		b (mm)	h (mm)	d_s (mm)	d_{sc} (mm)	bars no.	Ø (mm)	bars no.	Ø (mm)		
I	I11-UH-UN	120	163.6	128.6	39.6	2	8	2	6	8@100 c/c	Un-stre
	I12-UH-UN	120	162.8	130.7	32	2	8	2	6	6 @100c/c	Un-stre
	I13-OL-UN	120	168	135.7	42	2	16	2	6	6 @80 c/c	Un-stre
	I21-UL-UN	120	164.2	132.3	-	3	6	-	-	6 @50 c/c	Un-stre
	I22-UL-T	120	164.0	131	-	3	6	-	-	6 @50 c/c	T
	I23-UL-TC	120	164.0	131	-	3	6	-	-	6 @50 c/c	TC
	I24-UL-TC	120	164.5	132	-	3	6	-	-	6 @50 c/c	TC
	I25-UL-TC	120	164.8	131.8	-	3	6	-	-	6 @50 c/c	TC
II	II1-UH-T	120	163.8	127.8	30.8	1	16	2	8	8 @100 c/c	T
	II2-UH-TC	120	165.2	129.5	34.5	1	16	2	8	8 @100 c/c	TC
	II3-UH-TC	120	163.1	128.1	35.1	1	16	2	8	8 @100 c/c	TC
III	III1-OL-UN	120	164	140	36	2	16	2	6	6 @60 c/c	Un-stre
	III2-OL-T	120	164	138	30	2	16	2	6	6 @60 c/c	T
	III3-OL-TC	120	164	140	33	2	16	2	6	6 @60 c/c	TC
	III4-OL-UN	120	165	140	22	2	16	2	6	6 @60 c/c	Un-stre
	III5-OL-T	120	165	140	22.5	2	16	2	6	6 @60 c/c	T
	III6-OL-TC	120	167	142	23	2	16	2	6	6 @60 c/c	TC
IV	IV11-OL-TC	65	80	55	-	2	8	-	-	Non	TC
	IV12-OL-TC	65	80	55	-	2	8	-	-	Non	TCA
	IV21-OH-UN	65	75	50	-	2	10	-	-	Non	Un-stre
	IV22-OH-C	65	75	55	-	2	10	-	-	Non	C
	IV23-OH-C	65	75	55	-	2	10	-	-	Non	C
	IV24-OH-C	65	75	55	-	2	10	-	-	Non	C

d_s : effective depth, d_{sc}: concrete cover of compression reinforcement

T: tension strengthening; C: compression strengthening ; TC: tension and compression strengthening

TCA: tension and compression strengthening including bolt anchors

Ø : bar diameter

Table 3.9: Details of reinforcements and the shear to effective depth ratio

Series no.	Beam ref.	Shear span L_s (mm)	Effective depth d_s (mm)	Shear span to effective depth ratio L_s/d_s	Internal steel reinforcement ratio		External CFRP reinforcement ratio	
					Tension ρ_s (%)	Compress-ion ρ_{sc} (%)	Tension ρ_f (%)	Compress-ion ρ_{fc} (%)
I	I11-UH-UN	350	128.6	2.72	0.65	0.37	--	--
	I12-UH-UN	350	130.7	2.68	0.64	0.36	--	--
	I13-OL-UN	350	135.7	2.58	2.47	0.35	--	--
	I21-UL-UN	350	132.3	2.65	0.53	--	--	--
	I22-UL-T	350	131	2.67	0.54	--	0.92	--
	I23-UL-TC	350	131	2.67	0.54	--	0.92	0.61
	I24-UL-TC	350	132	2.65	0.54	--	0.91	0.61
	I25-UL-TC	350	131.8	2.66	0.54	--	0.91	0.61
II	II1-UH-T	350	127.8	2.74	1.31	0.66	0.31	None
	II2-UH-TC	350	129.5	2.70	1.29	0.65	0.31	0.13
	II3-UH-TC	350	128.1	2.73	1.31	0.65	0.31	0.13
III	III1-OL-UN	1000	140	7.14	2.39	0.34	--	--
	III2-OL-T	1000	138	7.25	2.43	0.34	1.74	--
	III3-OL-TC	1000	140	7.25	2.43	0.34	1.171	1.71
	III4-OL-UN	1000	140	7.14	2.39	0.34	--	--
	III5-OL-T	1000	140	7.14	2.43	0.34	1.71	--
	III6-OL-TC	1000	142	7.04	2.43	0.34	1.69	2.82
IV	IV11-OL-TC	450	55	8.18	2.81	--	1.34	1.34
	IV12-OL-TC	450	55	8.18	2.81	--	1.34	1.34
	IV21-OH-UN	450	50	9	4.40	--	--	---
	IV22-OH-C	450	55	9	4.40	--	--	1.34
	IV23-OH-C	450	55	9	4.40	--	--	2.70
	IV24-OH-C	450	55	9	4.40	--	--	4.0

Table 3.10: Strengthening scheme for all reinforced concrete beams investigated

Series no.	Beam ref.	External CFRP reinforcement					
		Compression laminate		Tension laminate			
		ply no	breadth (mm)	ply no	breadth (mm)	Laminate termination	End-Anchorage
I	I11-UH-UN	None	None	None	None	None	None
	I12-UH-UN	None	None	None	None	None	None
	I13-OL-UN	None	None	None	None	None	None
	I21-UL-UN	None	None	None	None	None	None (Control)
	I22-UL-T	None	None	3	120	A	120 mm U-shape
	I23-UL-TC	2	120	3	120	A	120 mm U-shape
	I24-UL-TC	2	120	3	120	B	None
	I25-UL-TC	2	120	3	120	B	None
II	II1-UH-T	None	None	1	120	A	200 mm U-shape
	II2-UH-TC	1	50	1	120	A	120 mm U-shape
	II3-UH-TC	1	50	1	120	A	2/120 mm U-shape
III	III1-OL-UN	None	None	None	None	None	None (Control)
	III2-OL-T	None	None	6	120	B	None
	III3-OL-TC	6	120	6	120	B	None
	III4-OL-UN	None	None	None	None	None	None (Control)
	III5-OL-T	None	None	6	120	B	None
	III6-OL-TC	10	120	6	120	B	None
IV	IV11-OL-TC	2	60	2	60	B	60 mm U-shape
	IV12-OL-TC	2	60	2	60	A	60 mm U-shape and steel anchor bolt
	IV21-OH-UN	None	None	None	None	None	None (Control)
	IV22-OH-C	2	60	None	None	None	400 mm U-shape
	IV23-OH-C	4	60	None	None	None	400 mm U-shape
	IV24-OH-C	6	60	None	None	None	400 mm U-shape

A: Prior to external supports, B: Beam tension ends

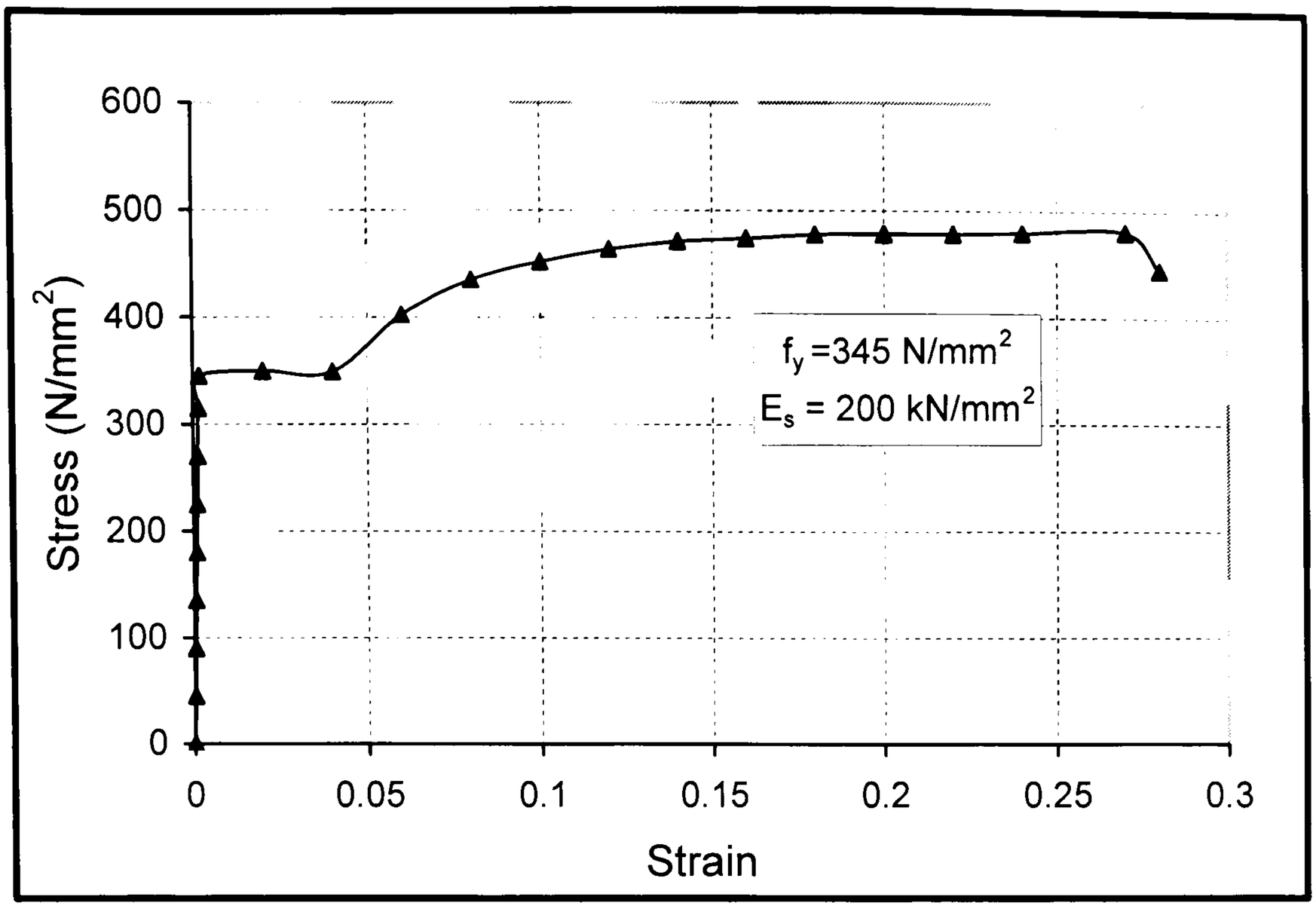

Figure 3.1a: Tensile test results for 6 mm

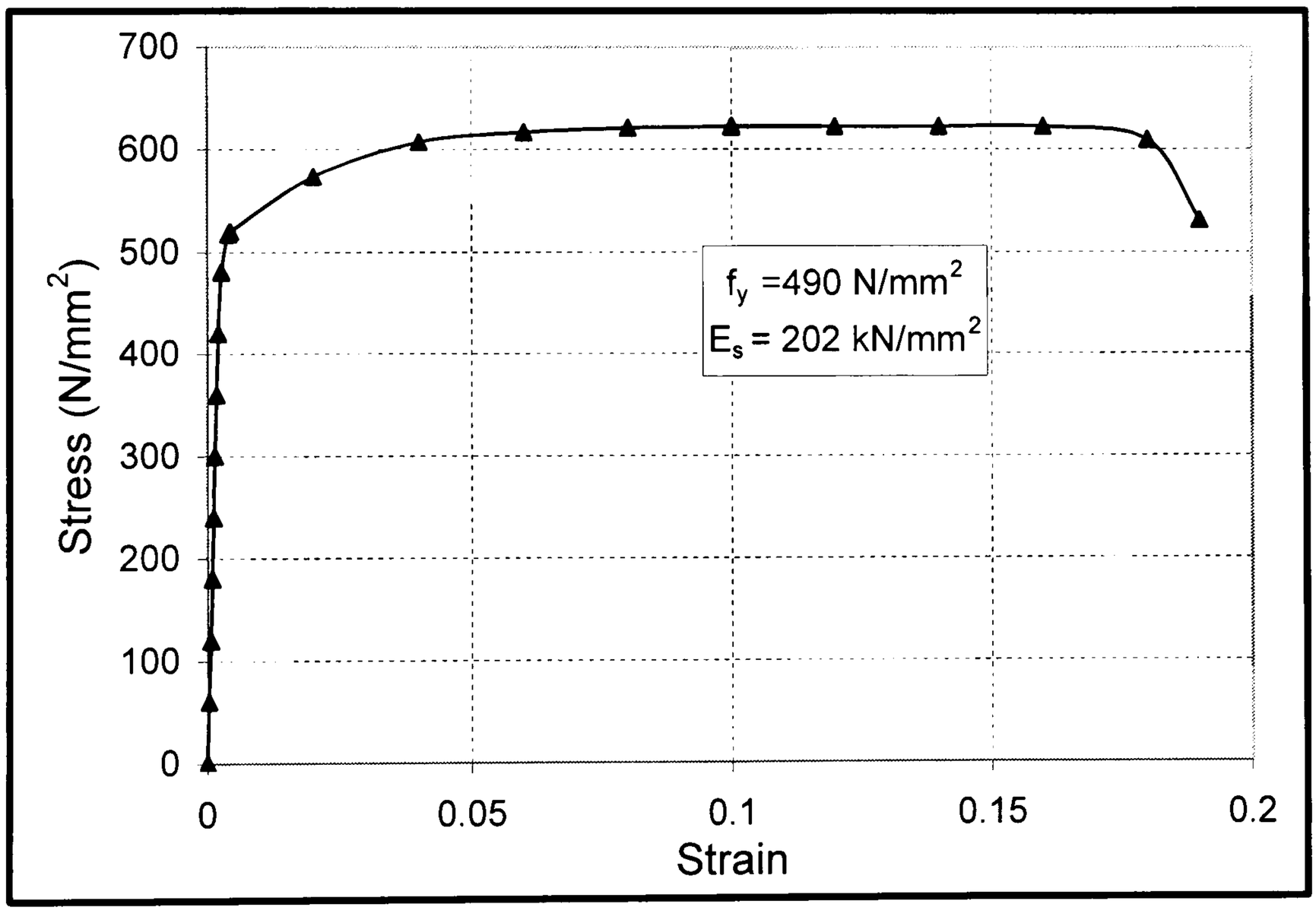

Figure 3.1b: Tensile test results for 8 mm

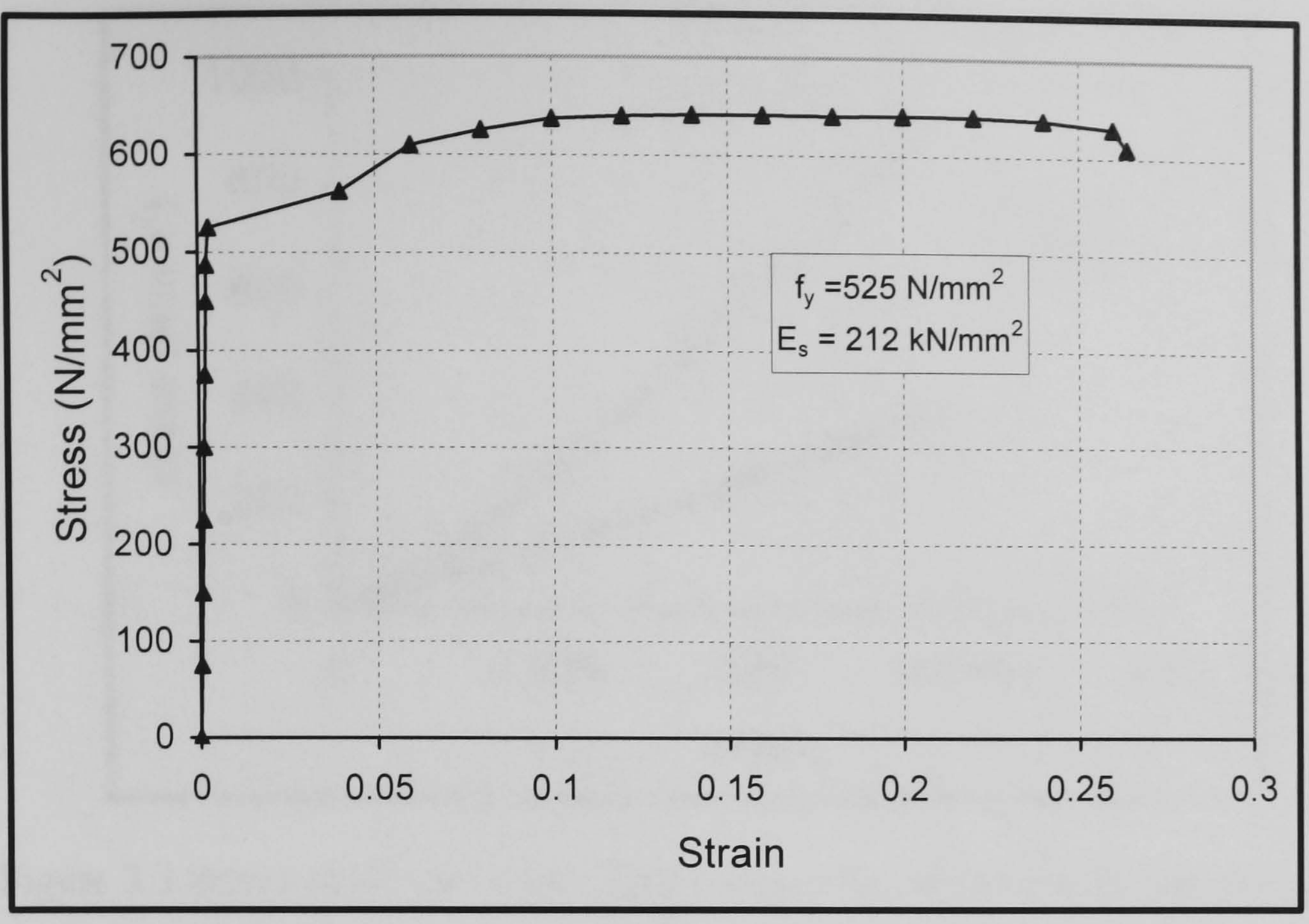

Figure 3.1c: Tensile test results for 16 mm

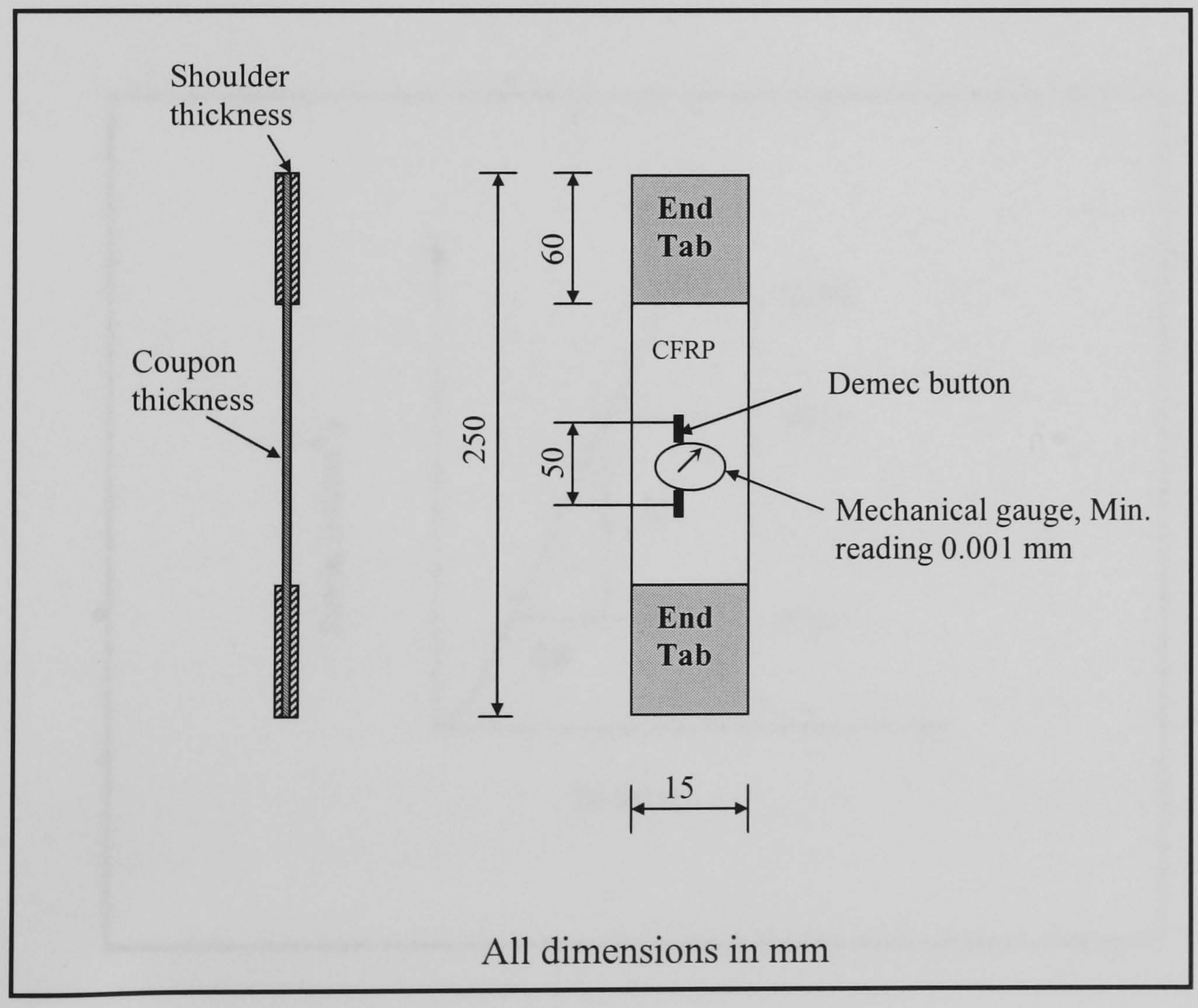

Figure 3.2: CFRP coupon specimen configuration with extension dial gauge

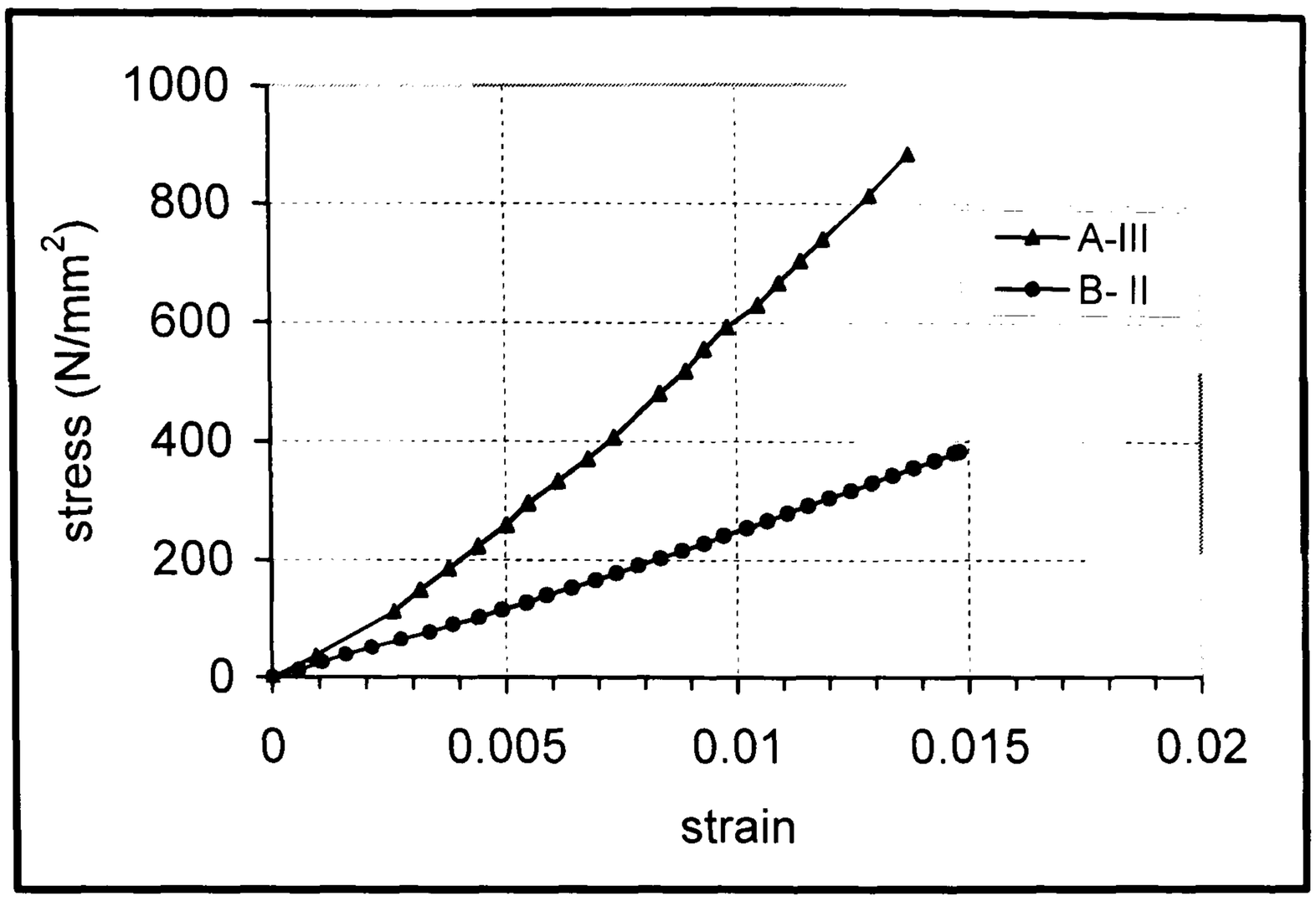

Figure 3.3 Stress-strain curve for CFRP coupon specimens (A-III) and (B-II)

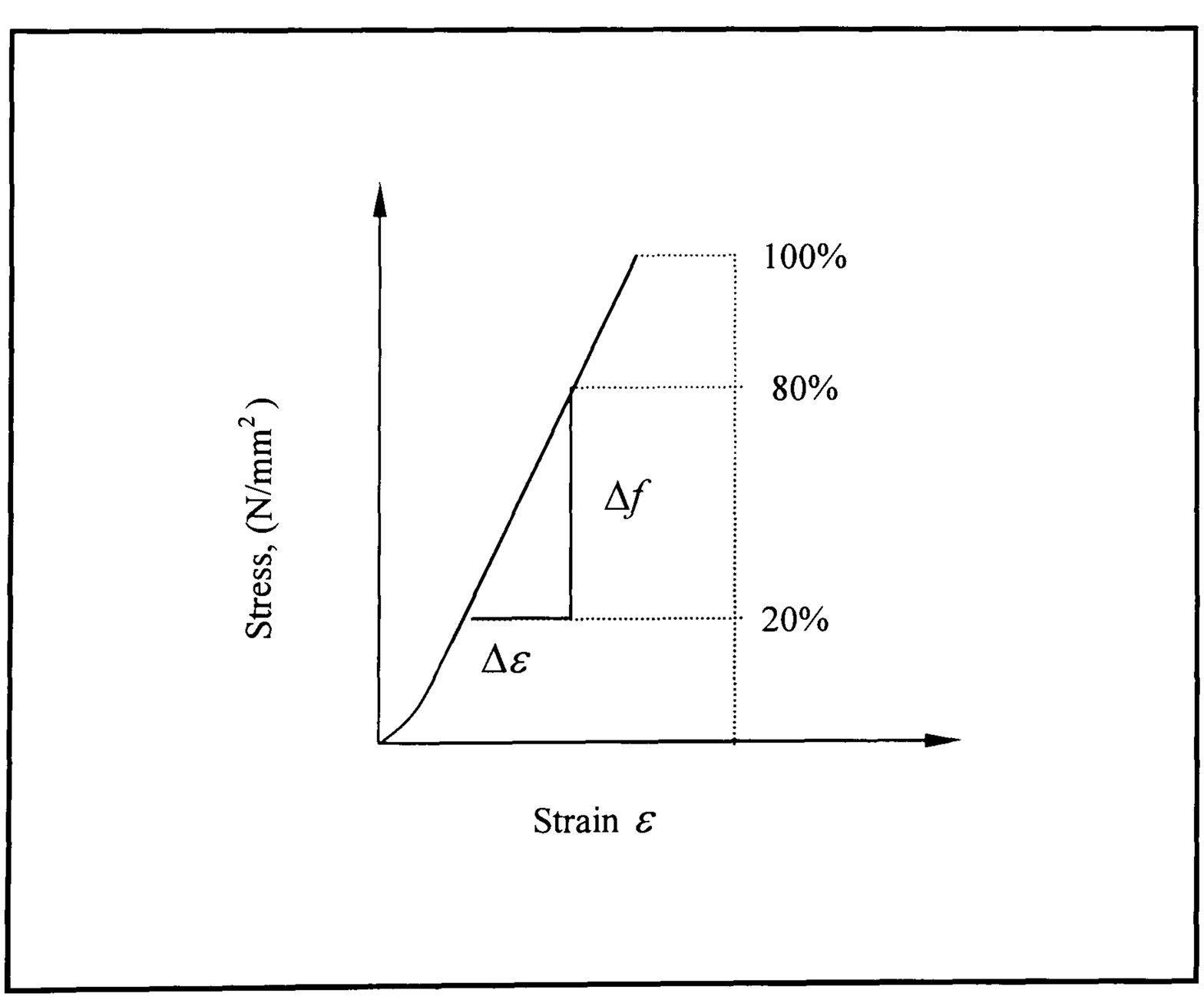

Figure 3.4: Method used to calculate elasticity modulus and tensile strength of the composite coupons

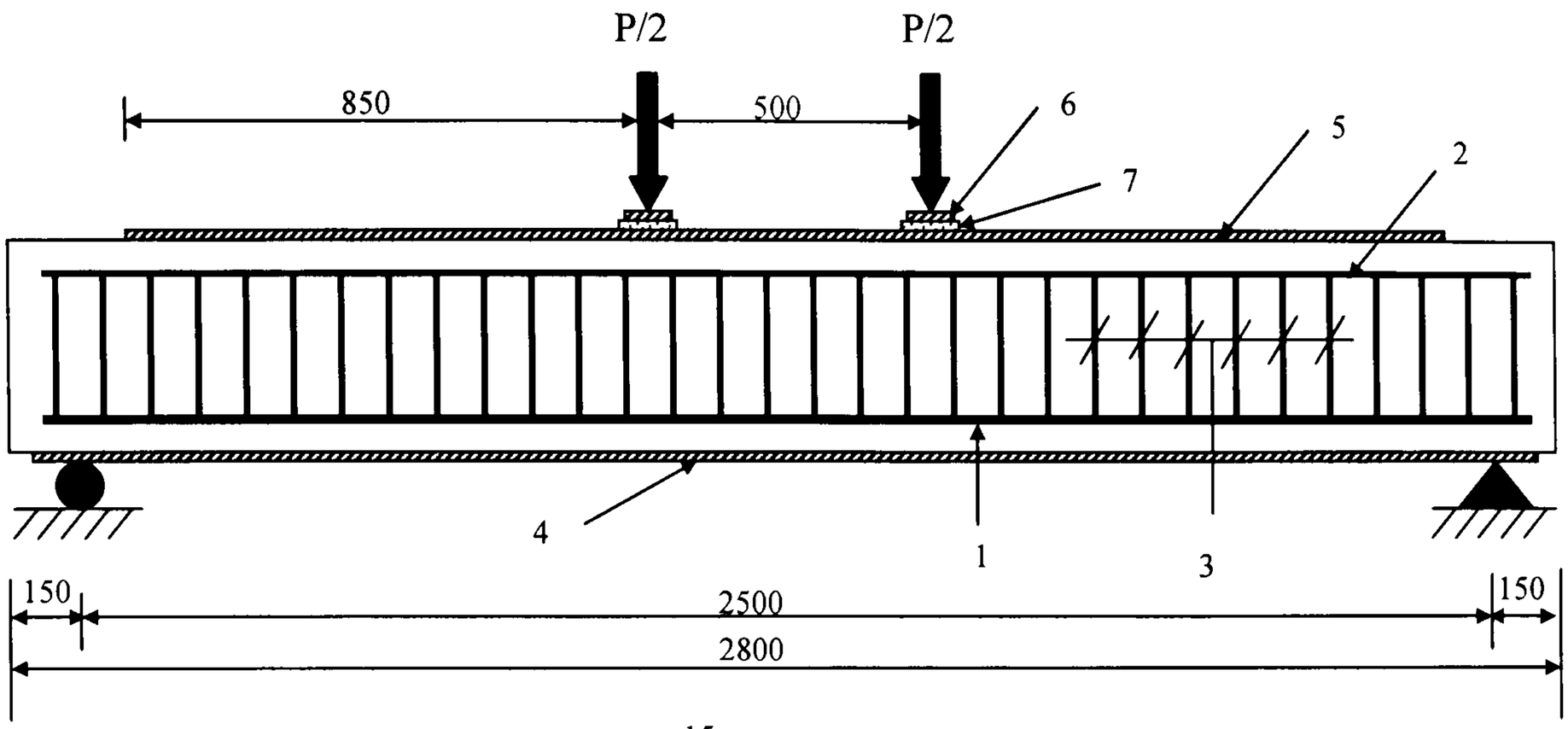

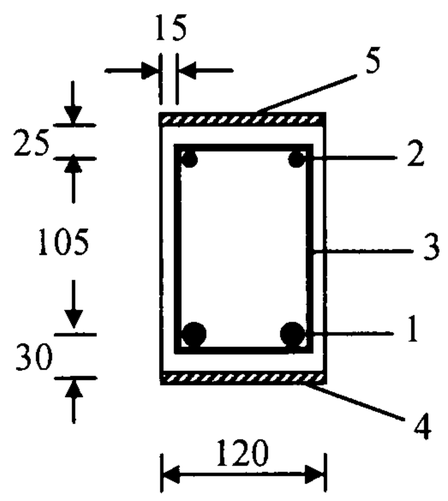

All dimensions are in mm

1:2 bars 16 mm diameter, tensile steel reinforcement

2: 2 bars 6 mm diameter, compression steel reinforcement

3: 2 bars 6mm diameter each 50 mm spacing vertical steel links

4: 6- CFRP tensile laminates, 120 mm width

5: 10- CFRP compression laminates, 120 mm width and 2200 mm length

6:150 mm x 60 mm x 20 mm solid steel plate

7:150 mm x 80 mm x 6 mm rubber pad

Figure 3.5: Test set-up for four points bending, III6-OL-TC; layout of the steel and CFRP laminates reinforcements.

I21-UL-UN, unstrengthened beam

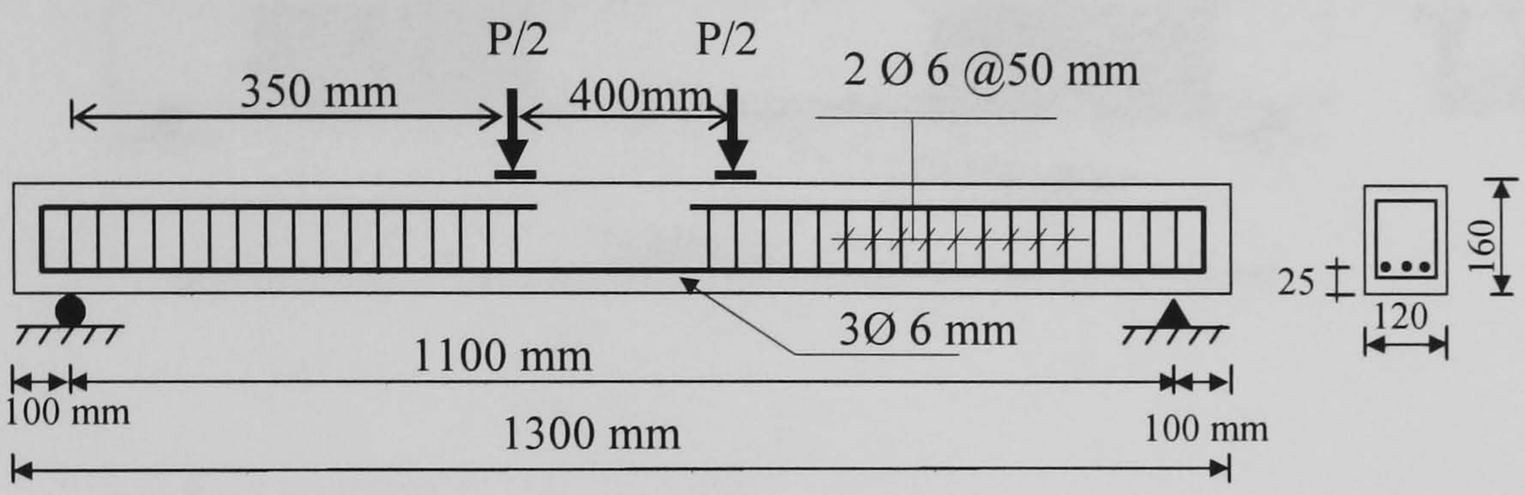

Beam I22-UL-T

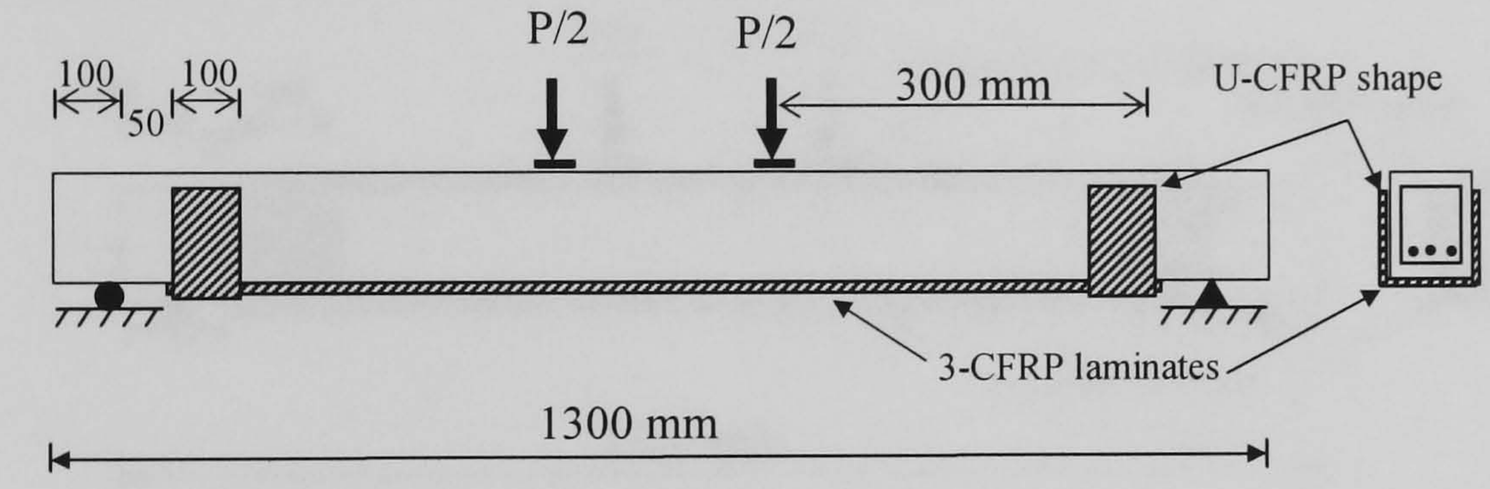

Beam I25-UL-TC

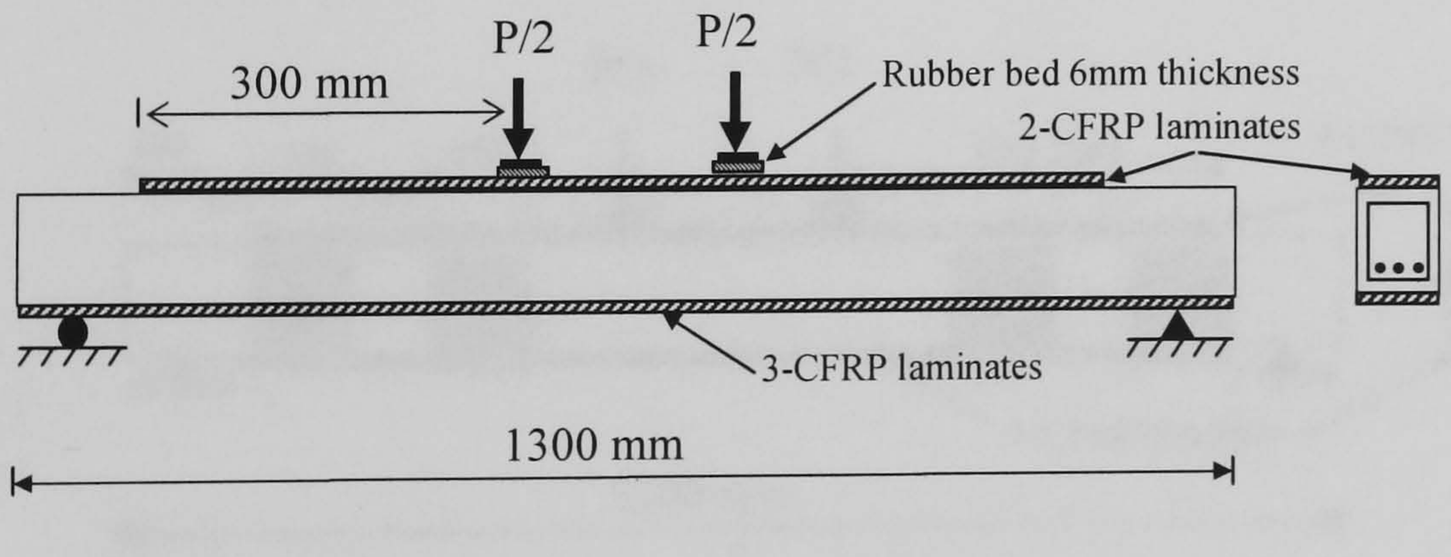

Figure 3.6: Beam descriptions of series-I

Beam II1-UH-T

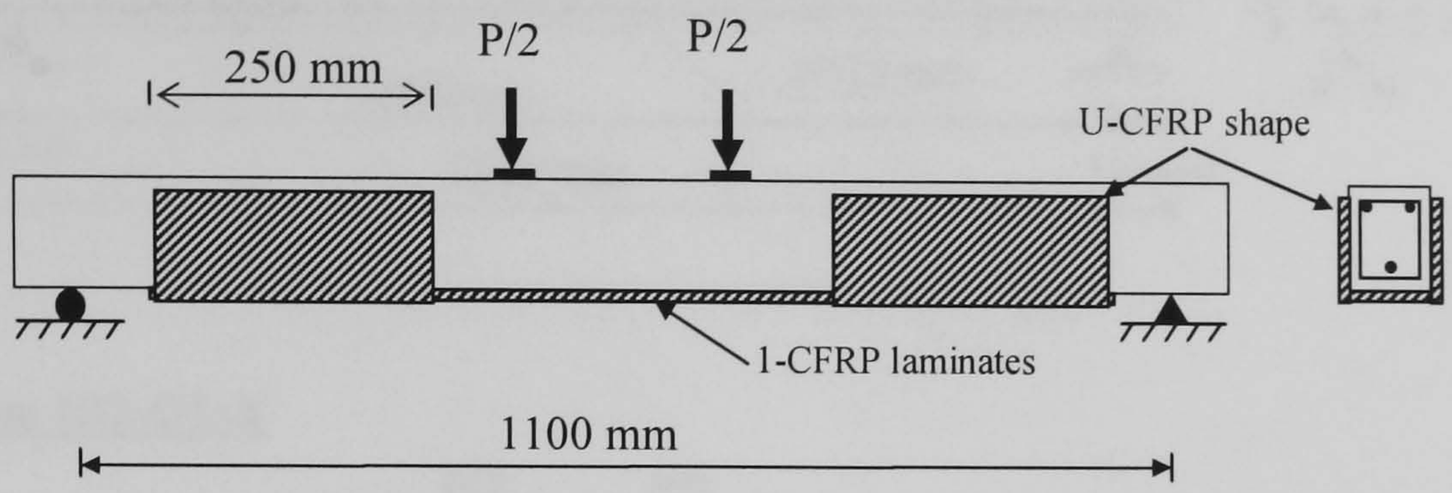

Beam II2-UH-TC

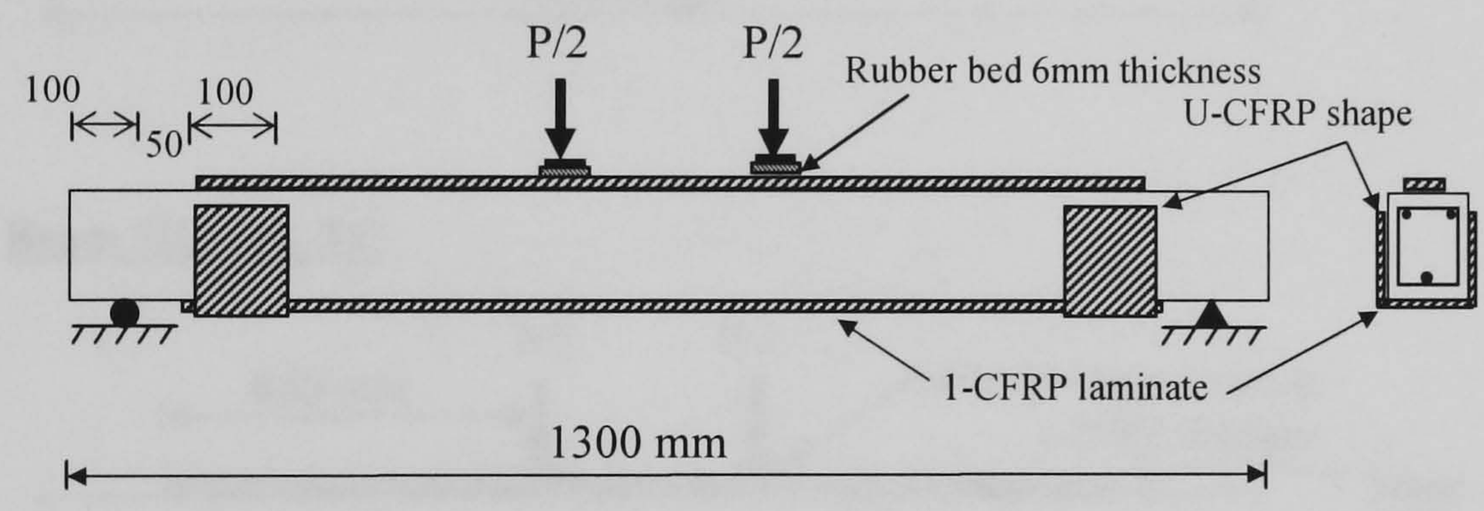

Beam II3-UH-TC

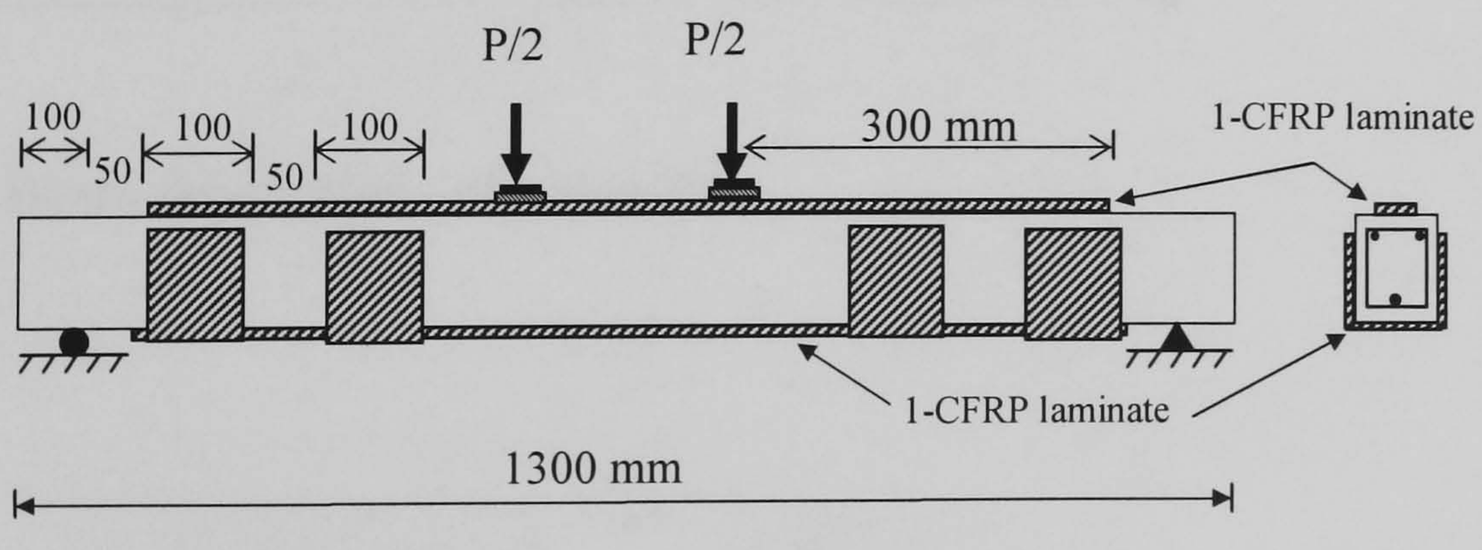

Figure 3.7: Beam descriptions of series-II

III1-OL-UN, unstrengthened beam

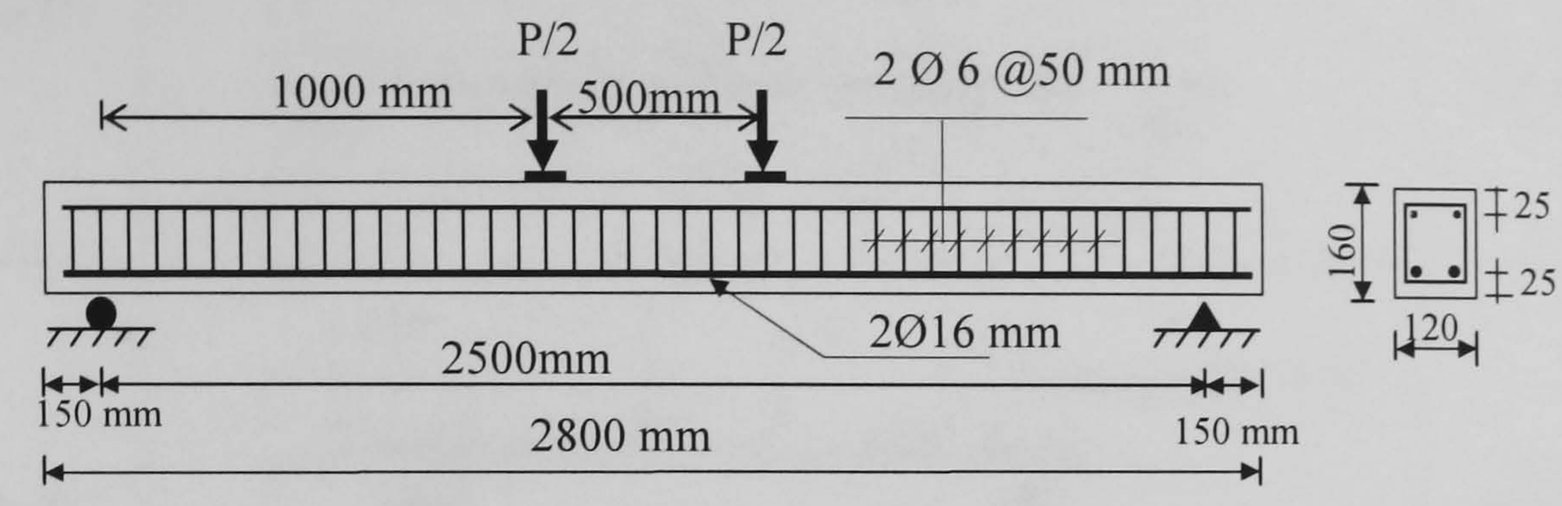

Beam III2-OL-T

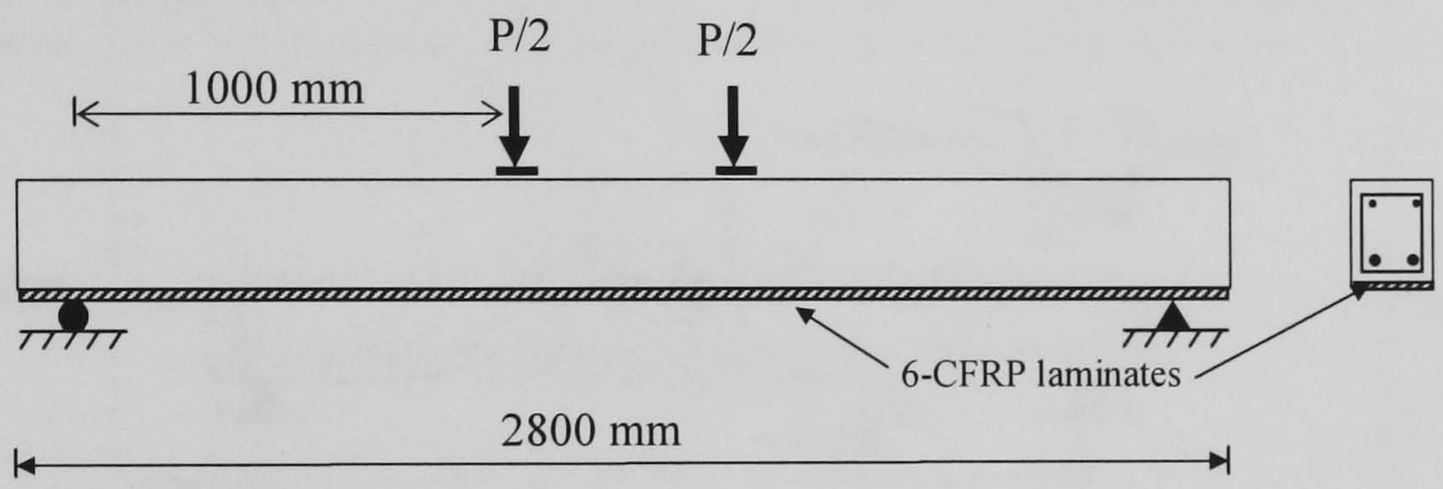

Beam III3-OL-TC

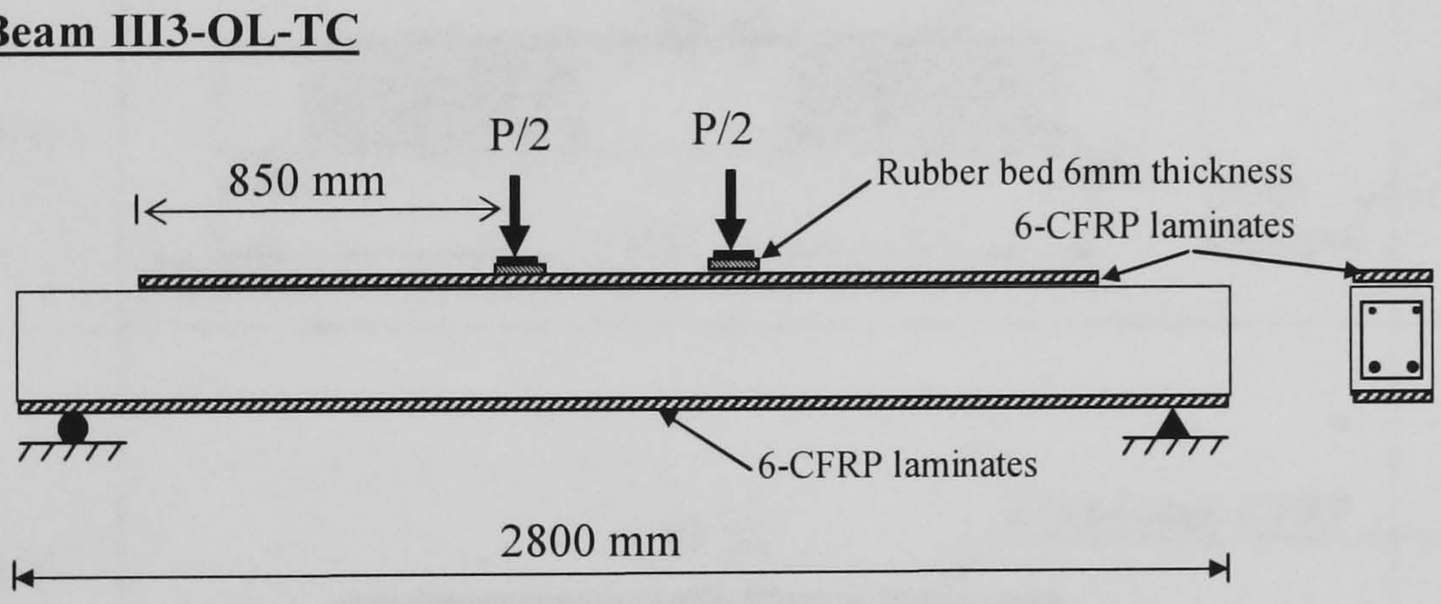

Figure 3.8: Beam descriptions of series-III

Beam no.	Beam Details	
IV11-OL-TC	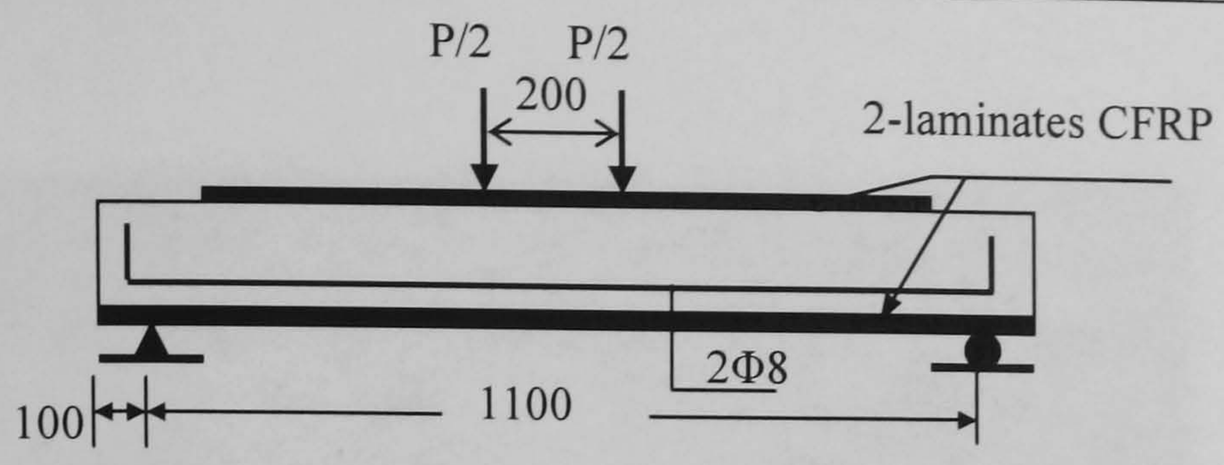	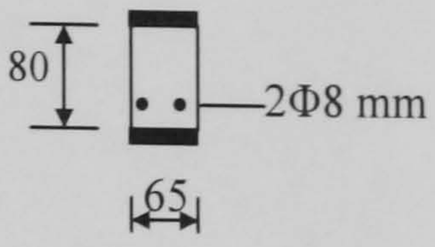
IV12-OL-TC	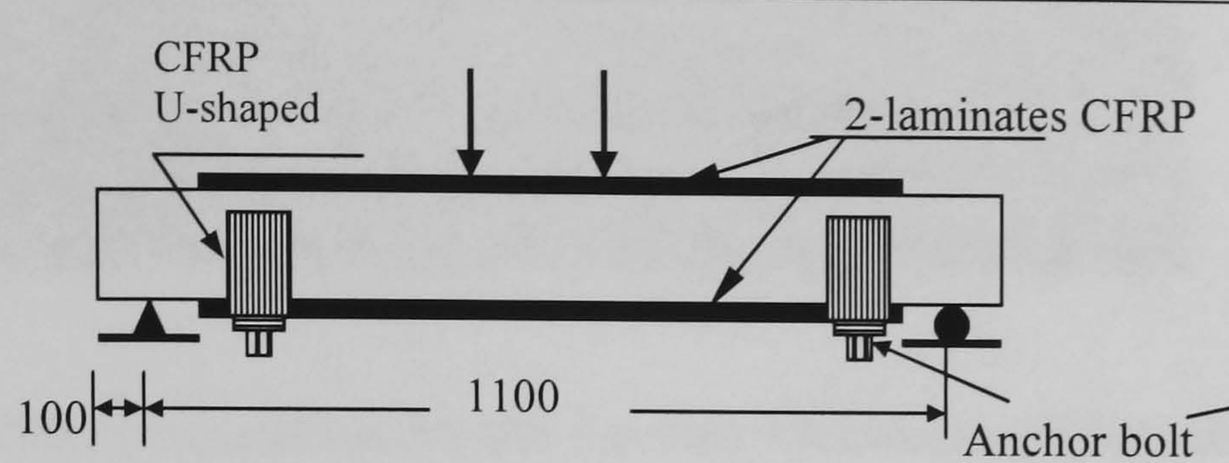	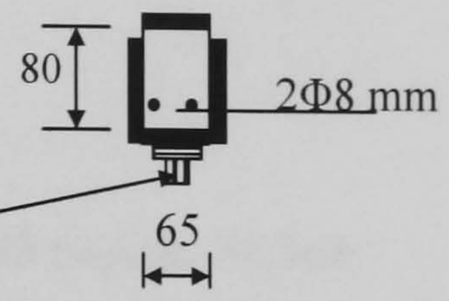
IV21-OH-UN	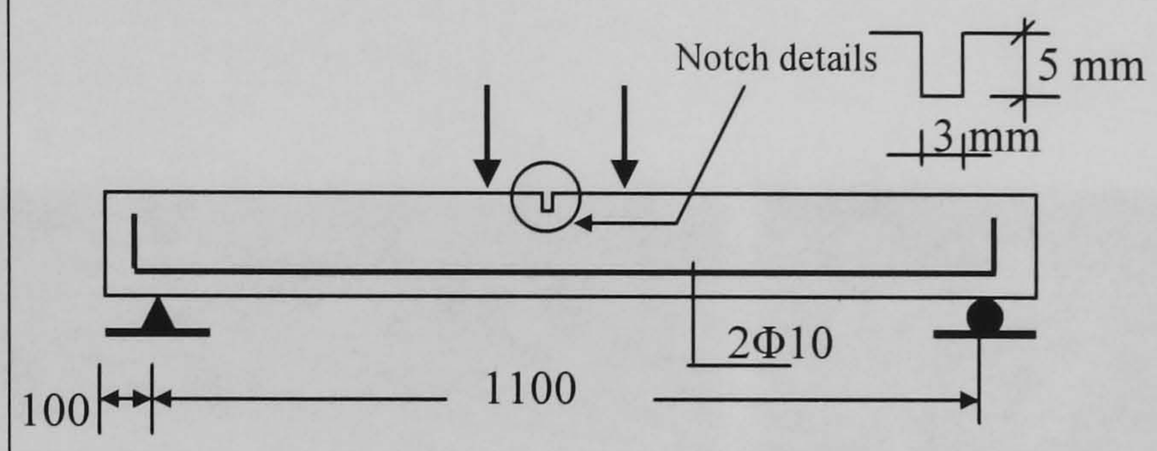	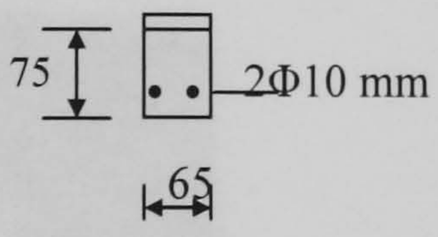
IV22-OH-C	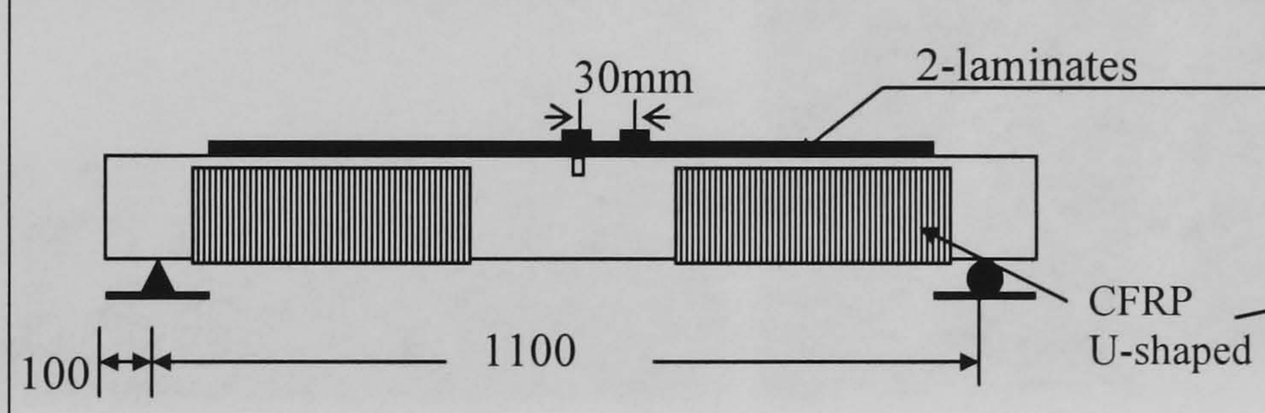	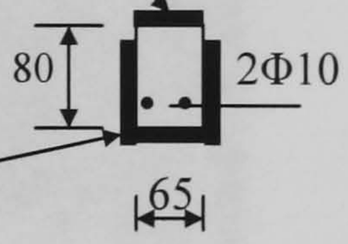
IV23-OH-C	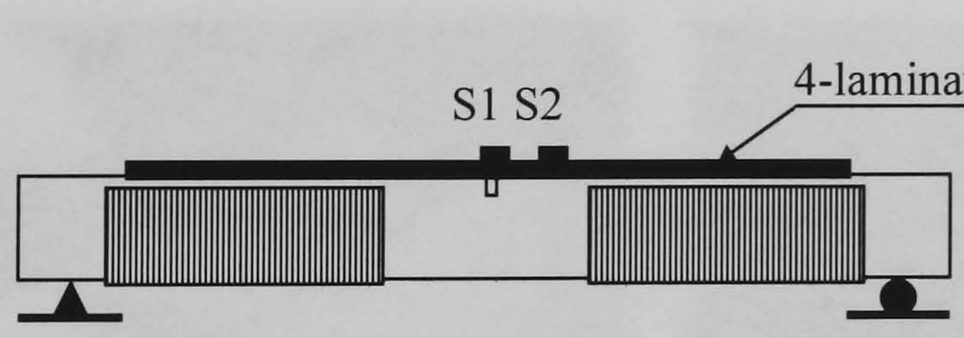	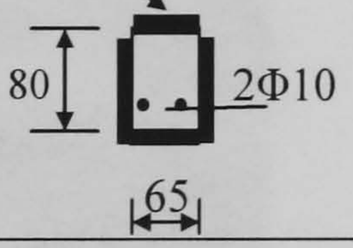
IV24-OH-C	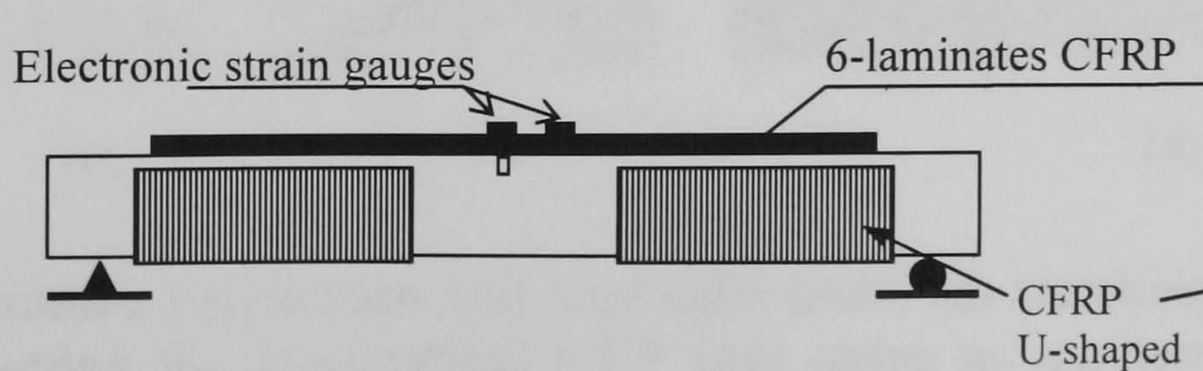	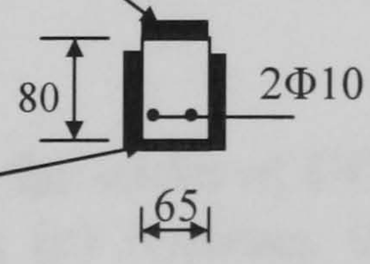

All dimensions in mm

Figure 3.9: Internal reinforcement and strengthening scheme of CFRP for the beams of series-IV

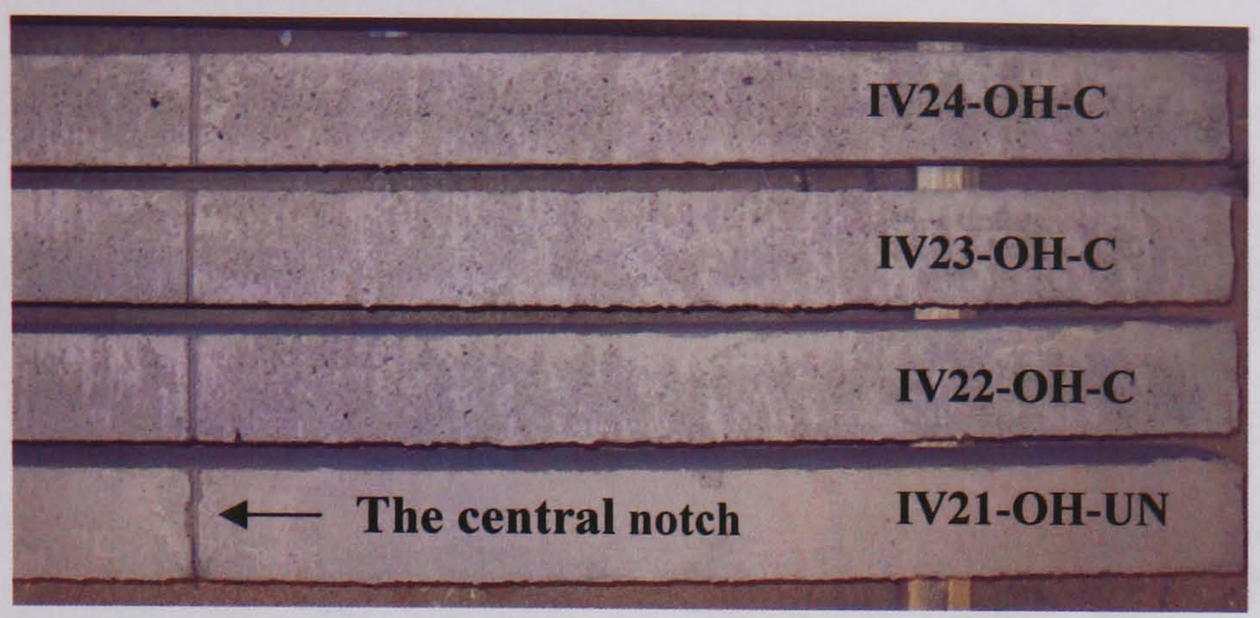

Figure 3.10: Surface preparation for the top face specimens of the second group; Series-IV

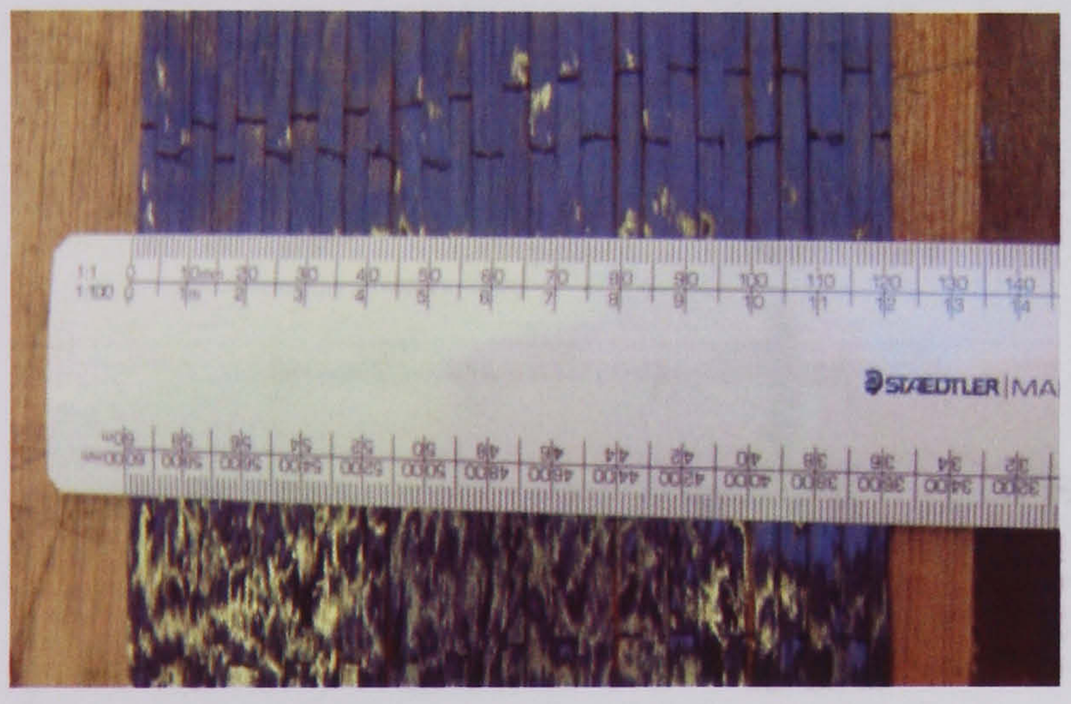

(a)

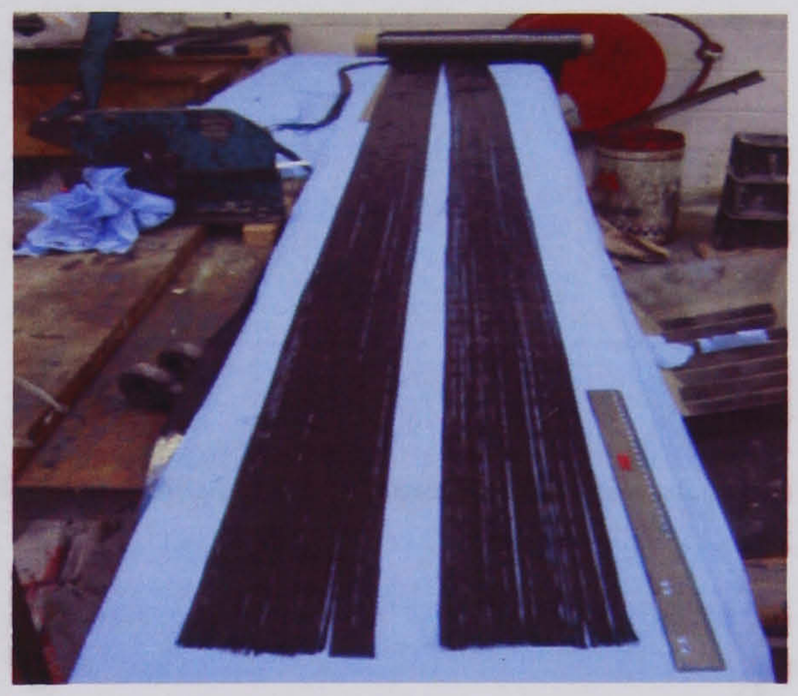

(b)

(c)

(d)

Figure 3.11: Specimen preparation and load cells units; (a) checking the width of UCF (UT-200); (b) cutting the longitudinal UCF into strips as required; (c) brushing the acetone on the concrete specimens immediately prior of applying epoxy resin and; (d) load cell held together with bolted steel frame and RDA-Transducer indicator E 308.

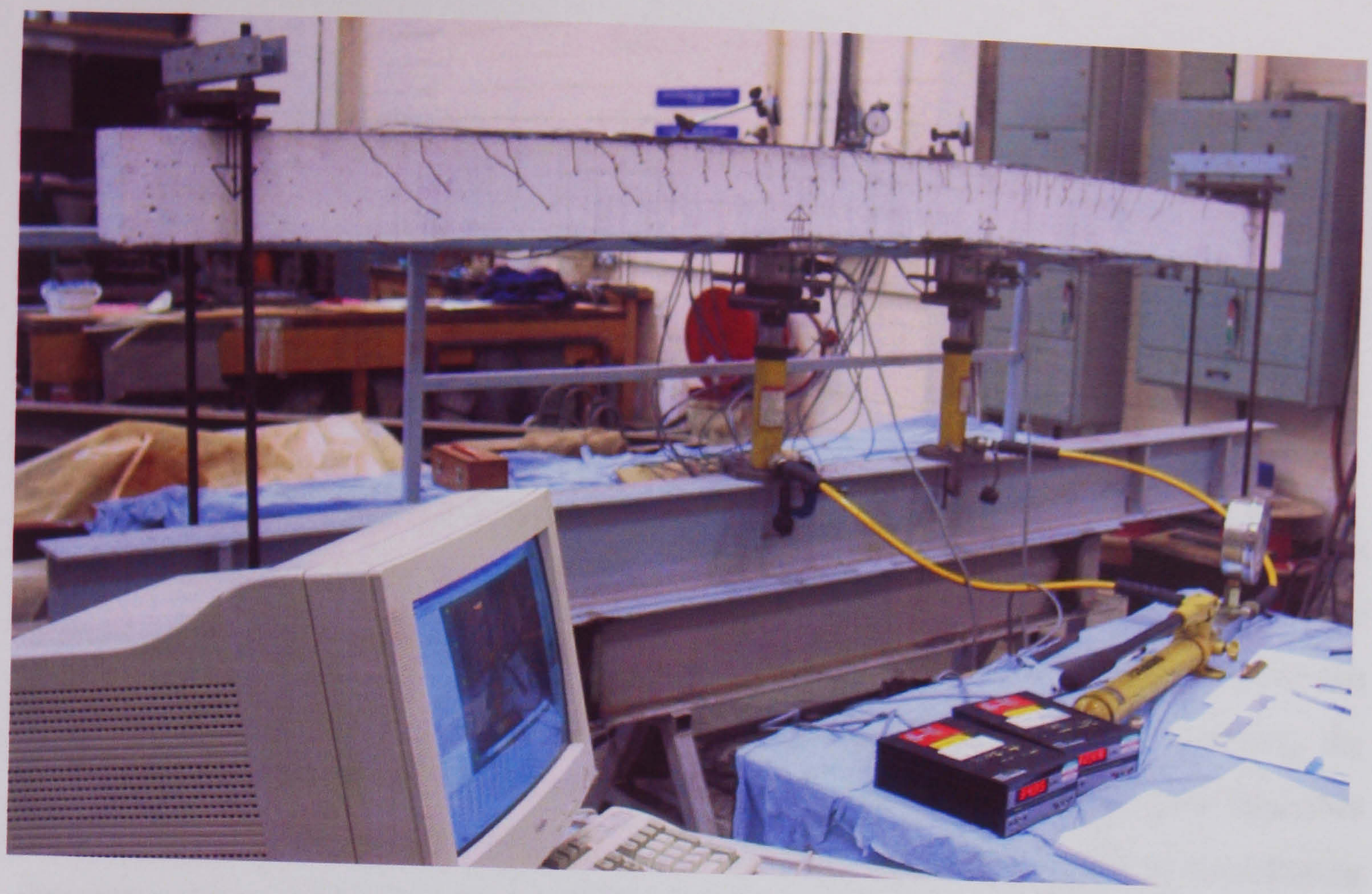

Figure 3.12: Test set-up for large beam of specimens of series-III, III6-OL-TC

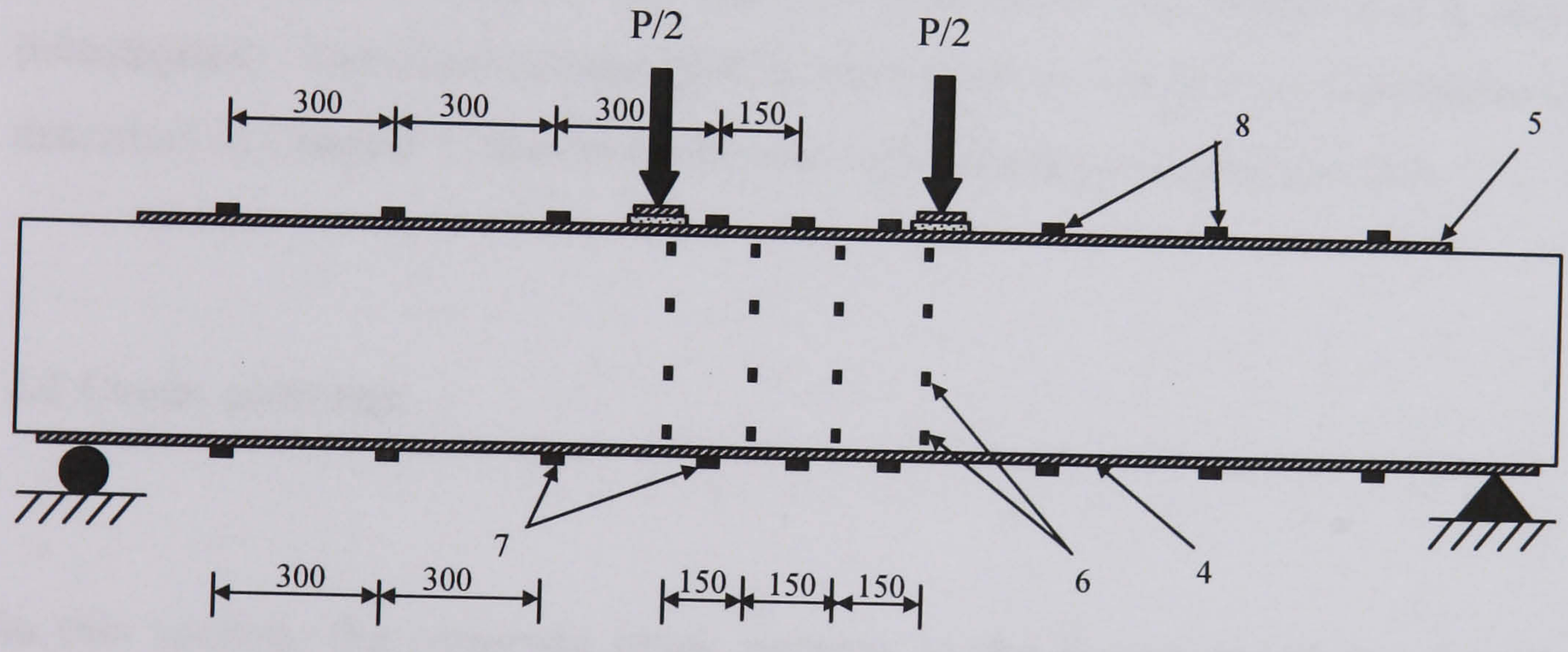

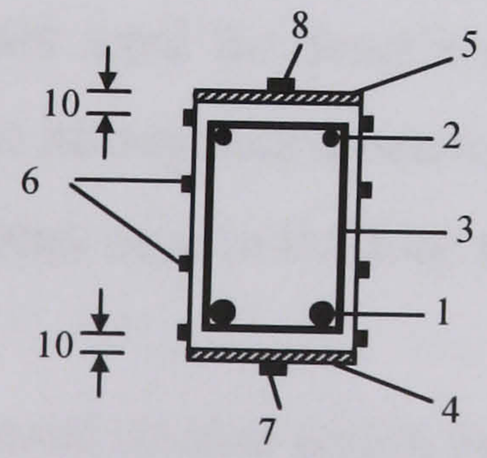

All dimensions are in mm

1. 2 bars 16 mm diameter, tensile steel reinforcement
2. 2 bars 6 mm diameter, compression steel reinforcement
3. 2 bars 6mm diameter each 50 mm spacing vertical steel links
4. 6- CFRP tensile laminates, 120 mm width
5. 10- CFRP compression laminates, 120 mm width and 2200 mm length
6. Demec buttons
7. electrical strains gauges are located on the tension CFRP laminate
8. electrical strains gauges are located on the compression CFRP laminate

Figure 3.13: Arrangement the strain gauges and demec buttons along III6-OL-TC beam

CHAPTER 4

EXPERIMENTAL RESULTS AND DISCUSSION

4.1 Introduction

The results of the experiments described in Chapter 3 are analysed and discussed in this Chapter. Several criteria have been investigated; in particular, the influence of the internal steel reinforcement ratio, the position of the external CFRP laminates on the beam (i.e. on the tension face, the compression face or both faces of the beam), the cross-sectional area of the CFRP laminates, and the beam scale. This Chapter describes crack patterns, failure modes, deflection and curvature responses, strains in the different elements of the section and the ductility for all the beams tests. In addition, the strength contribution obtained by adding the CFRP to the tension and compression faces of the beam, and the movement of the depth of the neutral axis as the load is increased are investigated. The experimental results were used to validate the numerical techniques described in Chapter 5, the comparisons of which are given in Chapter 6.

4.2 Crack patterns

In this section, the observed crack patterns in the beams tested are described. Two categories of specimens are used for describing the crack patterns. The categories are the unstrengthened and the strengthened beams. Due to the variation in the ratios of the tension steel in the specimens used in the four series tests, four cases are described:

1- An under-reinforced section which has a low steel ratio, less than 1%.

2- An under-reinforced section which has steel ratio between 1% and 2%.

3- An over-reinforced section which has a steel ratio between 2% and 3%.

4- An over-reinforced section which has a high steel ratio greater than 3%.

In all the tests the load corresponding to the first cracking observed was recorded. With hindsight it is unfortunate that the crack widths were not measured. Because of the

number of beams tested a selection of unstrengthened and strengthened specimens has been chosen to describe crack patterns at serviceability and at failure. The unstrengthened beams chosen were I11-UH-UN, I12-UH-UN, I21-UL-UN and III1-OL-UN while those strengthened on the tension face only were I22-UL-T and III2-OL-T. Those strengthened on both tension and compression faces were I25-UL-TC, III6-OL-TC and the second group of beams of series-IV.

Unstrengthened beams

In the unstrengthened beams, it was found that the load at which the first crack occurred varied, Table 4.1. This was in general related to the ratio of the tension steel in the section, to the variation of the section dimensions, and the span of the beams.

The three beams I11-UH-UN, I12-UH-UN and I21-UL-UN, which were reinforced with a low ratio of tensile steel reinforcement, exhibited flexural cracks. Cracks initiated from the tension face of the beam and propagated vertically towards the compression face, Figures 4.1, A.1a and A.1b, Appendix A. In each case close to the ultimate load, one of the flexural cracks between or under the point loads became a major crack; as the load was increased it propagated quickly towards the compression face and became wider, Figure 4.1.

In the over-reinforced beams, III1-OL-UN, Figure A.1c, Appendix A, and IV21-OH-UN, a large number of cracks developed along the beam spans. These cracks did not extend more than half of the beam depth before concrete crushing took place, as will be discussed in Section 4.3.3.

Strengthened beams

It was found that adding CFRP to the tension face of a beam increased the applied load required for the first crack to appear compared with the unstrengthened beam. Adding CFRP to both the tension and compression faces of a beam also increased the applied load required for the first crack to appear compared with the beams strengthened on the tension face only. The first crack in beams I22-UL-T and III2-OL-T, which were strengthened on the tension face, occurred when the load was approximately twice that of the unstrengthened beams, I21-UL-UN and III1-OL-UN, Table 4.1. However, in I25-UL-TC and III6-OL-TC, which were strengthened on both the tension and compression faces, the first crack occurred when the applied load was 1.34 and 1.17 respectively, times that of the beams strengthened on the tension face only, I22-UL-T and III2-OL-T, Table 4.1.

When the load at which the first crack appeared was compared with the ultimate load for the beams strengthened on the tension face only, two trends were found. In the strengthened beams which had a low ratio of tensile steel, i.e. I22-UL-T, the first crack load to the ultimate load ratio decreased, compared with the unstrengthened I21-UL-UN, while the opposite behaviour was found with beams that have a high ratio of tension steel, III2-OL-T, when compared with the unstrengthened beam III1-OL-UN. For example, the ratio of load at first crack to the ultimate load was 0.21 and 0.3 in the strengthened beam I22-UL-T and in the unstrengthened beam I21-UL-UN respectively. However, the strengthened beam failed by end-laminate peeling. Conversely, in the beams which had a high ratio of tension steel reinforcement, the first crack load to the ultimate load ratio was 0.24 and 0.13 respectively, in the strengthened beam III2-OL-T and the unstrengthened beam, III1-OL-UN, Table 4.1.

Similar behaviour was observed when the CFRP was added to the tension and compression faces of beam I25-UL-TC, which had a low ratio of tension steel. However, beam III6-OL-TC, which had a high ratio of tension steel and was strengthened in tension and compression, exhibited a lower crack load to ultimate load ratio than beam III2-OL-T, which was strengthened on the tension face only.

Adding CFRP only to the compression face of an over-reinforced beam which had a high area of tension steel, 4.4%, (i.e. the second group of beams of series-IV) the beams exhibited little change in the loads applied at which the first cracks appeared when compared with the unstrengthened beams.

The above confirms that strengthening of a reinforced concrete beam with CFRP delays the formation of the first crack. However, when the ratio of the first crack load to the ultimate load for the strengthened and unstrengthened specimens was compared, variable behaviour was found. This is because the increase in the flexural strength of the under-reinforced strengthened beam is higher than that of the over-reinforced strengthened beam.

It was also found that more shear and/or flexural-shear cracks occurred in the strengthened beams of the second group of series-I which had a small shear span to depth ratio, Figure A.1d, Appendix A.

4.3 Failure modes

Six failure modes were observed in the tests and these are described below. The failure mode for each of the beams tested in the current investigation is given in Table 4.2.

4.3.1 Steel yielding and FRP rupture

Steel yielding

This was a ductile flexural failure mode initiated by yielding of the tensile steel reinforcement at the mid-span of the beam. The yielding of the steel was followed by the concrete crushing in the constant moment area or under the load positions. This mode of failure occurred in unstrengthened beams with low tensile steel reinforcement ratios. Steel yielding was observed for unstrengthened beams, I11-UH-UN, I12-UH-UN and I21-UL-UN, Figures 4.1, A.1a and A.1b, Appendix A.

FRP rupture

Beam II1-UH-T, Figure 4.2, was strengthened on the tension face and designed to fail in concrete crushing. Because the spacing between the stirrups was relatively large U-shaped CFRP confinements had been added to cover approximately the whole shear span. This was to inhibit shear failure.

In the test, at 83 % of the failure load, a partial debonding at the ends of the U-shaped confinements from the concrete surface occurred, Figure 4.3. It was observed also that the CFRP failed by rupture at mid-span with a load close to the balanced load of the strengthened section. This failure was brittle and explosive and was accompanied by a loud noise.

4.3.2 Shear failure

Shear failure was associated with a major diagonal crack initiating from the tension face, near to the support, which propagated towards one of the point loads on the compression face. Shear failure was observed in II2-UH-TC with the crack occurring at 200 mm from the external support, Figure 4.4.

The beams of series-II were designed to fail by concrete crushing rather than in shear. The area of stirrups was higher than required for the increase in strength but the spacing between the stirrups was relatively large. U-shaped CFRP confinements with 120 mm width each were applied to the laminate ends to prevent peeling failure and to enhance the shear strength. Beam II2-UH-TC was the first of those tested in series-II. However, the CFRP confinement width was not sufficient to prevent the propagation of the inclined crack. Visual inspections, as the load increments were increased, showed that once shear cracks became wide at the concrete adjacent the CFRP on the tension face of the beam, the debonding of the CFRP laminate was hastened.

4.3.3 Concrete crushing

Failure due to concrete crushing occurred in both unstrengthened and strengthened over-reinforced beams. Adding CFRP to the tension face of an under-reinforced beam may also cause this failure to occur. This mode of failure is characterised by concrete crushing at the compression face of the beam at the mid-span.

Unstrengthened beams

Concrete crushing in unstrengthened beams was observed in the beams, III1-OL-UN, III4-OL-UN, I13-OL-UN and IV21-OH-UN. Normally, concrete crushing failure occurred somewhere in the middle section of the beam where the bending moment was constant.

Figure 4.5 shows a typical failure at the mid-span of the unstrengthened beam III1-OL-UN, in which concrete crushing was observed in the extreme compression fibre of the concrete beam before steel yielding.

Strengthened beams

As described in Section 3.4.3, three strengthening schemes were utilised: 1) adding CFRP laminates to the tension face of a beam; 2) adding CFRP laminates to both the tension and compression faces and 3) adding CFRP laminates to the compression face of a beam. However, none of the beams strengthened by adding CFRP to the compression face only, failed by concrete crushing.

Concrete crushing failure was observed in the over-reinforced beams which were strengthened on the tension face, for example, III2-OL-T, III5-OL-T of series-III. In

beam III2-OL-T, the failure zone occurred at the same location as that in the unstrengthened beam, III1-OL-UN, and exhibited approximately the same number of cracks along the beam span.

Concrete crushing was also observed in the over-reinforced beams strengthened on both the tension and compression faces, IV11-OL-TC and IV12-OL-TC, Figure 4.6. Concrete crushing failure was also observed in the under-reinforced beams strengthened on both the tension and compression faces, I25-UL-TC and II3-UH-TC.

In beams I25-UL-TC and II3-UH-TC, concrete crushing commenced at 97 % and 89% of the failure loads, respectively. Crushing always commenced just before the ultimate load was reached. At failure of the two beams, concrete crushing was followed by debonding of the CFRP from the beam tension face, Figures 4.7 and 4.8. In beam II3-UH-TC, tearing of the CFRP confinements at the laminate ends occurred, as will be discussed in Section 4.3.5. A loud noise due to debonding of the CFRP laminate or tearing of the CFRP confinements was heard at failure of the two beams.

It can be concluded that the concrete crushing mode in a beam strengthened in tension only is similar to that of an unstrengthened beam. However, in some beams the concrete crushing was followed with the debonding of the tension CFRP.

4.3.4 End-laminate peeling

End-laminate peeling was initiated by crack propagation from the end of the tension CFRP laminate to the steel reinforcement level leading to debonding of the concrete cover. This failure mode occurred in strengthened beams I22-UL-T and I23-UL-TC, but the crack patterns which caused the failure of the CFRP laminates were not seen because CFRP confinements, at the end of the laminates of the tension, were applied, Figure 4.9. Failure was brittle and explosive and was associated with a sudden

debonding of the CFRP confinements. The load noise which occurred at failure may be attributed to the debonding of the CFRP confinements from the beam sides.

The final failure occurred at 81 % and 68 % respectively of the predicted failure loads for beams I22-UL-T and I23-UL-TC. The predicted failure load was obtained, using the method given in Chapter 6, for each of the beams, which assumes that the failure occurred due to concrete crushing.

After failure, it was observed that cracks had developed at the end of the tension laminate and had propagated horizontally underneath the CFRP confinement leading to splitting of the concrete along the level of the tension steel in both beams, Figure 4.9.

To explain the development of cracks in the beams, I22-UL-T and I23-UL-TC, which finally caused the failure, Figure 4.9 is shown. The failure in the two beams was initiated by causing transverse cracks at the laminate ends at load 28.86kN and 30.31kN, respectively. As the applied load was increased further, the cracks increased in width. These cracks induced longitudinal cracks that propagated from the laminate end towards the beam midspan causing splitting of the concrete at the reinforcement level, Figure 4.10.

At the laminate ends, a high stress concentration is produced because of the abrupt termination of the laminate. So, the crack initiates at the laminate end and propagates to the level of the steel reinforcement. The tensile force released by the cracked concrete is transferred to the steel reinforcement. As a result, high local bond stresses between the steel reinforcement and concrete are induced near the crack. As the applied load is increased further, the tensile stresses in the steel reinforcement, and hence the bond stresses between the steel and the concrete near the crack also increase. When the bond fails at the crack tip, the crack propagates horizontally at the level of the steel reinforcement. End-laminate peeling can be prevented if anchorage techniques, such as CFRP confinements and anchor bolts, are utilized.

4.3.5 Debonding of CFRP failure

Debonding failure is a failure mode which can occur anywhere along the span of a beam strengthened with the CFRP. With CFRP laminate applied to the tension face of the beam, debonding failure may be initiated at a flexural or a flexural-shear crack. These cracks occur away from the laminate ends and propagate longitudinally towards one of the ends. Debonding failure occurred at the tension face of beam I24-UL-TC. Flexural cracks at the mid-span occurred at 38% of the failure load. Flexure-shear cracks occurred in the shear spans at 65% of the failure load. With further increases in load more cracks occurred and the existing cracks became wider. Finally, debonding of the CFRP laminates from the concrete surface occurred, Figure 4.11. Failure was accompanied by a loud noise. It was found the presence of flexure and flexure-shear cracks in the concrete adjacent to the CFRP tended to reduce the composite action and consequently affected the mechanism of failure.

When CFRP confinements at each end of beam II3-UH-TC were used, debonding of the laminate at the ends was delayed, Figure 4.12. Failure occurred because of concrete crushing. At failure, one of the CFRP confinements ruptured and caused a complete debonding of the CFRP laminates, Figure 4.12a. This may suggest that a number of cracks in the concrete adjacent to the CFRP interrupt the bond between the concrete and the CFRP.

4.3.6 Buckling of the CFRP

In this section the mechanism of buckling of the CFRP on the compression face of the beam, which has not been studied previously, is investigated.

Buckling of the CFRP at the mid-spans of the beams was observed at failure in some tests. When the thickness of the CFRP was small, e.g. beams I24-UL-TC and IV22-OH, buckling appeared to be initiated by longitudinal cracking of the concrete at the

concrete-adhesive layer. However, a sudden buckling was observed to occur when the thickness of the CFRP was increased, e.g. beams III3-OL-TC, III6-OL-TC, IV23-OH-C and IV24-OH-C. A typical buckling failure of a CFRP laminate is shown in Figure 4.13. The length of the buckle, after buckling of the CFRP, was measured. It was noted that the compression strain at the level of the CFRP in the beams at failure varied between 0.0026 and 0.0032, Table 4.4.

Given the strain in the CFRP laminate at failure measured in the test, Table 4.4, the modulus of elasticity of the CFRP, E_{fc}, Section 3.3.3, and the cross-section area of the laminates the failure load, P_b, was determined. The length of the buckled CFRP, assuming pinned ends and elastic behaviour was calculated using the following formulae derived from the formulae for the Euler's load

$$L = \sqrt{\frac{\pi^2 E_{fc} I_{fc}}{P_b}} \tag{4-1}$$

where L is the buckling length and I_{fc} is the moment of inertia of the CFRP.

The length was also calculated assuming fixed ends, to take the account of the bonding of the epoxy to the concrete surface, as:

$$L = 2\sqrt{\frac{\pi^2 E_{fc} I_{fc}}{P_b}} \tag{4-2}$$

The lengths obtained from equations 4-1 and 4-2 are shown in Figure 4.14.

Figure 4.14 compares the calculated and the measured buckled lengths of the CFRP for beams that failed by buckling of the CFRP. A better correlation between the measured and calculated buckling lengths was achieved with the fixed ended boundary condition than with the pin ended. When a small thickness, 0.8 mm, of CFRP was used, good

agreement between the measured and the calculated buckled lengths was achieved. Using a relatively thick CFRP, 4 mm, the measured buckled lengths were longer than the calculated ones, Figure 4.14. Further experimental work is required to show the effect of using a high ratio of CFRP with different mechanical properties, to test whether the measured buckled length will change. The use of either greater thickness of CFRP or with different material properties could delay the buckling failure.

4.4 Load-deflection and beam-stiffness relationships

Figures 4.15 to 4.18 show the relationship between the load and the mid-span deflection for beams of series I, II, III and IV respectively. The deflections and the loads for all beams at the onset of cracking, steel yielding and at ultimate load are recorded in Table 4.1. The deflection when the steel yields was assessed from the load-deflection curve.

At the early stages of loading, before the onset of the concrete cracking, all the strengthened beams in each of the series of I, II and III exhibited approximately similar deflections for a given load. After cracking, the beams strengthened on the tension faces exhibited smaller mid-span deflections, and thus higher stiffness than the corresponding unstrengthened beams at the same load level. Adding CFRP to the tension and compression faces of a beam with a similar amount of reinforcement decreased the mid-span deflection and also increased the stiffness at the same load level when compared with those strengthened in tension only.

Adding CFRP laminates to the tension face of the under-reinforced beam which had a low ratio of tension steel, I22-UL-T, increased both the yield load and the corresponding mid-span deflection compared with the unstrengthened, beam I21-UL-UN, Figure 4.15. However, no significant increase in the deflection was recorded in the over-reinforced beam III5-OL-T compared with the unstrengthened beam III4-OL-UN, Figure 4.17. The strengthened beams I22-UL-T and III5-OL-T each exhibited higher stiffness than the unstrengthened beams. The improvement in stiffness is due to adding the CFRP to the tension faces of the beams.

Adding CFRP laminates to the tension and compression faces of the under-reinforced beam which had a low ratio of tension steel, I25-UL-TC and III6-OL-TC. also decreased the mid-span deflections and increased the stiffness at the same load level compared with those strengthened in tension only, Figures 4.15 and 4.17. Beams I23-UL-TC, I24-UL-TC and I25-UL-TC, which had the same amount of CFRP applied to the compression face, showed very similar stiffnesses up to yielding of the tensile steel reinforcement, Figure 4.15.

The beams of series-II exhibited similar deflection values at similar loads up to the ultimate load, Figure 4.16. Beams of this series were strengthened with the same ratio of CFRP on the tension face, 0.31%. A CFRP ratio of 0.13% was used on the compression faces of those beams strengthened in compression. The compression CFRP appeared to make no difference to the stiffness of the beams. This is because the ratios of CFRP used on the compression were relatively small.

The test results though shown in Figure 4.17 indicated that increasing the ratio of CFRP on the compression face of an over-reinforced beam, i.e. beam III6-OL-TC, increased the beam stiffness compared to those with a lower ratio of CFRP, beam III3-OL-TC.

As shown in Figure 4.18, increasing the ratio of CFRP on the compression face of an over-reinforced beam which has a high tension steel ratio decreased the mid-span deflection for the same value of load. In other words, the stiffnesses of these beams at the load level, when the CFRP on the compression face increased, were increased.

4.5 Moment-curvature relationships

Figures 4.19 to 4.22 show the relationship between the applied moment and mid-span curvature for the beams of series I, II, III and IV respectively. The mid-span curvature was calculated from the measured tension and compression strains.

All beams of series-II exhibited similar moment-curvature relationships because the CFRP ratio used was similar, Figure 4.20. Adding CFRP to the tension and compression faces of the beams of series III and IV, Figures 4.21 and 4.22, lead to larger moments compared with those beams which were unstrengthened or strengthened on the tension face only. At similar moment levels the curvature, in the beams which were strengthened on the tension and compression faces, was lower than that on the beams strengthened on the tension face only.

However, at the failure point of the beams which were strengthened on the compression faces the final curvature value was controlled by the buckling failure of the CFRP. When the CFRP buckled in beam III6-OL-TC, which had a CFRP ratio of 2.82%, a higher moment capacity and curvature were exhibited compared with beam III3-OL-TC, which had a CFRP ratio of 1.71%, Figure 4.21. The increase in the curvature in beam III6-OL-TC was due to the yielding of the tensile steel.

4.6 Flexural strength enhancement

To assess the effect of adding CFRP to the beam faces on the flexural strength, the increase in the strength of the strengthened beam compared to an unstrengthened is expressed by the ultimate load enhancement ratio, η_1, defined as the ratio of the ultimate load of a strengthened beam to that of the corresponding unstrengthened beam. Additionally, for a beam strengthened on both the tension and the compression face a further enhancement ratio is given by η_2, which is defined as the load obtained from the strengthened beam divided by the beam strengthened in tension. Table 4.3 presents the ultimate loads and the load enhancement ratios η_1 and η_2 for all of the beams tested.

Table 4.3 shows that adding the CFRP to the tension and compression faces of a beam is an effective technique for strengthening purposes. Adding the CFRP to the tension face of an under-reinforced beam which has a low tension steel ratio achieved a high load enhancement ratio: e.g. for I22-UL-T η_1 was 3.5; however, the over-reinforced beam achieved only a relatively low enhancement: for example for III2-OL-T was

η_1=1.12. The enhancement in the strengthened under-reinforced beams noted here is similar to previous observations [64, 70, 84]. It was also observed [38] that adding a high ratio of CFRP or GFRP on to the tension face of over-reinforced beams achieved a small increase in the flexural strength compared with the unstrengthened beams.

Beams III2-OL-T and III5-OL-T which were strengthened on the tension face and had the same reinforcement ratios; however, the concrete strength was 10% higher in beam III5-OL-T, Table 3.4, had ultimate enhancement ratios, η_1, of 1.12 and 1.35 respectively, Figure 4.21.

When the CFRP was applied to the compression face of beams which had similar amounts of steel reinforcement and CFRP on the tension faces, a significant increase in the ultimate load enhancement ratio was achieved when compared with the unstrengthened beams. However, a small increase in the ultimate load enhancement ratio was achieved when compared with beams strengthened on the tension face only. For instance, beams I25-UL-TC and III3-OL-TC achieved an ultimate load enhancement ratio, η_1, of 4.12 and 1.28 respectively compared with unstrengthened beams, I21-UL-UN and III1-OL-UN. However, an ultimate load enhancement ratio, η_2, of 1.15 and 1.17 for the same beams respectively was obtained when compared with beams strengthened on the tension face only, I22-UL-T and III2-OL-T.

Adding a ratio of 2.82% of CFRP to the compression face of the over-reinforced beam III6-OL-TC increased the ultimate load enhancement ratio, η_1, to 1.55 compared with the unstrengthened beam III1-OL-UN. For the same beam the ultimate load enhancement ratio, η_2, was 1.40 compared with the beam III2-OL-T, which was strengthened in the tension face only. Even in the case when the CFRP was applied to the compression face of an over-reinforced beam IV24-OH-C, which had a high tension steel ratio, the ultimate load enhancement ratio, η_1, at failure was 1.30, Table 4.3. This beam was not strengthened on the tension face. From test observations, it is clear that the flexural strength of an over-reinforced beam strengthened on the compression face can be improved by increasing the amount of CFRP.

In conclusion, the use of CFRP on the tension face enhanced the load capacity of an under-reinforced section more than that of the over-reinforced section. However, the use of CFRP on the compression face of an over-reinforced section enhanced the load capacity compared to a similar beam strengthened on the tension face only or unstrengthened.

4.7 Compression strain

The test results described in Section 4.3.6 indicated that for most beams the CFRP failed by buckling before the beam reached the ultimate strength. Therefore, an investigation of the strains in the CFRP when it buckles is important. By knowing the strains in the CFRP at failure, a design model can be developed, as will be discussed in Chapter 5.

In this section the strain in the CFRP at the compression face of the beam is investigated. The strain was measured on the compression surface of concrete at the mid-span of the unstrengthened beams and on the CFRP for strengthened beams. Figures 4.23 to 4.26 show the relationship between the applied load and the compression strain for beams of series I to IV.

Compared to the unstrengthened beams, adding CFRP to the tension face of a beam increased the compression strain at the cracking load and decreased the compression strain at failure (e.g. I22-UL-T and III2-OL-T, Table 4.4). However, when the CFRP was added to both the tension and compression faces of a beam, a small decrease in the compression strain, at cracking and failure loads, was found compared with that strengthened on the tension face, Table 4.4.

Figure 4.25 shows the compression strain-load behaviour for the over-reinforced concrete beams of series-III. Adding CFRP laminates to the compression and tension faces of an over-reinforced beam achieved reductions in the compression strains at the

same load compared with that in the unstrengthened beam. For example, at a load of 30 kN, beam III3-OL-TC which was strengthened on the tension and compression faces, and the unstrengthened beam III1-OL-UN exhibited compression strains of 0.0009 and 0.0015, respectively. At the ultimate load, the over-reinforced beams strengthened on tension and compression faces also achieved reductions in the strains compared with the beams strengthened on the tension face only or unstrengthened. For example, the strains in the beams III3-OL-TC and III2-OL-T, strengthened in tension only, at the ultimate load were 0.0028 and 0.0034, respectively, Figure 4.25.

Figure 4.26 shows that increasing the ratio of CFRP on the compression face of an over-reinforced beam achieved reductions in the compression strains at the same load. The strengthened beams of the second group from series-IV, Figure 4.26, exhibited an ultimate compression strain between 0.0026 and 0.0032, Table 4.4.

It was found that increasing the ratio of CFRP on the compression face of an over-reinforced beam increased both the section capacity and the concrete strain at failure compared with those beams having lower ratios of CFRP; despite the fact that the final failure of those beams was buckling of the CFRP, Figures 24 and 26. The recorded failure strain in the CFRP for all beams strengthened in this investigation varied. For the unstrengthened beam III1-OL-UN, which failed by concrete crushing, the failure strain was 0.0040, while in beams III3-OL-TC, III6-OL-TC, IV23-OH-C and IV24-OH-C, which failed by CFRP buckling, the measured strain was 0.0028, 0.0032, 0.0026 and 0.0029 respectively. The variation of the measured strain in the beams strengthened on the compression faces was due to the buckling of the composite.

4.8 CFRP Laminate strain

In this section the strain measured in the tensile and compression CFRP laminates is discussed. Table 4.5 gives the load and the strains of the CFRP laminates at cracking, yielding of tension steel and at failure. Figures 4.27 to 4.29 show the applied load against the strains in both the tensile and the compression CFRP laminates at mid-span of beams for series I, II and III respectively.

In the under-reinforced beam, I22-UL-T, Figure 4.27, to which CFRP was added to the tension face, the tensile strain in the CFRP increased significantly after the concrete cracked. This is attributed to the increase in the additional tensile stress, which has carried by the external CFRP. However, when the CFRP was added to the tension face of the over-reinforced beam, III2-OL-T, Figure 4.29, no significant increase in the tensile strain in the CFRP laminate after cracking was found. This is attributed to the large amount of tension steel used, which carried most of the tensile stresses.

Adding CFRP laminates to the compression face of an under-reinforced beam strengthened on the tension face did not significantly change the strain in the tensile CFRP laminates at either cracking or yielding of tension steel, e.g. beam I25-UL-TC. compared with beam I22-UL-T which was strengthened on the tension face only, Figure 4.27 and Table 4.5. This might be attributed to the small amount of CFRP added on the compression face.

As indicated in Figure 4.29, the strain in the tension and compression CFRP reduced when CFRP was added to the compression face of an over-reinforced beam compared with that strengthened on tension face only at the same load level. On the other hand, adding a high ratio of the CFRP to the compression face of beam III6-OL-TC did not make significant reductions in the strains of the CFRP in either tension or compression compared with beam III3-OL-TC. However, the strain at failure in beam III6-OL-TC increased.

From the observations discussed above, it is clear that adding CFRP on the compression face of a strengthened over-reinforced beam reduces the strains in the concrete and the tension CFRP at a given value of the applied load compared with the unstrengthened beam. Furthermore, the strains at failure loads, particularly when the ratio of the CFRP is increased, are dependant on the amount of CFRP (the higher the ratio of CFRP added, the higher the applied load and strains that can be achieved).

Longitudinal strain distribution in the CFRP laminates

In order to investigate the distribution of the tensile and compression strains in the CFRP along the beam span, nine electrical resistance strain gauges were placed on each laminated face of the beams III5-OL-T and III6-OL-TC. Details of the spacing between the strain gauges are given in Figure 3.13. Figure 4.30 shows the strain distributions in the tension and compression CFRP laminates placed along the spans of these beams at a load of 61kN.

The results showed that the maximum strain in the CFRP laminates, in both tension and compression, occurred at the location where the bending moment is maximum and decreased towards the ends of the laminates. This behaviour was recorded in other experimental investigations [43,52] when the CFRP was added on the tension face of a beam. The addition of CFRP to the compression face of beam III6-OL-TC decreased the strain in the tension CFRP, for the same load, by 15% compared with that in III5-OL-T, Figure 4.30.

Figures 4.31 and 4.32 show the loads and the strains measured by the electrical strain gauges in the CFRP in both tension and compression along the span of beam III6-OL-TC. Figures 4.31 and 4.32 confirmed that the strain distribution of the beam along the span is symmetric about the centre.

Longitudinal tensile strain in the CFRP at failure

The largest tensile strain measured in the CFRP at mid-span of a strengthened beam from all tests was 0.0125, Figure 4.28 and Table 4.5. This strain was 95% of the maximum tensile strain measured from the direct tension test of the CFRP coupons, Section 3.3.4. The small difference resulted from the inability to measure the last reading of the strain in the CFRP at rupture. On the other hand, the smallest strain measured in the CFRP at mid-span of III3-OL-TC which failed by the buckling of the

CFRP was 0.0035, which corresponded to 27% of the maximum strain measured, also in Section 3.3.4. This strain measured when the CFRP laminates buckled at the mid-spam of the beam. It should be mentioned that bonding CFRP on the tension or tension and compression faces of a beam appeared to achieve perfect bonding with the concrete.

4.9 Internal reinforcement strain

In order to investigate the strains in the internal steel reinforcement, the strains were determined at the level of the internal steel reinforcement from the strain distribution through the beam depth. The strain distribution through the beam depth is shown in Figures 4.36 and 4.37. Figures 4.33, 4.34 and 4.35 show the applied load against the estimated strain, assuming full bond, in the tensile steel reinforcement at the mid-spans of beams for series I, III and IV respectively.

Adding CFRP to the tension face of beam I22-UL-T increased both the loads and the strains of the tension steel at cracking and yield compared with the unstrengthened beam I21-UL-UN, Figure 4.33. At ultimate load of the over-reinforced strengthened beam, III2-OL-T, no significant change in the strain of the tension steel was found, while the load increased compared with the unstrengthened beam, III1-OL-UN, Figure 4.34.

As can be seen from Figures 4.33 and 4.34, a beam with CFRP on the tension face had reduced tensile strains in the steel reinforcement at the same load level compared with the unstrengthened beam. Several experimental studies have recorded such behaviour when the CFRP was added to the tension face of a beam [1, 119,120].

Adding 0.61% of CFRP to the compression face of the under-reinforced beams strengthened on the tension face did not significantly affect the strains in the tensile steel compared with that beam strengthened on the tension face only, Figure 4.33.

Adding the CFRP to the compression face of the over-reinforced beam showed small reductions in the tensile steel strains compared with the beam strengthened on the tension face only, Figure 4.34. This might be due to the relative higher amount of CFRP added on the compression face of a beam.

The test results from the over-reinforced beams of the second group of series-IV, strengthened on the compression face only, showed that increasing the ratio of CFRP on the compression face decreased the strains in the tensile steel reinforcement at the same applied load compared with those in the unstrengthened beam, Figure 4.35.

4.10 The behaviour of the depth of the neutral axis

During the loading of section of a reinforced concrete beam in pure bending, the strains and the stresses at the tension and the compression faces of the beam increase. The position of the neutral axis at a given load is affected by the amount of the tensile reinforcement, the concrete stresses in compression and the cracking of concrete in the tension face of the beam. This section is focused on providing a better understanding of the movement of the neutral axis during loading. This behaviour has been compared with that predicted by the models, Chapter 6.

The position of the neutral axis, during loading, was calculated from the measured strains on the tension and compression faces of the beam at the mid-span, as shown in Figures 4.36 and 4.37. In beams where CFRP was applied to the tension and compression faces, the strains were measured using electrical resistance strain gauges placed on the CFRP; however, in the unstrengthened beams the strains were measured using demec gauges.

Figures 4.38 to 4.41 show the total applied load against the neutral axis, x/d_s, at mid-span for the beams of series I, II, III and IV respectively. The test results showed three

stages for the movement of the neutral axis in both strengthened and un-strengthened. These stages are:

Stage 1

This is the precracked stage. In this stage the distribution of longitudinal strains over any vertical section is initially linear. Strains in the longitudinal steel reinforcement are assumed to equal to those in the concrete surrounding it, and the values of all strains at any cross-section are very nearly proportional to the external bending moment there. During this stage deflections and rotations increase proportionally to the external load, and the behaviour of the beam is primarily determined by its cross-section and the characteristics of the concrete. The longitudinal steel reinforcement, being only lightly stressed, has little effect [121].

In the current study the external CFRP was added to the tension and compression face of a beam. Perfect bond with the concrete was assumed. Hence, the strains in the CFRP and those in the concrete surrounding it could behave in a way similar to that in the longitudinal steel and concrete. Therefore, based on the theory of elasticity assumptions, the strains at the maximum compression and tension faces of the beam in this stage are proportional to the external bending moment applied at any section, and no movement for the neutral axis during loading occurs. However, the test results, Figure 4.38 to 4.41, show that the movement of the neutral axis has been reduced during load increments. This might be caused by the variation of the measured strains over the vertical section of the beam.

Stage 2

This stage describes the position of the neutral axis, x/d_s, between the cracking load and for each of yielding of tension steel (under-reinforced beam), concrete crushing and/or buckling of the CFRP from the compression face of an over-reinforced beam. As the

applied load was increased in this stage, the variation in the neutral axis movement followed two criteria:

In the first criterion, the neutral axis x/d_s decreased with an increase in the yielding load; this occurred in the under-reinforced beam I21-UL-UN, Figure 4.38. However, for an under-reinforced strengthened beam I22-UL-T, yielding of tension steel was combined with a significant increase in the applied load and a small decrease in the neutral axis, compared with beam I21-UL-UN. The behaviour of the x/d_s observed from beam I22-UL-T was also confirmed from the under-reinforced strengthened beams of series-II, Figure 4.39.

In the second criterion, the neutral axis x/d_s showed relative increases from the cracking load up to concrete crushing, or buckling of the CFRP from the compression face of an over-reinforced beam, Figures 4.40 and 4.41. This increase in the neutral axis x/d_s, however, was not affected when the ratio of the CFRP on the compression face of the over-reinforced beam increased, as in beam III6-OL-TC, Figure 4.40. In both cases, the applied load was increased.

The behaviour of x/d_s in this stage is described as follows:

From the available theory of the behaviour of unstrengthened reinforced concrete beams in bending [121,122] it is understood that, when increasing the load beyond stage 1, the tension stress of the concrete exceeds the modulus of rupture; then the tension crack develops. This is by assuming an intermediate element at mid-span of the beam being considered. The tensile stresses are transmitted by tensile reinforcement; hence a considerable increase in the tensile strains is obtained. The movement of the x/d_s, after cracking, depends on the amount of the tension reinforcement.

Nilson and Winter (1991)[121] and Regan and Yu (1973)[122] have reported that, when a relatively moderate amount of tension reinforcement is employed as the load is

increased, the strain in the reinforcement and the deflection and rotation of the beam still increase in more or less direct proportion to the load, but at a faster rate than in stage 1. This is by assuming that strain distributions at vertical sections are also linear if the concrete stresses do not exceed approximately 50% of the compressive concrete stress[121]. On the other hand, the same investigators mentioned that if large amounts of reinforcement are employed, the compression strength of the concrete may reach its limit value before tension reinforcement yields. Concrete fails by crushing when the strains become so large that they disrupt the integrity of the concrete.

According to the experimental results obtained in this study, and with reference to the above mentioned previous studies, two main conclusions are drawn here:

1. At a relatively moderate amount of tension reinforcement, while the concrete stress is still within 50% of the compressive stress, the increase in the strain of the reinforcement may reduce x/d_s values. This is due to the crack propagation through the beam depth, which reduces the area of the uncracked section in compression.

2. At large amounts of reinforcement, as the concrete fails before yielding of tensile steel or CFRP rupture, the strains of both concrete and the tensile reinforcement are increased and consequently this would not significantly affect the movement of the neutral axis. This behaviour was observed in beams which failed by concrete crushing or buckling of the CFRP from the compression face of an over-reinforced beam, as in the second criteria of this stage.

Stage 3

This stage describes the movement behaviour of the neutral axis x/d_s between the loads for yielding of the tension steel and the failure. The neutral axis in this stage decreased with an increase in the applied load. The increase in the applied load depended on the ratios of the tension steel and CFRP reinforcement.

Adding high ratios of tension reinforcement, either steel, CFRP or both in the under-reinforced section, reduced the neutral axis; however, the applied load was improved, Figures 4.38 and 4.39.

Continuing with what was discussed in the first criterion in stage 2, as the applied load increases further the steel will reach its yield point. At that stress the reinforcement yields suddenly and produces large strains, and the tension cracks in the concrete widen visibly and propagate upward, with simultaneous significant deflection at the beam. When this happens, increases in the applied moment can no longer be balanced by increases in the force in the steel. Thus the difference in the load increases beyond this stage possibly necessitates an increase in the lever arm between the longitudinal tensile and compressive forces. This will correspondingly reduce the neutral axis [122]. In the current study, the reduction in the neutral axis in the strengthened section was associated with an increasing in the applied load. This was the result of adding the CFRP to the tension face of the beam which reduced the tensile strain of the steel reinforcement during load increments.

The interesting point found from this section is that adding CFRP to the tension face of an under-reinforced beam may cause behaviour similar to that of the over-reinforced beam, Figure 4.38. However, when a large ratio of CFRP was added to the compression face of the over-reinforced beam, the applied load on the beam could increase with no changes in x/d_s.

It can be concluded that the position of the neutral axis during loading of a reinforced concrete section in pure bending depends on several factors. The factors are the cracking load, the ratio of the tensile steel reinforcement, the ratio of the external CFRP-either on the tension or on the compression faces or both, the ratio of the compression steel, the bond strength between the concrete and the internal and the external reinforcement and the concrete strength.

4.11 Beam ductility

Ductility of a structural element can be defined as the ability to sustain large deformations before final failure [123]. To measure the ductility of reinforced concrete simply supported beams strengthened with external reinforcement at the tension face. three ductility indices have been developed [35,57,58]; the deflection ductility index, μ_D, the curvature ductility index, μ_φ, and the energy ductility index, μ_E, as described in Chapter 2.

In the current study, two types of failures were investigated. In the first type of failure, the tensile steel yielded before the final failure occurred, as in the beams of series I and II. In the second type of failure; however, the final failure occurred before yielding of the tensile steel reinforcement, as in the beams of series III and IV. The ductility indices could be calculated only for beams which failed in the former failure mode.

The ductility indices based on deflection, curvature and energy dissipation are given in Table 4.6 and were calculated using equations 2-1, 2-2, and 2-3, respectively. The deflections and curvatures for calculating ductility indices were obtained from Figures 4.15, 4.16, 4.17, 4.19, 4.20 and 4.21.

As can be seen from Table 4.6, all the strengthened under-reinforced beams of series-I exhibited less ductility than the corresponding unstrengthened beams. Beam I25-UL-TC which was strengthened with CFRP on the compression and tension faces of under-reinforced exhibited higher ductility indices than those obtained from beam I22-UL-T, which was strengthened on the tension face only.

Strengthening the over-reinforced beams III2-OL-T, III3-OL-TC, IV22-OH-C and IV23-OH-C increased the bending capacities compared with the unstrengthened beams: however, they exhibited no ductility, Figures 4.17 and 4.18. It can also be seen from the Figures that increasing the ratio of the CFRP on the compression face of an over-

reinforced concrete beam can increase the mid-span deflection at failure; however, the beams are not ductile.

4.12 Concluding remarks

The conclusions obtained from the experimental investigation reported in this chapter are summarised in the following:

Flexural strength enhancement

- Adding CFRP to the tension face of an under-reinforced beam, which has a low ratio of tension reinforcement, is an effective strengthening technique. The load capacity increased by up to three times that of the unstrengthened beams. Only a small increase in the flexural strength was achieved when the CFRP was added to the compression face of the beam which had a similar ratio of tension reinforcement, CFRP and steel.

- Adding the CFRP to the tension face of an over-reinforced concrete beam achieved little increase in the flexural strength compared with an unstrengthened beam. However, adding the CFRP to the compression face of an over-reinforced beam strengthened on the tension face was also considered an effective technique of strengthening beams, particularly with a CFRP ratio of 2.82% as been used in this study. The measured strength was enhanced by up to 40%.

- Increasing the ratio of CFRP on the compression face of an over-reinforced beam increased the section capacity and delayed the buckling failure of the CFRP. The compression strain in the CFRP when buckling occurred varied between 0.0026 and 0.0032.

Failure modes and crack patterns

The following failure modes were observed:

- For beams strengthened with CFRP on the compression face, buckling of the CFRP from the compression face was the dominant failure mode.

- Debonding of CFRP from the tension face of some strengthened beams which had low shear span to effective depth ratio was observed.

- End-laminate peeling failure, at the tension face of the strengthened beam, was explosive due to the sudden debonding of the CFRP confinements.

- Adding CFRP to the tension and compression faces of an over-reinforced beam, which had a tension steel ratio of approximately 3%, delayed the first crack formation. However, when the CFRP was added to the compression face there was not much difference compared with that strengthened on tension only. No noticeable change in the first crack formation exhibited when CFRP was added on the compression face of the over-reinforced beam which had a tension steel ratio of more than 3% compared to the unstrengthened beam.

- The occurrence of shear cracks at the laminate ends in the strengthened beams tended to hasten peeling and separation of the CFRP confinements. Increasing the width of the CFRP confinement at the laminate end played an important role in delaying the appearance of cracks and controlled the failure mode.

Other observations

- For the same load level, the beam with CFRP added to the tension face had smaller mid-span deflections and increased beam stiffness compared with those of the unstrengthened beam. For the same load level also, adding CFRP to the tension and compression faces of a beam led to reduced mid-span deflection and

so the beam stiffness was increased compared with those of the corresponding beam strengthened in tension only.

- After the internal tensile steel reinforcement yielded the tensile strain in the CFRP exhibited high strain values. This is due to the increase in the tensile stresses in the CFRP which were completely transferred by the external CFRP with a small contribution from the tensile steel reinforcement.

- In general, increasing the ratio of the CFRP on the tension face of the beam reduces the tensile strains in the CFRP at a given value of a load and at failure.

- Adding CFRP to the compression face of a beam strengthened on the tension reduced the tensile strains in the tension CFRP at the same load level. Both the failure load and the tensile strains at failure were increased.

- All the under-reinforced beams strengthened on the tension and compression faces exhibited less ductility than the unstrengthened ones. However, no ductility was observed, when CFRP was added on both tension and compression faces of an over-reinforced beam.

Table 4.1: Load and mid-span deflection at cracking, yielding of steel and ultimate load

Series no.	Beam ref.	Total load (kN)			Load ratios		Mid-span deflections (mm)		
		First crack	Yield *	Ultimate	Fs/Fc	Fcr/Fu	First crack	Yield	Ultimate
I	I11-UH-UN	11.65	34	44.76	NA	0.26	1.20	4.4	12.73
	I12-UH-UN	11.64	34	44.76	NA	0.26	1.37	5.1	12.43
	I13-OL-UN	36.12	-----	128	NA	0.28	2.33	----	14.16
	I21-UL-UN	6.24	18	20.74	1.00	0.30	0.88	4.6	25.07
	I22-UL-T	12.04	52	58.00	1.93	0.21	1.6	5.9	10.32
	I23-UL-TC	12.62	46	54.96	1.05**	0.23	1.02	5.0	7.13
	I24-UL-TC	16.4	52	78.16	1.36**	0.21	1.8	6.0	14.73
	I25-UL-TC	16.10	55	85.42	1.34**	0.19	1.46	5.8	17.90
II	II1-UH-T	11.46	81	97.00	NA	0.12	1.44	7.8	17.38
	II2-UH-TC	11.46	69	81.06	NA	0.14	1.18	8.2	10.80
	II3-UH-TC	11.46	81	95.60	NA	0.12	1.50	11.0	18.90
III	III1-OL-UN	6.00	--	46.06	1.00	0.13	2.56	--	29.9
	III2-OL-T	12.18	--	51.50	2.03	0.24	6.18	--	31.65
	III3-OL-TC	12.00	--	58.60	1.05**	0.20	5.03	--	28
	III4-OL-UN	5.66	---	45.10	1.00	0.13	3.32	---	28.35
	III5-OL-T	14.56	--	60.84	2.57	0.24	6.85	--	43.15
	III6-OL-TC	14.2	66	71.9	1.17**	0.20	5.18	28.0	42.58
IV	IV11-OL-TC	5.00	NA	10.8	NA	0.46	4.72	NA	15.57
	IV12-OL-TC	4.00	NA	12.48	NA	0.32	3.85	NA	14.12
	IV21-OH-UN	2.90	--	8.00	1.00	0.36	3.01	--	11.62
	IV22-OH-C	3.02	--	7.60	1.04	0.40	3.84	--	9.14
	IV23-OH-C	3.04	--	9.33	1.05	0.33	3.16	--	9.60
	IV24-OH-C	3.14	---	10.40	1.08	0.30	3.70	---	10.41

* assessed from load-deflection curves
Fs/Fc = Cracking load of strengthened beam/ Cracking load of unstrengthened beam
Fcr/Fu = Cracking load of a beam / Ultimate load of a beam
** assessed from the cracking load of unstrengthened beam in compression

Table 4.2: Failure modes of the beams tested

Series no.	Beam ref.	Strengthening scheme	Failure mode
I	I11-UH-UN	Unstrengthened	Steel yielding
	I12-UH-UN	Unstrengthened	Steel yielding
	I13-OL-UN	Unstrengthened	Concrete crushing
	I21-UL-UN	Unstrengthened	Steel yielding
	I22-UL-T	TU	Laminate-end peeling
	I23-UL-TC	TCU	Laminate-end peeling
	I24-UL-TC	TC	Debonding of tension CFRP followed by buckling of CFRP compression
	I25-UL-TC	TC	concrete crushing followed by debonding of tension CFRP
II	II1-UH-T	TU	FRP rupture
	II2-UH-TC	TCU	Shear
	II3-UH-TC	TCU	Concrete crushing simultaneously with tension CFRP debonding
III	III1-OL-UN	Unstrengthened	Concrete crushing
	III2-OL-T	T	Concrete crushing
	III3-OL-TC	TC	Buckling of CFRP laminates
	III4-OL-UN	Unstrengthened	Concrete crushing
	III5-OL-T	T	Concrete crushing
	III6-OL-TC	TC	Buckling of CFRP laminates
IV	IV11-OL-TC	TC	Concrete crushing
	IV12-OL-TC	TCB	Concrete crushing
	IV21-OH-UN	Unstrengthened	Concrete crushing
	IV22-OH-C	C	Buckling of CFRP laminates
	IV23-OH-C	C	Buckling of CFRP laminates
	IV24-OH-C	C	Buckling of CFRP laminates

T: tension CFRP laminate, C: compression CFRP laminate, U: confinements CFRP U-shaped, and B: steel anchor

Table 4.3: Load enhancement factors

Series no.	Beam ref.	Ultimate load Pu (kN)	Ultimate load enhancement		Remarks
			(η_1)	(η_2)	
I	I11-UH-UN	44.76	Non	Non	
	I12-UH-UN	44.76	Non	Non	
	I13-OL-UN	128	Non	Non	
	I21-UL-UN	20.74	1.00	-----	
	I22-UL-T	58.0 (71.60 [3])	2.80* (3.50 [3])	-----	
	I23-UL-TC	54.96	2.65*	-----	
	I24-UL-TC	78.16	3.77 [1+2]	-----	
	I25-UL-TC	85.42	4.12	1.15[3]	
II	II1-UH-T	97.00	1.55 [3]	-----	93.44 [3]
	II2-UH-TC	81.06	1.22 [3]	1.00 [3]	81.10 [3]
	II3-UH-TC	95.60	1.44 [3]	1.17 [3]	81.85 [3]
III	III1-OL-UN	46.06	1.00	-----	
	III2-OL-T	51.50	1.12	-----	
	III3-OL-TC	58.60	1.28	1.17 [2]	
	III4-OL-UN	45.10	1.00	-----	
	III5-OL-T	60.84	1.35	-----	
	III6-OL-TC	71.90	1.55[2]	1.40[2]	
IV	IV11-OL-TC	10.8	1.34[3]	1.10[3]	9.96 [3]
	IV12-OL-TC	12.48	1.49 [3]	1.22 [3]	10.26 [3]
	IV21-OH-UN	8.00	1.00	-----	
	IV22-OH-C	7.60	0.95 [2]	-----	
	IV23-OH-C	9.33	1.17 [2]	-----	
	IV24-OH-C	10.40	1.30 [2]	-----	

* onset of laminate end-peeling failure
1- debonding of tension CFRP followed by partial buckling of CFRP compression; 2- buckling of CFRP laminates; 3- predicted failure

η_1: ultimate load of strengthened beam in both tension and compression faces/ unstrengthened beam
η_2 : ultimate load of strengthened beam in both tension and compression faces/ strengthened in tension

Table 4.4: Compression strains for all beams tested

Series no.	Beam ref.	Characteristic layer	Total load P (kN)		Compression strain x10^{-2}	
			c	u	c	u
I	I11-UH-UN	concrete	11.65	44.76	0.037	0.44
	I12-UH-UN	concrete	11.64	44.76	0.03	0.70
	I13-OL-UN	concrete	36.12	128	0.072	0.37
	I21-UL-UN	concrete	6.24	20.74	0.017	0.43
	I22-UL-T	concrete	12.04	58.00	0.053	0.27
	I23-UL-TC	C-laminate	12.62	54.96	0.032	0.19
	I24-UL-TC	C-laminate	16.4	78.16	0.026	0.26
	I25-UL-TC	C-laminate	16.10	85.42	0.015	0.38
II	II1-UH-T	concrete	11.46	97.00	--	0.56
	II2-UH-TC	C-laminate	11.46	81.06	--	NA
	II3-UH-TC	C-laminate	11.46	95.60	--	0.56
III	III1-OL-UN	concrete	6.00	46.06	0.026	0.40
	III2-OL-T	concrete	12.18	51.50	0.037	0.34
	III3-OL-TC	C-laminate	12.00	58.60	0.034	0.28
	III4-OL-UN	concrete	5.66	45.10	0.017	0.37
	III5-OL-T	concrete	14.56	60.84	0.067	0.35
	III6-OL-TC	C-laminate	14.20	71.90	0.045	0.32
IV	IV21-OH-UN	concrete	2.90	8.00	0.18	0.5
	IV22-OH-C	concrete	3.02	7.90	0.083	0.3
		C-laminate			0.09	0.26
	IV23-OH-C	concrete	3.04	9.33	0.06	0.26
		C-laminate			0.07	0.26
	IV24-OH-C	concrete	3.14	10.40	0.064	0.29
		C-laminate			0.09	0.32

c and u are the load and strain at cracking and ultimate
u = the value at either ultimate load or buckling of CFRP laminate

Beams failed by CFRP buckling

Table 4.5: Tensile strains of the CFRP laminates

Series no.	Beam ref.	Total load P (kN)			Tensile CFRP strain x10^{-2}		
		c	y	u	c	y	u
I	I21-UL-UN	Unstrengthened					
	I22-UL-T	12.04	52	58.00	0.038	0.36	NA
	I23-UL-TC	12.62	46	54.96	0.042	0.32	NA
	I24-UL-TC	16.4	52	78.16	0.026	0.35	0.74
	I25-UL-TC	16.10	55	85.42	0.022	0.31	0.87
II	II1-UH-T	11.46	81	97.00	0.055	0.56	1.25
	II2-UH-TC	11.46	69	81.06	0.055	0.50	--
	II3-UH-TC	11.46	81	95.60	0.055	0.56	1.21
III	III1-OL-UN	Unstrengthened					
	III2-OL-T	12.18	--	51.50	0.067	---	0.37
	III3-OL-TC	12.00	--	58.60	0.046	--	0.35
	III4-OL-UN	Unstrengthened					
	III5-OL-T	14.56	--	60.84	0.089	--	0.73
	III6-OL-TC	14.20	66	71.90	0.056	0.37	0.40

c, y and u are the load and strain at cracking, tensile steel yielding and ultimate.
u = The total load either at ultimate or debonding of CFRP laminate

Table 4.6: Ductility of the tested beams

Series no.	Beam ref.	Deflection ductility	Curvature ductility	Energy ductility
		μ_D[1]	μ_φ[1]	μ_E[1]
I	I11-UH-UN	2.91	6.4	19.60
	I12-UH-UN	2.43	7.15	19.50
	I13-OL-UN	--	NA	1.67
	I21-UL-UN	5.45	16.67	10.73
	I22-UL-T*	1.73	1.73	2.10
	I23-UL-TC*	1.39	1.17	1.30
	I24-UL-TC**	2.46	2.23	5.00
	I25-UL-TC	3.11	2.74	6.10
II	II1-UH-T	2.24	1.85	2.42
	II2-UH-TC	1.32	1.04	1.28
	II3-UH-TC	1.72	1.88	2.31
III	III1-OL-UN	non	non	non
	III2-OL-T	non	non	non
	III3-OL-TC**	non	non	non
	III4-OL-UN	non	non	non
	III5-OL-T	non	non	non
	III6-OL-TC**	1.51	1.12	2.05
IV	IV11-OL-TC	non	non	non
	IV12-OL-TC	non	non	non
	IV21-OH-UN	non	non	non
	IV22-OH-C **	non	non	non
	IV23-OH-C **	non	non	non
	IV24-OH-C **	non	non	non

[1]: Calculated using equations 2-1, 2-2 and 2-3
* end-laminate peeling
** CFRP buckling

Figure 4.1: Typical flexural failure due to steel yielding near to the point load, beam I21-UL-UN

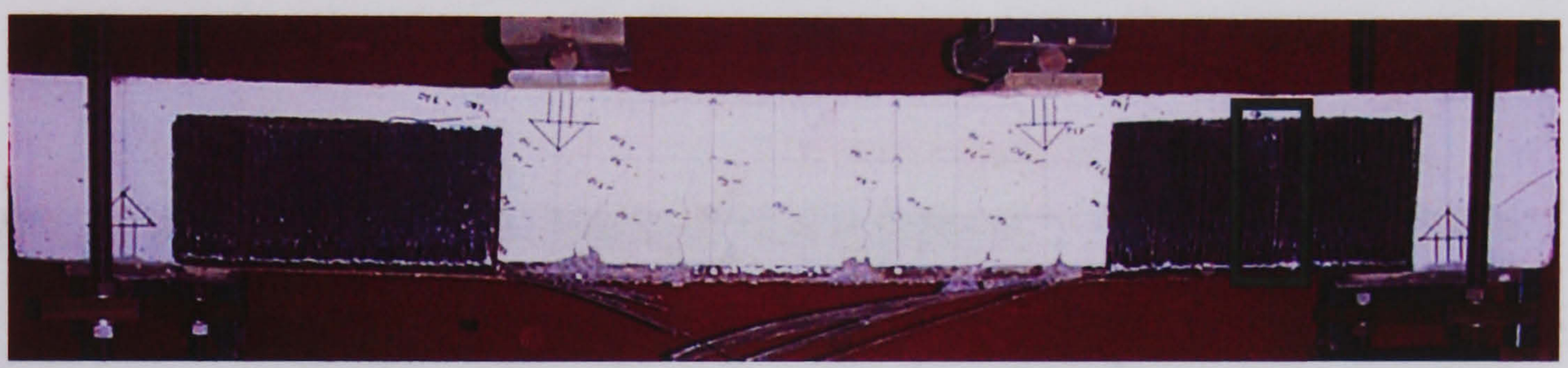

Figure 4.2: CFRP laminate rupture at the mid span, Beam II1-UH-T

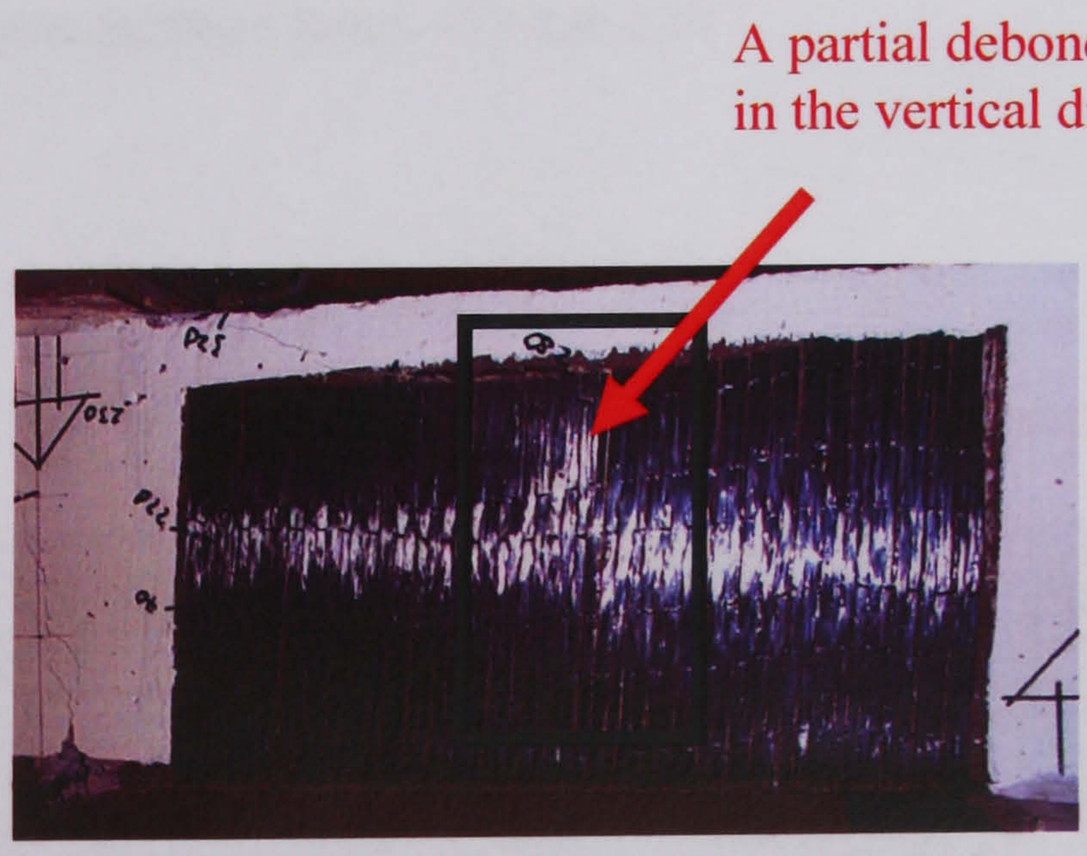

Figure 4.3: Debonding of the CFRP confinement, beam II1-UH-T

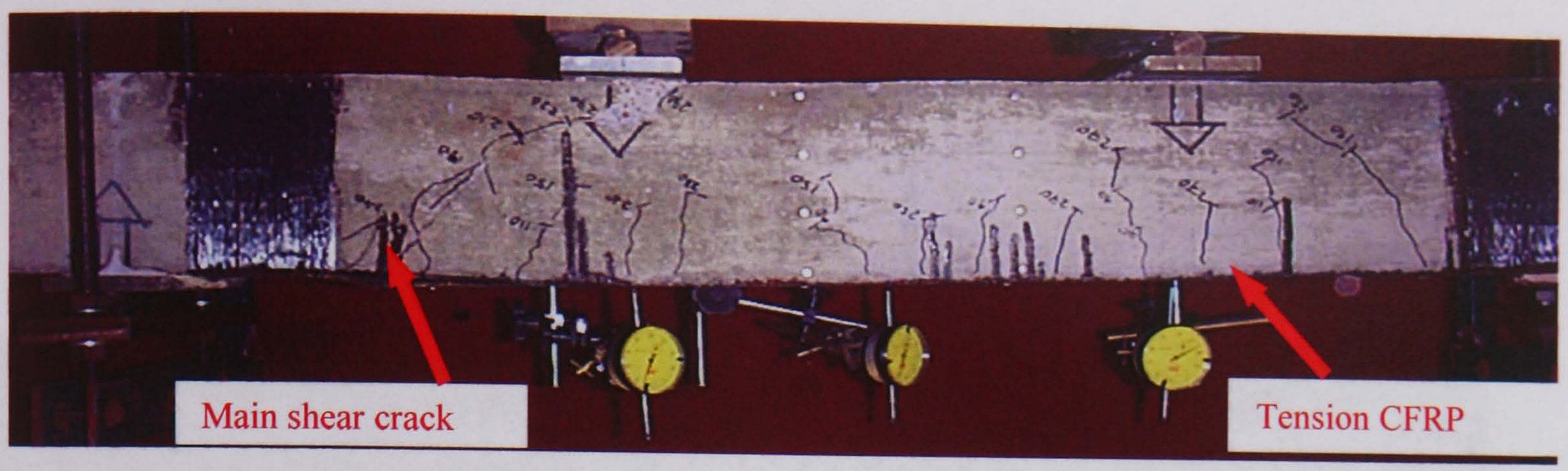

Figure 4.4: Shear failure in strengthened beam II2-UH-TC

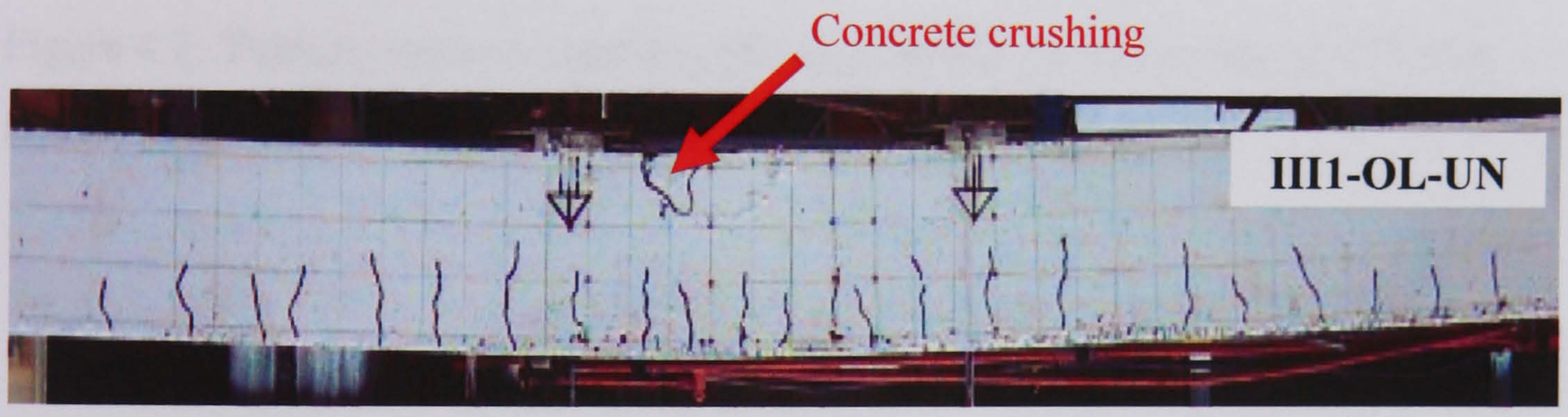

Figure 4.5: Typical flexural failure due to concrete crushing at the mid-span of the over-reinforced unstrengthened beam III1-OL-UN

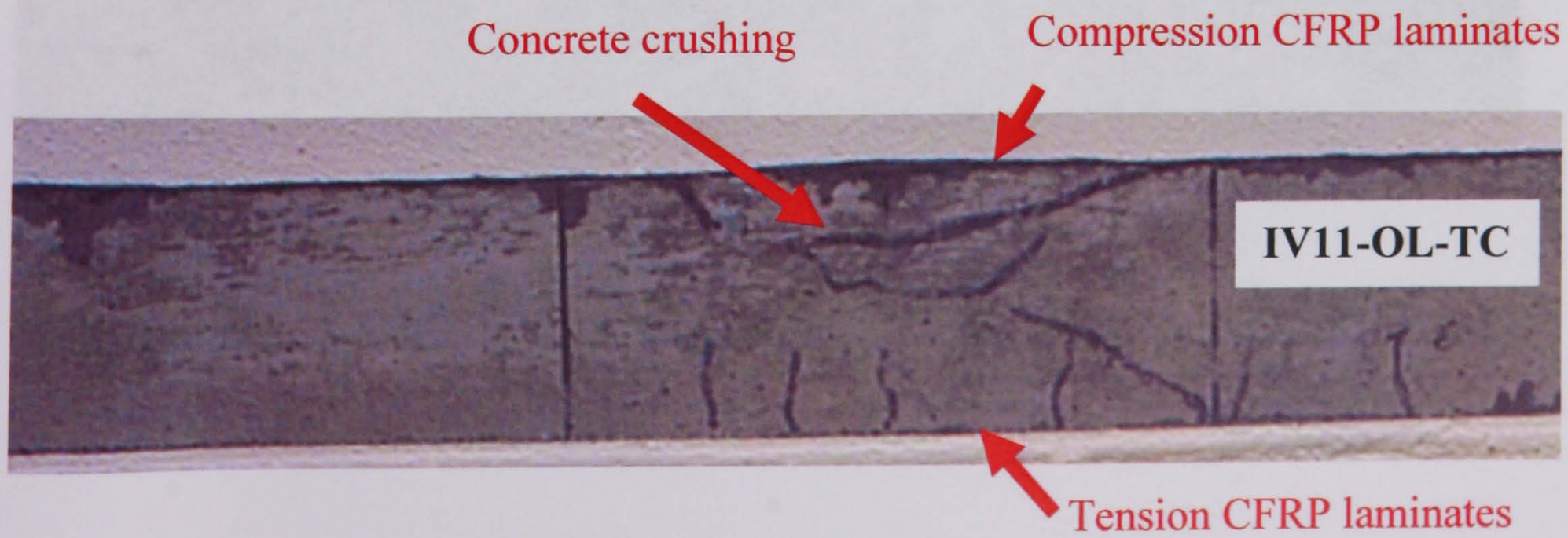

Figure 4.6: Flexural failure due to concrete crushing at mid-span of beam IV11-OL-TC

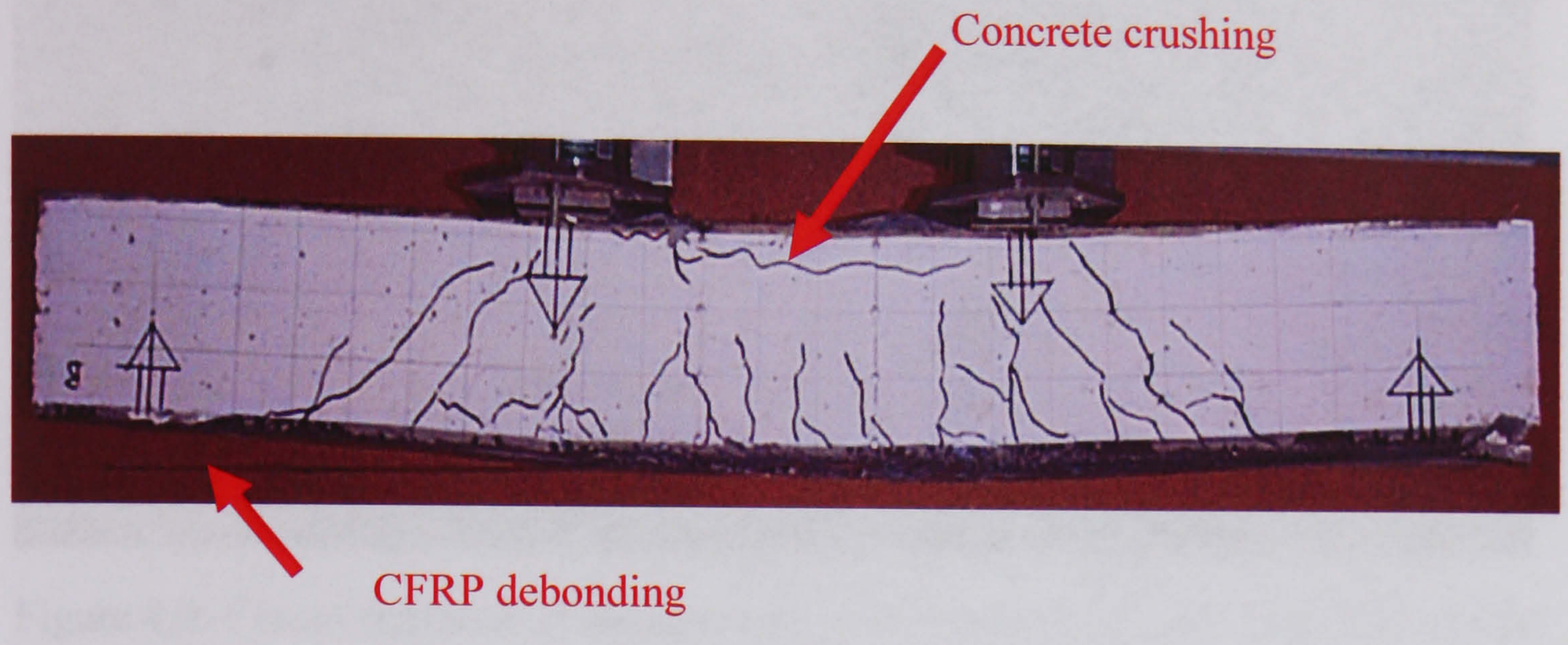

Figure 4.7: Typical concrete crushing failure followed by debonding of CFRP in tension, Beam I25-UL-TC

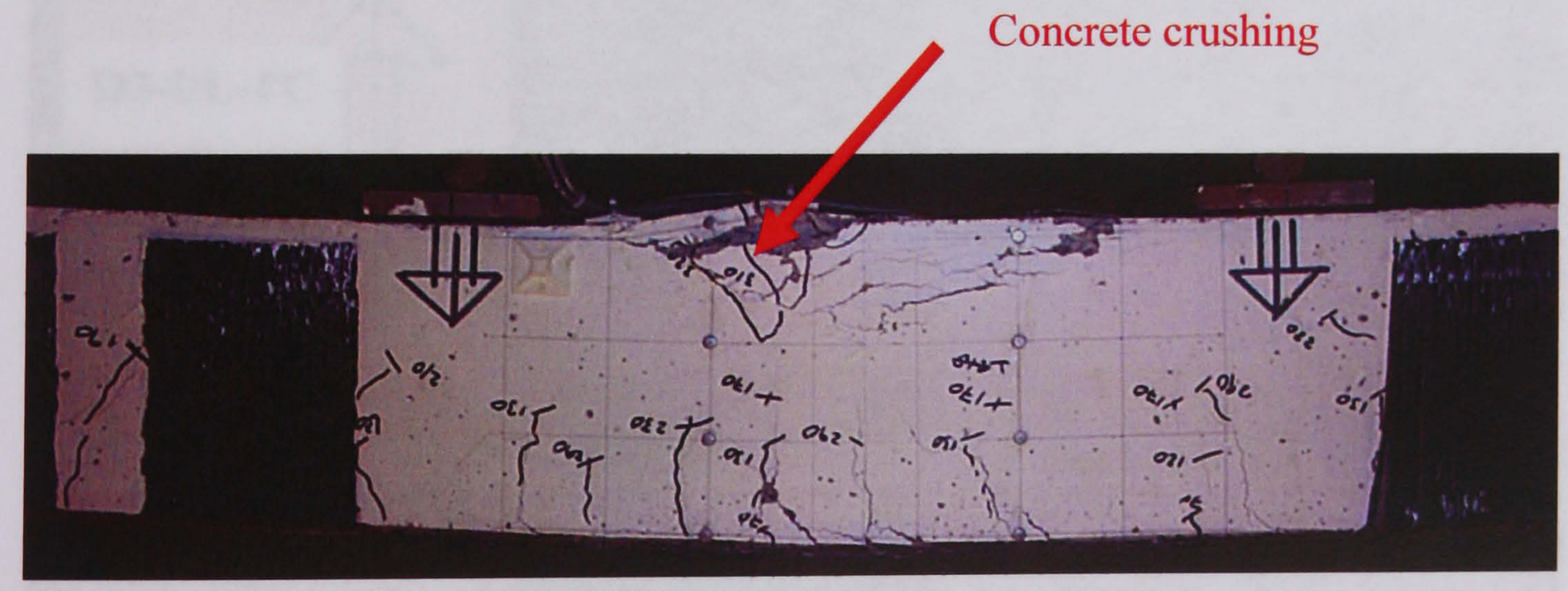

Figure 4.8: Concrete crushing, Beam II3-UH-TC

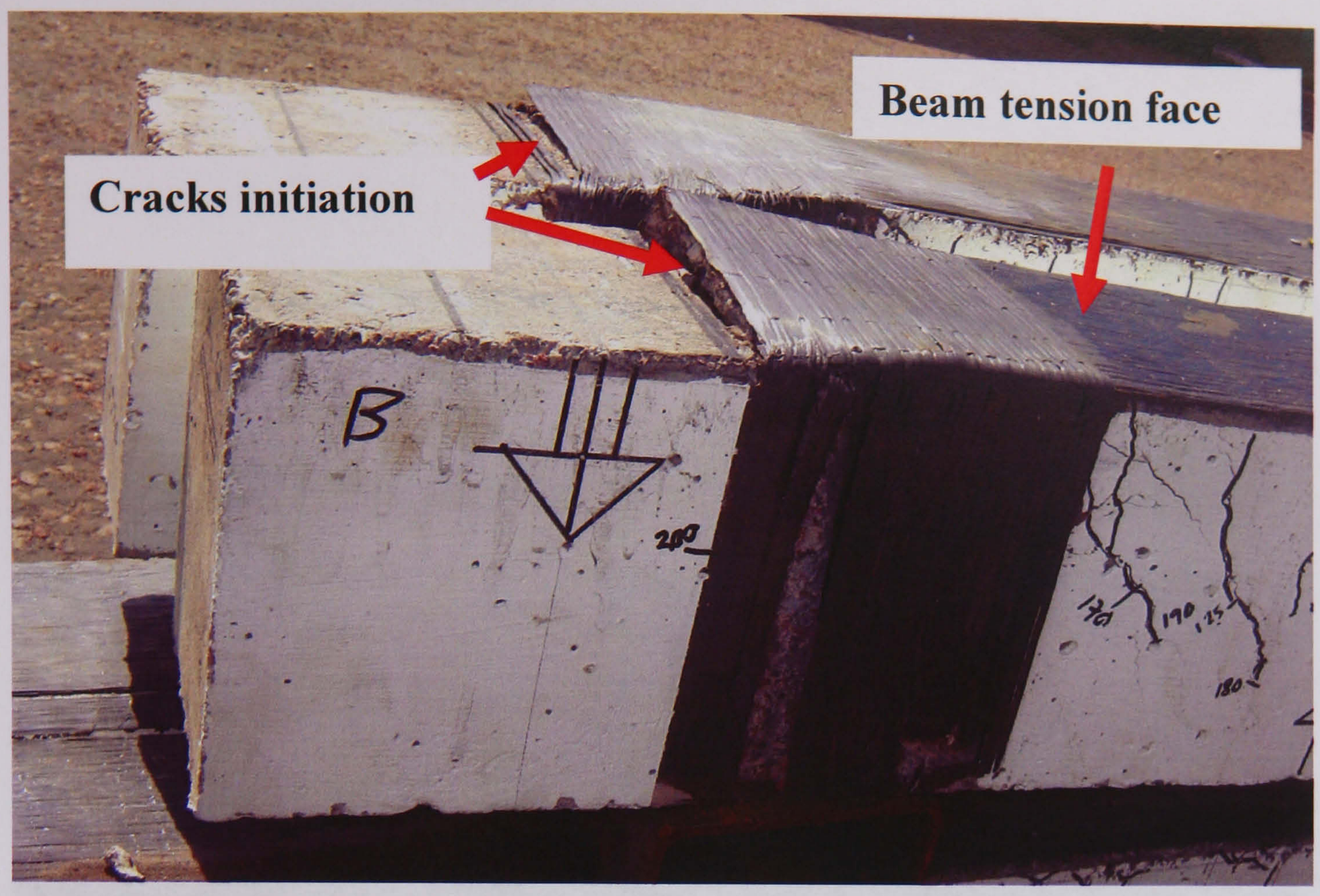

Figure 4.9: Cracks initiation at the laminate ends of beams I22-UL-T and I23-UL-TC

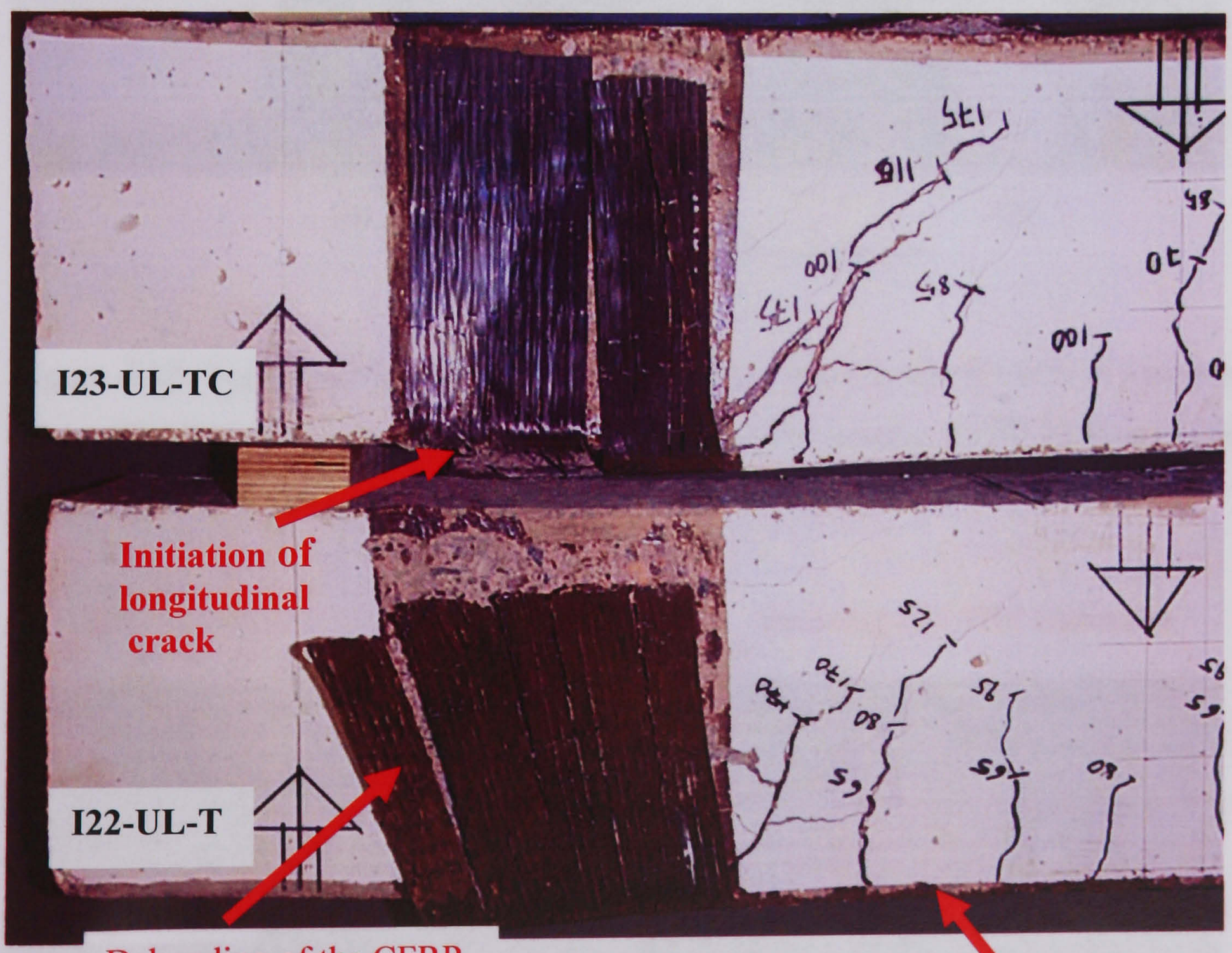

Figure 4.10: End-laminate peeling in beams of I22-UL-T and I23-UL-TC

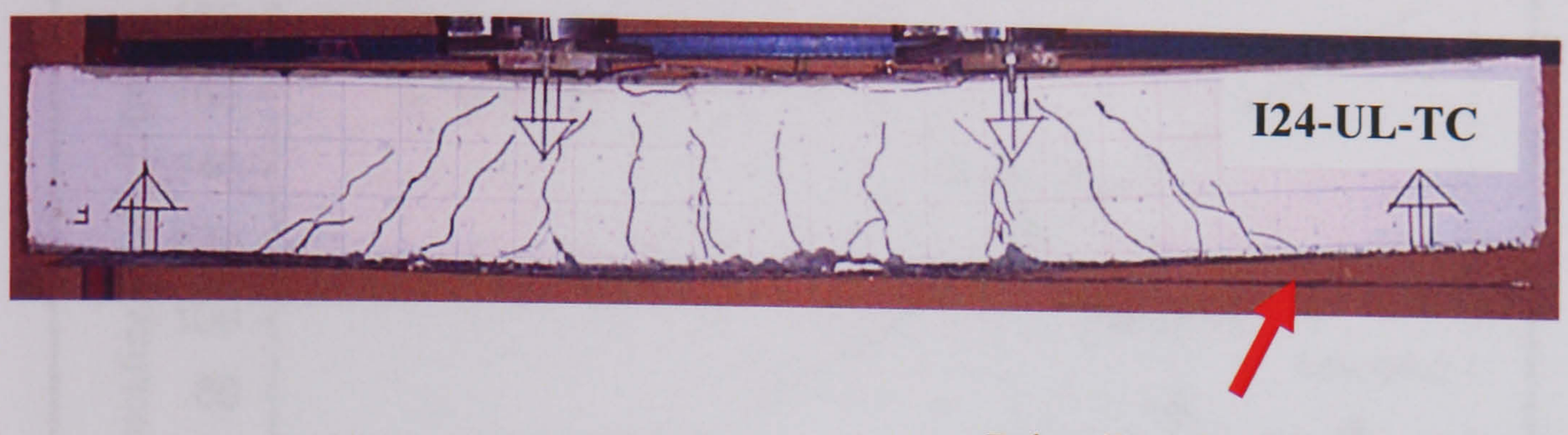

Debonding of CFRP tension laminates

Figure 4.11: Typical debonding of CFRP laminates from the tension face, beam I24-UL-TC

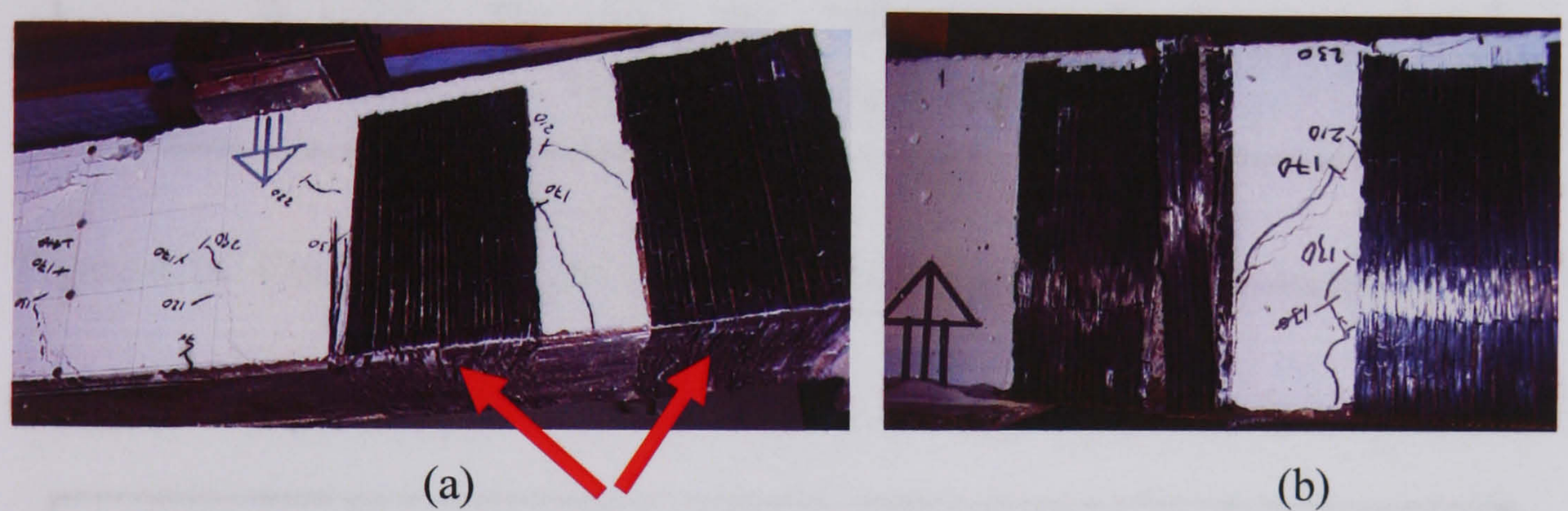

Tearing of U-shaped CFRP confinements

Figure 4.12: Typical debonding of CFRP confinements in beam II3-UH-TC: (a) tearing of the CFRP confinement caused by debonding of the tension CFRP laminates and (b) separation of the CFRP confinement from the beam sides.

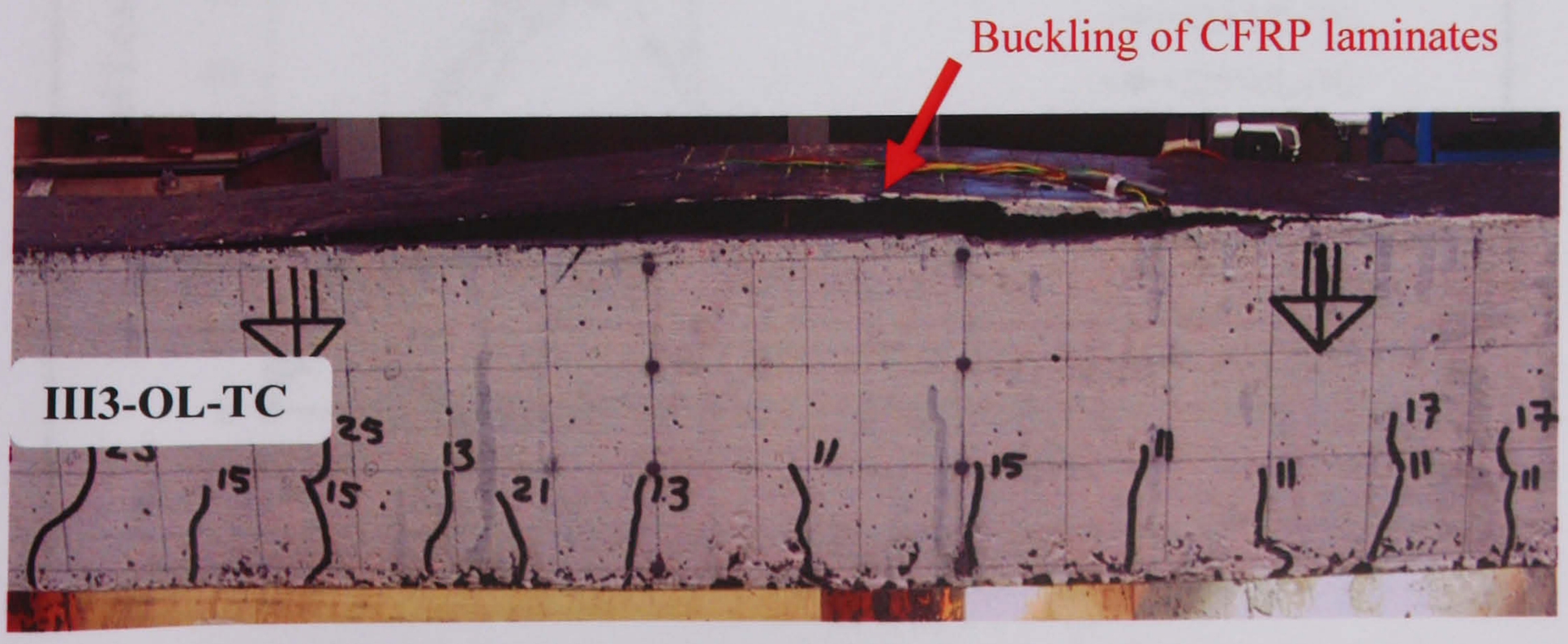

Figure 4.13: Typical buckling of CFRP laminates in the over-reinforced beam, III3-OL-TC

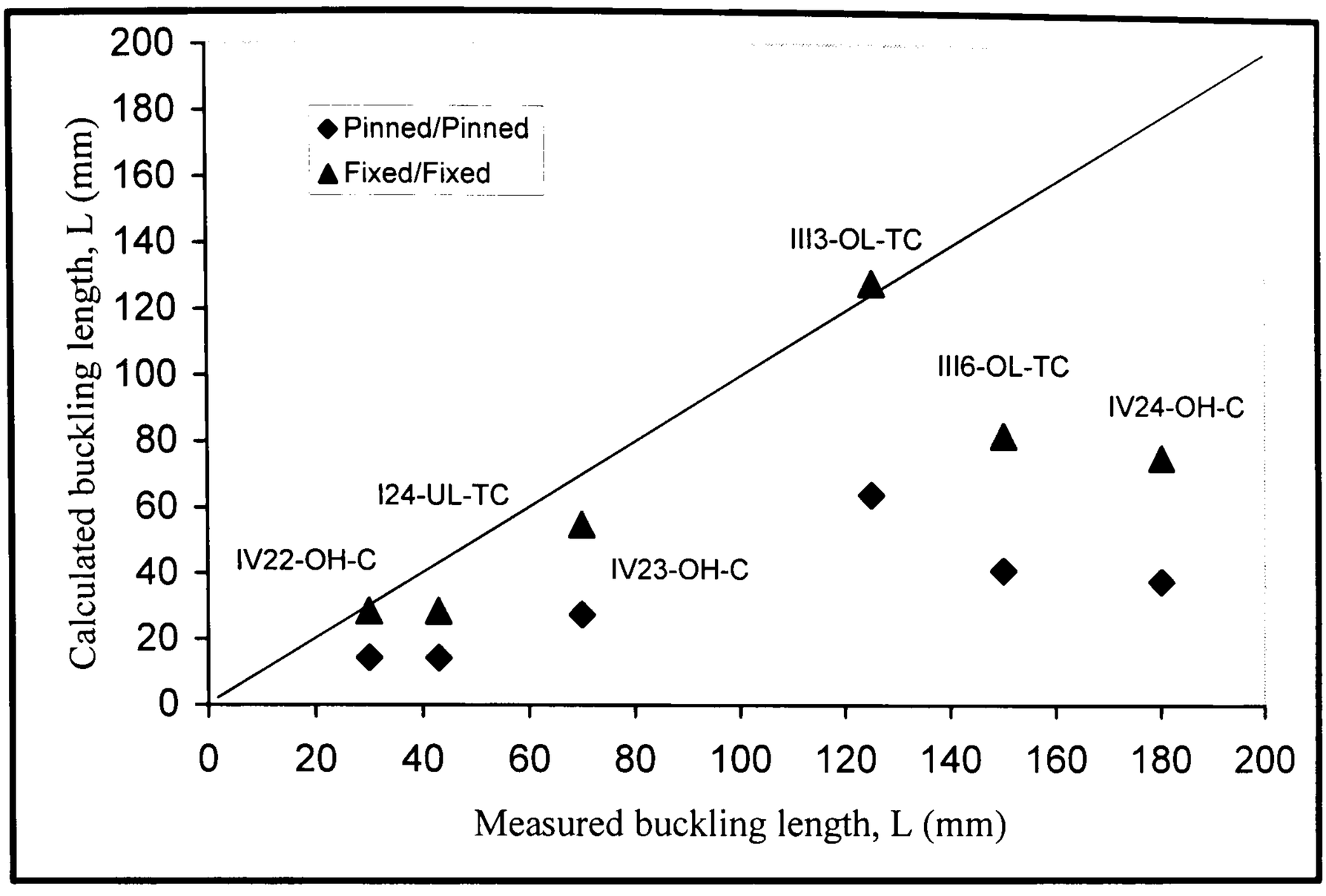

Figure 4.14: Comparison of the effective buckling lengths, the measured and calculated

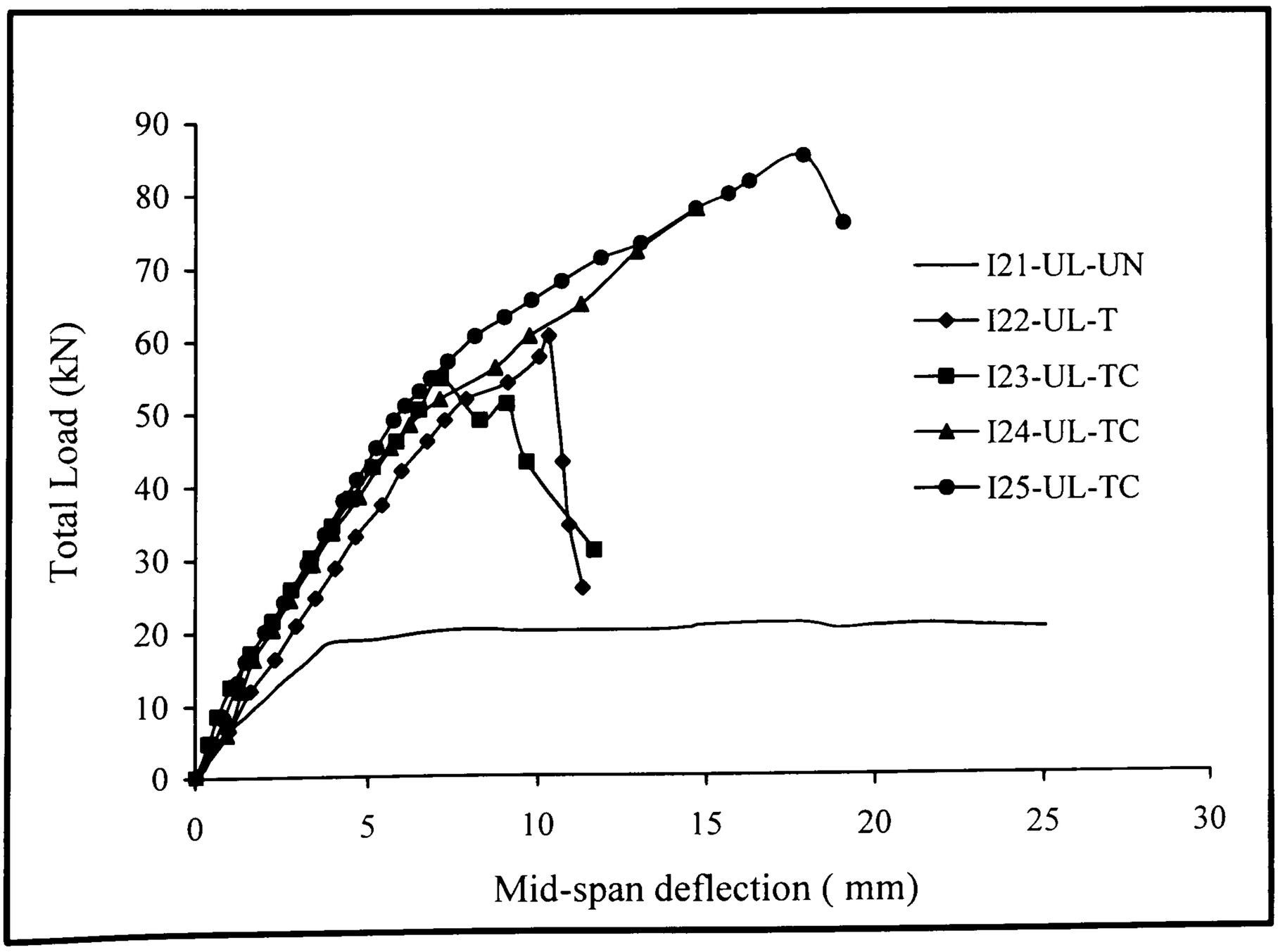

Figure 4.15: Load versus mid-span deflection for the beams tested in the second group of series-I

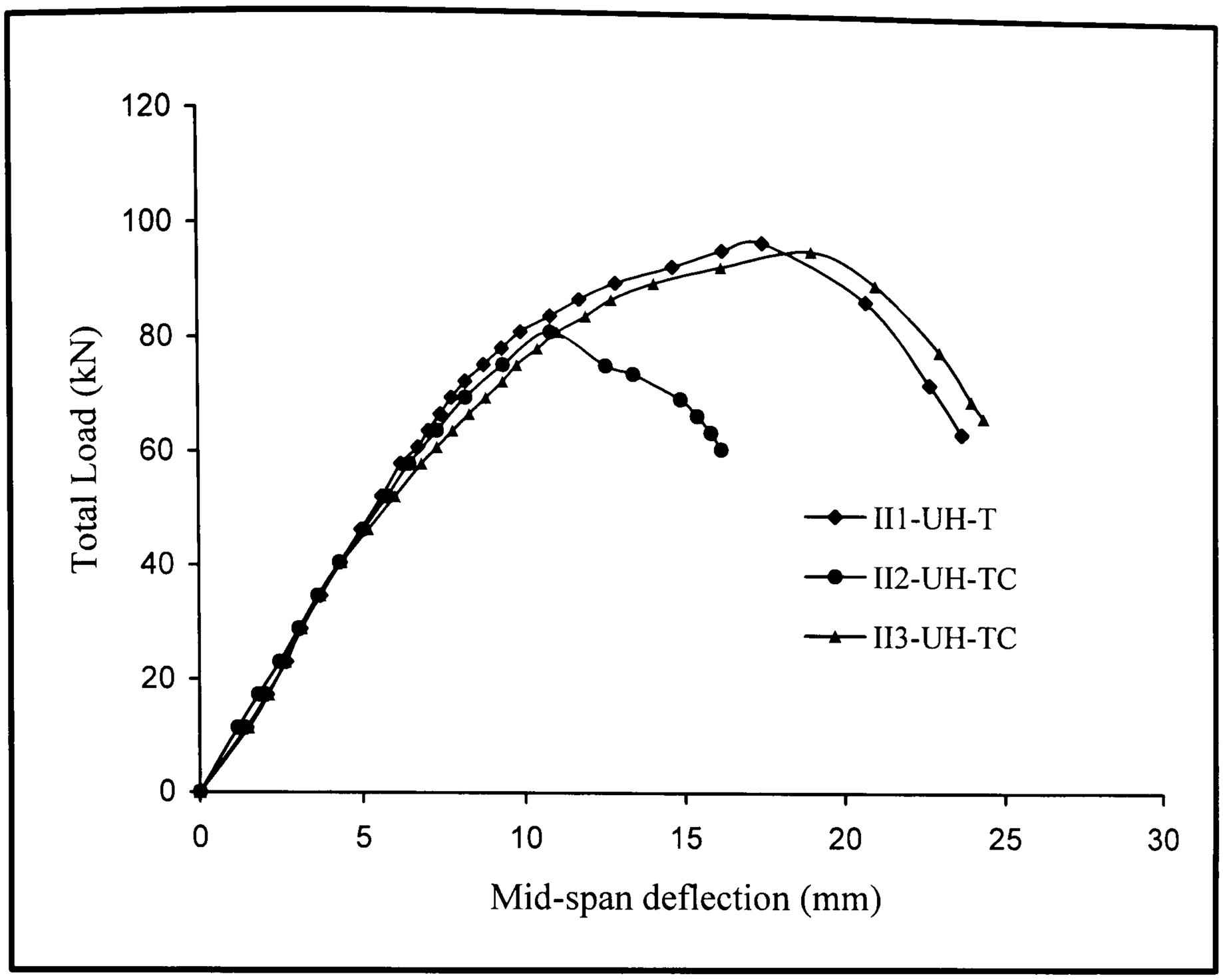

Figure 4.16: Load versus mid-span deflection for the beams tested in series-II

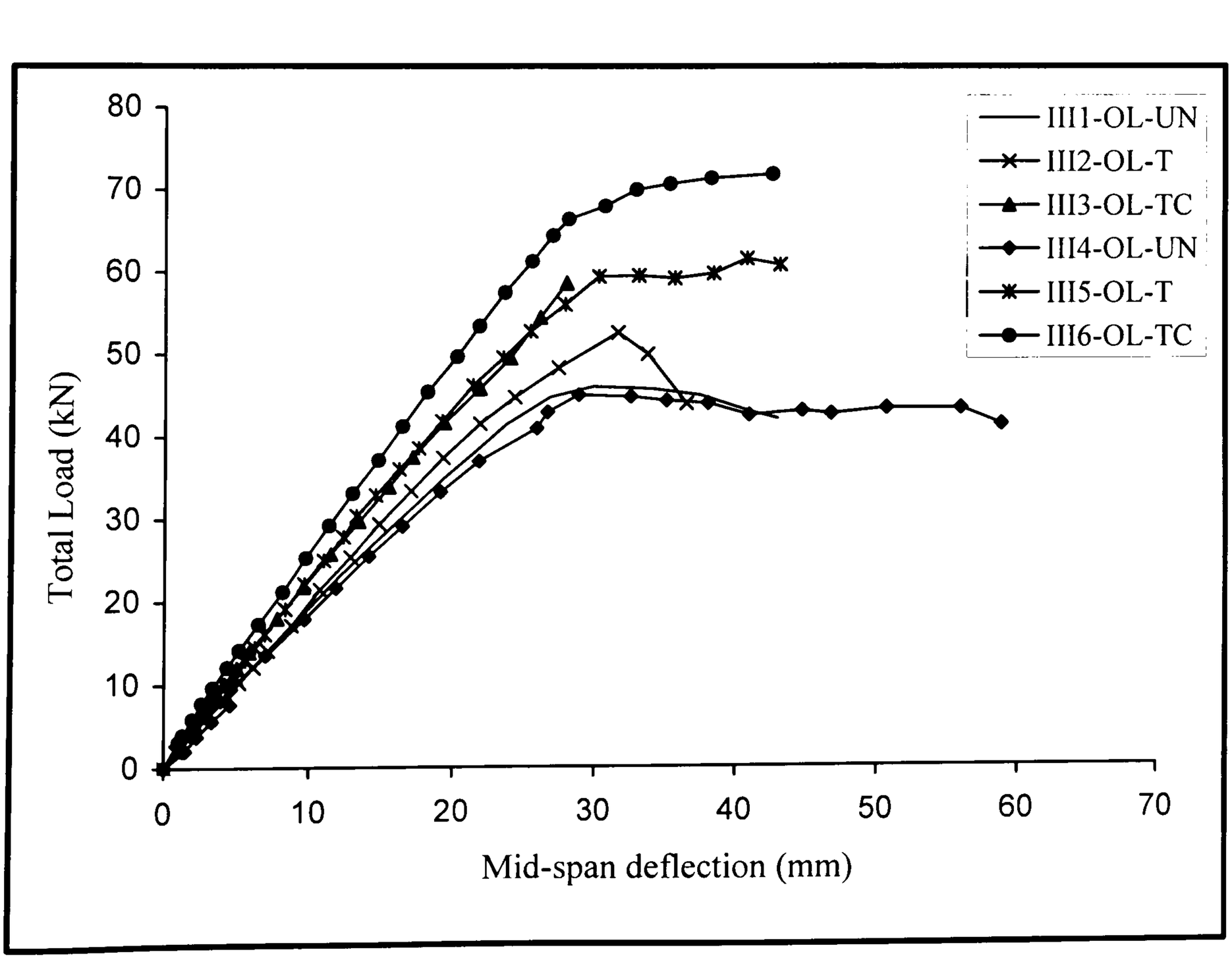

Figure 4.17: Load versus mid-span deflection for the beams tested in series-III

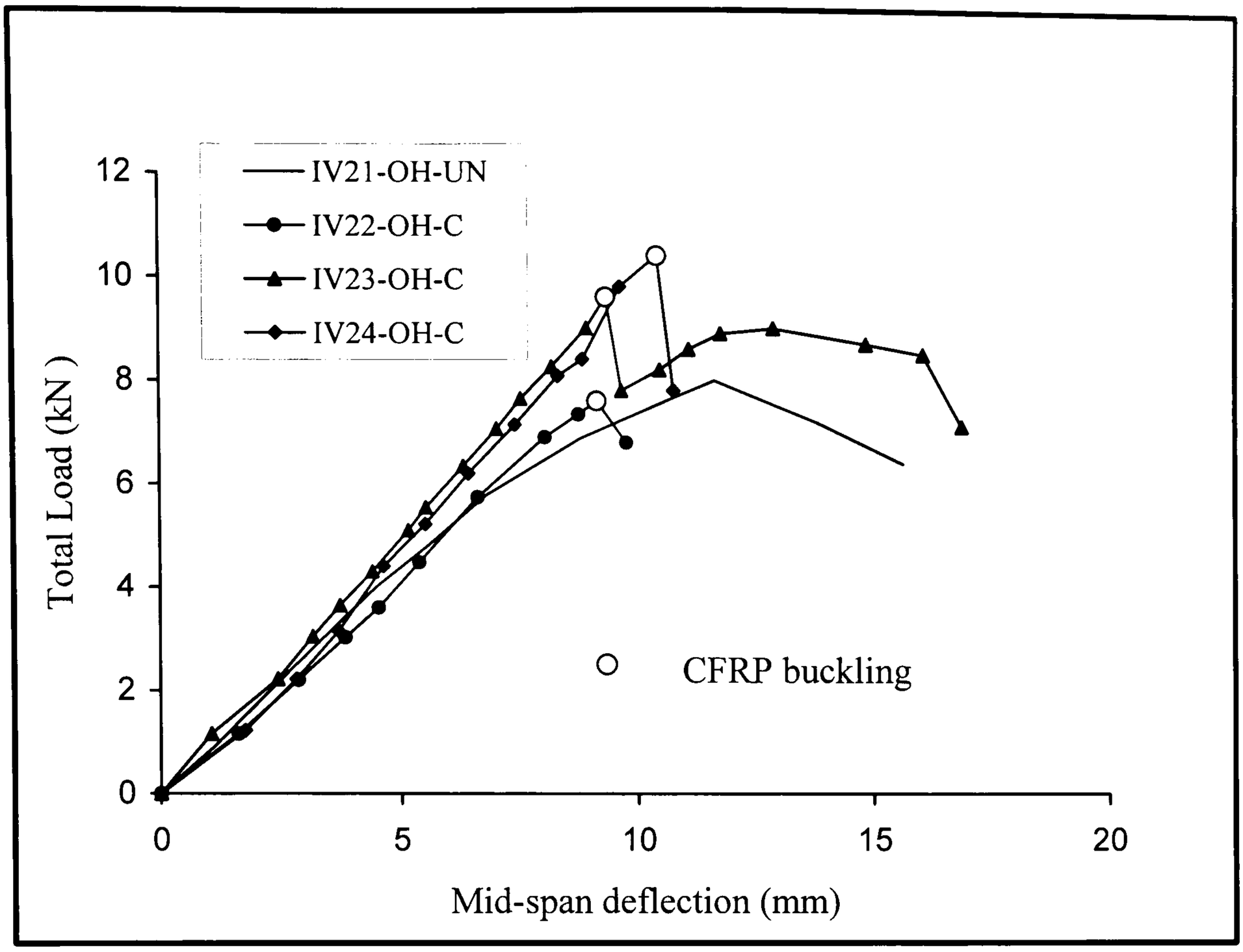

Figure 4.18: Load versus mid-span deflection for the beams tested in the second group of series-IV

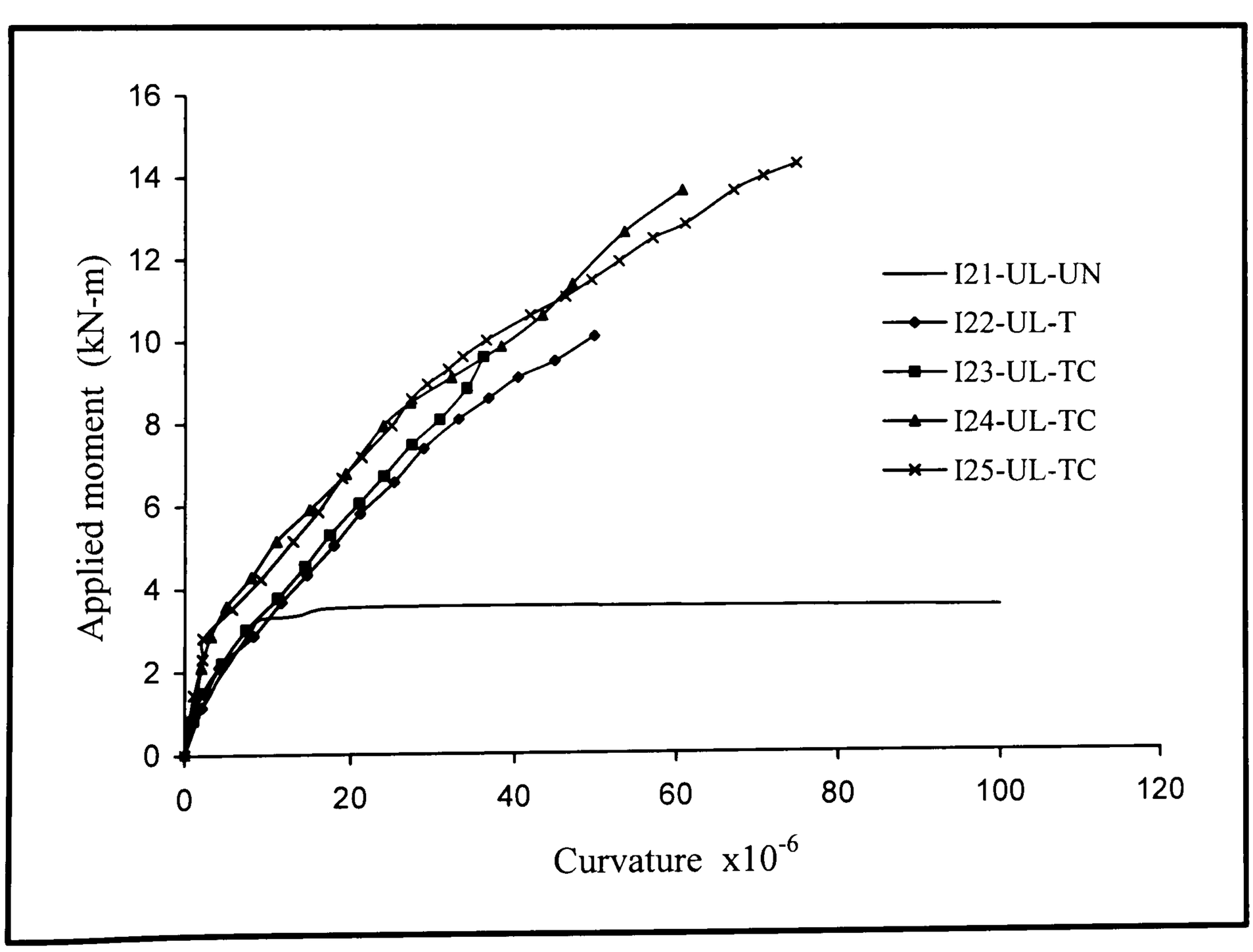

Figure 4.19: Moment-Curvature relationship for the beams tested in the second group of series-I

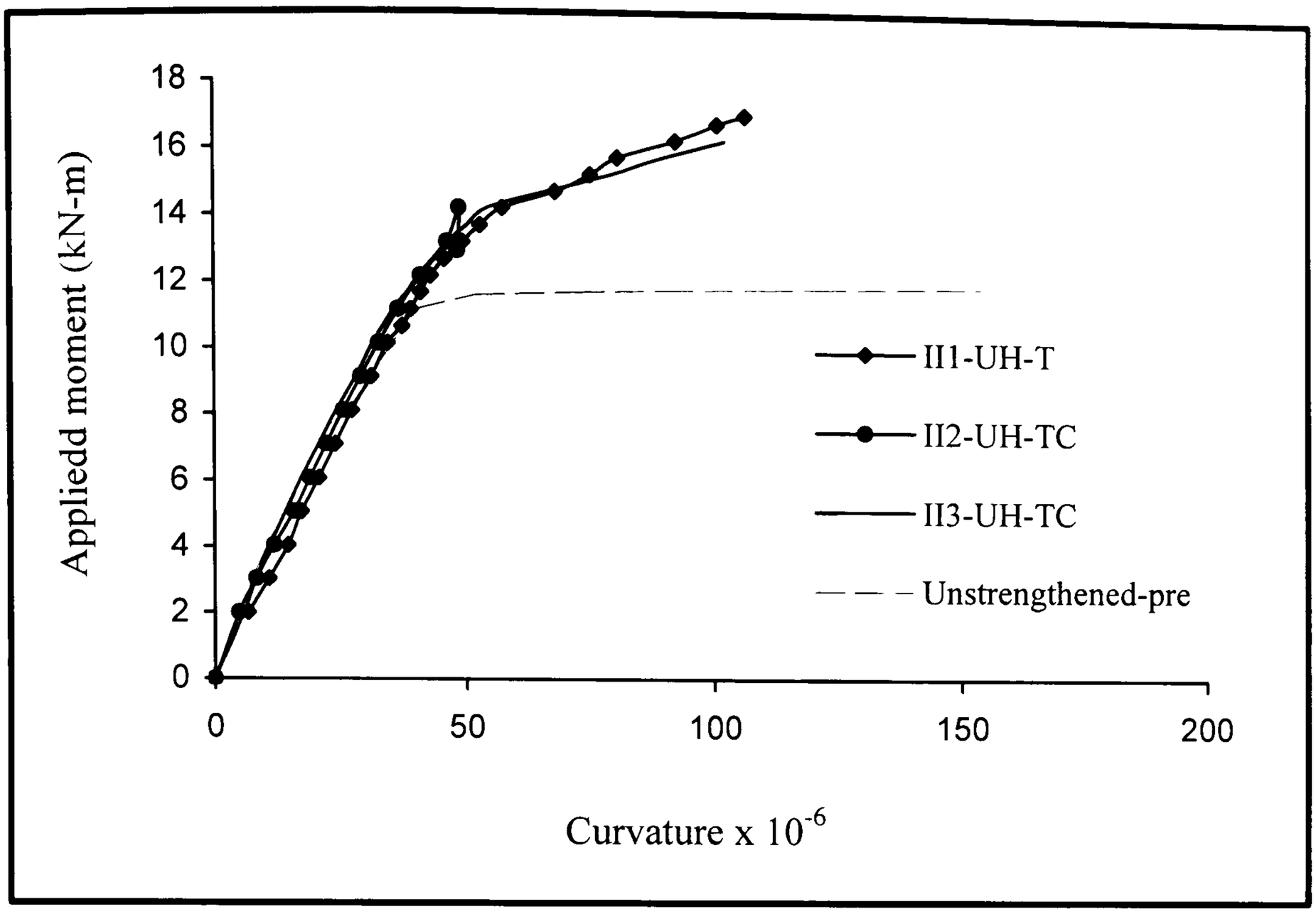

Figure 4.20: Moment-Curvature relationship for the beams tested in the series-II

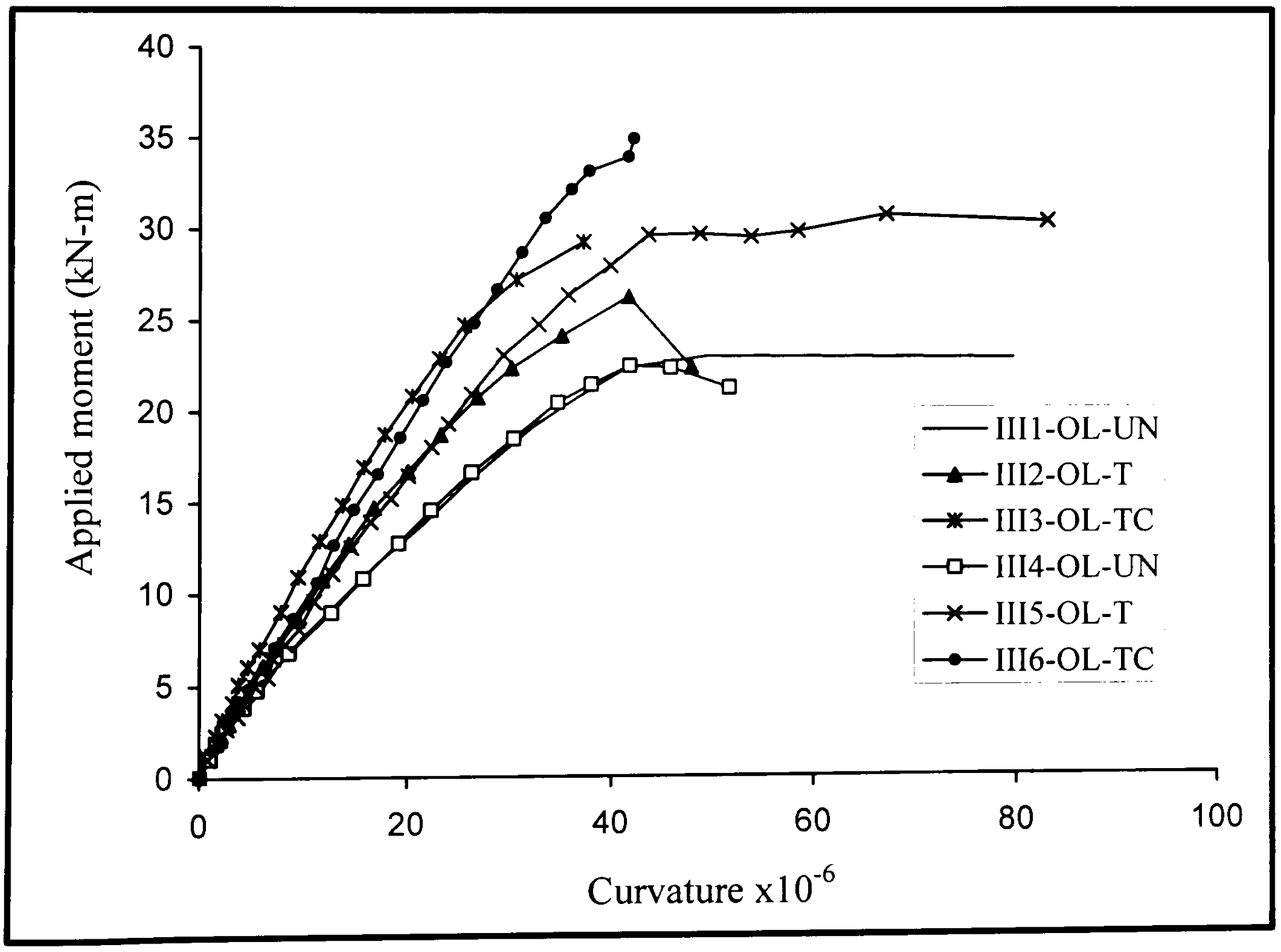

Figure 4.21: Moment-Curvature relationship for the beams tested in the series-III

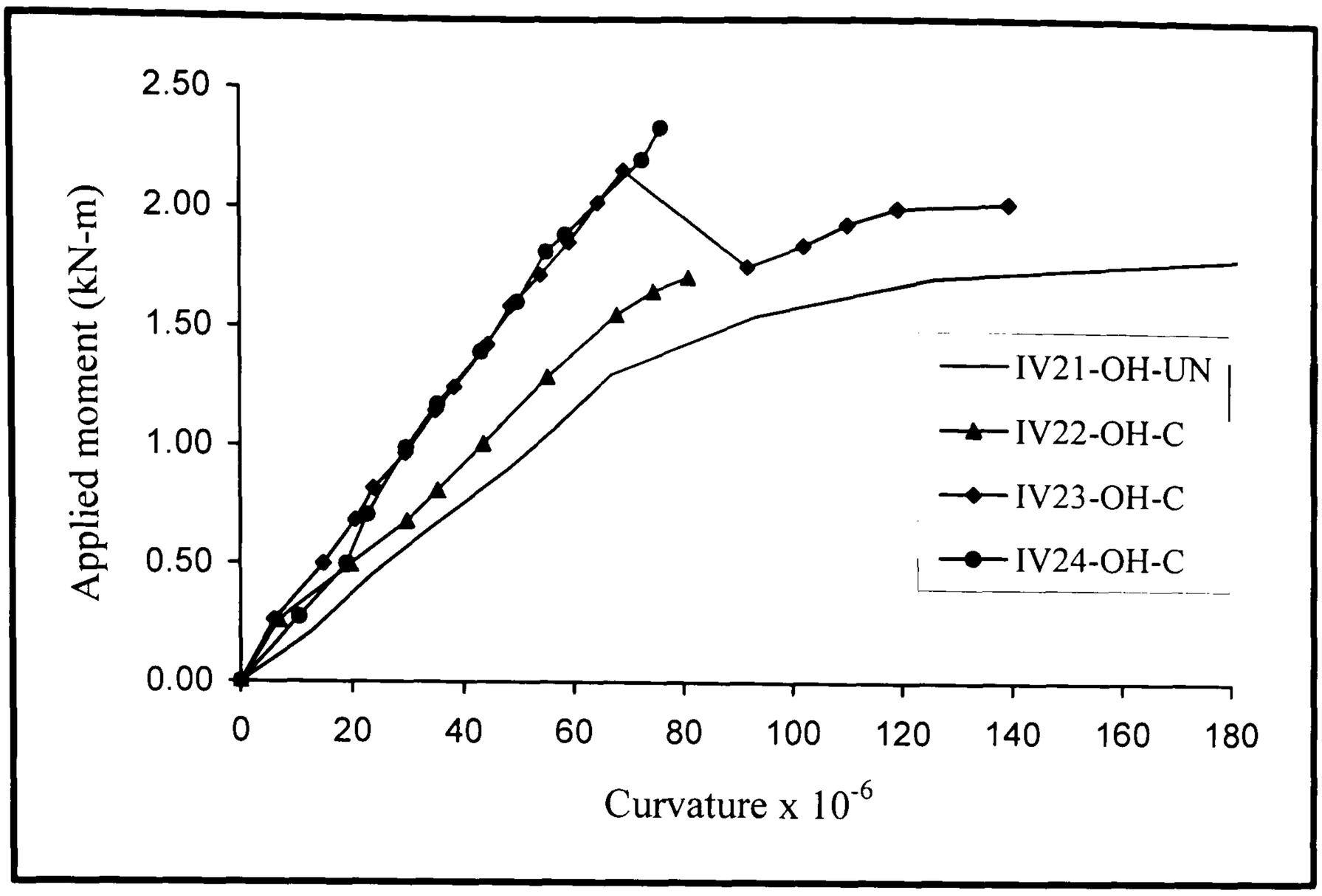

Figure 4.22: Moment-Curvature relationship for the second group beams tested in the series-IV

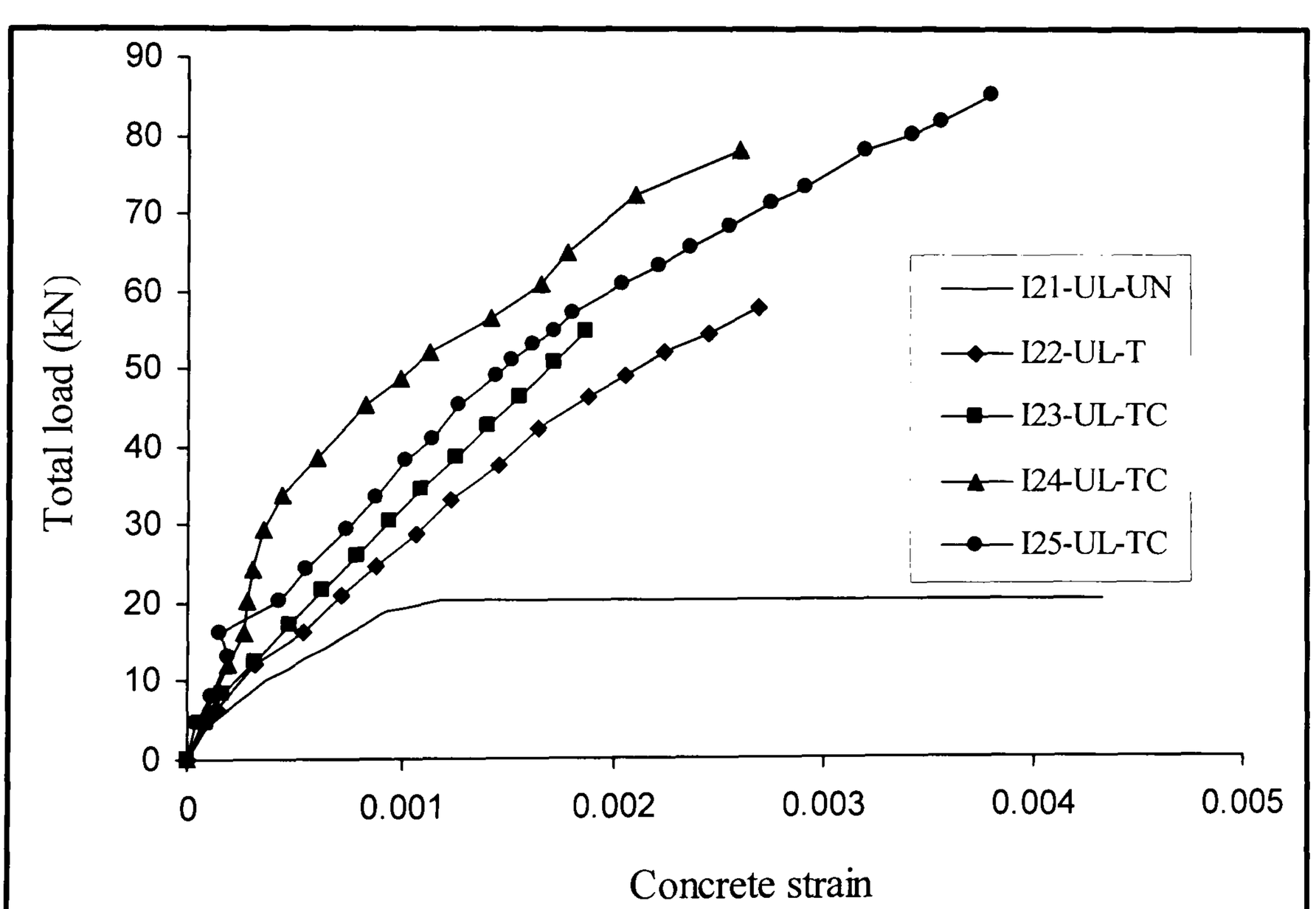

Figure 4.23: Total load versus concrete strain for the beams tested in the series-I

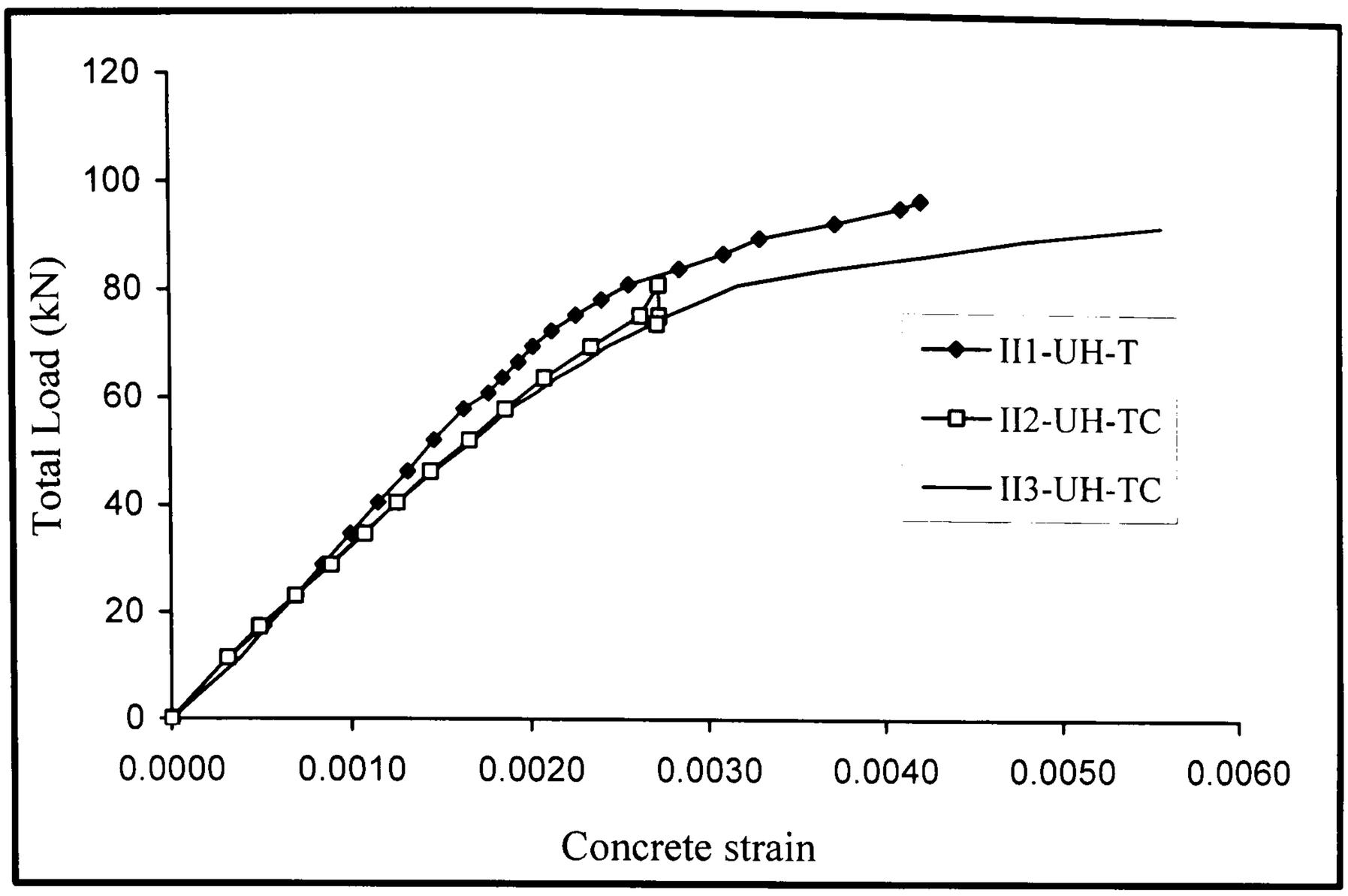

Figure 4.24: Total load versus concrete strain for the beams tested in the series-II

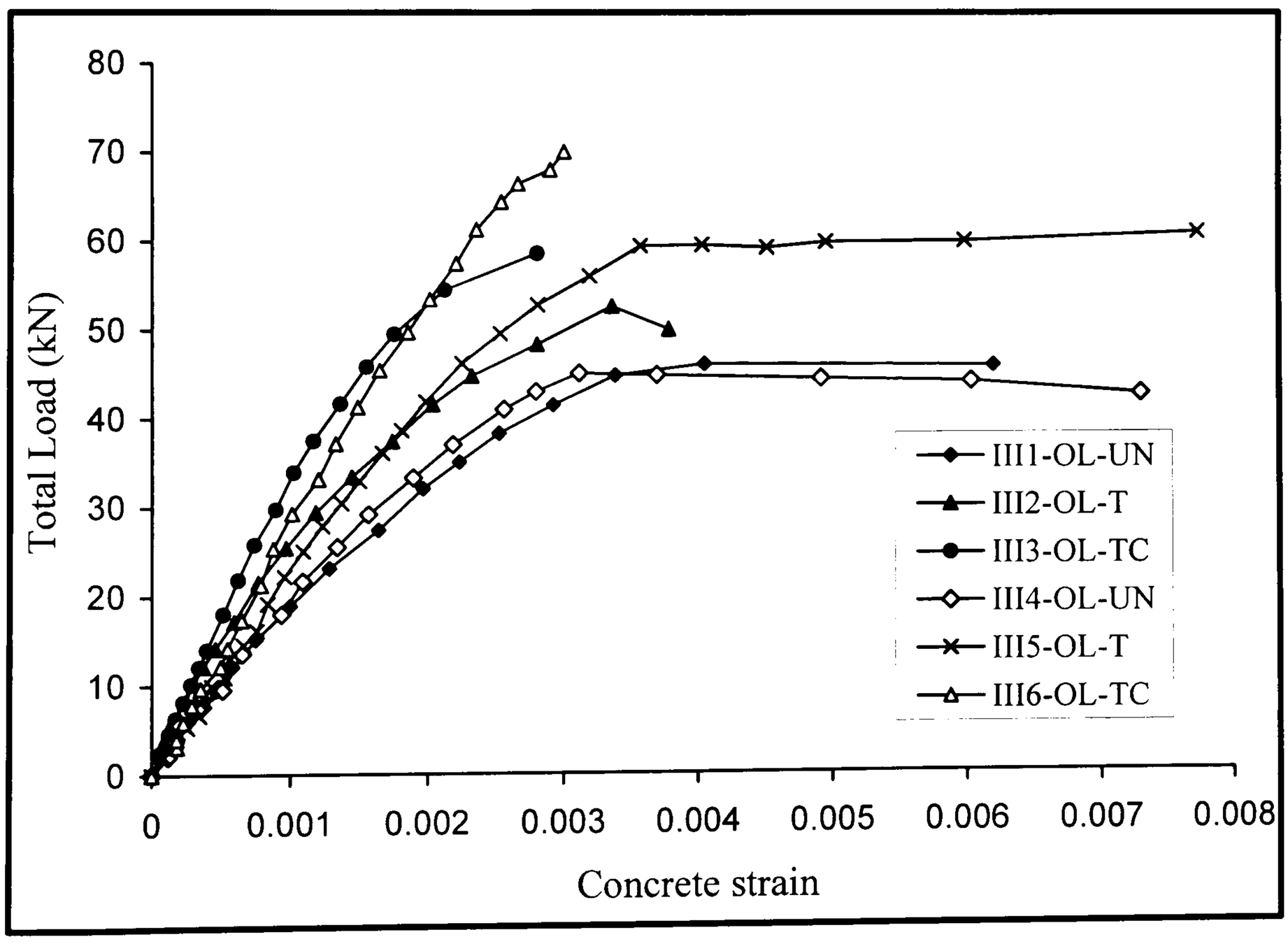

Figure 4.25: Total load versus compression strain for the beams tested in the series-III

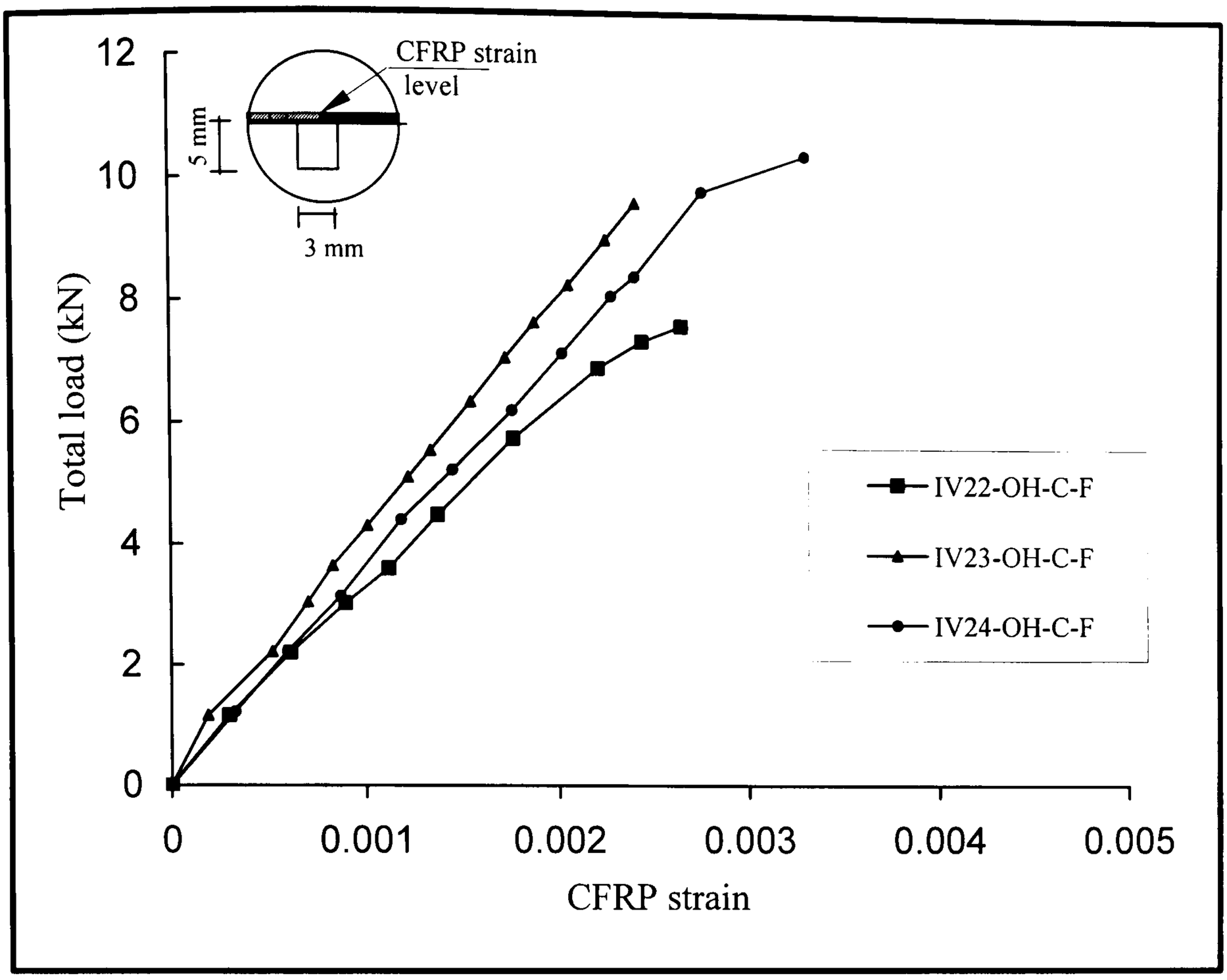

Figure 4.26: Total load versus compression CFRP strain for the second group specimens of IV-series

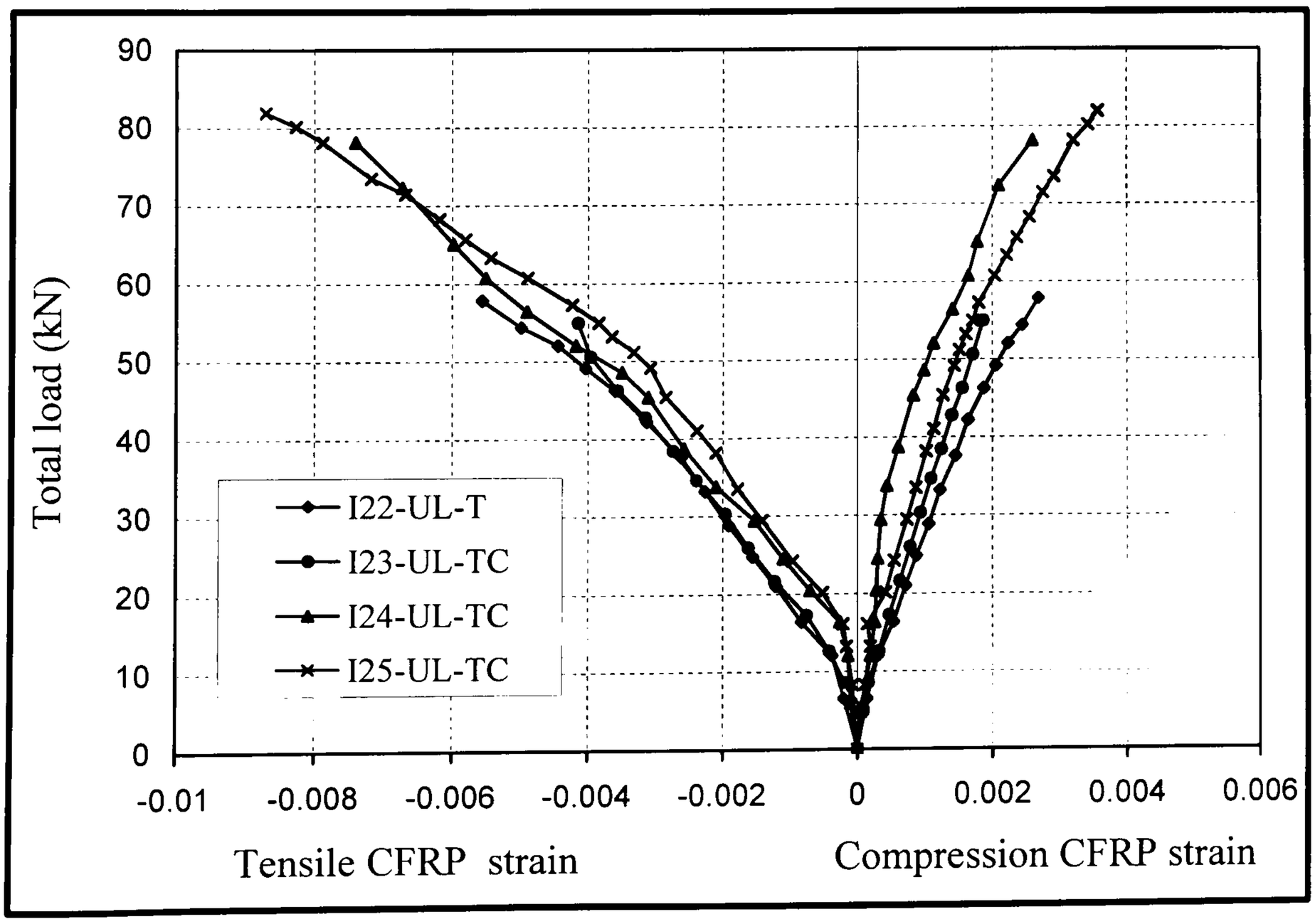

Figure 4.27: Total load versus CFRP laminate strain for the second group beams tested in the series -I

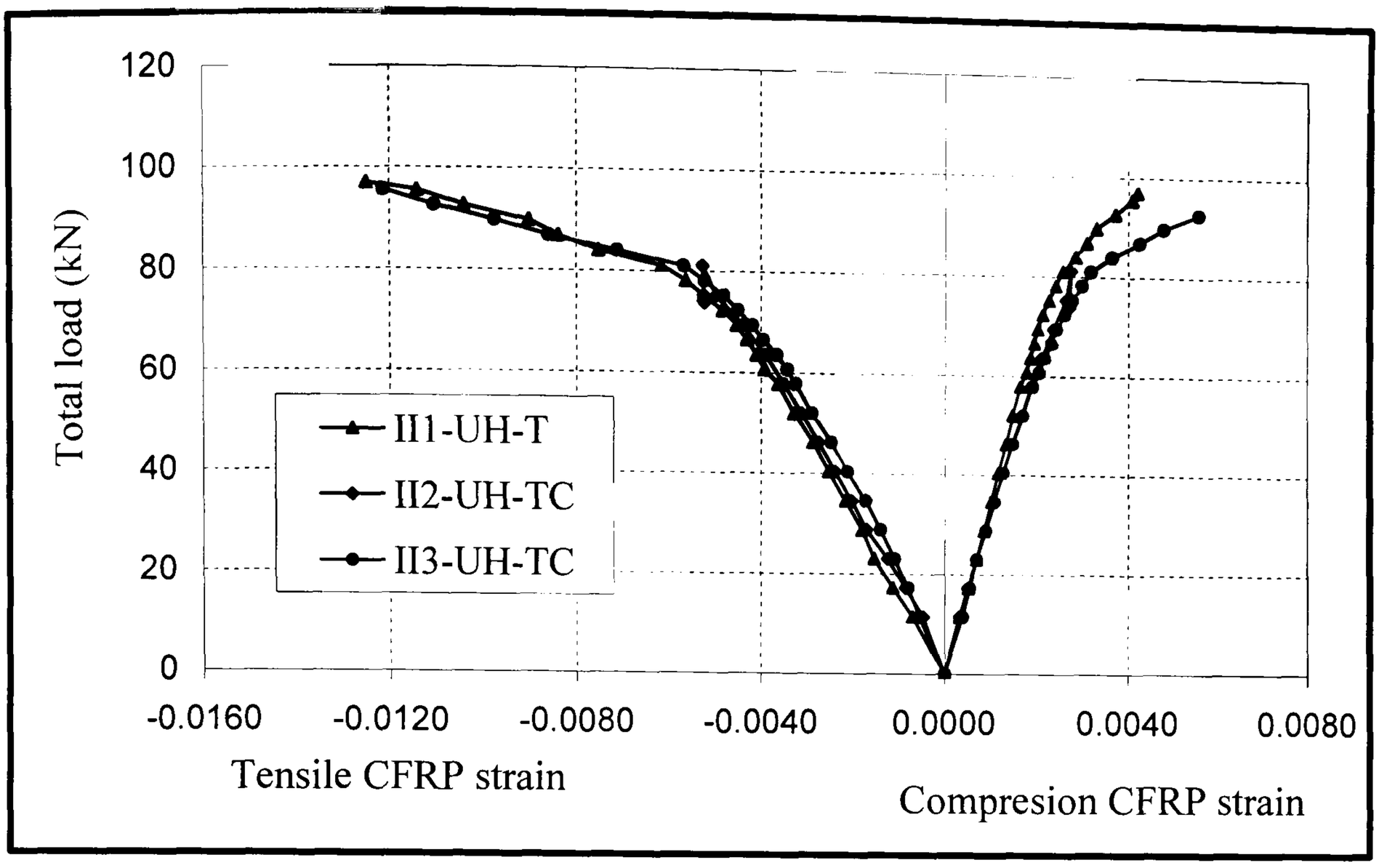

Figure 4.28: Total load versus CFRP laminate strain for the beams tested in the series-II

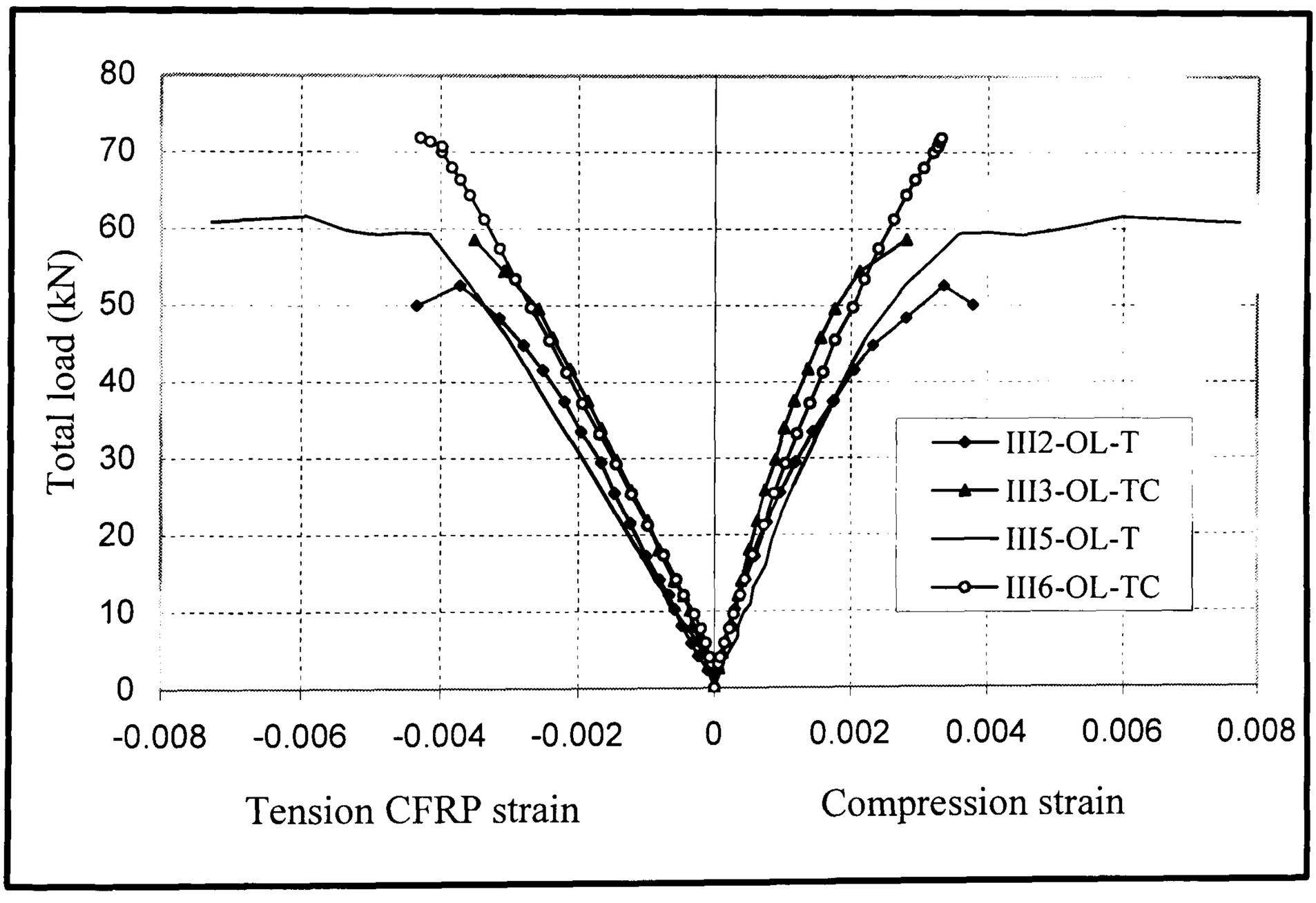

Figure 4.29: Total load versus CFRP laminate strain for the beams tested in the series-III

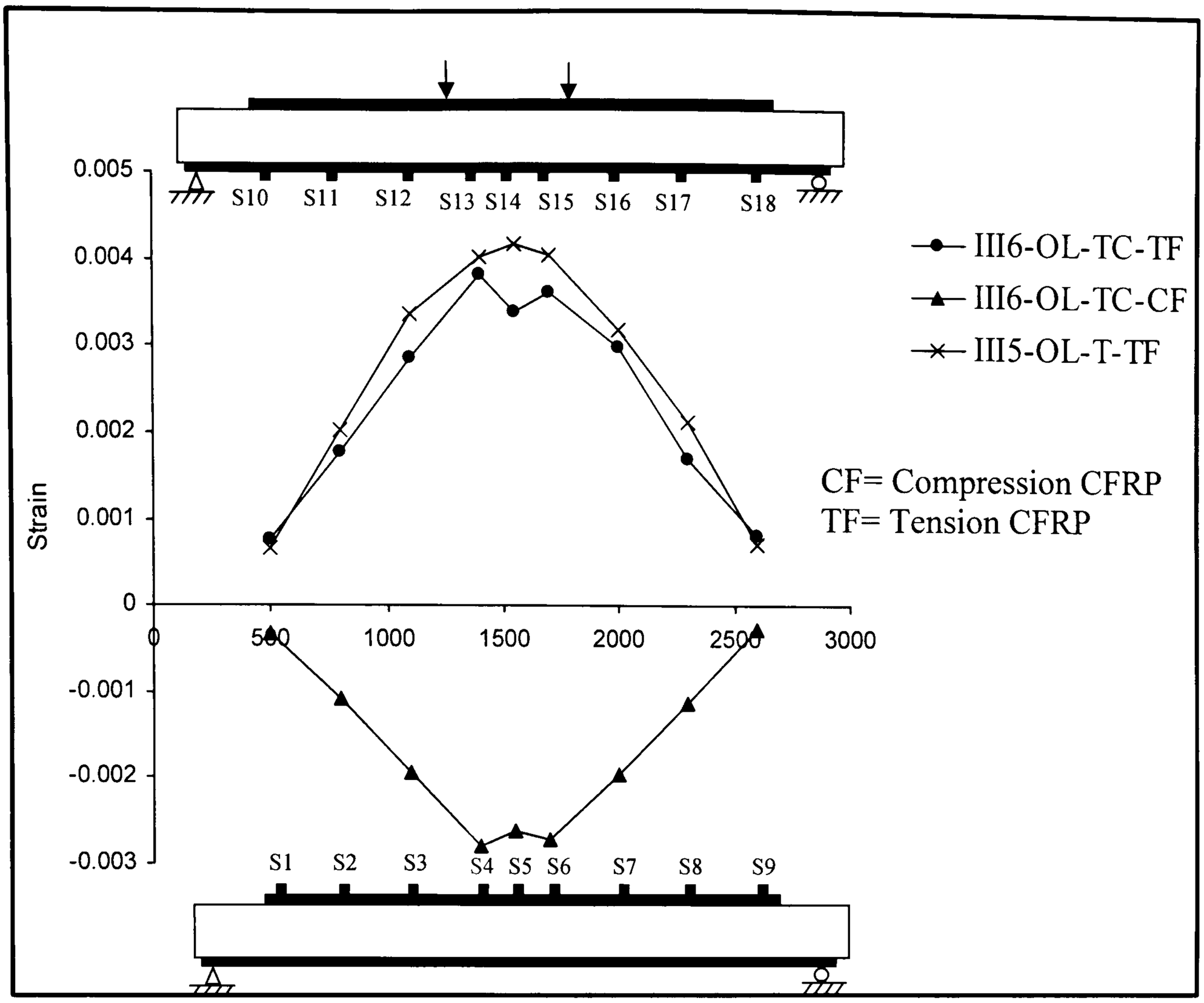

Figure 4.30: Strain distribution in the compression and tension CFRP laminates along the span of the beams III5-OL-T and III6-OL-TC at a load of 61kN.

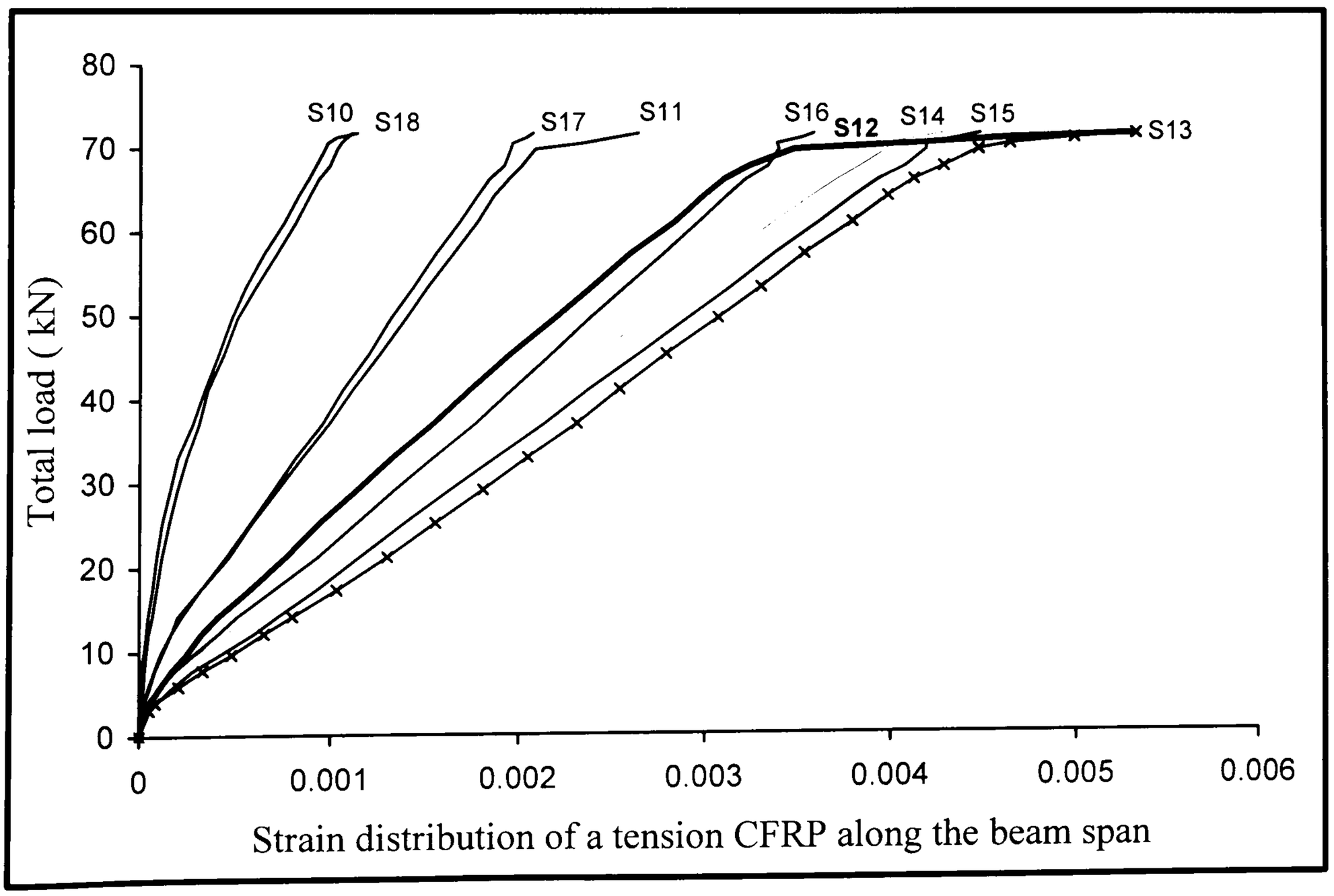

Figure 4.31: Strain distributions in the tension CFRP laminate along the spans of beam III6-OL-TC

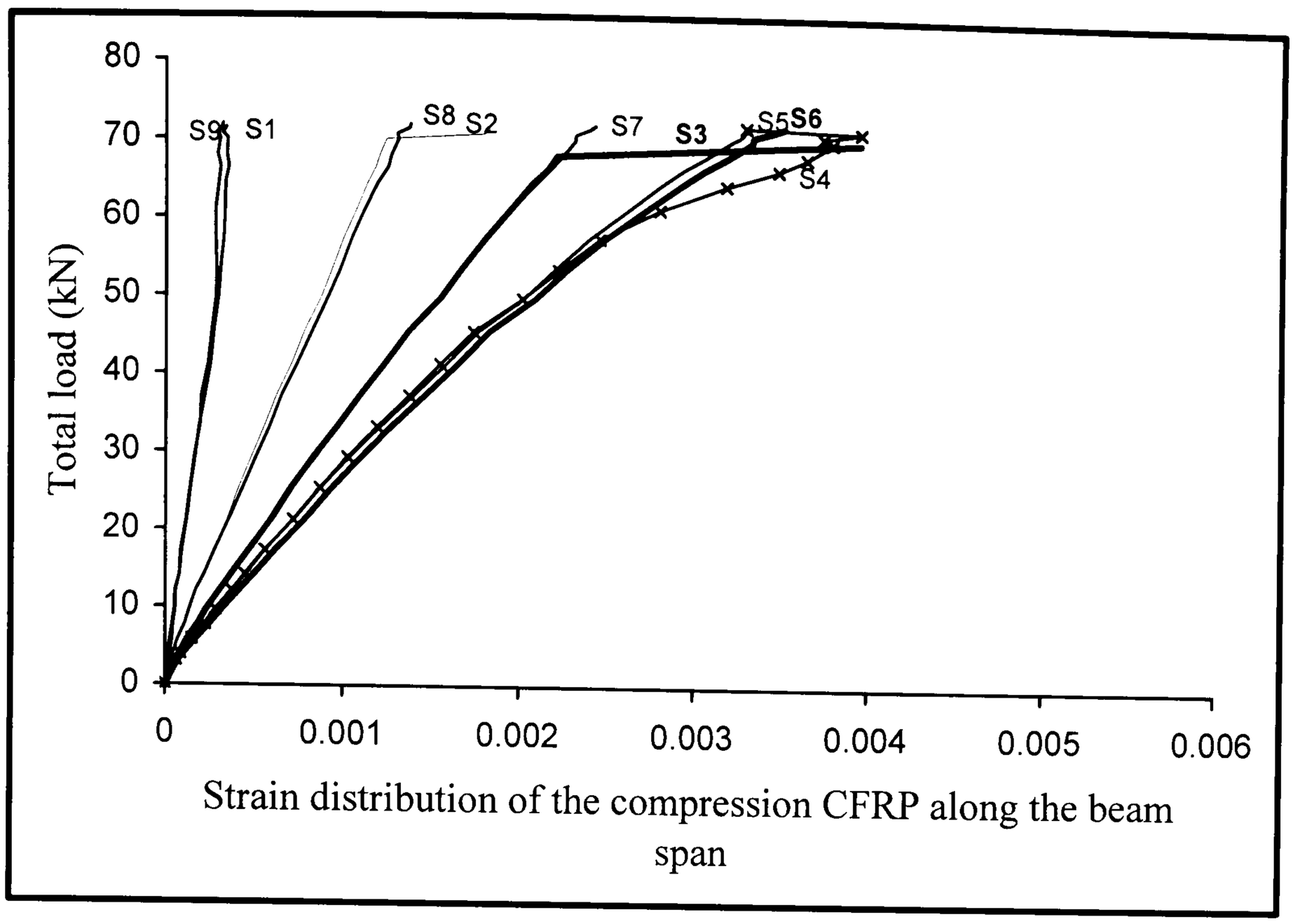

Figure 4.32: Strain distributions in the compression CFRP laminate a long the span of beam III6-OL-TC

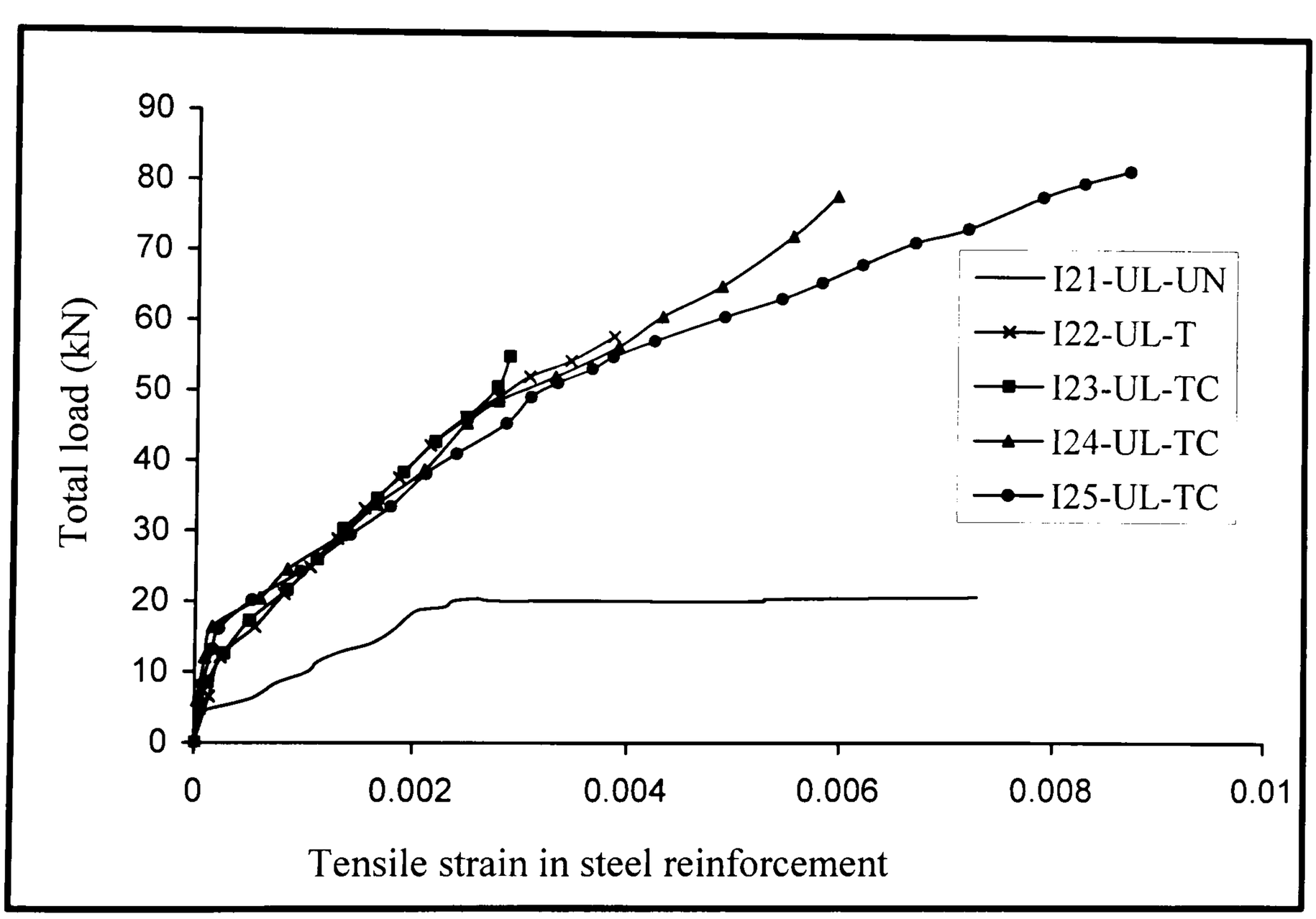

Figure 4.33: Total load versus internal tensile steel reinforcement strain for the second group beams of series-I

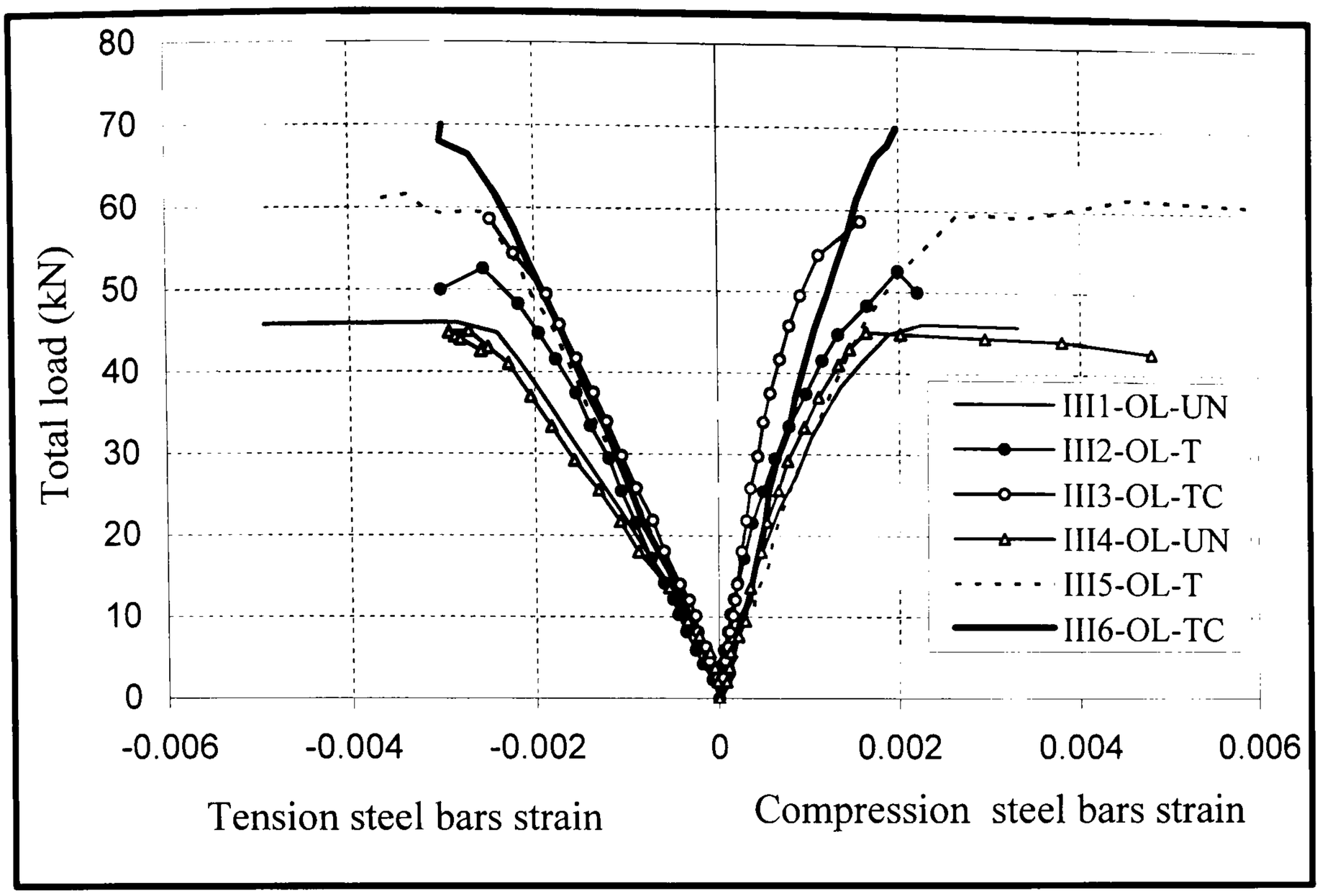

Figure 4.34: Total load versus internal steel reinforcement strain for the beams of series -III

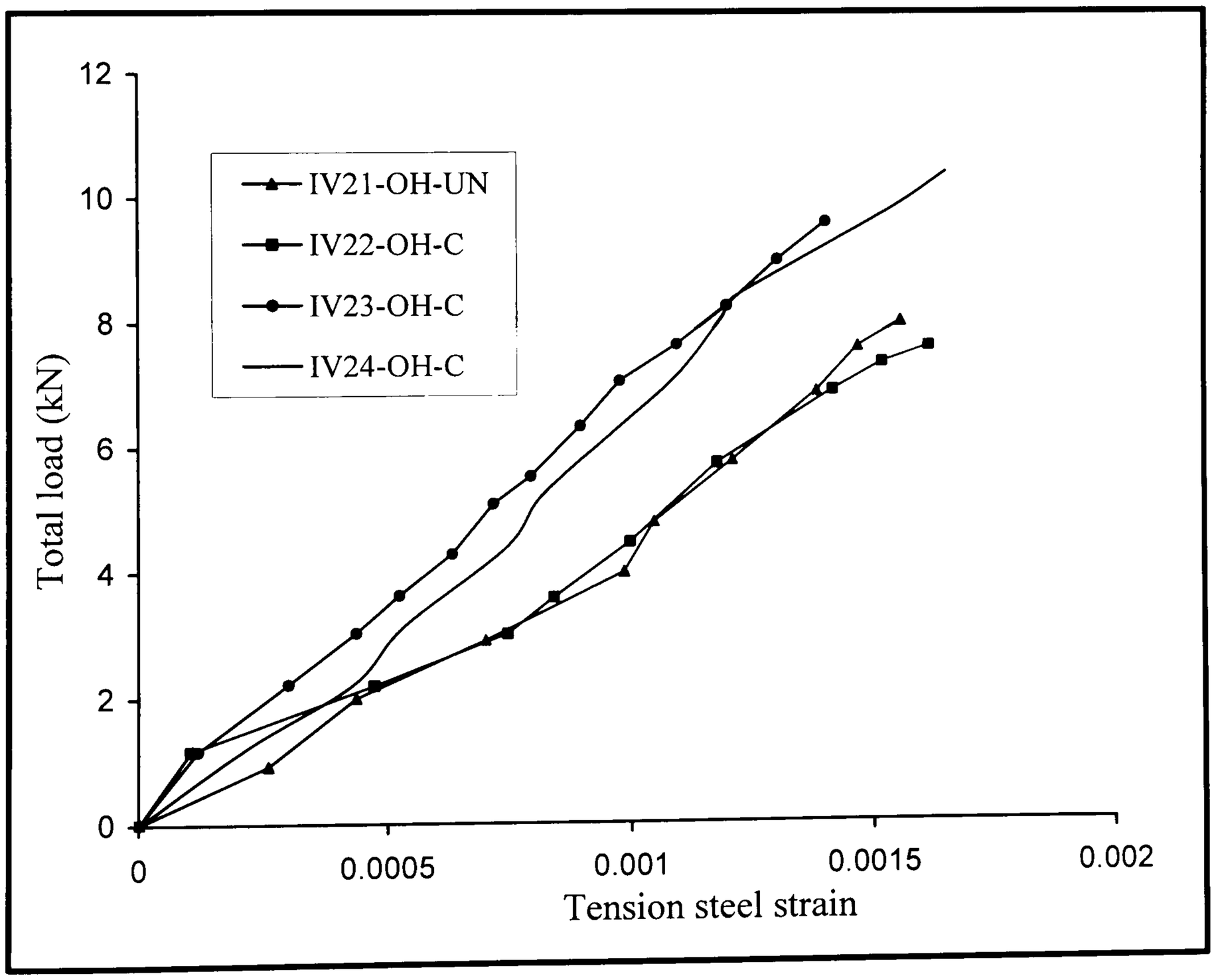

Figure 4.35: Total load versus internal steel reinforcement strain for the second group beams of series-IV

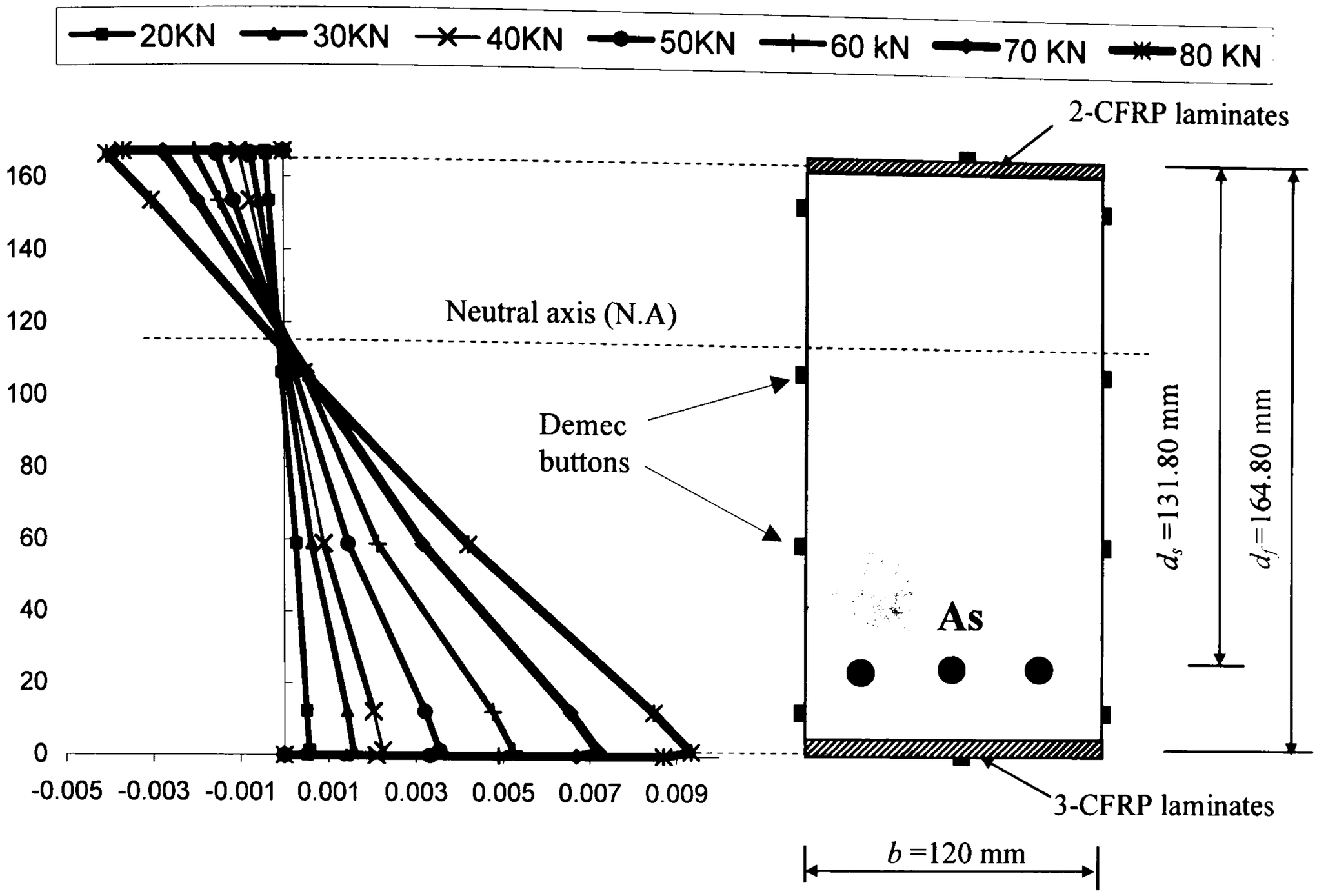

Figure 4.36: Distribution of the strain along the beam depth of lower steel ratio, beam I25-UL-TC

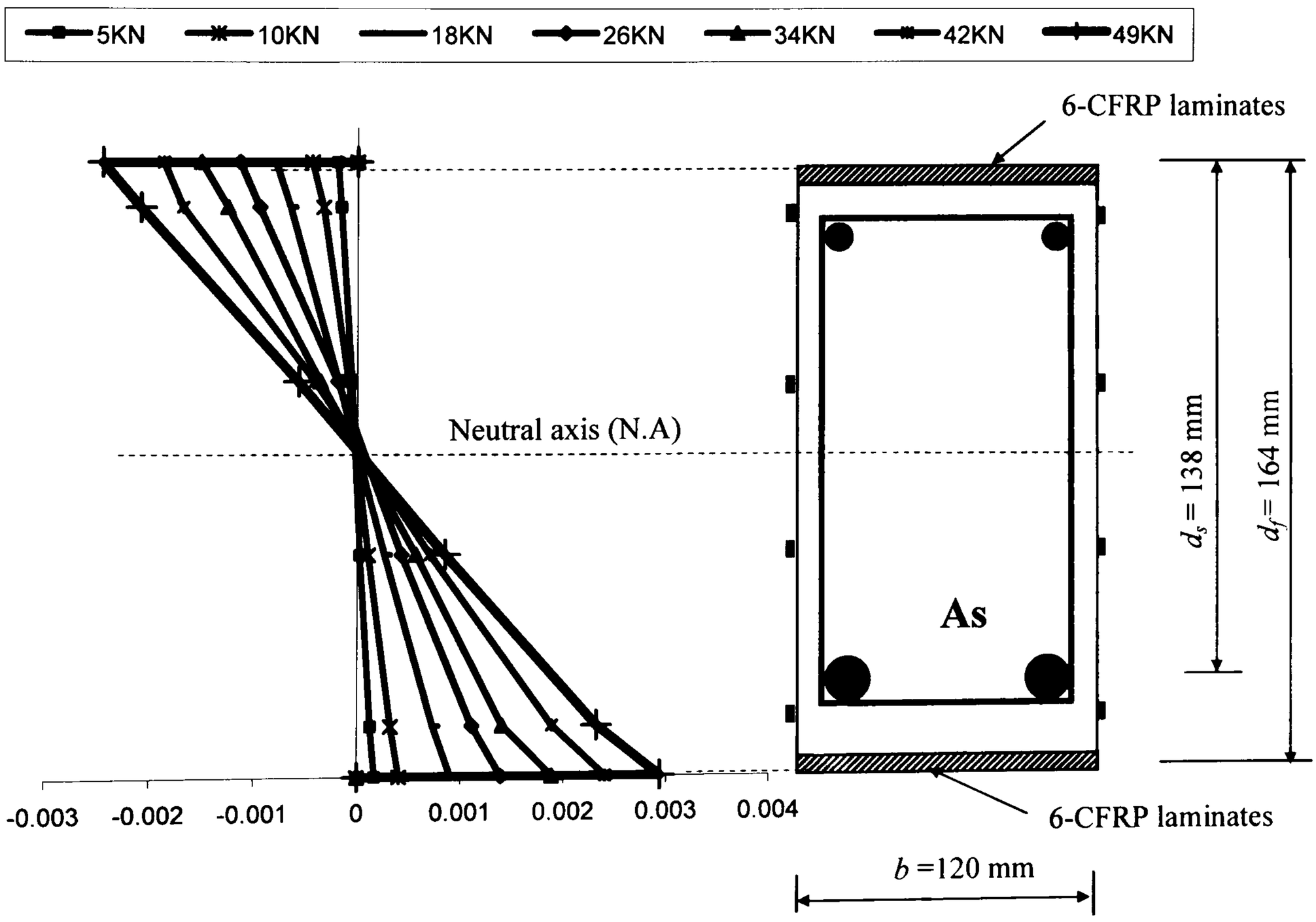

Figure 4.37: Distribution of the strain along the beam depth of higher steel ratio, beam III3-OL-TC

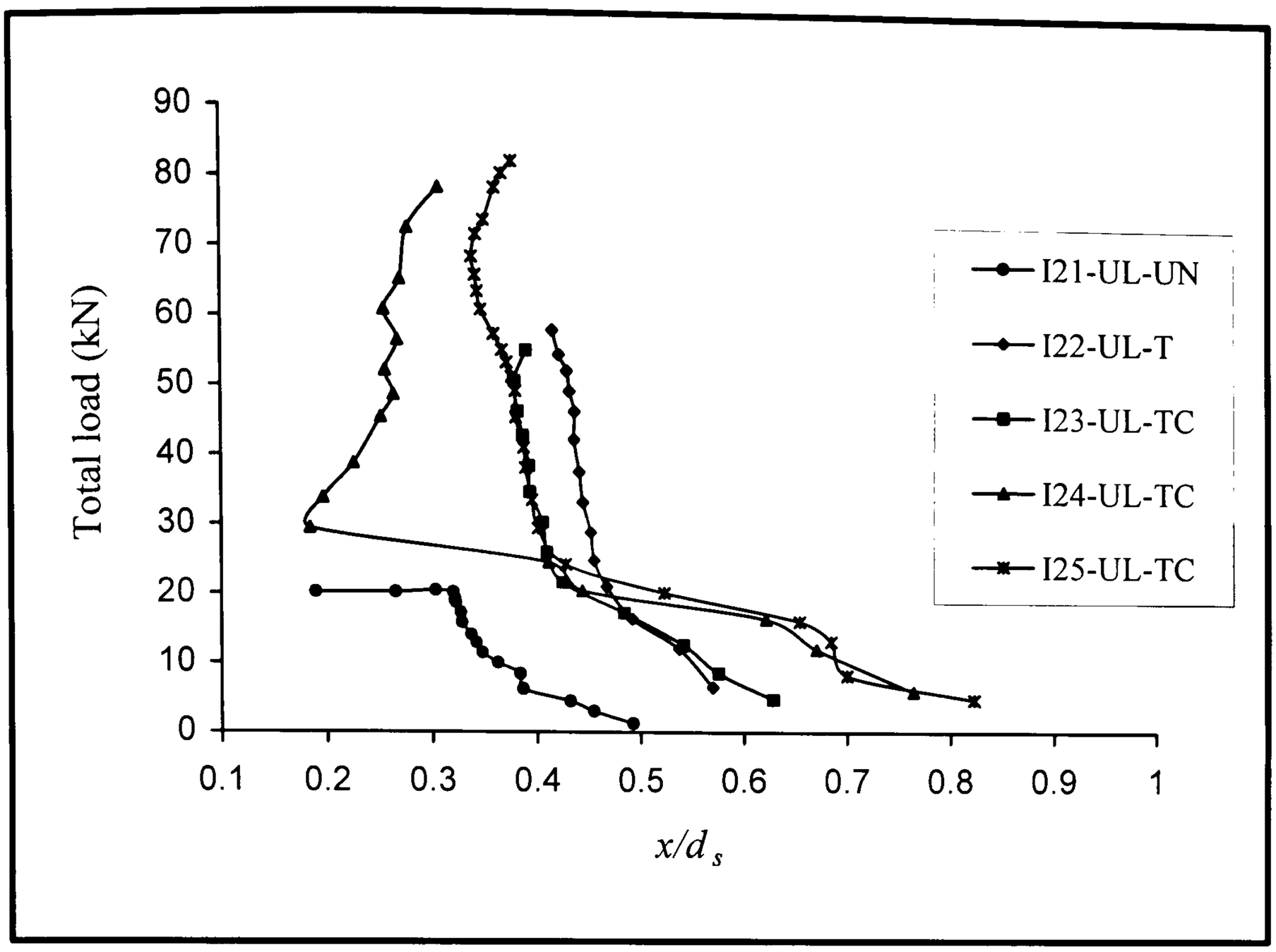

Figure 4.38: Total load versus the neutral axis of the second group beams of series-I

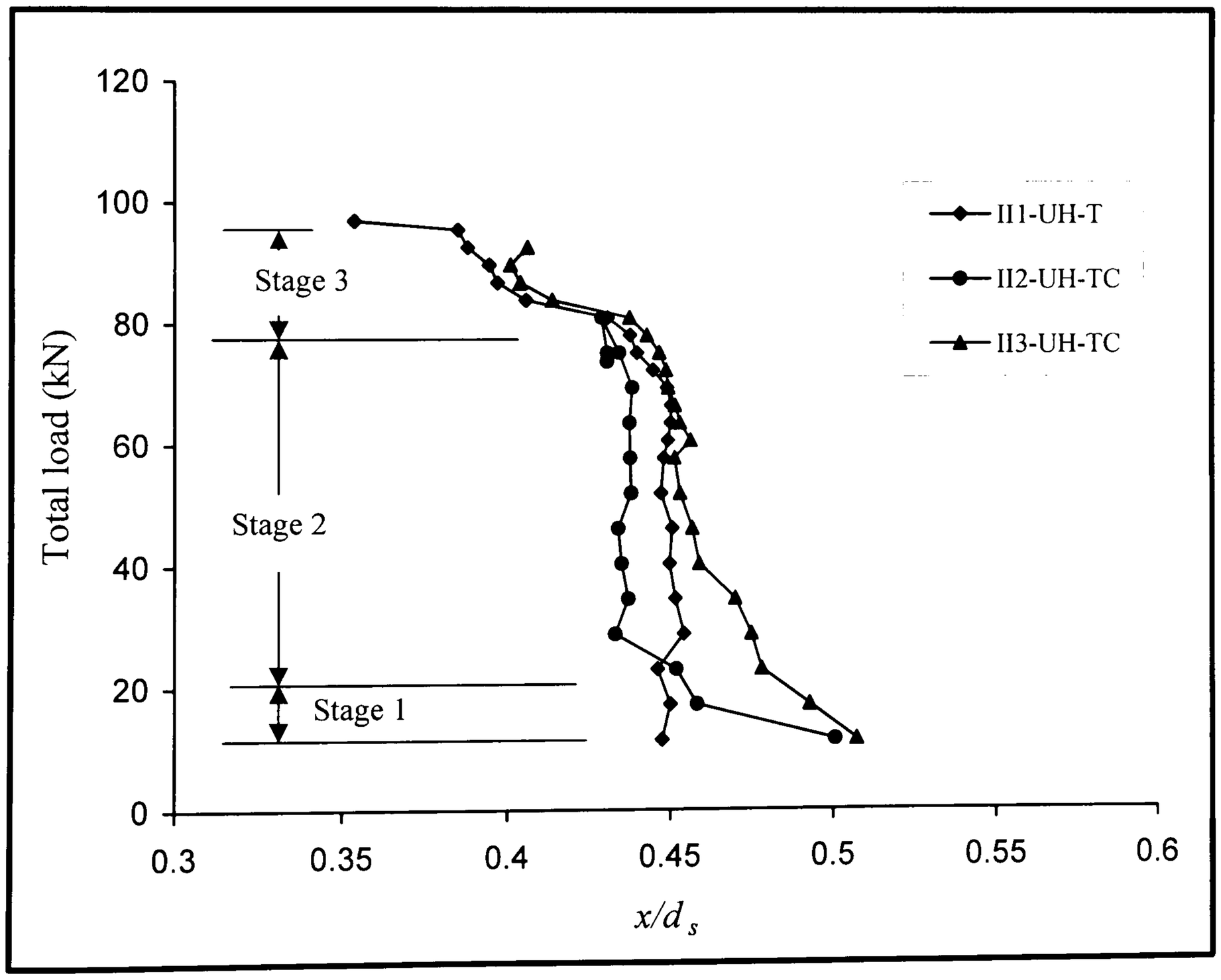

Figure 4.39: Total load versus the neutral axis of the strengthened beams of series-II

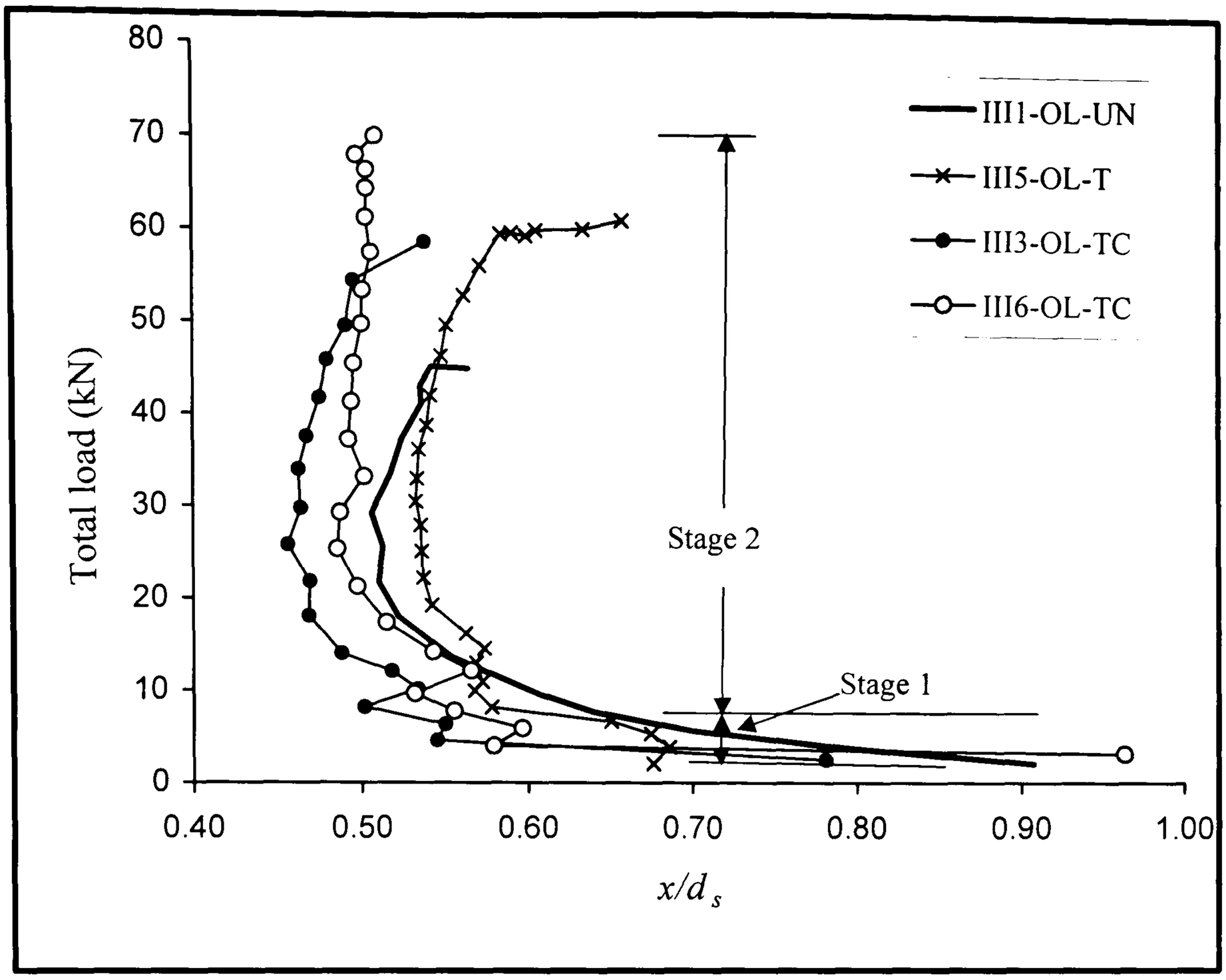

Figure 4.40: Total load versus the neutral axis in the beams of series-III

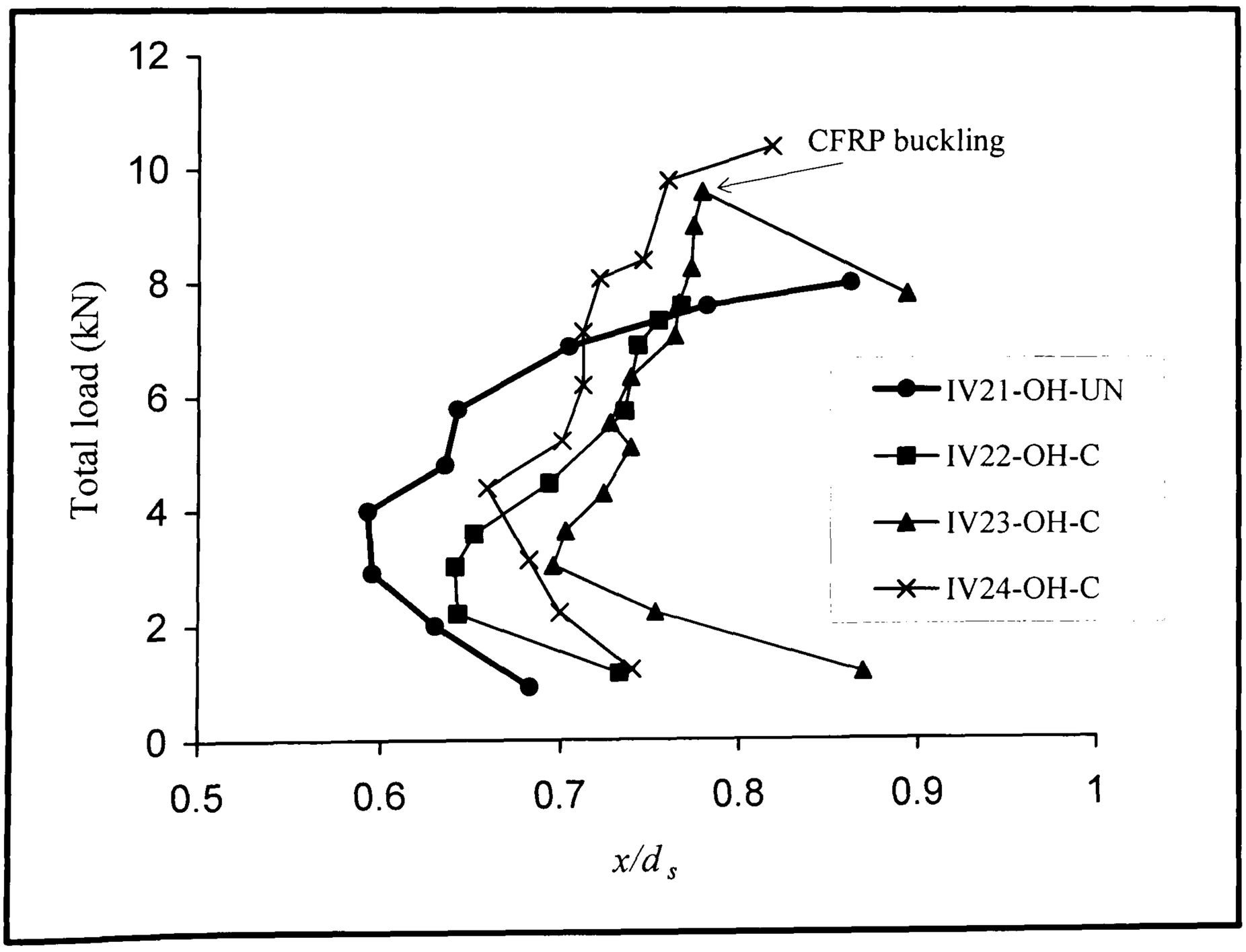

Figure 4.41: Total load versus the neutral axis of the strengthened beams of series-IV

CHAPTER 5

ANALYSIS, DESIGN AND NUMERICAL MODELS OF RC MEMBERS STRENGTHENED WITH CFRP LAMINATES

5.1 General

This Chapter describes the theoretical models used to predict the behaviour of the reinforced concrete members strengthened with CFRP. The results obtained from these models are compared in Chapter 6 with those measured in the laboratory experiments. The models are categorised into two types. The first are the analytical models, which are based on mathematical formulations and computer calculations. The analytical models comprise moment-curvature relationship, load-deflection and a simplified procedure for design. The second category is a finite element model, using the LUSAS software computer package.

5.2 Analytical modelling of structural behaviour

An analytical model has been developed to predict the behaviour of reinforced concrete beams strengthened with CFRP laminates bonded to the tension and compression zones of beams. This was done in order to gain an understanding of the factors that effect strengthening. In addition to predicting the behaviour of the strengthened beam, the analytical model was used to help develop a design procedure for strengthening beams using CFRP on the compression face.

The moment-curvature model predicts the behaviour of a section through the entire loading regime, and the load-deflection model predicts the behaviour of a member throughout the entire loading regime. The design method is used to determine the moment capacity of the section, based on strain compatibility and equilibrium of the forces. The models described in this chapter were used to examine the behaviour of the beams tested which were loaded in four point bending.

The three analytical models utilize equilibrium, strain compatibility of the cross sections, and the constitutive relations of the materials. The following assumptions were made when developing these analytical models:

1. Plane sections remain plane.
2. Flexural failure modes are studied only; no premature failure of the CFRP such as peeling or laminate separation is assumed.
3. The CFRP laminate is modelled as a membrane. It can resist axial load but has zero bending stiffness. The thickness of the CFRP is ignored due to the small value compared with the beam depth.
4. Perfect bond between CFRP and concrete surface up to failure is assumed.
5. The adhesive layer between the external reinforcement and the concrete beam is ignored.

5.3 Simplified models for flexural and deflection analysis

5.3.1 Introduction

In this section, two models for investigating the behaviour of simply supported reinforced concrete beams strengthened with CFRP are discussed. The models are the moment-curvature relationship and the load-deflection response. The material models for concrete, internal steel and external CFRP reinforcement are discussed in Section 5.3.2.

5.3.2 Material strength models

5.3.2.1 Concrete in compression

Concrete exhibits a nearly linear elastic stress-strain response up to about 30% of its compressive strength. This is followed by a reduction in the stiffness up to the

maximum concrete compressive strength. Beyond this compressive strength, the concrete stress-strain relation exhibits strain softening until failure takes place by crushing [124].

In order to model the above behaviour, the curve for the uniaxial stress-strain relationship introduced by Scott *et al.* (1982)[125], which modified the Kent and Park (1971)[126] model, was adopted in this study, Figure 5.1. In this model, the concrete stress-strain relationships in compression are described by three regions for concrete confined by rectangular shear reinforcement. In the current study the concrete was modelled as unconfined, by adopting the ratio of shear reinforcement $\rho_{sv} = 0$ and the factor $K = 1$ in equations 5-1 to 5-3. The relationship between the stress and strain for concrete is as follows:

Region I (AB, Figure 5.1):

$$f_c = Kf_{cy}\left[\frac{2\varepsilon}{\varepsilon_0} - \left(\frac{\varepsilon}{\varepsilon_0}\right)^2\right], \qquad \varepsilon \le \varepsilon_0 \tag{5-1}$$

Region II (BC, Figure 5.1):

$$f_c = Kf_{cy}\left[1 - Z\left(\varepsilon - \varepsilon_0\right)\right], \qquad \varepsilon_0 < \varepsilon \le \varepsilon_u \tag{5-2}$$

Region III (CD, Figure 5.1):

$$f_c = 0.2Kf_{cy}, \qquad \varepsilon > \varepsilon_u \tag{5-3}$$

where

$$\varepsilon_0 = 0.002K, \qquad K = 1 + \frac{\rho_{sv} f_{yv}}{f_{cy}}$$

$$Z = \frac{\tan\theta}{f_c} = \frac{0.5}{\varepsilon_{50uc} + \varepsilon_{50h} - 0.002K}$$

$$\varepsilon_{50uc} = \frac{3 + 0.29 f_{cy}}{145 f_{cy} - 1000}$$

$$\varepsilon_{50h} = \frac{3}{4}\rho_{sv}\sqrt{\frac{b_n}{s_h}}$$

where ε is the compressive concrete strain, ε_0 is the concrete strain at maximum stress, K is a factor which accounts for the strength increase due to confinement, Z is the strain softening slope, f_{cy} is the cylinder compressive strength of concrete in N/mm^2, f_{yv} is the yield strength of the stirrups, in N/mm^2, ρ_{sv} is the volume ratio of the stirrups and the concrete core measured to the out side of the stirrups, b_n is the width of the concrete core measured to the outside of stirrups and s_h is the spacing of the stirrups.

5.3.2.2 Concrete in tension

Until cracking occurs in the section, the stress-strain relationship of the concrete in tension is assumed to be linear elastic

$$f_t = E_c\varepsilon_t \qquad f_t \le \sigma_{c\,rack} \qquad (5\text{-}4)$$

where f_t, ε_t and E_c are the concrete tensile stress, tensile strain and the initial tangent modulus of the concrete, respectively, Figure 5.2. The parameter $\sigma_{c\,rack}$ is the cracking stress of the concrete.

Cracking of the concrete at any strip below the depth of the neutral axis was assumed to occur when the tensile stress in this particular strip was reached.

After the onset of cracking, the tensile forces across a crack are assumed to be zero. However, the concrete elements between the cracks are still able to resist the tension stress and this may increase the member stiffness. This effect is known as tension stiffening [127]. Fields and Bischoff (2004)[128] have reported that tension stiffening in reinforced concrete members depends on the effective area of concrete and the average

stress of concrete between cracks. The increase in the area of the tension steel was found to decrease the tension stiffening. Similar behaviour has been reported[128,129]. In the current investigation, tension softening is ignored due to the high ratio of tension steel reinforcement, in the majority of beams, used. In some beams the ratio of the tension steel reinforcement was 4.4%. Therefore, it is expected that the tension stiffening will not affect the results significantly.

5.3.2.3 Internal steel reinforcement

Ngo and Scordelies (1967)[131] and Vedo and Ghali (1977)[132] have reported that the strain hardening of the steel could be considered as linear from the yield stress point f_y up to the ultimate strain ε_{su}.

However, in the current study, the stress-strain relationship for the internal steel reinforcement in both tension and compression was modelled using a tri-linear relationship, Figure 5.3. This approximation gave a close value when compared with the steel stress-strain curves obtained from the tests of the reinforcement used, Figures 3.1a to 3.1c. In the elastic region, the stress-strain relationship was assumed to be linear up to yield, f_y. In the plastic region, strain hardening has been assumed using a linear relationship up to a strain of 0.5 of the failure strain ε_{su}, Figure 5.3. The limit of strain-hardening, ε_{sh}, was taken as $0.5\,\varepsilon_{su}$. In the final stage between a strain of $0.5\ \varepsilon_{su}$ and the ultimate strain ε_{su}, the stress was assumed to be constant, Figure 5.3.

Hence, the equations for the steel strength are divided into four regions:

1- Elastic region

$$f_s = \varepsilon_s E_s \qquad \varepsilon_s \le \varepsilon_y \tag{5-5}$$

2- Plastic strain hardening

$$f_s = f_y + (\varepsilon_s - \varepsilon_y) E_{s1} \qquad \varepsilon_y < \varepsilon_s \leq \varepsilon_{sh} \tag{5-6}$$

3- Plastic plateau

$$f_s = f_{su} \qquad \varepsilon_{sh} < \varepsilon_s \leq \varepsilon_{su} \tag{5-7}$$

4- Failure

$$f_s = 0 \qquad \varepsilon_s \geq \varepsilon_{su} \tag{5-8}$$

where, ε_s , ε_{su} , f_s , f_y and f_{su} are the steel strain, ultimate strain, stress in steel, yield stress and ultimate stress, respectively. The parameters E_s and ε_y, respectively, are the Young's modulus and yield strain of the steel reinforcement in the elastic region. Similarly, E_{s1} and ε_{sh} are the hardening slope and the strain at end of the strain hardening.

5.3.2.4 External CFRP

The CFRP which was bonded to both the tension and compression faces of the beams was assumed to exhibit linear elastic behaviour. In tension a maximum strain, ε_{fu}, in the CFRP was assumed. In compression, the maximum strain in the CFRP, $\varepsilon_{fcu} = 0.003$ was assumed, as observed in Section 4.7. Details of the stress-strain relationship of the CFRP are given in Figure 5.4.

The equations governing the relationship are:

CFRP tension

$$f_f = \varepsilon_f E_f \qquad \varepsilon_f \leq \varepsilon_{fu} \tag{5-9}$$

CFRP compression (by assuming different properties of the CFRP)

$$f_{fc} = \varepsilon_{fc} E_{fc} \qquad \varepsilon_{fc} \leq \varepsilon_{fcu} \tag{5-10}$$

where, ε_f , f_f and E_f are the strain, stress and Young's modulus, respectively, of the CFRP in tension. The ε_{fc} , f_{fc} and E_{fc} are the strain, stress and Young's modulus, respectively, of the CFRP in compression. The subscript u indicates to the ultimate strain. In the current study, Young's moduli of the CFRP in both the tension and compression face of the beam are equalled because same CFRP are used.

5.3.3 Moment-Curvature Model

The moment-curvature model is used to predict the behaviour of a section at any load. An iterative method is used in which the strain in the top fibre of concrete compression is incrementally increased from zero up to a value that gives the final bending moment. The proposed procedure developed for calculating the moment-curvature relationships are given in the flow chart, Figure 5.6. In addition to the assumptions given in Section 5.2, the moment-curvature relationship for the rectangular cross-section shown in Figure 5.5 is calculated using the following additional assumptions:

1. The concrete stress-strain relationship in tension behaves linearly until rupture, equation 5-4, Section 5.3.2.2.
2. The CFRP stress-strain relationships in tension and compression behave linear and satisfy equations 5-9 and 5-10 respectively, Section 5.3.2.4.

The procedure adopted for calculating the moment and the curvature of a beam, Figure 5.6, is:

1. The concrete cross-section depth is divided into l layers arranged parallel to the neutral axis. Figure 5.5a.
2. A small starting value of compression strain in the top fibre of the concrete is assumed.

3. An initial value for the depth of the neutral axis is assumed and the strain at the centroid of the layer is calculated based on plane sections remaining plane.
4. The stress in the layers of concrete, the steel reinforcing bars and the external CFRP laminates are obtained from the corresponding stress-strain relationships Figures 5.1 to 5.4, equations 5-1 to 5-10.
5. By considering the equilibrium, Figure 5.5c, the following equation is obtained.

$$F_c + F_{sc} + F_{fc} + T_c + F_s + F_f = 0 \tag{5-11}$$

where

$$F_c = a_c b \sum_{j=1}^{lc} f_{cj} \tag{5-12}$$

$$T_c = a_t b \sum_{p=1}^{lt} f_{tp} \tag{5-13}$$

F_c , T_c are the total compressive and the tensile forces in the concrete, respectively, Figure 5.5a and 5.5c and; a , b, h are the depth of each concrete strip layer, the beam width and depth respectively, Figure 5.5a; f , l , j , p are the concrete stress, number of concrete strips, concrete strip number in compression and tension, respectively. The subscripts c and t represent the concrete compression and tension, respectively. Compression is assumed to be positive.

Rewriting equation 5-11 in term of stresses and from equations 5-12 and 5-13 gives

$$a_c b \sum_{j=1}^{lc} f_{cj} + A_{sc} f_{sc} + A_{fc} f_{\mathrm{fc}} + a_t b \sum_{p=1}^{lt} f_{tp} + A_s f_s + A_f f_{\mathrm{f}} = 0 \tag{5-14}$$

Using the stress-strain relationship for steel and CFRP, the equation becomes

$$a_c b \sum_{j=1}^{lc} f_{cj} + A_{sc} \varepsilon_{sc} E_s + A_{fc} \varepsilon_{fc} E_{fc} + a_t b \sum_{p=1}^{lt} f_{tp} + A_s \varepsilon_s E_s + A_f \varepsilon_f E_f = 0 \qquad (5\text{-}15)$$

where

A_s, A_{sc}, E_s are the tension, compression steel area and Young's modulus of reinforcement in beams, respectively; A_f, A_{fc}, E_f, E_{fc} are the external tension, compression area and elasticity modulus of CFRP, respectively; $\varepsilon_s, \varepsilon_{sc}, \varepsilon_f, \varepsilon_{fc}$ are the strains in tension and compression for both the internal steel bars and the external CFRP, respectively. To calculate the strain at the centre of a strip, for example, the compression zone, Figures 5.5a and 5.5d, then from compatibility

$$\frac{\varepsilon_{aci}}{y_{ci}} = \frac{\varepsilon_i}{x} \qquad (5\text{-}16)$$

where

$$y_{ci} = x - \left(\sum_{j=1}^{lc-1} aci + \frac{aci}{2} \right)$$

substituting for y_{ci} in equation 5-16 and rearranging

$$\varepsilon_{aci} = \frac{\varepsilon_i}{x} \left\{ x - \left(\sum_{j=1}^{lc-1} aci + \frac{aci}{2} \right) \right\} \qquad (5\text{-}17)$$

ε_{aci} and ε_i are the strains at a centre of a compression strip aci and the top fibre of concrete compression, respectively; x is the distance from the extreme fibre of compression to the neutral axis and y_{ci} is the distance from the centroid of the compression strip to the neutral axis, *N.A*, Figure 5.5d. When the strains are negative,

i.e. tension, the parameters y_{ci} and ε_{aci} are replaced with y_{ti} and ε_{ati}. This means that the summation of the compression layer thicknesses ($\sum_{j=1}^{lc-1} {}_{aci}$) is less than the beam depth.

6. After tensile yielding of the steel occurs strain hardening is applied, equation 5-6, and then equation 5-15 becomes

$$a_c b \sum_{j=1}^{lc} f_{cj} + A_{sc}\,\varepsilon_{sc}\,E_s + A_{fc}\,\varepsilon_{fc}\,E_{fc} + a_t b \sum_{p=1}^{lt} f_{tp} + A_s\{f_y + (\varepsilon_s - \varepsilon_y)E_{s1}\} + A_f\,\varepsilon_f\,E_f = 0 \qquad (5\text{-}18)$$

7. The value of the depth of the neutral axis, x, is varied for the given value of concrete strain ε_{ci} until the force equilibrium condition is satisfied, equations 5-15 and 5-18.

8. When force equilibrium is satisfied for the given value of the concrete strain, the bending moment, M, is calculated, equation 5-19.

$$M = A_{fc}\,f_{fc}\,x + \sum_{j=1}^{lc} F_{cj}\,y_{ci} + A_{sc}\,f_{sc}\,(x\text{-}d_{sc}) + \sum_{p=1}^{lt} T_{tj}\,y_{ti} + A_s\,f_s\,(d_s\text{-}x) + A_f\,f_f\,(h\text{-}x) \qquad (5\text{-}19)$$

The corresponding curvature, φ, is given by Figure 5.5b.

$$\varphi = \frac{\varepsilon_i}{x_i} \qquad (5\text{-}20)$$

9. When the moment has been calculated the concrete strain at the compression face is recorded. The concrete extreme fibre compressive strain, ε_i, is then incremented and the previous procedure is repeated.

Spreadsheets using Microsoft Excel were developed to carry out the calculations.

5.3.4 Load-Deflection Model

The load-deflection model is used to predict the load-deflection behaviour of a reinforced concrete beam strengthened with CFRP laminates. The finite difference method was used to calculate the deflections of the beams for a given loading.

In the finite difference method, "difference" quantities are substituted for differential quantities. For example, the slope at point 2, Figure 5.7, is given by

$$\text{slope} = \theta_2 = \left(\frac{dv}{dx}\right)_2 \approx \left(\frac{\Delta v}{\Delta x}\right)_2 = \frac{v_3 - v_1}{2\Delta x} \tag{5-21}$$

in which the v is the deflection at the considered point. The grid spacing or the length of segment is designated as Δx, Figure 5.7. The grid spacing will influence the accuracy of the solution.

The approximation for curvature, φ, d^2v/dx^2 is obtained in a similar way,

$$\varphi_2 = \left(\frac{d^2v}{dx^2}\right)_2 = \left(\frac{d(\frac{dv}{dx})}{dx}\right)_2 \approx \frac{1}{\Delta x}\left[\left(\frac{v_3 - v_2}{\Delta x}\right) - \left(\frac{v_2 - v_1}{\Delta x}\right)\right] \tag{5-22}$$

$$= \frac{v_3 - 2v_2 + v_1}{(\Delta x)^2} \tag{5-23}$$

and in general, at points $n-1$, n and $n+1$, this gives

$$\varphi_n = \left(\frac{d^2v}{dx^2}\right)_n \approx \frac{v_{n+1} - 2v_n + v_{n-1}}{(\Delta x)^2} \tag{5-24}$$

where n and Δx are the segment number and the length of segment. And φ_n is the curvature at 'n' along the beam span.

The curvature, by assuming elastic behaviour, can be written as follows:

$$\left(\frac{d^2v}{dx^2}\right)_n = \varphi_n = \left(\frac{M(x)}{EI_z}\right)_n \tag{5-25}$$

where M and EI_z are the bending moment at the position n along the beam and the stiffness of the beam within the segment length.

In the current study, the bending moment and the corresponding curvature at the mid-span up to the failure of the beam were calculated, Section 5.3.3. The moment and the corresponding curvature diagrams were divided into ten and twenty segments along the length of the beam, Figure 5.8.

Because of symmetry only half of the beam was analysed.

Based on equation 5-24, for any structure divided into equal elements the finite difference method can be represented as

$$\frac{1}{\Delta x^2}\,[\mathrm{A}]\,v = \varphi \tag{5-26}$$

where φ and v are the curvatures and the displacements at the nodes, respectively. A is a rectangular asymmetrical matrix.

Boundary conditions

In dealing with boundary conditions, the end nodes (over the supports) and those immediately adjacent to them, nodes 0 and 2 and *n-1* and *n+1*, Figure 5.8 requires special consideration when the finite difference method is used.

If the beam end is a hinged support as in Figure 5.9, an auxiliary point 0 is introduced since $\theta_{1-0} = \theta_{1-2}$ then the boundary conditions are:

$$v_0 = - v_2 \tag{5-27}$$

similarly for the remote end

$$v_{n+1} = - v_{n-1} \tag{5-28}$$

and

$$v_1 = v_n = 0 \tag{5-29}$$

At the mid-span of the beam, point $n/2$, the rotation is zero. The maximum deflection also occurs at point $n/2$, Figure 5.8, thus the deflections at the points $n/2$-1 and $n/2$ +1, on either side of point $n/2$ are equal. Therefore

$$v_{(n/2)-1} = v_{(n/2)+1} \tag{5-30}$$

Matrix representation of solution

From equations 5-24 and 5-26 the general form of the matrix for the beam along the span is expressed by

$$\frac{1}{\Delta x^2}\begin{bmatrix} 1 & -2 & 1 & 0 & 0 & 0 & 0 & 0 \\ 0 & 1 & -2 & 1 & 0 & 0 & 0 & 0 \\ 0 & 0 & 1 & -2 & 1 & 0 & 0 & 0 \\ 0 & 0 & 0 & 1 & -2 & 1 & 0 & 0 \\ .. & .. & .. & .. & .. & .. & .. & .. \\ 0 & 0 & 0 & 0 & 1 & -2 & 1 & 0 \\ 0 & 0 & 0 & 0 & 0 & 1 & -2 & 1 \end{bmatrix}\begin{bmatrix} v_0 \\ v_1 \\ v_2 \\ v_3 \\ v_4 \\ \dots \\ v_{n-1} \\ v_n \\ v_{n+1} \end{bmatrix} = \begin{bmatrix} \varphi_1 \\ \varphi_2 \\ \varphi_3 \\ \varphi_4 \\ \dots \\ \varphi_{n-1} \\ \varphi_n \end{bmatrix} \tag{5-31}$$

The introduction of auxiliary points at the beam supports includes the displacements v_0 and v_{n+1} at the points 0 and *n+1*. The boundary equations 5-27, 5-28 and 5-29 are applied to the matrix equation 5-31. By eliminating the relevant values, the final form of the matrix for the beam becomes a tridiagonal symmetric singular matrix

$$\frac{1}{\Delta x^2}\begin{bmatrix} -2 & 1 & 0 & 0 \\ 1 & -2 & 1 & 0 \\ 0 & 1 & -2 & 1 \\ .. & .. & .. & .. \\ 0 & 0 & 1 & -2 \end{bmatrix}\begin{bmatrix} v_2 \\ v_3 \\ v_4 \\ \dots \\ v_{n-1} \end{bmatrix} = \begin{bmatrix} \varphi_2 \\ \varphi_3 \\ \varphi_4 \\ \dots \\ \varphi_{n-1} \end{bmatrix} \tag{5-32}$$

Because only half of the beam was analysed equation 5-30 was applied to the matrix equation 5-32, and the final form of the matrix was rewritten as

$$\frac{1}{\Delta x^2}\begin{bmatrix} -2 & 1 & 0 & 0 \\ 1 & -2 & 1 & 0 \\ 0 & 1 & -2 & 1 \\ .. & .. & .. & .. \\ 0 & 0 & 2 & -2 \end{bmatrix}\begin{bmatrix} v_2 \\ v_3 \\ v_4 \\ .. \\ v_{(n/2)} \end{bmatrix} = \begin{bmatrix} \varphi_2 \\ \varphi_3 \\ \varphi_4 \\ .. \\ \varphi_{(n/2)} \end{bmatrix} \quad (5\text{-}33)$$

Using equations 5-26 and 5-33, the displacements are given by

$$v = \mathrm{B}^{-1}\varphi \quad (5\text{-}34)$$

where B^{-1} is the inverse of $\frac{1}{\Delta x^2}$ [A]

Using MATLAB, the matrix B in equations 5-33 and 5-34, was inverted and multiplied by the curvature vector to obtain the displacements v_2, v_3..... $v_{(n/2)}$ at points 2, 3.... $(n/2)$. The curvature vector along half of the beam was calculated from the bending moments and the curvatures which were determined in Section 5.3.3.

The results calculated using this numerical technique for the beams tested will be compared with the experimental results in Chapter 6.

5.4 Simplified Model for Flexure Design

5.4.1 Introduction

The simplified model used to determine the ultimate flexural strength for the design of reinforced concrete members strengthened with CFRP. In addition to the assumptions presented in Section 5.2, for the simplified model the following further assumptions are made:

- The ultimate moment is reached when the concrete strain in the extreme compression fibre reaches a value of 0.0035 for unstrengthened beams or beams strengthened on the tension face only and 0.003 for beams strengthened on the compression face, Section 5.4.4.

- The tensile strength of concrete is ignored.

- The parabolic concrete stress distribution is replaced by an equivalent rectangular block with stresses as shown in Fig. 5.11e. This is in accordance with BS8110 [9]. The idealised rectangular stress block is represented by two parameters k_1, the mean concrete stress factor (the ratio of the average compressive stress to the concrete cube strength) and, k_2 the depth of the stress block factor (the ratio of the depth of the idealised rectangular stress block to the neutral axis depth). The values of the two factors are taken to be 0.67 and 0.9, respectively. The equivalent concrete strength is then expressed by

$$\sigma_c = k_1 f_{cu} \tag{5-35}$$

where f_{cu} is the compressive strength of the standard cube, N/mm^2.

- The ultimate stress of the CFRP in the tension face is used, Figure 5.4. The stress in the compression CFRP is that corresponding to a strain of 0.003, Figure 5.4. The stresses in the CFRP at tension and compression are obtained from equations 5-9 and 5-10, respectively.

- The stress-strain curve for the steel reinforcement is assumed to be elastic up to yield, Figure 5.3, and then plastic. The stresses and strains in the bars satisfy the following:

$$f_s = E_s \varepsilon_s \qquad \varepsilon_s < \varepsilon_y \tag{5-36}$$

$$f_s = f_y \qquad \varepsilon_s \geq \varepsilon_y \tag{5-37}$$

The terms in these equations are defined in Section 5.3.2.3.

- The strains and stresses of compression concrete, for all failure modes, are assumed positive.

5.4.2 Compatibility and equilibrium conditions

Since the assumption that plane sections remain plane during bending is made, the strain at any point through the section is linearly proportional to its distance from the neutral axis, x, Figure 5.11d. Assuming perfect bond between the concrete, the internal steel bars and the external CFRP, and considering the geometry, Figure 5.11d, the strain in each of the materials: ε_f in tension CFRP, ε_{fc} in the compression CFRP, ε_s in the tension steel bars and ε_{sc} compression steel bars can be calculated in terms of the maximum concrete compressive strain at collapse ε_{cu} as follows:

$$\varepsilon_f = \varepsilon_{cu} \frac{d_f - x}{x} \tag{5-38}$$

$$\varepsilon_f = \varepsilon_s \frac{d_f - x}{d_s - x} \tag{5-39}$$

$$\varepsilon_s = \varepsilon_{cu} \frac{d_s - x}{x} \tag{5-40}$$

$$\varepsilon_{sc} = \varepsilon_{cu} \frac{x - d_{sc}}{x} \tag{5-41}$$

similarly, the stress in each of the materials: σ_c in the concrete, f_s in the tension steel, f_{sc} in the compression steel, f_f in the tension CFRP and f_{fc} in the compression CFRP are calculated using the stress-strain relationships for each of the materials, equations 5-35, 5-36, 5-37, 5-9 and 5-10.

From consideration of equilibrium of the internal and external forces of the strengthened section, Fig.5.11e, the following equation is obtained

$$F_c + F_{sc} + F_{fc} + F_s + F_f = 0$$

$$k_1 k_2 f_{cu}\, b\, x + A_{sc} f_{sc} + A_{fc} f_{fc} + A_s f_s + A_f f_f = 0 \qquad (5\text{-}42)$$

where the compressive force in the concrete F_c is $k_1 k_2 f_{cu} b x$, the compressive force in the steel bars, F_{sc} is $A_{sc} f_{sc}$. The tensile force in the tension bars, F_s is $A_s f_s$, the tensile force in the external CFRP, F_f is $A_f f_f$, and the force in the external compression CFRP, F_{fc} is $A_{fc} f_{fc}$.

To solve equation 5-42 it is necessary to estimate the depth of the neutral axis x. Given the stresses and strains the terms in equation 5-42 can then be calculated to check if equilibrium is satisfied. An iterative process is normally adopted to determine the position of the neutral axis. However, an analytical method to determine the depth of the neutral axis, x, is described. The method is able to give directly the value of x, that achieves the equilibrium.

5.4.3 Flexural capacity and modes of failure in unstrengthened beam

In conventional reinforced concrete beams there are two flexural failure modes which depend on the ratio of tensile steel in the section, ρ_s. A low ratio of tension steel leads to yielding of the tensile steel initially at the ultimate moment. A higher ratio results in concrete crushing at the compression face before the tensile steel reaches the yield. Between the two failure modes, there is a critical value, that so-called balanced condition, ρ_b, as shown in Figure 5.10c. In this case the concrete strain ε_c reaches the

ultimate value in compression, $\varepsilon_{cu} = 0.0035$, at the same time as the tension steel reaches its yield strain ε_y.

The ratio of the neutral axis to the effective depth, x/d_s, has an unique value for the balanced condition and is obtained from equation 5-40, by replacing the steel strain with the yield strain ε_y, such that:

$$\frac{x}{d_s} = \frac{\varepsilon_{cu}}{\varepsilon_{cu} + \varepsilon_y} \tag{5-43}$$

5.4.3.1 Under-reinforced section

If the ratio of the tension steel is below this critical value ρ_b, the beam is under-reinforced, Figure 5.10b. In order to calculate the value of *x*, assuming a single reinforced unstrengthened section; the depth of the neutral axis is obtained from equation 5-42 assuming the steel yields.

$$x = \frac{A_s f_y}{k_1 k_2 f_{cu} b} \tag{5-44}$$

The ultimate bending moment, M_u, of the section can be calculated by taking the moments of force about the tension steel.

5.4.3.2 Over-reinforced section

If the ratio of the tension steel is greater than ρ_b, the section is said to be over-reinforced. The design procedure for calculating the depth of the neutral axis of this mode of failure shown in Figure 5.10d can be summarised in the following steps:

- Since the stress in the reinforcement is below the yield stress, the tensile stress of the steel, f_s, in equation 5-42 is given by $E_s \varepsilon_s$. From consideration of equilibrium, equation 5-42, the tensile strain in the tension steel is

$$\varepsilon_s = \frac{k_1 k_2 f_{cu}}{\rho_s E_s} \frac{x}{d_s} \tag{5-45}$$

- The ratio x/d_s is calculated from equation 5-40, and becomes

$$\frac{x}{d_s} = \frac{\varepsilon_{cu}}{\varepsilon_{cu} + \varepsilon_s} \quad \text{and}$$

- Combining with equation 5-45, the following quadratic equation is obtained

$$\frac{k_1 k_2 f_{cu}}{\rho_s E_s} \left(\frac{x}{d_s}\right)^2 + \varepsilon_{cu} \left(\frac{x}{d_s}\right) - \varepsilon_{cu} = 0$$

which can be solving to give the neutral axis depth; x

$$x = \left\{ \frac{\varepsilon_{cu}\, \rho_s\, E_s}{2 k_1 k_2\, f_{cu}} \left(-1 + \sqrt{1 + \frac{4 k_1 k_2\, f_{cu}}{\varepsilon_{cu}\, \rho_s\, E_s}} \right) \right\} d_s \tag{5-46}$$

- The moment capacity M_u can be determined by taking moment of force about the tension steel.

5.4.4 Flexural capacity and modes of failure in strengthened beam

For reinforced concrete beams which are strengthened with an external CFRP, the modes of failure are different. This difference may be due to the bond that is essential for stress transfer between the concrete and the tensile reinforcement. For example,

adding CFRP to the tension face of a beam in terms of increasing its flexural strength may cause peeling failure while this mode of failure is not going to occur in the unstrengthened beam. The ratio of external CFRP ρ_f plays an important role in controlling the failure mode and the moment capacity of strengthened reinforced concrete beams.

Adding CFRP to the compression face of a beam strengthened in tension can increase the ultimate capacity of the section to some extent; however, the failure mode may be changed compared with that strengthened in tension only. Buckling failure of the CFRP on the compression face is the dominant mode. The compression strain at the compression face, when buckling take place, is considered to be 0.003. This was determined from the experiments, Chapter 5.

Ashour (2002)[88] has reported limits for the areas of CFRP that controlled the flexural failure mode for reinforced concrete beams strengthened in tension only. These limits are the lower and upper of the CFRP area size which introduced three modes of failures to be defined later. These limits are considered in the current investigation.

In the simplified analytical method carried out here, the effect of the compression CFRP is considered. In addition, a direct calculation for the depth of the neutral axis x is developed for each failure mode rather than use of the iterative process [88]. Thus, the depth of the neutral axis x and the ultimate moment capacity of reinforced concrete beams strengthened with CFRP for the three modes of failure are calculated. The failure modes are Mode-I: Tensile rupture of CFRP, Mode-II: under-reinforced section and Mode-III: over reinforced section.

5.4.4.1 Mode-I: Tensile rupture of CFRP

In this mode, the lower limit of the CFRP ratio, for which no rupture of the CFRP occurs, is calculated. The design procedure for CFRP ruptures then, shown in Figure 5.11b, is determined. This can be calculated as follows:

- Calculate the neutral axis to depth ratio, x_l / d_f, by rearranging equation 5-38, where $x = x_l ; x_l$ is the minimum value of the depth of the neutral axis that avoids CFRP rupture. The strain in CFRP ε_f is replaced by the ultimate ε_{fu}.

$$\frac{x_l}{d_f} = \frac{\varepsilon_{cu}}{\varepsilon_{cu} + \varepsilon_{fu}} \tag{5-47}$$

- The stress in the tension CFRP is the ultimate f_{fu} and the stress in the tension steel is the yield stress f_y.

- The strain in the compression steel ε_{sc} is calculated using equation 5-41 with $x = x_l$. Subsequently, the stress in the compression steel f_{sc} is calculated from equations 5-36 and 5-37.

- Determine the depth ratio $n = d_s / d_f$.

- From longitudinal equilibrium of the internal forces, equation 5-42, the lower limit for the ratio of tension CFRP, which avoids its tensile rupture, is given

$$\rho_{fl} \ (\%) = \left\{ \frac{1}{f_{fu}} \left(k_1 k_2 f_{cu} \left(\frac{x_l}{d_f} \right) + n \left(\rho_{sc} f_{sc} - \rho_s f_y \right) + \varepsilon_{cu} E_{fc} \rho_{fc} \right) \right\} 100 \tag{5-48}$$

- If ρ_{fl} is negative, Mode-I, laminate rupture of CFRP, does not occur and the section fails in either Mode-II or Mode-III, which will be discussed later.

- Determine the CFRP ratio ρ_{fca} applied to the section, Figure 5-12.

- If ρ_{fca} is less than or equal to ρ_{fl}, Mode-I occurs.

- Calculate the depth of the neutral axis x, expressed here by x_1, which relates to failure Mode-I when ($x_1 \le x_l$). The following equation is used

$$x_1 = \frac{d_f}{2}\left(-k_3 + \sqrt{k_3{}^2 - 4k_4}\right) \tag{5-49}$$

where;

$$k_3 = \frac{1}{k_1 k_2 f_{cu}}\left(n\rho_{sc}E_{sc}\varepsilon_{cu} + \varepsilon_{cu}E_{fc}\,\rho_{fc} - n\rho_s\, f_y - \rho_f f_{fu}\right)$$

$$k_4 = \frac{-1}{k_1 k_2 f_{cu}}\left(n\,m\,\rho_{sc}E_{sc}\varepsilon_{cu}\right)$$

and, $m = d_{sc} / d_f$

- Calculate the stress in the compression steel f_{sc} and ε_{sc} from equations 5-36 and 5-41. The depth of the neutral axis x in equation 5-41 is replaced by x_1.

- Determine the flexural strength of the section, M_u, by taking the moment of the forces about any force level through the composite section depth. For example, it can be calculated by taking the moment of forces about the centroid of the tension CFRP laminates

$$M_u = k_1 k_2 f_{cu}\, b\, x_1\,(d_f - 0.5k_2\, x_1) + A_{sc} f_{sc}(d_f - d_{sc}) + \varepsilon_{cu}E_{fc}A_{fc}d_f$$
$$- A_s f_y (d_f - d_s) \tag{5-50}$$

5.4.4.2 Mode-II: Yielding of steel reinforcement followed by concrete crushing

In this mode, the calculated CFRP ratio ρ_{fca}, Figure 5.12, should be greater than ρ_{fl}, equation 5-48. In such cases, the tension steel often yields first and then this is followed by concrete crushing. Tearing of CFRP does not occur as long as this condition is satisfied. Hence, the upper value of the depth of the neutral axis, x_u, for which the tensile steel does not yield, is calculated. The design procedure for Mode-II is shown in Figure 5.11c. The steps are:

- Calculate the upper limit of the depth of the neutral axis x_u from equation 5-43, by replacing x by x_u.

$$\frac{x_u}{d_s} = \frac{\varepsilon_{cu}}{\varepsilon_{cu} + \varepsilon_y} \tag{5-51}$$

- Calculate the strains in the compression steel ε_{sc} and in the tensile CFRP ε_f from equations 5-41 and 5-38 with considering $x = x_u$.

- Similarly, calculate the stress in the compression steel f_{sc} from equation 5-36 and the stress in the tension CFRP f_f from equation 5-9.

- Considering the following strain in the tensile steel reinforcement ($\varepsilon_s = \varepsilon_y$) and by substituting with equation 5-42 where the ultimate tensile stress of the tensile steel f_s is replaced by the yield f_y. The upper limit for the ratio of the CFRP is given

$$\rho_{f\,u}\ (\%) = \left\{ \frac{n}{f_f} \left(k_1 k_2 f_{cu} \left(\frac{x_u}{d_s}\right) + \left(\rho_{sc}\, f_{sc} - \rho_s f_y\right) + \varepsilon_{cu} E_{fc} \rho_{fc} \right) \right\} 100 \tag{5-52}$$

The upper limit of CFRP ratio ρ_{fu} given by equation 5-52 is the limit above which yielding of steel is avoided; the section fails as in the over-reinforced case, Mode-III, which will be discussed later.

- Determine the CFRP ratio, ρ_{fca}, applied to the section, Figure 5.12.

- If the case satisfies the condition $\rho_{fl} < \rho_{fca} \leq \rho_{fu}$, Mode-II occurs.

- Calculate the depth of the neutral axis x, expressed by x_2, which relates to failure Mode-II, when $x_l < x_2 \leq x_u$. Equation 5-53 is used to determine x_2 in the case of reinforced concrete sections including compression steel.

$$x_2 = \frac{d_{sc}}{2}\left(-k_3 + \sqrt{k_3{}^2 - 4k_4}\right) \tag{5-53}$$

where

$$k_3 = \frac{1}{k_1 k_2 f_{cu}}\left[n_1\left(\rho_{sc} E_{sc} \varepsilon_{cu} - \rho_s f_y\right) + m_1\, \varepsilon_{cu}\left(\rho_f E_f + \rho_{fc} E_{fc}\right)\right]$$

$$k_4 = \frac{-\varepsilon_{cu}}{k_1 k_2 f_{cu}}\left(n_1\, \rho_{sc} E_{sc} + m_1{}^2\, \rho_f E_f\right)$$

and,

$n_1 = d_s / d_{sc}$, $m_1 = 1/m$ where m given in mode-I

- For the special case, no compression steel is included such as single reinforced section (e.g. reinforced concrete slabs); the depth of the neutral axis x_2, is then calculated by modifying equation 5-53 to the following

$$x_2 = \frac{d_f}{2}\left(-k_3 + \sqrt{k_3^{\,2} - 4k_4}\right) \tag{5-54}$$

where

$$k_3 = \frac{1}{k_1 k_2 f_{cu}}\left(\rho_{fc} E_{fc} \varepsilon_{cu} + \rho_f E_f \varepsilon_{cu} - n \rho_s f_y\right)$$

$$k_4 = \frac{-\rho_f E_f \varepsilon_{cu}}{k_1 k_2 f_{cu}}$$

- Determine the stress in the compression steel f_{sc} from equations 5-36 and 5-37, where ε_{sc} is calculated using equation 5-41 with $x = x_2$.

- Calculate the ultimate bending moment, M_u, by taking moments of forces about the external CFRP in tension.

$$M_u = k_1 k_2 f_{cu} b x_2 (d_f - 0.5 k_2 x_2) + A_{sc} f_{sc} (d_f - d_{sc}) + \varepsilon_{cu} E_{fc} A_{fc} d_f - A_s f_y (d_f - d_s) \tag{5-55}$$

5.4.4.3 Mode-III: Over-reinforced failure

In this mode, the applied CFRP ratio ρ_{fca}, Figure 5.12, should be greater than ρ_{fu}, equation 5-52. In such cases, the concrete strain reaches the ultimate value ε_{cu} before either yielding of steel or rupture of an external CFRP occur at the tension face.

The design procedure for this mode of failure, shown in Figure 5-11d, can be summarised in the following steps:

- Calculate the ratios of tension steel, ρ_s, compression steel, ρ_{sc}, tension CFRP ρ_f, and compression CFRP ρ_{fc}, respectively.

- Determine the ratio of n and m as in mode-I.

- Calculate the parameters k_3 and k_4:

$$k_3 = \frac{\varepsilon_{cu}}{k_1 k_2 f_{cu}} \left(n\rho_{sc} E_{sc} + n\rho_s E_s + \rho_f E_f + \rho_{fc} E_{fc} \right)$$

$$k_4 = \frac{-\varepsilon_{cu}}{k_1 k_2 f_{cu}} \left(n\, m\, \rho_{sc} E_{sc} + n^2 \rho_s E_s + \rho_f E_f \right)$$

- Calculate the depth of the neutral axis $x = x_3$ from the following equation

$$x_3 = \frac{d_f}{2}\left(-k_3 + \sqrt{k_3{}^2 - 4k_4} \right) \qquad (5\text{-}56)$$

The value x_3 is referred to the failure mode-III. Equation 5-56 can also be used for calculating the depth of the neutral axis of the conventional reinforced concrete beams by removing the term of CFRP from the parameters k_3 and k_4, and replacing d_f by h. This gives the same result as that achieved from equation 5-46.

- Determine the strains in the tension CFRP, the tension steel ε_s, and the compression steel ε_{sc} from equations 5-38, 5-40 and 5-41, respectively. The maximum concrete compressive strain considered, ε_{cu}, is 0.0035 and 0.003, respectively for reinforced concrete beams unstrengthened and strengthened with CFRP on the compression face.

- Calculate the material stresses respectively from equations 5-9, 5-10, 5-36 and 5-37 for the tension CFRP f_f, the compression CFRP f_{fc}, tension steel f_s, and compression steel f_{sc}.

- Calculate the ultimate bending moment, M_u, by taking moments of forces about the external tension CFRP.

$$M_u = k_1 k_2 f_{cu}\, b\, x_3\, (d_f - 0.5 k_2\, x_3) + A_{sc} f_{sc} (d_f - d_{sc}) + \varepsilon_{cu} E_{fc} A_{fc} d_f - A_s f_s (d_f - d_s) \quad (5\text{-}57)$$

Derivation of equations 5-49, 5-53, 5-54 and 5-56 is given in Appendix C. A schematic process of generating the different flexural failure modes of reinforced concrete sections strengthened with external CFRP in both faces tension and compression is presented in form of a flow chart, Figure 5.12. The described method for designing the reinforced concrete beams strengthened with CFRP accommodates all kinds of external FRP composites reinforcement. This theoretical procedure is validated with the experiments from the current study as well as from the literature and is given in Chapter 6.

5.5 Numerical Finite Element Model

5.5.1 Introduction

In this section an analysis using the finite element method, FEM, is presented in order to further investigate the behaviour of the CFRP strengthened reinforced concrete beams tested in the laboratory. The LUSAS Finite Element Program [10] version 13.8 was used.

Three unstrengthened reinforced concrete beams I11-UH-UN, I13-OL-UN, I21-UL-UN, one beam strengthened in tension I22-UL-T and one beam I25-UL-TC was strengthened in tension and compression were analysed. The results of the analysis of each beam were compared with the experimental results and are given in Chapter 6.

5.5.2 Material models

In the current investigation material models were required for the concrete, the internal steel reinforcement and the external CFRP.

5.5.2.1 Concrete models

The concrete models used are LUSAS material models 82 and 84; the first model accounts for cracking in tension while the second accounts for cracking in tension and concrete crushing. Because the beams modelled involved strengthened and unstrengthened specimens from Series-I, which had a low ratio of tension steel; the unstrengthened specimens failed by yielding of steel in which crushing of concrete was not significant. In contrast, in the strengthened ones the crushing of the concrete was significant. Therefore both models were used. Further details on concrete models used in this investigation are given in the following sections.

Concrete model 82

This model represents the nonlinear material effects associated with the tensile cracking of concrete. The model assumes that, at any one point in the material, there are defined numbers of permissible cracking directions. The model also assumes that the material can soften and eventually lose strength. An exponential softening curve is assumed and, for direct tensile loading in one direction, it is defined by the tensile strength and the strain at the end of the softening curve, Figure 5.13. In this model, the crushing of concrete in compression was not considered and linear stress-strain behaviour was assumed.

Concrete model 84

In this model, the nonlinear behaviour of the concrete in both tension and compression is represented by a multi-crack concrete and crushing material model which is based on a multi-surface plasticity approach. The model simulates directional softening and crushing in compression using the same yield functions. Cracks in tension are assumed to form when the major principal stress reaches the tensile strength, after which a permanent crack plane is formed. Multiple cracks can form at non-orthogonal directions to one another. The model simulates nonlinear behaviour in compression with hardening and softening functions applied to the local yield surfaces.

In tension zones permanent crack planes result in a directional loss of strength, whereas in compression zones the planes are not permanent but rather may rotate and result in an isotropic loss of strength. In both tension and compression, unloading from the yield surface is assumed to be elastic [10].

The following material properties are required for the models, Figures 5.13 and 5.14.

1. The maximum uniaxial tensile, f_t, stress after which softening in tension begins.
2. Tensile strain at the end of softening curve, ε_{to}, Figure 5-13.

3. The maximum uniaxial compressive stress, f_c, after which softening in compression begins.
4. The uniaxial strain at the peak uniaxial compressive stress, ε_{cp}. As a guide, any value of the ε_{cp} should lie in the range $0.002 \leq \varepsilon_{cp} \leq 0.003$.
5. The uniaxial strain at the end of the uniaxial compressive softening curve, ε_{co}. If no data for the strain at the end of the compressive softening curve, ε_{co}, is available, then a reasonable value to use is $\varepsilon_{co} = 5\,\varepsilon_{cp}$.
6. The uniaxial strain at the end of the uniaxial tensile softening curve, ε_{to}. Strain at end of tensile softening curve for cases of distributed spaced cracks, which is typically the case for reinforced concrete, should be entered. If no data is available then a value of $\varepsilon_{to} = 0.004$ is reasonable to use for most concretes.
7. The ratio of the uniaxial compressive yield stress to the peak uniaxial compressive stress, r_{op}. A typical value for most concrete structures with moderate degrees of confinement is 0.5. The parameter r_{op} governs the initial position of the compressive yield surface.

5.5.2.2 Longitudinal steel reinforcement model

The longitudinal steel reinforcement bars were modelled using Von Mises nonlinear hardening properties.

5.5.2.3 External CFRP model

CFRP laminates are anisotropic materials. Several independent elastic stiffness parameters for different planes are required to define a fully anisotropic material. However, the tensile strength and the Young's modulus of the CFRP in the longitudinal fibre direction are the most important parameters, because the transverse stresses are negligible. Consequently, for modelling purposes, the tensile strength and the Young's modulus of the CFRP in the longitudinal fibre direction were considered.

5.5.3 Modelling procedure

5.5.3.1 Mesh configuration

The concrete surface was modelled by 2D continuum plane stress quadrilateral 8 noded, QPM8, elements, Figure 5.15b. It should be noted that the 8-noded elements have more nodes per element and consequently are more accurate than the 4-noded element.

A mesh of rectangular elements of different size was required. Larger elements, particularly with respect to the important locations that need to be analysed, were needed. Smaller elements were used in the shear span of the beam, the left-hand side, whereas larger elements were applied to the mid-portion of the beam, the right-hand side, Figure 5.15a. To avoid any local failure in the concrete underneath the load points, particularly in the strengthened beams, the element sizes at these locations were increased, Figure 5.15a.

The steel reinforcing bar was modelled using a discrete 3-noded quadratic element, BAR3, Figure 5.15b.

Similarly, the CFRP both in tension and compression was modelled using a discrete 3-noded quadratic element, BAR3. Each CFRP element was bounded by the concrete element adjacent.

5.5.3.2 Geometric and material properties

As the section comprised different materials, a grouping process for the steel bars, the CFRP and the concrete was used. After the mesh configuration was completed, geometric and material properties were assigned to each group of elements. Geometric

properties were assigned to the steel bars and CFRP, by defining their cross sectional areas, and the concrete elements were defined by the thickness of the section, 120 mm. All reinforcement and concrete properties were defined using the data obtained from experimental work, Chapter 3.

Non-linear properties for steel and concrete were assigned to the model. Concrete models 82 and 84 were assigned to the concrete, depending on the predicted flexural failure of each beam. For example, model 84 was used for the section where the concrete crushing is significant.

5.5.3.3 Loading and boundary conditions

When using the finite element approach to nonlinear beam analysis, the stiffness matrix is constantly updated in order to take account of the nonlinear effects that are present. Since the equilibrium configuration of the structure changes constantly, it is necessary to carry out the analysis in a series of load increments. The equilibrium and kinematic states of the structure at the end of the load increment are used to formulate the stiffness relationship for the solution for the next load incurrent. Based on this, a solution for the nonlinear problem is obtained by a series of linearized iterations [133]. Two different methods were experienced, the load control method and displacement control method. In the load control method, the unit point load is applied to a specified point on the structure, whereas a unit displacement is applied at the nodal position in the displacement control method. The displacement control method is applicable for limit point problems since iterations are carried out at a constant displacement rather than at a constant load, as in the case of the load control method. On the other hand, the selection of a proper control displacement has a significant influence on the convergence characteristics of the problem. Tracing of a targeted control displacement, however, is not an easy task. Therefore, the load control method was adopted in the analysis. The method was carried out by applying a single concentrated load of -1 kN in the y direction.

In FE modelling, boundary conditions must be applied to restrain the model so as to prevent a rigid body rotation. In LUSAS, boundary conditions are described by restraints, support conditions. Each support comprises three degree of freedom: Free, fixed, and spring stiffness. In the current study, the beam was simply supported, fixed in the y and x directions at the support and at the mid-span of the beam, Figure 5.15a. Considering the boundary condition fix in the x direction at the mid-span was to satisfy the symmetry requirements of the beam.

5.5.4 Summary

Based on the analytical and numerical models presented in this chapter, a summary for each model is written below.

Moment-Curvature Model

An analytical modelling programme has been developed to investigate the moment-curvature relationship of reinforced concrete sections strengthened with external CFRP laminates. The model considers only flexure failure. The model considers an incremental process for the compression strain, and eventually the depth of the neutral axis that achieves forces equilibrium and the corresponding bending moment for each increment are determined. The incremental process was repeated up to the final bending moment of a section reached for unstrengthened beams and those strengthened in tension face only, while a strain of 0.003 was assumed for beams strengthened in the compression face.

Load-Deflection Model

A load-deflection model was developed to predict the deflection behaviour of a reinforced concrete beam strengthened with CFRP laminates under load increments.

The model was based on the application of finite difference equations, simple bending theory using direct relationships between deflection, slope and bending moment in terms of differential derivatives.

Simplified Design Model

A simplified analytical method is described for design of reinforced concrete members strengthened with CFRP. This method uses both the strain compatibility and equilibrium formulae, based on a rectangular stress block, to derive equations are able to determine the exact value of the depth of the neutral axis x for the different flexural modes. The ultimate moment of the section is then determined.

Numerical Finite Element Model

In the LUSAS model, a nonlinear model for a simply supported four point loaded reinforced concrete beam subjected to inelastic large deformations was described. A 2D model was adapted to model the three unstrengthened reinforced concrete beams I11-UH-UN, I13-OL-UN, I21-UL-UN, the beam strengthened in tension I22-UL-T and the beam I25-UL-TC was strengthened in the tension and the compression.

In the LUSAS model, perfect bond was assumed between the concrete and the CFRP.

The results from the analysis using analytical and numerical models for unstrengthened reinforced concrete beams and those strengthened with CFRP laminates are discussed in Chapter 6. These include strengthened beams on the tension and both the tension and compression faces.

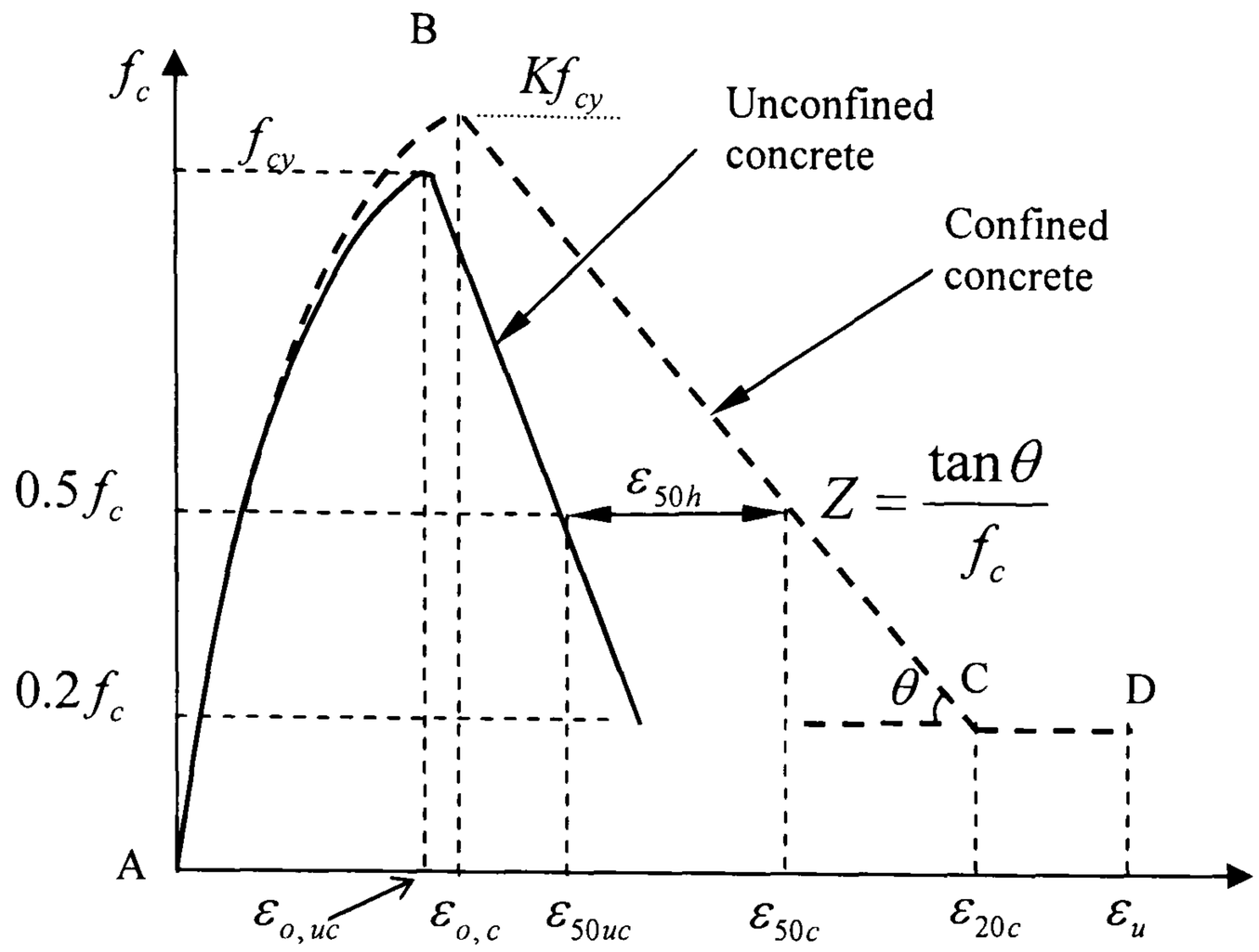

Figure 5.1: Stress-strain relationship for concrete in compression (Kent and Park, 1971[126] and modified later by Scott *et al.*1982 [125])

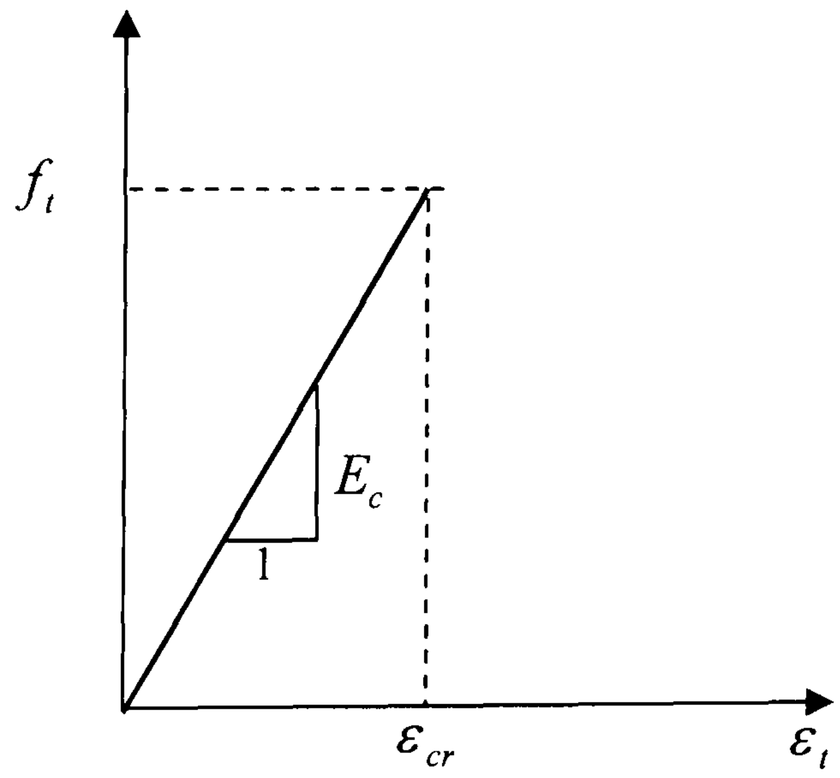

Figure 5.2: Stress-strain relationship for concrete in tension

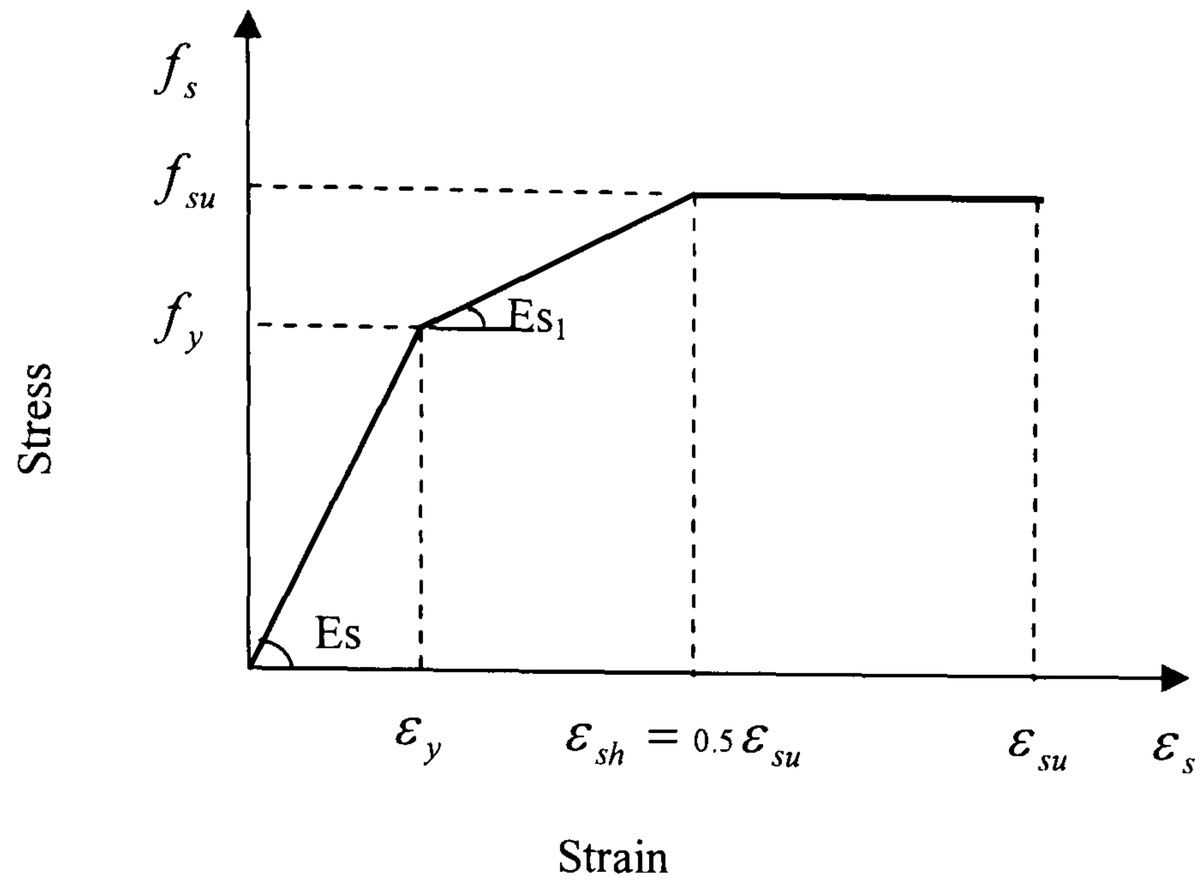

Figure 5.3: Stress-strain relationship of steel reinforcement

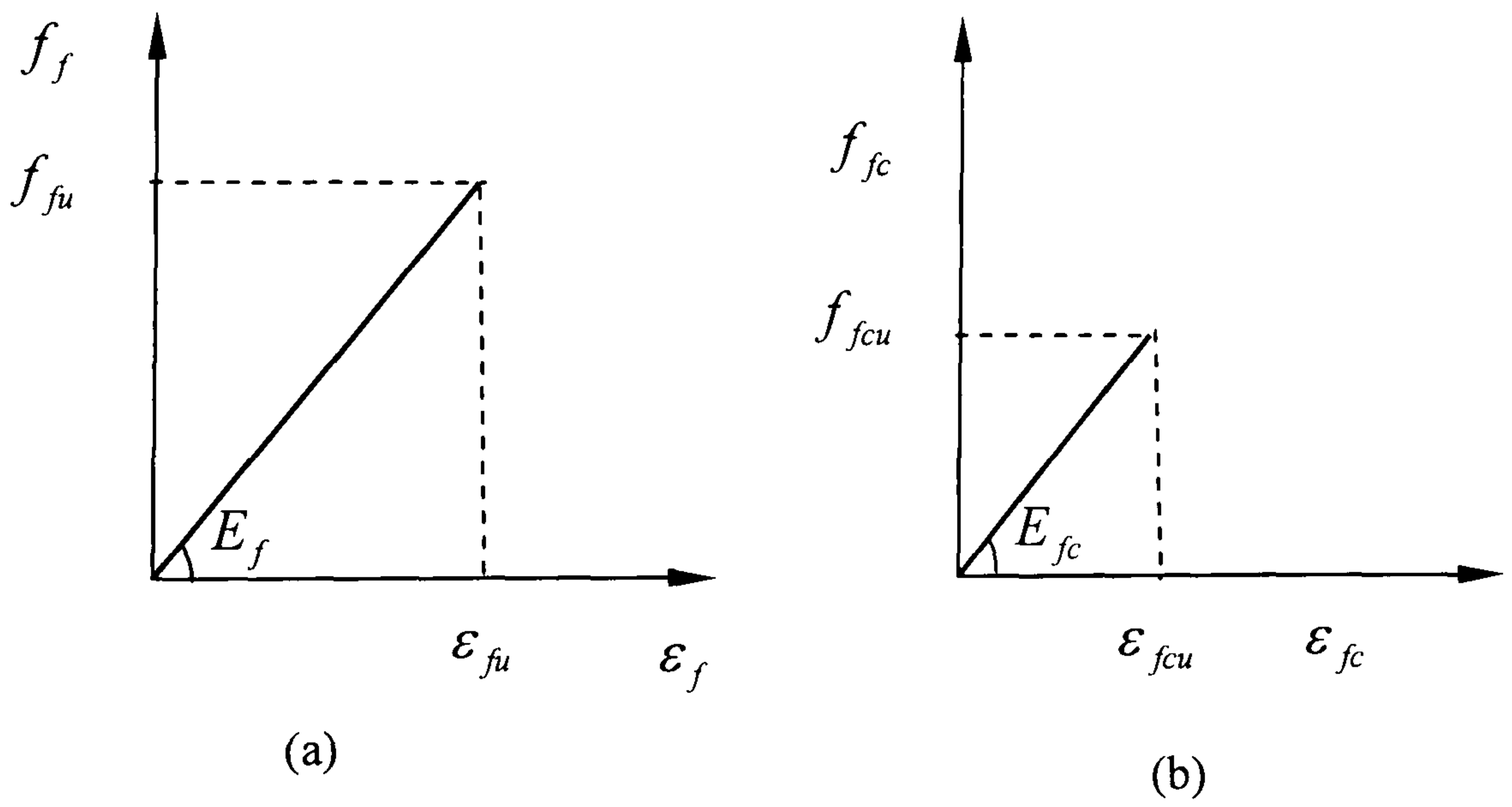

Figure 5.4: Stress-strain relationship of CFRP: (a) tension and (b) compression

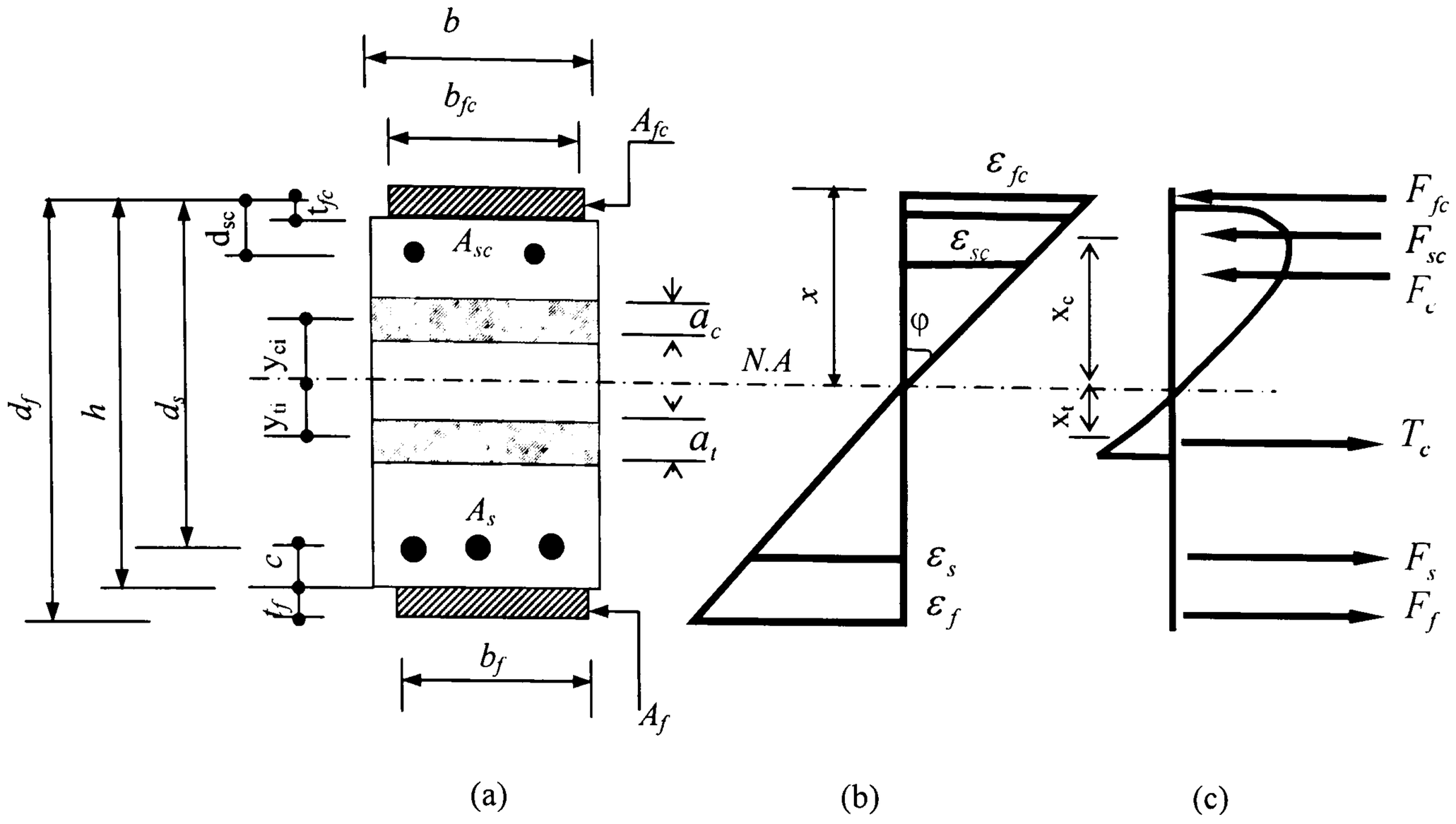

Figure 5.5: Stress and stress distribution in a strengthened reinforced concrete beam section: (a) Cross-section; (b) Strain distribution; (c) Stress and force distribution.

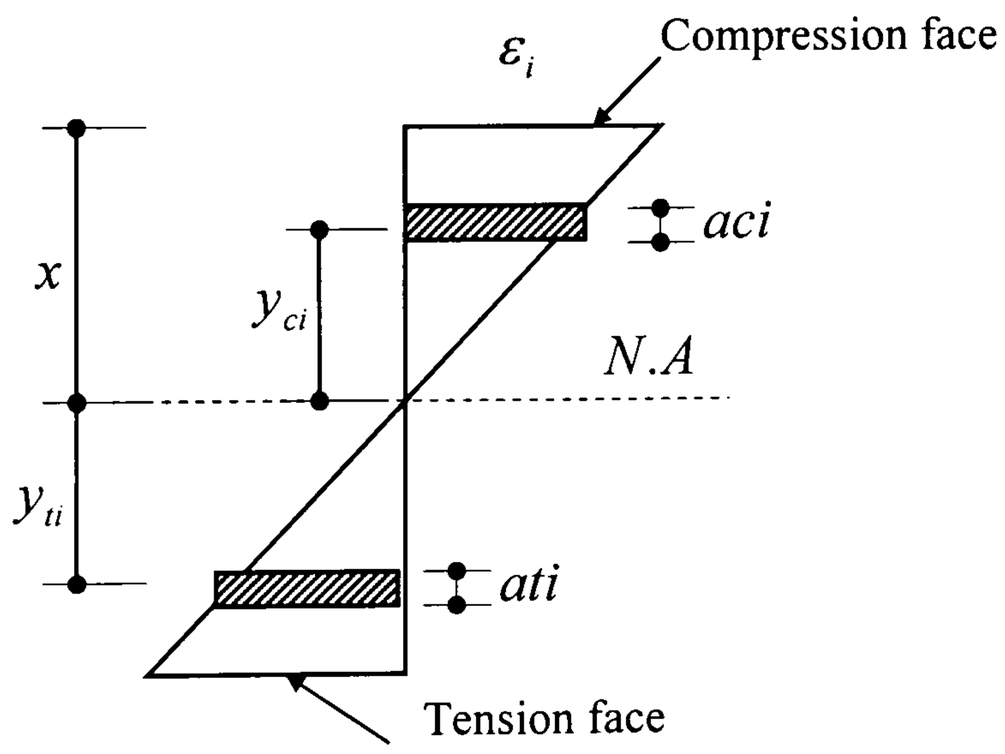

Figure 5.5d: Tension and compression strips along the beam depth

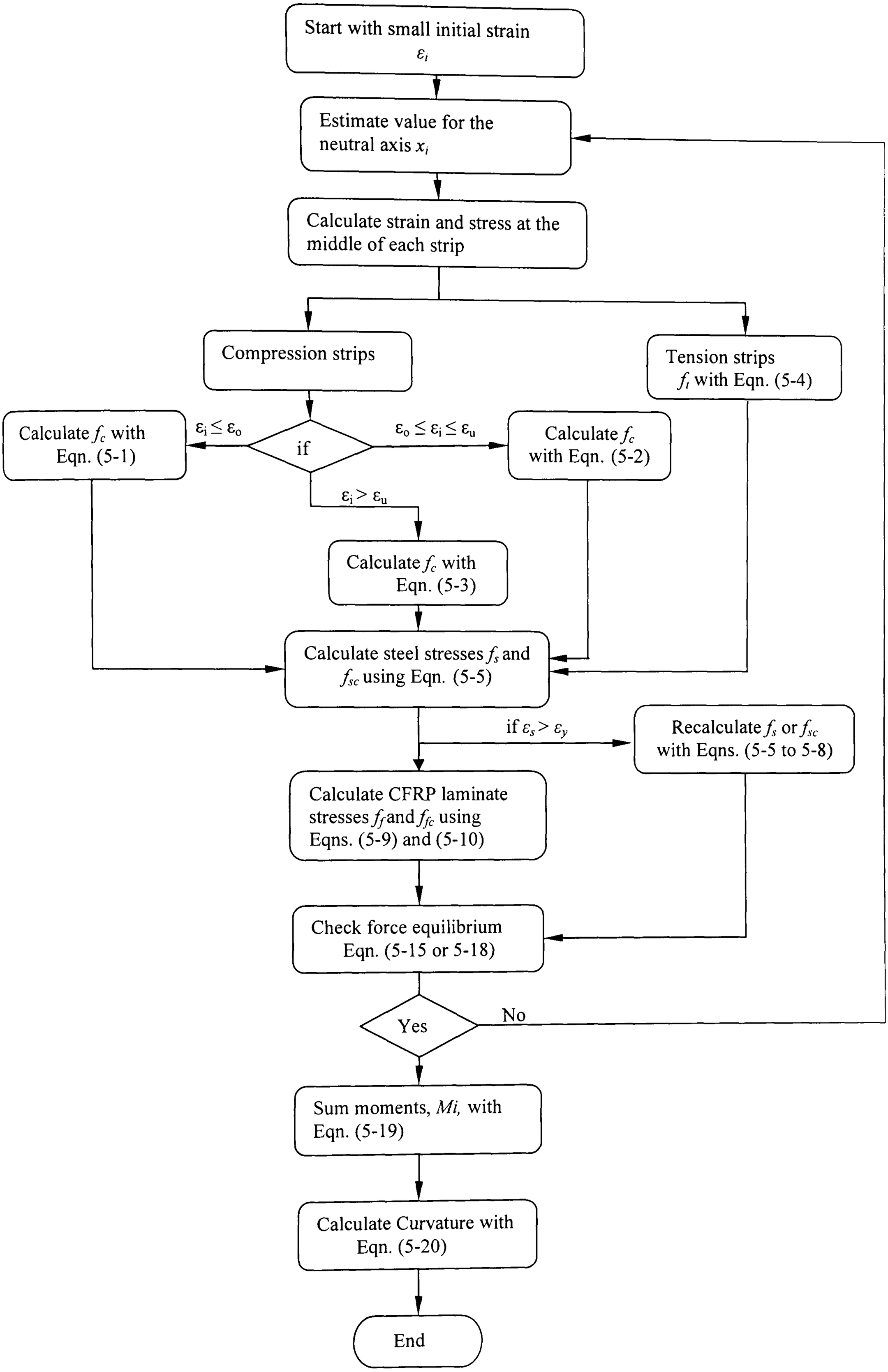

Figure 5.6: Flow chart to develop moment-curvature relationship of a beam

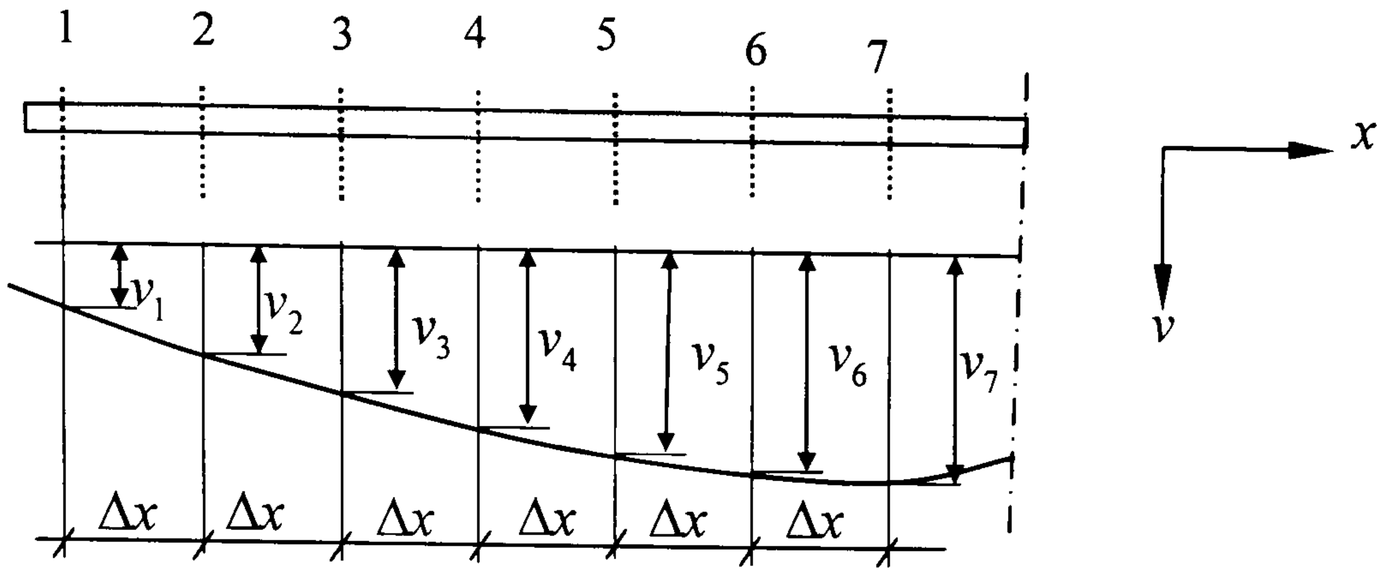

Figure 5.7: Division of the beam span into equal differential quantities

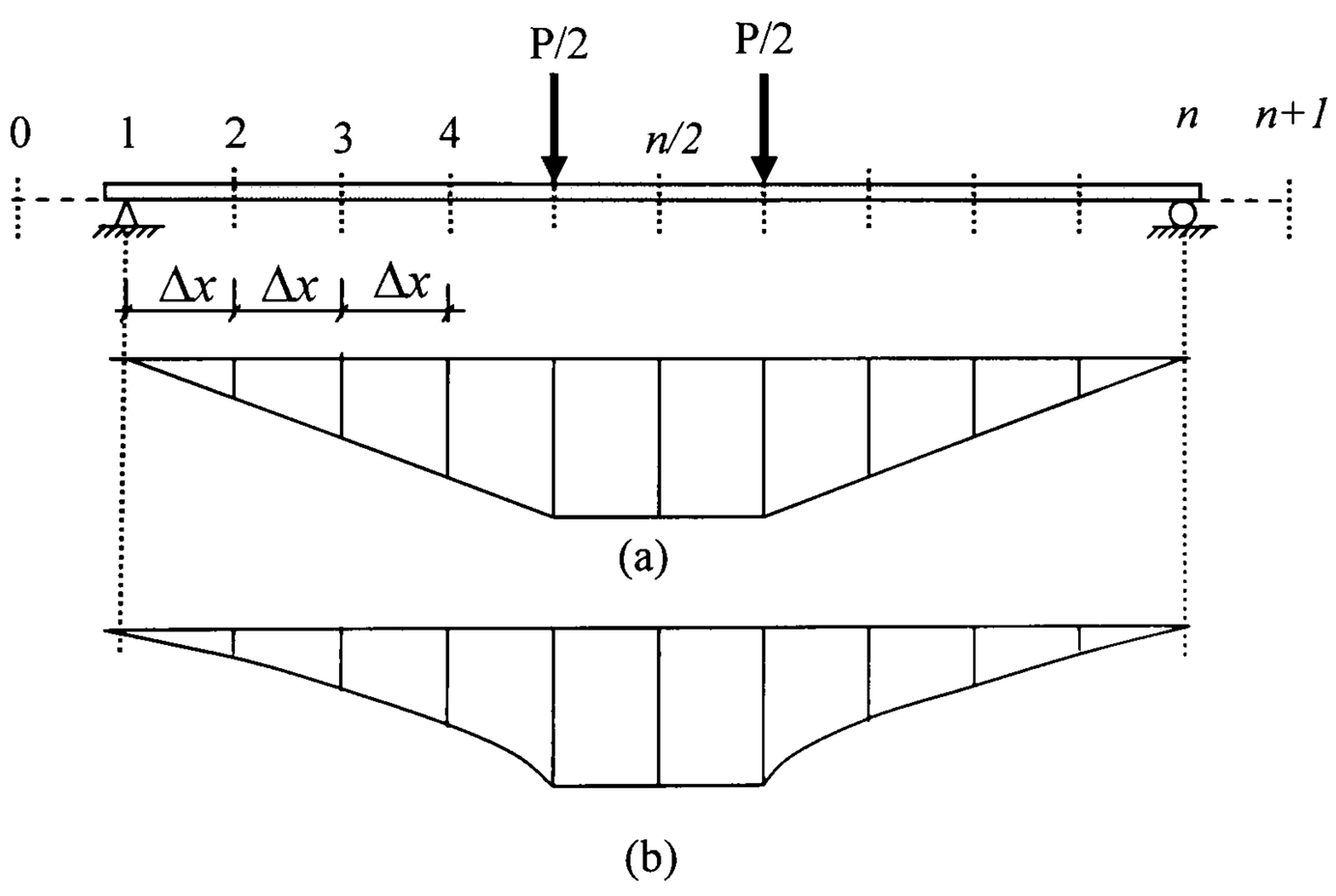

Figure 5.8: a) Bending moment and b) Curvature: diagrams for four point loaded beam

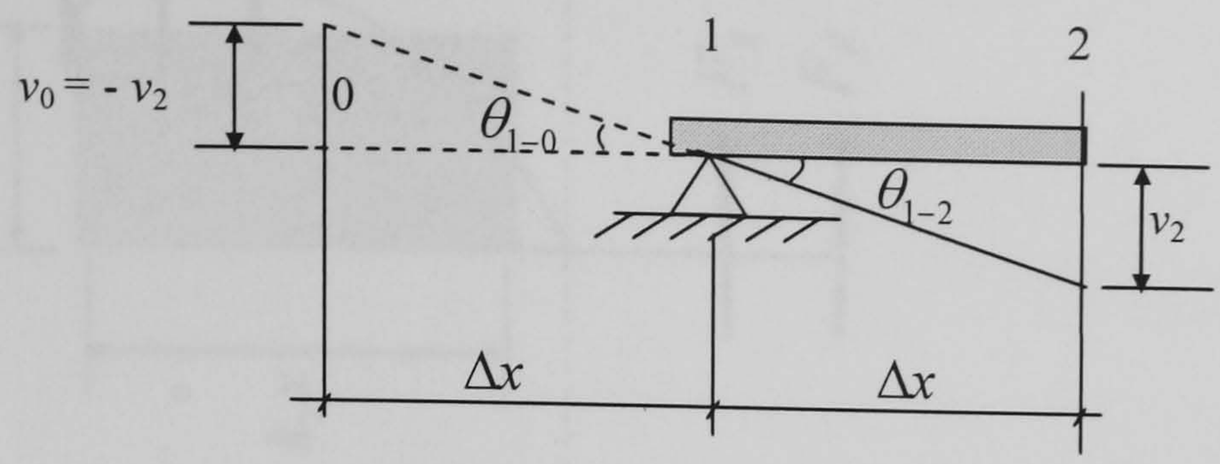

Figure 5.9: Boundary conditions at a simple support

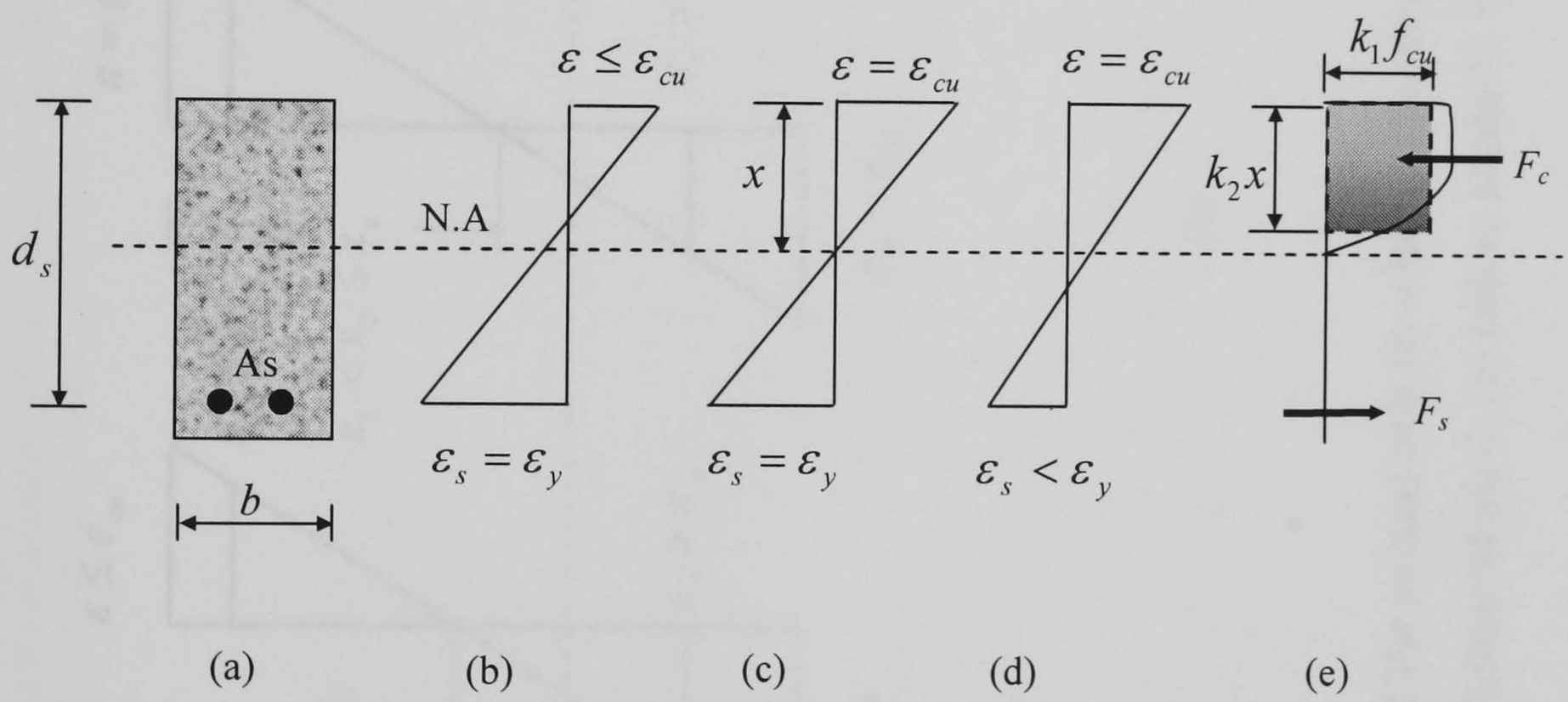

Figure 5.10: Movement of neutral axis on the depth reinforced concrete unstrengthened beam: (a) RC section; (b) steel yielding; (c) balanced section; (d) Concrete crushing; (e) stresses and forces based on case (c).

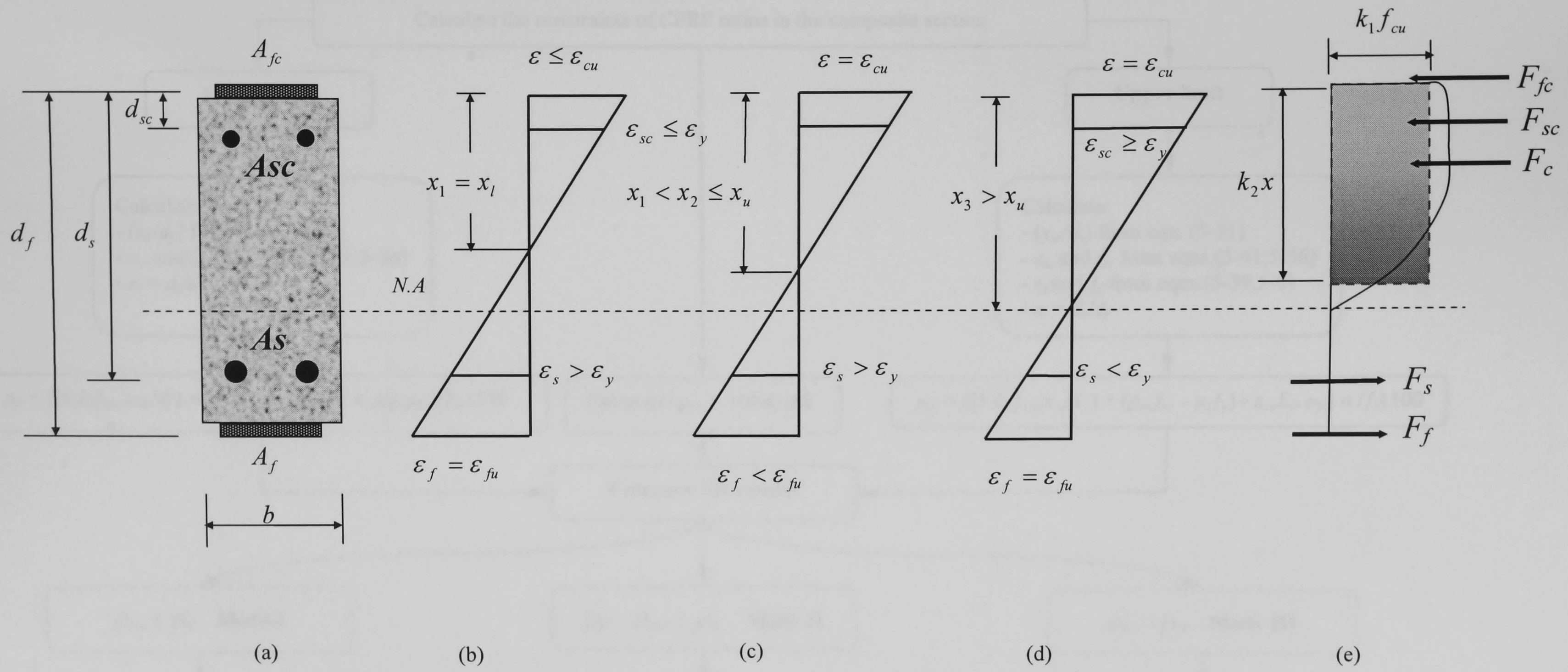

Figure 5.11: Movement of the depth of the neutral axis on reinforced concrete beam strengthened by CFRP: (a) RC section with CFRP at tension and compression faces; (b) failure Mode-I; (c) failure Mode-II; (d) failure Mode-III; (e) stresses and forces based on case (d)

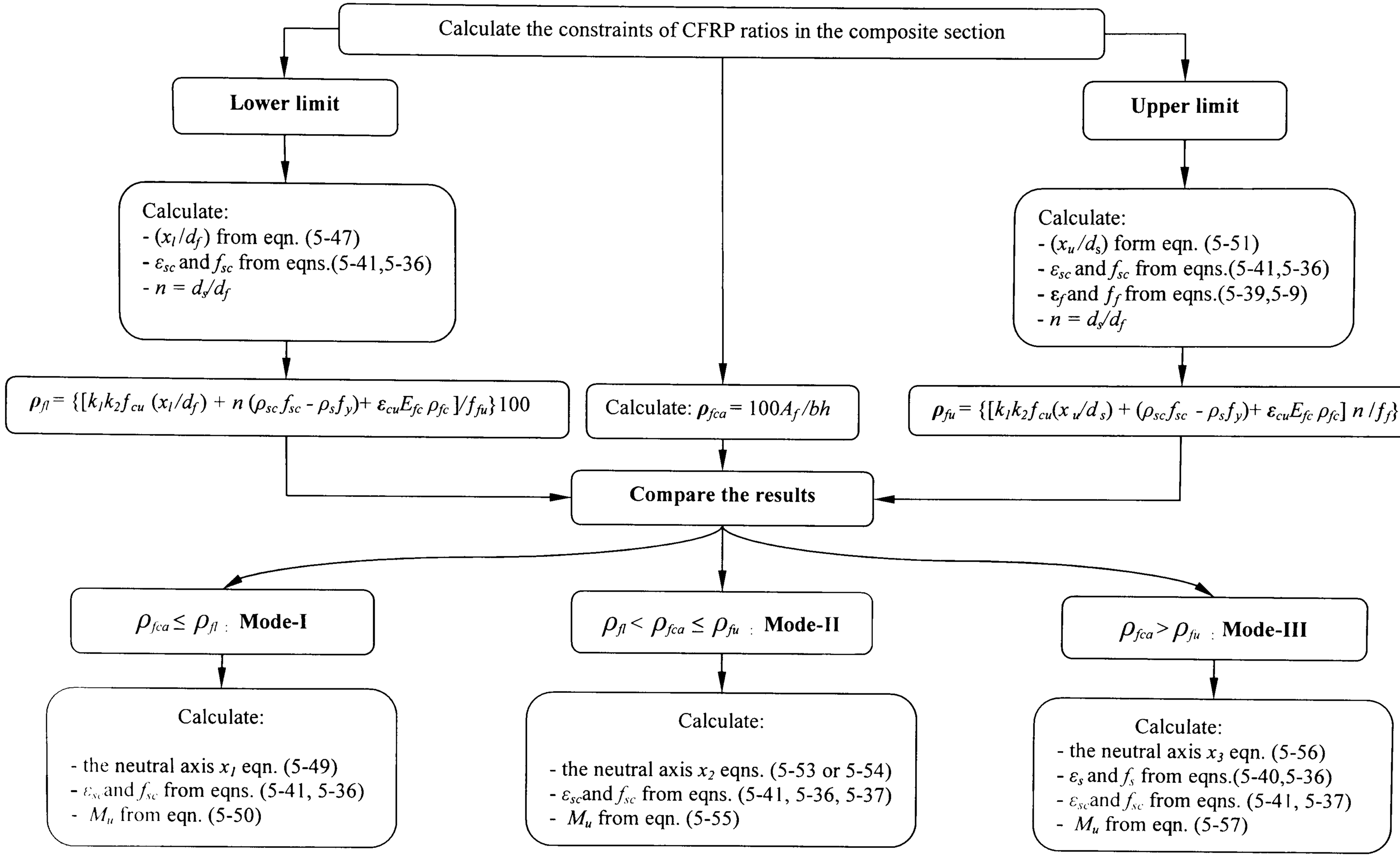

Figure 5.12: Schematic process for generating of flexure modes of reinforced concrete beams strengthened with CFRP

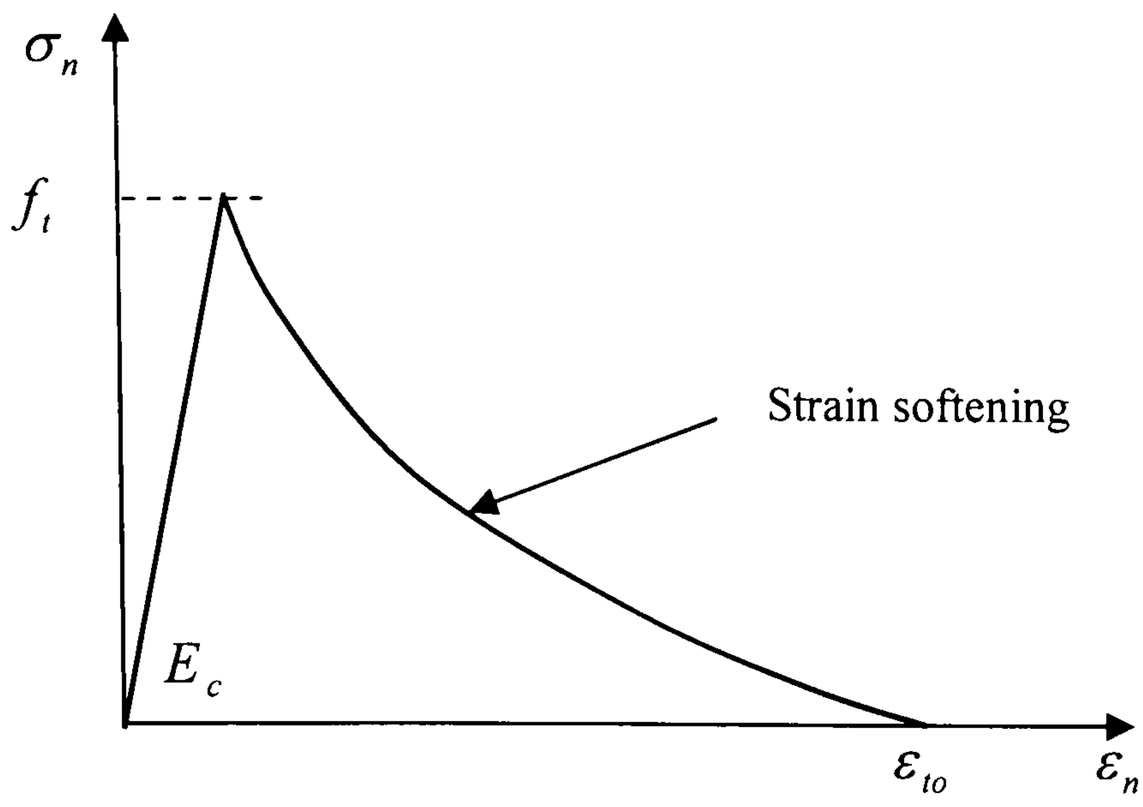

Figure 5.13: Stress-strain behaviour normal to a crack plane [10]

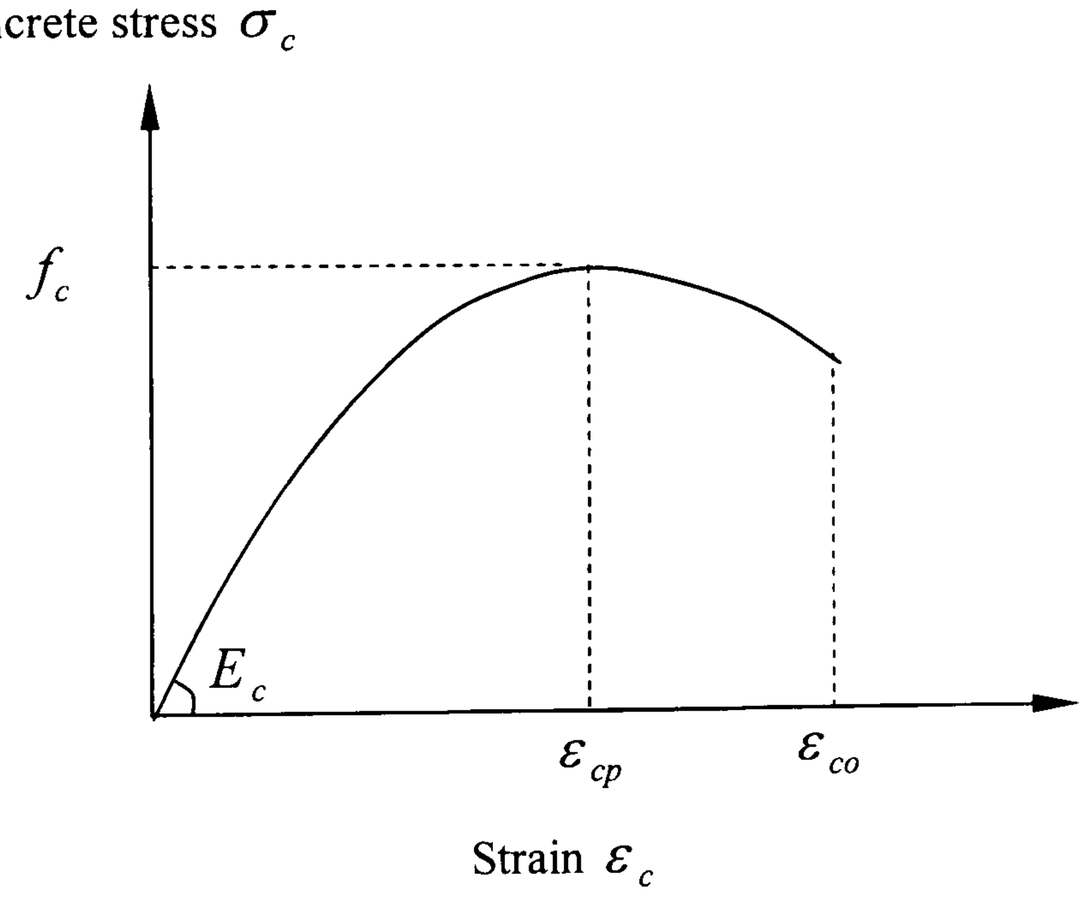

Figure 5.14: Stress-strain behaviour of concrete in compression [10]

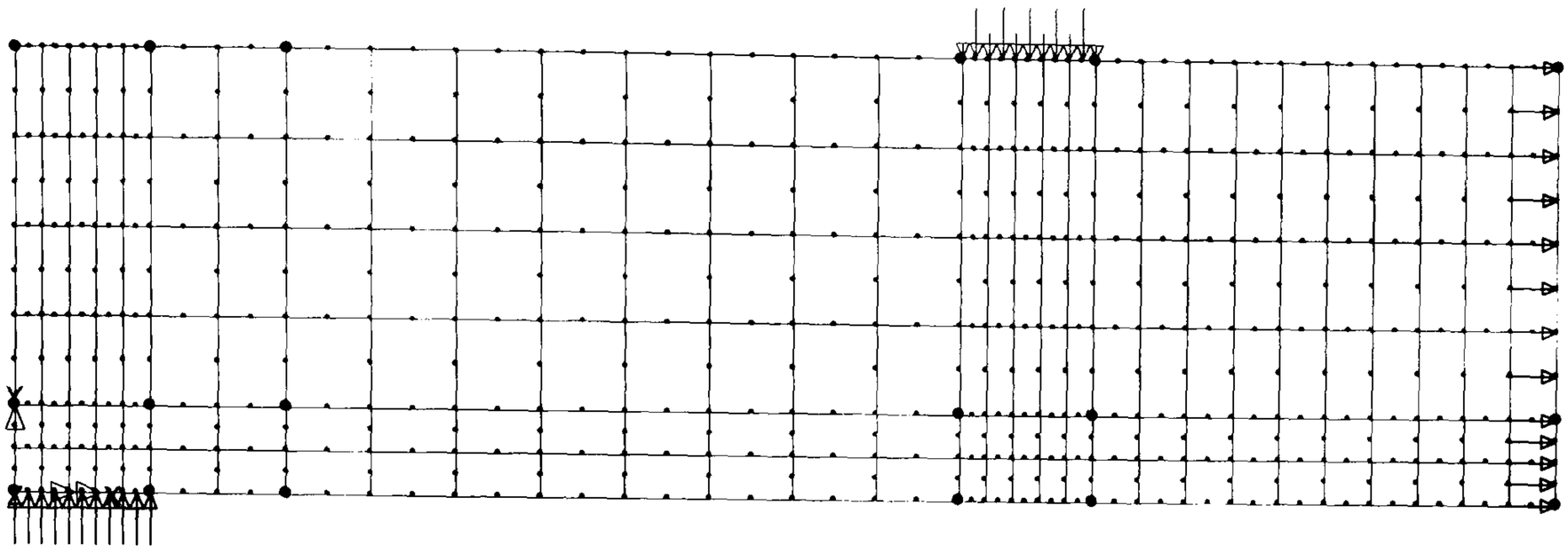

a) 2D FE model for half of beam

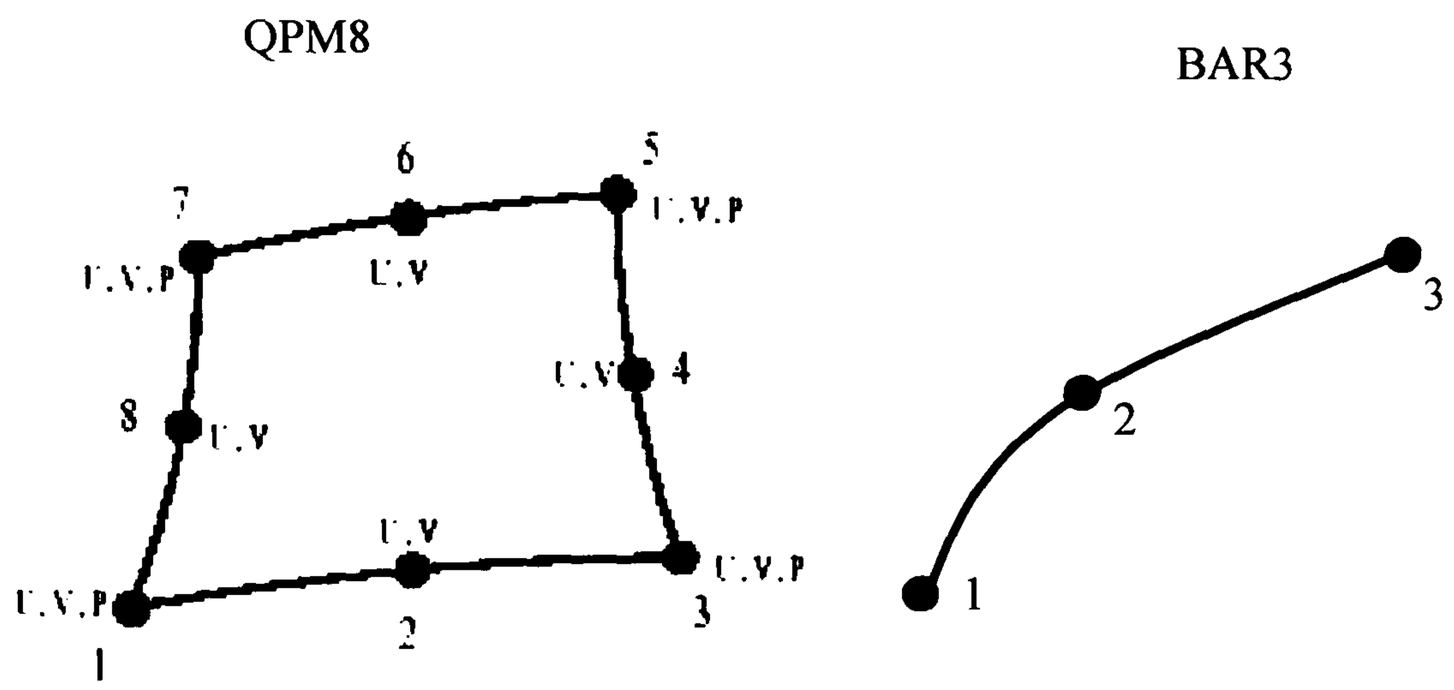

b) Both element types used in modelling concrete and reinforcement

Figure 5.15: Beam mesh configuration and elements used in modelling

CHAPTER 6

COMPARISON OF TEST RESULTS AND ANALYTICAL PREDICTIONS

6.1 Introduction

This chapter deals with the comparison of the experimental results with those obtained from the modelling using the finite element program LUSAS and the theories described in Chapter 5. It comprises two main sections. The first section compares the experimental results with those calculated using the simplified analysis, the finite difference procedure, the design procedure and the FE analysis models. The second section validates the results obtained from both the simplified analysis and the design procedure, described in Chapter 5-Section 5.3.3 and Section 5.4, with reference to the experimental results from the literature and those carried out by the author.

6.2 Comparisons of results

This section compares the experimental results obtained in the current investigation with those of the models which are described in Chapter 5. Several parameters are compared, the load-deflection relationships, moment-curvature relationships, strains in the internal tension steel, strains in the CFRP on the tension and compression faces, the movement of the neutral axis through the beam depth as the applied load is increased, and the maximum strength of the sections. The crack patterns obtained from the FE analysis were assessed and also compared with those obtained in the experiments. The predicted results were considered at the same location as in the experimental beams.

From the beams that were tested the following specimens were chosen for the comparison of the above parameters.

- Three unstrengthened beams I11-UH-UN, I13-OL-UN and I21-UL-UN were analysed using LUSAS. Beam I22-UL-T which was strengthened on the tension face and beam I25-UL-TC which was strengthened on both the tension and compression faces were also analysed using LUSAS.

- Four beams were chosen from series-III. Beam III1-OL-UN was unstrengthened and considered as the control beam. Beam III2-OL-T was strengthened on the tension face. Beams III3-OL-TC and III6-OL-TC were strengthened on the tension and the compression faces.

- The second group of beams from series-IV was chosen, IV21-OH-UN, IV23-OH-C and IV24-OH-C. Beam IV21-OH-UN was unstrengthened and the rest were strengthened at the compression face only with different ratios of CFRP, Section 3.4.3.3.

It should be noted that the term load in this section refers to the sum of the two loads applied at the two points on a beam. In all tests, deflection, curvature, strains in the tension and compression reinforcement, the strain in the concrete and the depth of the neutral axis behaviour were recorded at the mid-span of the beams.

6.2.1 Load-deflection relationships

Figures 6.1 to 6.5 show the load-deflection plots from the finite element analyses, those calculated using the finite difference procedure, Section 5.3.4, and experimental results for beams I11-UH-UN, I13-OL-UN, I21-UL-UN, I22-UL-T and I25-UL-TC. Figures 6.6 to 6.10 show the load-deflection plots calculated using the finite difference procedure and the experimental results for beams of series III and IV. The predicted ultimate load, calculated from the design procedure, Section 5.4, is also shown.

Generally, the load-deflection plots for all five beams, Figures 6.1 to 6.5, show that the predictions from the LUSAS analysis, the calculated results obtained from the finite difference procedure and the experimental observations, all have a similar trend. Figures 6.6 to 6.10 show plots of the results of the finite difference procedure and the experimental deflections. These have a similar trend also; however, the load-deflection plots calculated using the finite difference procedure exhibited stiffer behaviour.

The results from the experiments, the LUSAS analysis and finite difference procedure in the unstrengthened beams I11-UH-UN, I13-OL-UN and I21-UL-UN, Figures 6.1 to 6.3 respectively, show good agreement.

In the strengthened beams I22-UL-T and I25-UL-TC, Figures 6.4 and 6.5 respectively, the results of LUSAS and those calculated using the finite difference procedure are generally in good agreement although both exhibited stiffer behaviour than the experimental results. The LUSAS analysis for beam I25-UL-TC, Figure 6.5, did not reach the ultimate load due to a failure to converge.

The unstrengthened over-reinforced beams III1-OL-UN and IV21-OH-UN, Figures 6.6 and 6.10 respectively, exhibited good agreement between the experimental results and those calculated using the finite difference procedure. The experimental results and those calculated using the finite difference procedure for the strengthened over-reinforced beams, Figures 6.7 to 6.10, show a similar trend; however, the loads and deflections behaviour obtained from the finite difference procedure are stiffer than the experiments. The strengthened beams IV23-OH-C and IV24-OH-C, Figure 6.10, show unpredictable behaviour, where the measured deflections at the same load level are smaller than those of the finite difference procedure. For all beams, Figures 6.1 to 6.9, and beam I21-OH-UN, Figure 6.10, the calculated ultimate strengths using the design procedure, Section 5.4, approximately agree with the experimental results and those of FE analysis and finite difference procedure.

Assuming perfect bond between the concrete, the CFRP and the steel bars in the finite difference procedure and the FE analysis might be the cause of the higher stiffness compared with the experiments.

6.2.2 Moment-Curvature relationship

Figures 6.11 to 6.15 show the moment-curvature relationships from the FE analysis, the simplified analysis and the experimental results for beams I11-UH-UN, I13-OL-UN, I21-UL-UN, I22-UL-T and I25-UL-TC. Figures 6.16 and 6.17 show the moment-curvature relationships for the experimental results and the simplified analysis results for beams of series III and IV. For beams when buckling of the CFRP occurred, the moments and curvatures were calculated using the simplified analysis up to a maximum compressive strain in the concrete adjacent to CFRP of 0.003, for the reasons discussed in Chapter 4.

The experimental moment-curvatures relationships for all beams, Figures 6.11 to 6.17, approximately agreed with those from the FE analysis and those calculated using the simplified analysis. After cracking, Figures 6.11 to 6.15, the experimental results were in good agreement with the FE analyses and those calculated using the simplified analysis. After yielding of the steel in beam I25-UL-TC, lower experimental moments were exhibited for a given curvature or a moment than those obtained from the FE analyses and the calculated using the simplified analyses, Figure 6.15. This might be due to the perfect bond assumed between the concrete, the CFRP and the steel bars in the simplified analysis and the FE analysis.

The experimental moment-curvature relationships for each beam, unstrengthened and strengthened, of series-III and IV, Figures 6.16 and 6.17, are in good agreement with those calculated using the simplified analysis.

In general, the results obtained from the FE analyses and the simplified analyses for calculating moment and curvature for reinforced concrete beams strengthened with CFRP are in agreement with the experimental values. This confirms that when perfect bond between the CFRP and the concrete at both the compression face and the tension face of a beam is achieved the bending capacity efficiently improves. Additionally, the bending capacity can be easily predicted.

6.2.3 Tensile strain in longitudinal steel reinforcement

Figures 6.18 to 6.22 show the variation of the tensile strains in the steel reinforcement bars with the load at the mid-span, obtained from the FE analyses, the simplified section analysis results and the experimental results for beams I11-UH-UN, I13-OL-UN, I21-UL-UN, I22-UL-T and I25-UL-TC. Similarly, Figures 6.23 and 6.24 show the variation of the tensile strains in the steel reinforcement bars with the load at the mid-span, obtained from the simplified section analysis results and the experimental results for the beams of series III and IV.

Figures 6.18 to 6.22 show that the FE analyses, the simplified section analyses and the experimental results are generally in good agreement. The FE analysis, in some cases, predicted lower strains than the experimental results, but the results agree with the simplified analysis ones to some degree. Similarly, good agreement was achieved between the simplified analysis and the experimental results for the beams of series III and IV, Figures 6.23 and 6.24.

6.2.4 Tensile strain in CFRP

Figures 6.25 and 6.26 show the variation of the tensile strains in the external CFRP laminates with the load at mid-span obtained from the FE analyses, calculated using the simplified analyses and the experimental results for beams I22-UL-T and I25-UL-TC respectively. Figure 6.27 shows the variation of the tensile strains in the external CFRP

laminates with the load at the mid-span obtained from the simplified analyses and the experimental results for the strengthened beams of series-III. Generally, good correlation was achieved between the results of the FE analyses, the simplified analyses results and the experimental results for beams I22-UL-T, I25-UL-TC, III2-OL-T, III3-OL-TC and III6-OL-TC, Figures 6.25 and 6.27.

6.2.5 Compression strain

Figures 6.28 to 6.32 show the variation of the compression strains with the load at the mid-span obtained from the results of the FE analyses, the results calculated using the simplified analyses and the experimental results of beams I11-UH-UN, I13-OL-UN, I21-UL-UN, I22-UL-T and I25-UL-TC. Figures 6.33 and 6.34 show the variation of the compression strains with the load at the mid-span obtained from the results calculated using the simplified analyses and the experimental results for the beams of series III and IV.

Good correlation was achieved between the results of the FE analysis, the results calculated using the simplified analysis and the experimental results for beams, Figures 6.28 to 6.31. A small difference in the strains between the predicted and the measured observations in beam I25-UL-TC, Figure 6.32, particularly after yielding of the steel reinforcement, was found.

Figure 6.33 shows that the results calculated using the simplified analysis are in good agreement with the experimental results for all beams of series-III, both strengthened and unstrengthened. The strengthened beam IV24-OH-C, Figure 6.34, show unpredictable behaviour, where the experimental strains in the CFRP are larger than that of the simplified analysis at the same load; however, both the simplified analysis and the experimental results have similar trends.

6.2.6 Movement of the depth of the neutral axis

Figures 6.35 to 6.37 show the variation of the ratio of the depth of the neutral axis to the effective depth of the section with the load for the FE analysis, the results calculated using the simplified analysis and the experimental results for the beams I21-UL-UN, I22-UL-T and I25-UL-TC. Figures 6.38 and 6.39 show the variation of the ratio of the depth of the neutral axis to the effective depth of the section with the load for the results calculated using the simplified analysis and the experimental results, for beams of series III and IV.

The experimental results obtained from beams I21-UL-UN, I22-UL-T and I25-UL-TC are in a good agreement with the FE analysis and the calculated results. The calculated results using simplified analysis for series-III also agree well with the experimental results. Beams IV23-OH-C and IV24-OH-C, which were strengthened on the compression face only, Figure 6.39, showed a difference between the experimental results and the simplified analyses results. However, the trends are similar. This difference in the ratio of the depth of the neutral axis in the two beams, when is assessed at the failure load obtained from the experiments, is approximately 12%.

Generally, the plots of load versus movement of the neutral axis obtained from the FE analyses, and the results calculated using the simplified analysis have trends similar to those from the experiments. Thus, the movement of the neutral axis behaviour observed in Chapter 4 is confirmed by the predicted results.

6.2.7 Assessment of crack patterns

Figures 6.40 and 6.41 show the development of cracking and crushing at various loads from the FE analysis for beams I21-UL-UN, I22-UL-T and I25-UL-TC.

Figure 6.40 and 6.41 show that as the applied load is increased, vertical flexural cracking appears at the mid-span of a beam. At increasing the applied load, additional flexural and diagonal cracks are induced. These cracks propagate towards the compression face of a beam. Finally, concrete crushing appears at the middle portion of the compression face of the beam.

Figure 6.40 shows that for the unstrengthened beam I21-UL-UN increasing the load did not cause flexural-shear cracks and / or and shear cracks along the shear span compared with the beam I24-UL-T, which was strengthened on the tension face. This is because beam I21-UL-UN failed by steel yielding while beam I24-UL-T failed by concrete crushing. Beam I25-UL-TC, which was strengthened on the tension and compression faces, exhibited similar crack patterns to that of beam I25-UL-TC, Figure 6.41.

The cracking predicted by the FE analyses gives a good indication of the crack patterns and crack development as the load is increased. When the crack patterns from the LUSAS analysis are compared with those that occurred in the test of beam I25-UL-TC, Figure 6.42, good agreement is observed.

It can be concluded that using the LUSAS finite element analysis for modelling a reinforced concrete beam, either unstrengthened or strengthened can give good agreement for the crack patterns and their development when compared with the experiments.

6.2.8 Ultimate loads

The experimental ultimate loads, P_m, for all beams tested in the current study, Section 4.5, are compared with the loads, P_c, calculated using the simplified analysis, Section 5.3.3, and both are given in Table 6.1. Because the analyses could not predict some of the experimental failure load, the beams are divided into two groups, Table 6.1. The

first group includes specimens which failed in the modes assumed in the analyses whereas the second group includes the specimens which exhibited different failure modes.

Table 6.1 shows that the average values of the ratios between calculated and experimental ultimate loads for the first and the second group are 0.92 and 1.21 respectively. In all considered beams in the first group, the failure mode and the ultimate load obtained from the calculated using the simplified analyses models agreed with those observed in experiments.

It can be concluded that the simplified analysis model based on moment-curvature analysis is able to predict the flexural failure modes and the ultimate loads of a beam strengthened into both tension and compression faces when perfect bond is assumed.

6.3 Corroboration with results taken from the literature

The ultimate loads of 76 reinforced concrete beams and slabs both unstrengthened and strengthened with externally bonded FRP materials, taken from the literature and from the current research have been used to validate the results obtained from the simplified analysis, Section 5.3.3 and the design procedure, Section 5.4. It should be noted that the strengthened specimens taken from the literature were strengthened on the tension face only. In Table 6.2 comparisons of the flexural strength and failure mode of unstrengthened and strengthened sections. The experimental flexural strength, *M1*, was compared with that predicted by the simplified analysis, *M2,* and the design procedure, *M3*. Three modes of flexural failure were reported:

Mode-I: yielding of the internal tensile steel reinforcement in the case of the unstrengthened section, followed by FRP rupture in the case of the strengthened section

Mode-II: yielding of the internal steel reinforcement followed by concrete

crushing

Mode-III: concrete crushing before yielding of tensile steel and rupture of the FRP

Table 6.2 shows the mean and the standard deviation for the comparison of the predictions by the simplified analysis and experimental ultimate moments are 1 and 0.10, respectively. Similarly, the mean and the standard deviation for ultimate moments calculated from the design procedure and the experimental ultimate moments are 0.99 and 0.099, respectively.

The predicted failure mode obtained from the simplified flexural analysis and design procedure for all beams agreed with those observed in the experiments, Table 6.2. A comparison of the ultimate moments obtained from experiments and those from the design procedure is given in Table 6.2 and is plotted in Figure 6.43. This figure shows a good correlation between the calculated ultimate moments from the design procedure and the experimental moments.

6.4 Conclusions

The following conclusions can be drawn from the comparison of the experimental results, finite element analyses, simplified analyses and design procedure reported in this chapter:

- The results predicted by the finite element analysis and the simplified analysis models are in a good agreement with the experimental results for the reinforced concrete beams strengthened with CFRP, either on the tension face or on both the tension and compression face.

- The deflections predicted by the finite difference procedure compared well with those predicted by the FE analysis and the experimental results.

- The design procedure can be used to determine the ultimate moment and the flexural failure mode of the reinforced concrete section with external bonded CFRP when perfect bond is assumed. This design procedure can be used for all kinds of FRP materials.

- Achieving good agreement between the experiment and the theory, particularly when the design procedure approach is used, can give more confidence to the use of CFRP on the compression face of reinforced concrete members which behave in flexure.

Table 6.1: Comparison between the ultimate loads of the experimental and simplified analysis

	Beam ref.	Failure mode	P_m (kN)	P_C (kN)	P_C / P_m	Average
First Group	I11-UH-UN	S	44.76	36.60	0.82	0.92
	I12-UH-UN	S	44.76	36.29	0.81	
	I21-UL-UN	S	20.74	23.07	1.11	
	I25-UL-TC	C	85.42	97.74	1.14	
	I13-OL-UN	C	128.00	110.00	0.86	
	II3-UH-TC	C	95.60	91.50	0.96	
	III1-OL-UN	C	46.06	42.76	0.93	
	III2-OL-T	C	51.50	49.64	0.96	
	III4-OL-UN	C	45.10	43.85	0.97	
	III5-OL-T	C	60.84	51.65	0.85	
	IV11-OL-TC	C	10.80	11.38	1.05	
	IV12-OL-TC	C	12.48	11.60	0.93	
	IV21-OH-UN	C	8.00	6.83	0.85	
Second Group	III3-OL-TC	B	58.60	64.65	1.10	1.21
	III6-OL-TC	B	71.90	72.47	1.01	
	IV22-OH-C*	B	7.60	10.23	1.35	
	IV23-OH-C*	B	9.33	12.51	1.34	
	IV24-OH-C*	B	10.40	14.83	1.43	
	I24-UL-TC	TD	78.16	90.28	1.16	
	II2-UH-TC	SH	81.06	88.00	1.09	
	I22-UL-T	EP	58.00	71.60	1.23	
	I23-UL-TC	EP	54.96	81.14	1.48	
	II1-UH-T	R	97.00	93.40	0.96	

C: Concrete crushing; EP: End peeling; S: Steel yielding ; TD : Tension debonding; B: CFRP buckling; R: FRP rupture; SH: shear failure

P_m : The experimental ultimate load; P_c : The ultimate load calculated using the simplified analysis.

* Bonding of the CFRP composite to the concrete surface was early lost in the mid span in experiments.

Authors and Beam reference	Section geometry (mm)				ρ_s %	ρ_{sc} %	ρ_f %	Bending Moment (kN-m)			$\frac{M2}{M1}$	$\frac{M3}{M1}$	Failure Mode	Remarks
	b	d_s	h	d_{sc}				$M1$	$M2$	$M3$				
Lam & Teng- 2001[75]														
I	500	74.00	104.0		0.678	--	0.55	11.3	11.22	11.28	0.99	1.00	I	
II	500	81.7	102.1		0.614	----	0.50	12.3	12.61	12.8	1.03	1.04	I	
III	500	49.3	102.1		1.018	----	0.51	11.0	10.01	10.2	0.91	0.93	I	
IV	500	73.6	101.8		1.54	----	0.56	19.4	20.33	17.4	1.05	0.90	II	
Teng *et al.* 2000 [74]											0.00	0.00	I	
A2	500	90.2	102.2	-	0.557	----	0.30	9.47	10.07	10.3	1.06	1.09	I	
B2	500	90.2	100.2	--	0.376	----	0.34	11.9	11.28	11.3	0.95	0.95	I	
C2	500	73.5	102.5	-	1.068	----	0.36	12.41	12.73	12.9	1.03	1.04	I	
A1	500	73	104	-	0.688	----	----	5.4	5.88	5.89	1.09	1.09	I	Unstrengthened slab
B1	500	87.9	101.9	-	0.322	----	----	5.94	5.23	5.49	0.88	0.92	I	Unstrengthened slab
C1	501	79.2	103.2	--	0.99	----	----	10.24	9.00	9.29	0.88	0.91	I	Unstrengthened slab
Chajes *et al.* 1994 [50]											0.00	0.00		
A2	127	50.8	76.2		1.100	----	2.05	3.00	3.16	3.14	1.05	1.05	II	
A3	127	50.8	76.2		1.100	----	2.05	3.43	2.94	2.84	0.86	0.83	II	
E1	127	50.8	76.2		1.104	----	2.77	3.11	3.21	3.19	1.03	1.03	I	
E2	127	50.8	76.2		1.104	----	2.77	3.11	3.30	3.30	1.06	1.06	I	
E3	127	50.8	76.2		1.104	----	2.77	3.13	3.31	3.3	1.06	1.05	I	
G1	127	50.8	76.2		1.104	----	2.38	3.06	3.59	3.58	1.17	1.17	I	
G2	127	50.8	76.2		1.104	----	2.38	3.46	3.59	3.58	1.04	1.03	I	
G3	127	50.8	76.2		1.104	----	2.38	2.94	3.52	3.5	1.20	1.19	I	
Ritchie *et al.* 1991[29]											0.00	0.00		
E	152.4	250.8	305		0.675	----	1.90	57	57.52	57.4	1.01	1.01	I	
F	152.4	250.8	305		0.675	----	1.90	61	57.24	57.0	0.94	0.93	I	
L	152.4	250.8	305		0.675	----	0.50	56.1	57.6	57.0	1.03	1.02	I	
Bonacci *et al.* 2000 [134]											0.00	0.00		
B1	270	350	400	40	0.952	0.15	---	131.3	137.07	136.2	1.04	1.04	I	Unstrengthened beam
B5[1]	270	350	400	40	0.952	0.15	0.04	157.3	156.42	167.0	0.99	1.06	II	
B7[2]	270	350	400	40	0.952	0.15	--	118.95	137.07	136.2	1.15	1.15	I	Unstrengthened beam
Sharif *et al.* 1994 [30]														
CB	150	114	150	36	0.918	0.333	---	6.88	7.78	7.98	1.13	1.16	I	Unstrengthened beam
P1	150	114	150	36	0.918	0.333	0.88	13.2	10.98	11.13	0.83	0.84	I	
P3J	150	114	150	36	0.918	0.333	1.75	16.11	14.21	14.20	0.88	0.88	II	
P2BW	150	114	150	36	0.918	0.333	1.75	15.33	14.21	15.46	0.93	1.01	II	

Nguyen *et al.* 2001 [64]														
A1500	120	120	150		1.64	----	0.67	25.96	21.25	20.58	0.82	0.79	II	
A1500	120	120	150	28	1.64	1.09	0.67	25.96	23.99	23.91	0.92	0.92	II	
Swamy *et al.* 1999 [35]														
B1	150	217	259	-	1.85	----	0.72	75.71	76.52	76.36	1.01	1.01	II	
B2	150	217	259	-	1.85	----	0.72	76.09	77.12	77.03	1.01	1.01	II	
Andreou *et al.* 2000 [135]											0.00	0.00		
110	100	174	200		0.9	----	0.17	20	19.89	19.7	0.99	0.99	II	
111	100	174	200		0.9	----	0.17	20	19.89	19.7	0.99	0.99	II	
109	100	174	200		0.9	----	0.33	24.5	23.43	23.1	0.96	0.94	II	
Arduni *et al.* 1997 [32]														
B2	300	350	400	50	0.379	0.253	0.05	96.3	103.04	103.26	1.07	1.07	I	
Lamanna *et al.* 2001 [136]														
F-2I-S-102-I	153	114	153	40	1.48	0.58	1.87	11.9	13.63	13.58	1.15	1.14	II	
F-2I-F-102-I	153	114	153	40	1.48	0.58	1.87	12.4	14.27	14.32	1.15	1.15	II	
F-2I-H-102-I	153	114	153	40	1.48	0.58	1.87	13.3	16.70	15.95	1.26	1.20	II	
F-2I-S-102-2	153	114	153	40	1.48	0.58	1.87	13.3	13.73	13.7	1.03	1.03	II	
F-2I-S-102-2R	153	114	153	40	1.48	0.58	1.87	12.7	13.73	13.7	1.08	1.08	II	
F-2I-S-51-I	153	114	153	40	1.48	0.58	0.94	11.91	12.21	12.13	1.03	1.02	II	
Rahimi *et al.* 2001 [38]														
C3	200	120	150	30	1.68	0.42	0.25	28.13	31.58	31.03	1.12	1.10	II	
C4	200	120	150	30	1.68	0.42	0.25	28.95	31.58	31.03	1.09	1.07	II	
C5	200	120	150	30	1.68	0.42	0.75	38.7	39.98	38.84	1.03	1.00	II	
C6	200	120	150	30	1.68	0.42	0.75	38	39.98	38.84	1.05	1.02	II	
C7	200	120	150	30	1.68	0.42	1.13	32.7	33.00	32.41	1.01	0.99	II	
C8	200	120	150	30	1.68	0.42	1.13	32.5	33.00	32.41	1.02	1.00	II	
Ross *et al.* 1999 [84]														
4B	200	152	200	36	1.87	0.33	0.30	49.2	52.75	52.22	1.07	1.06	II	
4C	200	152	200	36	1.87	0.33	0.30	47.8	52.75	52.22	1.10	1.09	II	
4D	200	152	200	36	1.87	0.33	0.30	50.8	52.75	52.22	1.04	1.03	II	
5B	200	152	200	36	2.55	0.33	0.30	67.1	58.13	57.60	0.87	0.86	II	
5C	200	152	200	36	2.55	0.33	0.30	67.1	58.13	57.60	0.87	0.86	II	
5D	200	152	200	36	2.55	0.33	0.30	66.5	58.13	57.60	0.87	0.87	II	
6B	200	152	200	36	3.35	0.33	0.30	77.3	64.18	63.86	0.83	0.83	II	
6C	200	152	200	36	3.35	0.33	0.30	70	64.18	63.86	0.92	0.91	II	
6D	200	152	200	36	3.35	0.33	0.30	70.3	64.18	63.86	0.91	0.91	II	

Grace 2001 [44] II - B2	250	402	457	65	1.47	1.47	0.13	301.2	335.12	331.94	1.11	1.10	II	
Mukhopadhyaya *et al.* 1998[58] FS2	150	215	250		2.92	----	1.63	91.85	92.10	90.89	1.00	0.99	II	
Yasutaka *et al.* 01 [137]														
U 45 -1	160	225	260	35	0.78	0.158	0.06	42.96	37.79	37.38	0.88	0.87	I	
U 45-2	160	225	260	35	0.78	0.158	0.06	41.53	37.79	37.38	0.91	0.90	I	
Holdane and Ziara 1999 [16]														
D	200	162	200	35	2.29	0.48	--	60.95	57.78	57.83	0.95	0.95	III	Unstrengthened beam
C	200	370	400	35	1.3	0.21	--	153	150.77	152.78	0.99	1.00	I	
Beams are selected from the current study														
I12-UH-UN	120	130.7	162.8	32	0.64	0.36	--	7.83	6.35	6.27	0.81	0.80	I	Unstrengthened beam
I13-OL-UN	120	135.7	168	42	2.47	0.35	--	22.40	19.25	19.25	0.86	0.86	III	Unstrengthened beam
I21-UL-UN	120	132.3	164.2	---	0.55	--	--	3.63	4.04	3.97	1.11	1.09	I	Unstrengthened beam
I25-UL-TC *	120	131.8	164.8	--	0.54	--	0.92	14.95	17.1	16.67	1.14	1.12	II	
II1-UH-T	120	127.8	163.8	30.8	1.31	0.66	0.31	16.97	16.35	14.5	0.96	0.85	I	
II3-UH-TC *	120	128.1	163.1	35.1	1.31	0.65	0.31	16.73	16.94	14.84	1.01	0.89	II	
III1-OL-UN	120	140	164	36	2.39	0.34	--	23.03	21.38	22.34	0.93	0.97	III	Unstrengthened beam
III2-OL-T	120	138	164	30	2.43	0.34	1.74	26.30	24.82	25.51	0.94	0.97	III	
III4-OL-UN	120	140	165	22	2.39	0.34	--	22.55	22.83	22.65	1.01	1.00	III	Unstrengthened beam
III5-OL-T	120	140	165	22.5	2.43	0.34	1.71	30.42	26.00	26.7	0.85	0.88	III	
IV11-OL-TC *	65	55	80	-	2.81	--	1.34	2.43	2.71	2.75	1.12	1.13	III	
IV12-OL-TC *	65	55	80	-	2.81	--	1.34	2.81	2.72	2.81	0.97	1.00	III	
IV21-OH-UN	65	50	75	-	4.83	--	--	1.80	1.54	1.68	0.86	0.93	III	Unstrengthened beam
* the ratios of the compression CFRP mentioned in Table 3.9 *M1*, *M2* and *M3* are the ultimate moment from experiments, simplified analysis and design procedure, respectively. I = FRP rupture for strengthened beams and steel yielding for unstrengthened beams II- concrete crushing followed by yielding of tensile steel for strengthened beams III- concrete crushing								Average			1.00	0.99		
								Standard deviation			0.10	0.099		

Table 6.2: Comparison the ultimate bending moments from experiments, simplified analysis model and design procedure model

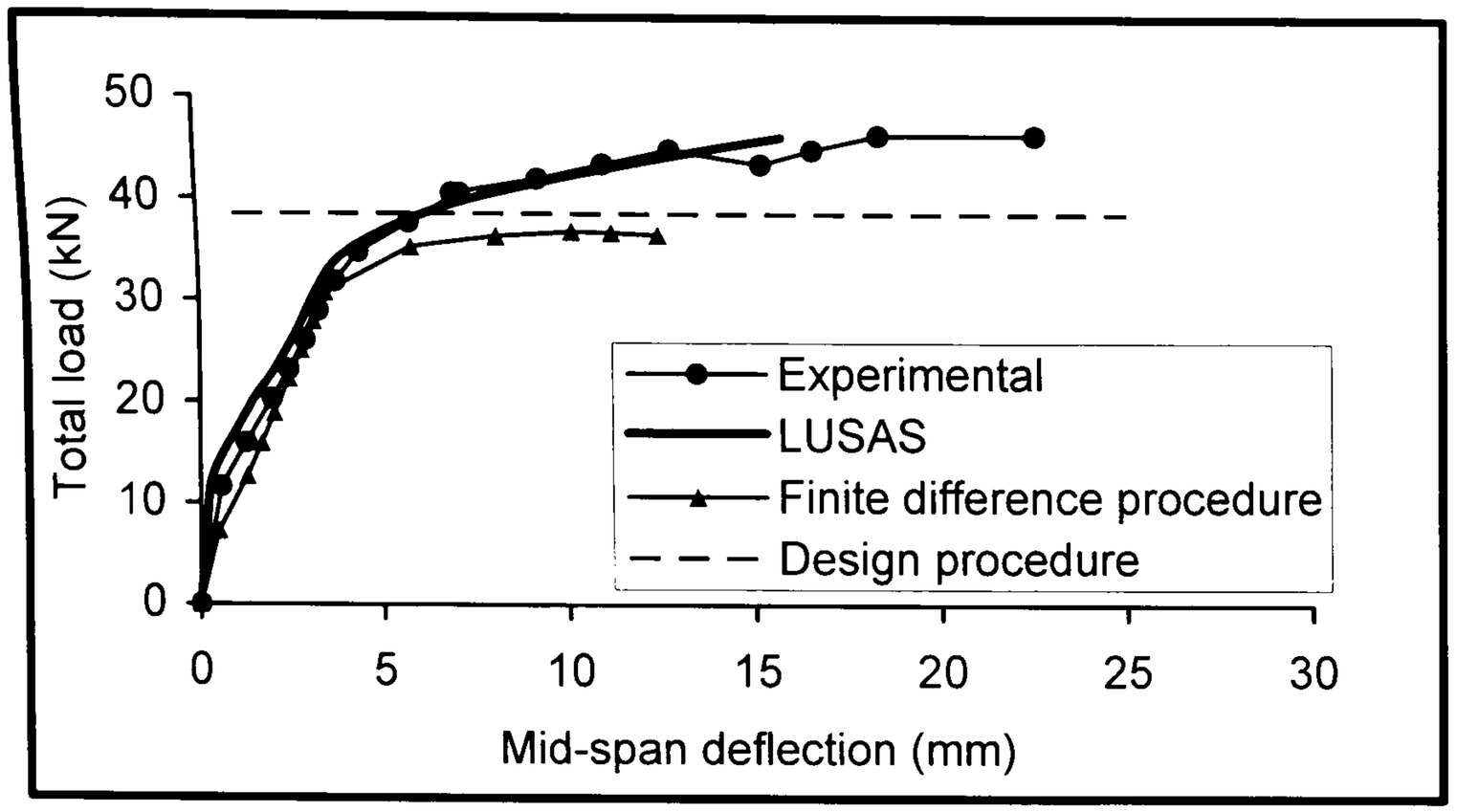

Figure 6.1: Total load versus mid-span deflection for beam I11-UH-UN

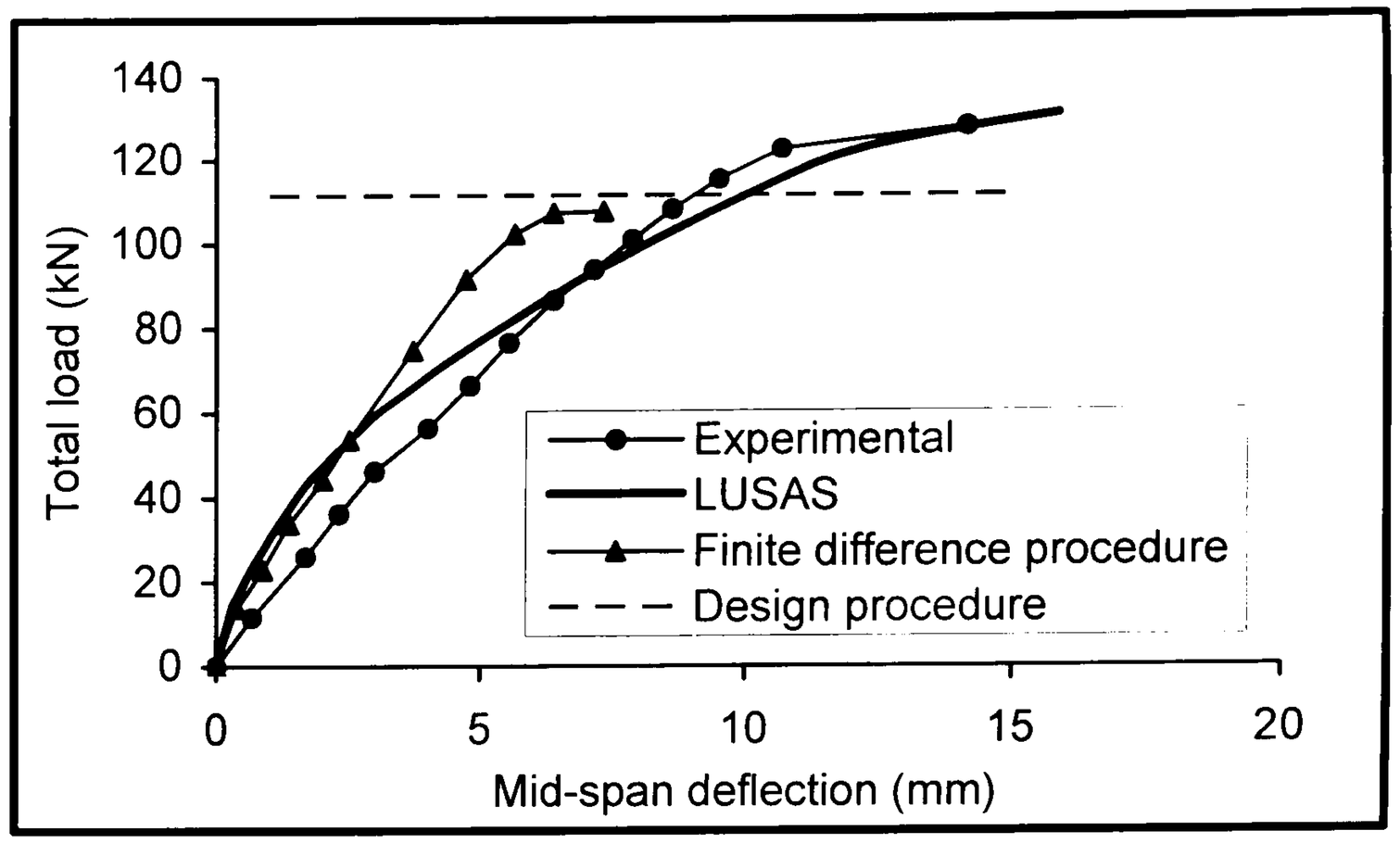

Figure 6.2: Total load versus mid-span deflection for beam I13-OL-UN

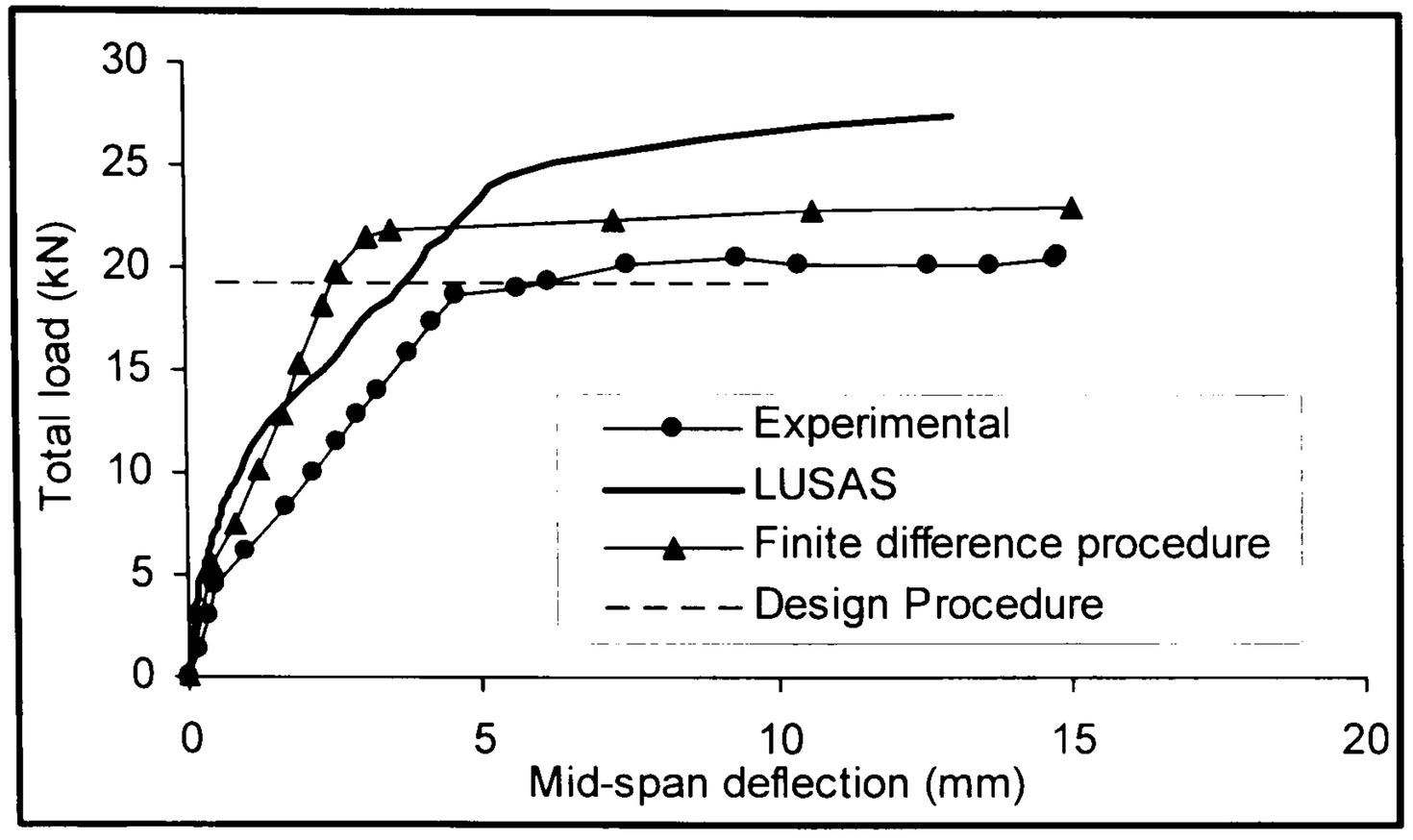

Figure 6.3: Total load versus mid-span deflection for beam I21-UL-UN

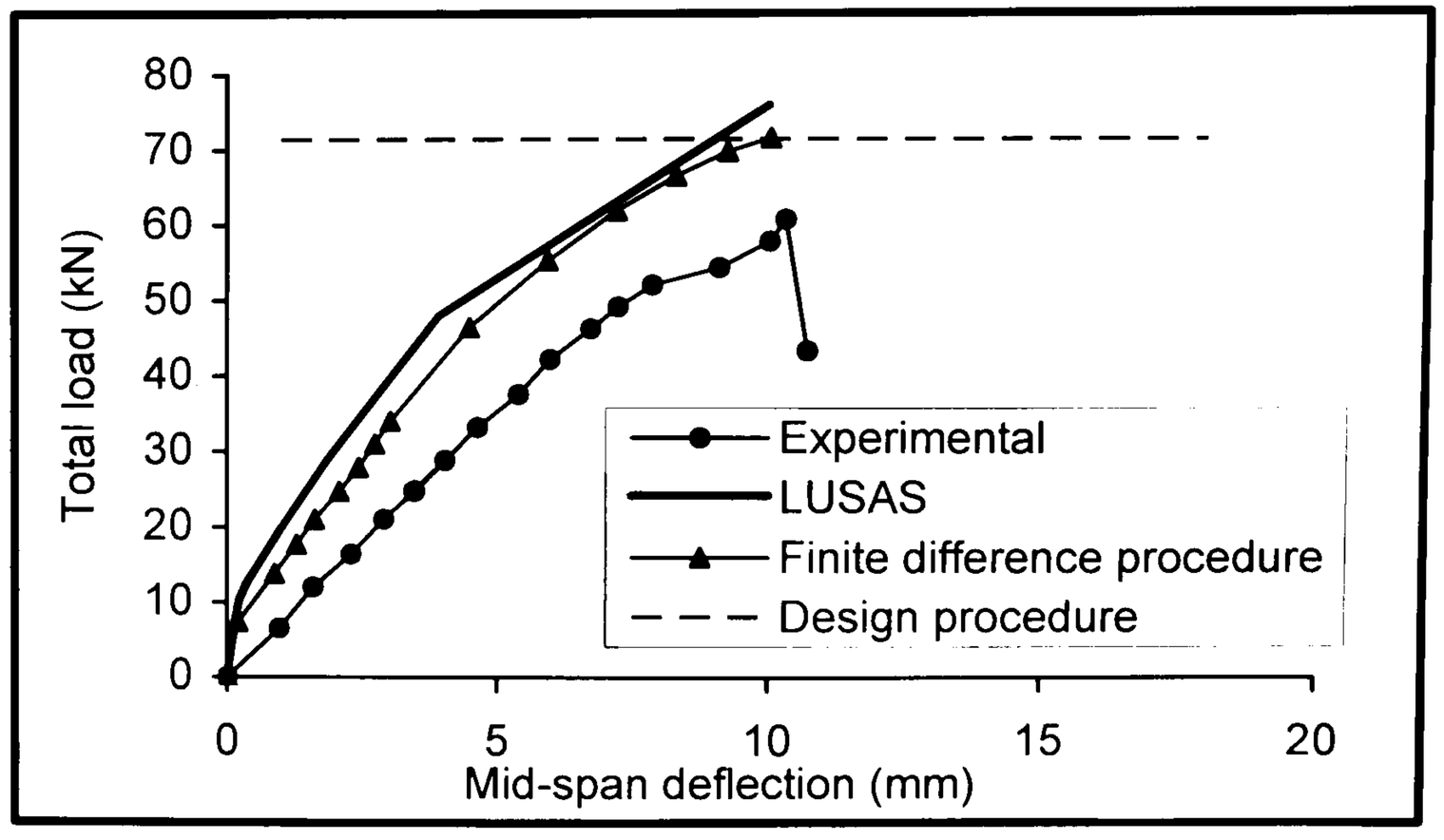

Figure 6.4: Total load versus mid-span deflection for beam I22-UL-T

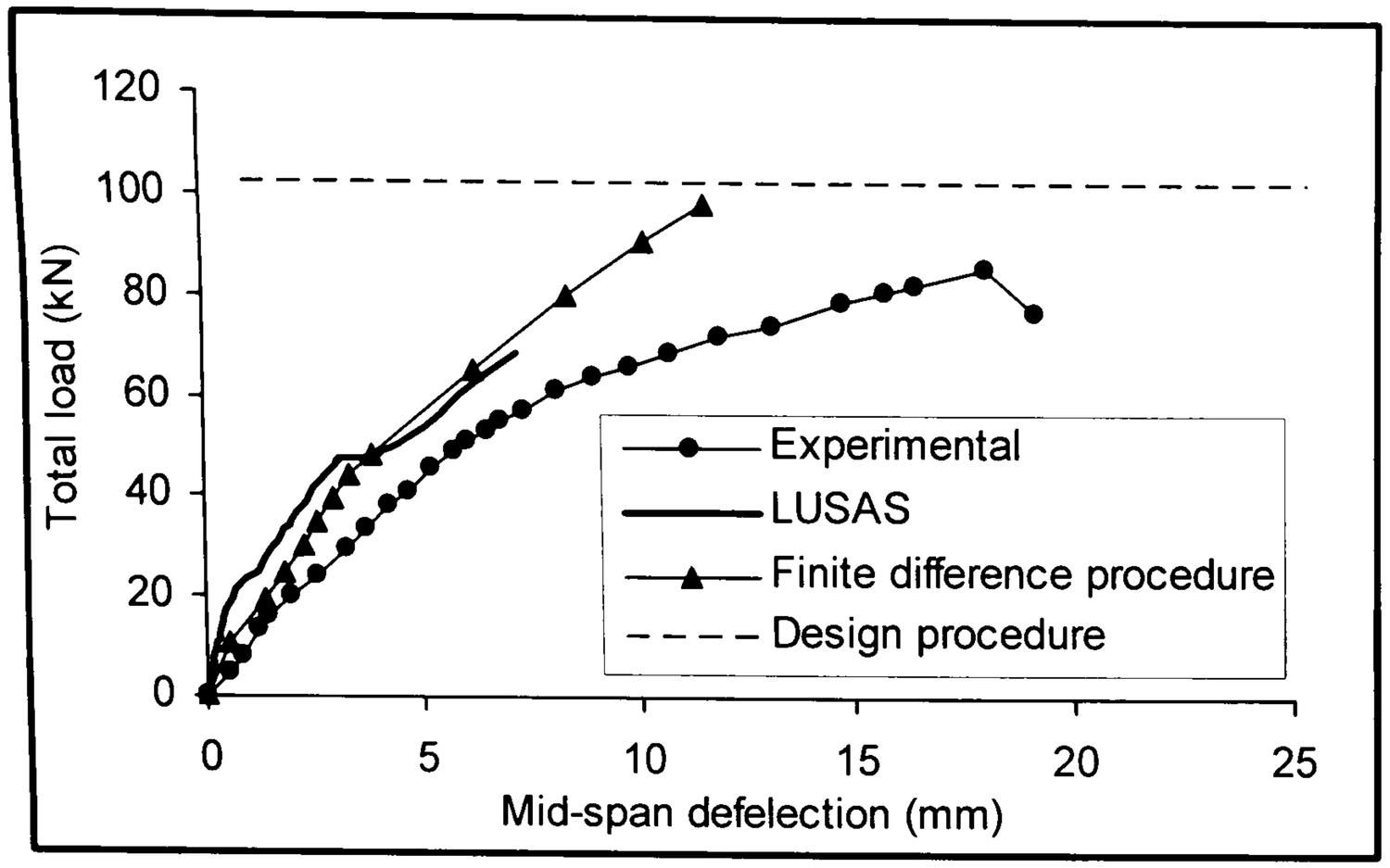

Figure 6.5: Total load versus mid-span deflection for beam I25-UL-TC

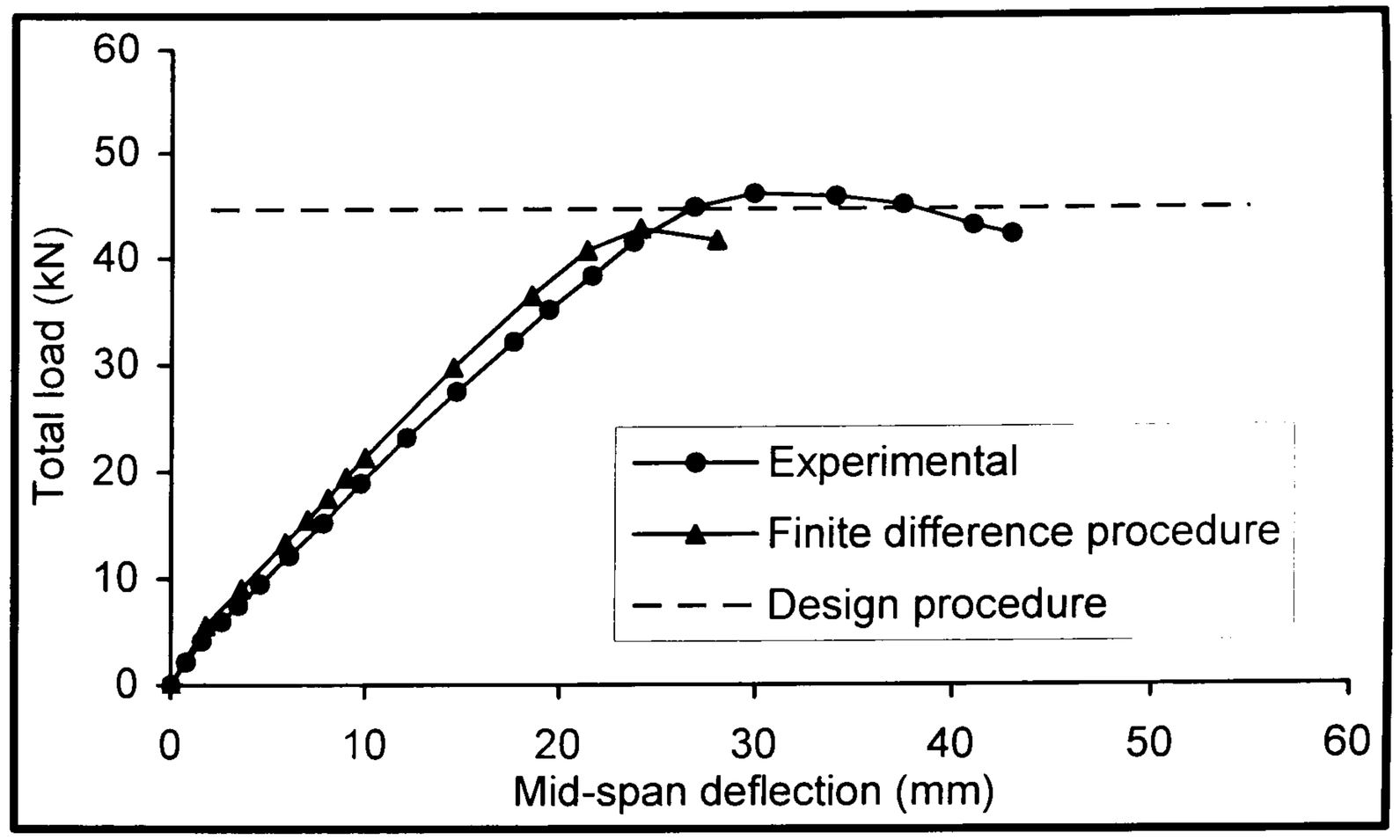

Figure 6.6: Total load versus mid-span deflection for beam III1-OL-UN

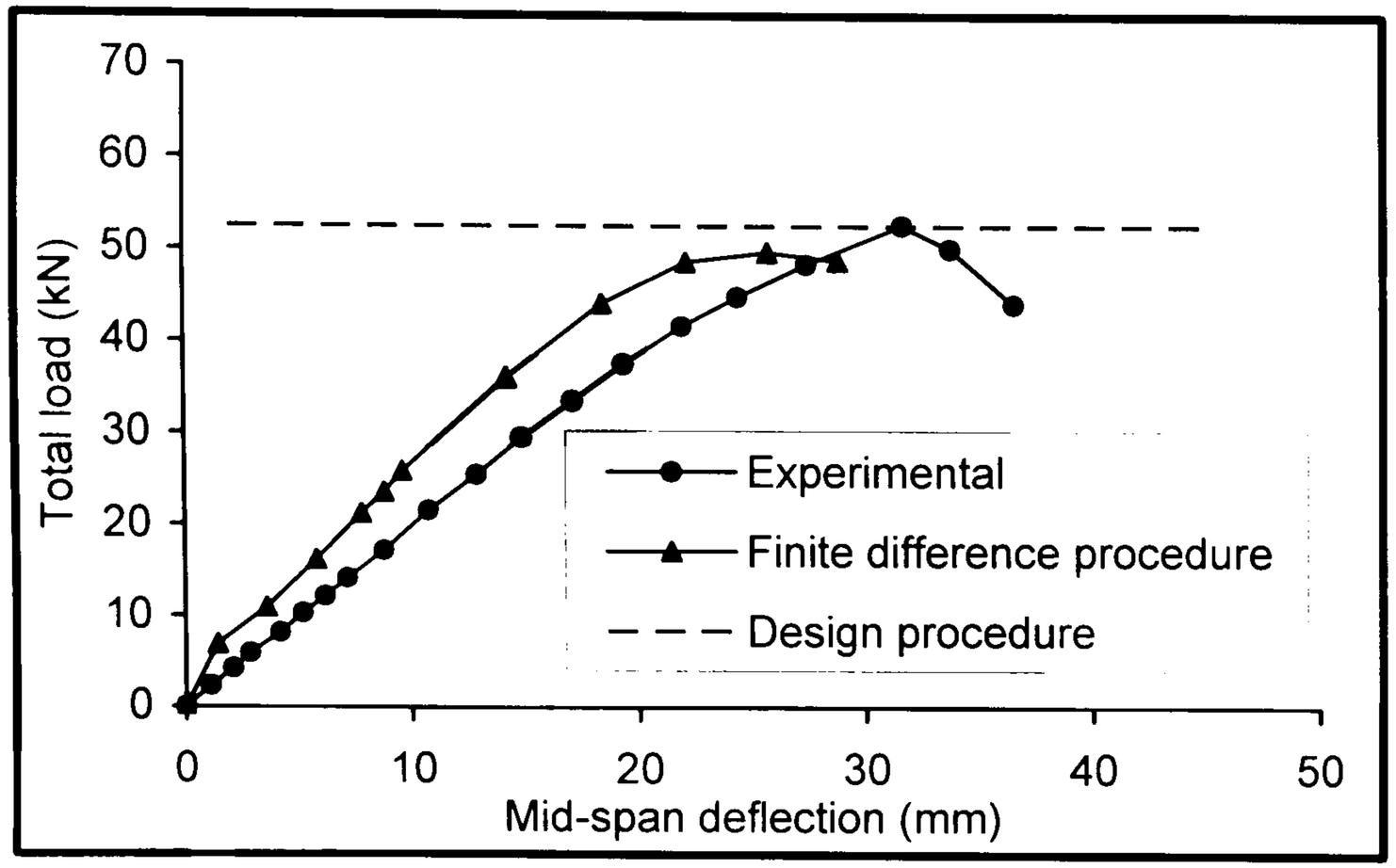

Figure 6.7: Total load versus mid-span deflection for beam III2-OL-T

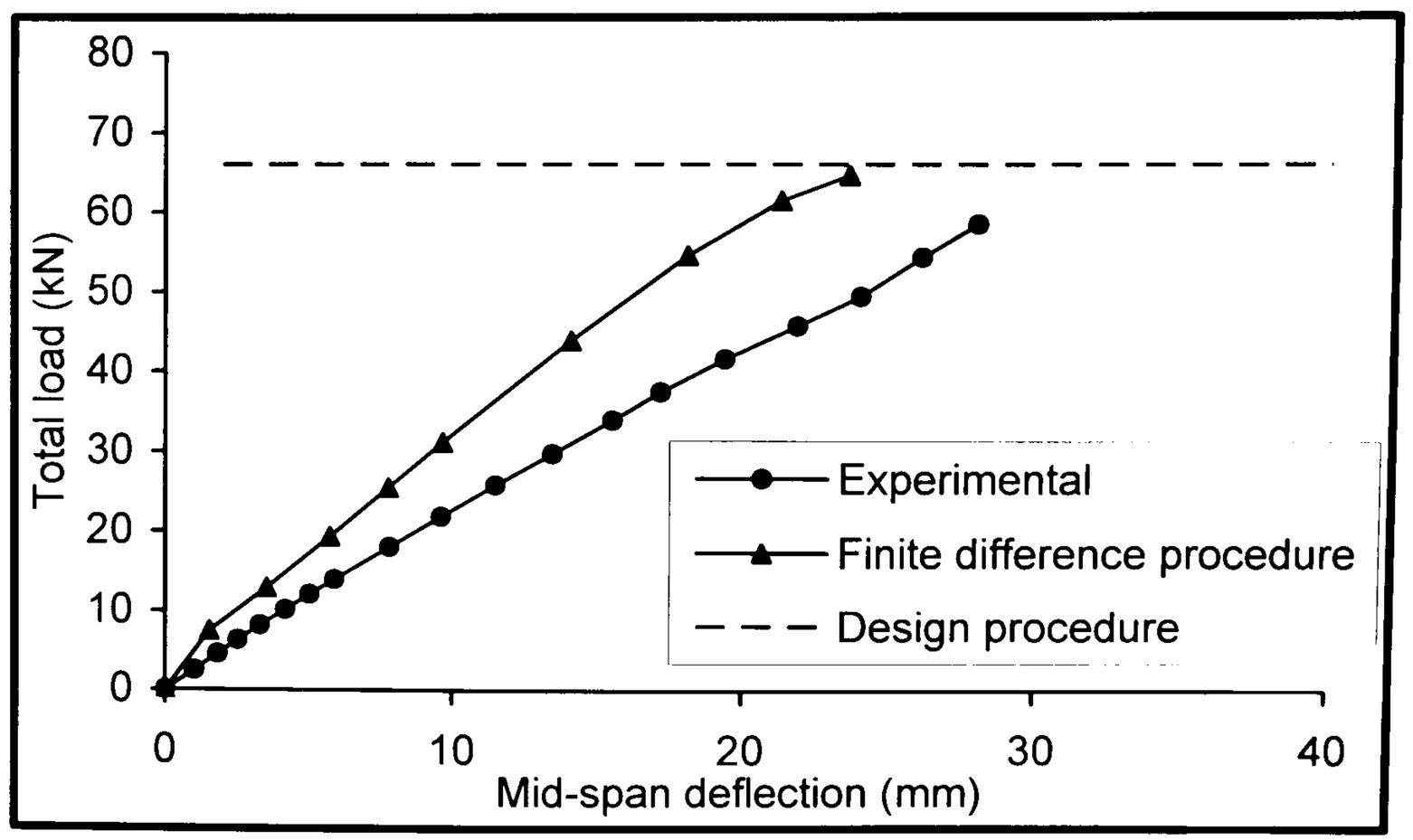

Figure 6.8: Total load versus mid-span deflection for beam III3-OL-TC

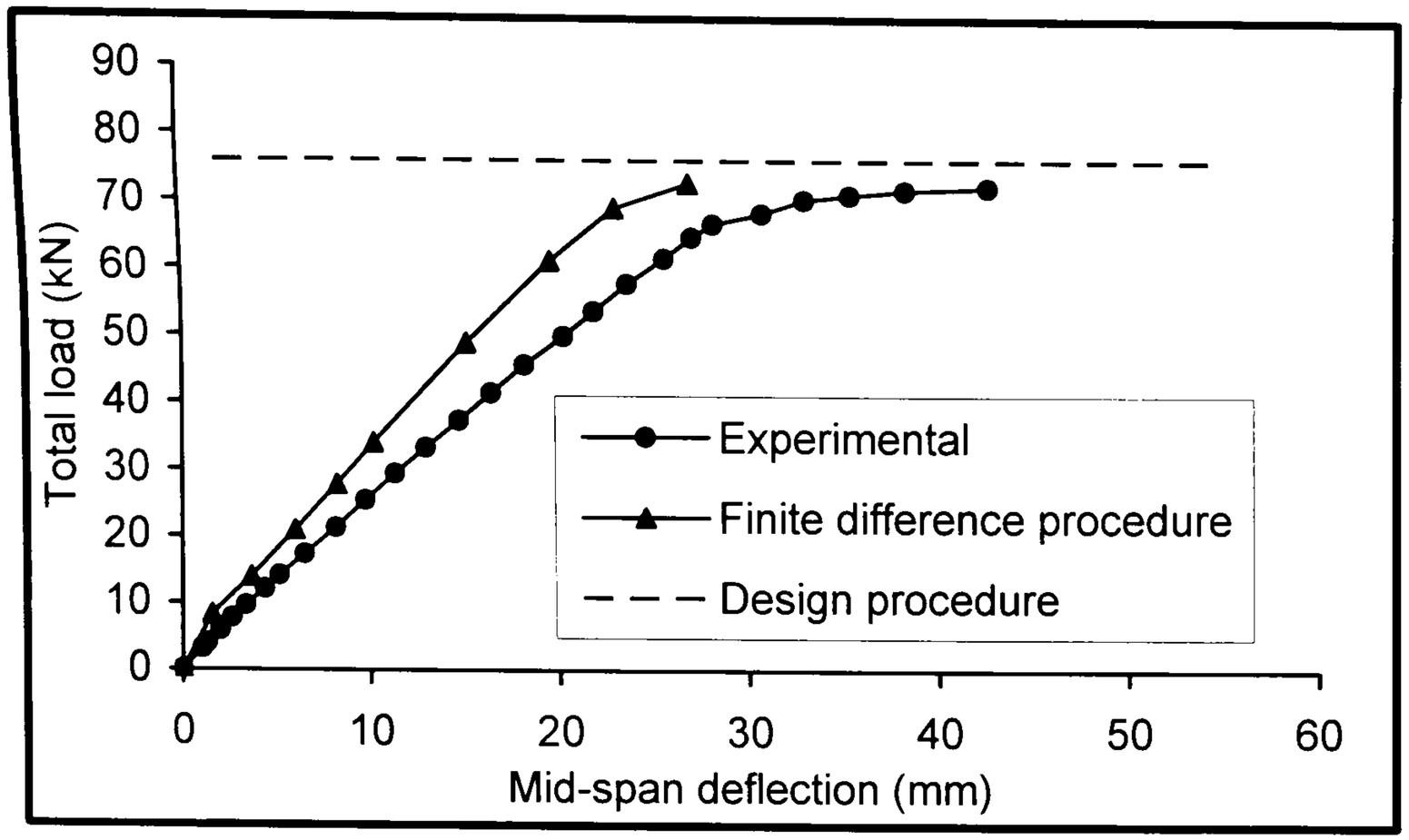

Figure 6.9: Total load versus mid-span deflection for beam III6-OL-TC

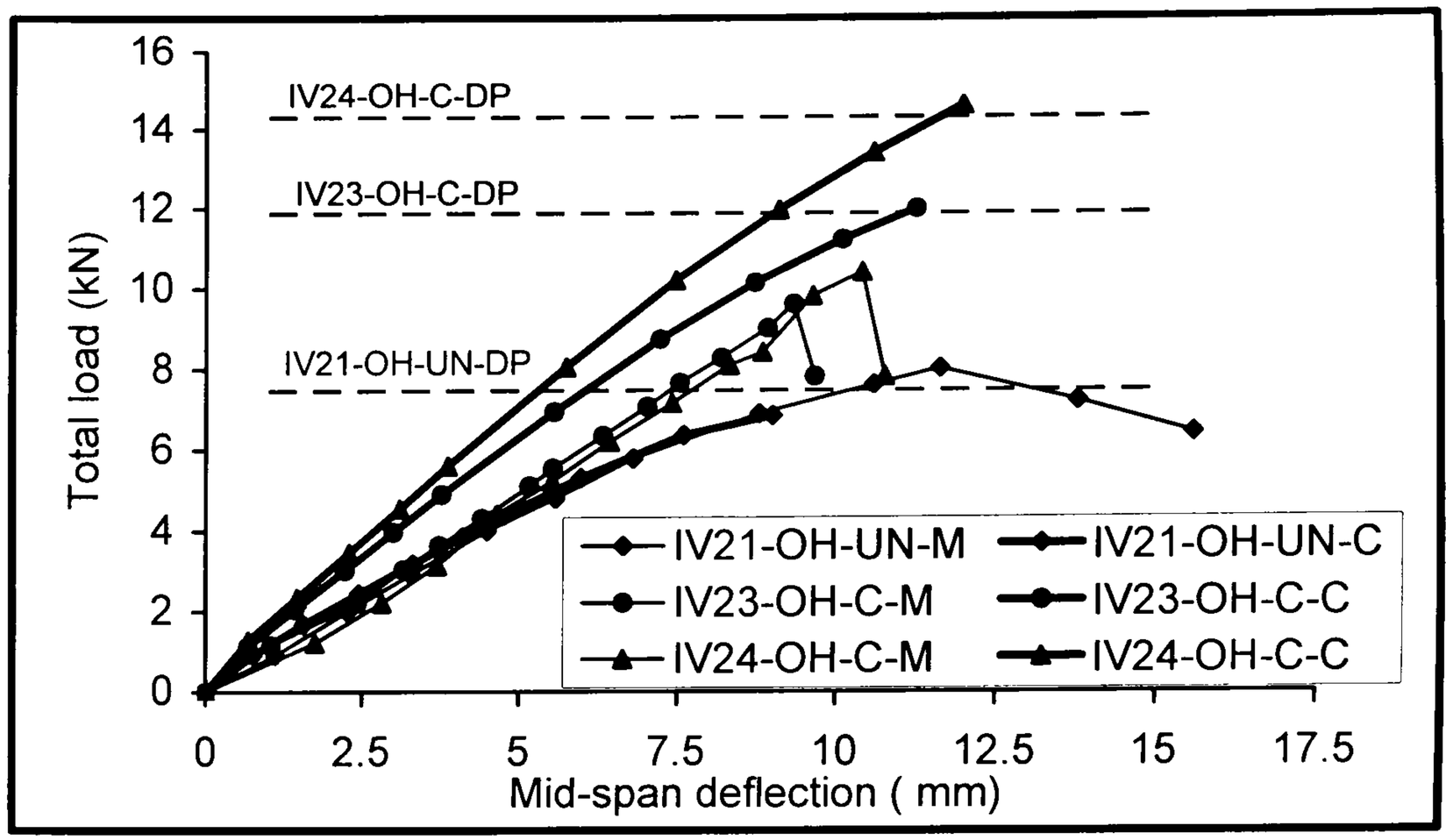

Figure 6.10: Total load versus mid-span deflection for beams of series-IV

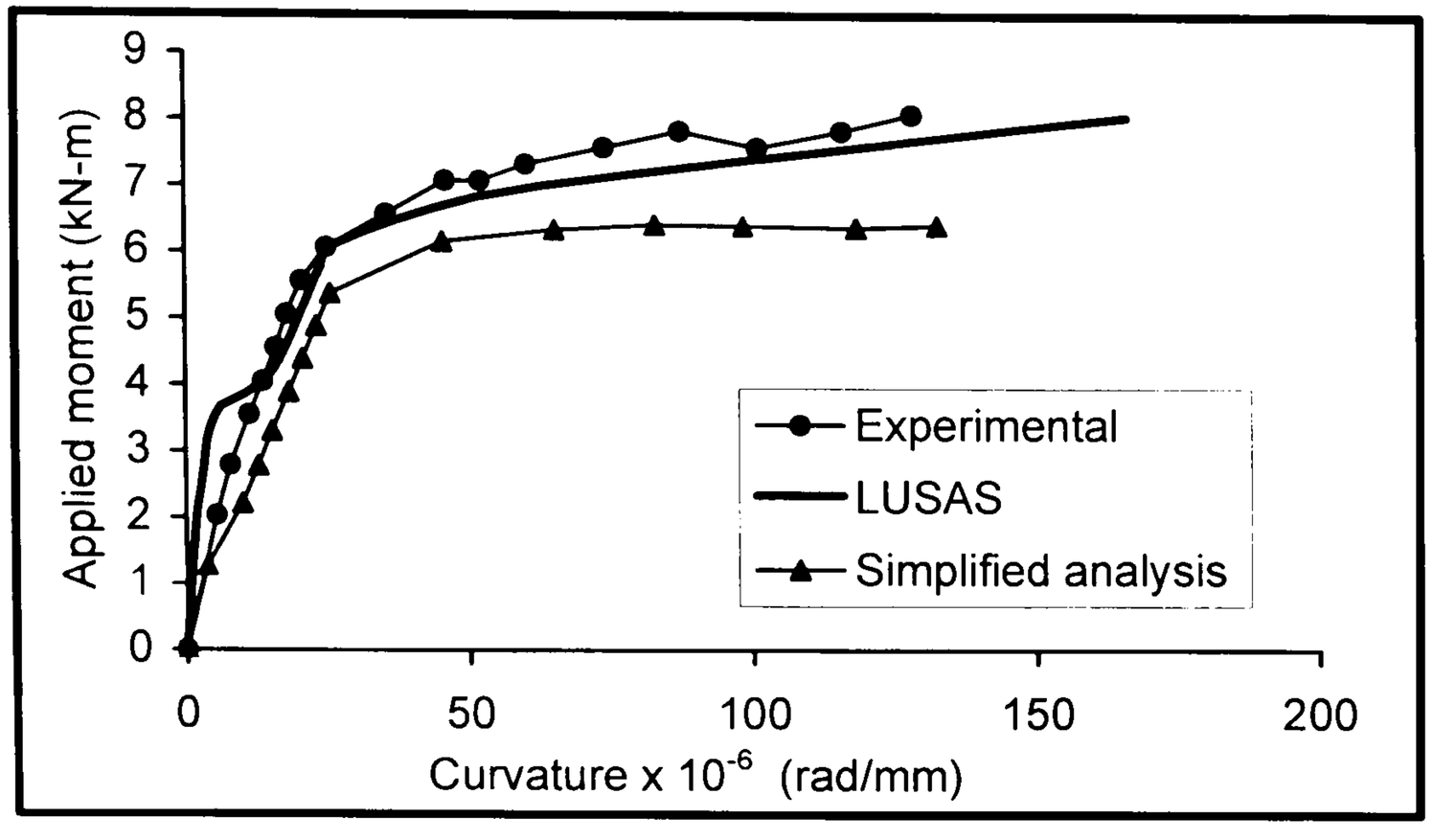

Figure 6.11: Applied moment versus curvature for beam I11-UH-UN

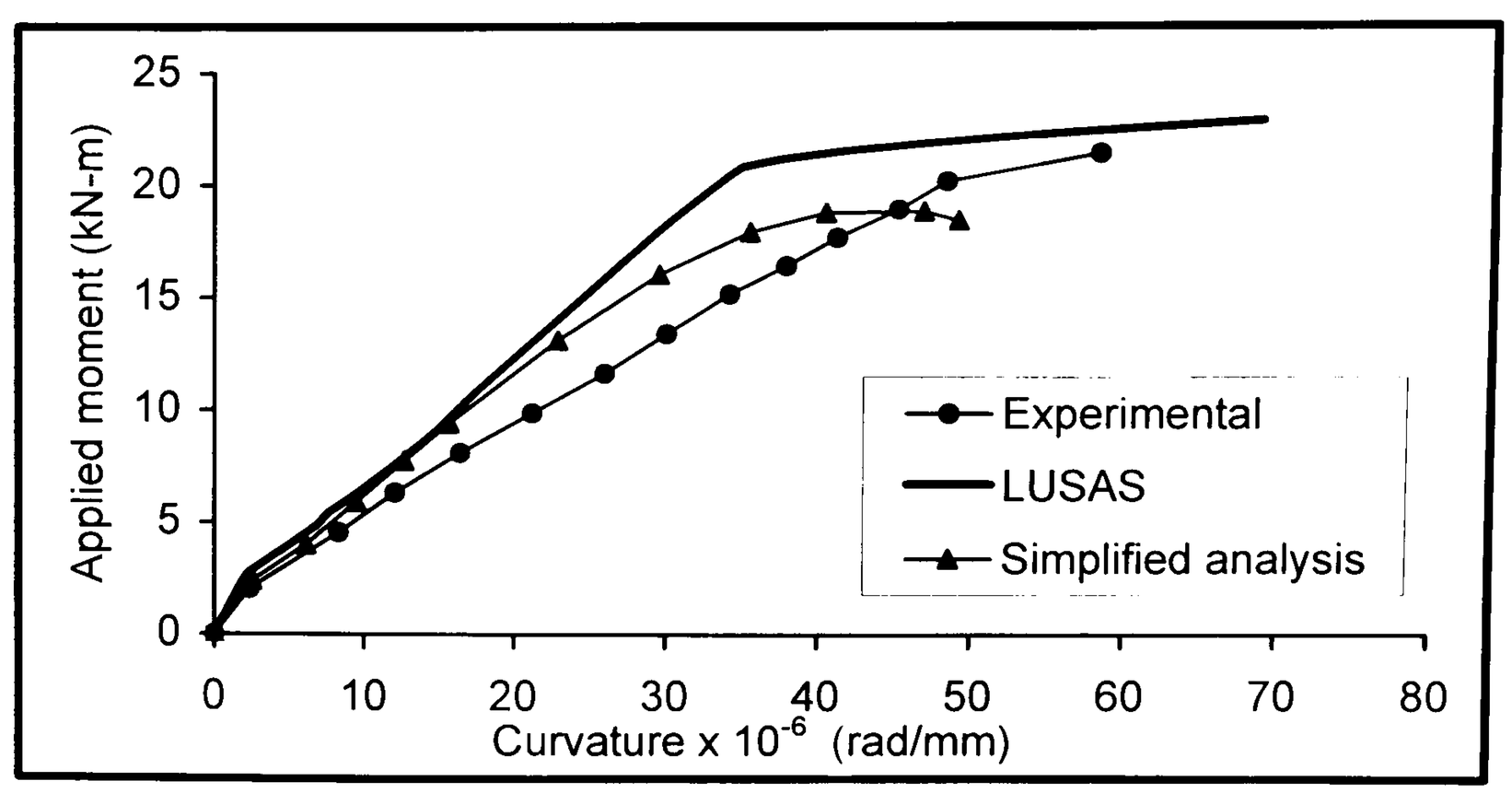

Figure 6.12: Applied moment versus curvature for beam I13-OL-UN

In Figure 6.10 M: Experimental; C: Finite difference procedure and; DP: Design procedure

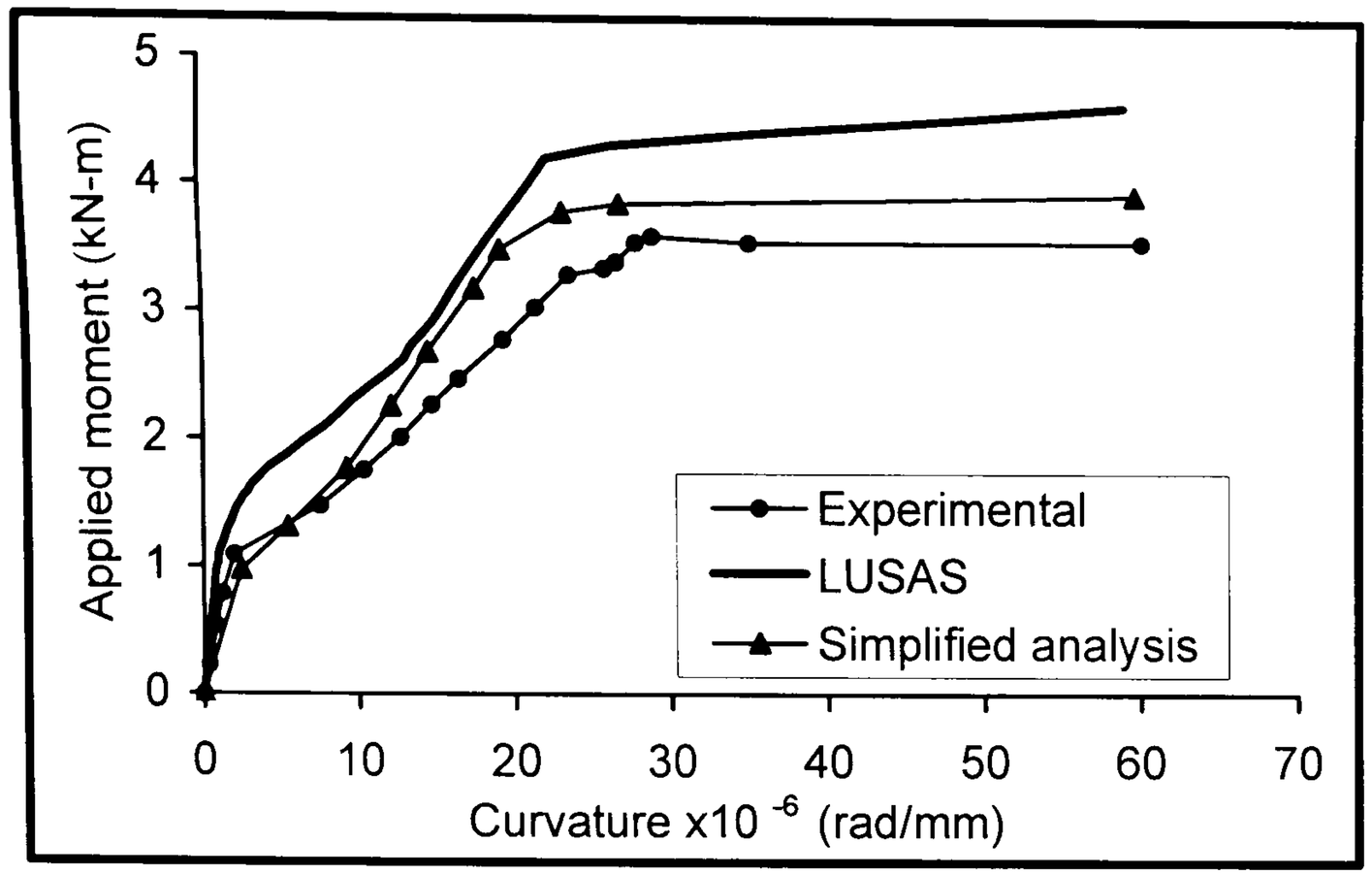

Figure 6.13: Applied moment versus curvature for beam I21-UL-UN

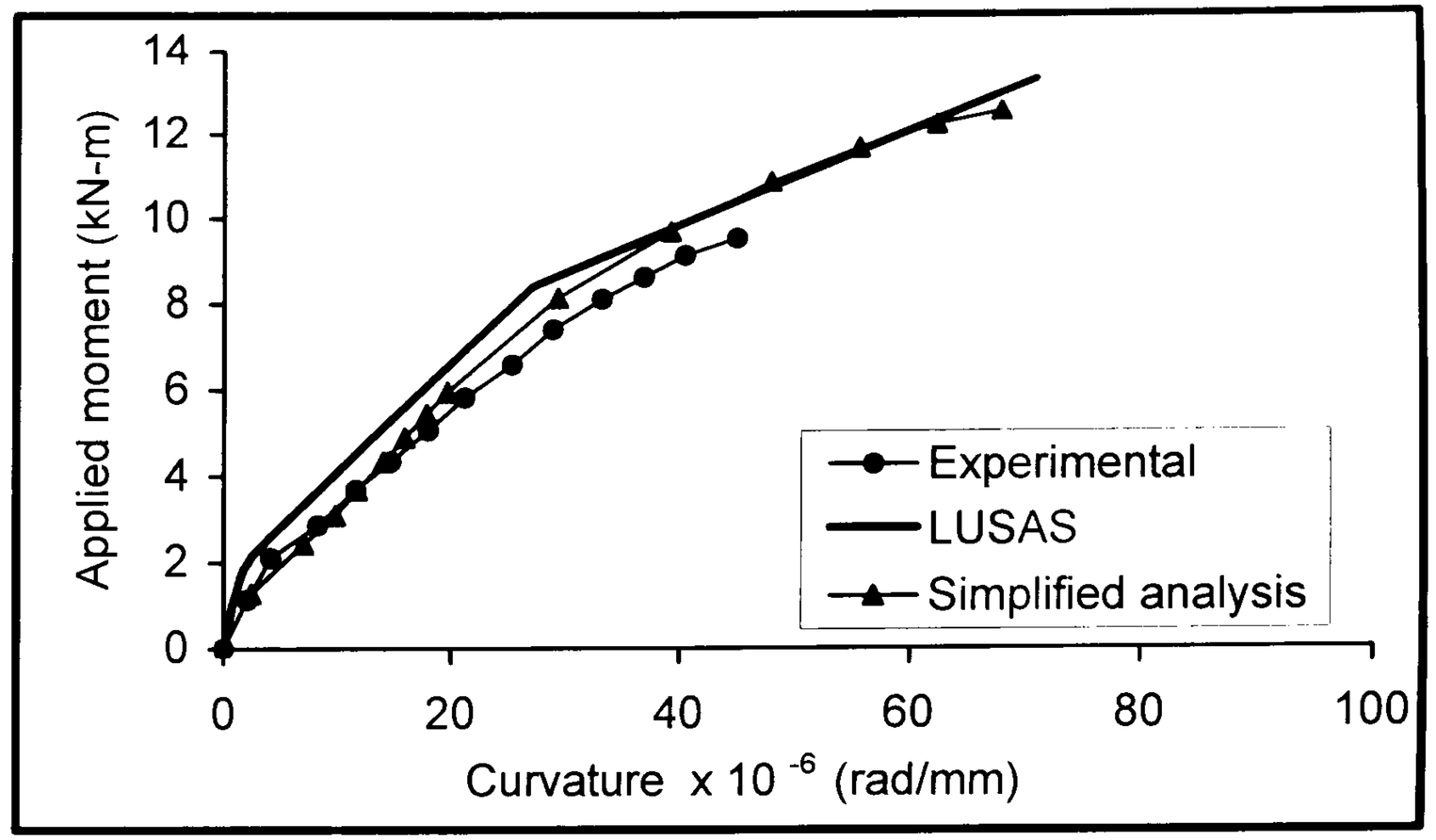

Figure 6.14: Applied moment versus curvature for beam I13-OL-UN

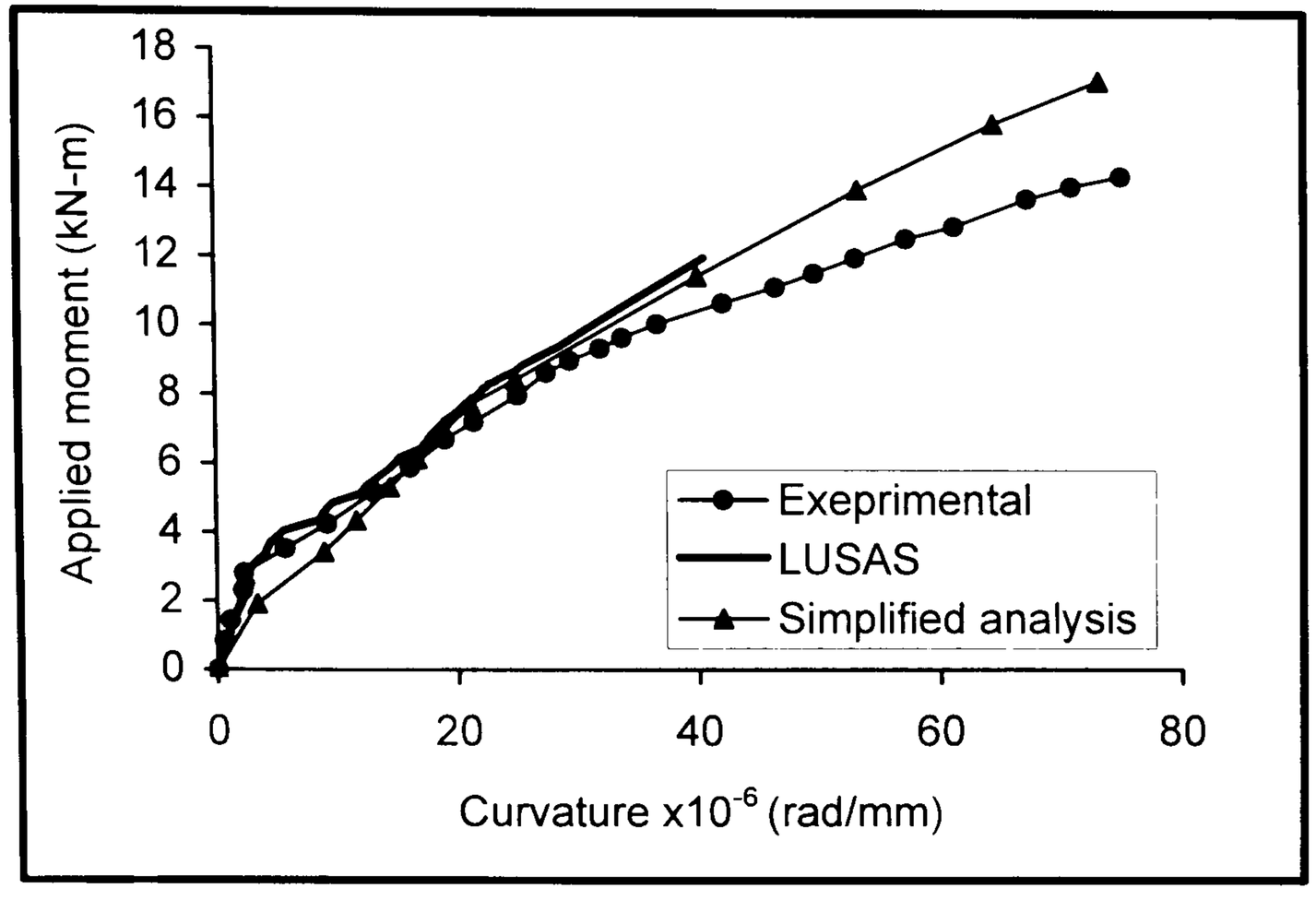

Figure 6.15: Applied moment versus curvature for beam I25-UL-TC

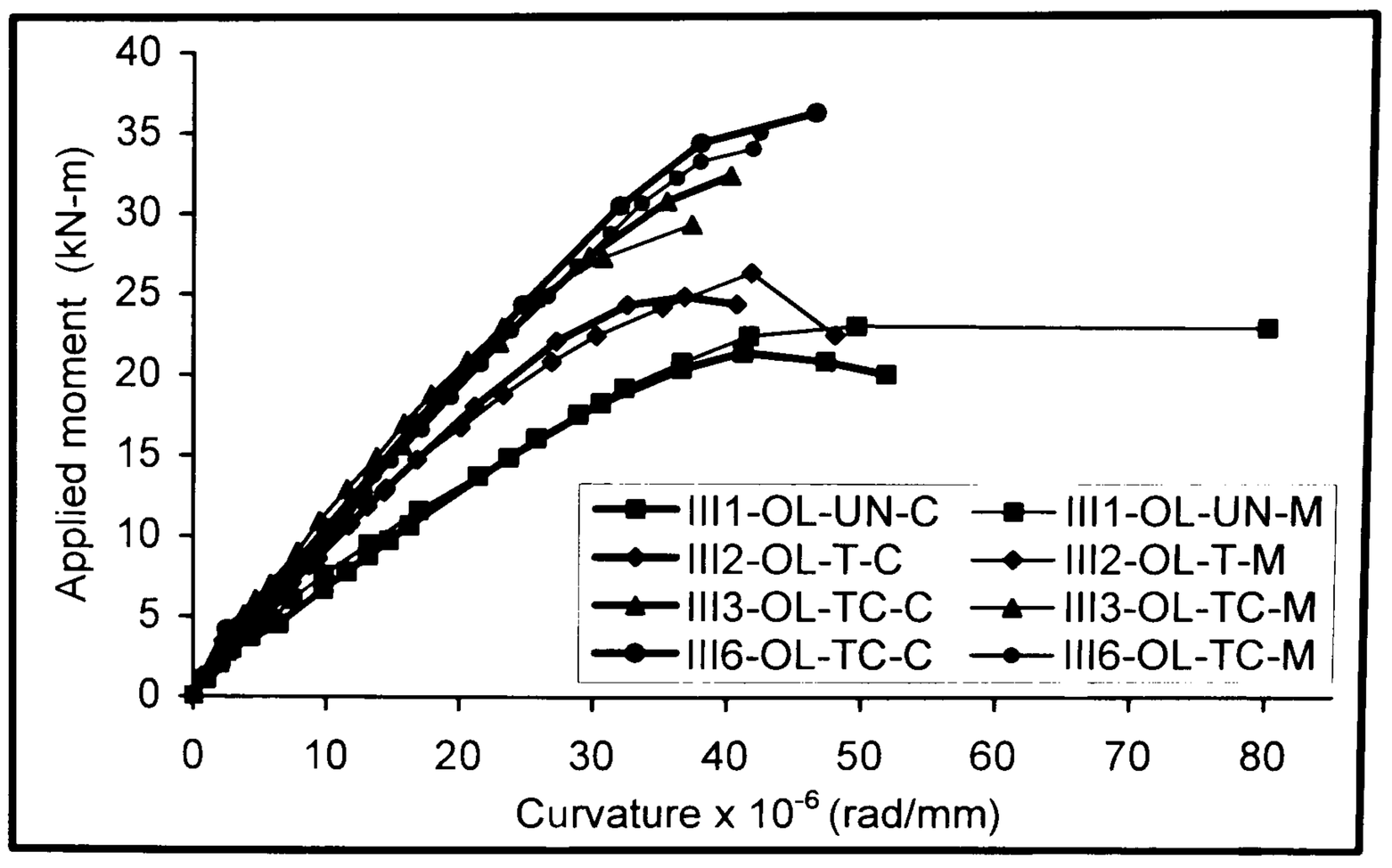

Figure 6.16: Applied moment versus curvature for beams series-III

In Figure 6.16 M: Experimental and; C: Simplified analysis

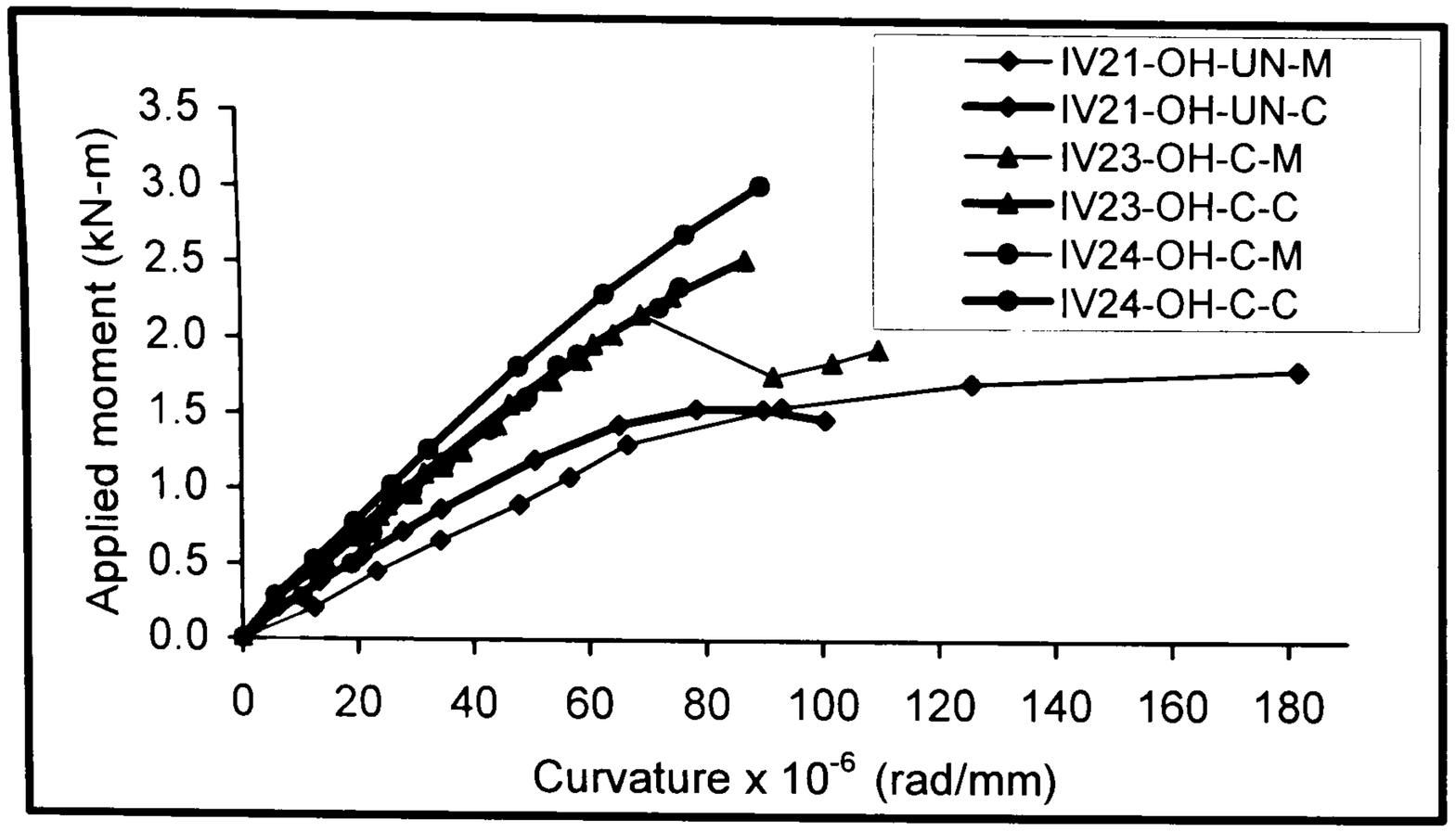

Figure 6.17: Applied moment versus curvature for beams of series-IV

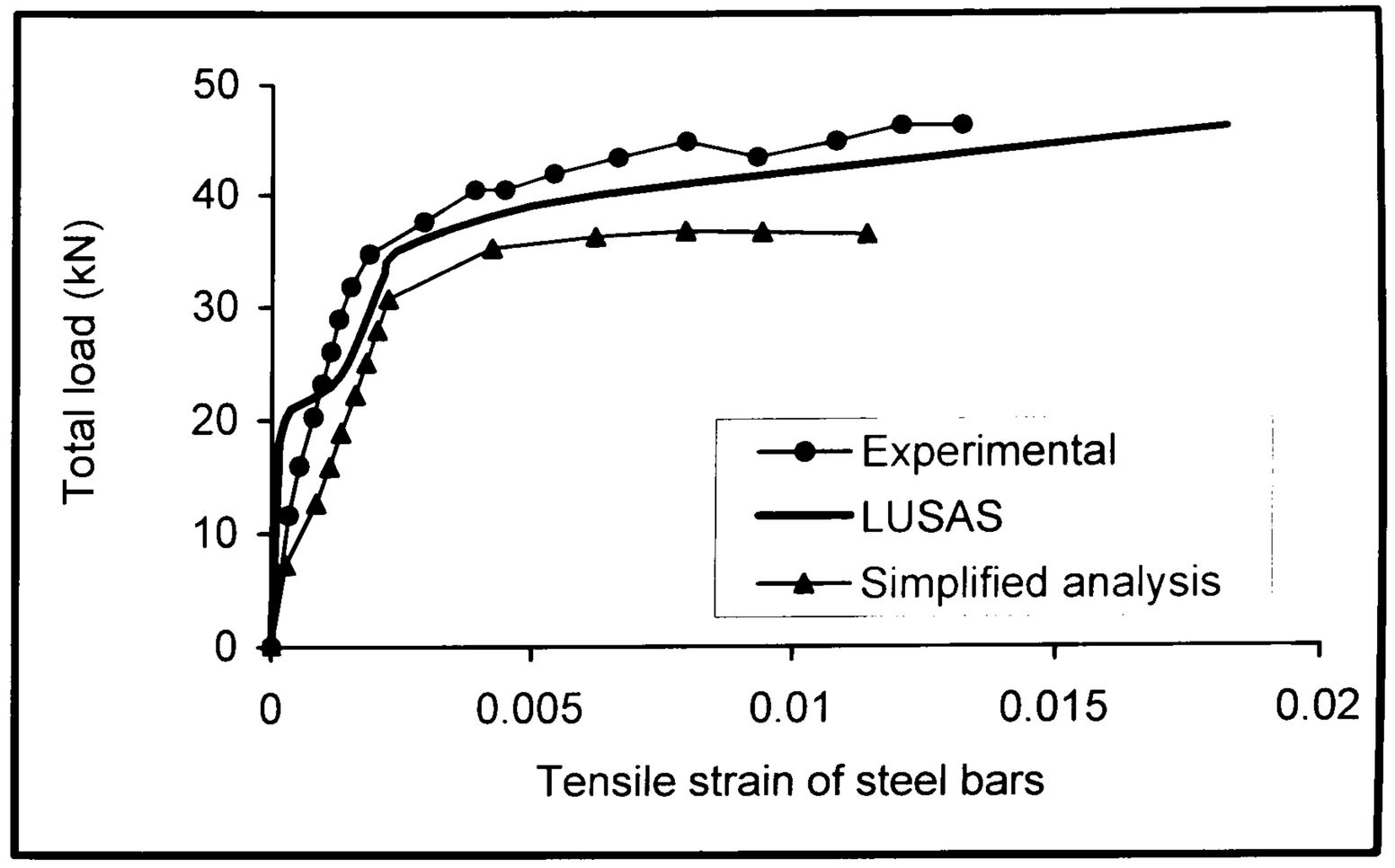

Figure 6.18: Total load-tensile strain in the steel bars, beam I11-UH-UN

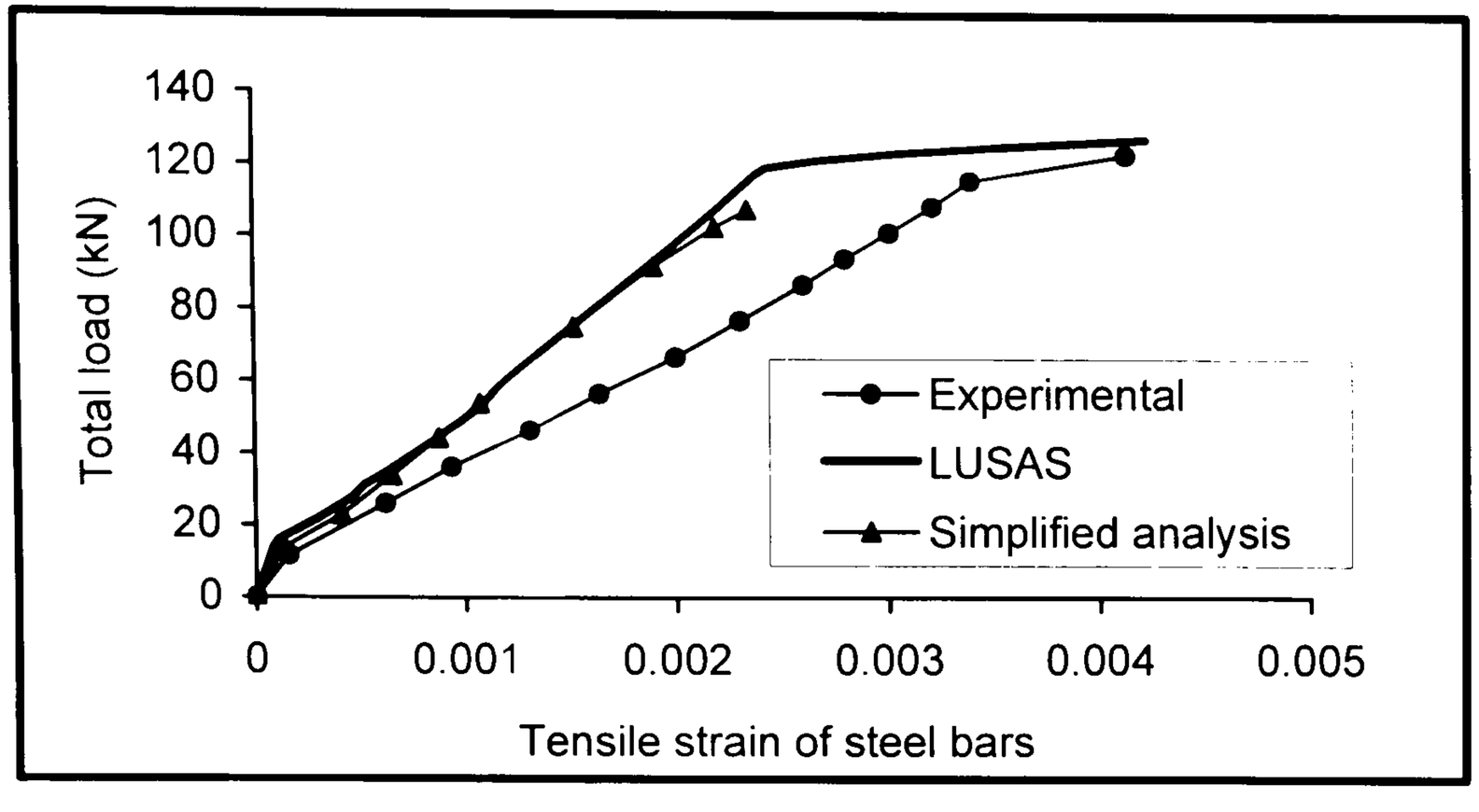

Figure 6.19: Total load-tensile strains of the steel bars, beam I13-OL-UN

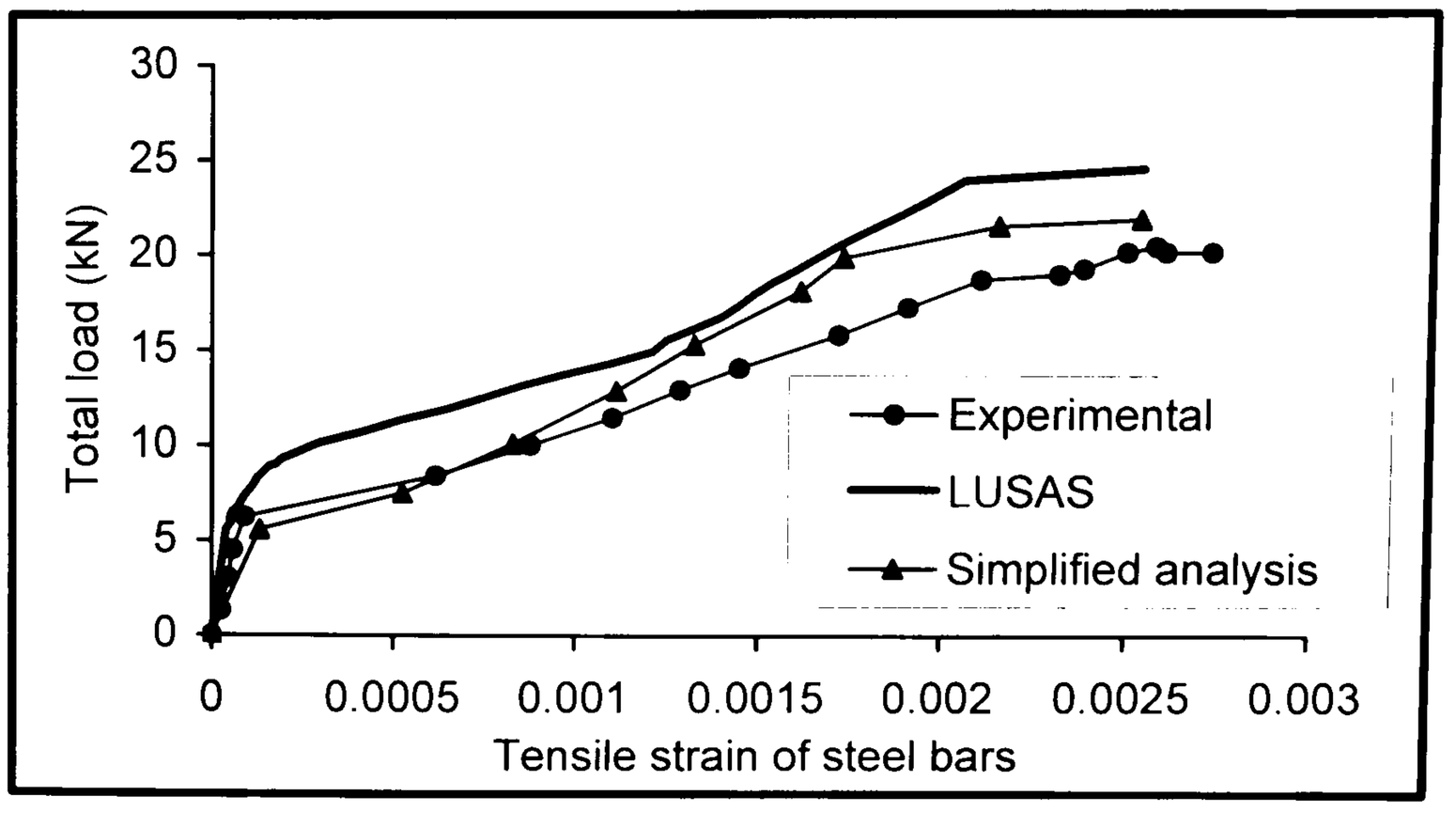

Figure 6.20: Total load versus strains in the tensile steel bars, beam I21-UL-UN

In Figure 6.17 M: Experimental and; C: Simplified analysis

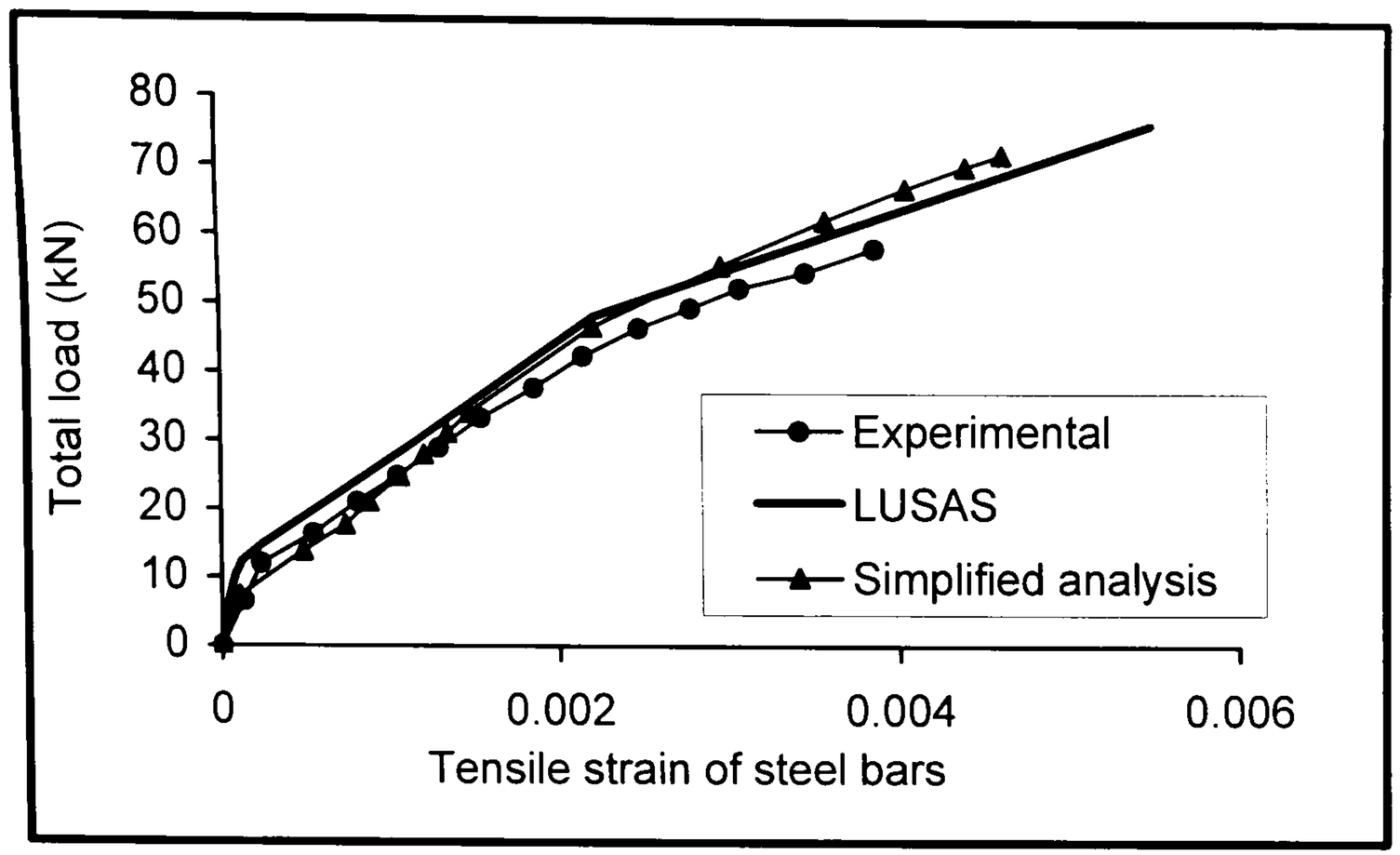

Figure 6.21: Total load - tensile strain in the steel bars, I22-UL-T

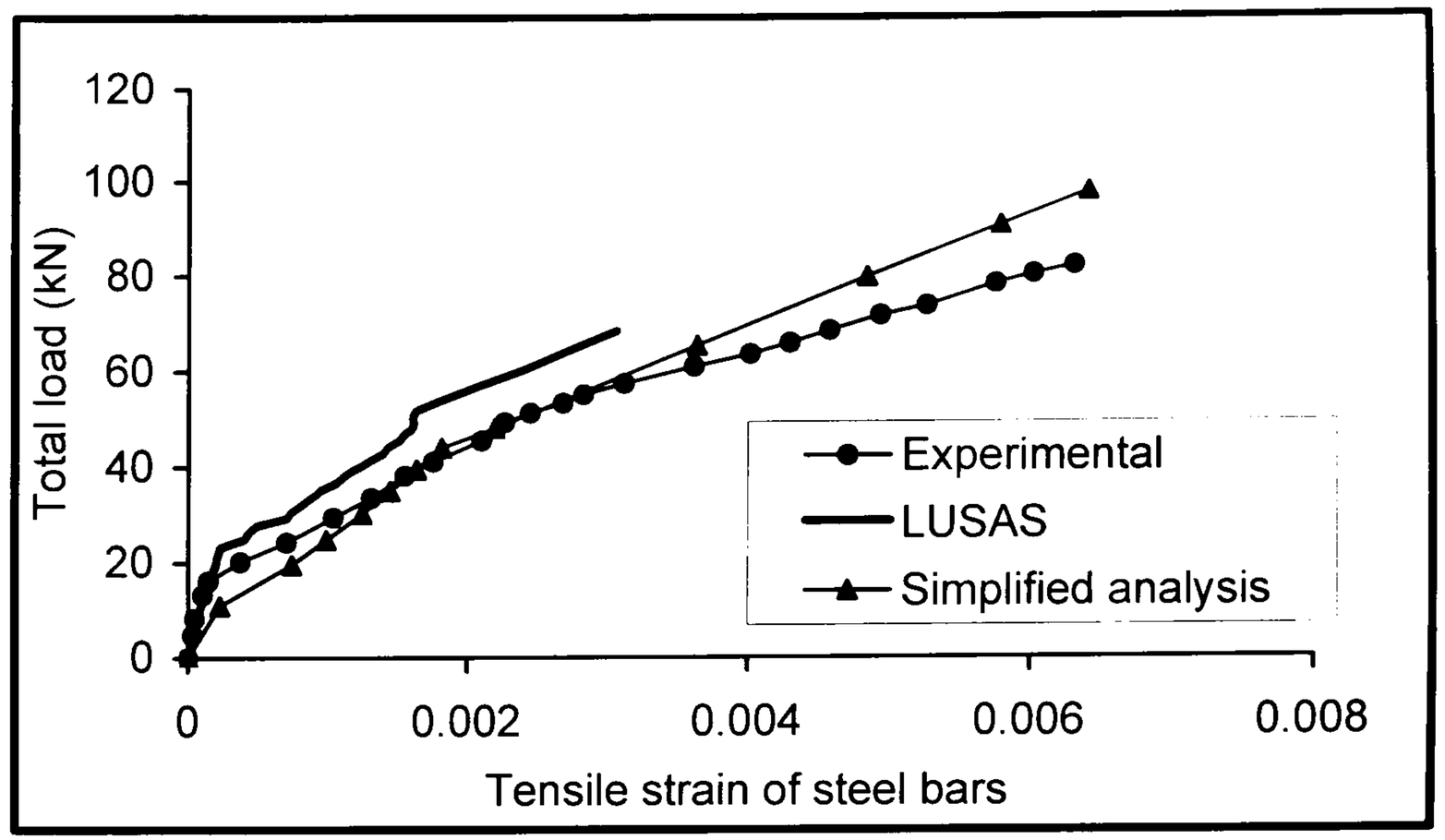

Figure 6.22: Total load versus strains in the tensile steel bars, beam I25-UL-TC

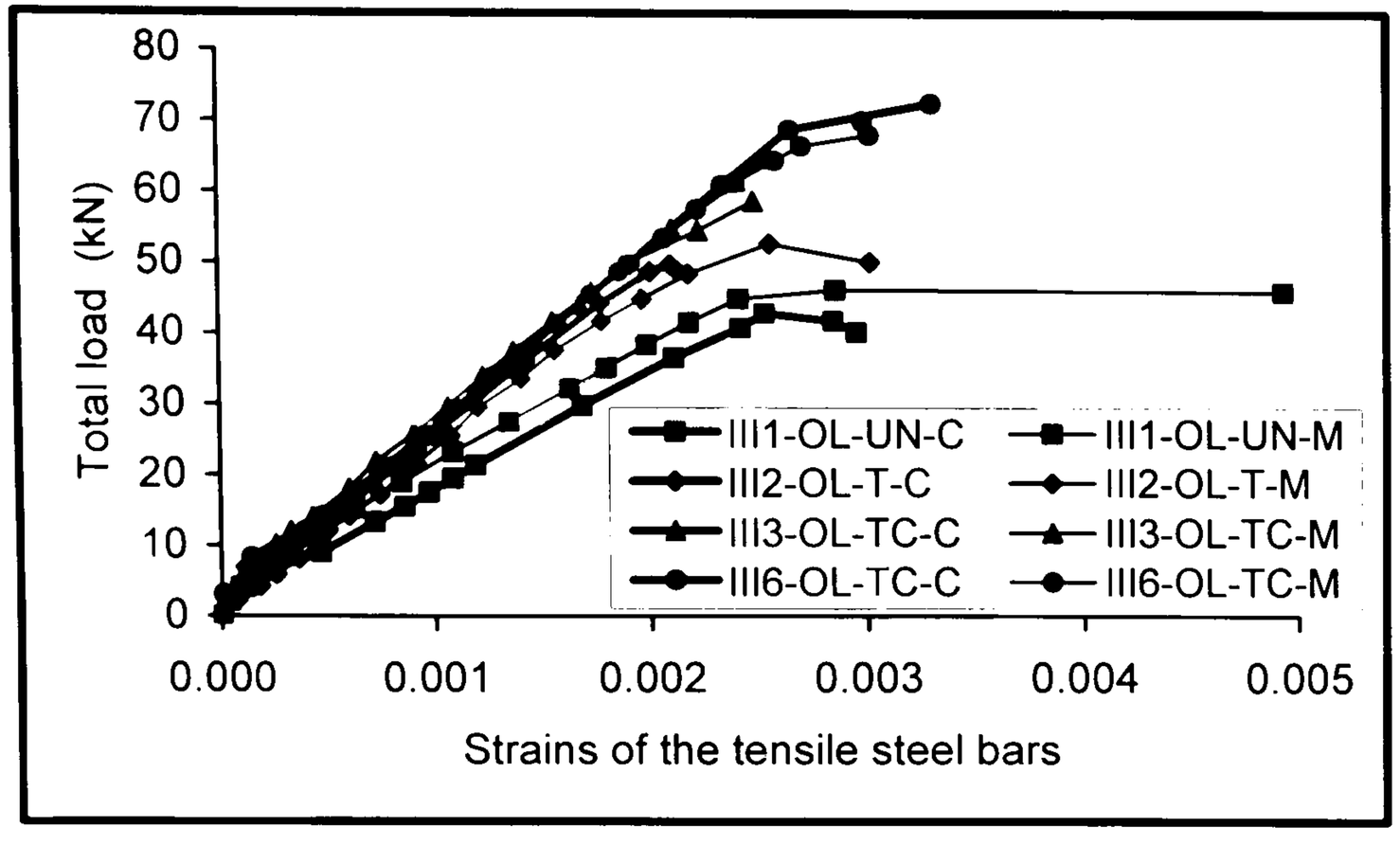

Figure 6.23: Total load-tensile strains in the steel bars, beams of series-III

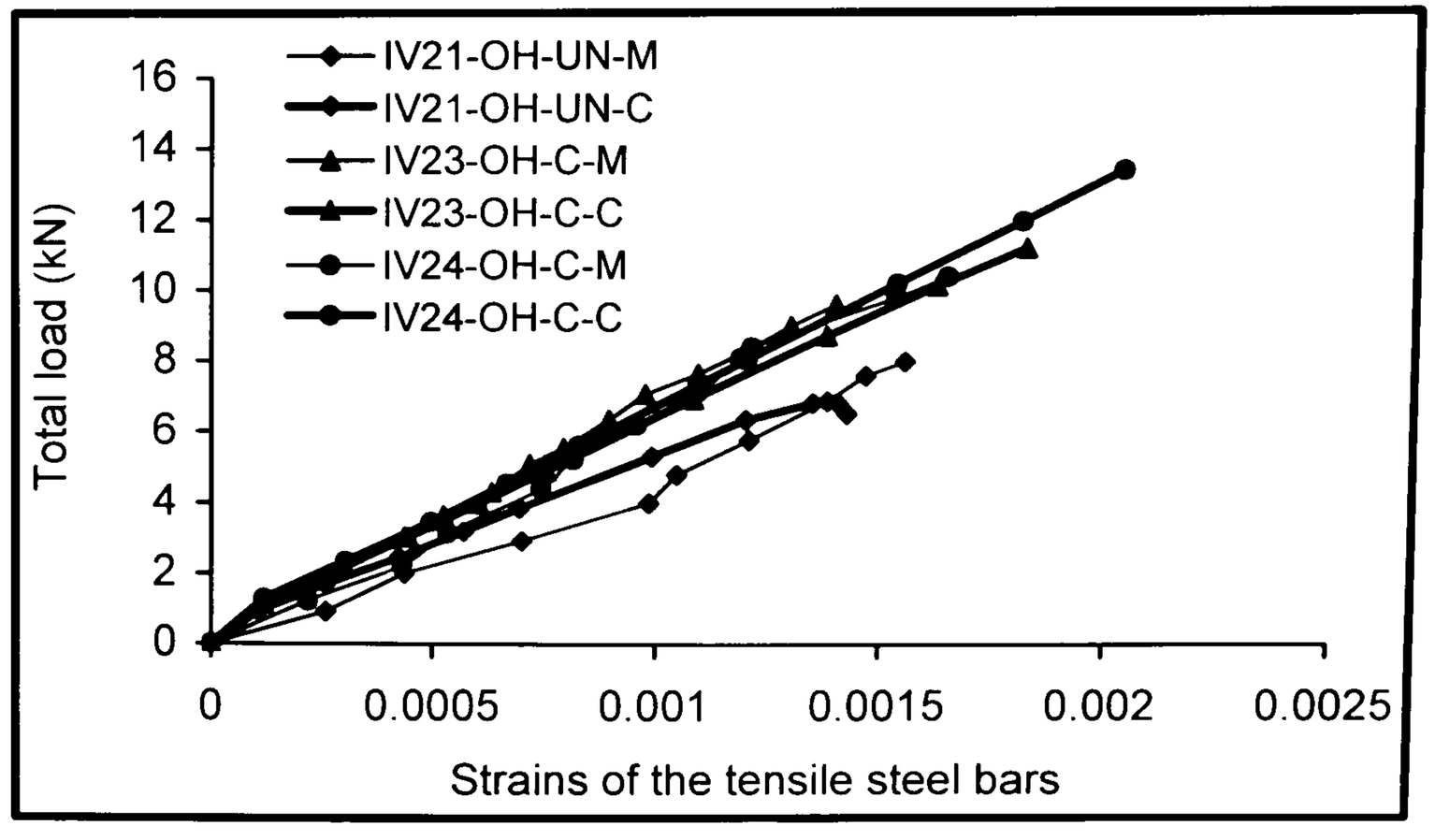

Figure 6.24: Total load-tensile strains in the steel bars, beams of series-IV

In Figures 6.23 and 6.24 M: Experimental and; C: Simplified analysis

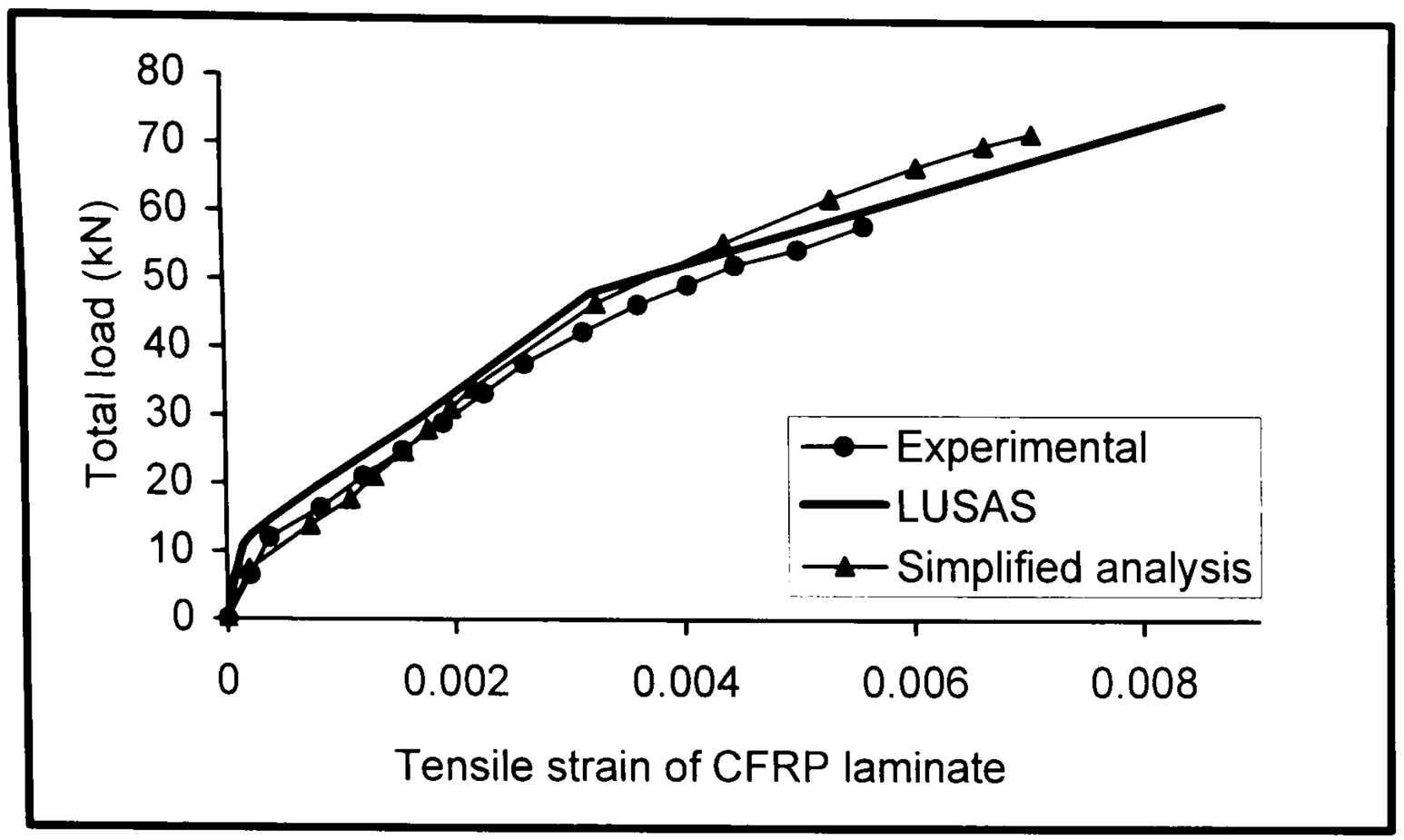

Figure 6.25: Total load versus CFRP laminate strain for beam I22-UL-T

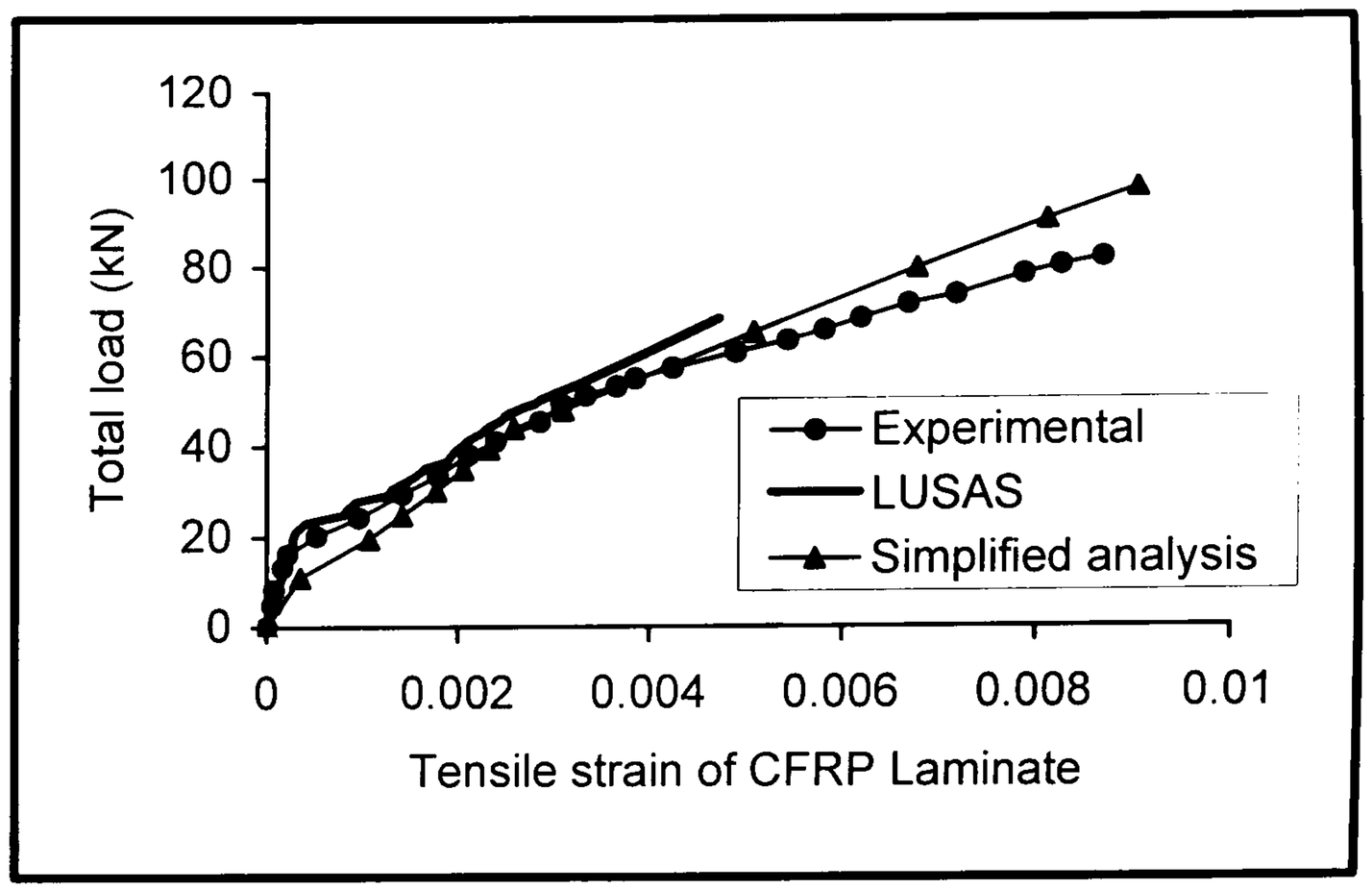

Figure 6.26: Total load versus CFRP laminate strain for beam I25-UL-TC

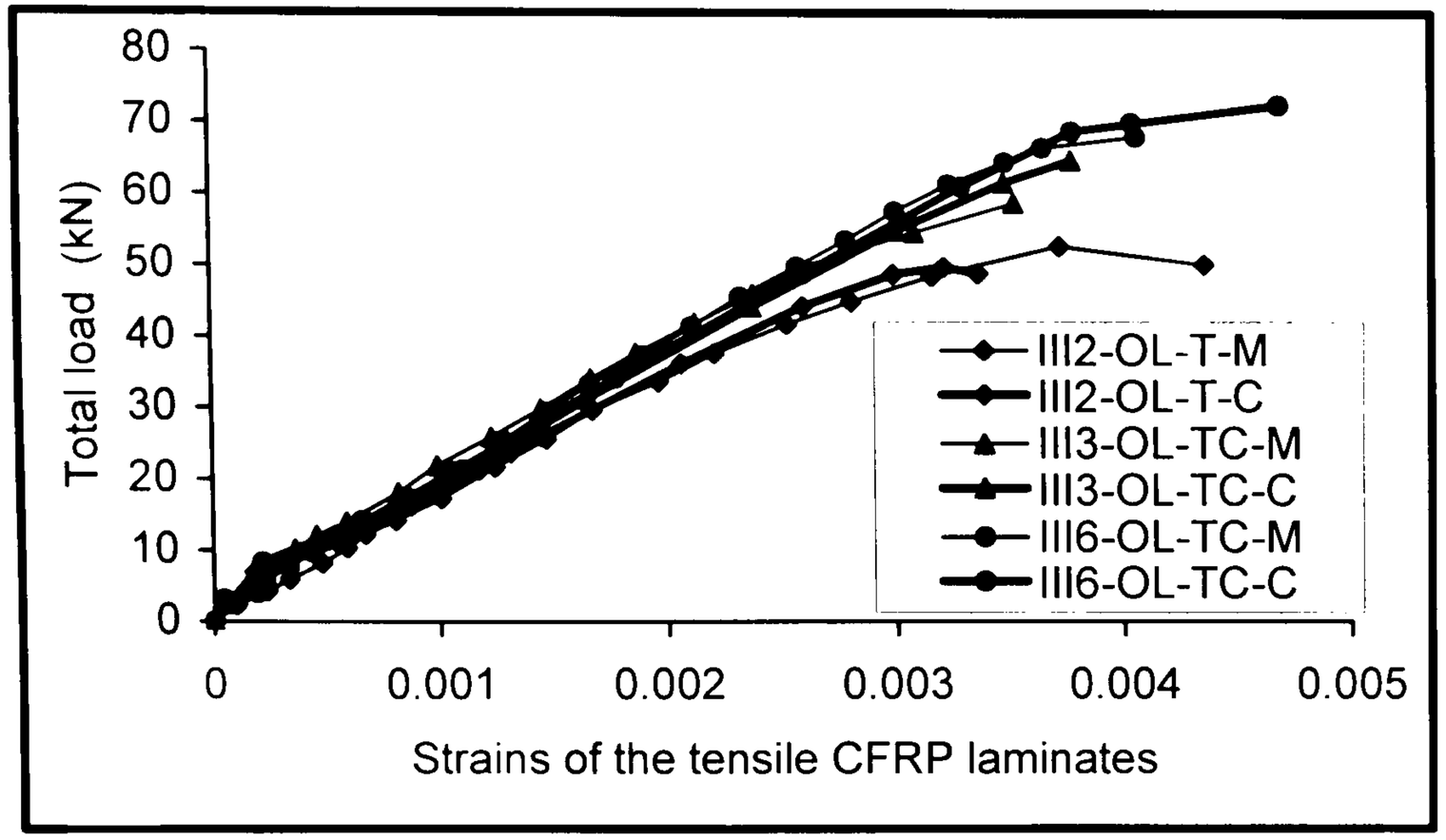

Figure 6.27: Total load -CFRP laminate strain, beams of series-III

In Figure 6.27 **M: Experimental** and; C: Simplified analysis

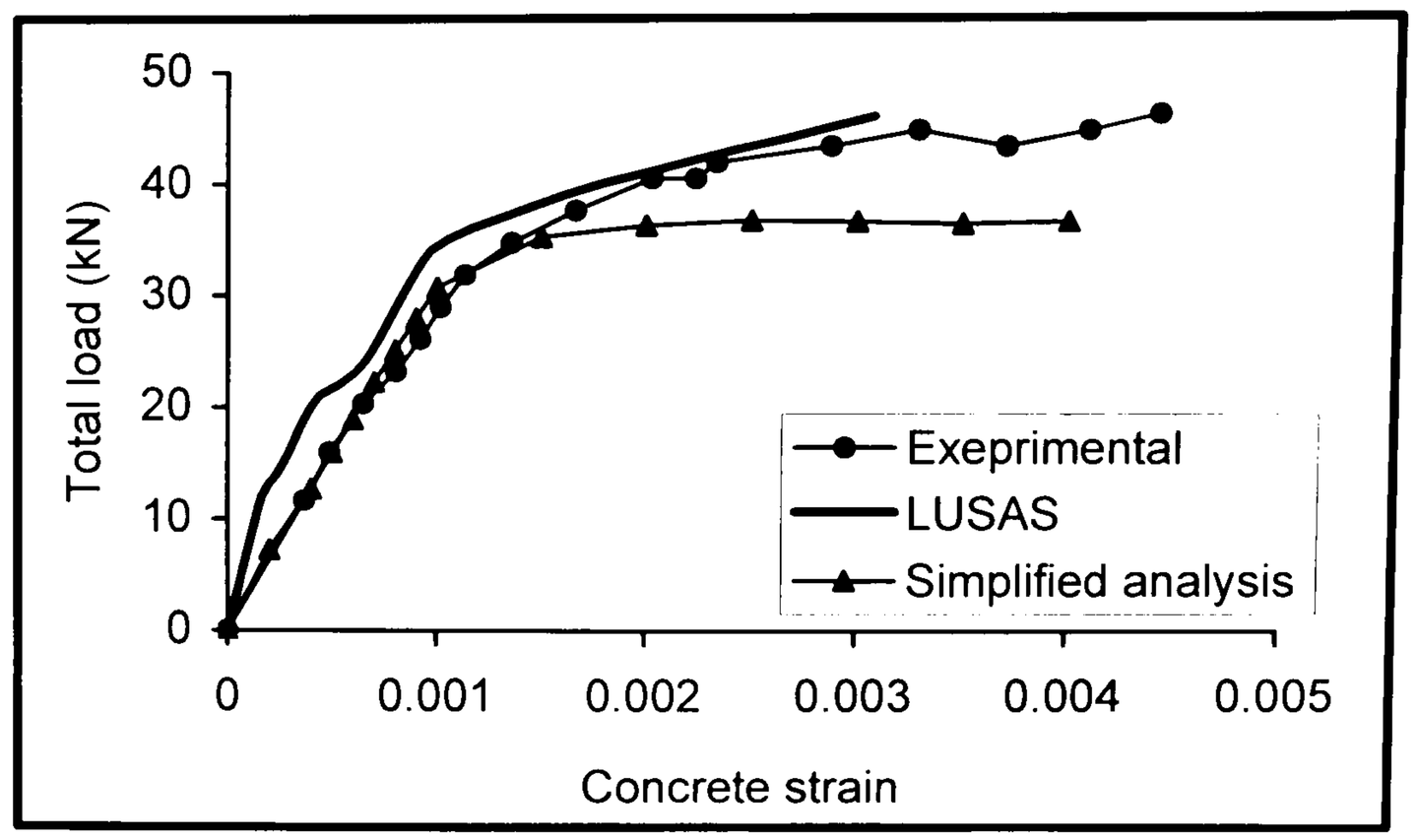

Figure 6.28: Total load versus concrete strains for beam I11-UH-UN

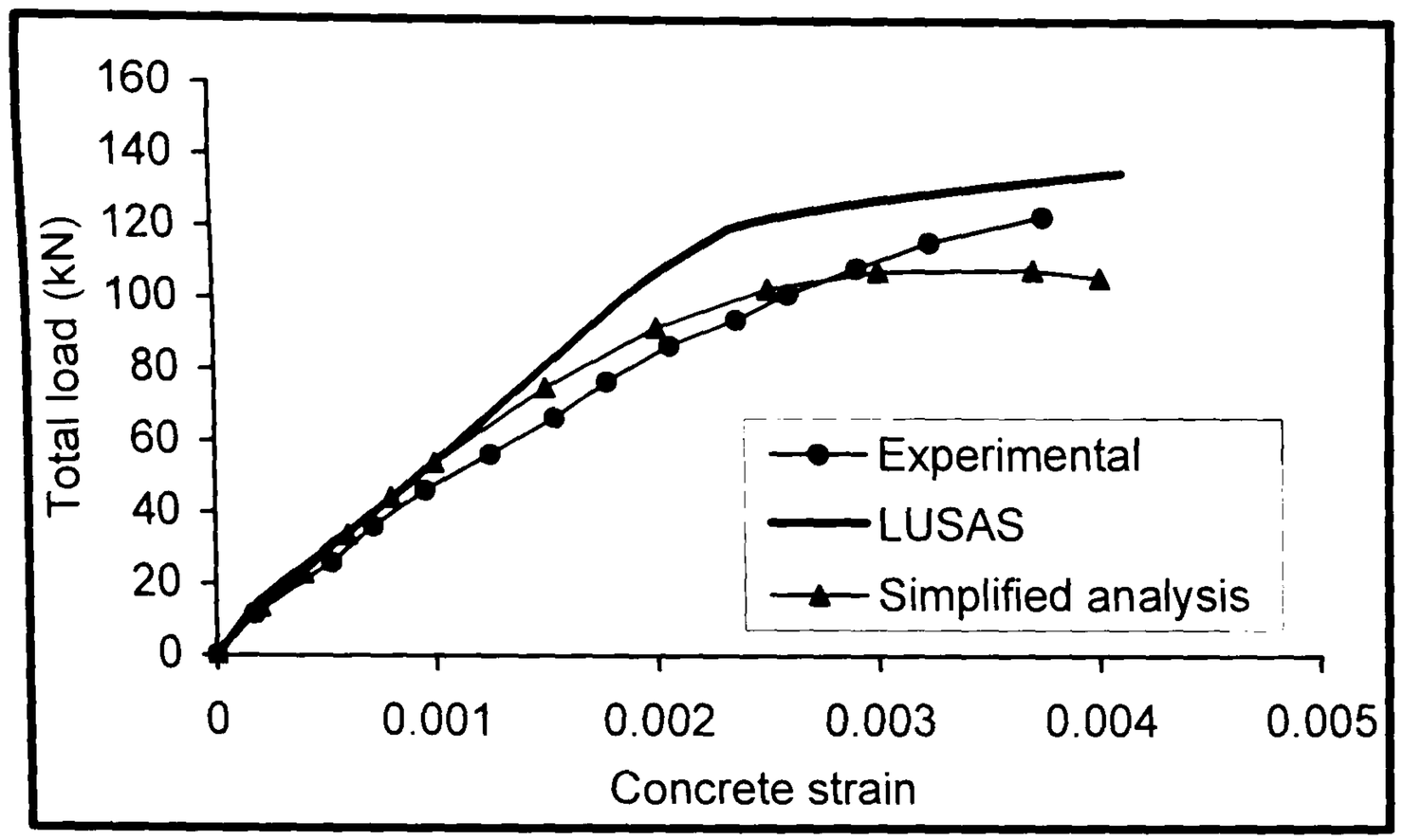

Figure 6.29: Total load versus concrete strains for beam I13-OL-UN

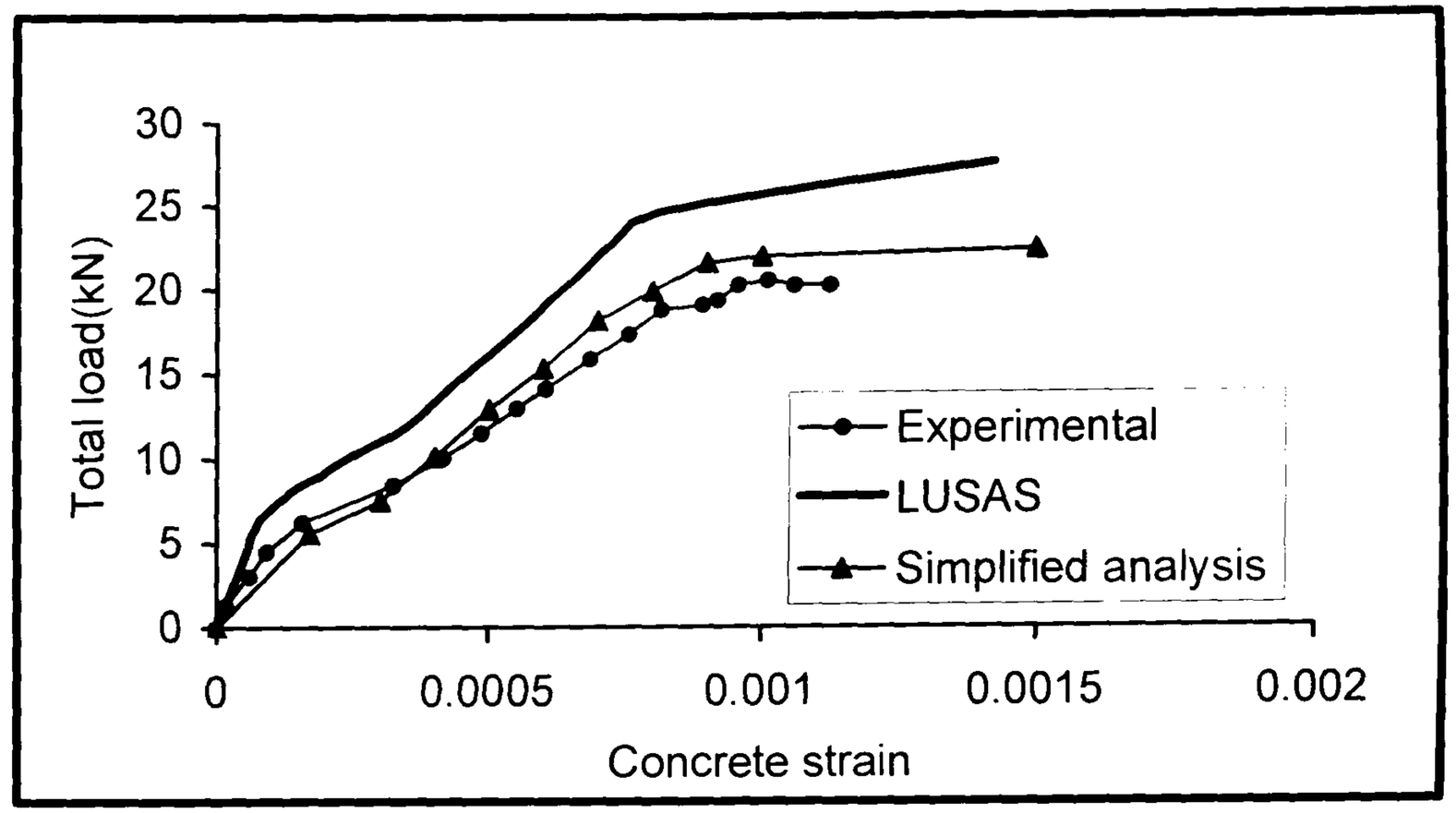

Figure 6.30: Total load versus concrete strains for beam I21-UL-UN

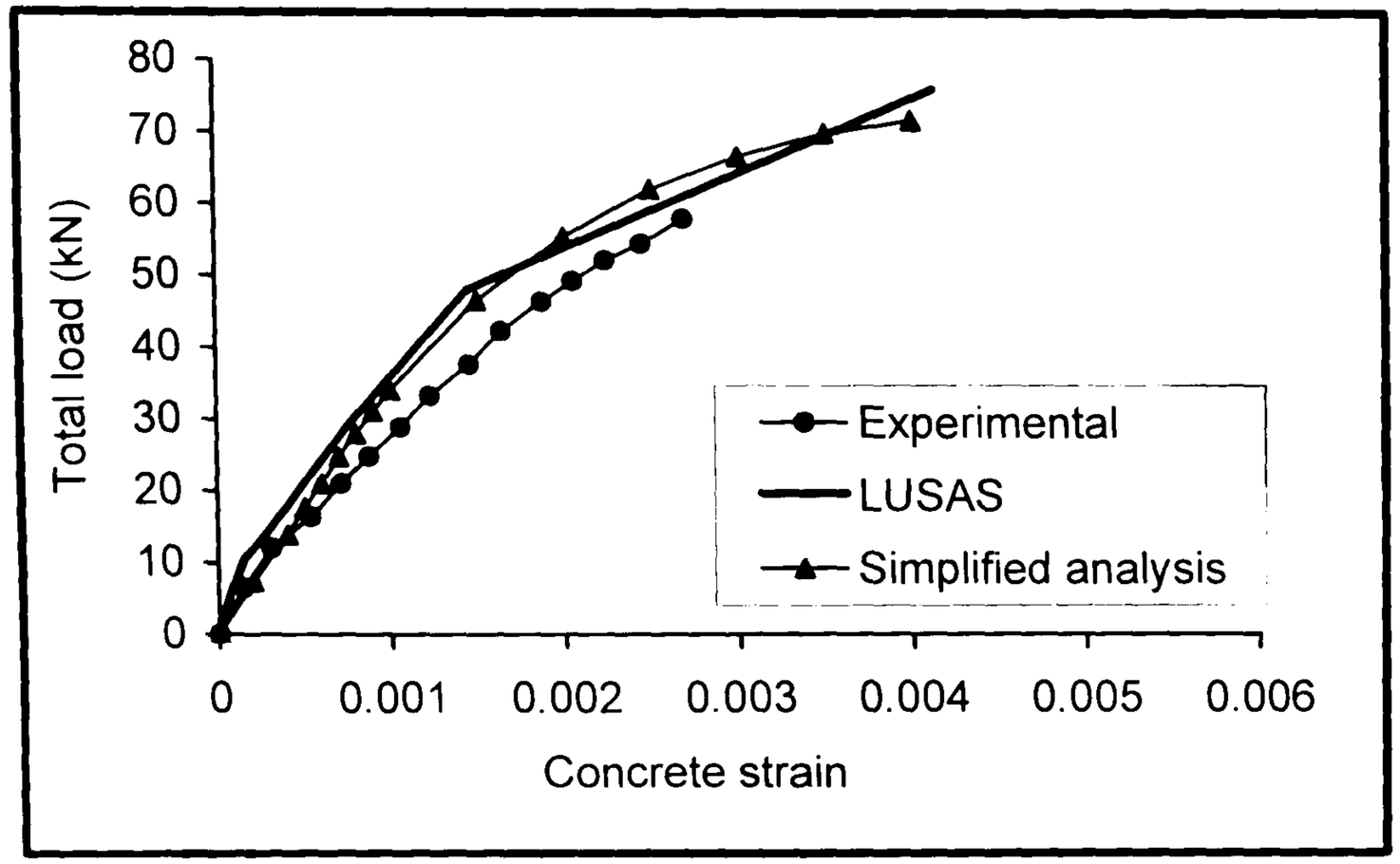

Figure 6.31: Total load versus concrete strains for beam I22-UL-T

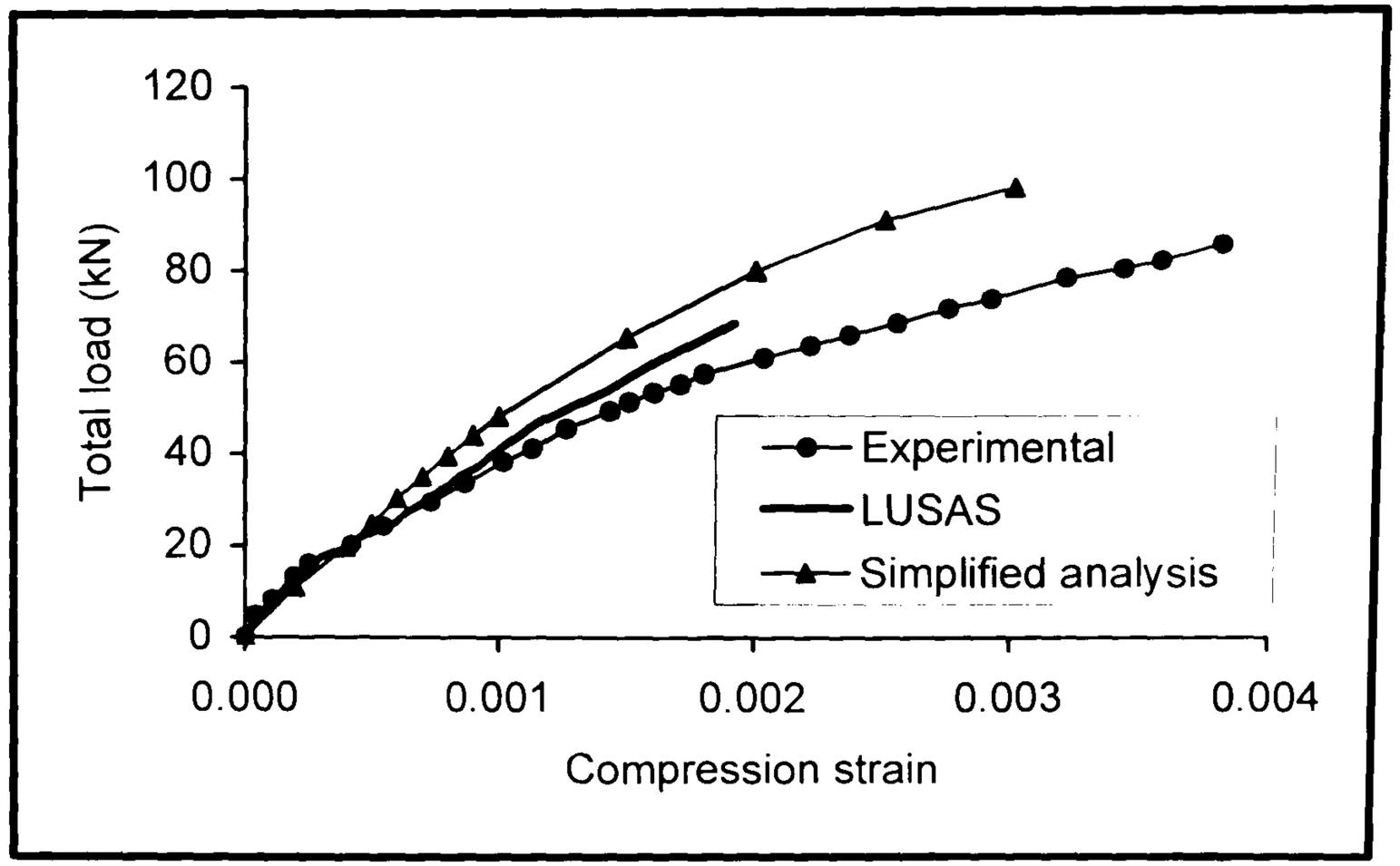

Figure 6.32: Total load versus concrete strains for beam I25-UL-TC

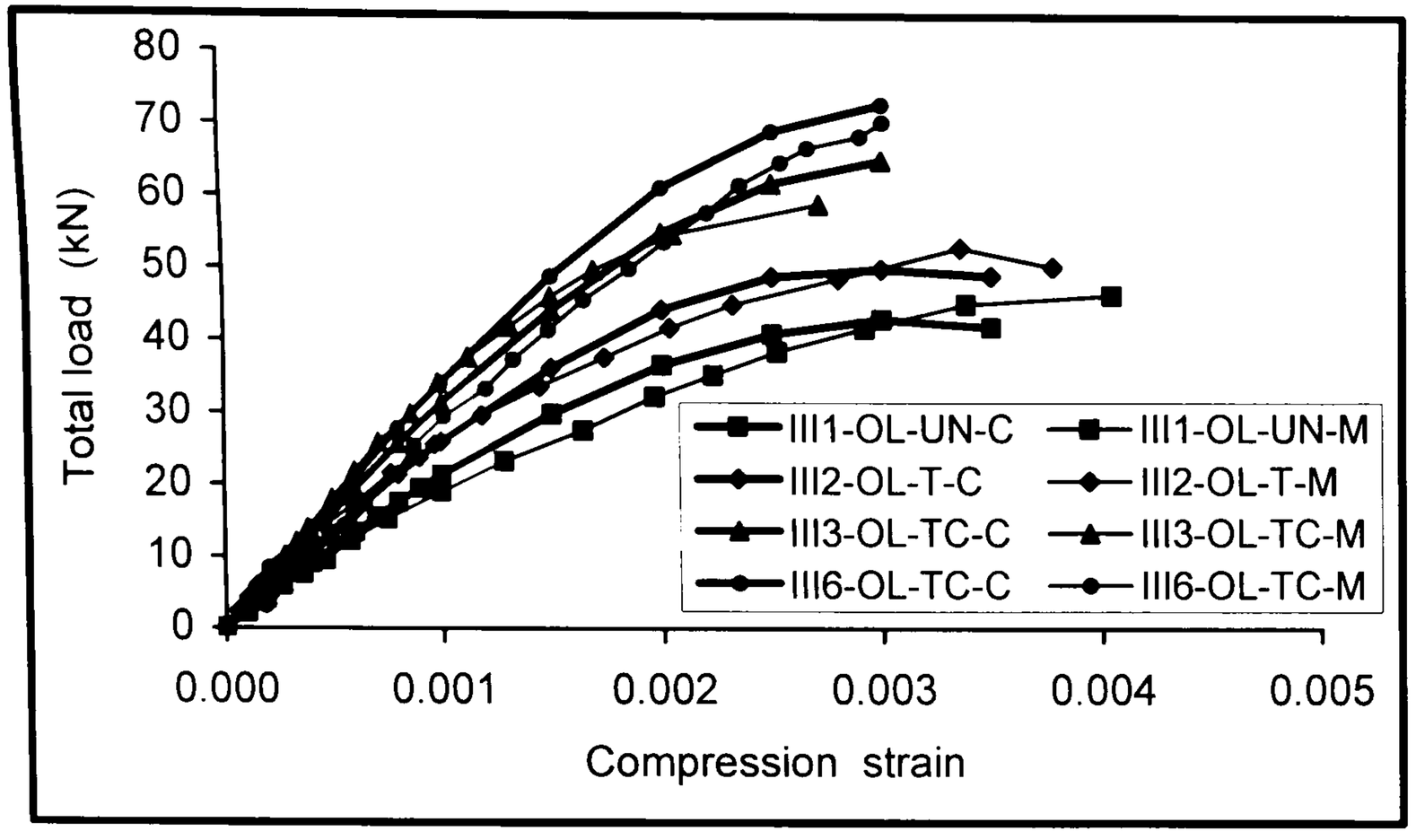

Figure 6.33: Total load versus concrete strain for beams of series-III

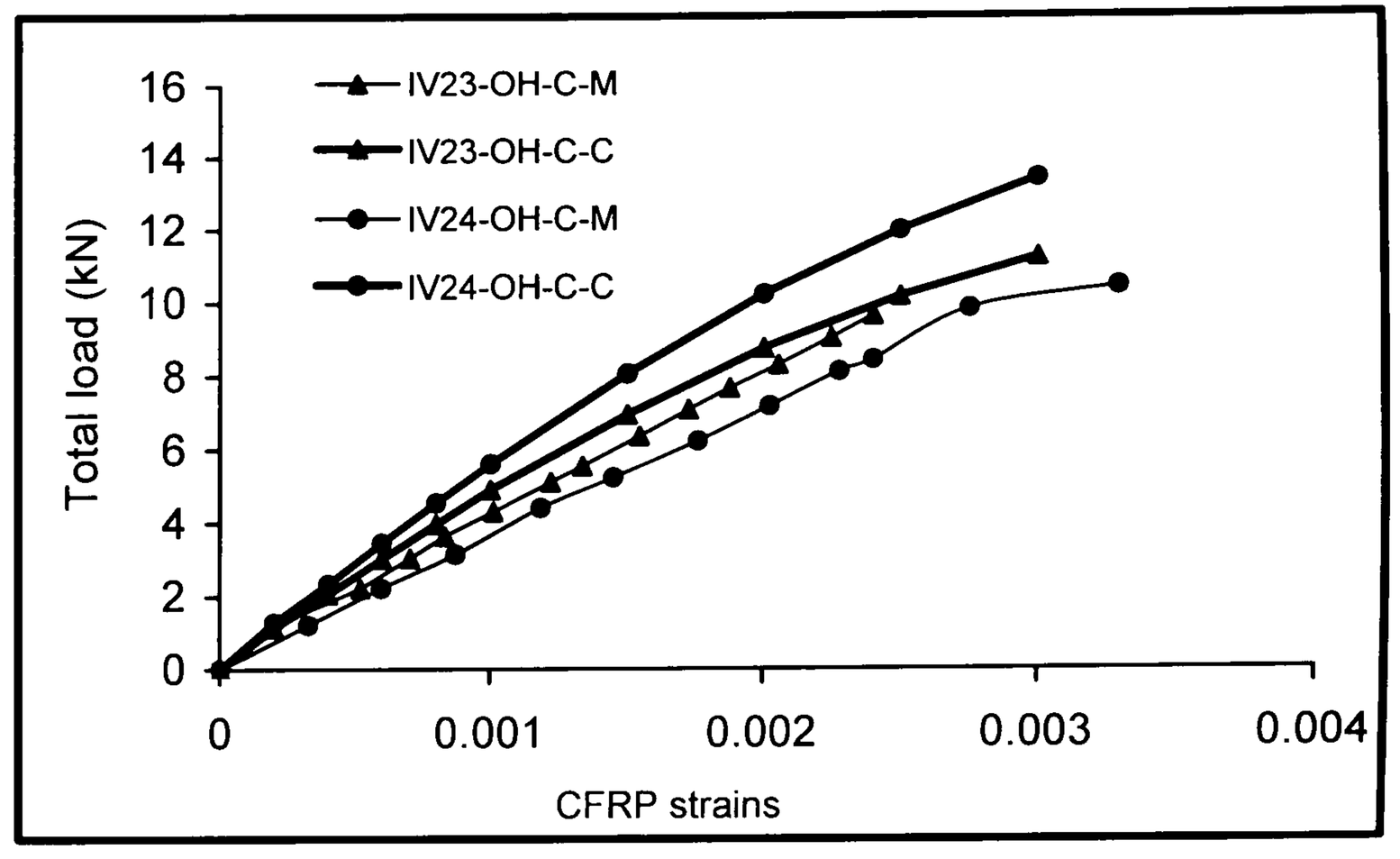

Figure 6.34: Total load vers. CFRP laminate strain for beams of series-IV

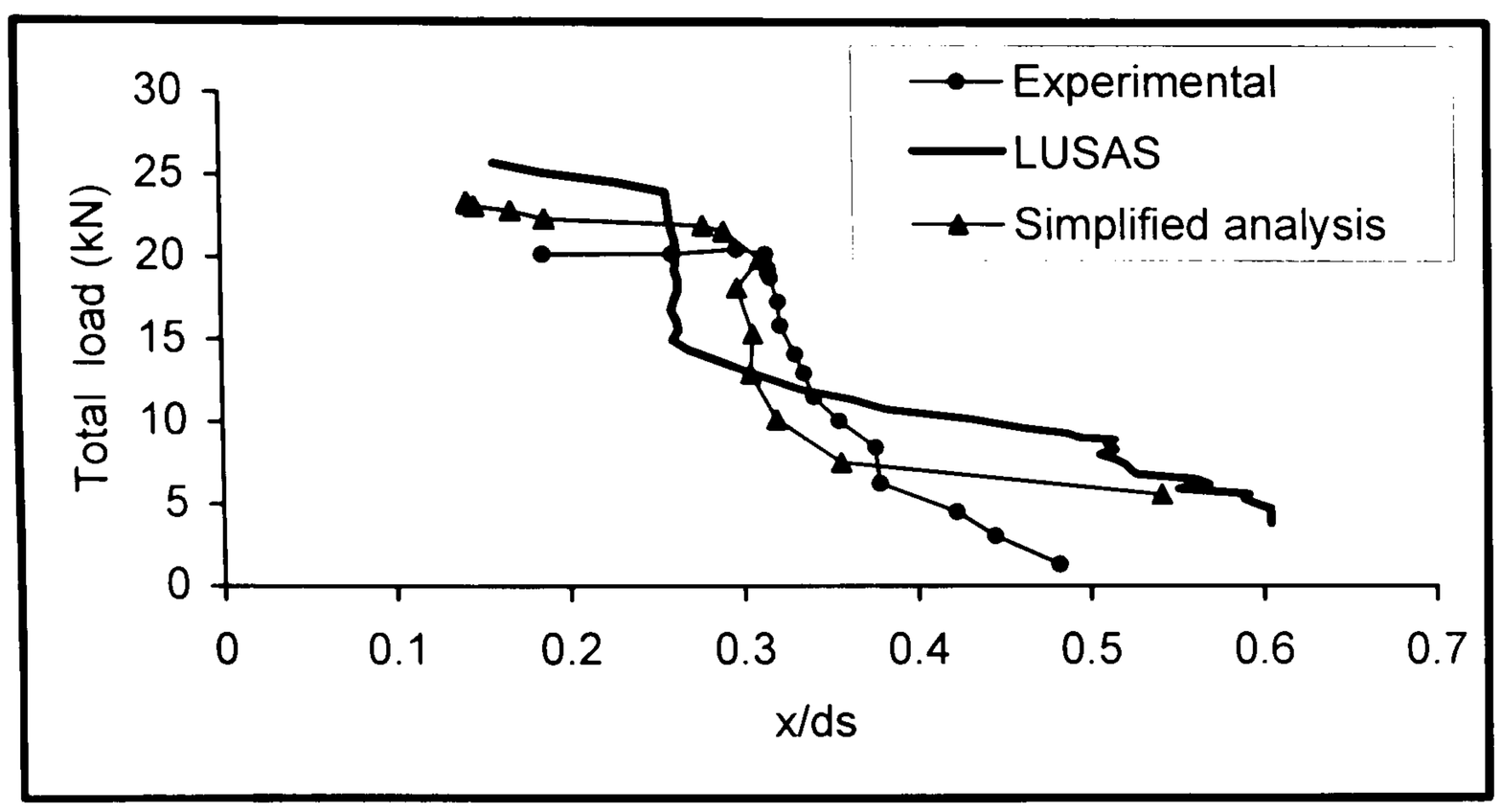

Figure 6.35: Total load versus neutral axis for beam I21-UL-UN

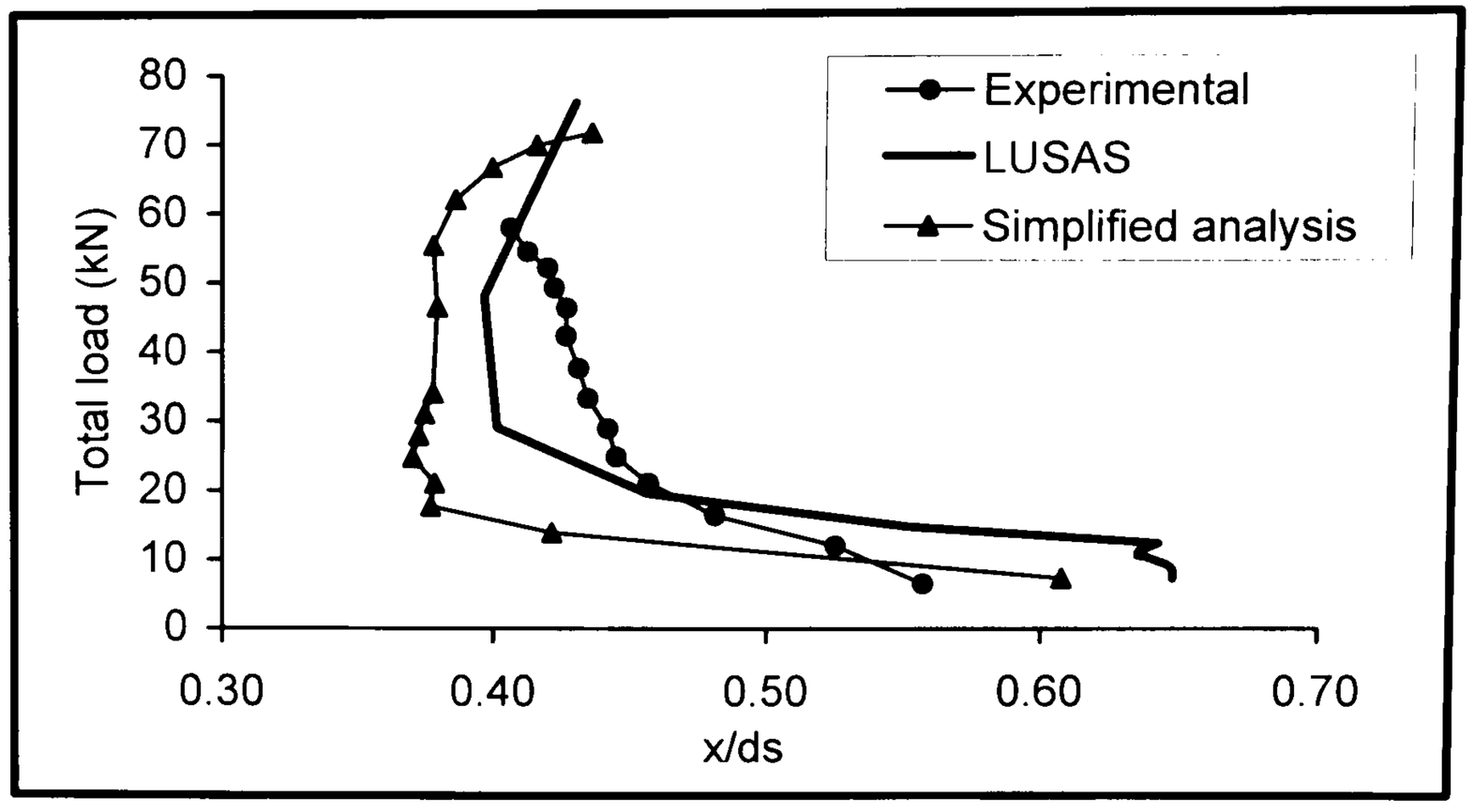

Figure 6.36: Total load versus neutral axis for beam I22-UL-T

In Figures 6.33 and 6.34 M: Experimental and; C: Simplified analysis

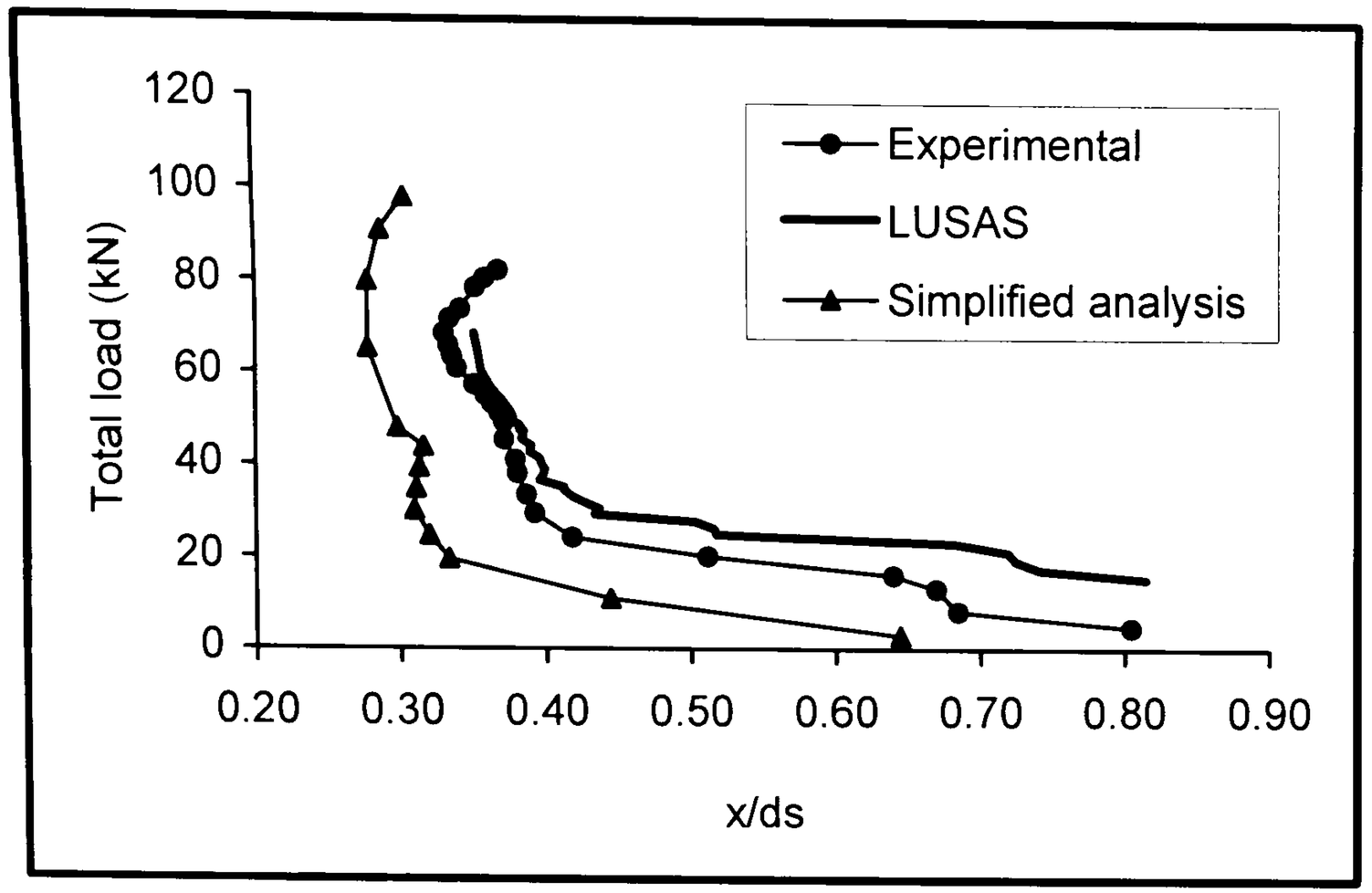

Figure 6.37: Total load versus neutral axis for beam I25-UL-TC

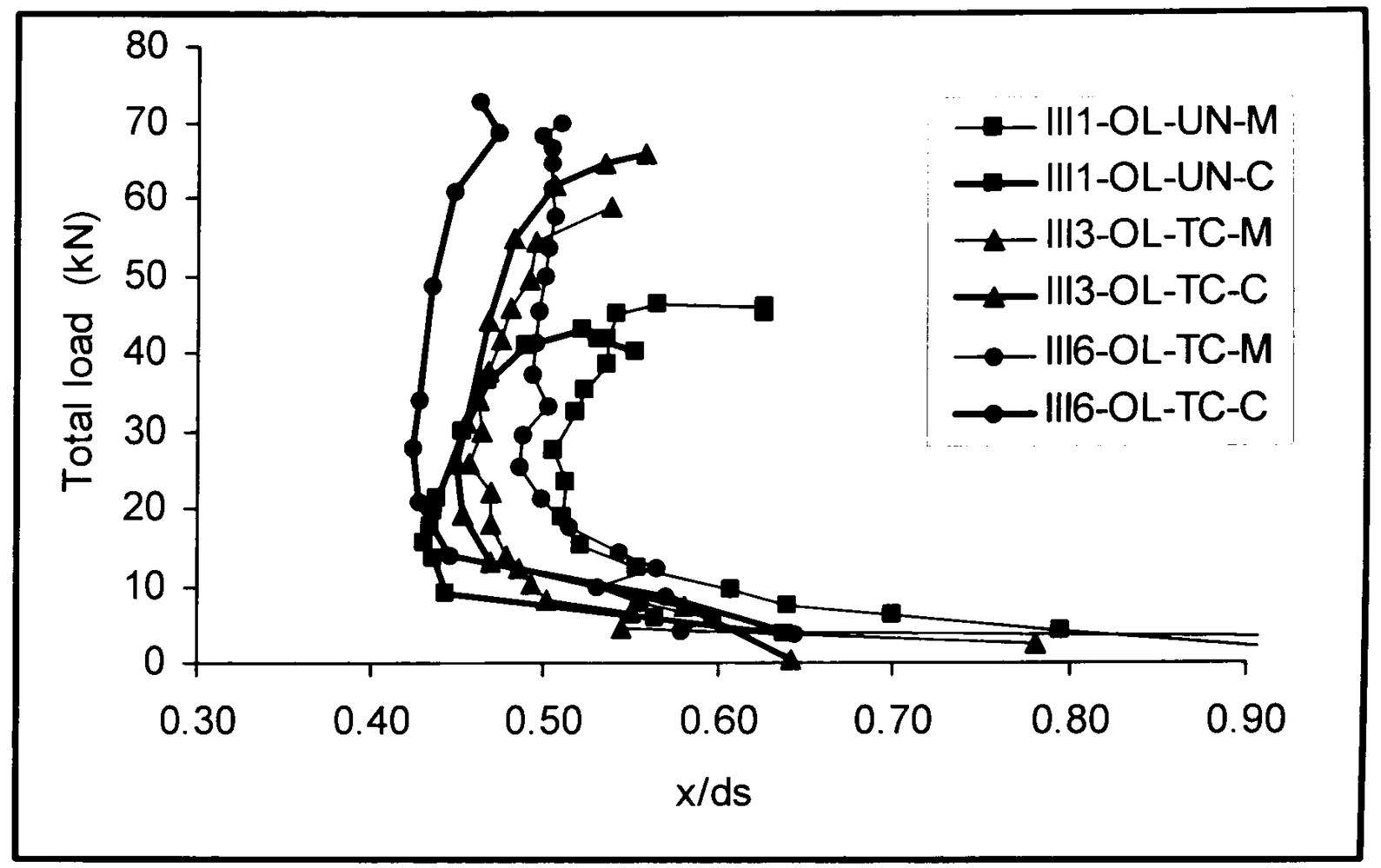

Figure 6.38: Total load versus neutral axis for beams of series-III

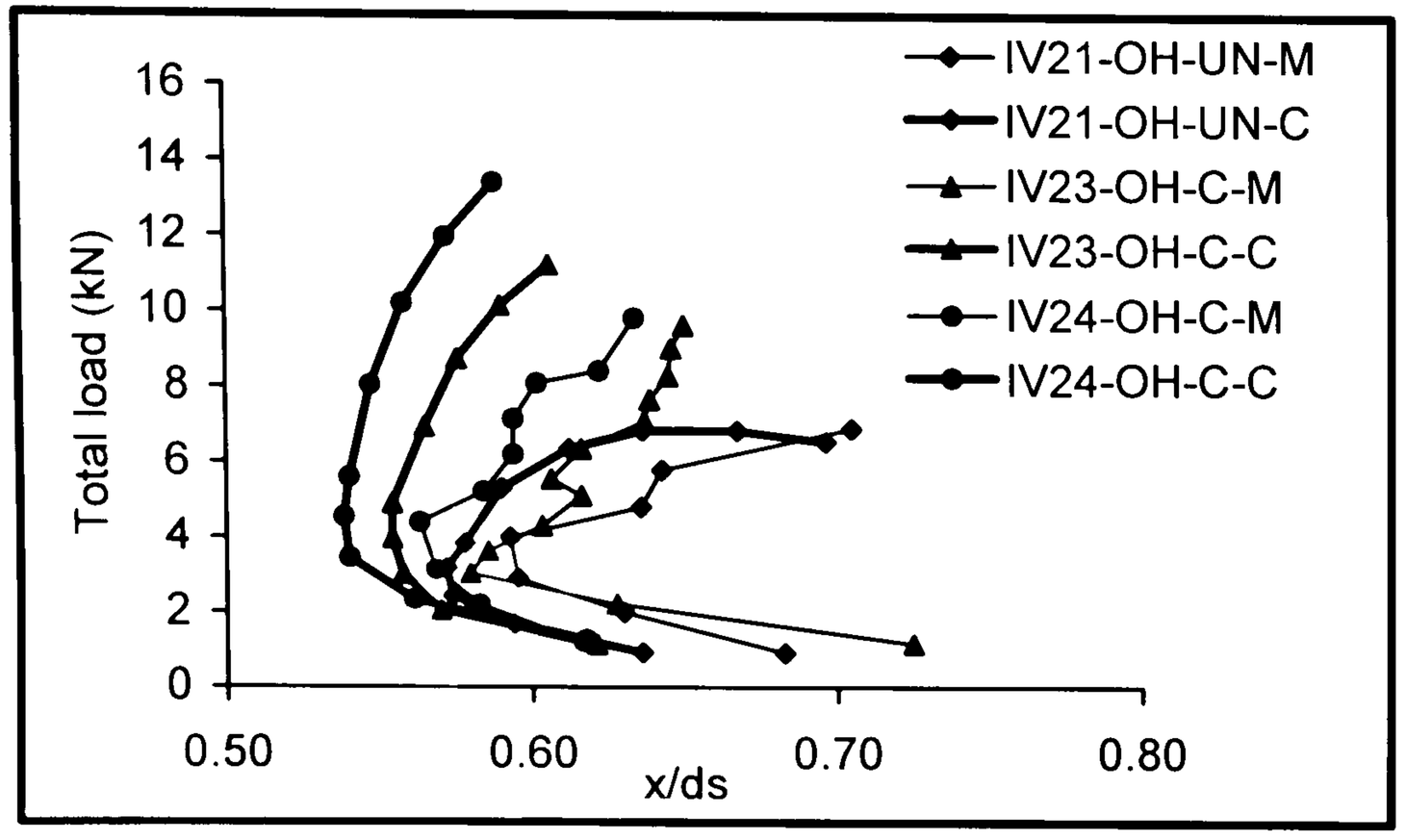

Figure 6.39: Total load versus neutral axis for beams of series-IV

In Figures 6.38 and 6.39 M: Experimental and; C: Simplified analysis

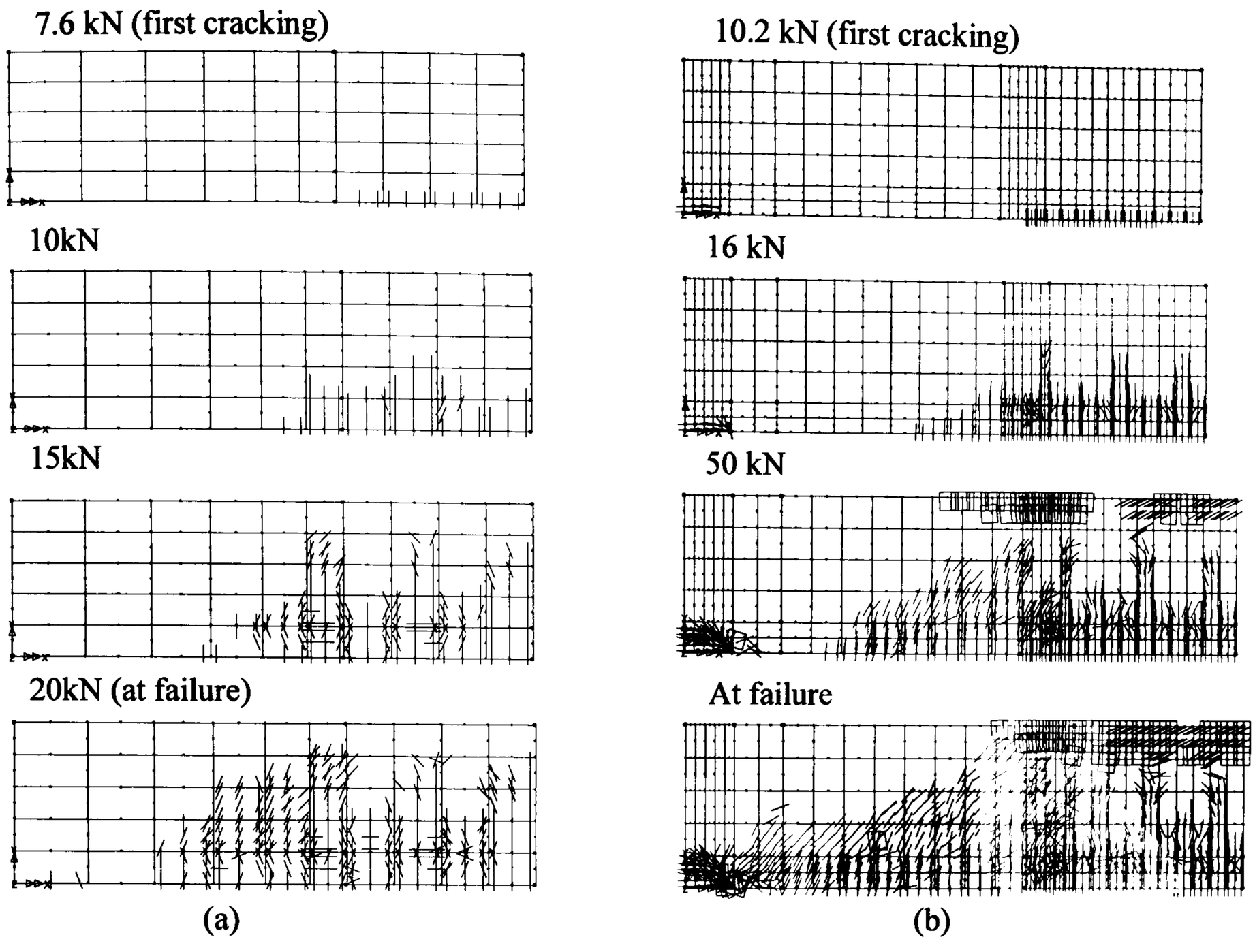

Figure 6.40: Evaluation of crack patterns (a) Unstrengthened beam I21-UL-UN, Model 82: (b) Strengthened I22-UL-T, Model 84.

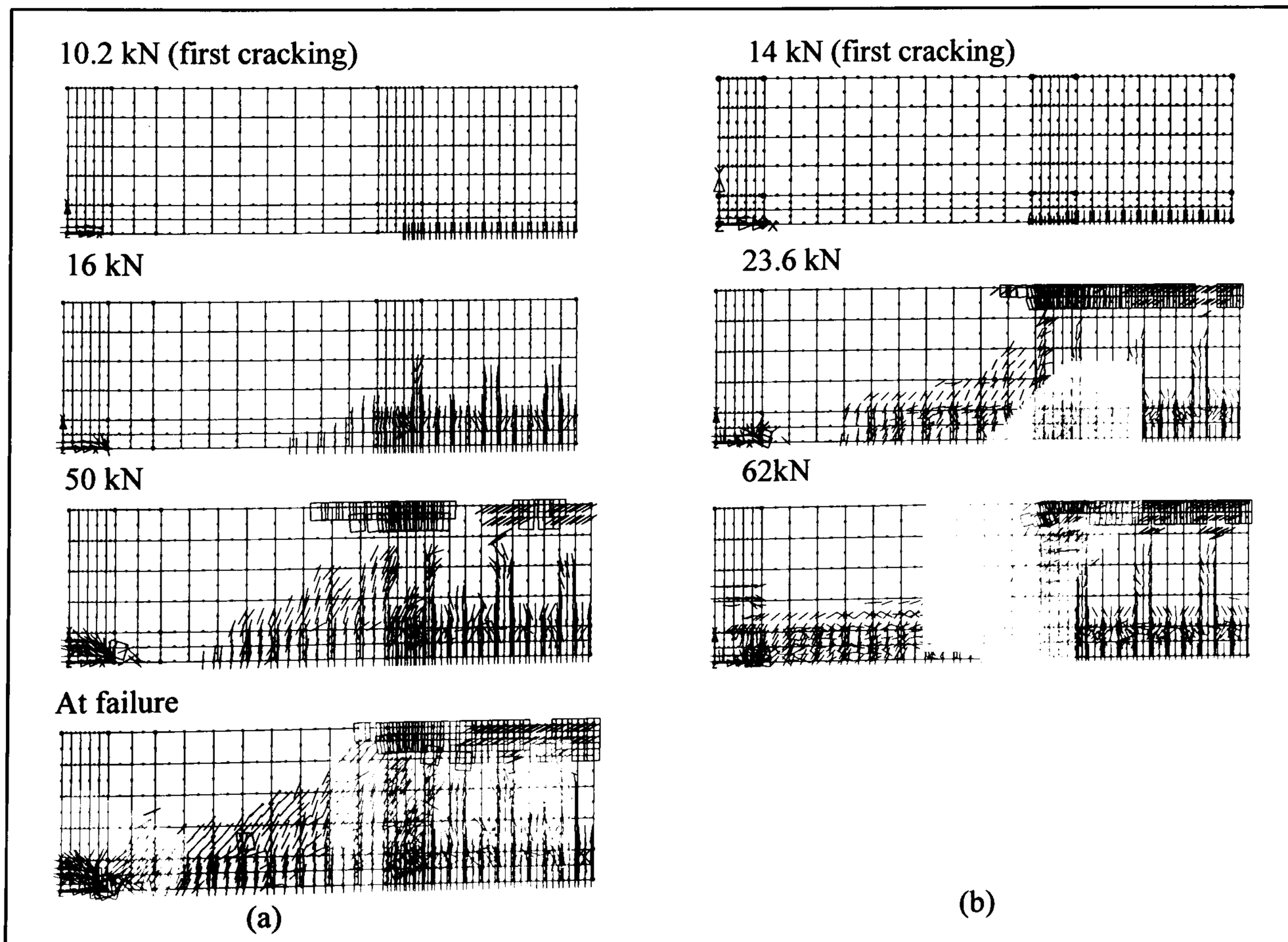

Figure 6.41: Evaluation of crack patterns (a) strengthened beam I22-UL-T: (b) strengthened beam I25-UL-TC

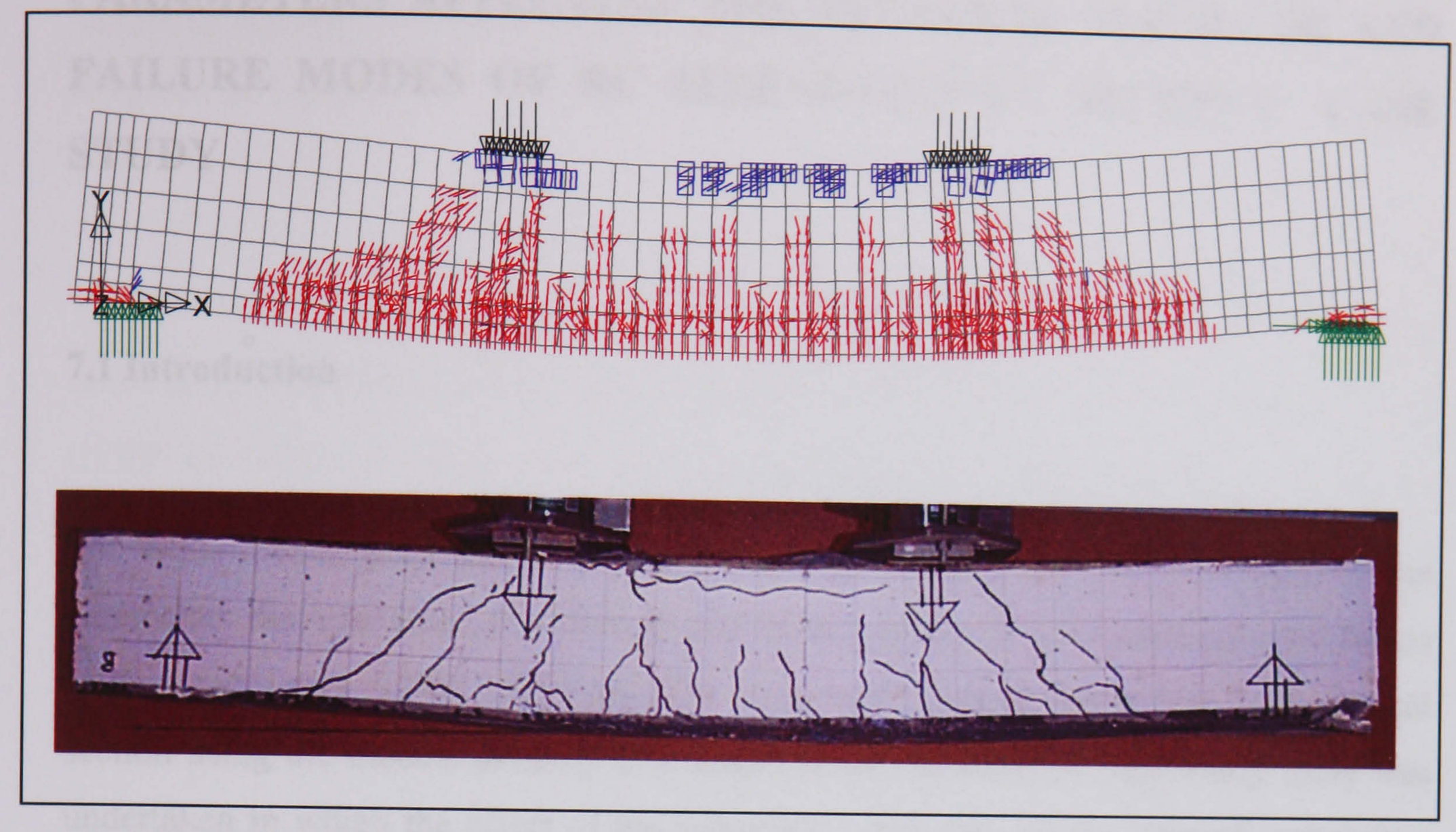

Figure 6.42: Comparison for crack patterns from the test and LUSAS analysis for beam I25-UL-TC, Full beam modelled.

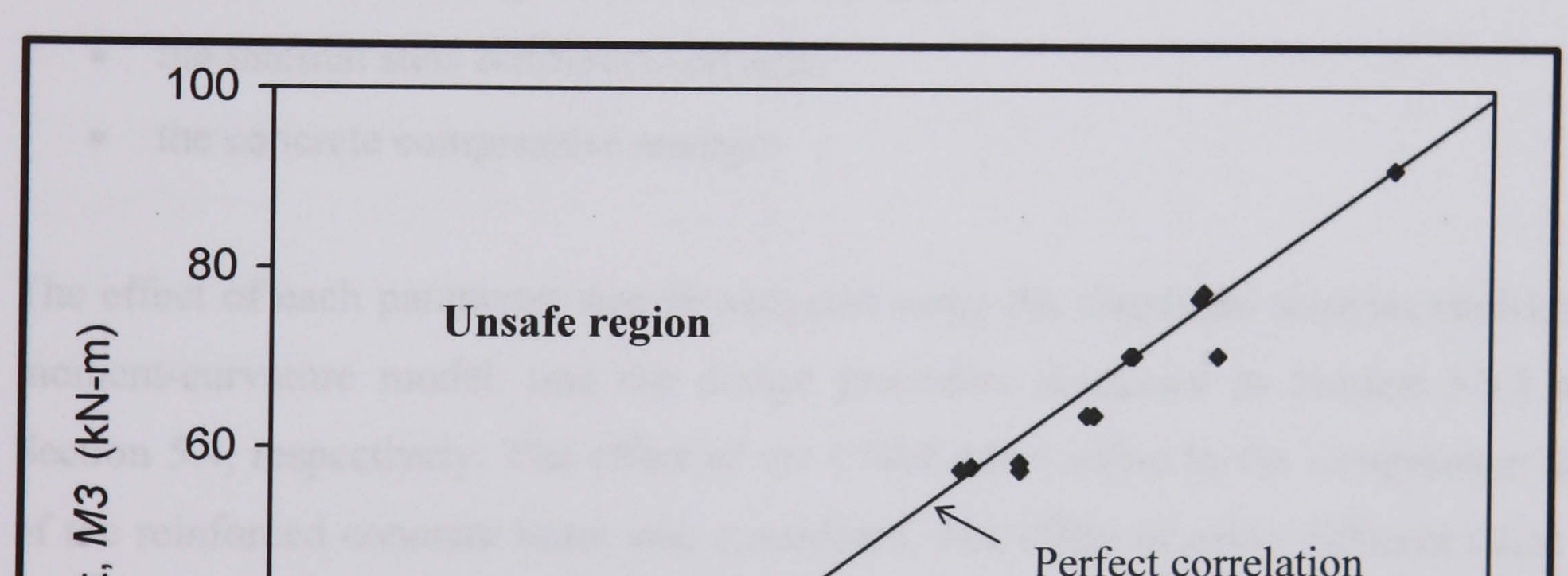

Figure 6.43: Comparison of ultimate bending moments of the experiments with the design procedure

CHAPTER 7

PARAMETERS AFFECTING THE FLEXURAL STRENGTH AND FAILURE MODES OF RC STRENGTHENED SECTION: CASE STUDY

7.1 Introduction

The experimental programme carried out in this research did not investigate all the parameters that can affect the strength and failure modes of reinforced concrete beams strengthened with CFRP materials. The influence of these parameters for a typical section using the models developed is described in this Chapter. Sensitively study was undertaken in which the effect of the following parameters on the strength and failure modes of reinforced concrete beams were investigated:

- the FRP ratio acting in tension and compression
- the internal steel reinforcement ratio
- the concrete compressive strength

The effect of each parameter was investigated using the simplified analysis model, the moment-curvature model, and the design procedure discussed in Section 5.3.3 and Section 5.4, respectively. The effect of the CFRP when added to the compression face of the reinforced concrete beam was considered. The effect of using different ratios of CFRP and GFRP laminates on the tension face of the beam was investigated. The parametric study identified the effect of each variable on the flexural capacity and the flexural failure mode of a reinforced concrete section, either unstrengthened or strengthened with an external CFRP or GFRP.

Figure 7.1 shows the details of the geometry of the section, the internal steel reinforcement and the external CFRP or GFRP reinforcements on both the tension and compression faces. The types of the CFRP and GFRP laminates used and their properties are given in Table 2.2. Perfect bond between the CFRP, GFRP and the

concrete surface in tension and compression has been assumed. The material properties and the ratios or values of the internal steel reinforcement, the external CFRP and GFRP laminates and the concrete compressive strength that were used in the parametric study are given in Table 7.1.

The ratios of the internal tensile steel reinforcement used were $\rho_s = 0$, 1 and 3% and the ratios of the compression steel were $\rho_{sc} = 0$, 1 and 2%. The ratio of the external tensile CFRP or GFRP reinforcement used, varied from 0 to 4%, and the ratio of the compression CFRP used was by $\rho_{fc} = 0$, 1, 1.5 and 3%. The compressive strength of concrete was normally 30 N/mm^2 for all cases, except in the analysis in section 7.5 when the concrete strength was varied, as reported in Table 7.1.

7.2 CFRP, GFRP and internal steel in tension

In this section the ratios of the CFRP and the GFRP used on the tension face of a beam were varied with the same ratios, Table 7.1. The differences between CFRP and GFRP are the Young's moduli and the ultimate strengths. For each beam, three ratios of tensile steel reinforcement were used: 0, 1 and 3%. No compression CFRP or compression steel was included.

Figure 7.2 shows the variation of the ultimate moment with both the internal tensile steel ratio and the ratio of external bonded CFRP and GFRP laminates. The boundaries of failure modes, Mode-I and Mode-III, as defined in 5.4.4, are shown in Figure 7.2. Figure 7.2 shows that using GFRP laminates for strengthening a reinforced concrete section results in a lower ultimate moment than using CFRP laminates for a given tension steel ratio. This is due to the lower Young's modulus and the ultimate strength of the GFRP laminates.

Adding CFRP or GFRP to the tension face of a beam with no tension steel leads to increase in the ultimate moment in a similar way to reinforcing it with internal steel.

When CFRP or GFRP is added to the tension face of an under-reinforced section, a high increase in the flexural strength compared with that in the over-reinforced section is achieved, Figure 7.2.

Figure 7.2 shows that by increasing the ratio of the external CFRP on the tension face of an under-reinforced section, the ultimate moment increases to a similar value to that for an over-reinforced section. A higher ratio of GFRP, therefore, on the tension face of a beam is required to reach the same ultimate moment. For example, at a ratio of 3% of CFRP, the ultimate moment for the under-reinforced section is similar to that of the over-reinforced section. However, using GFRP with the same ratio exhibited a lower ultimate moment than the over-reinforced. This suggests that using a high ratio of CFRP or GFRP on the tension face of a reinforced concrete beam, either the under-reinforced or the over-reinforced, can increase the ultimate moment of the beam to some stage and no further significant increases beyond can be achieved. Therefore, to prevent or to minimise the risk of the peeling failure that occurred at the laminate ends, it would be appropriate to add CFRP to the compression face of the beam.

Figure 7.2 shows that the ratio of CFRP or GFRP that is added to the tension face of a beam controls the mode of failure. For example, in the under-reinforced beams which were no tension steel, failure mode-III occurred at ratios of 1.2% and 0.4% of GFRP and CFRP respectively. For under-reinforced section, the failure mode-III, Section 5.4.4.3, occurred at ratios of 3.95% and 1.3 %, for GFRP and CFRP respectively.

7.3 CFRP in compression

Figure 7.3 illustrates the variation of the ultimate moment for sections with adding CFRP on both the tension and compression faces. The unstrengthened section is over-

reinforced. The ratio of the tensile reinforcement was 3%. No compression steel was used. The ratios of the external compression CFRP were set at 0, 1.5 and 3%. The ratio of the tension CFRP was varied between 0 and 4%.

Figure 7.3 shows that increasing the ratio of the CFRP on the tension face of an over-reinforced beam does not lead to a significant increase in the flexural strength. For example, adding a ratio of 3% of the CFRP to the tension face of the beam achieved an increase of the flexural strength of 1.28 compared to the unstrengthened beam. Adding CFRP laminates to the compression face of the beam achieved significant increases in the flexural strength. For example, adding compression CFRP ratios of 1.5% and 3% respectively, with the same ratio of the tension CFRP exhibited flexural strength increases of 1.34 and 1.67, compared to a beam strengthened in tension only.

Figure 7.3 indicates that strengthening an over-reinforced beam with CFRP ratios of 1% on the tension face and 1.5% on the compression face exhibited a flexural strength increase of 1.60, compared with that strengthened with 1% on the tension face only. However, if 2% of CFRP was added to the tension face of an over-reinforced beam that has the same ratio of compression CFRP, the flexural strength increased by 1.06 compared with that strengthened with 1% and 1.5% of the CFRP on the tension and compression.

Strengthening an over-reinforced beam, which has a high ratio of CFRP on the compression face, with high ratios of CFRP on the tension face does not lead to a significant increase in the flexural strength compared with that of a beam strengthened with a lower ratio of CFRP on the tension, Figure 7.3. Using low ratios of CFRP on the tension face of the beam, as reported in the literature, can prevent end-laminate peeling. Hence, adding CFRP on the compression face of a beam strengthened with low ratios of the CFRP on the tension face can increase the flexural strength of the section and at the same time the risk of end-laminate peeling can be reduced. The increase in the flexural strength of the section strengthened on the compression face is due to the large lever arm of the force of the CFRP compared to that of the compression steel.

Figure 7.3 shows that the ratio of CFRP on the compression face of an over-reinforced beam also strengthened in tension controls the failure mode. The higher the ratio of CFRP on the compression face in the presence of a low ratio of tension CFRP, the more likely the occurrence of rupture of the tension CFRP, Mode-I, Section 5.4.4. However, crushing of concrete before steel yielding, Mode-III, Section 5.4.4, occurs when the section is strengthened on the tension face only.

Adding CFRP on both the tension and the compression faces of an over-reinforced section improves the flexural strength of the composite section. However, using a high ratio of the CFRP on the tension face of the section does not lead to a significant increase in the flexural strength, compared with the section that has a high ratio of tension CFRP.

7.4 Effect of compression steel reinforcement

In Section 7.3, it was shown that adding CFRP to the compression face of an over-reinforced beam, strengthened in tension, increases the flexural strength. In a similar way, the ratio of the compression steel included in the existed reinforced concrete section can influence the flexural strength of a beam. The effect of the compression steel reinforcement ratios included in the section on the flexural strength of the beam, with the presence of the CFRP, is described in this Section.

Figure 7.4 shows the variation of the ultimate moment of a section with the ratio of the external CFRP on the tension face and ratio of the internal compression steel. The ratio of tensile steel reinforcement was 3%; ratios of the compression steel reinforcement were 0, 1%, and 2%. The compression CFRP ratio was 1.5%. The ratio of the external CFRP which was applied to the tension face varied between 0 and 4%.

Figure 7.4 illustrates the increase of the ultimate moment in beams which have high ratios of compression steel compared with beams which have low ratios of compression

steel and beams without compression steel. Using high ratios of CFRP on the tension face of beam sections, which have a high ratio of compression steel or without compression steel, does not lead to significant differences in the ultimate moments compared with beams strengthened with low ratios of tension CFRP. For example, adding CFRP ratios of 3% and 1% on the tension face of a beam with a compression steel ratio 2% increased the ultimate moment by about 1.4 and 1.34 times those of beams without compression steel. This implies that adding a high ratio of CFRP on the tension face of an over-reinforced beam does not significantly increase the flexural strength of the beam compared with a beam that has a low ratio of CFRP. However, the significant improvement in the flexural strength is caused by the presence of the higher ratio of the compression steel that had been included in beam, not the amount of the CFRP.

Figure 7.4 shows that strengthening an over-reinforced section which has a high ratio of compression steel reinforcement, with CFRP on both the tension and the compression faces, changes the failure mode compared with a section that has a low ratio of tension CFRP. The higher the ratio of compression steel in the presence of low ratios of tensile CFRP the quicker the yielding of tensile steel compared with a beam without compression steel. In such a case, the tensile steel reinforcement yields before concrete crushes, but the ultimate moment of the beam will still increase because the contribution in it comes from the tensile CFRP and the compression steel; in a beam with no compression steel, the failure occurs either by yielding of the tensile steel followed by concrete crushing or by concrete crushing before steel yielding. In both failure modes lower ultimate moments, compared with beams that have compression steel, are achieved.

The ratio of the compression steel reinforcement included in the over-reinforced concrete section can increase the flexural capacity, and controls the failure modes compared with a section without compression steel.

7.5 Compressive strength of concrete

Changes in the ratios of the reinforcement, internal and external, or the compressive strength of the concrete or both together, affect the ultimate bending moment of the beam section. In this section the effect of these two parameters on the ultimate bending moment capacity of the various beam sections, unstrengthened, strengthened on the tension and strengthened on both the tension and compression faces, was investigated. The external reinforcement used was CFRP.

The internal steel ratio was 3% and 1%, in tension and compression, respectively. The ratio of the external CFRP on the tension was 1%. Similar ratios of the external CFRP were used on the tension and the compression faces of the beams strengthened on both faces. The compressive strength of the concrete was varied from 20 to 50 N/mm^2.

Figure 7.5 shows the variation of the ultimate moment enhancement ratio which is defined as the ratio of the ultimate bending moment of the strengthened beam to the unstrengthened beam against the compressive strength of the concrete for an over-reinforced section. Increasing the compressive strength of the concrete from 20 to 50 N/mm^2 in an over-reinforced unstrengthened section does not lead to a significant increase in the ultimate moment, Figure 7.5. This is due to yielding of the tensile steel at a concrete compressive strength of 30 N/mm^2. For a beam strengthened with a ratio of 1% of CFRP on the tension face, when the same compressive strength of the concrete and the same amount of internal steel reinforcement are used, the ultimate moment enhancement ratios are 1.09 and 1.45 compared with that of an unstrengthened section. The increase in the ultimate enhancement ratio of the strengthened beam when high compressive strength of concrete is used is due to the premature yielding of the tensile steel because of the addition of the compression steel. Figure 7.5 shows also that adding 1% of CFRP on the compression face of a beam strengthened with 1% of CFRP on the tension face increased the ultimate moment enhancement ratios by 1.49 and 1.65 compared with that of unstrengthened sections. It should be noted that using relatively lower concrete compressive strengths in beams strengthened on both the tension and compression faces exhibited higher ultimate enhancement ratios compared with those strengthened on tension face. On the other hand, Swamy and Mukhopadhyaya, (1999) [35] recalled that increasing the compressive strength of concrete may result in plate

separation from the tension face due to the large amount of energy released when concrete cracks. Therefore, adding CFRP to the compression face simultaneously with the tension CFRP of a section that has low compressive strength of concrete may improve the ultimate moment enhancement ratio and reduce the risk of plate separation from the tension face of a beam.

When the effect of increasing the compressive strength of the concrete on the ultimate moment of the over-reinforced beams (unstrengthened, strengthened on the tension face and strengthened on both the tension and compression faces) is considered, Figure 7.6 shows the gradient of the ultimate moment with the concrete compressive strength. The gradient is calculated by dividing the difference in the ultimate moments to that of the concrete compressive strengths. Figure 7.6 reveals that the gradient of the ultimate moment is relatively enhanced, particularly with the strengthened beams. However, the gradient of the ultimate moment is decreased with the increased compressive strength of concrete. The possible reason behind that is when the compressive strength of the concrete in a beam, which has the same amount of the external and the internal reinforcement, is increased the movement of the neutral axis is decreased (goes up). Subsequently, a bending moment by the tension force, due to the increase in the lever arm of the tension force, is increased, compared with that in the compression force. So, the contribution to the ultimate moment of a beam is reduced with the increasing of the strength of the concrete.

Increasing the compressive strength of concrete from 20 N/mm^2 to 30 N/mm^2 in the unstrengthened over-reinforced concrete beam changed the failure mode of the beam from yielding of the tensile steel reinforcement followed by concrete crushing to crushing of the concrete before yielding of the tensile steel reinforcement, Figure 6.7. A similar mode of failure in beams strengthened on the tension face occurred only when the compressive strength of the concrete increased from 30 N/mm^2 to 40 N/mm^2, Figure 6.7.

It is evident from the previous discussion that adding the CFRP on the compression face of an over-reinforced beam strengthened on the extreme tension face increases the

ultimate bending moment with using lower compressive strength of concrete compared with that of beam strengthened on tension only. Increasing the compressive strength of the concrete for an over-reinforced beam that has the same internal and external reinforcement relatively enhances the ultimate moment of the beam and changes the failure mode.

7.6 Summary

The following conclusions can be drawn from the results of the parametric study described in this chapter:

- By increasing the ratios of CFRP and GFRP on the tension face of either under-reinforced beam or over-reinforced beam, the flexural strength of the strengthened section was found to increase. However, beams which were strengthened with GFRP exhibited lower flexural strength improvements because of its lower mechanical properties compared with those of CFRP. Under-reinforced beams strengthened with CFRP or GFRP showed higher strength increases compared to over-reinforced beam which had similar ratios of CFRP or GFRP.

- Using high ratios of CFRP on the tension face of the over-reinforced sections strengthened on the compression face did not significantly improve the flexural strength compared with that strengthened with low ratios. CFRP strengthening applied to the compression face of an over-reinforced section strengthened with CFRP on the tension face has been shown to improve the flexural strength compared with a beam strengthened on tension face only. Increasing the ratio of the CFRP on the compression face of a beam having similar tension reinforcement changes the failure modes. For example, concrete crushing before yielding of tensile steel in a beam strengthened on tension only has changed to steel yielding followed by CFRP rupture in a beam strengthened on both the tension and compression.

- The parametric study described in this Chapter showed that using low compressive strength of concrete with an over-reinforced beam strengthened on both tension and compression face can lead to a significant increase in the ultimate moment compared to that strengthened on tension face only. It has been found also that increasing the compressive strength of the concrete for an over-reinforced beam relatively enhances the ultimate moment and changes the failure mode.

Material / Property	Internal steel reinforcement		External FRP reinforcement	
	Tensile bars	Compression bars	Tension laminates	Compression laminates
Yield or tensile strength (N/mm^2)	460	460	1200 [1]	1200 [1]
			400 [2]	Non [2]
Elasticity modulus, (kN/mm^2)	200	200	120 [1]	120 [1]
			40 [2]	Non [2]
Reinforcement ratio %	0 to 3	0 to 2	0 to 4	(0, 1.5, 3) [1]
				Non [2]
Concrete compressive strength f_{cu} (N/mm^2)	varied from 20 to 50*			
1= CFRP Laminates; 2 = GFRP Laminates * used in Section 7.5				

Table 7.1: Material properties and reinforcement ratios used in the parametric analysis

1- Tensile steel reinforcement bars

2- Compression steel reinforcement bars

3- CFRP, or GFRP tensile laminates

4- CFRP compression laminates

All dimensions in mm

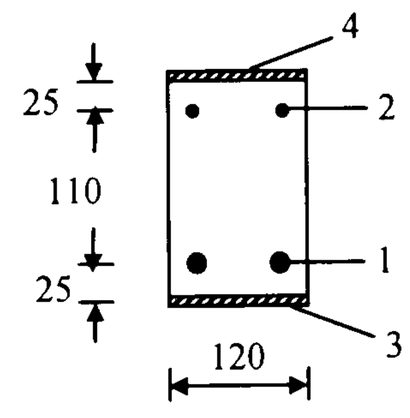

Figure 7.1: Details of reinforced concrete beam section used in the parametric analysis

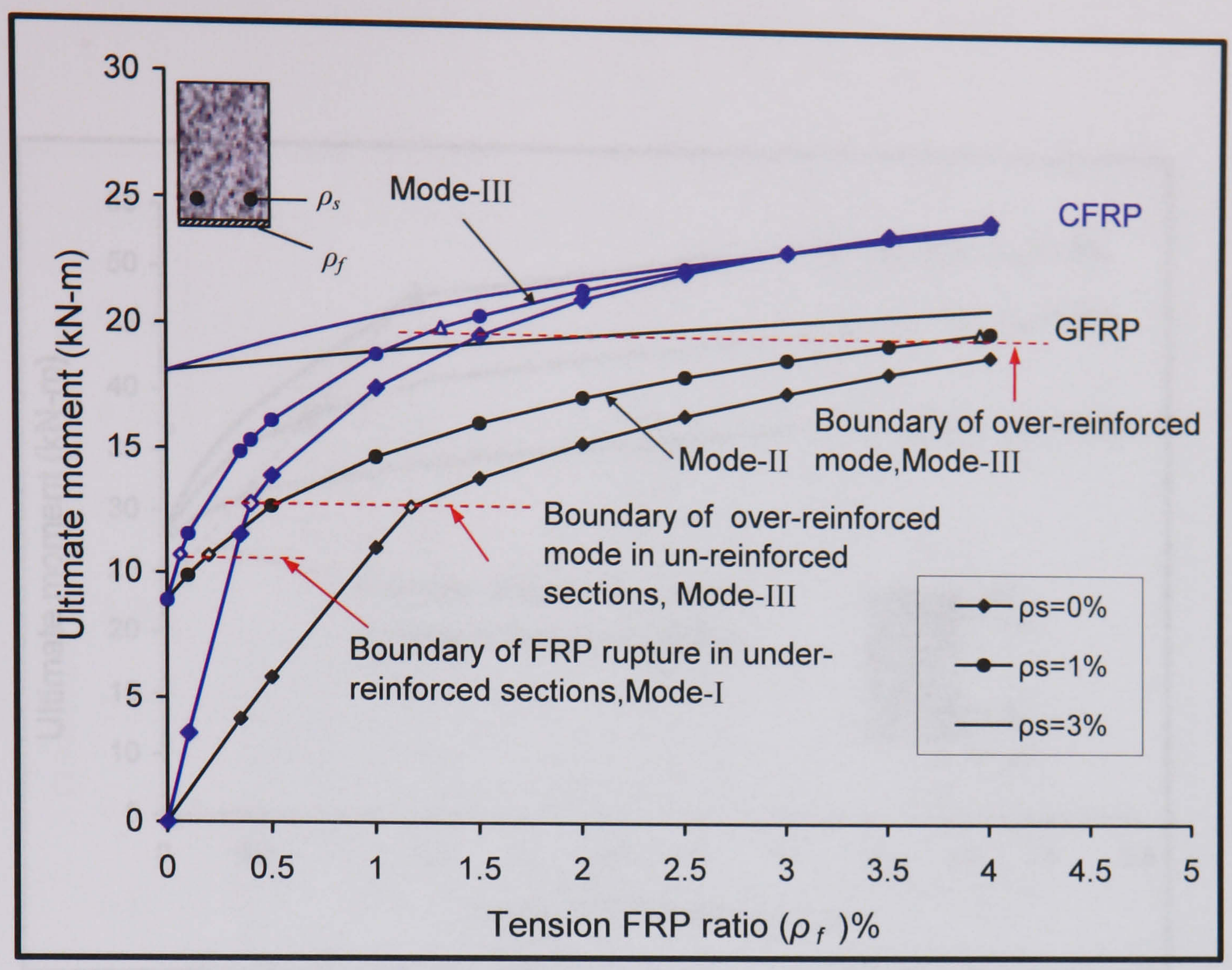

Figure 7.2: Variation of moment capacity against the ratios of internal tensile steel and the external FRP reinforcements

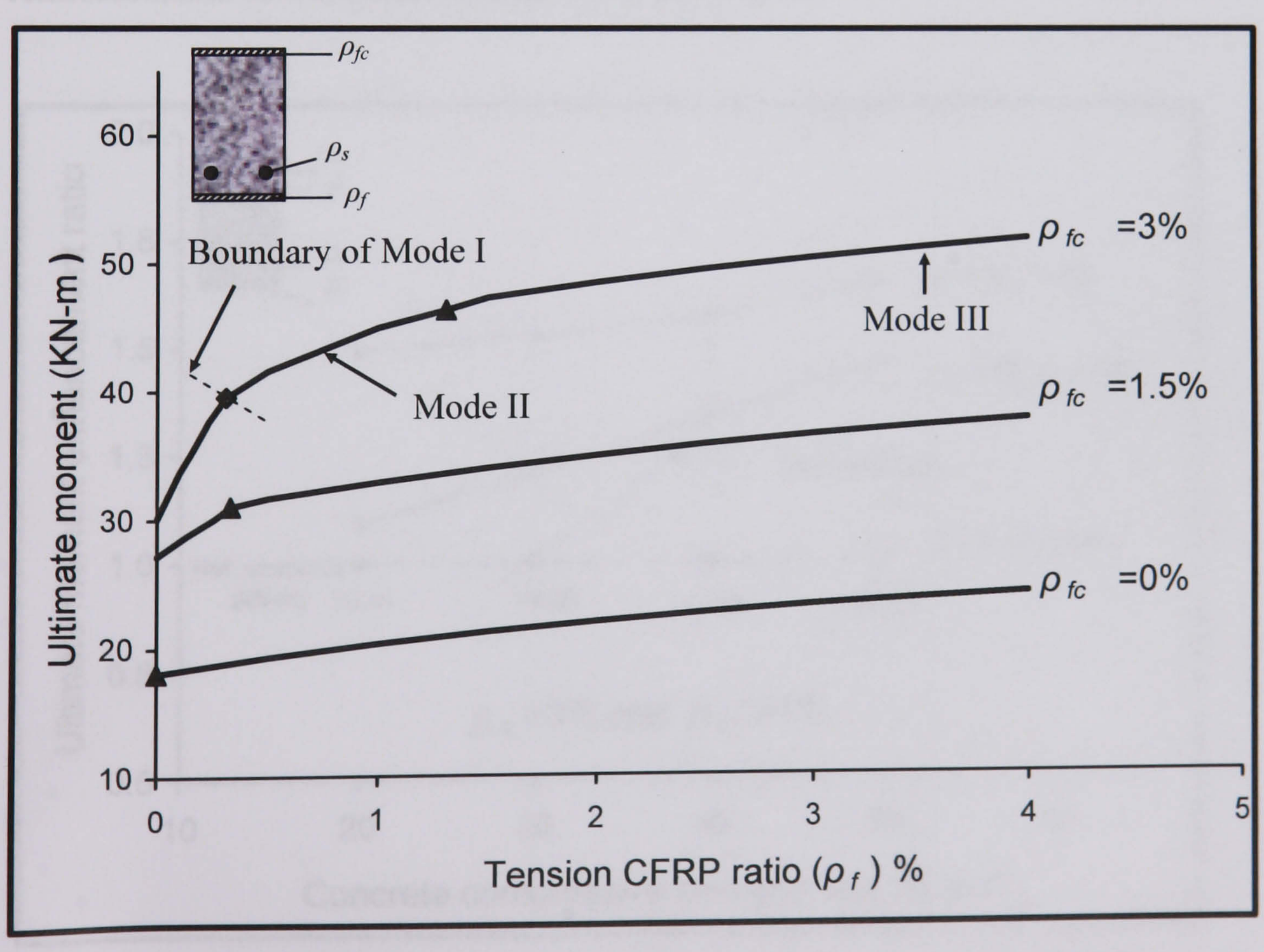

Figure 7.3: Variation of moment capacity against the ratios the external CFRP reinforcements on tension and compression beam faces

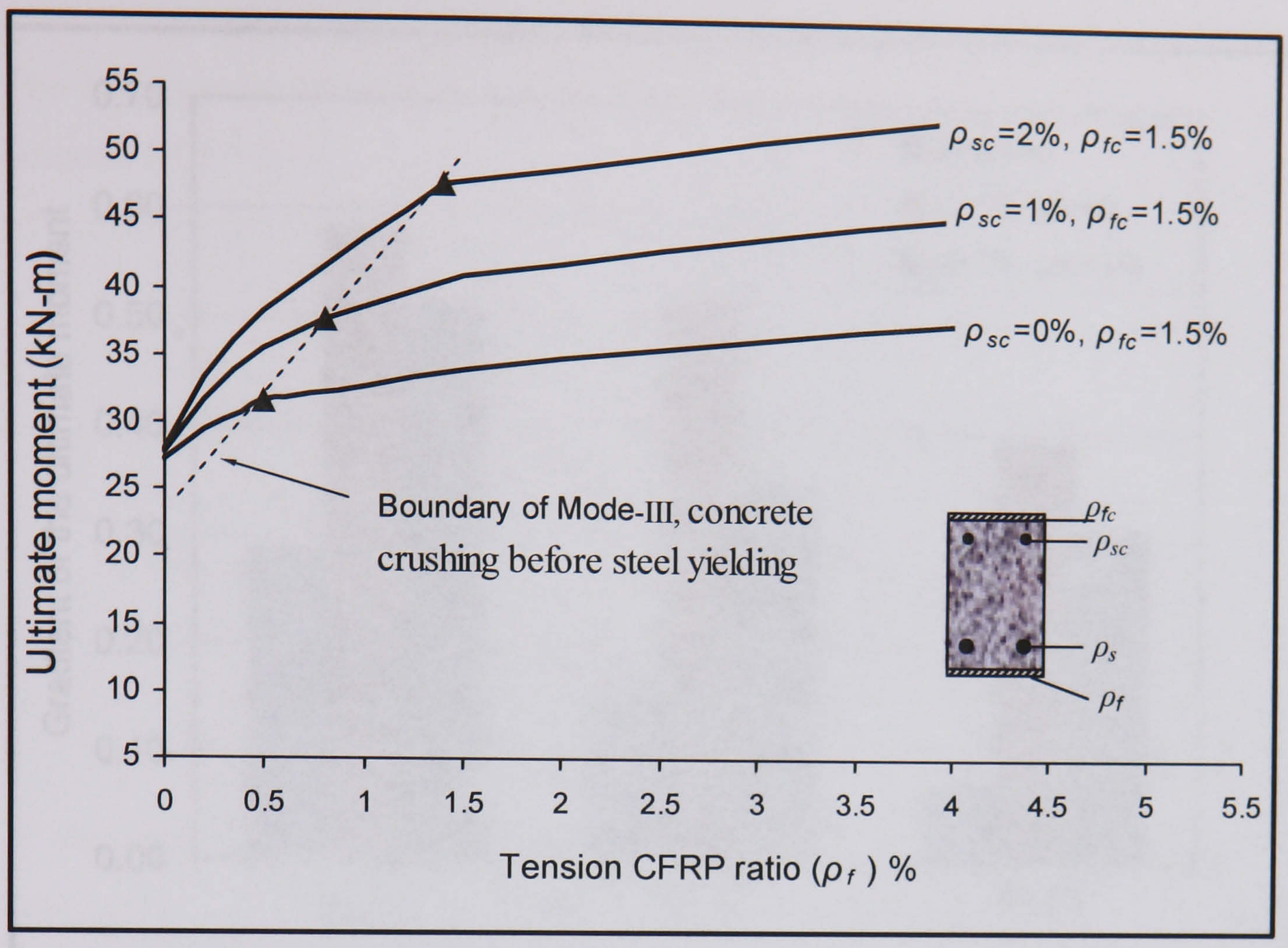

Figure 7.4: Variation of moment capacity against the ratios the external CFRP reinforcements on tension and compression beam faces

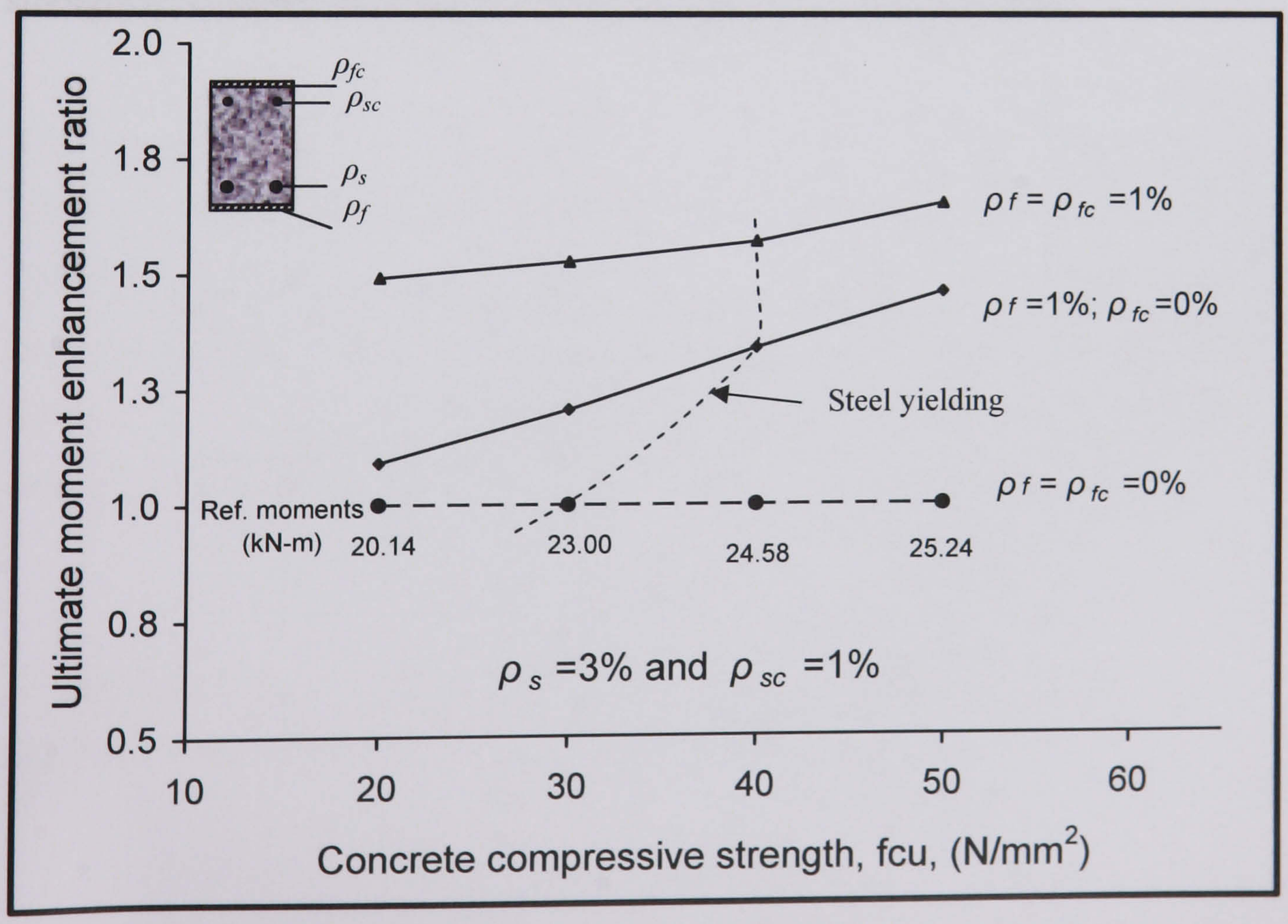

Figure 7.5: Variation of the ultimate moment enhancement ratio against the compressive strength of concrete with ratios of the external CFRP reinforcements

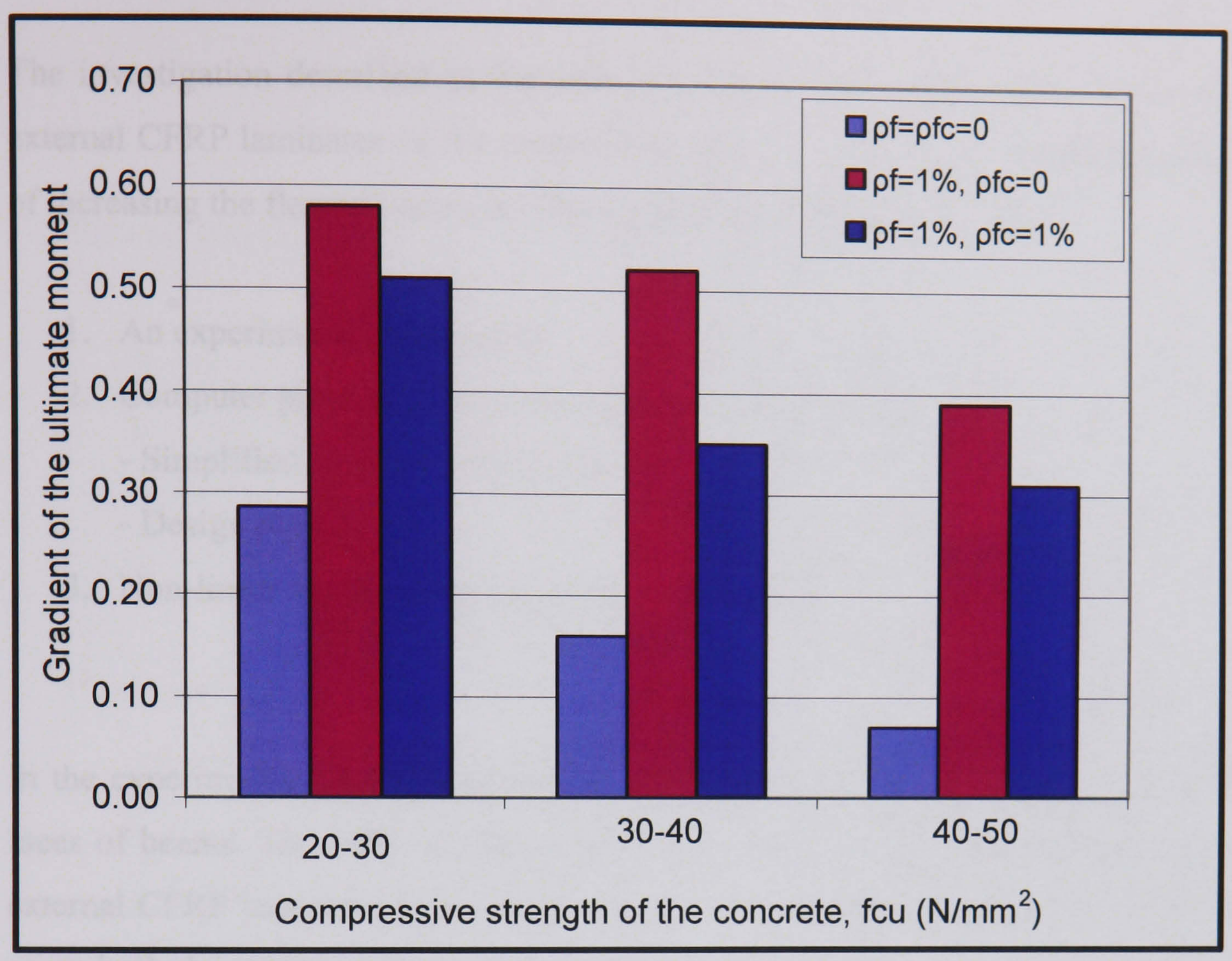

Figure 7.6: Variation of the gradient of the ultimate moment against the compressive strength of concrete with ratios of the external CFRP reinforcements.

CHAPTER 8
CONCLUSIONS AND RECOMMENDATIONS

The investigation described in this study has demonstrated the effectiveness of using external CFRP laminates on the compression face of reinforced concrete beam in terms of increasing the flexural strength. The research comprised three aspects:

1. An experimental programme
2. Computer programs have been developed for the following:
   - Simplified flexural analysis models
   - Design procedures
3. Non-linear finite element analyses

In the experiments, CFRP laminates were added to both the compression and tension faces of beams. The effect of the internal steel reinforcement ratio, the position of the external CFRP laminates on the beam (i.e. on the tension face, on the compression face or on both the tension and compression faces), the thickness of the CFRP laminates on the compression face and the dimensions of the beam cross-section were investigated.

The simplified flexural analysis models comprise a moment-curvature relationship based on section analysis, and load-deflection relationship based on longitudinal analyses of the member using the finite difference procedure. The ultimate moment of the section, using a design procedure based on the simplified material models given in BS 8110, was determined. The simplified flexural analysis and design procedure models included mathematical formulations and computer calculations.

A two-dimensional finite element model was used to analyse some of the unstrengthened and strengthened concrete beam sections.

The results of the research provide a better understanding of the potential for flexural strengthening using CFRP on over-reinforced beams. Conclusions have been given at

the end of each chapter; only the principal findings from the study are summarised below. A number of recommendations for further work are also given.

From the experimental work, the principal findings are:

For flexural strength enhancement

- The tests showed that for an under-reinforced beam strengthened on the tension face, the flexural strength is increased by up to three times compared with the unstrengthened beam. A small increase in flexural strength can be achieved for an over-reinforced strengthened beam compared with the unstrengthened one.

- A small increase in the flexural strength was achieved by adding CFRP to the compression face of an under-reinforced strengthened beam. Adding the CFRP to the compression face of an over-reinforced strengthened beam was found to be an effective technique for strengthening beams. The increase in the strength was up to 1.4 of that of the beam strengthened in tension only.

For the cracking and failure modes

- The occurrence of the first crack at the mid-span of the beam is delayed when CFRP is added to either the tension and/ or the compression faces of an over-reinforced beam which has less than 3% of the steel. No significant difference in the occurrence of the first crack is observed in the section which is strengthened on the compression face. However, no significant change is exhibited when the CFRP is added to the compression face of the over-reinforced beam which has a tensile steel ratio of more than 3%.

- The occurrence of cracks at the laminate ends in the tension face of a strengthened beam tended to hasten end-laminate peeling even if the CFRP confinements are provided. Thus, from some stage of the loading of a beam, the

end confinements become an ineffective technique for hindering crack propagation.

- End-laminate peeling was more prone to occur at the ends of the CFRP laminates when the laminates were cut off within the span of the beam.

- Debonding of the CFRP from the tension face of some beams which had a low shear span to effective depth ratio was observed. It was also observed that crack initiations at the concrete adjacent to the concrete-adhesive interface along the beam span hasten debonding of the CFRP.

- The failure mode for the majority of beams strengthened on the compression face was buckling of the CFRP.

Further observations from the experimental work were made:

- The strain at the extreme compression fibre of concrete, at which the buckling of the CFRP on the compression face occurred, varied between 0.0026 and 0.0032.

- A beam to which CFRP laminates had been added to both the tension and compression faces exhibited less mid-span deflection and hence curvature at the same load level compared to that strengthened on the tension face only or an unstrengthened beam.

- A beam to which CFRP laminates had been added to both the tension and compression faces also decreased the strains in the internal steel reinforcement and the external CFRP at the same load level compared to that strengthened on tension face only or an unstrengthened beam.

In the analytical work the principal findings were:

- The 2D FE models tested in the current study produced reasonable agreement with the experimental results. The comparisons showed that these models are able to predict the nonlinear behaviour of both unstrengthened and strengthened reinforced concrete beams.

- Concrete model 82 is appropriate for analysing a section when concrete crushing is not significant. This numerical model simulates tensile cracks of the concrete but crushing failure in compression is neglected.

- Concrete model 84 is suitable when FE analysis of the nonlinear behaviour of the concrete in tension and compression is considered. This numerical model simulates the tensile cracks and concrete crushing in compression.

- A simplified analytical model based on the moment-curvature relationship was presented which successfully predicted the ultimate moment and the curvature of the unstrengthened and strengthened beams.

- Limits for the ratio of the external CFRP in the tension face of a beam were calculated in order to ascertain if the section was ductile, ignoring laminate peeling, debonding and buckling of the CFRP.

- Equations which have been derived based on the external CFRP limits can be used to determine the flexural failure mode and the ultimate flexural strength of the beam section.

- The parametric study described in Chapter 7 showed that when CFRP was applied only on the tension face of a beam, there was an optimum ratio of the external CFRP in tension at which no further increase in the ultimate moment of the beam could be achieved.

- The results obtained from the FE analysis, the simplified analyses and the design procedure were in good agreement with the experimental results.

Recommendations for future research

The following recommendations for future research should be considered:

- The experimental investigation carried out in this research showed that buckling of the CFRP at the mid-span of a beam was dominant. Further experimental work is needed to test whether buckling failure of the CFRP might be delayed when different thicknesses and properties of CFRP are used.

- The efficiency of using both mechanical anchors and U-shaped confinements at the ends of the external tension reinforcement to prevent peeling failure needs to be investigated.

- Similarly, the efficiency of using mechanical anchors, either steel or fibre, for the external compression reinforcement to prevent or delay buckling failure of the CFRP, needs to be investigated.

- Adding CFRP on the compression face of a continuous reinforced concrete beam might be effective to prevent or delay the occurrence of the formation of the plastic hinges along the beam spans as the load is increased. The formations of the plastic hinges are due to the redistribution of the moments along the beam spans. Hence, adding CFRP on the compression face of the beam should be investigated.

- The current investigation has shown that adding CFRP to the compression face of a beam, particularly an over-reinforced one, leads to a significant improvement in the flexural strength. Hence, CFRP is promising in strengthening the compression faces of other structural elements, i.e. reinforced concrete cantilever parts and masonry walls. Further experimental work using CFRP in strengthening such elements is needed.

- The durability, fatigue and fire resistance of strengthened reinforced concrete beams have not been fully investigated. More research is required to investigate

these factors, considering the development of a suitable technique that can be used for continuous monitoring of the deterioration of these strengthened beams.

REFERENCS

[1] Arduini M., and Nanni A., 1997, "Behaviour of precracked RC beam strengthened with CFRP sheets," Journal of Composites for Construction, Vol. 1, No. 2, 63-70

[2] FIP-Guide to good practice, 1991, "Repair and strengthening of concrete structures," Thomas Telford, London

[3] Reddy D.V., Grevois G.B. and Carlsin L.A., 1996, "Laminate bonding for concrete repair and retrofit," Materials for New Millennium, In: Proceedings of the Materials Engineering Conference, Vol.2, Washington, DC, 1579-1591

[4] Dussek I. J., 1980, "Strengthening of bridge beams and similar structures by means of epoxy-resin-bonded external reinforcements," Transportation Research Record 785, Transportation Research Board, 21-24

[5] Jones R., Swamy R. N. and Charif A., 1988, "Plate separation and anchorage of reinforced concrete beams strengthened by epoxy-bonded steel plates," The Structural Engineer, V. 66, No. 5, 85-94 March

[6] Oehlers D. J., 1992, "Reinforced concrete beams with plates glued to their soffits," Journal of Structural Engineering, Vol.118, No. 8, 2023-2038

[7] Garden H.N., Quantrill R.J., Hollaway L.C., Thorne A.M. and Parke G.A.R., 1998, "An experimental study of the anchorage length of carbon fibre composite plates used to strengthen reinforced concrete beams," Construction and Building Materials, Vol.12, 203-219

[8] MATLAB Program, Version 5.3 (R11.1), September 1999

[9] British Standards Institution. Structural use of Concrete: Code for practice Design and Construction. BSI, London, 1997. BS 8110.

[10] LUSAS," A finite element computer program", Version 13.8, Forge House, 66 High Street, Kingston upon Thames, Surry, KT1 1HN, UK

[11] Misara A.K., Bungy J.H., Ghazalii M.Z.M. and Hassan M., 1995," Performance of gunite repaired reinforced concrete beams," Proceedings of the Sixth International Conference on Structural Faults and Repairs, "extending the life of concrete", London, UK, Vol.2, 411-418

[12] Rafeeqi S. F.A., 2000," Flexural behaviour of reinforced concrete beams strengthened by external unbonded reinforcement," PhD Thesis, Heriot-Watt University, Edinburgh

[13] Allen D.C. and Roper H., 1991," Concrete structures: Materials, Maintenance and Repair," Concrete Design and Construction Series, Longman Scientific & Technical, UK, p 369

[14] Pham-Thanh D., Rigden S.R. and Burley E., 1995," Strengthening of concrete bridges using sprayed concrete," Proceedings of the Sixth International Conference on Structural Faults and Repairs, "extending the life of concrete", London, UK, Vol.1, 175-182

[15] Diab Y.G., 1998, "Strengthening of RC beams by using sprayed concrete: experimental approach," Engineering Structures, Vol.20, No. 7, 631-643

[16] Haldane D. and Ziara M., 1999," Strengthening of reinforced concrete girders using mechanically bonded overlayers," The 9th BCA Annual Conference on Higher Education and the Concrete Industry, Cardiff University, Wales, 207-218

[17] Ziara M. M., 2000," Structural upgrading of RC beams using composite overlays," Construction and Building Materials, 14. 397-406

[18] ÖZTÜ H. and AYVAZ Y., 2002, "Comparative study of behaviour of reinforced concrete beams strengthened and repaired-strengthened by using V connecting bars and U connecting stirrups," Construction and Building Materials. 16, 321-329

[19] Virlogeux M.P., 1990," External prestressing: From construction history to modern technique and technology," External prestressing in bridges," edited by Naaman, A. and Breen, J., ACI, SP 120-1, 1-60

[20] Carins J. and Rafeeqi S., 1997, "Behaviour of reinforced concrete beams strengthened by external unbonded reinforcement," Construction and Building Materials, Volume 11, Issues 5-6, 309-317

[21] Cairns J. and Rafeeqi S., 2003, "Strengthening reinforced concrete beams with external unbonded bars: experimental investigation," Proceedings of the Institution of Civil Engineers; Structures and Buildings 156, Issue I. 27-37

[22] Cairns J. and Rafeeqi S., 2003," Strengthening reinforced concrete beams with external unbonded bars: Theoretical investigation," Proceedings of the Institution of Civil Engineers, Structures and Buildings 156, Issue I. 39-48

[23] Alaee F. J. and Karihaloo B. L., 2003, "Retrofitting of reinforced concrete beams with CARDIFRC," Journal of Composites for Construction, Vol. 7, No. 3,175-186

[24] Raithby K.D., 1980, "External strengthening of concert bridges with bonded steel plates," Transport and Road Research Laboratory, Supplementary Report 612

[25] Jones R., Swamy R. N., Bloxham J. and Bouderbalah A., 1980, "Composite behaviour of concrete beams with epoxy bonded external reinforcement," The International Journal of Cement Composites 2, No. 2, 91-107

[26] Swamy R. N., Jones R. and Bloxham J. W., 1987, "Structural behaviour of reinforced concrete beams strengthened by epoxy-bonded steel plates," The Structural Engineer, Vol. 65 A, No. 2, 59-68

[27] Oehlers D. J. and Moran J. P., 1990, "Premature failure of externally plated reinforced concrete beams," Journal of Structural Engineering, Vol.116, No. 4. 978-993

[28] An W., Saadatmanesh H. and Ehsani, R., 1991," RC beams strengthened with GFRP plates II: Analysis and Parametric study," Journal of Structural Engineering, ASCE, 117, 11, 3434-3455

[29] Ritchie P.A., Thomas D.A., Lu L. W. and Connelly G. M., 1991, "External reinforcement of concrete beams using fibre reinforced plastics," ACI Structures Journal, 88, 4, 490-500

[30] Shrif A., Al-Sulimani G. J., Basunbul I. A., Balush M. H. and Ghaleb, B. N., 1994, "Strengthening of initially loaded reinforced concrete beams using FRP plates," ACI Structural Journal, V.91, No.2,160-168

[31] Meier U. and Winstorfer A., 1995, "Retrofitting of structures through external bonding of CFRP sheets," Proceedings, 2nd international RILEM symposium, non metallic FRP reinforcement for concrete structures, E & FN Spon, London, 509-516

[32] Arduini M., Tommaso D. A. and Nanni A., 1997," "Brittle failure in FRP plate and sheet bonded beams," ACI Structural Journal, Vol. 94, No. 4, 363-370

[33] Malek A. M., Saadatmanesh H. and Ehsani, M. R., 1998, "Prediction of failure load of RC beams strengthened with FRP plate due to stress concentration at the plate end," ACI Structural Journal, Vol. 95, No. 1, 142-152

[34] Saadatmanesh H. and Malek M., 1998, "Design guidelines for flexural strengthening of RC beams with FRP plates," Journal of Composites for Construction, Vol. 2, No. 4, 158-164

[35] Swamy R. N. and Mukhopadhyaya P., 1999, "Debonding of carbon-fibre-reinforced polymer plate from concrete beams," Proceedings of the instantiation of civil engineering, Structures and Buildings, 134, 301-317

[36] Spadea G., Bencardino F. and Swamy R. N., 2000, "Optimizing the performance characteristics of beams strengthened with bonded CFRP laminates." Materials and Structures, Vol. 33, 119-126

[37] Mukhopadhyaya P. and Swamy, 2001, "Interface shear stress: a new design criterion for plate debonding," Journal of Composites for Construction (ASCE), Vol. 5, No. 1, 35-43

[38] Rahimi H. and Hutchinson A., 2001," Concrete beams strengthened with externally bonded FRP plates," Journal of Composites for Construction (ASCE), 5, No.1, 44-56

[39] Pham H., and Al-Mahaidi R., 2004, "Experimental investigation into flexural retrofitting of reinforced concrete bridge beams using FRP composites." Composite Structures, 66, 617-625

[40] Thomsen H., Spacone E., Limkatanyu S. and Camata G., 2004, "Failure mode analysis of reinforced concrete beams strengthened in flexure with externally bonded fibre-reinforced polymers," Journal of Composites for Construction (ASCE), Vol. 8, No.1, 123-131

[41] Arduini M., Nanni A., Ditommaso A. and Focacci F., 1997," Shear response of continuous RC beams strengthened with carbon FRP sheets," Non-metallic (FRP) reinforcement for concrete structures, Proceedings of the Third International Symposium, Vol. 1,459-469

[42] Grace N.F., Soliman A. K., Abdel-Sayed G. and Saleh K. R., 1999," Strengthening of continuous beams using fibre reinforced polymer (FRP) laminates," In: Fourth International Symposium on Fibre Reinforced Polymer Reinforcement for Reinforced Concrete Structures, American Concrete Institute, 647-657

[43] Tann D. B. and Delpak R., 2000," Shear strengthening of continuous reinforced concrete beams using externally bonded carbon fibre sheets, "Proceedings of the 10th BCA Annual Conference on High Education and the Concrete Industry, Birmingham, UK,325-338

[44] Grace N.F., 2001, "Strengthening of negative region of reinforced concrete beams using carbon fibre-reinforced polymer strips," ACI Structural Journal, Vol. 98, No. 3, 347-358

[45] Ashour A. F., El-Refaie S.A. and Garrity S.W., 2004, "Flexural strengthening of RC continuous beams using CFRP laminates," Cement and Concrete composites, Vol.26, 765-775

[46] ICE, Design and Practice Guides, FRP composites: Life extension and strengthening of metallic structures, Thomas Telford, Institution of Civil Engineers, 2001

[47] Teng J. G., Chen J. F., Smith S. T. and Lam L., 2002, "FRP-strengthened RC structures," John Wiley & Sons, Ltd, England

[48] SP Systems, Composite Engineering Materials, Guideline Instructions Manual, Newport, UK (2002)

[49] Saadatmanesh H. and Ehsani M. R., 1990, "Fiber composite can strengthen beams," American Concrete International, ACI, 12, 3, 65-71

[50] Chajes M., Thomson T. A., Januszka T. F. and Finch W. W., 1994," Flexural strengthening of concrete beams using externally bonded composite materials," Construction and Building Materials, 8, 3, 191-201

[51] Bonacci J. F. and Maalej M., 2000, "Externally bonded fibre-reinforced polymer for rehabilitation of corrosion damaged concrete beams," ACI Structural Journal, 97, 5, 703-711

[52] Ramana V. P. V., Kant T., Morton S. E., Dutta P. K., Mukherjee A. and Desai Y. M., 2000, "Behaviour of CFRPC strengthened reinforced concrete beams with varying degrees of strengthening," Composites Part B 31, 461-470

[53] Bonacci J. F. and Maalej M., 2001, "Behavioural trends of RC beams strengthened with externally bonded FRP," Journal of Composites for Construction (ASCE), Vol. 5, No. 2, 102-113

[54] Shin Y. and Lee C., 2003, "Flexure behaviour of reinforced concrete beams strengthened with carbon fibre-reinforced polymer laminates at different levels of sustaining load," ACI Structural Journal, Vol.100, No.2, 231-239

[55] Grace N. F., Ragheb W. F. and Abdel-Sayed G., 2003, "Flexure and shear strengthening of concrete beams using new triaxially braided ductile fabrics," ACI Structural Journal, Vo. 100, No. 6, 805-814

[56] Alagusundaramoorthy P., MAsce Harik L. E., and Choo C. C., 2003," Flexural behaviour of RC beams strengthened with carbon fibre reinforced polymer sheets or fabric," Journal of Composite for Construction (ASCE), 292-300

[57] Spadea, G., Bencarding, F. and Swamy, R. N., 1998, "Structural behaviour of composite RC beams with external bonded CFRP", Journal of Composite for Construction, ASCE, Vol. 2, No. 3, 132-137

[58] Mukhopadhyaya B., Swamy N., ASCE F. and Lynsdale C., 1998, "Optimizing structural response of beams strengthened with GFRP plates", Journal for Composites for Construction, ASCE, Vo. 2, No. 2, 87-95

[59] Spadea G., Swamy R. N. and Bencardino F., 2001, "Strength and ductility of reinforced concrete beams repaired with bonded CFRP laminates," Journal of Bridge Engineering, Vol. 6, No. 5, 349-355

[60] Arya C., Clarke J. L., Kay E. A. and O'Regan P. D., 2002," Technical Report No. 55: Design guidance for strengthening concrete structures using fibre composite materials: a review," Engineering Structures, Vol. 24, Issue 7, 889-900

[61] Buyukozturk O. and Hearing B., 1998, "Failure behaviour of pre-cracked concrete beams retrofitted with FRP," Journal of Composites for Construction ASCE, Vol. 2, No. 3, 133-144

[62] Seim W., Hörmann M., Karbhari V. and Seible F., 2001, "External FRP post-strengthening of scaled concrete slabs," Journal of Composites for Construction. Vol. 5, No. 2, 67-75

[63] Mohamed Ali M. S., Oehlers D. J. and Park S., 2001, "Comparison between FRP and steel plating of reinforced concrete beams," Composites: part A: Applied Science and Manufacturing, 32, 1319-1328

[64] Nguyen D. M., Chan T. K. and Cheong H. K., 2001, "Brittle failure and bond development length of CFRP-concrete beams," Journal of Composites for Construction (ASCE), 5, No.1, 12- 17

[65] Ziraba Y. N., Balush M. H., Basunbul I. A., Sharif A. M., Azad A. K. and Al-Sulimani G. J., 1994, "Guidelines toward the design of reinforced concrete beams with external plates, " ACI Structural Journal, 639-646

[66] Garden H.N. and Hollaway L.C., 1998, "An experimental study of failure modes of reinforced concrete beams strengthened with prestressed carbon composite plates," Composites Part B, Vol.29, No. 4, 411-424

[67] Oehlers D., 2001, "Development of design rules for retrofitting by adhesive bonding or bolting either FRP or steel plates to RC beams or slabs in bridges and building," Composites Part A: Applied science and manufacturing, Vol. 32, 1345-1355

[68] Olivier J.G., 1999, "Fracture in reinforced concrete computational and analysis studies," PhD Thesis, Heriot-Watt University, Edinburgh

[69] Sebastian, W. M., 2001, "Significance of midspan debonding failure in FRP-plated concrete beams," Journal of Structural Engineering, 127, No. 7, 792-798

[70] Saadatmanesh H. and Ehsani M. R., 1991, "RC beams strengthened with GFRP plates, I: Experimental study," Journal of Structural Engineering, Vol.117, No.11, 3417-3433

[71] Meier U., 1995, "Strengthening of structures using carbon fibre/epoxy composites," Construction and Building Materials, Vol. 9, No.6, 341-351

[72] Triantafillou T. C. and Plevris N., 1992, "Strengthening of RC beams with epoxy-bonded fibre-composite materials," Materials and Structures, 25, 201-211

[73] Teng J. G., Lam L., Chan W. and Wang J., 2000, "Retrofitting of deficient RC cantilever slabs using GFRP strips," Journal of Composites for Construction (ASCE), 4, 2, 75- 83

[74] Teng J. G., Cao S.Y. and Lam L., 2001, "Behaviour of GFRP-strengthened RC cantilever slabs," Construction and Building Materials, 15, 339-349

[75] Lam L. and Teng J. G., 2001," Strengthening of RC cantilever slabs bonded with GFRP strips," Journal of Composites for Construction (ASCE), 5, 4, 221-227

[76] Smith S. T. and Teng J. G., 2002, "FRP-strengthened RC beams. I: Review of debonding strength models", Engineering Structures, Vol. 24, Issue 4, 385-395

[77] Zhang S., Raoof M. and Wood L.A., 1995," Prediction of peeling failure of reinforced concrete beams with externally bonded steel plates", Proceedings of the Institution of Civil Engineers: Structures and Buildings, 110, 257–268

[78] Raoof M. and Zhang S., 1997," An insight into the structural behaviour of reinforced concrete beams with externally bonded plates," Proceedings of the Institution of Civil Engineers: Structures and Buildings, 122, 477–492

[79] Wang C.Y. and Ling F. S., 1998, "Prediction model for the debonding failure of cracked RC beams with externally bonded FRP sheets," Proceedings of the

Second International Conference of Composites in Infrastructure (ICCI), Arizona, USA, 548–562

[80] Roberts T. M., 1989, "Approximate analysis of shear and normal stress concentrations in the adhesive layer of plated RC beams," The structural Engineer, the Institution of Structural Engineers, London, June, Vol.67, No.12/20, 229-233

[81] Ziraba Y.N., Baluch M.H., Basunbul I.A., Sharif A.M., Azad A.K. and Al-Sulaimani G.J., 1994, "Guidelines towards the design of reinforced concrete beams with external plates", ACI Structural Journal, 91, 6, 639–646

[82] Smith S. T. and Teng J.G., 2001, "Interfacial stresses in plated beams", Engineering Structures, Vol.23, 857-871

[83] ACI Committee 318, 1999, "Building code requirements for structural concrete (ACI 318-99)", American Concrete Institute

[84] Ross C. A., Jerome D. M., Tedesco J. W. and Hughes M. L., 1999, "Strengthening of reinforced concrete beams with externally bonded composite laminates," ACI Structural Journal, 96, No. 2, 212- 220

[85] El-Mihilmy M. and Tedesco J. W., 2000, "Deflection of reinforced concrete beams strengthened with fibre-reinforced polymer (FRP) plates", ACI Structural Journal, V. 97, No.5, 679-688

[86] Triantafillou T. C. and Plevris N., 1992, "Strengthening of RC beams with epoxy bonded fibre-composite materials", Materials and Structures, Vol.25, 201-211

[87] R 55: Design guidance for strengthening concrete structures using fibre composite materials: The Concrete Society Technical Report 55, 35-38, 2000

[88] Ashour A. F., 2002," Size of FRP laminates to strengthen reinforced concrete sections in flexure," Structures and Buildings, Proceedings of the Institution of Civil Engineers, 152, 3, 225-233

[89] Hong He., Pilakoutas K. and Waldron P., 1997, "Analysis of externally strengthened RC beams with steel and FRP plates," Proceedings 7th International Conference on Structural Faults and Repairs, 83-92

[90] Hutchinson A. R. and Rahimi H., 1993, "Behaviour of reinforced concrete beams with externally bonded fibre reinforced plastics," Proceedings of the 5th International Conference Structural Faults and Repairs, University of Edinburgh. 221-228

[91] Tripi M. T., Bakis C.E., Boothby T .E. and Nanni A., 2000, "Deformation in concrete with external CFRP sheet reinforcement," Journal for Composites for Construction. ASCE, May, 85-97

[92] Adhikary B. B., Mutsuyoshi H. and Sano M., 2000, "Shear strengthening of reinforced concrete beams using steel plates bonded on beam web: experiments and analysis", Construction and Building Materials, 14, 5, 237-244

[93] Arduini M. and Nanni A., 1997, "Parametric study of beams with externally bonded FRP reinforcement", ACI Structural Journal, 94, 5, 493-501

[94] Toutanji H. and Ortiz G., 2001, "The effect of surface preparation on the bond interface between FRP sheets and concrete members" Composite Structures 53, 457-462

[95] Clarke J. I., 2000, "Strengthening concrete structures with fibre composites", Proceeding of the 10th BCA Annual Conference on High Education and the Concrete Industry, Birmingham, 277-287

[96] Täljsten B. and Elfgren L., 2000," Strengthening concrete beams for shear using CFRP- materials: evaluation of different application methods", Composites: Part B: Engineering, 31, 87-96

[97] Smith S. T. and Teng J. G., 2001, "Debonding failures in FRP-plated RC beams with or without U strips end anchorage", Proceedings of the International Conference on FRP Composites in Civil Engineering, Hong Kong, 607-615

[98] Bencardino F., Spadea G. and Swamy R. N., 2002, "Strength and ductility of reinforced concrete beams externally reinforced with carbon fibre fabric", ACI Structural Journal, Vo. 99, No. 2, 163-171

[99] British Standard Institution, 2001, "Tensile testing of metallic materials: Method of test at ambient temperature," BS EN 10002-1:2001

[100] British Standard Institution, 1992, "Specification for aggregates from natural sources for concrete," BS882

[101] British Standard Institution, 1991, "Methods for specifying concrete mixes," BS 5328: Part 2

[102] British Standard Institution, 1983, "Method for making test cubes from fresh concrete," BS 1881: Part108

[103] British Standard Institution, 1983, "Method for making test cylinders from fresh concrete," BS 1881: Part 110

[104] Test for splitting tensile strength of cylindrical concrete specimens, American Society for Testing and Materials ASTM C496 (1990)

[105] MacGregor J.G., 1988, "Reinforced concrete: Mechanics and design", Prentice Hall, Englewood Cliff, New Jersey, USA

[106] Hassoun M. N., 1985, "Design of concrete structures. PWS Publishers", PWS Publishers, USA

[107] British Standard Institution., 1997. "Structural use of concrete: code of practice for design and construction". BS 8110: Part 1

[108] Standard practice for injection molding test specimens of thermoplastic molding and extrusion materials, American Society for Testing and Materials, ASTM D3641-02

[109] British Standard Institution, 1997 , " Injection moulding of test specimens of thermoplastic materials: General principles, and moulding of multipurpose and bar test specimens", BS EN ISO 294-1

[110] British Standard Institution, 1997, "Plastics: Preparation of test specimens by machining", BS EN ISO 2818

[111] British Standard Institution, 1997, "Plastics: Multipurpose-test specimens", BS EN ISO 3167

[112] ASTM D 792-0, 2001, "Density and specific gravity (relative density) of plastics by displacement", Annual Book of ASTM Standard, American Society for Testing and Materials, Vol. 08.01, 156-161

[113] ASTM D3039/D3039M, 1995, "Tensile properties of polymer matrix composite materials", Annual Book of ASTM Standard, American Society for Testing and Materials, Vol. 08.01, 111-121

[114] British Standard Institution, 1997, "Determination of tensile properties: Test conditions for unidirectional fibre-reinforced plastic composites", BS EN ISO 527-5

[115] Barbero E. J.," Introduction to composite materials design", Taylor and Francis, Philadelphia, PA

[116] Weeton J. W., Peters D. M. and Thomas K. L., 1987, "Engineers' guide to composite materials," American Society for Metals

[117] Marcus L., 1973, "Carbon fibres in engineering" McGraw-Hill Book Company, UK, Limited

[118] Kuriger R. J., Shad M. S., Ryan B. and Alam M. K., 1999, "Analysis of composite reinforced concrete beams," Russ College of Engineering and Technology Ohio University, USA

[119] EL-Refaie S. A., 2001, "Repair and strengthening of continuous reinforced concrete beams," PhD Thesis, University of Bradford, UK

[120] EL-Refaie S. A., Ashour A S. and Garrrity S W., 2000, "Tests of reinforced concrete continuous beams strengthened with carbon fibre sheets," Proceeding of the 10th BCA Annual Conference on high education and the concrete industry. Birmingham 29-30 June

[121] Nilson A. H. and Winter G., 1991, "Design of concrete structures," McGraw-Hill, 11th edition

[122] Regan P. E. and YU C. W., 1973, "Limit state design of structural concrete," Chatto & Windus London

[123] Swamy R. N., Lynsdale, C. J. and Mukhopadhyaya P., 1996, "Effective strengthening with ductility: uses of externally bonded plates of non-metallic composite materials", 2nd International Conference on Advanced Composite Materials in Bridges and Structures, the Canadian Society for Civil Engineering, Montreal, 481-488.

[124] Kwak H.G. and Kim S.P., 2002, "Nonlinear analysis of RC beams based on moment-curvature relation", Computers and Structures, 80, 615-628

[125] Scott B. D., Park R. and Priestly M. J. N., 1982, Stress-strain behaviour of concrete confined by overlapping hoops at low and high strain rates," ACI Journal, January-February, 79(1): 13-27

[126] Kent D.C. and Park R..1971, " Flexural members with confined concrete", Journal of the structural Division, Proceedings of the American Society of Civil Engineers, July, Vol. 97, ST7,1969-1990

[127] Jones R., Swamy R. N. and Bloxham J., 1986, "Crack control of reinforced concrete beams through epoxy bonded steel plates", Adhesions between polymers and concrete Proceeding of international SYMP, Aix en Provence France,542-555

[128] Fields K. and Bischoff P. H., 2004, "Tension stiffening and cracking of high-strength reinforced concrete tension members," ACI Structural Journal, V.101, No.4, 447-456

[129] Marzouk, H. and Chen Z. W., 1993, "Nonlinear analysis of normal and high strength concrete slabs," Canadian Journal of Civil Engineering, V.20, No.4, 696-707

[130] CEB-Comitte Euro-International dubeton (CEB-FIP), 1990, Model Code for Concerte Structure

[131] Ngo D. and Scordelis A. C., 1967, "Finite element analysis of reinforced concrete beams," ACI Journal, Vol. 64, No. 3, 152-163

[132] Vebo A. and Ghali A., 1977, "Moment-curvature relation of reinforced concrete slabs," Journal of the Structural Division, ASCE, Vo. 103, No. 3, 515-531

[133] Chen W. F. and LUI E. M., 1991, "Stability design of steel structure frames," CRC Press, Inc, Florida, USA

[134] Bonacci J. F. and Maalej M., 2000, "Externally bonded fibre-reinforced polymer for rehabilitation of corrosion damaged concrete beams," ACI Structural Journal, 97, No. 5, 703- 711

[135] Andreou E., Delpak R., Pinelli R. and Chang K., 2000, "The application of composite based on Kevlar for the strengthening of RC beams," Proceedings of the 10th BCA, Annual Conference on Higher Education and the Concrete Industry, Birmingham, 310-311

[136] Lamanna A. J., Bank L. C. and Scott D.W., 2001, "Flexural strengthening of reinforced concrete beams using fasteners and fibre-reinforced polymer strip," ACI Structural Journal, Vo. 98, No. 3, 368-376

[137] Yasutaka S., Hiromichi M. and Hiroaki T., 2001, " Anchoring method of carbon fibre sheet for strengthening of reinforced concrete beams," Proceedings of the 5th International Conference on Fibre-reinforced Plastics for Reinforced Concrete Structures, Cambridge, UK, 409-417

APPENDIX A

CRACK PATTERNS AND FAILURE MODES OF TEST BEAMS

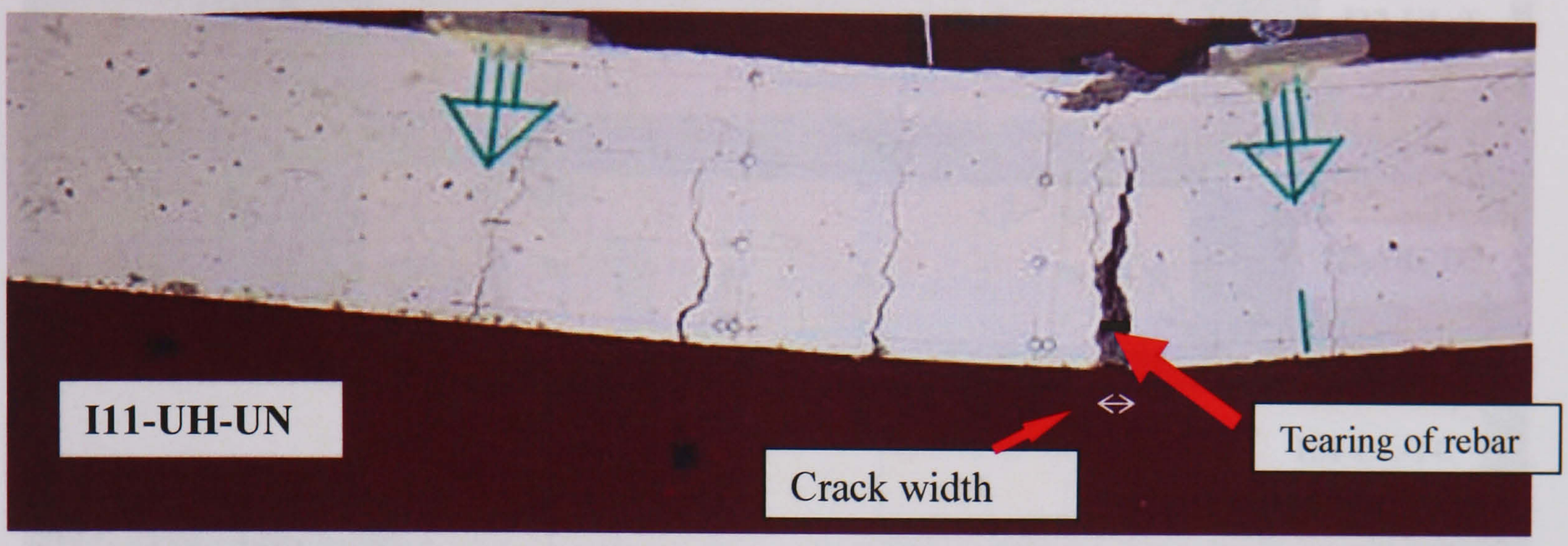

FigureA.1a: Typical flexure failure due to steel yielding near to the right point load, beam I11-UH-UN.

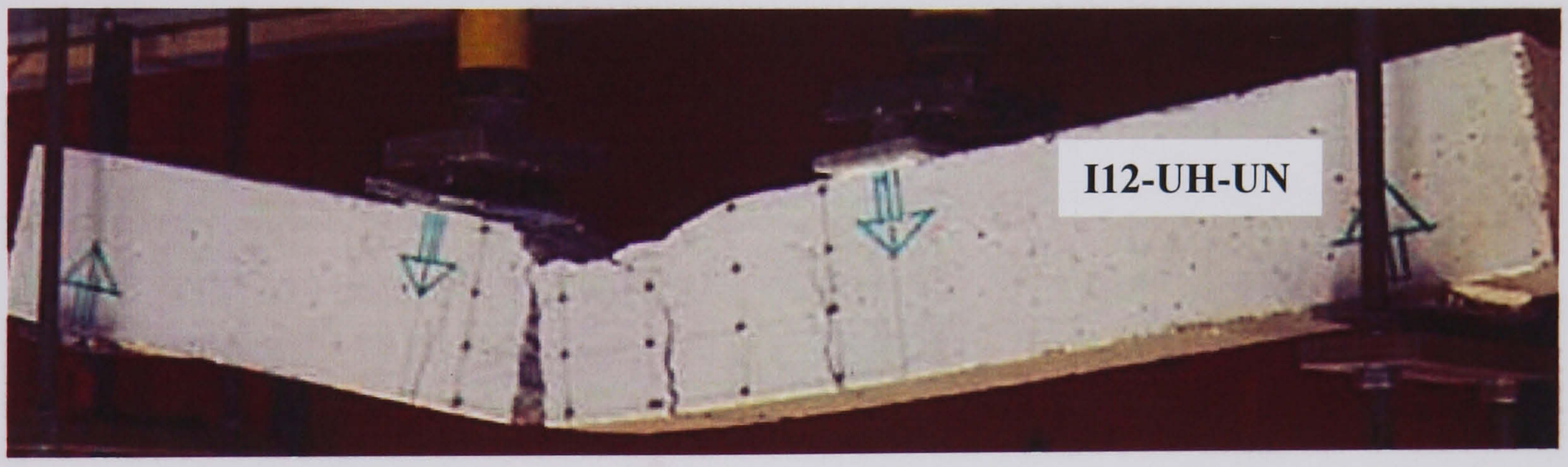

Figure A.1b: Typical flexure failure due to steel yielding near to the left point load, beam I12-UH-UN.

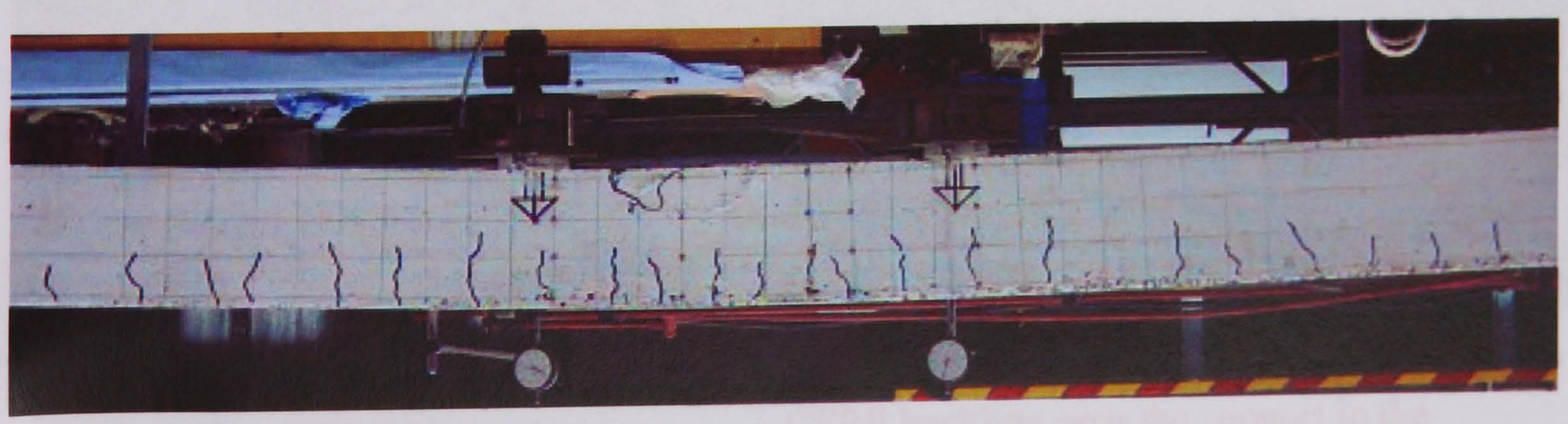

Figure A.1c: Typical cracks at failure for strengthened beams III1-OL-UN

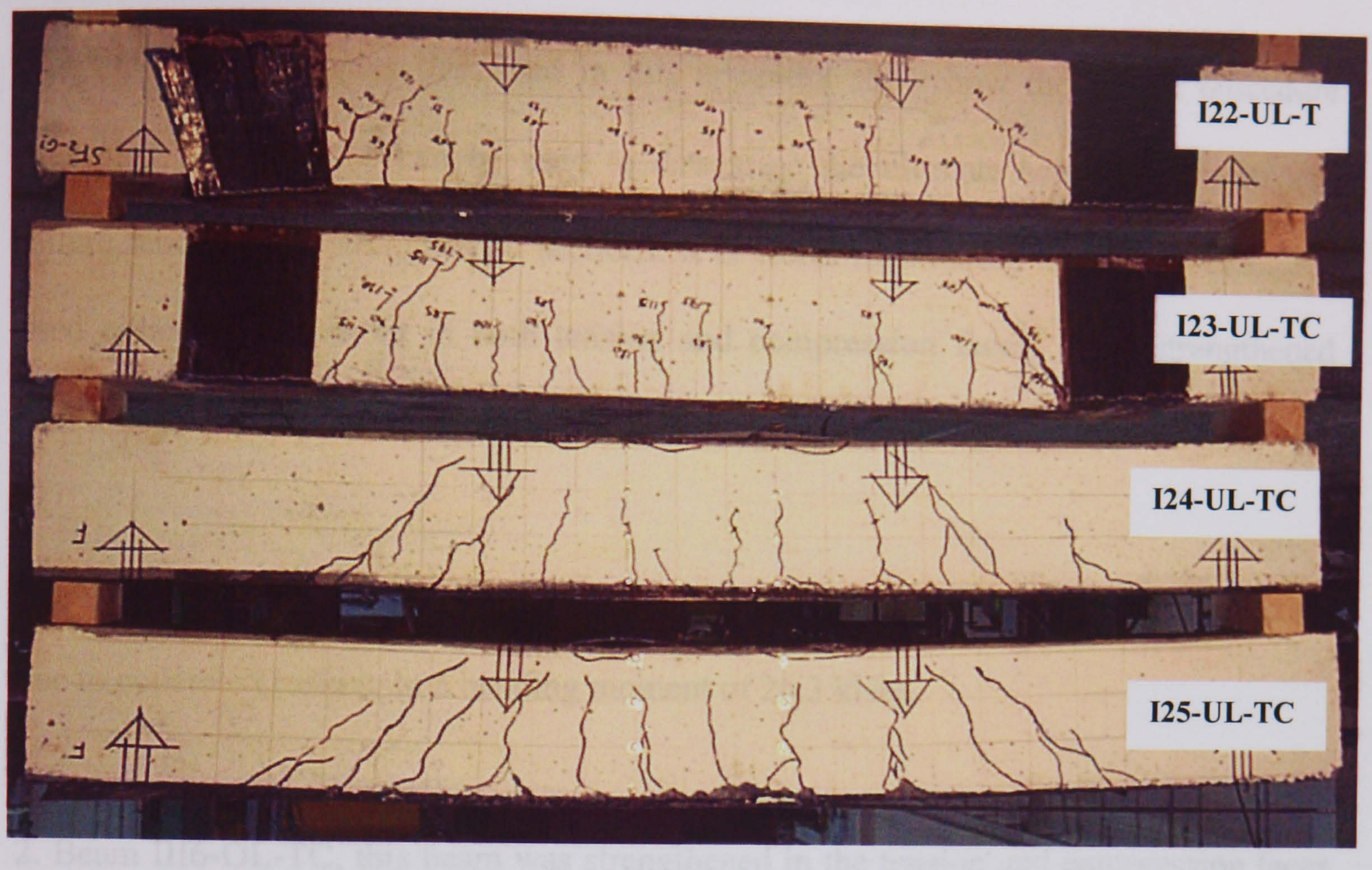

Figure A.1d: Typical cracks at failure for strengthened beams in second group of series-I

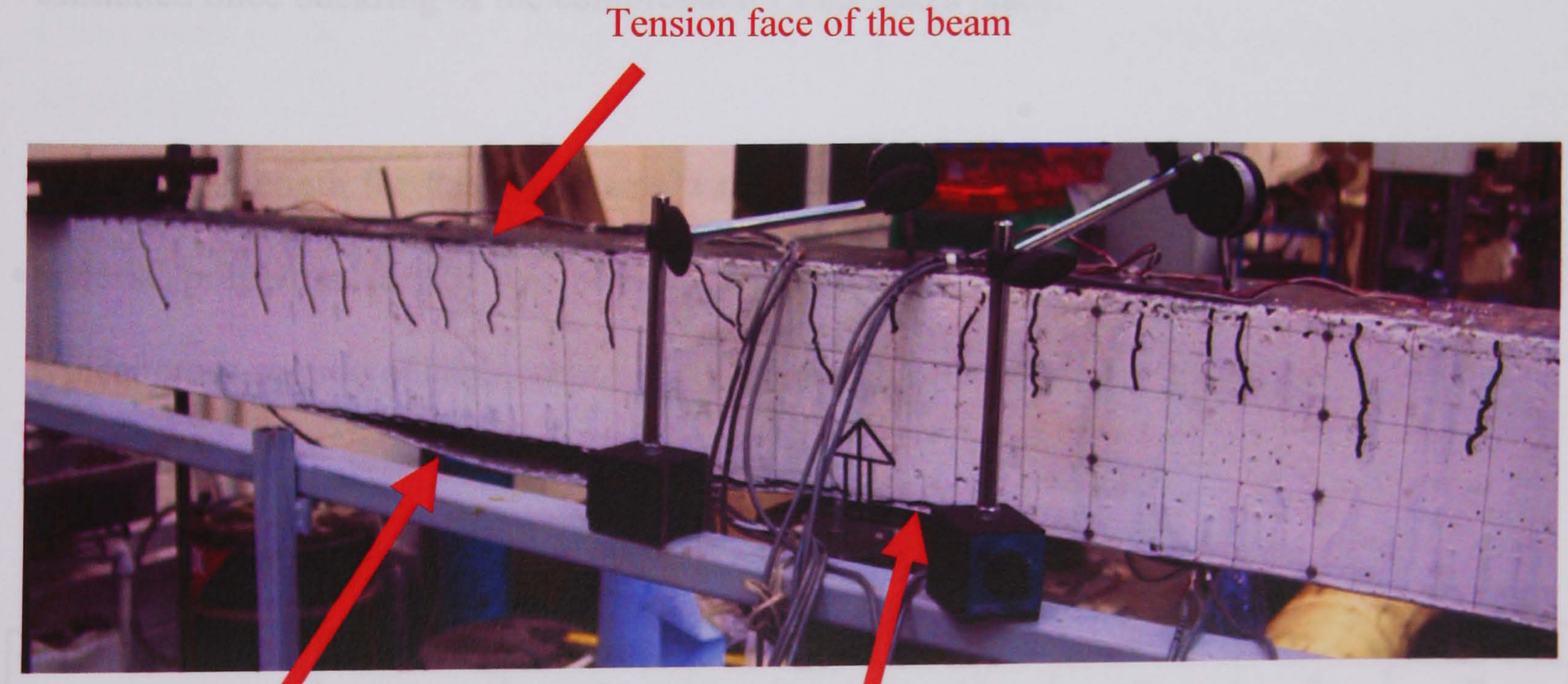

Figure A.3: Buckling of CFRP laminate in beam III6-OL-TC.

APPENDIX B
WORKED EXAMPLES

The following examples described in this appendix show how the design procedure presented in Chapter 5 can be used to determine the ultimate bending moment and failure mode of the strengthened sections. It is worth mentioning that the procedure is used either in tension or in both tension and compression faces. Two strengthened reinforced concrete beams were chosen from the current investigation.

1. Beam III2-OL-T, this beam was strengthened in the tension face and failed by flexure due to concrete crushing at a bending moment of 26.3 kNm.

2. Beam III6-OL-TC, this beam was strengthened in the tension and compression faces and failed by buckling of the CFRP laminates at a bending moment of 71.90 kNm. The ultimate concrete strain when buckling occurred was taken as 0.003, Section 5.4. In this beam, the design procedure proved that the ultimate bending moment of a beam can be estimated once buckling of the compression CFRP takes place.

The shear strength for the two beams was calculated in accordance with BS8110. The material properties for the two beams are presented in Table B-1. Figure B1 shows a typical cross-section of each beam.

Table B-1: Material properties of the worked examples

Material property	Concrete	Longitudinal steel		Stirrups		CFRP	
	f_{cu} (N/mm^2)	f_y (N/mm^2)	E_s (kN/mm^2)	f_{yv} (N/mm^2)	E_{sv} (kN/mm^2)	f_f (N/mm^2)	E_f (kN/mm^2)
Beam III2-OL-T	37.48	530 [1] 368 [2]	212 [1] 200 [2]	368	200	802.37	61.94
Beam III6-OL-TC	40.50						
[1]: tension steel bars ; [2]: compression steel bars							

Figure B1: Two reinforced concrete strengthened beams tested in the current study; a) beam III2-OL-T; b) beam III6-OL-TC

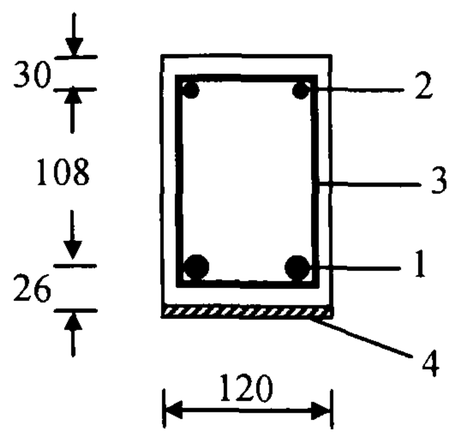

(a)

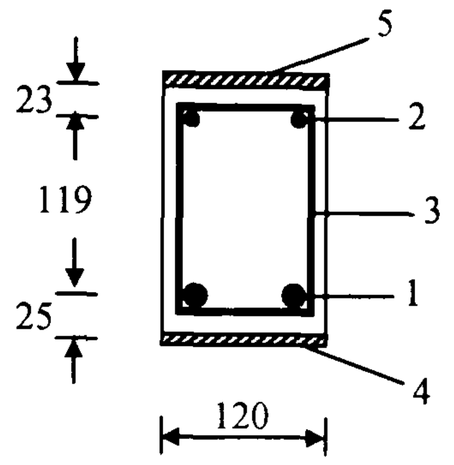

(b)

1:2 bars 16 mm diameter 2:2 bars 6 mm diameter 3:2 bars 6mm diameter each 50 mm spacing between stirrups 4: 6 CFRP tensile laminates, (A_f=288 mm^2) All dimensions in mm	1: 2 bars 16 mm diameter 2: 2 bars 6 mm diameter 3 :2 bars 6mm diameter each 50 mm spacing between stirrups 4: 6 CFRP tensile laminates, (A_f=288 mm^2) 5: 10 CFRP compression laminates, (A_{fc} = 480mm^2)

B.1 Beam III2-OL-T

B.1.1 Design for flexure failure

As reported in Section 5.4.4, the design procedure starts by calculating the constraints ratio of CFRP which controls the mode of failure as shown in Figures 5.11 and 5.12. Consequently, the type and design procedure for a given strengthened section can be determined.

a) CFRP ratio applied ρ_{fca}

Calculate the CFRP ratio applied on section, (6 laminates, 120 mm width and 0.4 mm thickness each).

$$\rho_{fca} = \frac{0.4x120x6}{120x164} x100 = 1.46\ \%$$

b) CFRP rupture (lower limit)

- Calculate the ratio, x_l / d_f, from equation (5-38), where the beam depth d_f = 164 mm, the strains in concrete and CFRP are ε_{cu}=0.0035 and ε_{fu}= 0.0130. respectively.

$$\frac{x_l}{d_f}=\frac{0.0035}{0.013+0.0035}=0.213,\quad x_l=34.88\ \text{mm}$$

- The stresses in the tension CFRP, f_f, and tension steel, f_s, respectively, are $f_f=f_{fu}=802.37\ \text{N/mm}^2$ and $f_s=f_y=530\ \text{N/mm}^2$, Table B1.
- Calculate ε_{sc} and f_{sc} from equations 5-41 and 5-36, respectively.

  $\varepsilon_{sc}=0.00049<0.0018,\ f_{sc}=98.02\ \text{N/mm}^2<368\ \text{N/mm}^2$
- Calculate the depth ration $n=d_s/d_f=0.84$, the tension steel ratio $\rho_s=A_s/bd_s=0.0242$ and the compression steel ratio $\rho_{sc}=A_{sc}/bd_s=0.0034$.
- Calculate the ratio of lower limit of the CFRP in tension face from eq.5-48.

$$\rho_{fl}(\%)=\left\{\frac{1}{802.37}\left(0.67x0.9x37.48x0.213+0.84\left(0.0034x98.02-0.0242x530\right)\right)\right\}100$$

$$=-0.708\ \%<1.46\ \%$$

This means that as long as ρ_{fl} is negative, the tensile rupture of the CFRP laminate with the properties given in Table B.1 will not occur for any given ratio of the CFRP laminate. Accordingly, the failure mode tends to occur by either Mode-II or Mode-III, Section 5.4.4.1. Therefore, the ratio of the CFRP will be calculated for the steel balanced section. This ratio represented by upper limit of CFRP.

c) CFRP upper limit

- Calculate the ratio x_u/d_s from equation 5-51, where the effective beam depth $d_s=138$ mm, the strain in the tensile steel bar is $\varepsilon_y=0.0025$.

$$\frac{x_u}{d_s}=\frac{0.0035}{0.025+0.0035}=0.583,\quad x_u=80.50\ \text{mm}$$

- Calculate the strains ε_{sc} and ε_f from equations 5-41 and 5-38 with $x=x_u$ respectively.

  $\varepsilon_{sc}=0.0022>0.0018,\ \varepsilon_f=0.0036$
- $f_{sc}=368\ \text{N/mm}^2$ (from equation 5-37) and $f_f=224.87\ \text{N/mm}^2$ (from equation 5-9).
- Considering the calculated values of the depth ratio $n=0.84$, $\rho_s=0.0242$ and $\rho_{sc}=0.0034$, in Section b.

- Calculate the ratio of upper limit of the CFRP in tension face which makes steel balanced section from equation 5-52.

$$\rho_{fu}(\%)=\left\{\frac{0.84}{224.87}\left(0.67x0.9x37.48x0.583+\left(0.0034x368-0.0242x530\right)+0\right)\right\}100$$

$$= 0.613\ \% < 1.46\ \%$$ (the CFRP ratio applied on the beam section).

Consequently, the flexure failure will be due to concrete crushing before both steel yielding and rupture of the CFRP laminates such as over-reinforced section. Hence, the failure satisfies Mode-III, Section 5.4.4.3.

d) Ultimate bending moment of the section

- Calculate the depth of the neutral axis x_3 from equation 5-56, where $m = 0.183$, the parameters

$$k_3 = \frac{0.0035}{0.67x0.9x37.48}\left(0.842x0.0034x200000+0.842x0.0242x212000+0.0146x61940+\right.$$

$$= 0.897$$

$$k_4 = \frac{-0.0035}{0.67x0.9x37.48}\left(0.842x0.183x0.0034x200000+0.842^2\,x0.0242x212000+0.0146x6194\right.$$

$$= -0.718$$

$$x_3 = \frac{164}{2}\left(-0.897+\sqrt{(0.897)^2-4(-0.718)}\right)= 83.71\ \text{mm}$$

- Calculate the ultimate bending moment, *Mu,* from equation 5-57

$$M_u = 0.67x0.9x37.48x120x83.71\,(164-0.5x0.9\,x83.71)+56.5x368(164-30)+0$$

$$-400x481.26(164-138) = 26.46\text{x}10^6\ \text{Nmm} = 26.46\ \text{kNm} \cong 26.30\ \text{kNm}$$

(Observed from the test)

B.1.2 Design shear resistance of beam

The ultimate bending moment calculated from the previous section was 26.46 kNm. Because the shear span of the beam tested was 1m, the shearing force due to ultimate loads at the beam support is $V = 26.46$kN. Consequently, the average shear stress v that is required, at any vertical cross-section along shear span, according to BS 8110, should be calculated from:

$$v = \frac{V_c}{bd_s} = \frac{26.46x10^3}{120x138} = 1.60 \text{ N/mm}^2$$

The resisting shear stress, includes shear stress caused from the concrete, v_c, and that from stirrups, v_s, is

$v_c = \frac{0.79}{\gamma_m}\left(\frac{100A_s}{bd_s}\right)^{\frac{1}{3}}\left(\frac{400}{d_s}\right)^{\frac{1}{4}}$, where $\left(\frac{100A_s}{bd_s}\right) \leq 3$, $\left(\frac{400}{d_s}\right) \geq 1$ and for characteristic concrete strength $f_{cu} > 25$ N/mm^2 the value of v_c should be multiplied by $(f_{cu}/25)^{1/3}$. Hence,

$$v_c = \frac{0.79}{1}\left(\frac{100x400}{120x138}\right)^{\frac{1}{3}}\left(\frac{400}{138}\right)^{\frac{1}{4}}\left(\frac{37.48}{25}\right)^{\frac{1}{3}} = 1.57 \text{ N/mm}^2$$

Because the test specimen was required to achieve flexure failure, the average shear stress of the section is assumed to be fully resisted by the stirrups. Two bars 6 mm diameter with 50 mm spacing were selected.

$$v_s = \frac{0.95 f_{yv} A_{sv}}{sb} = \frac{0.95x368x56.5}{50x120} = 3.30 \text{ N/mm}^2$$

A small spacing between the stirrups was used to accommodate shear stress produced in beam III6-OL-TC, as will be discussed later, where the CFRP was applied on the compression face. The total shear resistance obtained from stirrups was $v_s = 3.30$ N/mm^2 > 1.6 N/mm^2 (the average shear stress). Therefore, failure was caused by flexure due to concrete crushing as had been predicted.

B.2 Beam III6-OL-TC

B.2.1 Design for flexure failure

Beam III6-OL-TC was strengthened in both tension and compression faces and was assumed to fail by flexure due to concrete crushing. However, the CFRP was buckled before concrete crushing took place. As observed in Section 4.3.6, buckling of CFRP laminates occurred when the average concrete strain reached a value of 0.003. This value of strain is considered as the ultimate strain when the design procedure, section

5.4.4, is used to calculate ultimate bending moment of reinforced concrete beam strengthened on compression. Similar design procedures to that in beam III2-OL-T are carried out.

a) CFRP ratio applied ρ_{fca}

ρ_{fca} = 1.44 %, where $d_f = h$ = 167 mm

b) CFRP rupture (lower limit)

- $\frac{x_l}{d_f} = \frac{0.003}{0.013 + 0.003}$ = 0.188, from equation 5-38, where the strains in concrete and CFRP laminates are ε_{cu} =0.003 and ε_{fu} = 0.0130, respectively.

  x_l = 31.40 mm

- The stresses in the tension CFRP and the tension steel, respectively, are $f_f = f_{fu}$ = 802.37 N/mm^2 and $f_s = f_y$ =530 N/mm^2, Table B1.
- Calculate ε_{sc} and f_{sc} from equations 5-41 and 5-36, respectively.

  ε_{sc} = 0.0008 < 0.0018, f_{sc} =160.55 N/mm^2 < 368 N/mm^2
- Calculate $n = d_s / d_f$ = 0.85, $\rho_s = A_s / bd_s$ =0.0235, $\rho_{sc} = A_{sc} / bd_s$ =0.0033 and $\rho_{fc} = A_{fc} / bd_f$ =0.024.
- Calculate the ratio of lower limit of the CFRP in tension face from eq.5-48.

$$\rho_{fl}(\%) = \left\{\frac{1}{802.37}\left(0.67x0.9x40.5x0.188 + 0.85\left(0.0033x160.55 - 0.0235x530\right) + 0.003x61940x0.024\right)\right\}100$$

= -0.135 % < 1.43 %,

This confirms the same case that was discussed in beam III2-OL-T. The ratio of the CFRP will be calculated for the steel balanced section, which is represented by the upper limit of CFRP.

c) CFRP upper limit

- Calculate the ratio $\frac{x_u}{d_s} = \frac{0.003}{0.025 + 0.003}$ = 0.546. from equation 5-51. where the strain in the tensile steel bar is ε_y = 0.0025.

$x_u = 77.45$ mm

- Calculate the strains ε_{sc} and ε_f from equations 5-41 and 5-38 with $x = x_u$. respectively.

  $\varepsilon_{sc} = 0.0021 > 0.0018$, $\varepsilon_f = 0.0035$

- $f_{sc} = 368$ N/mm^2 (from equation 5-37) and $f_f = 214.83$ N/mm^2 (from equation 5-9).
- Considering the calculated values of the depth ration $n = 0.85$, $\rho_s = 0.0235$, $\rho_{sc} = 0.0033$ and $\rho_{fc} = 0.024$, in Section b.
- Calculate the ratio of upper limit of the CFRP in tension face that makes steel balanced section from equation 5-52.

$$\rho_{fu}(\%) =$$

$$\left\{\frac{0.85}{214.83}\left(0.67x0.9x40.5x0.546 + \left(0.0033x368 - 0.0235x530\right) + 0.003x61940x0.024\right)\right\}100$$

$= 2.59\ \% > 1.46\ \%$ (the actual ratio of the CFRP laminates).

Accordingly, the steel reinforcement will be yielded before concrete crushing takes place such as under-reinforced section. So, the failure satisfies Mode-II, Section 5.4.4.3.

d) Ultimate bending moment of the section

- Calculate the depth of the neutral axis x_2 from equation 5-53, where $n_1 = 6.17$, $m_1 = 7.26$, the parameters

$$k_3 = \frac{1}{0.67x0.9x40.5}\left(6.17(0.0033x200000x0.003 - 0.0235x530)\right)$$
$$+ \left(7.26x0.003x61940(0.0144 + 0.024)\right) = -0.525$$

$$k_4 = \frac{-0.003}{0.67x0.9x40.5}\left(6.17x0.0033x200000 + 7.26^2 x\, 0.0144x61940\right) = -6.27$$

$$x_2 = \frac{23}{2}\left(-(-0.525) + \sqrt{(-0.525)^2 - 4(-6.27)}\right) = 63.94 \text{ mm}$$

- $\varepsilon_{sc} = 0.0019 > 0.0018$ (from equation 5-41), hence, $f_{sc} = 368$ N/mm^2 (from equation 5-37).
- Calculate the ultimate bending moment, M_u from Equation (5-55)

$$M_u = 0.67x0.9x40.5x120x63.94\,(167 - 0.5x0.9\,x63.94) + 56.5x368(167 - 23)$$
$$+ 0.003x61940x480x167 - 400x530(167 - 142) = 38.50\text{x}10^6\,\text{Nmm}$$
$$= 38.50\ \text{kNm} > 35.95\ \text{kNm}\ \text{(which observed from the test).}$$

The calculated moment indicts 6.5% higher than the measured.

B.2.2 Design shear resistance of beam

The ultimate bending moment calculated from the previous section was 38.50 kNm. Because the shear span of the beam tested was similar to that of III2-OL-T, the ultimate shearing force at the beam supports is V = 38.50 kN. Accordingly, the average shear stress v at any vertical cross-section along shear span can be calculated from:

$$v = \frac{V_c}{bd_s} = \frac{38.50x10^3}{120x142} = 2.26\ \text{N/mm}^2$$

Similar procedures for calculating the shear resistance of beam III2-OL-T were carried out. Same area and arrangement of shear reinforcement, stirrups, in beam III2-OL-T were also used. This is because the average shear stress calculated from beam III6-OL-TC is less than that calculated from the stirrups of beam III2-OL-T (2.26 N/mm^2 < 3.30 N/mm^2).

Notice that, the examples previously explained that the simplified design procedures presented in this study are able to estimate the ultimate bending moment of reinforced concrete beam strengthened with CFRP either on tension or both the tension and compression face.

APPENDIX C
DERIVATION OF NEUTRAL AXIS DESIGN FORMULA FOR RC BEAM STRENGTHENED WITH CFRP COMPOSITE

Appendix C shows the derivation of the values of the depth of the neutral axis x that cause ultimate capacity of RC beam strengthened with CFRP given in chapter 4. Four equations based on failure mode are described.

- Equation (5-49): FRP rupture, Mode-I.
- Equation (5-53): steel yielding followed by concrete crushing, Mode-II, double reinforced section.
- Equation (5-54): steel yielding followed by concrete crushing, Mode-II, single reinforced section.
- Equation (5-56): concrete crushing before steel yielding, Mode-III.

Derivation of the four equations is given as follow:

C.1 Equation (5-49)

- In the failure mode characterised by this equation, the stresses in the tension CFRP and the tension steel are $f_f = f_{fu}$ and $f_s = f_y$, respectively. The strain in the concrete is $\varepsilon_{fc} = \varepsilon_{cu}$. However, in the case where the compression steel has been included in the composite section, the compression steel is not necessary to reach yielding. By replacing the stresses in equation 5-42 the following equation is obtained

$$k_1 k_2 f_{cu}\, b\, x + A_{sc} E_{sc} \varepsilon_{sc} + A_{fc} f_{fc} + A_s f_y + A_f f_{fu} = 0 \qquad \text{(C-1)}$$

- By substituting the areas of reinforcement in the composite section A_s, A_{sc}, A_f, A_{fc} by the reinforcement ratios, $A_s = \rho_s b d_s$, $A_{sc} = \rho_{sc} b d_s$, $A_f = \rho_f b d_f$, $A_{fc} = \rho_{fc} b d_f$, in the above equation and considering sign conversions, we can get the following equation:

$$k_1 k_2 f_{cu} x + \rho_{sc} E_{sc} \varepsilon_{sc} d_s + \rho_{fc} f_{fc} d_f - \rho_s f_y d_s - \rho_f f_{fu} d_f = 0 \qquad \text{(C-2)}$$

- Dividing the right hand side of equation 5-41 by the effective depth of external reinforcement d_f, the strain in the compression steel is then calculated as follows

$$\varepsilon_{sc} = \varepsilon_{cu} \left(\frac{x/d_f - d_{sc}/d_f}{x/d_f} \right) \qquad \text{(C-3)}$$

- Substituting the strain from equation C-3 in equation C-2, multiplying by $x/d_f{}^2$ and rearranging in terms of finding the depth of the neutral axis x of the composite section, also consider $n = d_s/d_f$ and $m = d_{sc}/d_f$, the following quadratic equation is obtained.

$$(\frac{x}{d_f})^2 + k_3(\frac{x}{d_f}) + k_4 = 0 \qquad \text{(C-4)}$$

- By considered the depth of the depth of the neutral axis $x = x_1$, which refers to failure Mode-I, and by solving the above quadratic equation into the basic roots the depth of the neutral axis x_1 of composite section is obtained

$$x_1 = \frac{d_f}{2}\left(-k_3 + \sqrt{k_3{}^2 - 4k_4} \right) \qquad \text{(5-49)}$$

where;

$$k_3 = \frac{1}{k_1 k_2 f_{cu}} \left(n\rho_{sc} E_{sc} \varepsilon_{cu} + \varepsilon_{cu} E_{fc} \rho_{fc} - n\rho_s f_y - \rho_f f_{fu} \right)$$

$$k_4 = \frac{-1}{k_1 k_2 f_{cu}} \left(nm\rho_{sc} E_{sc} \varepsilon_{cu} \right)$$

C.2 Equation (5-53)

- In this mode of failure, the strain in tension steel reaches the yielded values followed by concrete crushing, simultaneously, while the tensile FRP composite is not reach the rupture limit. Hence, $f_s = f_y$, $\varepsilon_{fc} = \varepsilon_{cu}$ and $f_f < f_{fu}$. The compression steel is included in this case; however, the yield stress does not

necessary to be reached. By replacing of these stresses in equation 5-42 the following equation is obtained

$$k_1 k_2 f_{cu}\, b\, x + A_{sc} f_{sc} + A_{fc} f_{fc} + A_s f_y + A_f f_f = 0 \qquad \text{(C-5)}$$

- By substituting of the areas of reinforcement in the composite section A_s, A_{sc}, A_f, A_{fc} by the reinforcement ratios as in C-2 in the above equation,we c an obtain the following equation:

$$k_1 k_2 f_{cu} x + \rho_{sc} f_{sc} d_s + \rho_{fc} f_{fc} d_f + \rho_s f_y d_s + \rho_f f_f d_f = 0 \qquad \text{(C-6)}$$

- By replacing the stresses, f_{sc} and f_f equation (C-6) by $E_{sc}\varepsilon_{sc}$ and $E_f \varepsilon_f$ for compression steel and the tension CFRP, receptively, then the following equation is governed

$$k_1 k_2 f_{cu} x + \rho_{sc} E_{sc} \varepsilon_{sc} d_s + \rho_{fc} E_{fc} \varepsilon_{fc} d_f + \rho_s f_y d_s + \rho_f E_f \varepsilon_f d_f = 0 \qquad \text{(C-7)}$$

- The strains in the tension CFRP and the compression steel are calculated from equations (5-38) and (5-41), respectively, and by dividing the right hand side of each by the concrete cover in compression d_{sc}, getting the following

$$\varepsilon_f = \varepsilon_{cu}\left(\frac{d_f / d_{sc} - x / d_{sc}}{x / d_{sc}}\right) \qquad \text{(C-8)}$$

$$\varepsilon_{sc} = \varepsilon_{cu}\left(\frac{x / d_{sc} - 1}{x / d_{sc}}\right) \qquad \text{(C-9)}$$

- Substituting the calculated strains from equations (C-8) and (C-9) in equation (C-7), assuming the strains in tension CFRP and tension steel yield are negative and multiplying by $x / d_{sc}{}^2$. Take ratios $n_1 = d_s / d_{sc}$ and $m_1 = 1/m$ and rearranging in terms of finding the depth of the depth of the neutral axis x. the following quadratic equation is obtained.

$$(\frac{x}{d_{sc}})^2 + k_3(\frac{x}{d_{sc}}) + k_4 = 0 \qquad \text{(C-10)}$$

- Considering the depth of the depth of the neutral axis $x = x_2$, which refers to failure Mode-II, and by solving the above quadratic equation into the basic roots. ignore the negative vale, the depth of the depth of the neutral axis x_2 is obtained

$$x_2 = \frac{d_{sc}}{2}\left(-k_3 + \sqrt{k_3{}^2 - 4k_4}\right) \qquad \text{(5-53)}$$

where

$$k_3 = \frac{1}{k_1 k_2 f_{cu}}\left(n_1(\rho_{sc}E_{sc}\varepsilon_{cu} - \rho_s f_y) + m_1\varepsilon_{cu}(\rho_f E_f + \rho_{fc}E_{fc})\right)$$

$$k_4 = \frac{-\varepsilon_{cu}}{k_1 k_2 f_{cu}}\left(n_1\ \rho_{sc}E_{sc} + m_1{}^2\ \rho_f E_f\right)$$

C.3 Equation (5-54)

- Equation 5-54 is derived for similar failure mode to that in equation 5-53, but the compression steel reinforcement is omitted. Eliminating the term of compression steel from equations C-5, C-6 and C-7 and following similar process in equation 5-53, is leading to the following equation.

$$k_1 k_2 f_{cu} x + \rho_{fc} f_{fc} d_f + \rho_s f_y d_s + \rho_f E_f \varepsilon_f d_f = 0 \qquad \text{(C-11)}$$

- The strain in the tension CFRP is calculated from equation 5-38 by dividing the right hand side by the beam depth d_f, and consider sign conversion for ε_f getting the following

$$\varepsilon_f = -\varepsilon_{cu}\left(\frac{1 - x/d_f}{x/d_f}\right) \qquad \text{(C-12)}$$

- Substituting the strain from equation C-12 in equation C-11, the tensile yield stress is assumed to be negative, and multiplying by $x/d_f{}^2$. Take ratio $n = d_s/d_f$ and rearranging in term of finding the depth of the depth of the

neutral axis x of the composite section, the following quadratic equation is obtained.

$$(\frac{x}{d_f})^2 + k_3(\frac{x}{d_f}) + k_4 = 0 \qquad \text{(C-13)}$$

- Solving the above quadratic equation into the basic roots, ignore the negative value, the depth of the depth of the neutral axis x_2 of composite section is determined

$$x_2 = \frac{d_f}{2}\left(-k_3 + \sqrt{k_3{}^2 - 4k_4}\right) \qquad \text{(5-60)}$$

where

$$k_3 = \frac{1}{k_1 k_2 f_{cu}}\left(\rho_{fc} E_{fc} \varepsilon_{cu} + \rho_f E_f \varepsilon_{cu} - n \rho_s f_y\right)$$

$$k_4 = \frac{-\rho_f E_f \varepsilon_{cu}}{k_1 k_2 f_{cu}}$$

C.4 Equation (5-56)

- The failure mode characterised by this equation is flexure due to concrete crushing while the stresses in tension steel and in the tension FRP composite do not reach either yield stress in steel or the rupture limit of FRP $f_s < f_y$ and $f_f < f_{fu}$. However, the compression steel, $f_{sc} \le f_y$.
- By replacing the stresses, f_s, f_f and f_{sc} from equation 5-42 and substituting of strains and elasticity module, respectively, for each, the following equation obtained

$$k_1 k_2 f_{cu}\, b\, x + A_s E_s \varepsilon_s + A_{sc} E_{sc} \varepsilon_{sc} + A_{fc} E_{fc} \varepsilon_{cu} + A_f E_f \varepsilon_f = 0 \qquad \text{(C-14)}$$

- By substituting of the areas of reinforcement A_s, A_{sc}, A_f, A_{fc} by the reinforcement ratios ,as in C-2, and dividing by the effective depth of CFRP d_f and substituting, getting the following equation

$$k_1 k_2 f_{cu}(\frac{x}{d_f}) + \rho_s E_s \varepsilon_s (\frac{d_s}{d_f}) + \rho_f E_f \varepsilon_f + \rho_{sc} E_{sc} \varepsilon_{sc} (\frac{d_s}{d_f}) + \rho_{fc} E_{fc} \varepsilon_{fc} = 0 \quad \text{(C-15)}$$

Take $n = d_s / d_f$, consider the negative strains values in the tensile CFRP and the steel and equating for ε_f

$$\varepsilon_f = \frac{1}{\rho_f E_f}\left(k_1 k_2 f_{cu}(\frac{x}{d_f}) + n\rho_{sc} E_{sc} \varepsilon_{sc} - n\rho_s E_s \varepsilon_s + \rho_{fc} E_{fc} \varepsilon_{cu} \right) \quad \text{(C-16)}$$

- By substituting of ε_f from equation 5-39 and rearrangement

$$\varepsilon_s = \frac{1}{z_1 \rho_f E_f}\left(k_1 k_2 f_{cu}(\frac{x}{d_f}) + n\rho_{sc} E_{sc} \varepsilon_{sc} + \rho_{fc} E_{fc} \varepsilon_{cu} \right) \quad \text{(C-17)}$$

where, $z_1 = \left(\frac{1 - x/d_f}{n - x/d_f} + \frac{n\rho_s E_s}{\rho_f E_f} \right)$

- The strain in the tension steel ε_s may exist from equation 5-40 and dividing the right hand side by d_f, the following form is obtained

$$\varepsilon_s = \varepsilon_{cu} \frac{n - x/d_f}{x/d_f} \quad \text{(C-18)}$$

- By equating the two equations C-17 and C-18 in terms of finding the tensile strain in the compression steel ε_{sc}

$$\varepsilon_{sc} = \frac{1}{n\rho_{sc} E_{sc}}\left(\varepsilon_{cu} z_1 \rho_f E_f (\frac{n - x/d_f}{x/d_f}) - k_1 k_2 f_{cu}(\frac{x}{d_f}) - \rho_{fc} E_{fc} \varepsilon_{cu} \right) \quad \text{(C-19)}$$

- The strain in compression steel ε_{sc} may exist from equation 5-41 with similar way of that in tension and dividing the right hand side by d_f and take $m = d_{sc} / d_f$, the following form is given

$$\varepsilon_{sc} = \varepsilon_{cu}\left(\frac{x/d_f - m}{x/d_f} \right) \quad \text{(C-20)}$$

- By equating the two equations C-19 and C-20 and rearranging in terms of finding the depth of the depth of the neutral axis x of the composite section, the following quadratic equation is governed

$$(\frac{x}{d_f})^2 + k_3(\frac{x}{d_f}) + k_4 = 0 \qquad \text{(C-21)}$$

- By considering the depth of the depth of the neutral axis $x = x_3$, which refers to failure Mode-III, and by solving the above quadratic equation into the basic roots, ignore the negative value, the depth of the neutral axis x_3 of composite section is obtained

$$x_3 = \frac{d_f}{2}\left(-k_3 + \sqrt{k_3{}^2 - 4k_4}\right) \qquad \text{(5-56)}$$

where

$$k_3 = \frac{\varepsilon_{cu}}{k_1 k_2 f_{cu}}\left(n\rho_{sc}E_{sc} + n\rho_s E_s + \rho_f E_f + \rho_{fc}E_{fc}\right)$$

$$k_4 = \frac{-\varepsilon_{cu}}{k_1 k_2 f_{cu}}\left(n\,m\rho_{sc}E_{sc} + n^2\rho_s E_s + \rho_f E_f\right)$$